Report
R-23-04
October 2023

Control of deterministically modelled structures on the stress variability at Forsmark

Jouni Valli
Matti Hakala
Jussi Mattila
Rodrigo Winderholler

SVENSK KÄRNBRÄNSLEHANTERING AB

SWEDISH NUCLEAR FUEL
AND WASTE MANAGEMENT CO

Box 3091, SE-169 03 Solna
Phone +46 8 459 84 00
skb.se

SVENSK KÄRNBRÄNSLEHANTERING

ISSN 1402-3091
SKB R-23-04
ID 2008333
October 2023

Control of deterministically modelled structures on the stress variability at Forsmark

Jouni Valli, Matti Hakala, Jussi Mattila, Rodrigo Winderholler
Rock Mechanics Consulting Finland Oy

Keywords: 3D modelling, Numerical simulations, In situ stress, Mean stress, Stress variability, Shear displacement, Slip, Deformation zones.

Abstract

The Swedish Nuclear Fuel and Waste Management Company (SKB) has selected the Forsmark site for the construction of a deep nuclear waste repository at a preliminary target depth of 470 m. In the design of such a repository, many factors must be considered to meet all functional requirements for long-term safety, including the in situ rock stress state. The current stress state in the Fennoscandia area is dominated and driven by Mid-Atlantic ridge push and collision of the Eurasian and African plates in the Alps. Past glaciation has been interpreted to have caused stress changes and promoted deformation zone slip. Shallow dipping deformation zones (DZ) have been and are at present prone to slip in the prevailing thrust fault conditions.

Between 1991–2007, approximately 130 rock stress measurements with overcoring and 240 measurements with hydraulic methods have been carried out in the Forsmark area. These have been interpreted by Martin (2007) along with borehole breakout, core disking and non-linear strain rock sample data, resulting in an interpretation with notable variation in horizontal stress components that did not address variability.

This study functions as an update to a previous study by Hakala et al. (2019) that examined the interaction of brittle DZs and the in situ stress state in the Forsmark area by means of 3D numerical simulations. The first phase of this study validated the applicability of a new approach using FLAC3D instead of the previously used 3DEC code, using geometrically identical models with a limited number of DZs and coarse discretisation. The second phase applied this new approach to update the Forsmark stress model using the latest Deterministic Model for Structures (DMS), including 152 DZs in a higher resolution model. Seven cases, with different target stress magnitudes and trends, were simulated to cover the uncertainties of the current in situ stress model.

Phase 1 demonstrated a sufficiently similar result, particularly with respect to stress changes between the two codes, while DZ slip was not exactly identical. FLAC3D was therefore selected for use in Phase 2 given computation time was also significantly reduced.

All the target stress states of Phase 2 were achieved at the repository depth (470 m) using boundary thrust conditions and the defined rock mass elastic parameters and DZ shear strength parameters. The depth dependent stress magnitudes and orientations in Martin (2007) were also matched fairly well: all cases were deemed physically plausible.

Of the simulated cases, the Base case and Case 4 results matched the overcoring stress measurements best with the σ_1 and σ_2 magnitude elevated by 15 % and 20 %, respectively, relative to the Base case. The uncertainty of the field stress measurements is, however, quite high. The simulated stresses were in good agreement with the Martin (2007) stress model, although simulations indicate a steeper σ_1 gradient above a depth of 200 m.

Sammanfattning

Svensk Kärnbränslehantering AB (SKB) har valt Forsmark som plats för att bygga ett slutförvar för använt kärnbränsle, på ett preliminärt djup av 470 m. Vid utformningen av ett sådant förvar måste hänsyn tas till många faktorer för att uppfylla alla funktionskrav för långsiktig säkerhet, bland annat bergspänningstillståndet in situ. Det nuvarande spänningsfältet i Fennoskandien domineras och drivs av tektonisk plattförskjutning via Mittatlantiska ryggen och kollisionen mellan den Eurasiska och Afrikanska plattan. Tidigare glaciation har tolkats ha orsakat spänningsförändringar och främjat rörelser i deformationszoner. Flackt stupande deformationszoner (DZ) har varit, och är för närvarande, de mest benägna att skjuvas i de rådande förkastningsförhållandena.

Under perioden 1991–2007 har cirka 130 bergspänningsmätningar med överborrning och 240 mätningar med hydrauliska metoder utförts i Forsmarksområdet. Dessa har tolkats av Martin (2007) tillsammans med data från borrhålsutfall (”borehole breakouts”), uppsprickning i kärnor (”core disking”) och icke-linjära töjningsdata. Martin (2007) visade på en signifikant variation för båda de horisontella spänningskomponenterna, men presenterade inte någon förklaring till dessa variationer.

Denna studie kan ses som en uppdatering av en tidigare studie av Hakala et al. (2019) som undersökte betydelsen av DZ för variation i spänningstillståndet in situ, med hjälp av numeriska 3D-simuleringar. Den första fasen av denna studie validerade tillämpligheten av ett nytt tillvägagångssätt där programmet FLAC3D används istället för den tidigare 3DEC, i båda fallen med geometriskt identiska modeller med ett begränsat antal DZ och grov diskretisering. I den andra fasen tillämpades bergmodellen för strukturer (DMS), inklusive 152 DZ i modellen och med högre upplösning. Sju fall med olika målspänningsmagnituder och spänningsriktningar simulerades för att täcka osäkerheterna i den nuvarande in situ-spänningsmodellen.

Fas 1 visade ett tillräckligt likartat resultat, särskilt med avseende på spänningsförändringar mellan de två datorprogrammen, medan skjuvningsbeloppen i DZ inte var exakt identiska. Med hänsyn till den betydligt kortare beräkningstid valdes FLAC3D för användning i fas 2.

Alla ”målspänningstillstånd” i fas 2 uppnåddes på förvarsdjupet (470 m) med de använda randvillkoren och de definierade elastiska parametrarna för bergmassan och skjuvhållfasthetsparametrarna för DZ. De djupberoende spänningsmagnituden och riktningarna i Martin (2007) stämde också rätt väl överens med spänningarna modellerna, dvs alla beräkningsfall ansågs vara fysiskt rimliga.

Av de simulerade fallen överensstämde resultaten från basfallet och fall 4 bäst med bergspänningsmätningarna i fält. Där fall 4 har en förhöjd magnitud på σ_1 och σ_2 med 15 respektive 20 % i förhållande till basfallet. Osäkerheten i bergspänningsmätningarna är dock ganska hög. De simulerade spänningarna överensstämde väl med spänningmodellen som tolkats av Martins (2007), även om simuleringarna indikerar en brantare σ_1 gradient ned till 200 m djup.

Contents

1 Introduction

1.1 Background

The safe final disposal of spent nuclear fuel is critical in the design of a deep bedrock nuclear waste repository and is affected by several factors, including the in situ stress state as well as any identified geological features such as structures/deformation zones (DZ) at the selected site. The Swedish Nuclear Fuel and Waste Management Company (SKB) has selected the Forsmark site for the construction of a repository at a preliminary target depth of −470 m, which is in Northern Uppland approximately 100 km north of Stockholm (Figure 1-1). Site investigations have yielded a great deal of data that has resulted in the development of a Deterministic Model for Structures (DMS), which includes detailed three-dimensional models of all the deformation zones (DZ) at the Forsmark site, currently totalling 153 DZ (Hultgren and Petersson 2022). Such models have been used in previous studies for stress modelling purposes where the interaction of geological features such as faults or deformation zones and the stress state was simulated (Tonon et al. 2001, Tonon and Amadei 2003, Hakami 2006, Hakami and Min 2009, Valli et al. 2011, Valli et al. 2016, Hakala et al. 2019, Kaisko et al. 2023). A previous version of the DMS has been used for stress modelling in Hakala et al. (2019).

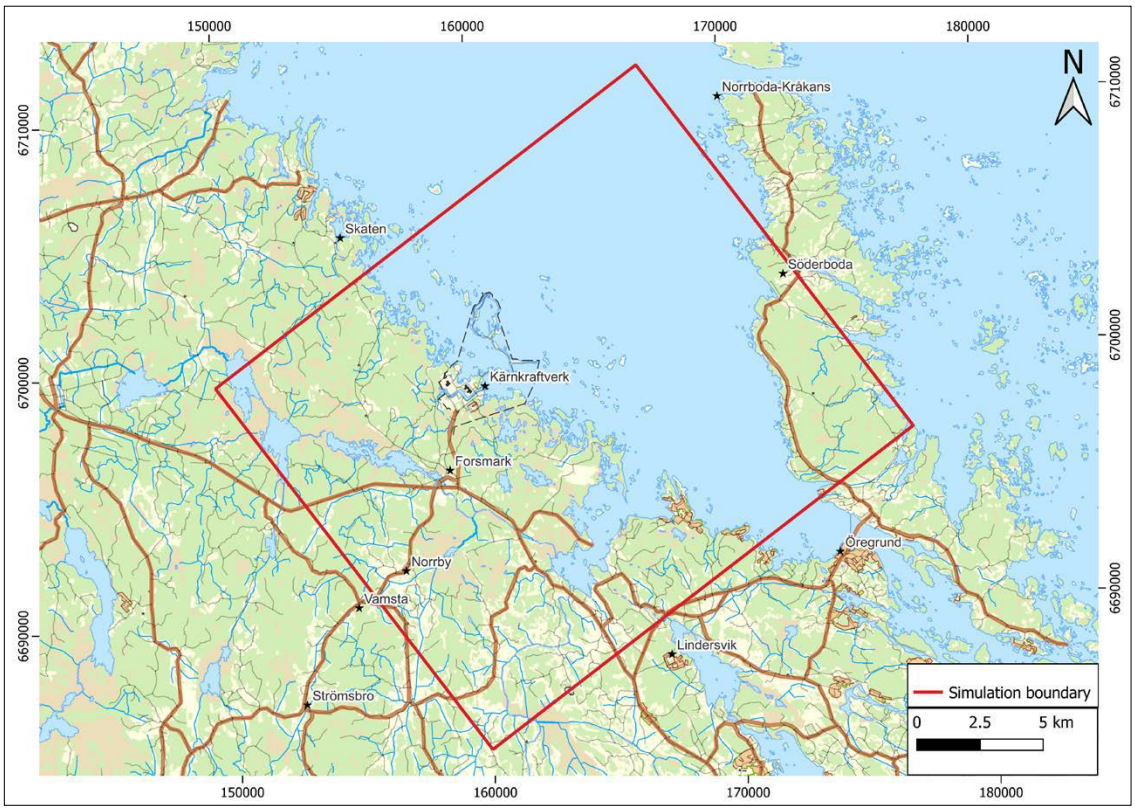

Figure 1-1. *The Forsmark site and the simulation area.*

1.2 Goals

This study was divided in two phases with the following objectives:

1. Verify a new numerical analysis approach available in FLAC3D (Itasca 2022a) for the simulation of the interaction of structures such as DZs with the in situ stress state at the Forsmark site against 3DEC (Itasca 2022b) and selecting the numerical code to be used in the next phase.
2. Once selected, the primary objective of this study was to update the Forsmark rock stress model by updating and taking the latest DMS model into account in the previous simulations (Hakala et al. 2019), where the interaction of the in situ stress state and all of the pertinent DZ in the Forsmark area were simulated.

Phase 2 simulations were set to analyse several aspects of seven cases to be simulated, including a Base case and six other stress field scenarios to cover the uncertainties of the current in situ stress model (Table 1-1). These aspects include:

- DZ shear displacements.
- The variation of the in situ stress state.
- The correlation with the in situ stress measurements.
- The sensitivity of the results to changes in DZ parameters.
- The sensitivity of the results to the orientation of applied thrust.

Table 1-1. The target stress fields for the cases in Phase 2.

Stress case	Depth range	Maximum horizontal stress		Minimum horizontal stress		Vertical stress
	(m)	σ_H (MPa)	Trend (°)	σ_h (MPa)	Trend (°)	σ_v (MPa)
Base case (Martin 2007, R-07-26)	0–150	19 + 0.008z	145	11 + 0.006z	55	0.0265z
	150–400	9.1 + 0.074z	145	6.8 + 0.034z	55	0.0265z
	400–600	29.5 + 0.023z	145	9.2 + 0.028z	55	0.0265z
Case 1 (Trend − 20°)	0–150	19 + 0.008z	125	11 + 0.006z	35	0.0265z
	150–400	9.1 + 0.074z	125	6.8 + 0.034z	35	0.0265z
	400–600	29.5 + 0.023z	125	9.2 + 0.028z	35	0.0265z
Case 2 (Trend + 20°)	0–150	19 + 0.008z	165	11 + 0.006z	75	0.0265z
	150–400	9.1 + 0.074z	165	6.8 + 0.034z	75	0.0265z
	400–600	29.5 + 0.023z	165	9.2 + 0.028z	75	0.0265z
Case 3 ($\sigma_h = \sigma_v$)	0–150	19 + 0.008z	145	0.0265z	55	0.0265z
	150–400	9.1 + 0.074z	145	0.0265z	55	0.0265z
	400–600	29.5 + 0.023z	145	0.0265z	55	0.0265z
Case 4 (σ_{Hmax}, σ_{hmax} and σ_{vmax})	0–150	1.20 × (19 + 0.008z)	145	1.25 × (11 + 0.006z)	55	0.0265z + 0.0005z
	150–400	1.15 × (9.1 + 0.074z)	145	1.25 × (6.8 + 0.034z)	55	0.0265z + 0.0005z
	400–600	1.15 × (29.5 + 0.023z)	145	1.20 × (9.2 + 0.028z)	55	0.0265z + 0.0005z
Case 5 (σ_{Hmax}, σ_{hmin} and σ_{vmin})	0–150	1.20 × (19 + 0.008z)	145	0.75 × (11 + 0.006z)	55	0.0265z − 0.0005z
	150–400	1.15 × (9.1 + 0.074z)	145	0.75 × (6.8 + 0.034z)	55	0.0265z − 0.0005z
	400–600	1.15 × (29.5 + 0.023z)	145	0.80 × (9.2 + 0.028z)	55	0.0265z − 0.0005z
Case 6 (σ_{Hmax} and $\sigma_{hmin} = \sigma_{vmin}$)	0–150	1.20 × (19 + 0.008z)	145	0.0265z − 0.0005z	55	0.0265z − 0.0005z
	150–400	1.15 × (9.1 + 0.074z)	145	0.0265z − 0.0005z	55	0.0265z − 0.0005z
	400–600	1.15 × (29.5 + 0.023z)	145	0.0265z − 0.0005z	55	0.0265z − 0.0005z

2 Initial data

The data used for this study include the most recent DMS (Hultgren and Petersson 2022), the in situ stress state interpretations defined in Martin (2007), as well as the rock mechanics (of the rock mass and the deformation zones) properties defined in Glamheden et al. (2007, 2008).

2.1 Deformation zones

The DZs in the most recent DMS are based on pre-existing models (Stephens and Simeonov 2015) but have been updated using the most recently available data in the Sicada database as of September 2022. All the DZs within the simulation area have been included in the simulation model, apart from ZFM1189 (see Section 3.2.2). This results in a total of 152 DZs being modelled in the simulation model out of the 153 in the DMS (Figure 2-1).

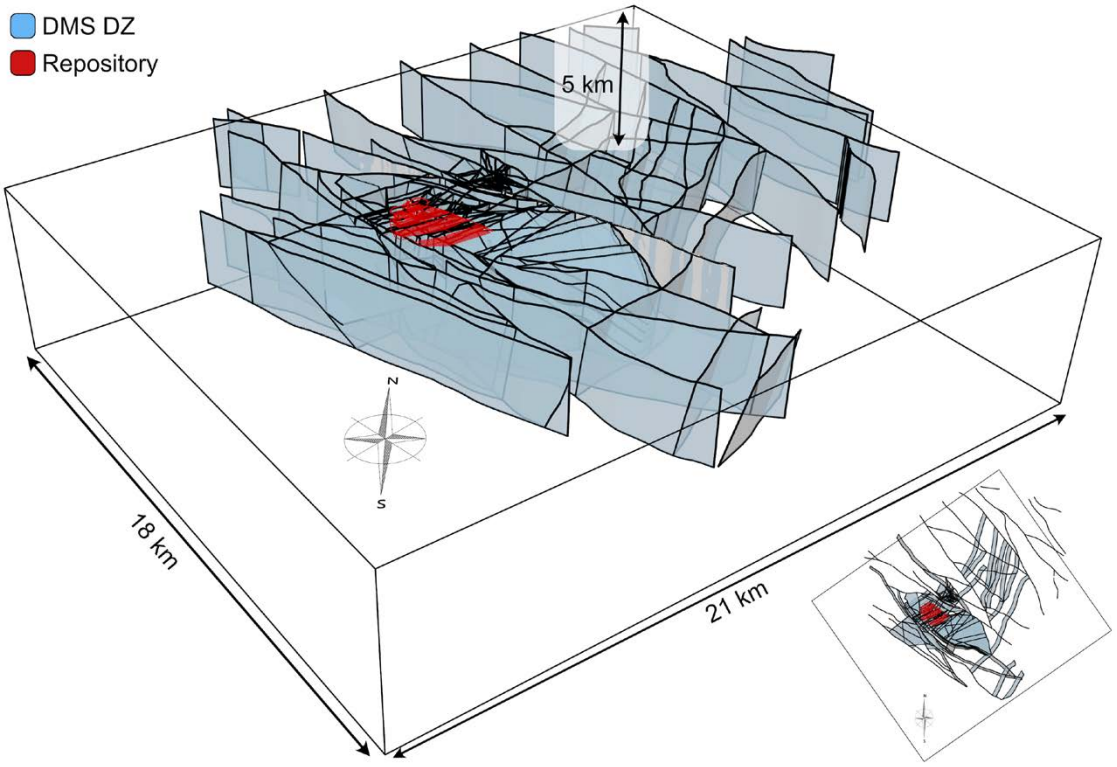

Figure 2-1. *The DZs of the updated DMS, with a top-down view as an inset in the bottom-right corner.*

2.2 In situ stress

The Forsmark site in situ stress state interpretation was originally established in 1991 when Stephansson et al. (1991) used data in a Rock Stress Database to evaluate the stress state in Fennoscandia. 500 entries from location in Sweden, Finland and Norway were used resulting in the conclusion that in the first 1 000 meters there is a high horizontal stress component and both the maximum and minimum horizontal stress components exceed the vertical stress, assuming that the vertical stress is proportional to the weight of the overburden (Martin 2007).

This has been followed with several stress measurement campaigns in Forsmark, consisting of over-coring (~ 130 measurements), hydraulic fracturing (HF) (~ 70 measurements) and hydraulic tests on pre-existing fractures – HTPF (~ 170 measurements). The conclusions of Stephansson et al. (1991) were supported by the overall results of these measurements, since some HF showed intermediate stresses or minimum horizontal stresses lower than the vertical stress (Chapter 6.4 in Martin 2007, R-07-26). Additionally, survey programs of borehole breakouts and core disking, evaluation of nonlinear strains in laboratory samples and determination of stress magnitudes to cause core disking (Martin 2007) were performed to aid in the interpretation of in situ stress. Based on the above, the in situ stress state has been defined in detail in Martin (2007) and presented in Glamheden et al. (2007).

Both direct and indirect in situ stress state measurements clearly indicate a NW–SE orientation of the major horizontal stress. The magnitude variation can be constrained based on measurements and indirect damage observations. Based on the rock mechanics site descriptive modelling stage 2.2 for the Forsmark area (Glamheden et al. 2007) and the inherent assumptions, the mean magnitudes of the major and minor horizontal stresses at a depth of 500 m are approximately 41 MPa and 23 MPa, respectively. According to Glamheden et al. (2007), discrete features such as faults can cause local spatial variability of ± 9 degrees in orientation and ± 5 MPa in magnitude.

Additional studies of borehole breakout frequency and orientations have been conducted in holes KFM08A, KFM08C, KFM09A and KFM09B after Martin (2007). The results are fairly similar to those reported by Martin (2007) and support the stress model presented in Glamheden et al. (2007). There is no observed increase in borehole breakouts with depth according to these studies. Increasing Young's modulus as a function of depth in a finite difference model shows a gradual increase in the in situ stress magnitude which is in reasonable agreement with the observed state of in situ stress, but the measured data exhibits larger variation. The influence of an increase in rock mass quality by depth on the in situ stress was confirmed by Glamheden et al. (2008), although no distinct local heterogeneities or geological features were modelled. This modelling resulted in higher magnitudes and less agreement with the measured data than the previous numerical modelling presented in stage 2.2 (Glamheden et al. 2007).

2.3 Rock properties

Glamheden et al. (2007, 2008) describe the multidisciplinary characterisation of the Forsmark site including geology, surveying and measurement programs, laboratory tests and interpretation of the in situ stress state, intact rock, fracture and rock mass mechanical properties. The rock mass quality in Forsmark is very good and the rock is stiff, strong and homogeneous based on the laboratory tests of rock samples and fractures and geomechanical classification indices. The rock mass properties have been estimated with empirical and theoretical methods and integrated through a process called harmonisation (Glamheden et al. 2007). Theoretical analysis of rock mass properties parallel and perpendicular to the major principal stress and tensile strength tests conducted both parallel and perpendicular to foliation resulted in similar values regardless of direction, indicating a reasonably isotropic rock mass. Volumes with lower rock mass quality are mainly related to the increased fracture intensity in DZs (Glamheden et al. 2007).

3 Simulation approach and input data

3.1 Approach

Much of the general description related to the simulation approach applied in this study is the same or similar to the previous study published in Hakala et al. (2019). As described in Hakala et al. (2019) and originally in Heidbach et al. (2018), the current stress state in the Fennoscandia area is dominated and driven by Mid-Atlantic ridge push and collision of the Eurasian and African plates in the Alps. Additionally, earlier glaciation cycles have changed stress conditions remarkably and potentially promoted the slip of brittle deformation zones thereby causing changes in the stress field. In the thrust fault conditions that have been dominant for a long time, shallow dipping deformation zones have been, and are still, more prone to slip than subvertical zones. As a result, the in situ stress state is affected by the background stresses and potentially perturbed by deformation zone slip, which has been studied by numerical simulations of the interaction of geological features and the stress state (Tonon et al. 2001, Tonon and Amadei 2003, Hakami 2006, Hakami and Min 2009, Valli et al. 2011, 2016). This study applies the same methodology as described in Hakala et al. (2019) by modelling the interpreted deformation zones in the focus area and applying velocity boundary conditions to form the interpreted in situ stress state at repository depth, simulating the stages leading up to the currently interpreted stress state. Simulation results are interpreted using the methods applied in the previous study. Note that DZs are modelled as surfaces using the surface geometry of the DMS and therefore the potential thickness of DZs is not explicitly included which would lead to further complexity in the simulation model.

Numerical simulations were performed in two phases. The first phase verified the use of a new contact logic available in FLAC3D (Itasca 2022a) by comparing results to 3DEC (Itasca 2022b). The new contact logic makes use of zone-joints: the zone-joint logic in FLAC3D provides an alternative to the current FLAC3D interface implementation (Itasca 2022c) in small strain. The logic has not been extended to large strain at this time. Unlike the one-sided interface logic, the zone-joint logic creates contacts between zone gridpoints and faces that are on opposing/touching surfaces. Unlike in the interface implementation, several contact models can be used to undertake force-displacement computations with zone joints. The formulation computes relative velocities between the gridpoint and face in contact, at the gridpoint location, and passes this value along with the contact area to a contact model to compute contact forces. The forces are subsequently applied to the gridpoint and face. A Mohr-Coulomb model, basically identical to the 3DEC Mohr-Coulomb implementation, is also available for zone joints. The original interface logic in FLAC3D uses a similar model but with some notable differences (Itasca 2022c). This contrasts with 3DEC where subcontacts are created, even in small strain. Subcontacts are useful when large relative motions exist between objects in contact but have minimal physical impact in small strain simulations as subcontacts are not updated in small strain. This comparison was performed to further verify the applicability of the method as at the time of use, it was in development. Additionally, FLAC3D computation is significantly faster than 3DEC.

Phase 1 simulations were performed solely using the Base case parameters of Phase 2 (Section 3.7). To ensure reasonable computation times and to avoid unnecessary complexity, the geometry of the first phase model included sixteen deformation zones that were selected to form sufficient complexity in the repository area and included both low-dipping and subvertical to vertical deformation zones. Although the deformation zones were modelled according to the DMS geometry, they were simplified to a degree as a result of purposefully coarse discretisation to improve computation times. All the stages previously simulated in the Hakala et al. (2019) study were simulated in phase 1 and 2, including the development of the in situ stress state using velocity boundary conditions, the following glaciation and finally, the re-establishment of the in situ stress state using velocity boundary conditions. Phase 2 proceeded to use the code selected to be most suitable and included all 152 deformation zones in the DMS determined to be feasible to model. Phase 2 simulations included in total, seven different cases (Section 3.7).

3.2 Geometry

3.2.1 Phase 1 model

The model geometry for Phase 1 was constructed similar to the previous study but as undulating surfaces and included sixteen deformation zones from the DMS (Table 3-1). The deformation zone geometry was simplified to accommodate an average edge length of ca 200 m using triangulation when discretising the deformation zone surfaces. The same geometry i.e., the same discretisation was used for both the FLAC3D and 3DEC models, as at this time of method development the process involved exporting the 3DEC geometry into FLAC3D. Similarly, gridpoints were identical between the two models.

Table 3-1. The DZs included in the Phase 1 model geometry.

DZ ID	Area (km^2)
ZFMA2	4.8
ZFMA3	11.9
ZFMA8	1.8
ZFMENE0060A	6.6
ZFMENE0061	5.2
ZFMENE0401A	5.6
ZFMENE1192A	1.1
ZFMENE2254	0.7
ZFMNE0810	5.7
ZFMNE2282	0.6
ZFMNW0017	16.9
ZFMWNW0001 (Singö)	23.5
ZFMWNW0019	11.5
ZFMWNW0023	9.8
ZFMWNW0123	11.1
ZFMWNW0809A	7.8

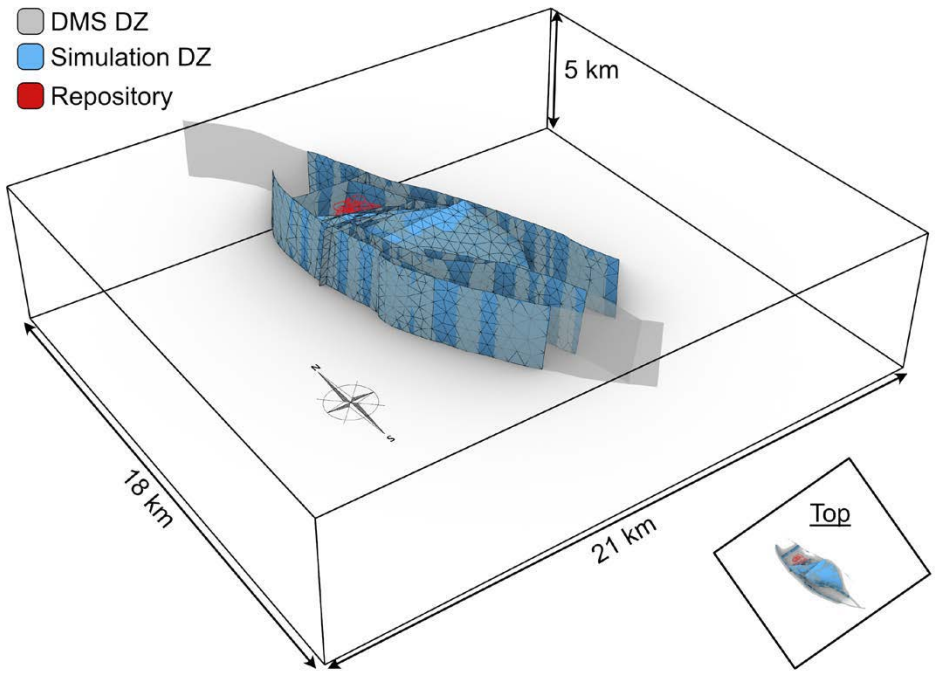

Figure 3-1. *The selected DZs from the DMS in grey and the simulation geometry in blue in the Phase 1 model.*

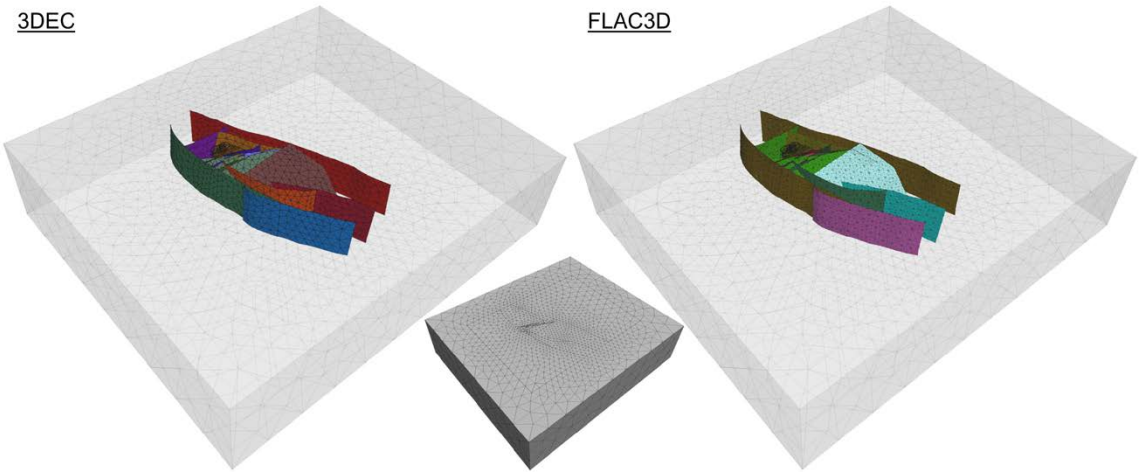

Figure 3-2. *The model geometry in the 3DEC model (left) and the FLAC3D model (right). The centre illustrates overall mesh size in the model.*

3.2.2 Phase 2 model

The DZs in Phase 2 were modelled to match the original DMS geometry as closely as possible while still being computationally reasonable (Figure 3-3). The overall mesh size was < 20 m in the repository area, increasing to ca 750 m at the boundaries of the model (Figure 3-4). Only large-scale deformation zone undulation was modelled, small-scale asperities were not included. Geometrical accuracy was within 10 meters (at maximum, generally maximum deviation is 5 m) near the underground facilities and at a distance of 2000 meters from the repository, DZ geometry was allowed to deviate at maximum 40 meters. Due to geometrical issues with intersecting DZs leading to very narrow and poor quality elements, some additional simplification to the undulating surfaces was necessary. This required trimming the deformation zone surfaces or in one case, excluding the deformation zone entirely: ZFM1189 was excluded (Figure 3-5). Exclusion of this DZ does not, like the other simplifications, affect the simulation outcome given the overall size of the model. Additionally, ZFM1189 is the smallest DZ in the DMS, with a surface area of 0.017 km^2. Finally, all joint Forsmark (JFM) features were excluded along with nine deformation zones that fell outside the modelling volume:

- ZFMNE3542
- ZFMNNE3546A
- ZFMNNW3524
- ZFMNNW3534
- ZFMNW3511
- ZFMNW3552
- ZFMWNW3512
- ZFMWNW3519
- ZFMWNW3520

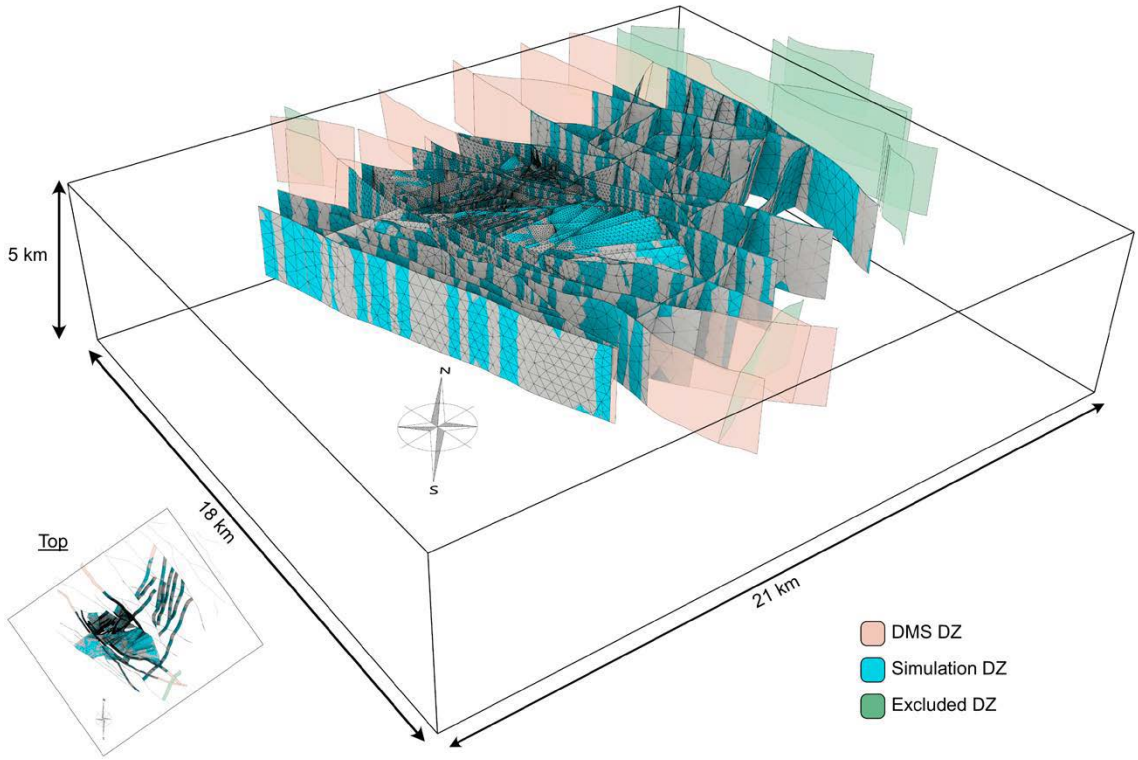

Figure 3-3. *Phase 2 model deformation zone geometry. Note that deformation zone geometry that extended well outside the area of interest was excluded: the discretised geometry is simulated.*

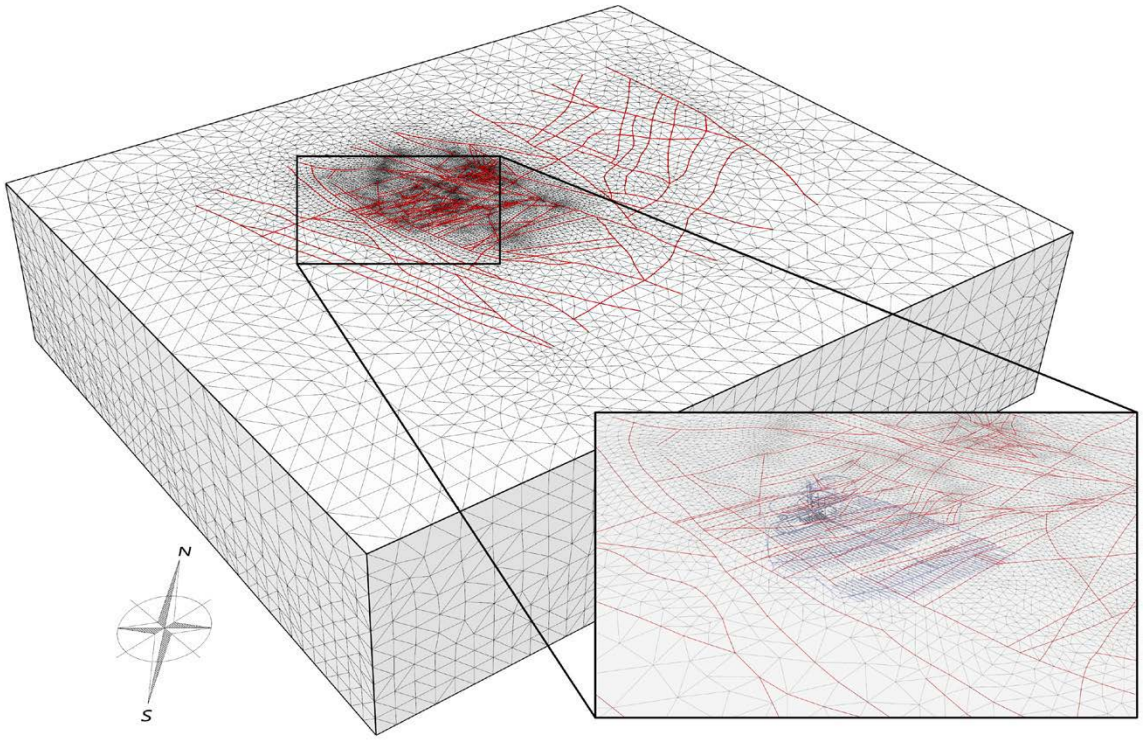

Figure 3-4. *Phase 2 model meshing.*

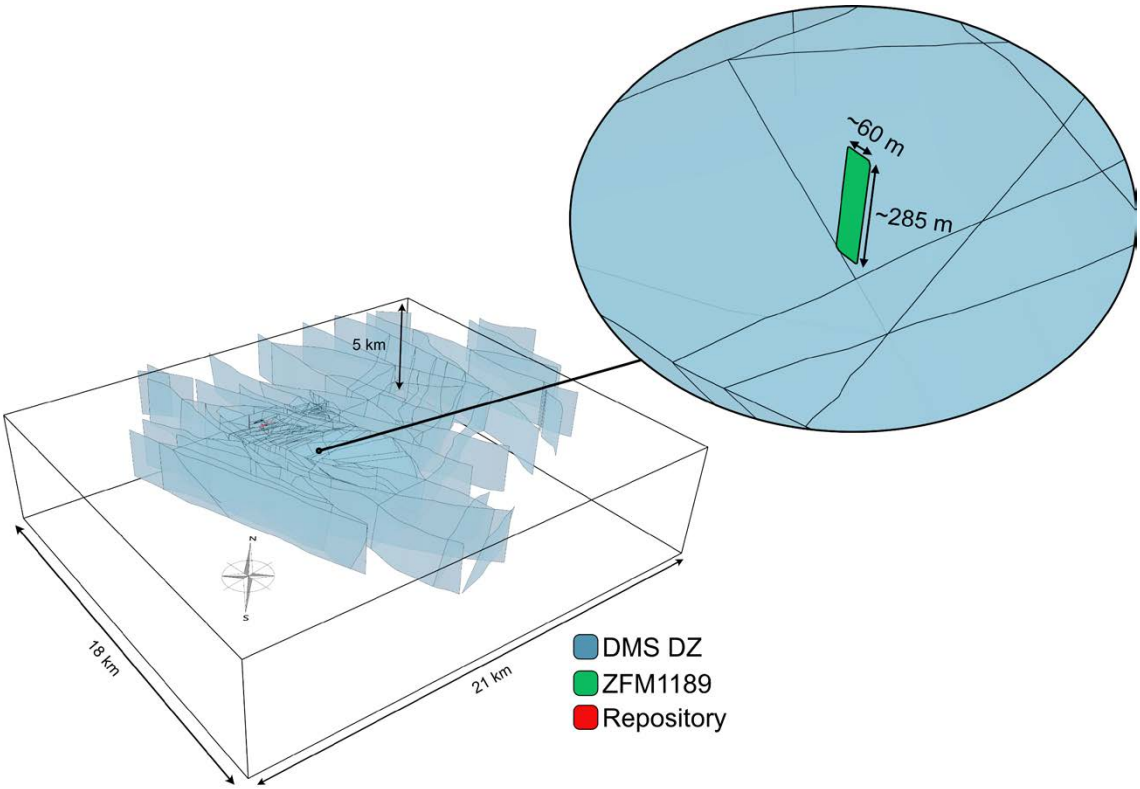

Figure 3-5. *Excluded deformation zone ZFM1189 in the DMS geometry.*

3.3 Rock mass properties

As in the previous study, the rock mass was considered to be isotropic and elastic and was divided into four different geological domains: the main rock mass and three fracture domains surrounding the facilities (FFM01, FFM02, FFM06) (Figure 3-6). The applied elastic parameters consider the fracturing and only the DZs were modelled explicitly. Young's modulus values were estimated based on the rock mechanics Forsmark modelling stage 2.3 (Glamheden et al. 2008) and Poisson's ratio values were based on empirical analysis of Fracture domains in Glamheden et al. (2007) (Table 3-2). FFM01 and FFM06 were considerably stiffer than FFM02, and the stiffness increased with depth. Rock mass density was 2 650 kg/m^3.

Table 3-2. Rock mass elastic parameters after Glamheden et al. (2007) and Glamheden et al. (2008).

Depth range	**Above 400 m**		**Below 400 m**	
Elastic parameters	**E (GPa)**	**v ()**	**E (GPa)**	**v ()**
Fracture domain				
Rock mass	65	0.24	65	0.24
FFM01	65	0.24	70	0.24
FFM02	55	0.18	-	-
FFM06	65	0.30	70	0.24

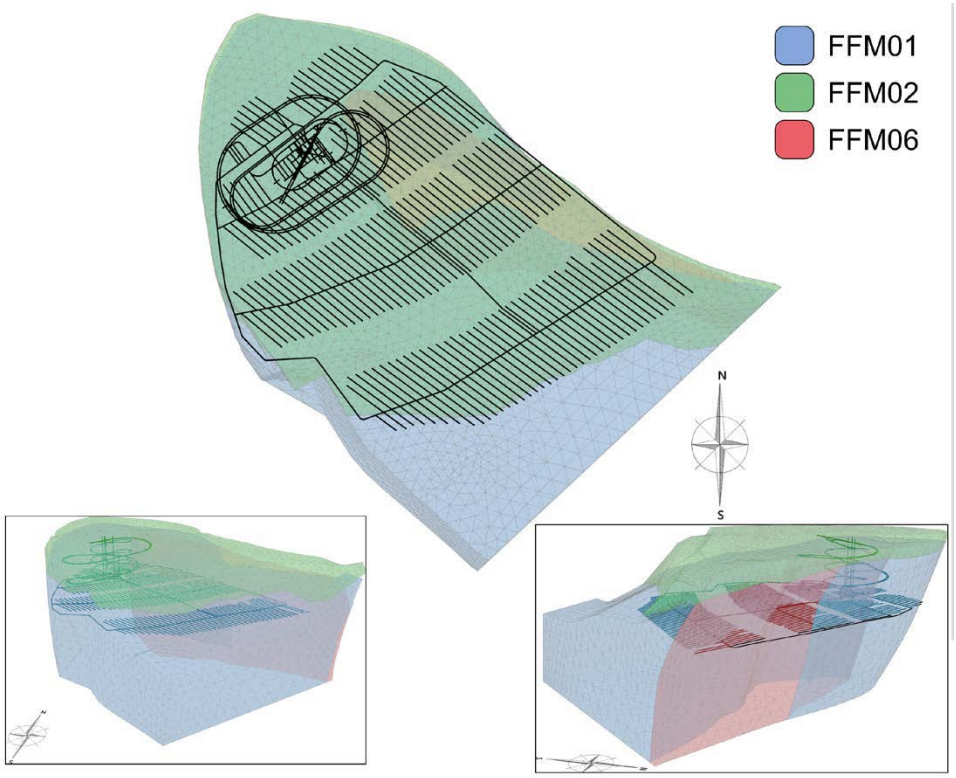

Figure 3-6. *Fracture domains surrounding the facilities.*

3.4 Deformation zones

Like in the previous study, all DZs except the Singö DZ were assigned the same basic deformation and strength parameter values based on the Forsmark site descriptive model v2.2 and its completion at the end of site investigations (Glamheden et al. 2007, SKB 2008) (Table 3-3). The initial values for cohesion and friction were maintained in contacts after failure (perfectly elastoplastic constitutive model). Note that the parameters were not varied in any of the cases of this study, like they were in Hakala et al. (2019).

Table 3-3. Basic stiffness and strength values for DZs. kn: normal stiffness, ks: shear stiffness, coh: cohesion, fric: friction angle, ten: tensile strength.

Parameter	kn (MPa/mm)	ks (MPa/mm)	coh (MPa)	fric (°)	ten (MPa)
Deformation zone					
All, except Singö	80	20	0.7	36	0.001
Singö	0.2	0.01	0.4	31.5	0.001

3.5 In situ stress state and ground water pressure

As described in Hakala et al. (2019), the primary in situ stress state interpreted for the Forsmark area to be applied in the simulations was based on the Martin (2007) interpretation presented in the form of horizontal and vertical stress components (Table 3-4 and (Figure 3-7). The interpretation is based on the average mean stresses at depth levels of 0 m (extrapolated), 150 m, 300 m, 400 m and 500 m, with a horizontal stress ratio of 1.7 in addition to a criterion that borehole breakout can initiate at a depth of 1 000 m. The assumption is that σ_H increases slowly for the first 150 m, then has a higher gradient between 150–400 m and then continues with a lower gradient. For the first 150 m, σ_h has a similar gradient to σ_H and after that continues more or less linearly with depth. The vertical component (σ_v) increases linearly with depth, with the same gradient for all depth ranges. The gradients for the deepest depth range are assumed to be valid up to a depth of 2.1 km. Gravity was applied as 9.81 m/s^2.

Table 3-4. The primary in situ stress state based on Martin (2007).

Depth range (m)	σ_H (MPa)	σ_H trend (°)	σ_h (MPa)	σ_h trend (°)	σ_v (MPa)
0–150	19 + 0.008z, ±20 %	145	11 + 0.006z, ±25 %	55	0.0265z, ±2 %
150–400	9.1 + 0.074z, ±15 %	145	6.8 + 0.034z, ±25 %	55	0.0265z, ±2 %
400–600	29.5 + 0.023z, ±15 %	145	9.2 + 0.028z, ±20 %	55	0.0265z, ±2 %

z is depth below rock surface in metres, vertical stress variation ±0.0005z.

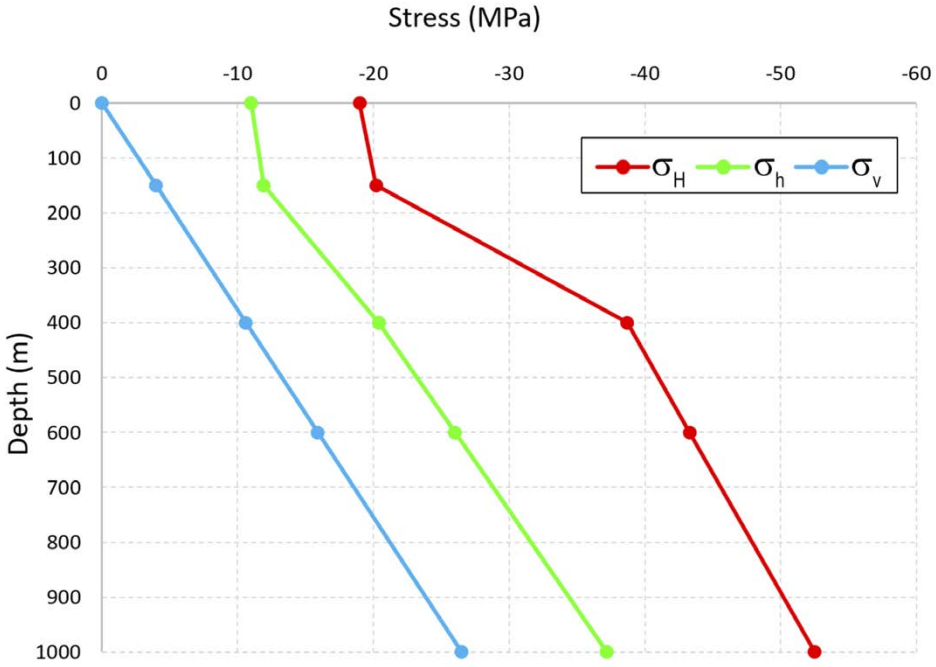

Figure 3-7. *The primary in situ stress state based on Martin (2007).*

The latest stress state interpretation for the Forsmark area is detailed in Martin (2007), which was slightly modified in (Glamheden 2007). Hakala et al. (2019) indicated that where the measurements in the Sicada database were studied in Martin (2007), some measurements were ranked as unreliable, but without clear measurement specific basis or listing. The interpretation figure (Figure 3-8 in this report and Figure 7-3 in Martin 2007) included a greater number of measurements than those listed as acceptable/reliable in the study Appendix A in Martin (2007). Some of the magnitudes or depths in the Sicada database (Sicada all in Figure 3-8) also deviate from the values presented in Figure 3-7 in Martin (2007) (orange pentagons in Figure 3-8 in this report). The simulation results of this study were compared with the "Sicada simulation reference" data (see Figure 3-8) which includes the data presented in Appendix A of Martin (2007). This set excludes borehole KFK001 (DBT1 in Martin (2007)) results which have probable thermal issues as well as measurements with major principal stress magnitudes less than 10 MPa, which were also omitted in the Martin (2007) interpretation. Finally, the most likely range of variation for the vertical stress in Martin (2007) is ±0.0005, but was interpreted in this study to be depth dependent, i.e. ±0.0005z or 2 % given such a low variation range without a depth gradient is likely not the intent of Martin (2007).

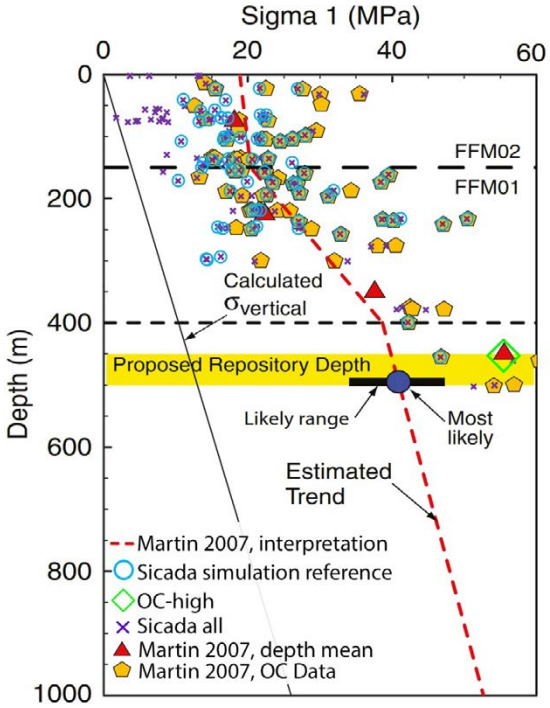

Figure 3-8. *Measured major principal stress values versus depth and the Martin (2007) interpretation—the measured values have three data sets, the one used for the Martin (2007) interpretation (orange), SICADA-all and SICADA simulation reference (modified after Martin 2007).*

In Phase 1 and 2 simulations the stress state was established by applying thrust to opposite vertical model boundaries. “Thrust” in the context of the simulations in this study is the application of a velocity boundary condition in the normal direction of the model boundary surfaces. Put simply, the model was compressed from all sides at varying velocities to achieve a target stress state at a given location. For the simulation target stresses, the principal stresses are defined based on the horizontal stresses defined in Martin (2007), where $\sigma_1 = \sigma_H$, $\sigma_2 = \sigma_h$ and $\sigma_3 = \sigma_v$. The velocities along the major and minor horizontal stress orientations were different but were not depth dependent: depth dependency had been concluded to be of negligible impact in the previous study (Hakala et al. 2019). The effect of thrust orientation compared to DZ-geometry was studied by varying the thrust orientation by ±20° (Figure 3-9). In all Phase 2 calculations the thrust was servo-controlled and stopped when primary in situ conditions were reached at repository depth (470 m) at the centre of the repository (Figure 3-10). “Servo-controlled” refers to the use of a proprietary script written to cycle or solve the model an arbitrary number of cycles to a target stress state resulting in small increments of displacement. After an increment of thrust displacement has been applied, the model boundaries are fixed in the normal direction and the model is cycled to a quasistatic state. Based on the difference of the current stress state at the monitoring point and the target magnitude, the thrust velocities for the opposing boundaries are recalculated and applied for the next increment. Smaller differences result in the servo decreasing velocities on the corresponding boundaries or if the target magnitude is close to be exceeded, extensional boundary conditions are applied. The script obtains the average principal stresses based on the average of the tensors within a set radius of a sphere at the monitoring location. Once the maximum and intermediate principal stresses were within set tolerances (0.2 MPa), the script terminates, the boundaries are fixed in their normal directions (surface free, all others fixed in normal direction) and the model is equilibriated. The target stresses were individually determined for each principal stress and based on the Martin (2007) interpretation, with a target range of ±1 % at the monitoring location. The different variants of in situ stress states are summarised in Section 3.7.2.

Full hydrostatic water pressure was assumed for all DZs with a water level equal to the rock surface. In Phase 2 simulations, variable excess pore pressure was applied during the glaciation cycle (Section 3.6). Water density was 1 000 kg/m^3.

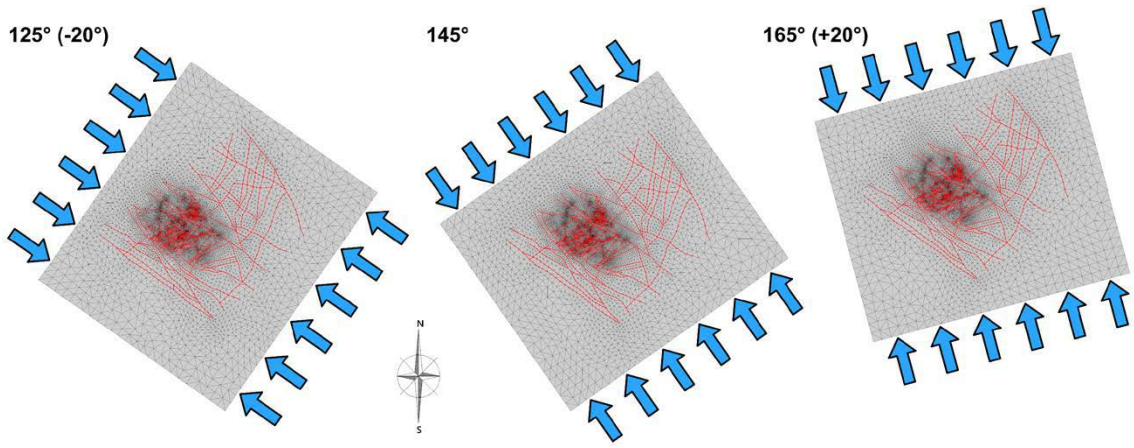

Figure 3-9. *The varying major thrust orientations used in the simulations.*

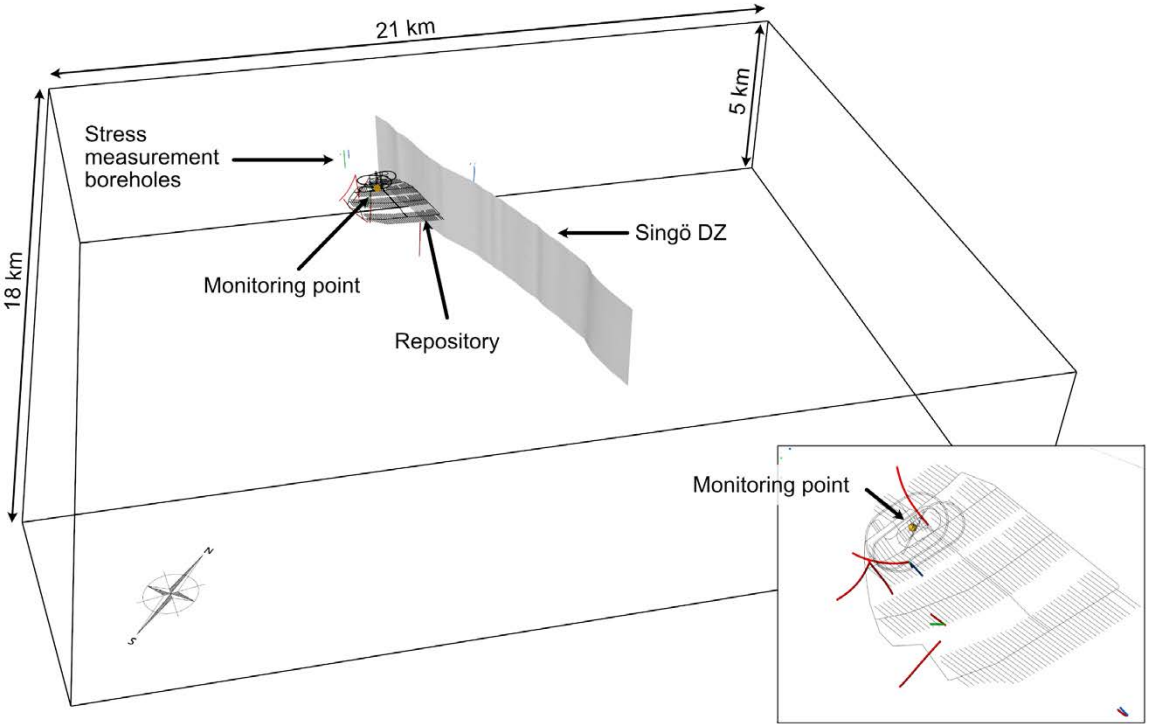

Figure 3-10. *Location of the monitoring point used to control thrust, viewed from above in the inset in the bottom right.*

3.6 Glaciation

The same glacial cycle as simulated in Hakala et al. (2019) was applied in Phase 1 and 2 of this study. As before, the simulation cycle for the glaciation consisted of four phases; Forebulge, Glacial maximum, Edge passing and the Removal of glaciation (Table 3-5, Table 3-6, Figure 3-11, Figure 3-12). The glacially induced stresses were assumed to be constant with depth and equal to the values calculated for the 500 m level. The maximum error caused by this assumption was about 0.5 MPa. The glacially induced excess pore pressure model was the same as the alternative pore pressure model in Hökmark et al. (2010), equivalent to 98 % of the glacially induced vertical load (Figure 3-13). In this pore pressure model the pressure was constant with depth except in the edge passing phase. Unlike the thrust in the formation of the in situ stress state, the glacially induced stresses and pore pressures corresponding to each simulation phase were set directly on the DZ surfaces and model elements. The vertical stresses in the glaciation phases are achieved by applying a layer on top of the model that is assigned a density required to generate the vertical load required to reach the specified vertical stress at each respective stage. Similar to the thrust, the density was increased or decreased incrementally to avoid dynamic effects. Pore pressure changes were applied incrementally along with the stress changes. This approach maintained a quasistatic state. In the removal phase all excess stresses and pore pressures were removed.

Table 3-5. Additional stresses induced by the simulated second glaciation cycle.

	Forebulge			Second maximum			Edge passing		
	Stress (MPa)	dip [°]	dd [°]	Stress (MPa)	dip [°]	dd [°]	Stress (MPa)	dip [°]	dd [°]
σ_1	0	0	3	28.9	0	95	11	0	76
σ_2	−5.4	0	93	24.8	0	185	7.6	0	166
σ_3	0.3	90	0	25.7	90	0	−0.2	90	0

Table 3-6. Total stresses during simulated second glaciation cycle at repository depth (465 m).

	Pre-glaciation			Forebulge			Second maximum			Edge passing		
	Stress (MPa)	dip [°]	dd [°]	Stress (MPa)	dip [°]	dd [°]	Stress (MPa)	dip [°]	dd [°]	Stress (MPa)	dip [°]	dd [°]
σ_1	43.5	0	145	41.7	0	152	73.2	0	312	62.0	0	323
σ_2	22.6	0	55	19	0	62	52.0	0	42	39.2	1	53
σ_3	12.3	90	0	12.7	90	0	37.7	90	212	38.2	89	226

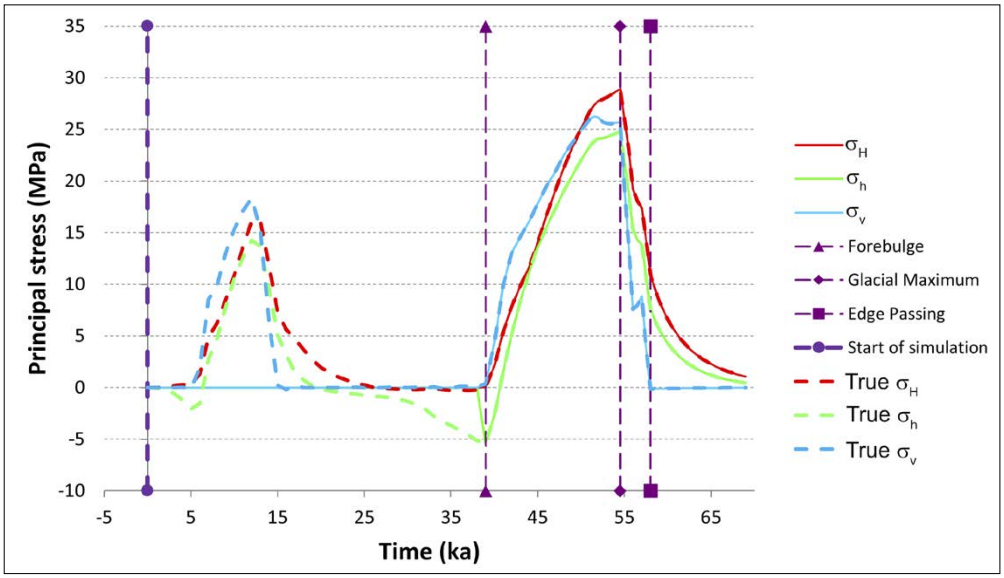

Figure 3-11. *Development of glacially induced changes of horizontal and vertical stresses at 500 m depth level after Hökmark et al. (2010). Compression = positive.*

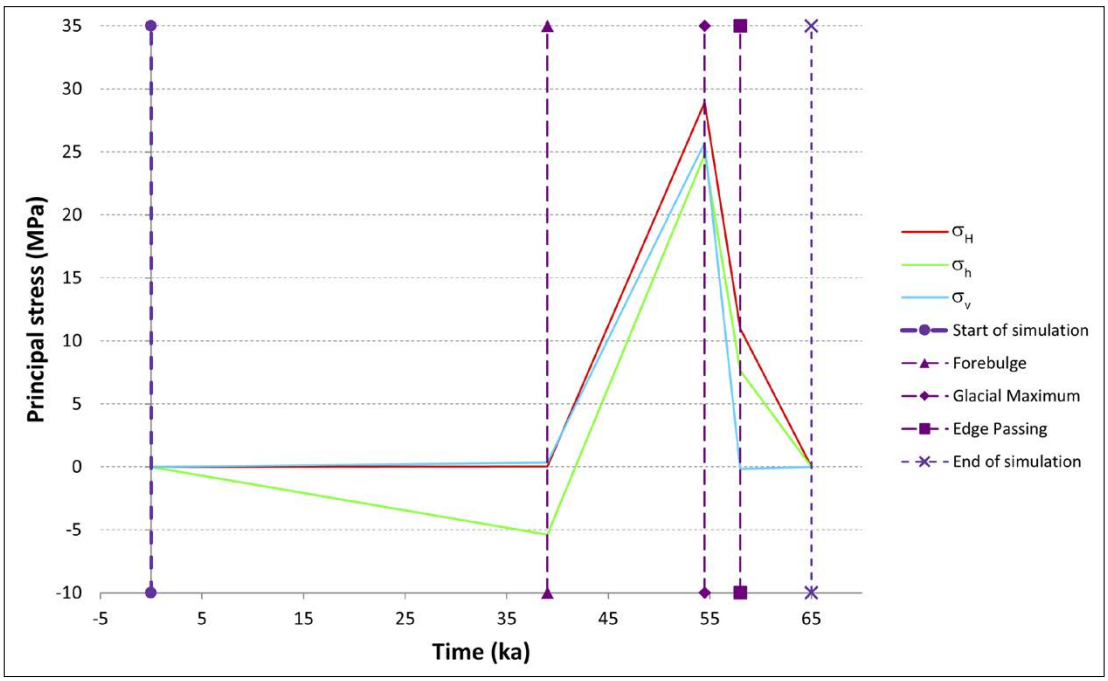

Figure 3-12. *The development of the simulated glacially induced changes of horizontal and vertical stresses at the 500 m depth level. Compression = positive.*

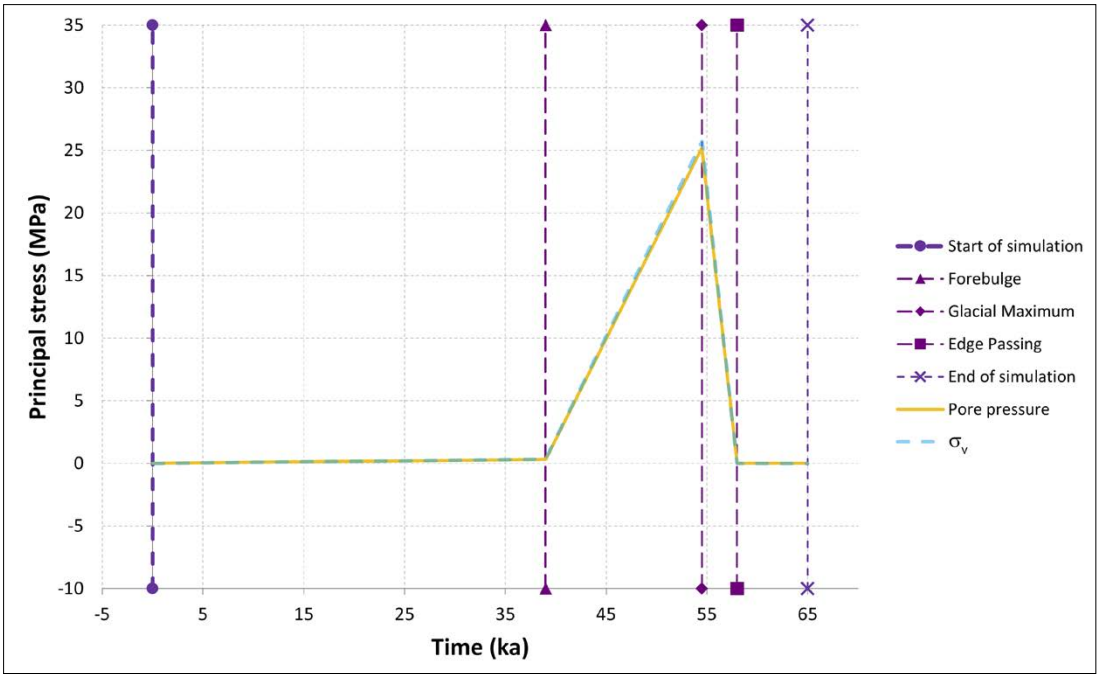

Figure 3-13. *Glacially induced excess pore pressure model for Forsmark, after Hökmark et al. (2010). Compression = positive.*

3.7 Simulation cases

3.7.1 Simulation Phase 1

Phase 1 simulations were performed using the Base case parameters of Phase 2, with both 3DEC and FLAC3D. Sixteen undulating deformation zones were modelled (Section 3.2.1). Rock mass and deformation zone properties were assigned according to Sections 3.3 and 3.4. Both 3DEC and FLAC3D models were simulated with a fully elastic rock mass. The deformation zones were simulated both as elastic or elastoplastic in 3DEC and FLAC3D. The in situ stress state as defined in Section 3.5 and Table 3-7 was established using thrust boundary velocity conditions and by applying the glacial cycle presented in Section 3.6. Finally, the defined in situ stress state was re-established if the stress state after glaciation deviated from the target defined in Table 3-7. Apart from the limit used to evaluate convergence during thrust, 3DEC and FLAC3D simulations were identical. This limit was higher in 3DEC due to extended computation times, while still achieving equilibrium at all stages including during the application of thrust or glaciation. The effect of using the same convergence limit in 3DEC was tested and determined to be negligible.

3.7.2 Simulation Phase 2

Phase 2 included all 152 undulating DMS deformation zones with greater accuracy. Deformation zones are grouped into three sets:

- Set 1 dipping mostly to the southeast with a dip less than 50° i.e., these deformation zones have a dip direction close to the mean major thrust trend of 145°, ranging from 0 to 360°.
- Set 2 is subvertical (50–90°) dipping mainly to the northeast (dip direction 170–260° and 350–080°), i.e., the strike is along the major thrust trend.
- Set 3 is also subvertical (50 – 90°) and dips mainly towards the southeast (dip direction 080–170° and 260–350°), i.e., the strike is perpendicular to the major thrust trend.

This geometry was used in seven simulation cases (Table 3-7). Mesh size was optimised to improve computation time by grading the mesh outwards from the repository area from an edge length of < 20 m to ca 750 m at the boundaries of the model (Section 3.2.2). Rock mass and deformation zone properties were identical to Phase 1. Before applying thrust, the model was first run to elastic equilibrium with only the lithostatic stress gradient according to a rock mass density of 2 650 kg/m³.

The model was compressed to seven different repository level target in situ stress states based on the Martin (2007) interpretation. The Base case adopts the mean magnitudes and orientations while the further six cases are mostly within the variation limits of Martin (2007) stress model. The compressing velocities on opposite model boundaries were equal in magnitude and constant at all depths. The applied glaciation cycle was according to Hökmark (2010) and applied as stress increments. Special care was taken to prevent dynamic, overstressed, conditions. In Cases 1 and 2 the major thrust trend is rotated horizontally ± 20° from the mean trend of 145°. This is performed using model geometries where the internal part of the model is identical throughout the cases, but the external part of the model domain is modified so that the boundaries are orthogonal to the applied major thrust trend. In Cases 3 and 6 the target value of the minor horizontal stress component is reduced to be equal to the vertical component and in Case 6 the target for the maximum horizontal stress is also increased by 15 %. In Cases 4 and 5 the target for the major horizontal stress is increased 15 % and the target for the minor horizontal stress is either increased or decreased by 20 %. In other words Cases 3 to 6 increase the horizontal shear stresses. Note that the increases or decreases are those applicable to a depth of 470 m, given the models are controlled according to the stresses monitored at this depth; e.g. a maximum horizontal stress that is increased by 15 % applies to all depth levels in Case 6. Additionally, all increases and decreases specified in percentages are relative to the Base case. The vertical stresses were defined in Case 4 by setting the density to 2 700 kg/m^3, and in Cases 5 and 6 by setting the density to 2 600 kg/m^3, as opposed to the default density of 2 650 kg/m^3.

Table 3-7. Parameter values and calculation conditions for Phase 2 simulation cases, where the differences compared to the Base case are highlighted with colour: blue for a decrease, orange for an increase, according to a depth of 470 m.

Case	Maximum horizontal stress		Minimum horizontal stress		Vertical stress	Excess glacial pore pressure
	σ_H (MPa)	Trend (°)	σ_h (MPa)	Trend (°)	σ_v (MPa)	
Base case (Martin 2007, R-07-26)	40.3	145	22.4	55	12.5	98 %
Case 1 (Trend − 20°)	40.3	125	22.4	35	12.5	98 %
Case 2 (Trend + 20°)	40.3	165	22.4	75	12.5	98 %
Case 3 ($\sigma_h = \sigma_v$)	40.3	145	12.5	55	12.5	98 %
Case 4 (σ_{Hmax}, σ_{hmax} and σ_{vmax})	46.4	145	26.8	55	12.7	98 %
Case 5 (σ_{Hmax}, σ_{hmin} and σ_{vmin})	46.4	145	17.9	55	12.2	98 %
Case 6 (σ_{Hmax} and $\sigma_{hmin} = \sigma_{vmin}$)	46.4	145	12.2	55	12.2	98 %

4 Simulation results

4.1 Presentation of results

Only the key figures that explain the observed behaviour for phases 1 and 2 are included in the main text whereas majority of the result figures are presented in the Appendices. Phase 1 and 2 figures include the following:

- 3D figures of DZ shear displacement contours with maximum values (Appendix 1, Appendix 2).
- Equal area lower hemisphere plots of DZ normals for DZs which have sheared more than 0.1 m, defined according to whether shear of over 0.1 m has occurred anywhere along the DZ (Appendix 3, Appendix 4).
- Cumulative shear displacement multiplied by associated area versus depth for major orientations sets of deformation zones for Phase 1 (Appendix 5).
- The change of the principal stress magnitudes in a horizontal cross-section at the repository (Appendix 14, Appendix 15, Appendix 16, Appendix 17, Appendix 18, Appendix 19).
- The change of the major principal stress trend in a horizontal cross-section at the repository (Appendix 20, Appendix 21).
- The major principal stress magnitude, trend and σ_1/σ_2 ratio with mean and 95 % variation limits for each hundred meter depth interval in two 1 900 m diameter vertical cylinders (Figure 4-1) covering the majority of the repository area up to a depth of 2 000 m for Phase 1 (Appendix 7).
- Principal stress trends and magnitudes in lower hemisphere projection polar plots for the data obtained in Phase 1 from cylinders 1 and 2 (Appendix 10).
- The major principal stress magnitude and trend distributions from a 100 m thick section of the 1 900 m diameter vertical cylinder 1 (Figure 4-1) covering the majority of the repository area centered at the repository depth 470 m, i.e., between 420–520 m (Appendix 12).

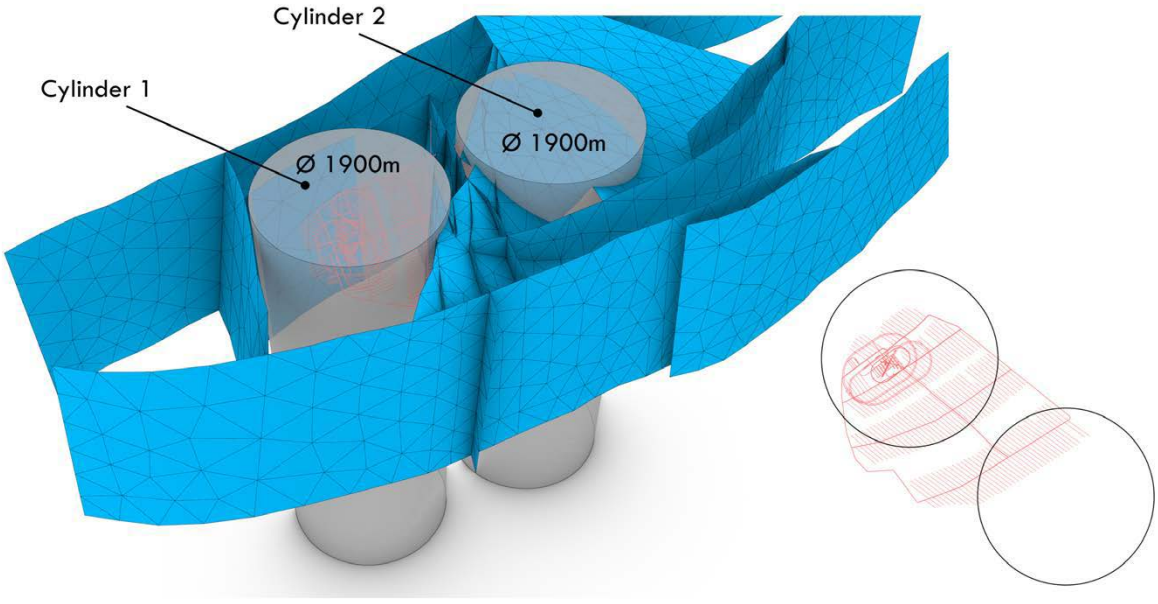

Figure 4-1. *Cylindrical data acquisition volumes in Phase 1 for average stress magnitudes and trends.*

Phase 2 results also include the following modified or additional figures:

- Cumulative shear displacement multiplied by associated area versus depth for major orientations sets of deformation zones by type (Appendix 6).
- The major principal stress magnitude, trend and σ_1/σ_2 ratio with mean and 95 % variation limits for each hundred meter depth interval in a 2 400 m wide vertical cylinder (Figure 4-2) covering the majority of the repository area up to a depth of 2 000 m (Appendix 8). The location of the existing overcoring stress measurements are shown in Figure 4-4 and their magnitudes are included in the plots of Appendix 8 for comparison.
- The major principal stress magnitudes with mean and 95 % variation limits for each hundred meter depth interval in a 2 400 m wide vertical cylinder covering the majority of the repository area versus stress measurements up to a depth of 2 000 m (Appendix 9).
- Principal stress trends and magnitudes in lower hemisphere projection polar plots for the data obtained from the 2 400 m wide vertical cylinder (Figure 4-2) covering the majority of the repository area (Appendix 11).
- The major principal stress magnitude and trend distributions in a rectangular volume (2 950 × 2 160 × 100 m) encompassing the repository area from a depth range of 420 to 520 m (Figure 4-3 and Appendix 13).

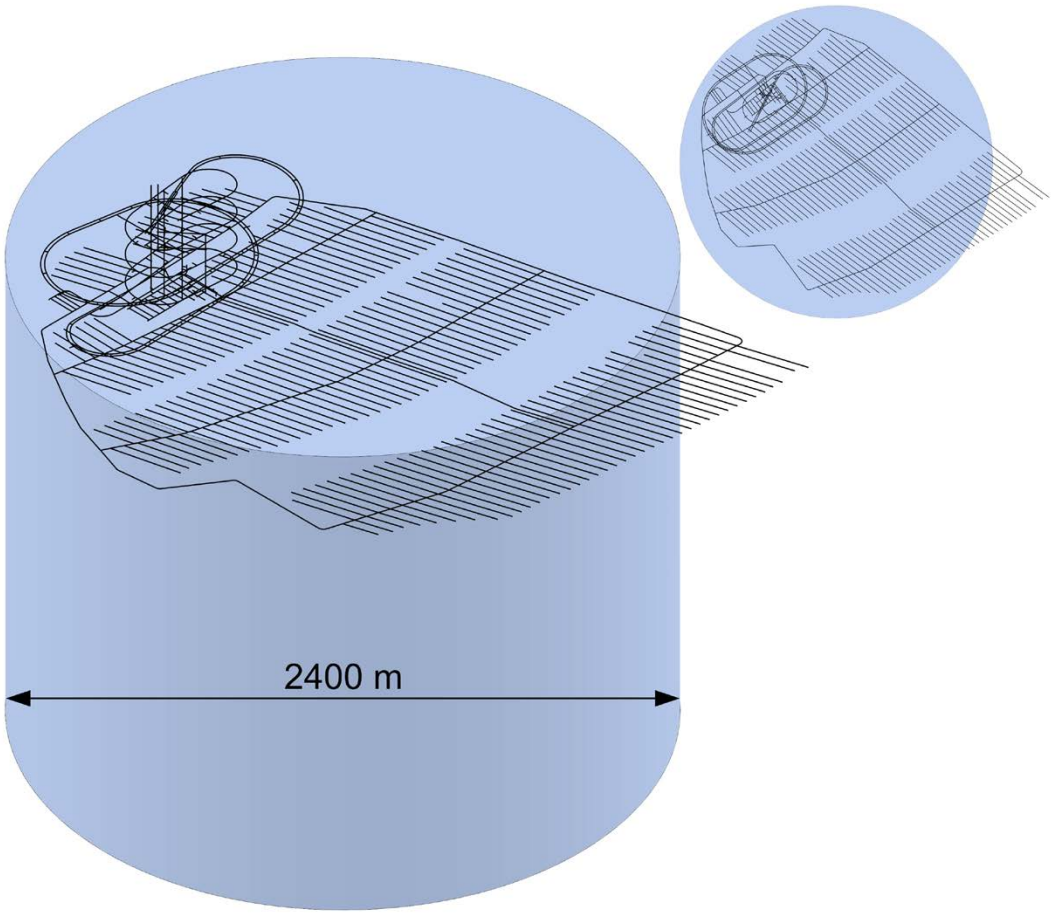

Figure 4-2. *Cylindrical data acquisition volume for average stress magnitude and trend values in Phase 2.*

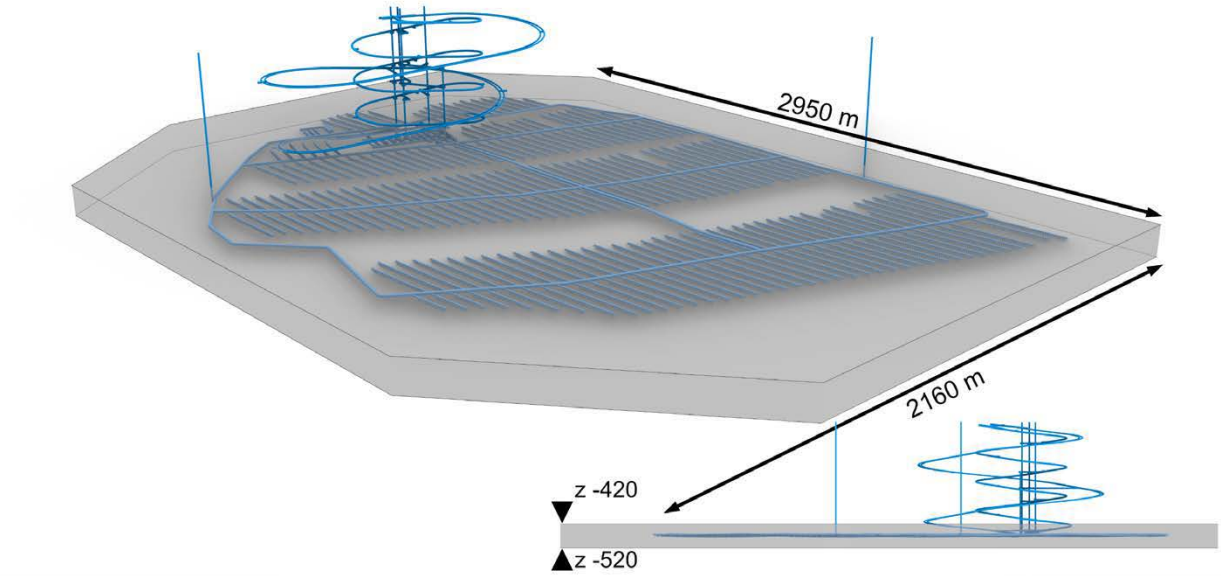

Figure 4-3. *The data acquisition volume for frequency analysis of the distributions of the magnitude and trend of σ_1 at repository depth.*

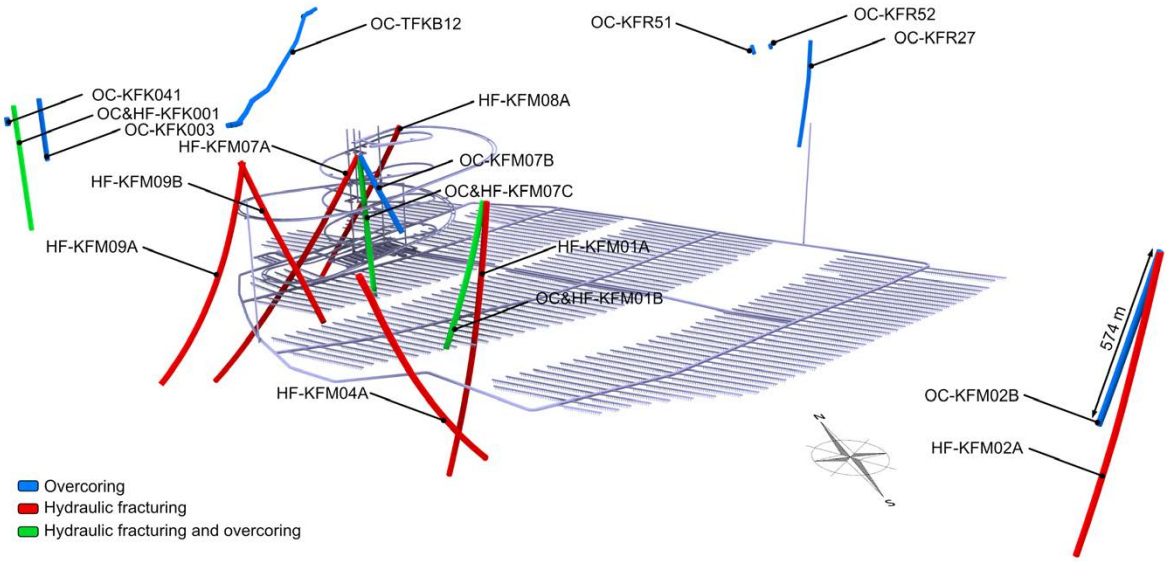

Figure 4-4. *The locations of the stress measurements plotted in major principal stress magnitude and trend figures.*

4.2 Phase 1

Phase 1 simulations were performed with 3DEC and FLAC3D using the Base case parameters. The results are focused on the comparison of the results of the two codes. Both fully elastic and elasto-plastic simulations were performed. Note that the deformation zones are separated into sets for cumulative shear plots and lower hemisphere projections of which deformation zones sheared in elastoplastic simulations. The sets are defined as in Hakala et al. (2019), see Section 3.7.2.

The total displacements of the fully elastic simulation were compared to verify that the required thrust in FLAC3D and 3DEC was identical to confirm equivalent model stiffnesses (Figure 4-5). Deformation zone shear was determined to be largely comparable (Figure 4-6), but based on the accumulated shear and number of sheared contacts, 3DEC indicates at a maximum 25 % more accumulated shear in Set 2 between a depth of 300 to 400 m (Figure 4-7). This is apparent at all stages of the simulation. The average maximum principal stress magnitude and trend as well as the σ_1 and σ_2 ratio are also practically identical at all stages (Figure 4-8). The same observation applies to principal stress orientations between a depth of 400 to 500 m (Figure 4-9) and for median values and distributions of the maximum principal stress component in the repository volume (Figure 4-10 and Figure 4-11). The distribution of the maximum principal stress magnitude at repository depth is nearly identical, while the distribution of the trend of σ_1 is identical (Figure 4-12). Overall, elastic results are nearly the same.

Elastoplastic, shallow-dipping deformation zone Set 1 exhibits 50 % or more accumulated shear in 3DEC than in FLAC3D. 3DEC also resulted in minor shear in three deformation zones of Set 3 (Figure 4-13 to Figure 4-15). The average maximum principal stress magnitude and trend are, however, practically identical (Figure 4-16) as is also apparent from the distributions from cylinder 1 (Figure 4-17), although the scatter in the trend of the maximum principal stress up to a depth of ca 300 m is slightly higher in FLAC3D based on results from the second cylinder (Figure 4-18). Elastoplastic simulations are therefore virtually identical, supporting the use of FLAC3D for Phase 2 simulations. The reason for the observed differences between the two codes could not be identified but is related to the difference in deformation zone slip. The difference in deformation zone slip in geometrically identical models is most probably due to the developing contact logic.

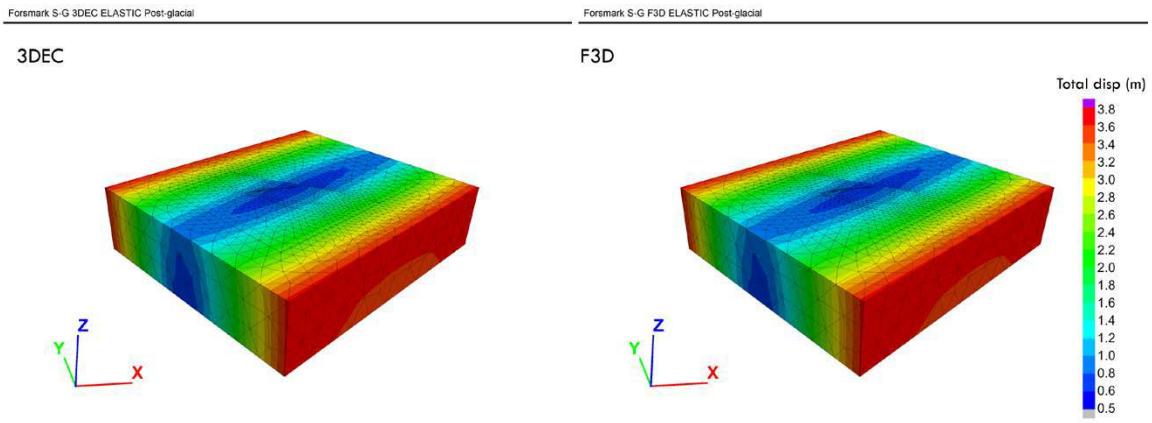

Figure 4-5. *3DEC versus FLAC3D total displacements after glaciation. F3D refers to FLAC3D and is used interchangeably throughout the report.*

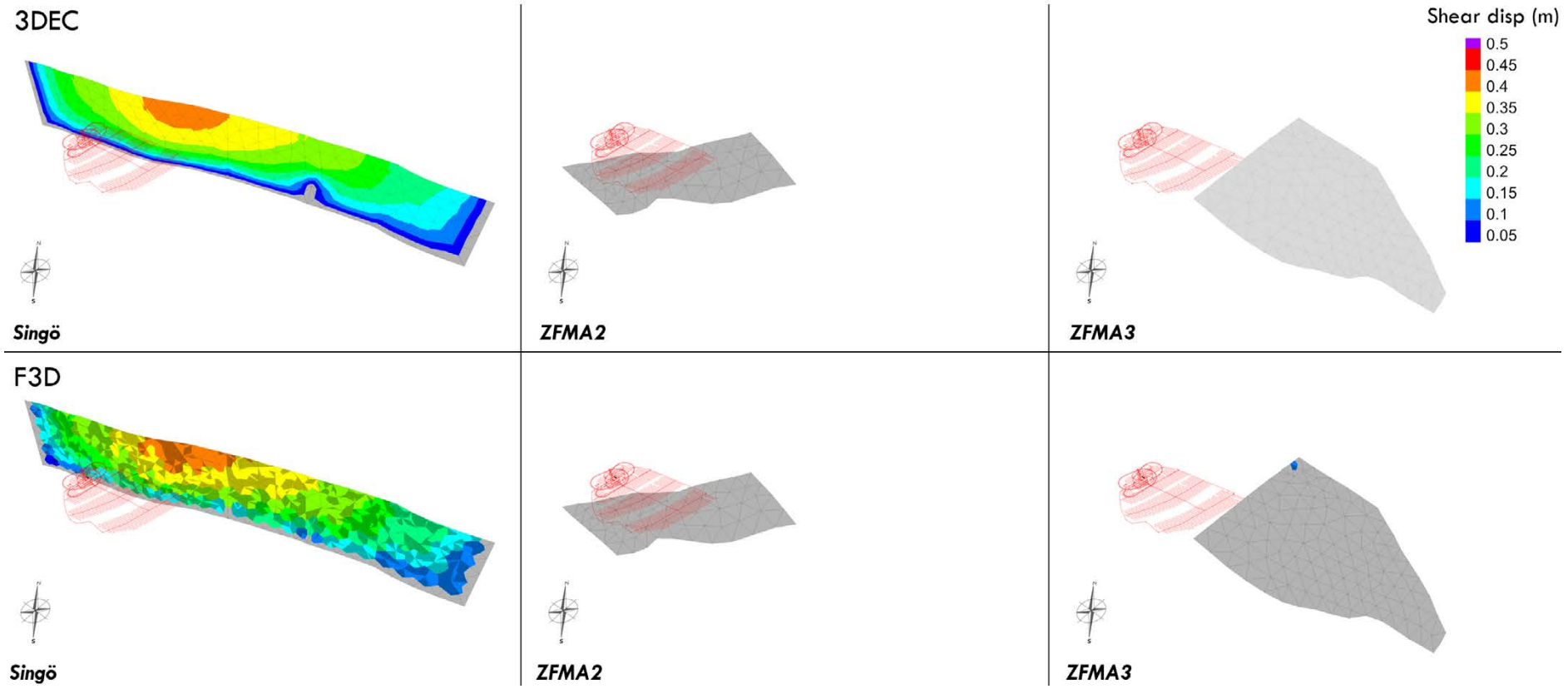

Figure 4-6. *Elastic deformation zone shear displacement in three deformation zones after glaciation, limited to a minimum of 5 cm to avoid presenting displacements that are negligible at this scale. The repository is illustrated in red.*

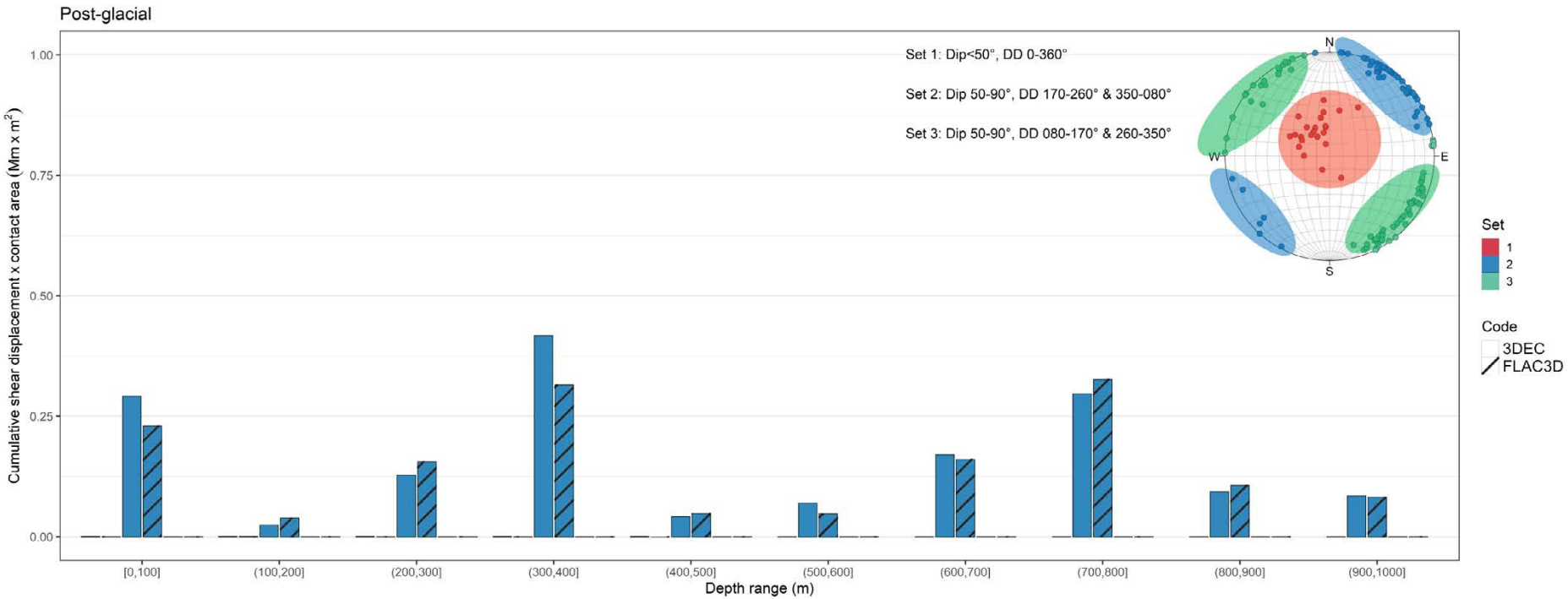

Figure 4-7. *Cumulative shear displacement multiplied by associated area versus depth for major orientations sets of DZ for 3DEC and FLAC3D after glaciation in a fully elastic simulation.*

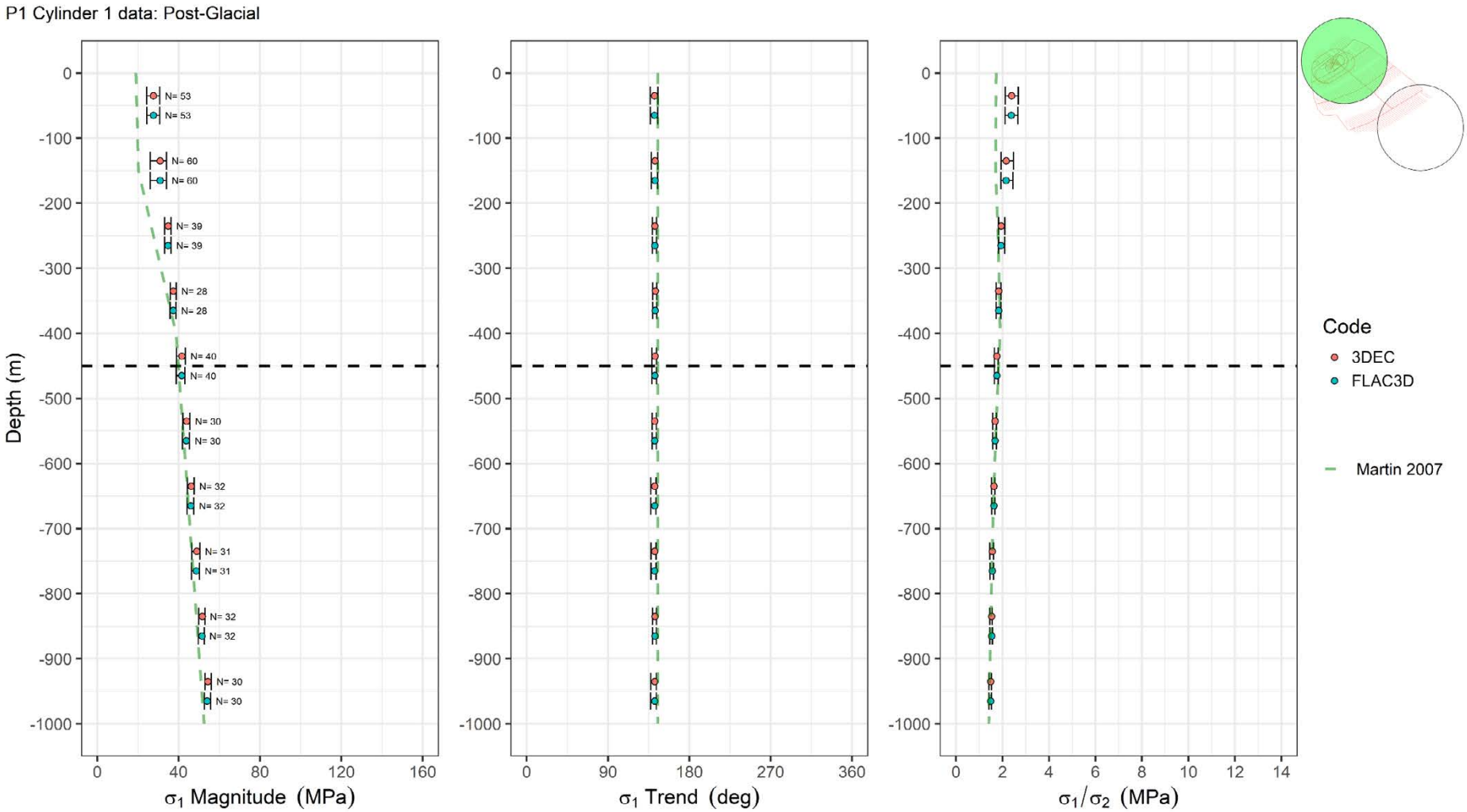

Figure 4-8. *Mean and 95 % variation interval of σ_1 magnitude and trend at hundred meter intervals for 3DEC and FLAC3D after glaciation in an elastic simulation for cylinder 1 (in green in top right inset). The Martin (2007) interpretation is indicated with a green dashed line and the repository depth with a horizontal dashed black line.*

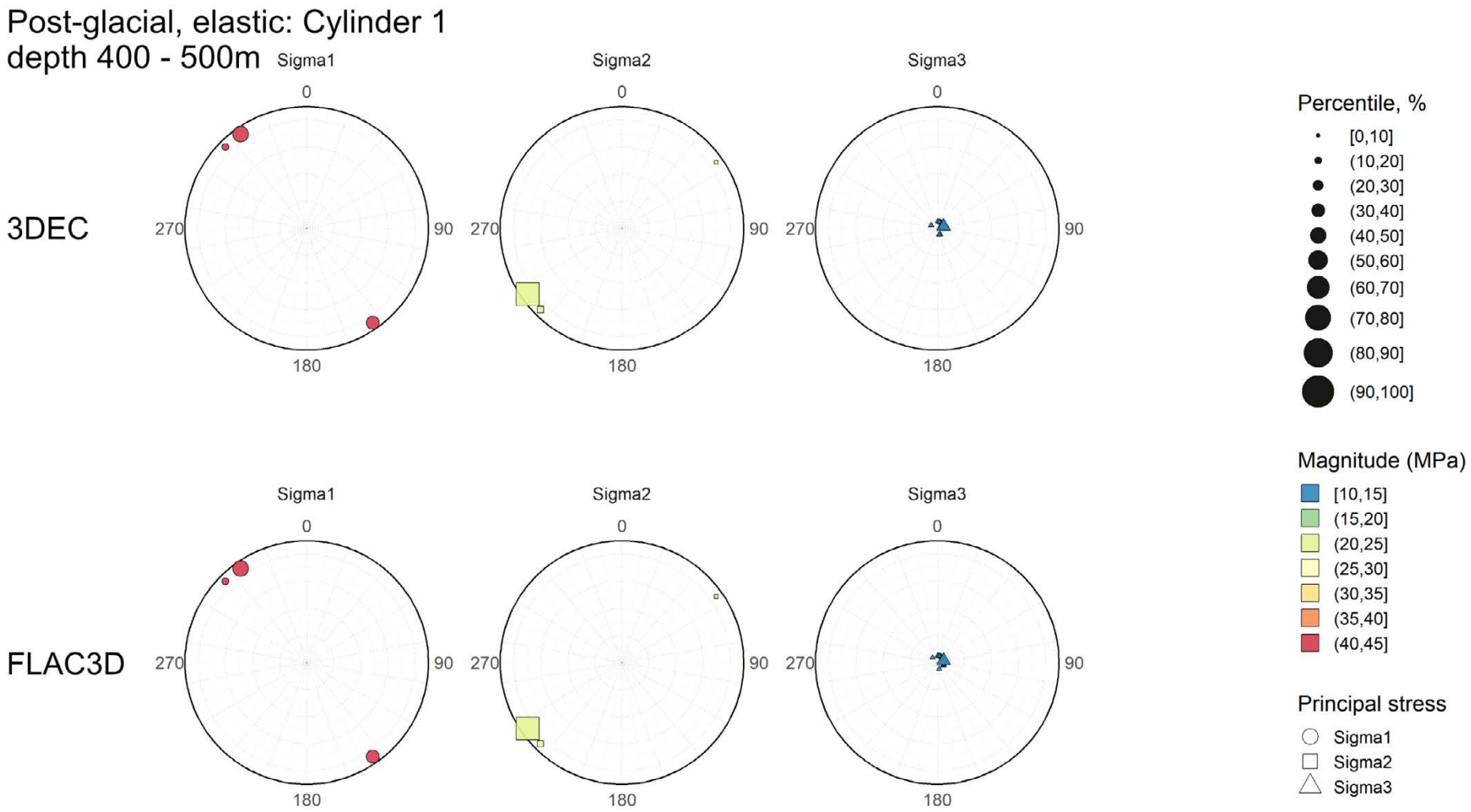

Figure 4-9. *Lower hemisphere projection polar plots of the principal stresses at 20° intervals obtained from cylinder 1 of fully elastic Phase 1 simulations, coloured according to magnitude and symbol sizes by percentile. z = 400–500 m.*

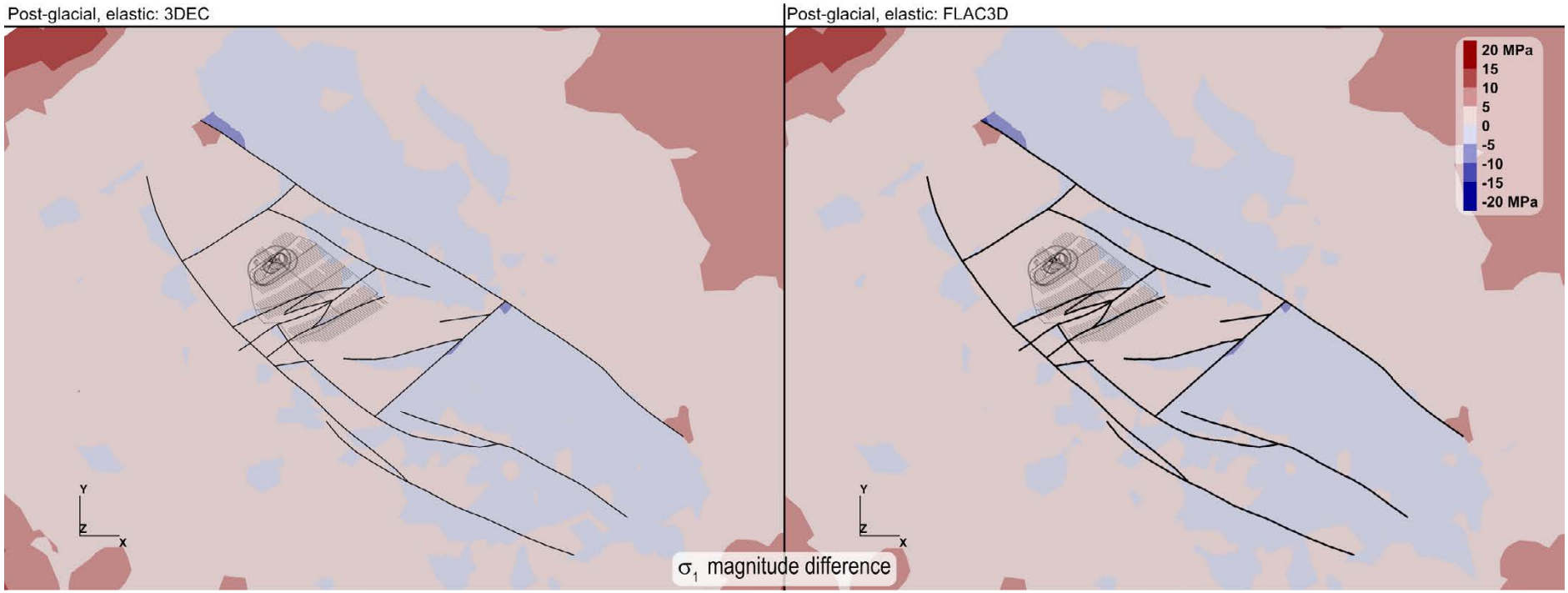

Figure 4-10. *Horizontal cross sections of 3DEC and FLAC3D simulations at repository depth −470 m of the maximum principal stress magnitude difference to the Martin (2007) interpretation, after glaciation in a fully elastic simulation.*

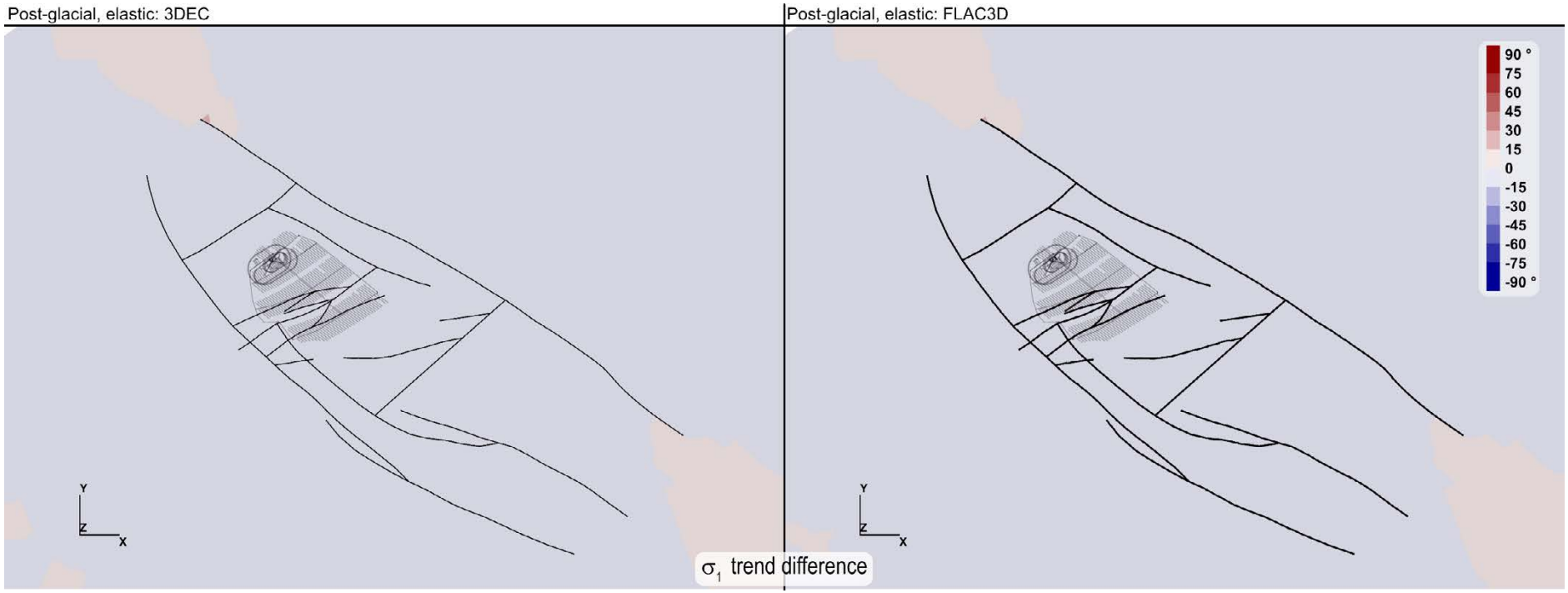

Figure 4-11. *Horizontal cross sections of 3DEC and FLAC3D simulations at repository depth −470 m of maximum principal stress trend difference to the Martin (2007) interpretation, after glaciation in a fully elastic simulation.*

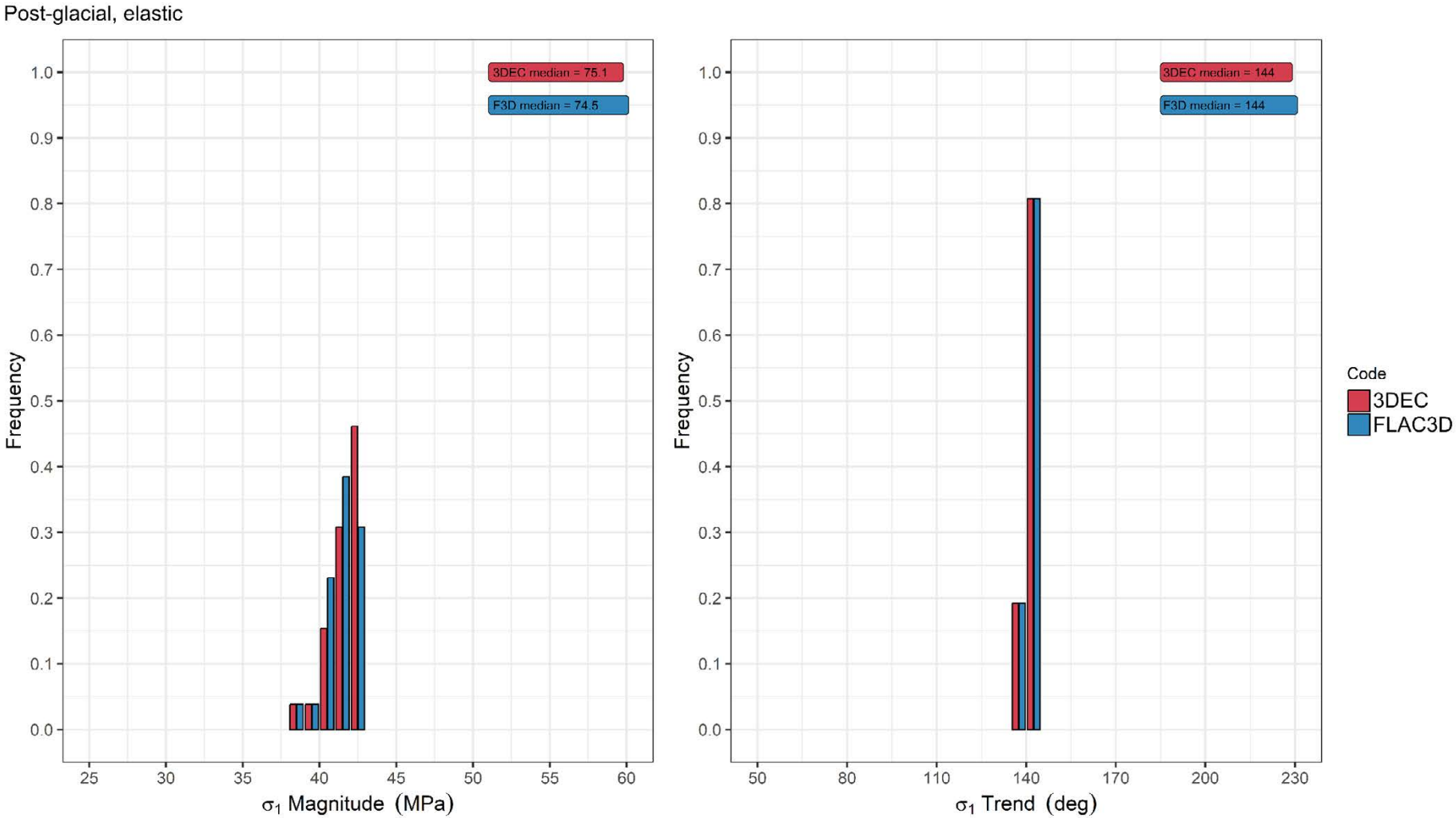

Figure 4-12. *Distribution of σ_1 trend and magnitude at repository depth from cylinder 1 after glaciation in a fully elastic simulation.*

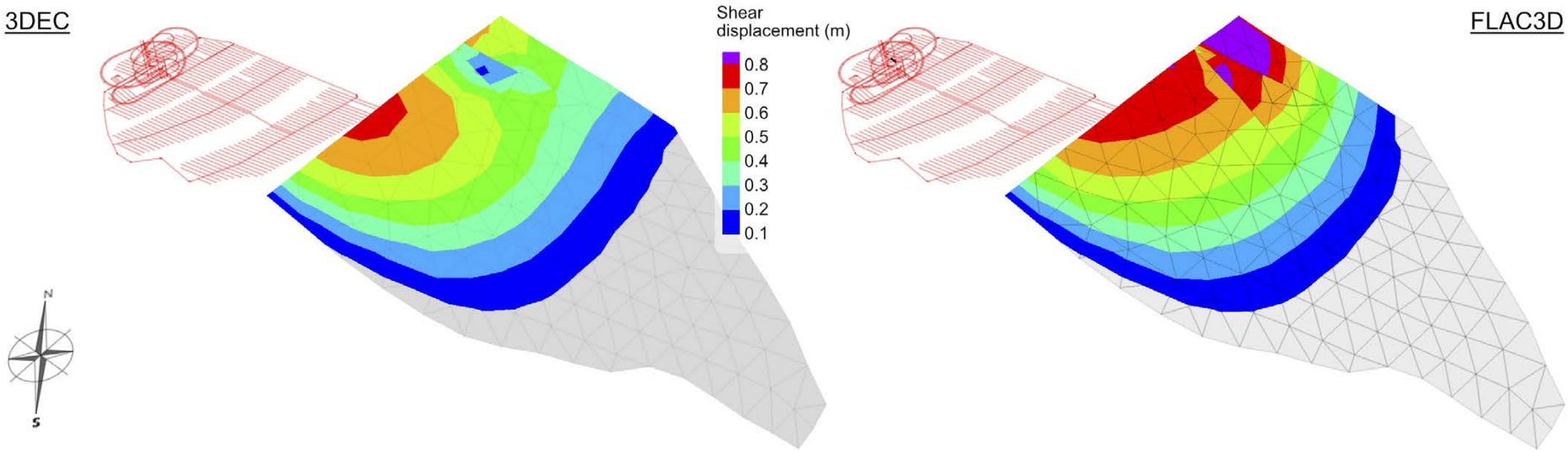

Figure 4-13. *ZFMA3 deformation zone shear displacement in meters after glaciation in an elastoplastic simulation.*

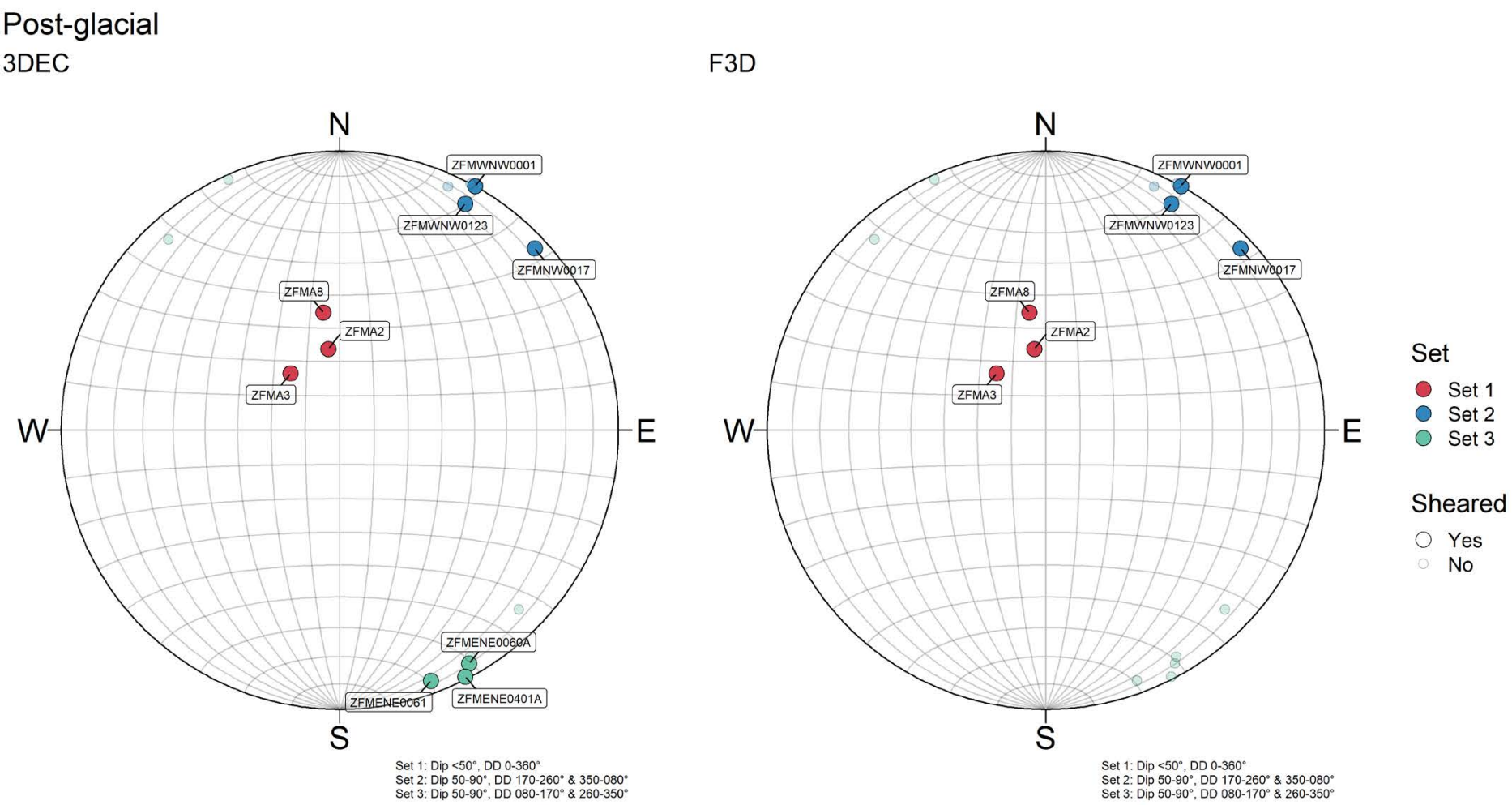

Figure 4-14. *Lower hemisphere projections of sheared deformation zones according to set definitions after glaciation in an elastoplastic simulation for 3DEC and FLAC3D. Sheared = shear displacement > 10 cm.*

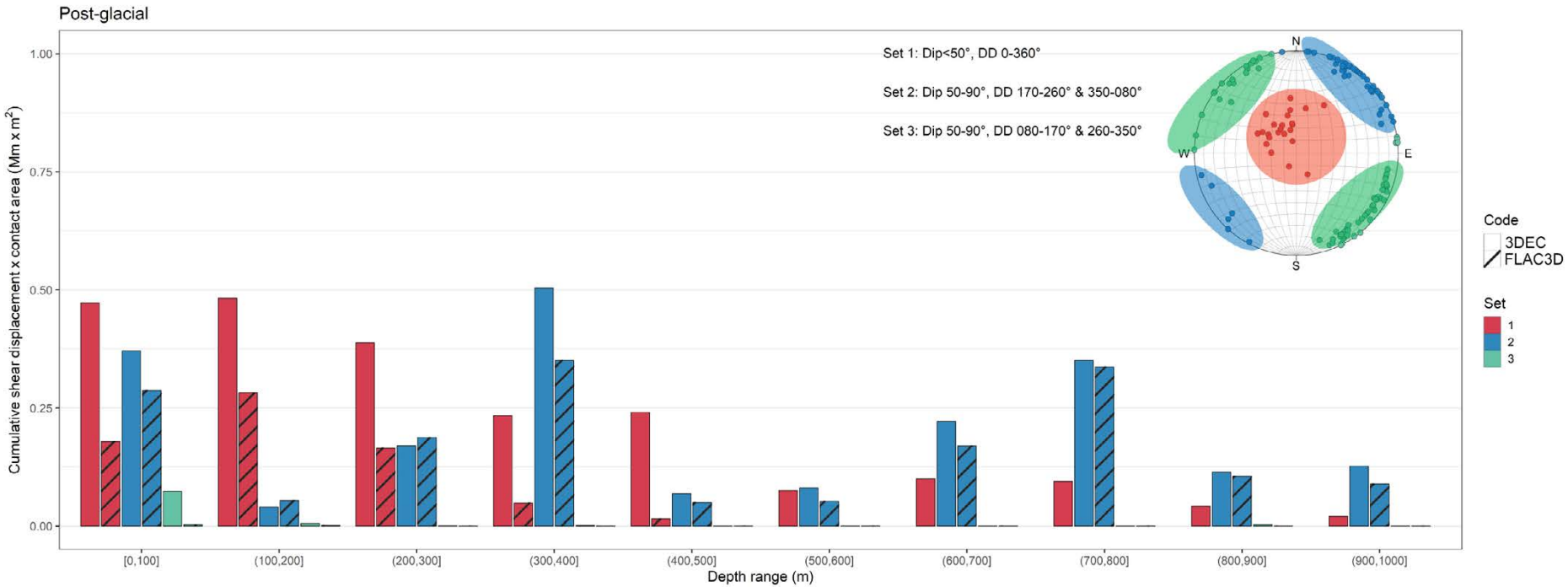

Figure 4-15. *Cumulative shear displacement multiplied by associated area versus depth for major orientations sets of DZ for 3DEC and FLAC3D after glaciation in an elastoplastic simulation.*

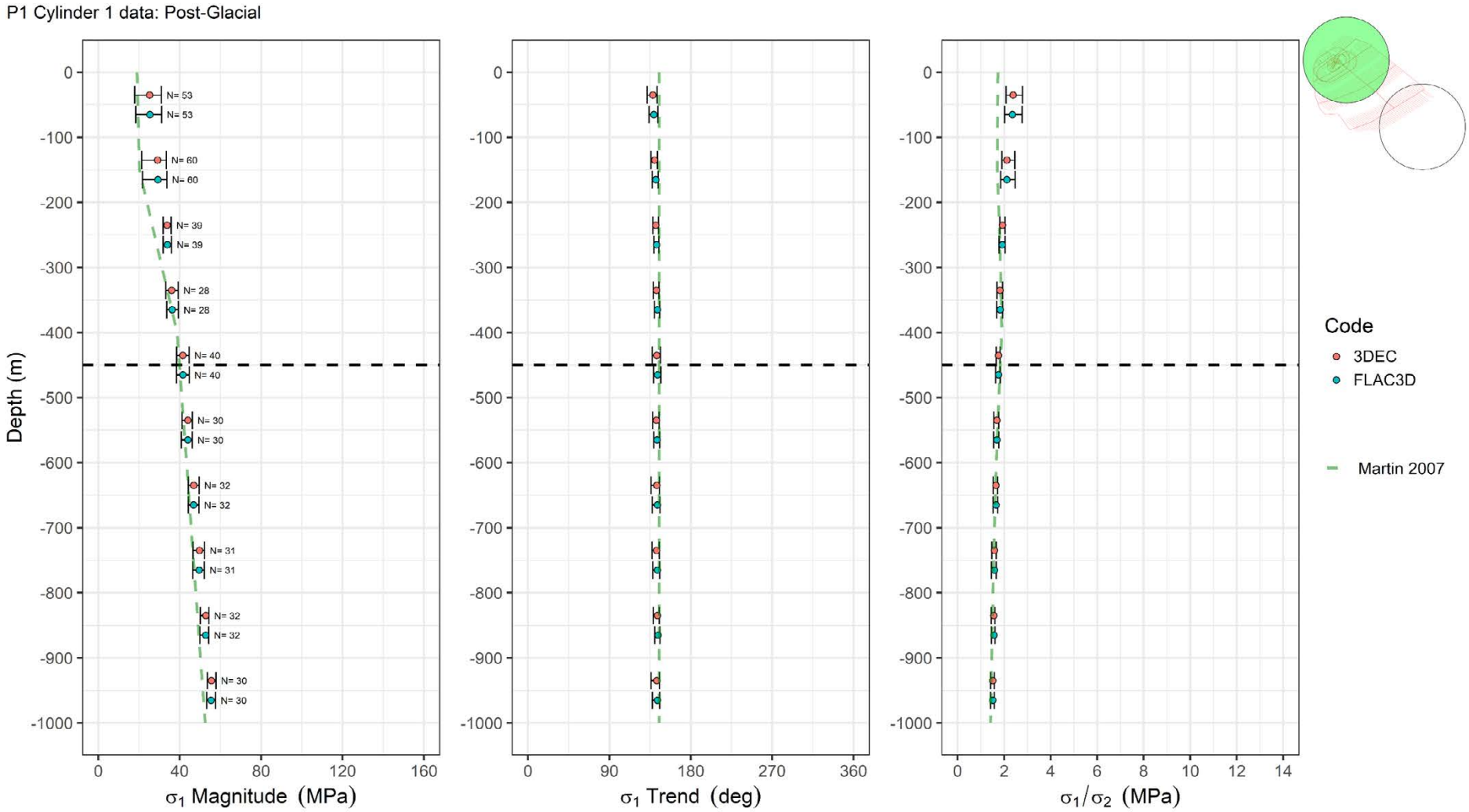

Figure 4-16. *Mean and 95 % variation interval of σ_1 magnitude, trend and the ratio of σ_1 and σ_2 at hundred meter intervals for 3DEC and FLAC3D after glaciation in an elasto-plastic simulation for cylinder 1 (in green in top right inset). The Martin (2007) interpretation is indicated with a green dashed line and the repository depth with a horizontal dashed black line.*

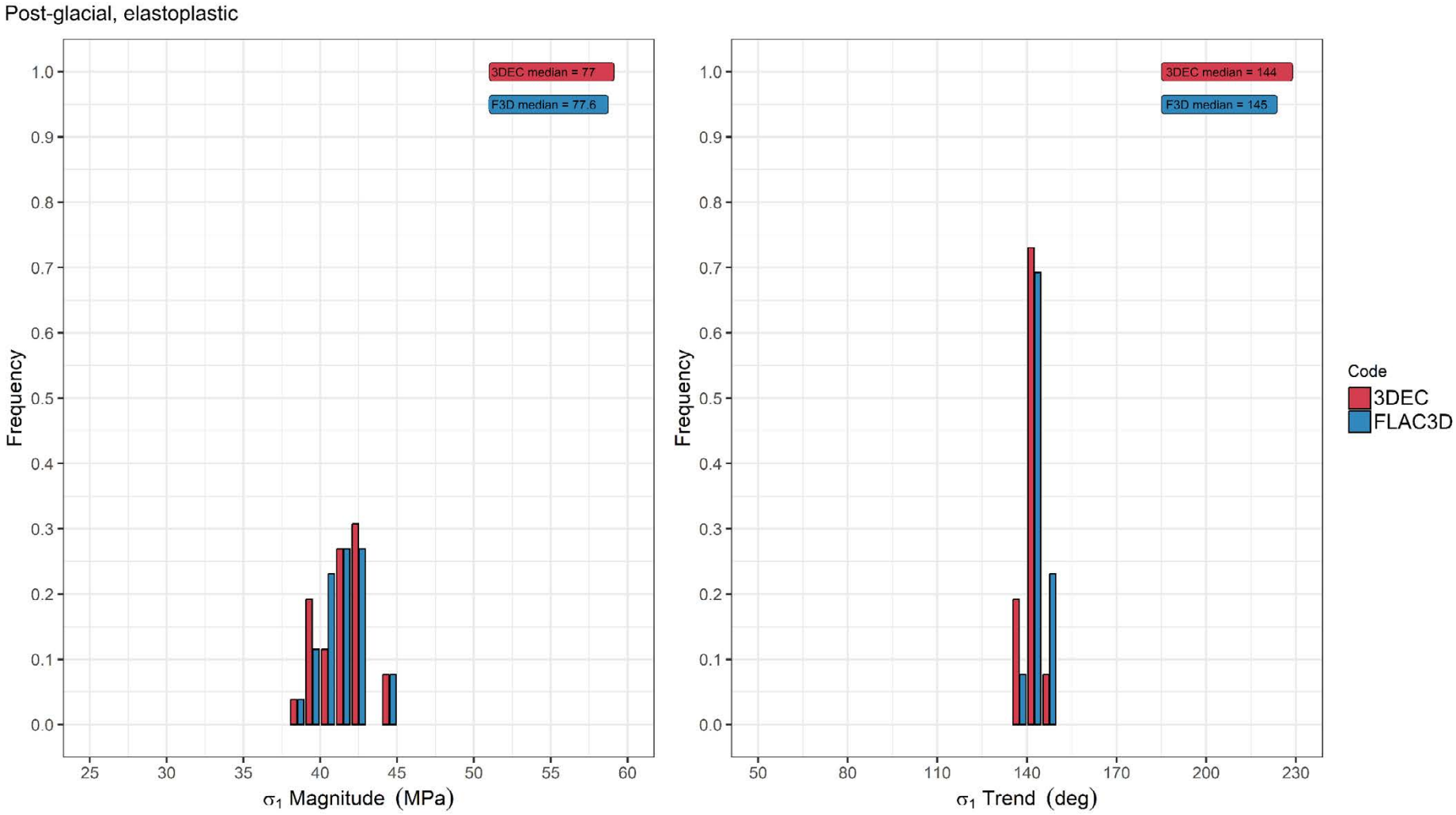

Figure 4-17. *Distribution of σ_1 trend and magnitude at repository depth from cylinder 1 after glaciation in an elastoplastic simulation.*

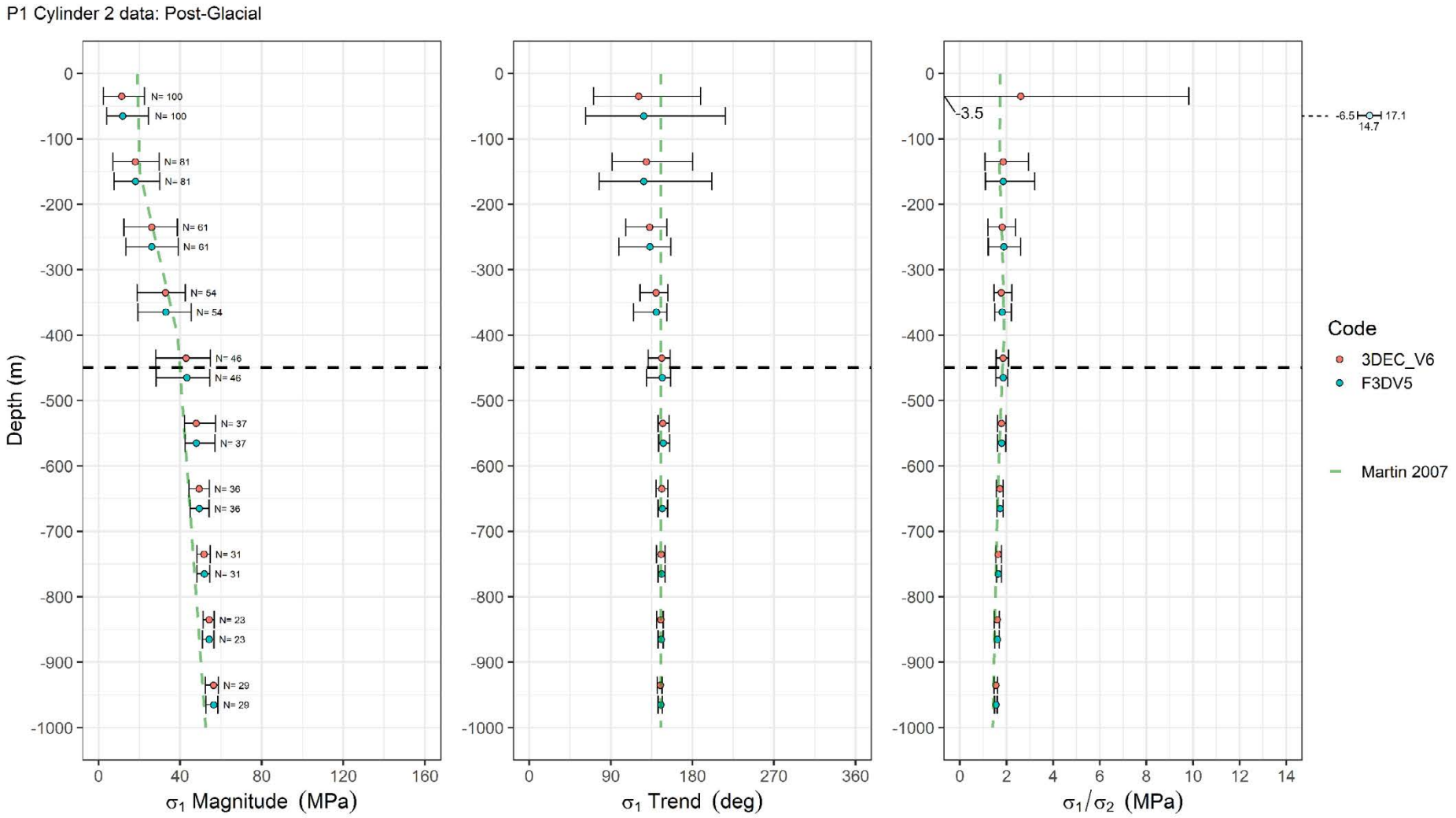

Figure 4-18. *Mean and 95 % variation interval of σ_1 magnitude and trend at hundred meter intervals for 3DEC and FLAC3D after glaciation in an elastoplastic simulation for cylinder 2 (top right:green). The Martin (2007) interpretation is indicated with a green dashed line and the repository depth with a horizontal dashed black line.*

4.3 Phase 2

Base case

The applied boundary thrust macro logic was able to produce target stress states at the repository depth level for all the seven cases modelled, with the applied deformation zone shear strength parameters. The thrust for the Base case mainly caused plastic shear but also combined shear and tension of deformation zone Set 1, extending down to a depth of 600 m (Figure 4-19, Figure 4-20). Set 2, mainly the Singö deformation zone (ZFMWNW0001), exhibits elastic shear displacement to a depth of 1 000 m. Set 3 does not shear. The glaciation cycle increases plastic shear of Set 1 only (Figure 4-21).

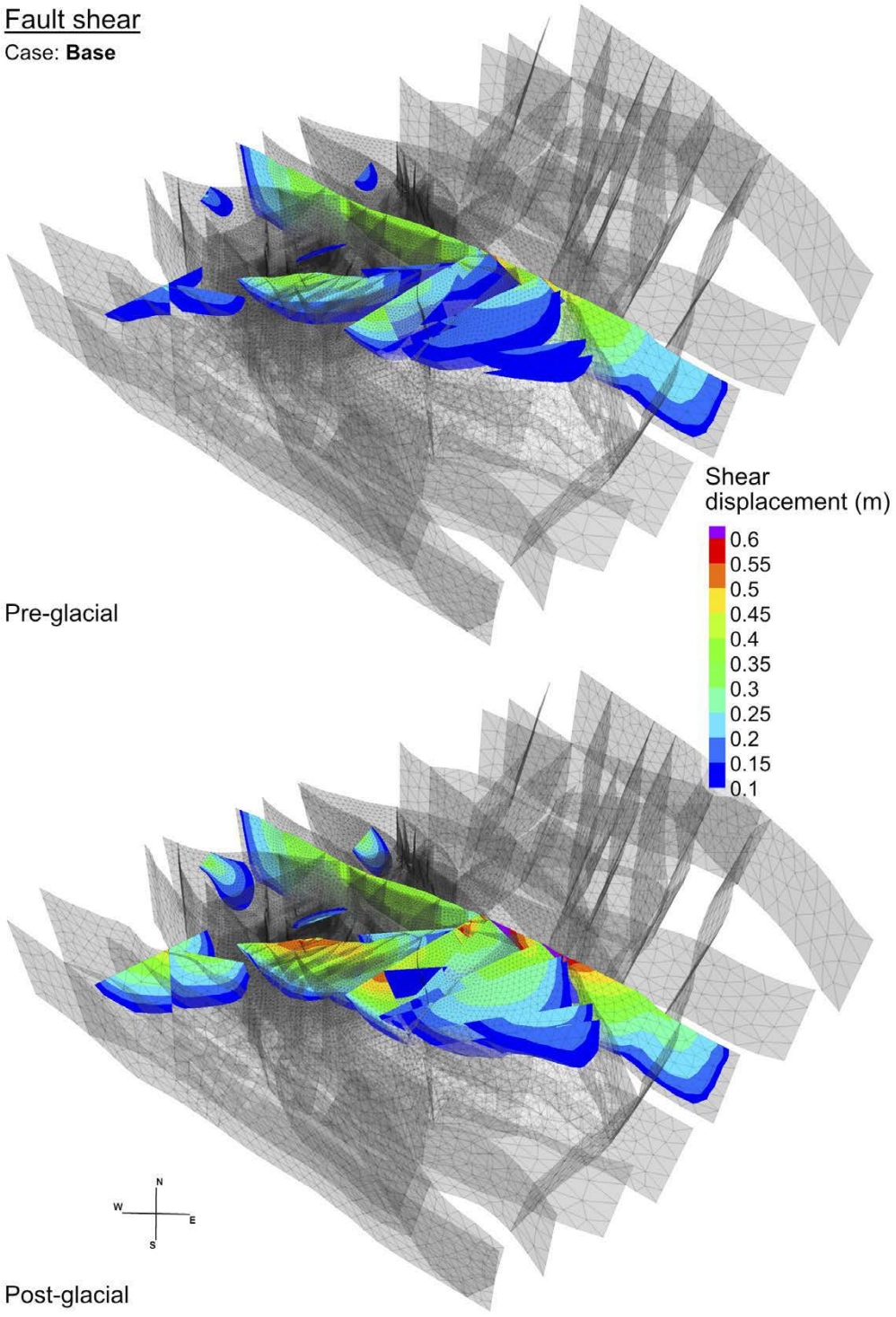

Figure 4-19. *Phase 2 deformation zone shear contours before and after glaciation for the Base case.*

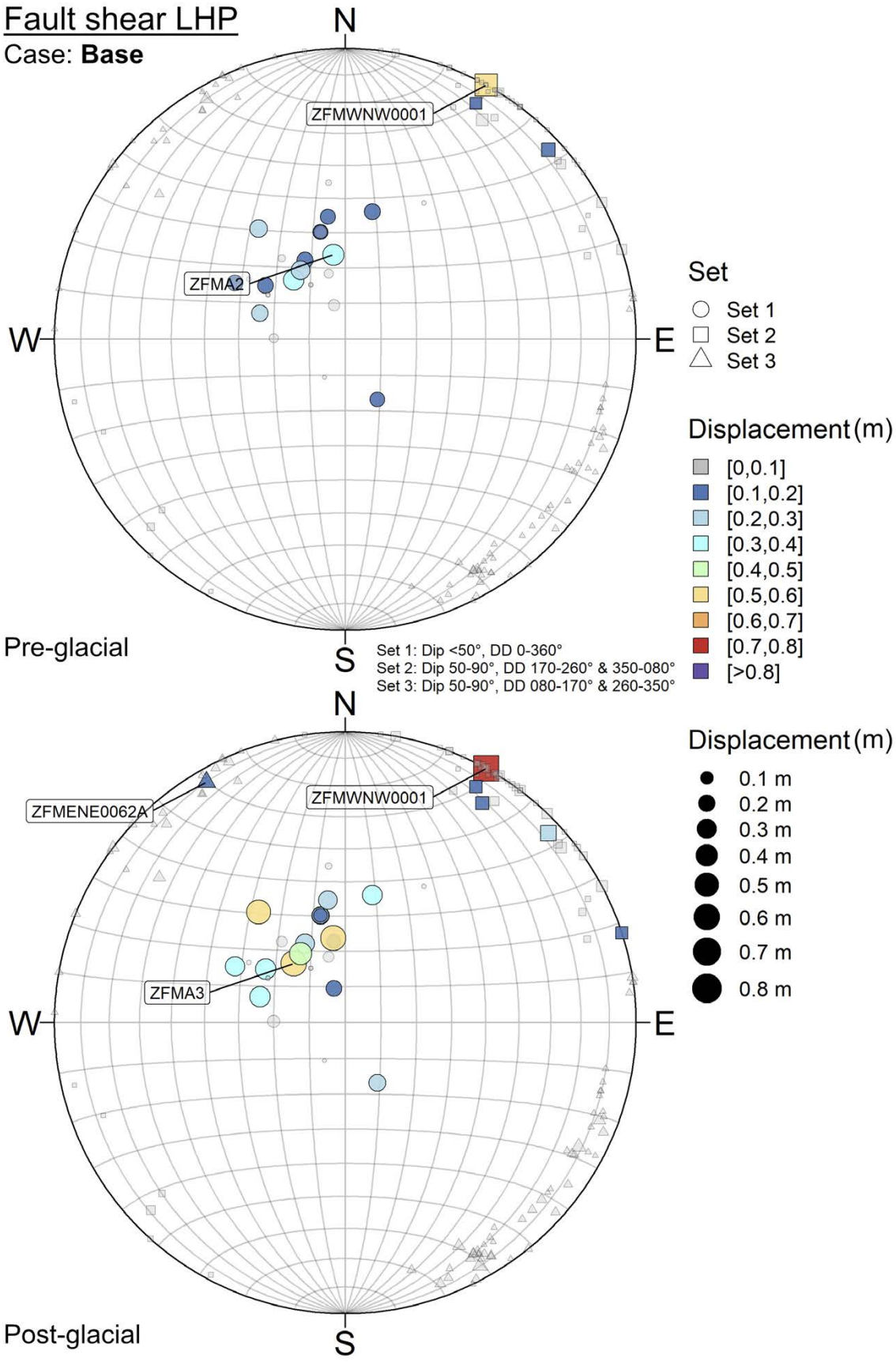

Figure 4-20. *Deformation zone shear before and after glaciation by set group on an equal area lower hemisphere projection (LHP) for the Base case. Both symbol size and colour indicate displacement magnitude in metres.*

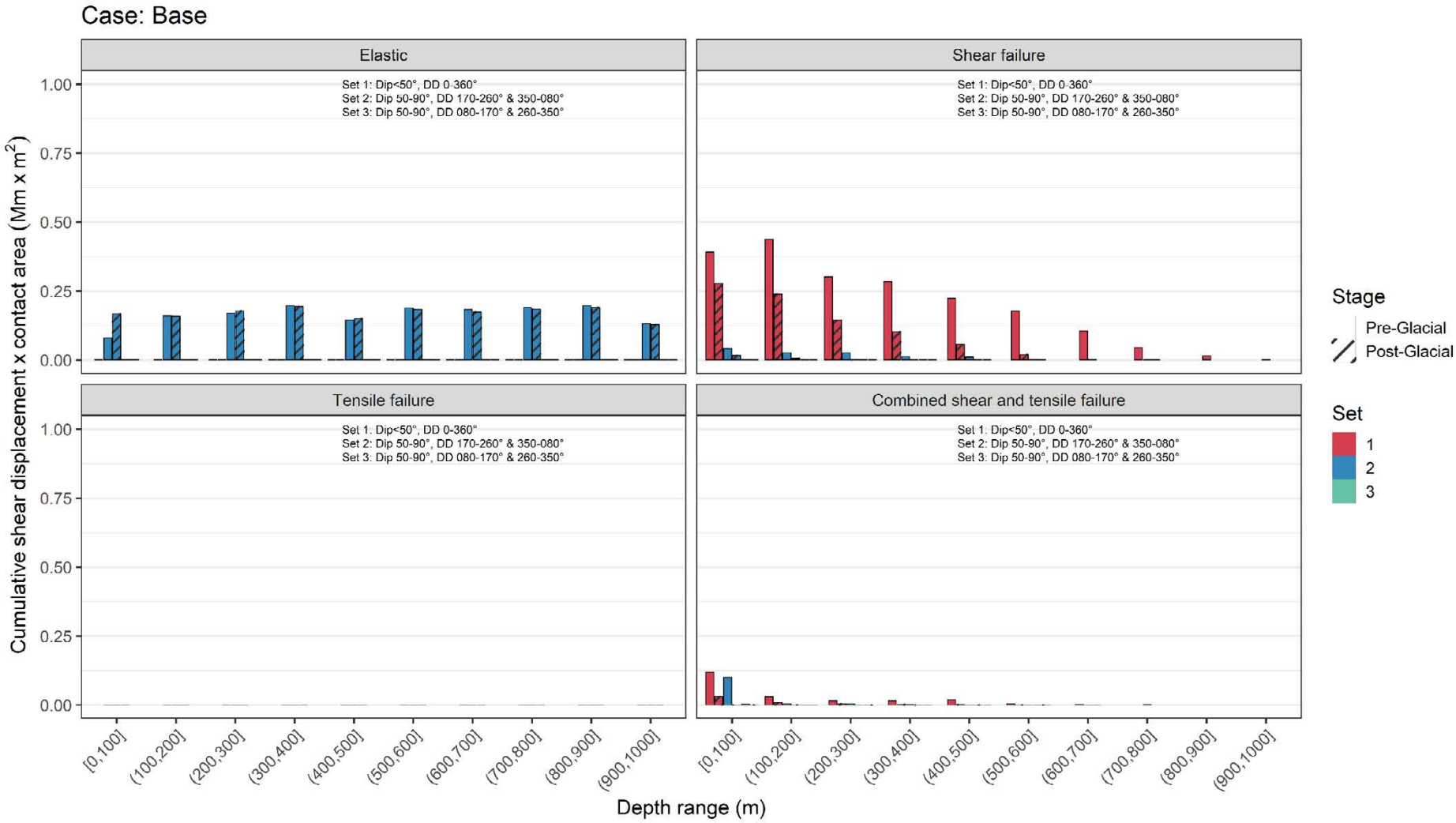

Figure 4-21. *Cumulative shear displacement multiplied by associated area versus depth for major orientation sets of DZ for the Base case of Phase 2 before and after glaciation.*

Analysis of the depth-based distribution of principal stress data across the repository footprint indicates that at the pre-glacial phase the mean trend of the maximum compression rotates a maximum of 12° counterclockwise from the trend of thrust above a depth 200 m but below 200 m the mean trend is relatively constant and does not deviate significantly from the thrust direction (Figure 4-22). Compared to the stress gradients given in Martin (2007), the σ_1 magnitude is 5–10 MPa greater at depths of 100 m to 300 m and slightly increased below 700 m. At the repository level, however, the σ_1 magnitude matches the target magnitude. The glacial cycle decreases the σ_1 mean magnitude down to the 300 m level and widens variation on the lower magnitude side, while a minor increase of magnitude variation can be seen down to a depth of one kilometre (Figure 4-23). In the repository volume (±50 m from the repository level), the median horizontal stress magnitudes are equal to the targets and the mean trend only deviates −3° (Figure 4-24). The variation of σ_1 is less than ±5 MPa, ±2.5 MPa for σ_2 and σ_3 and the variation of the trend of σ_1 is below ±10° (Figure 4-25 to Figure 4-28). This applies both to the pre- and post-glacial stages.

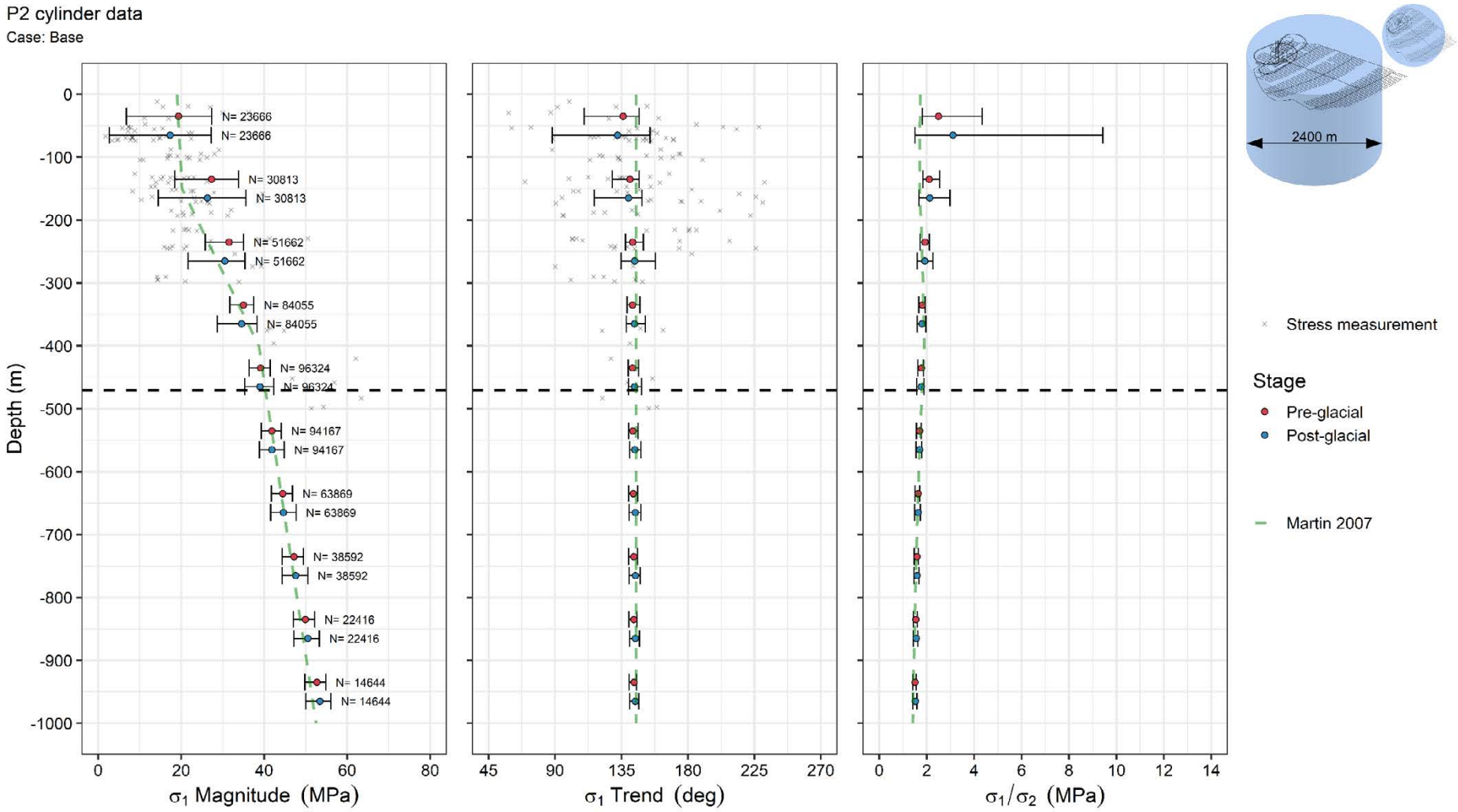

Figure 4-22. *Mean and 95 % variation interval of σ_1 magnitude, trend and the ratio of σ_1 and σ_2 at hundred meter intervals for the Base case of Phase 2 before and after glaciation for a cylinder covering the repository footprint (in blue in top right inset). The Martin (2007) interpretation is indicated with a green dashed line and the repository depth with a horizontal dashed black line. Field stress measurements indicated with grey markers.*

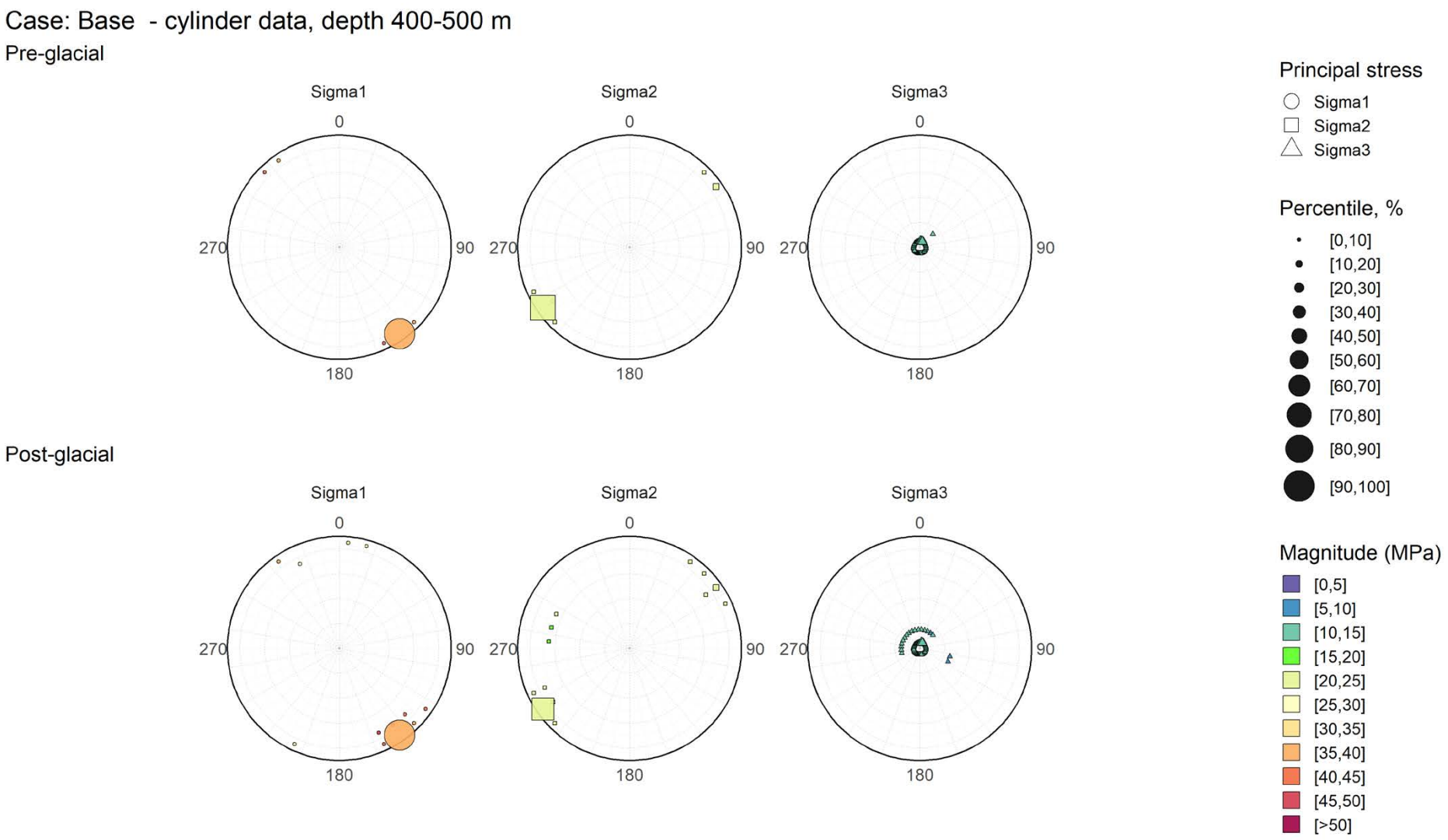

Figure 4-23. *Lower hemisphere projection polar plots of the principal stresses at 20° intervals obtained from a cylinder covering the repository footprint of the Base case of Phase 2 simulations, coloured according to magnitude and symbol sizes by percentile. z = 400−500 m.*

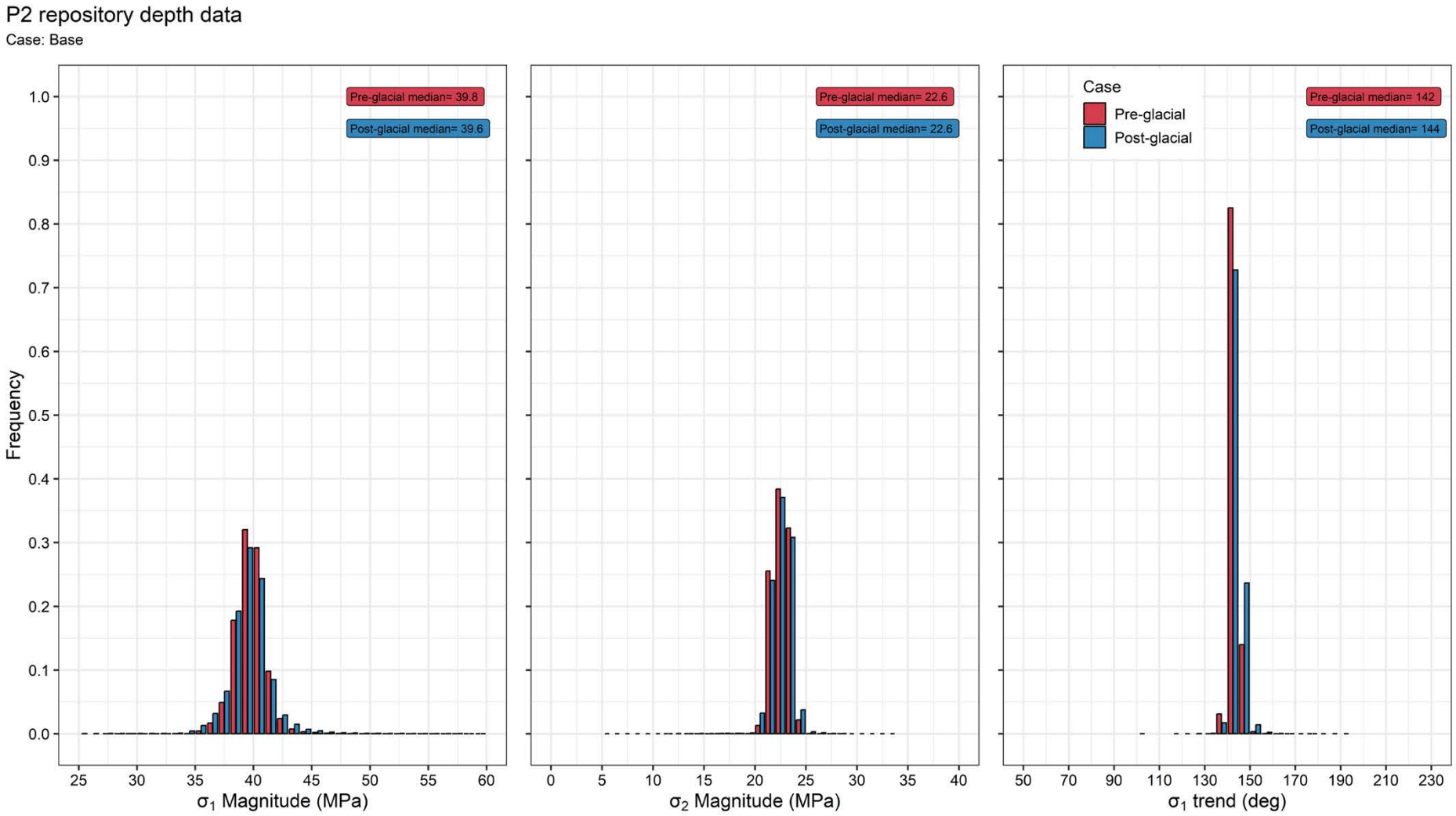

Figure 4-24. *Distribution of σ_1 and σ_2 magnitude and σ_1 trend at repository depth before and after glaciation for the Base case of Phase 2 simulations.*

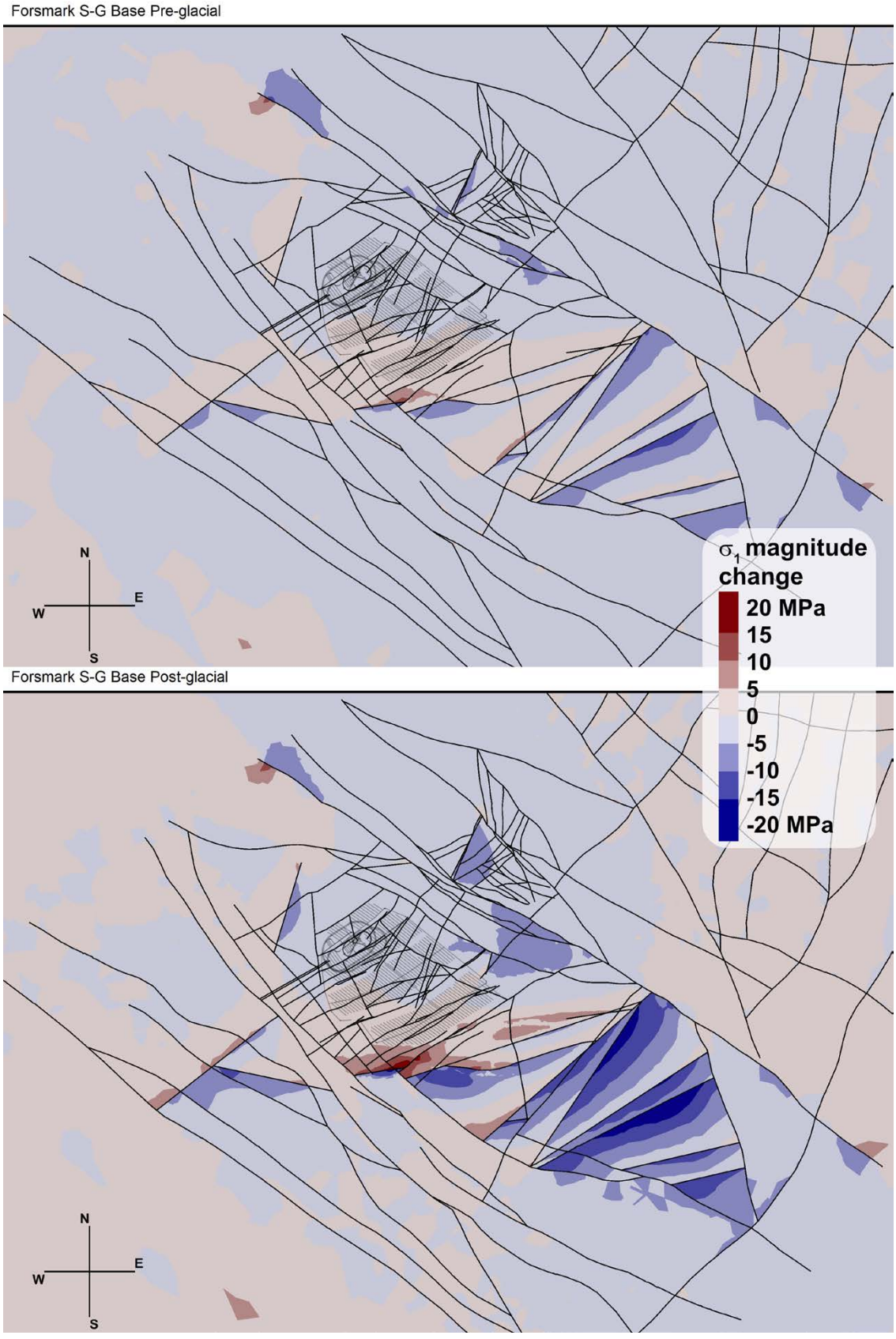

Figure 4-25. *The change in σ_1 magnitude before and after glaciation for the Base case of Phase 2 simulations in a horizontal cross-section at repository depth (470 m). The reference value is case-dependent.*

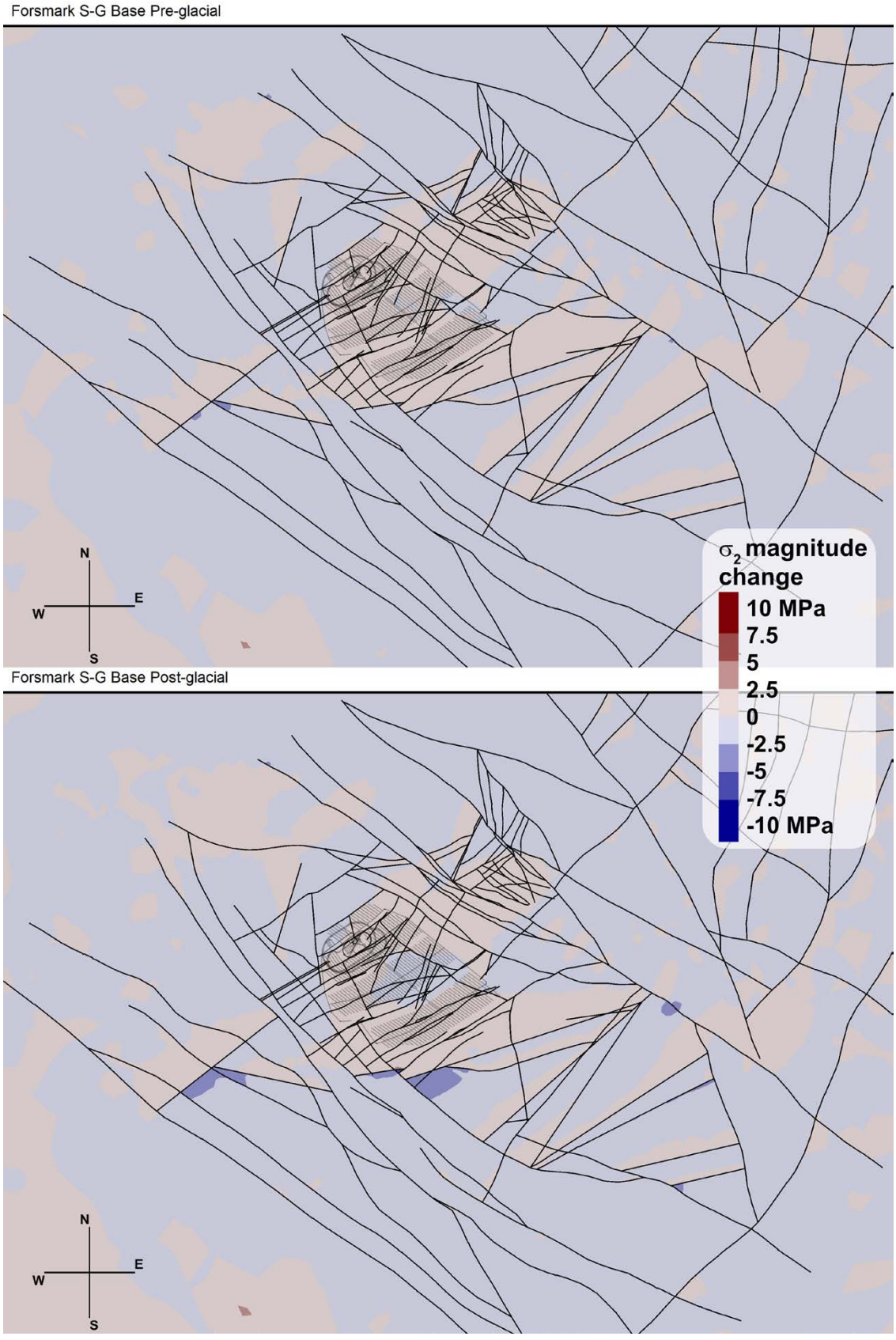

Figure 4-26. *The change in σ_2 magnitude before and after glaciation for the Base case of Phase 2 simulations in a horizontal cross-section at repository depth (470 m). The reference value is case-dependent.*

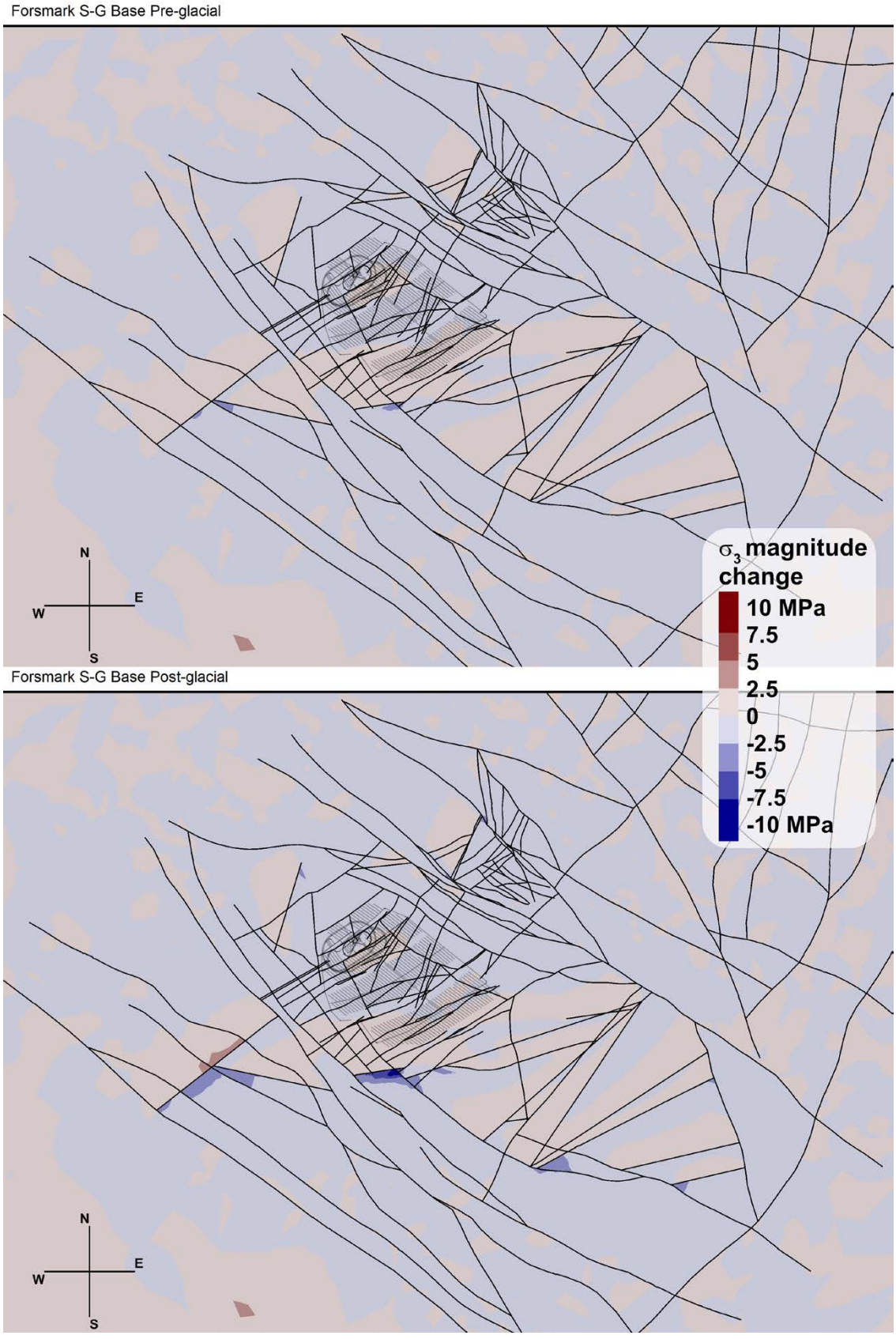

Figure 4-27. *The change in σ_3 magnitude before and after glaciation for the Base case of Phase 2 simulations in a horizontal cross-section at repository depth (470 m). The reference value is case-dependent.*

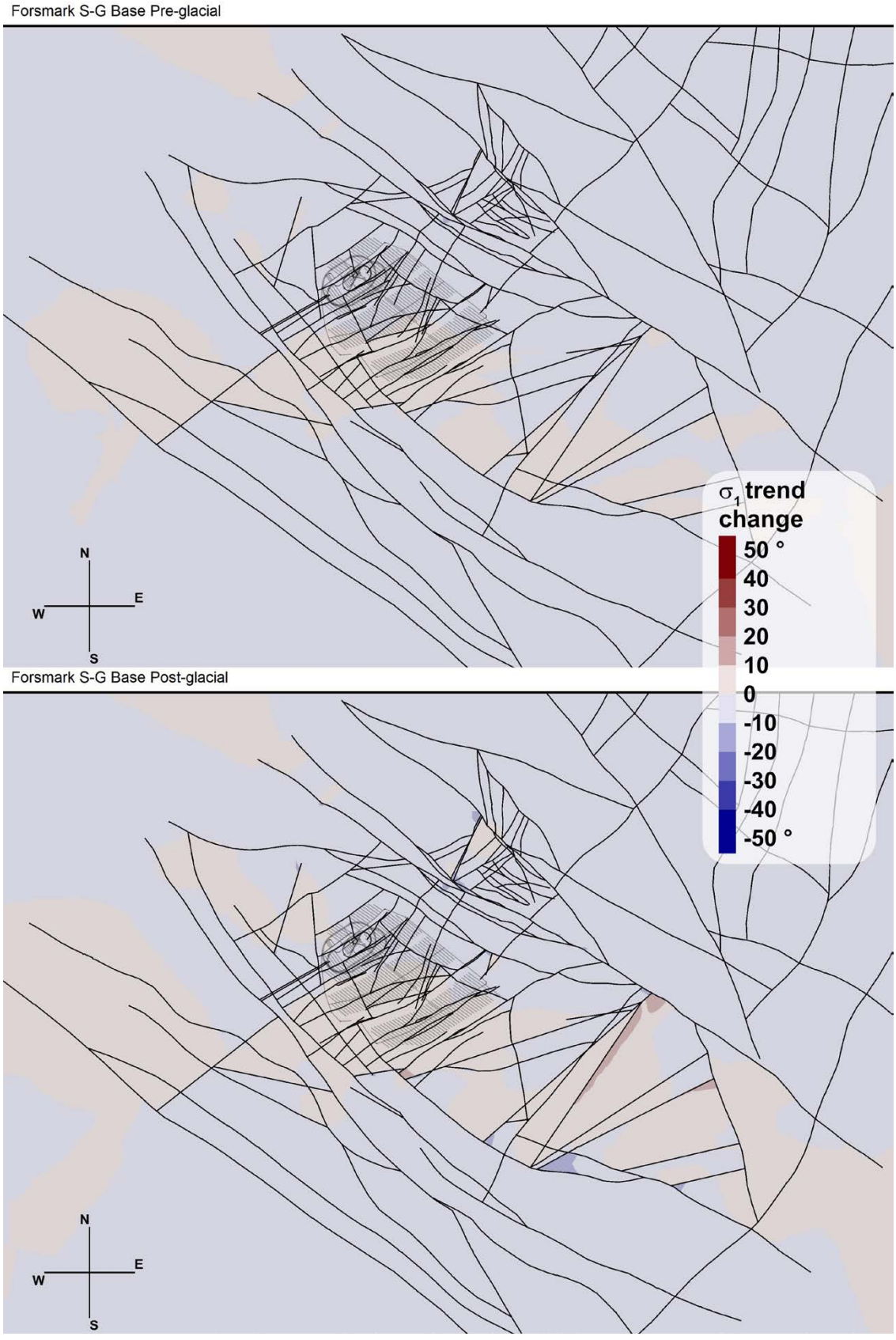

Figure 4-28. *The change in σ_1 trend before and after glaciation for the Base case of Phase 2 simulations in a horizontal cross-section at repository depth (470 m). The reference value is case-dependent.*

A comparison of the simulated stress confidence limits with the stresses measured in the field shows that a moderate number of measured σ_1 values down to the 300 m level are outside the simulated 95 % confidence limits (Figure 4-29). A moderate number of measured σ_2 values up to a depth of 500 m from the surface are clearly above the 95 % confidence limits but between a depth of 100 m to 300 m some are also below the 95 % confidence limits (Figure 4-30). Above the 300 m level the simulated variation of the major principal stress trend is considerably lower than the measured variation (Figure 4-22).

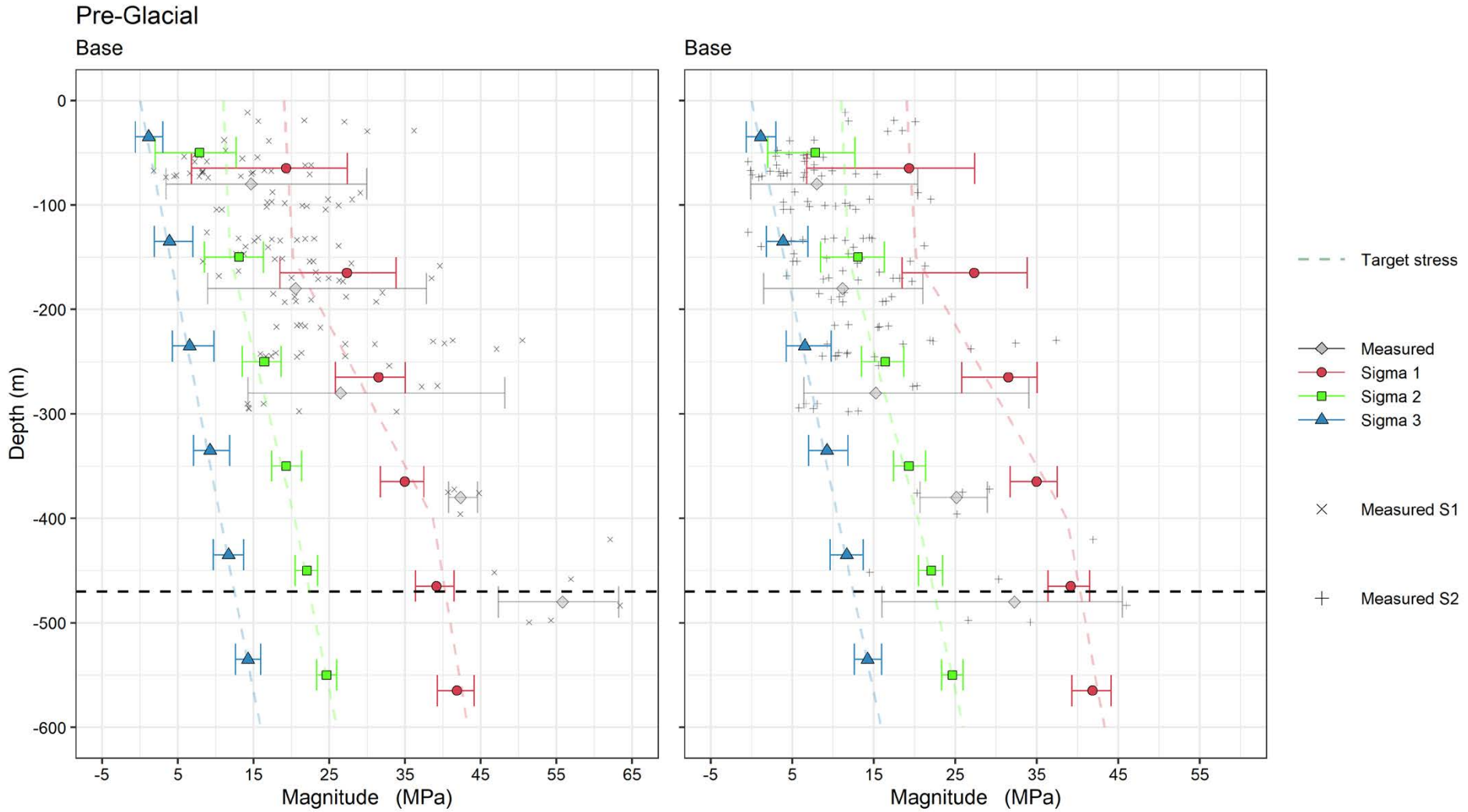

Figure 4-29. *Mean and 95 % variation interval of the principal stress magnitudes versus measured stresses at hundred-meter intervals for the Base case of Phase 2 simulations* ***before*** *glaciation from a cylinder covering the repository. Left: simulation results versus σ_1 from field stress measurements. Right: simulation results versus σ_2 from field stress measurements. The Martin (2007) interpretation is indicated with coloured dashed lines and the repository depth with a horizontal dashed black line. Field stress measurements indicated with grey cross or plus symbols, with the mean and 95 % variation interval also in grey.*

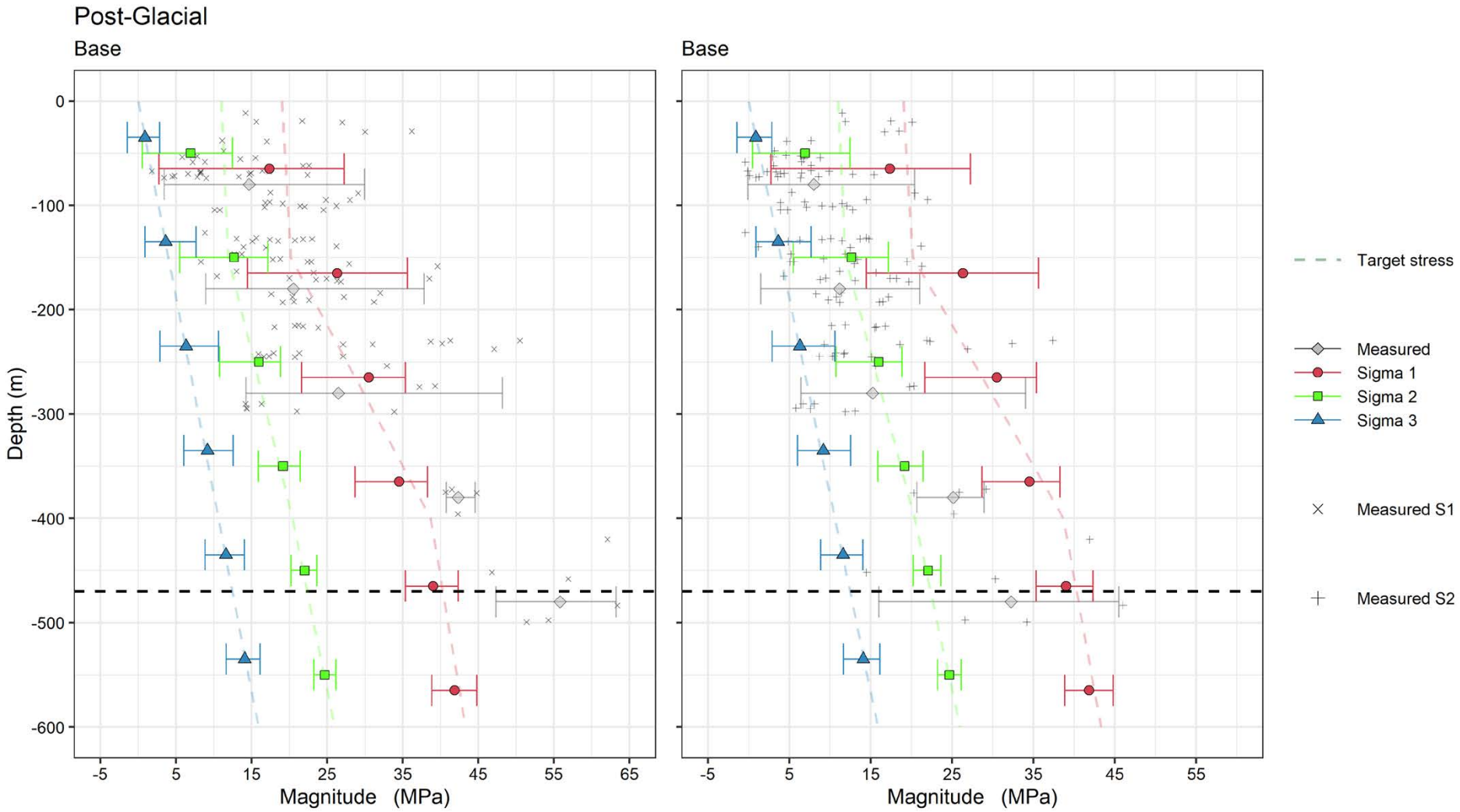

Figure 4-30. *Mean and 95 % variation interval of the principal stress magnitudes versus measured stresses at hundred meter intervals for the Base case of Phase 2 simulations* ***after*** *glaciation from a cylinder covering the repository. Left: simulation results versus σ_1 from field stress measurements. Right: simulation results versus σ_2 from field stress measurements. The Martin (2007) interpretation is indicated with coloured dashed lines and the repository depth with a horizontal dashed black line. Field stress measurements indicated with grey cross or plus symbols, with the mean and 95 % variation interval also in grey.*

Cases 1 and 2

In Cases 1 and 2, the thrust was either rotated −20° (counterclockwise) or +20° (clockwise) compared to the default orientation of 145° and the deformation zone geometry. Counterclockwise rotation increased plastic shear of deformation zone Set 1 but reduced elastic shear of Set 2 almost to zero (Figure 4-31). Clockwise rotation did not affect Set 1 shear notably, but elastic shear of Set 2 increased by about 40 % (Appendix 6). In these cases, Set 2 activity is mainly due to shear of the Singö deformation zone (Figure 4-32). For both cases glaciation only increased shear of Set 1, although one deformation zone in Set 3 also exhibited minor plastic shear (Appendix 6). Plastic shear extends to a depth of 900 m in Case 1 (Appendix 6).

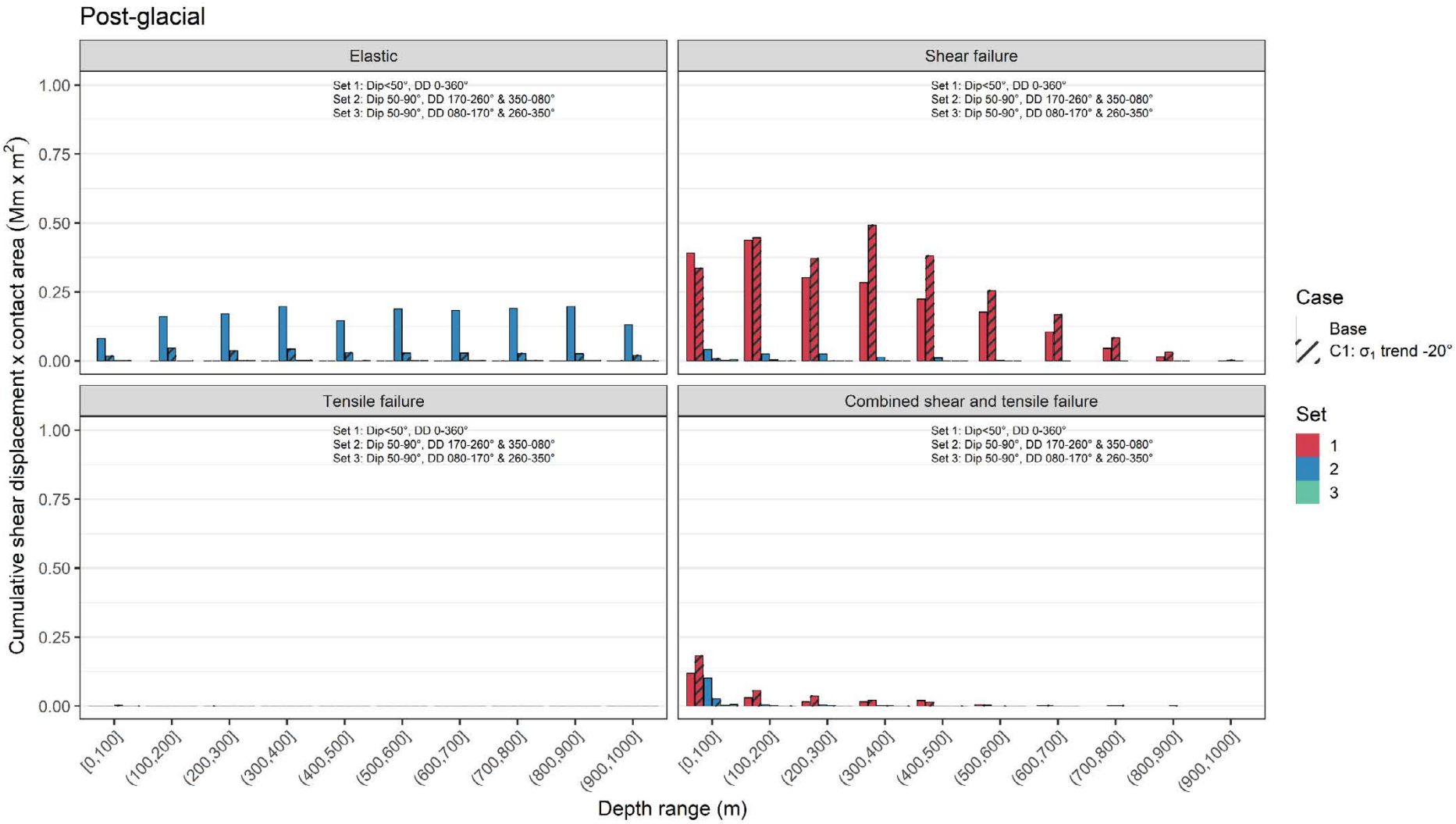

Figure 4-31. *Cumulative shear displacement multiplied by associated area versus depth for major orientation sets of DZ for the Base case and Case 1 (C1) of Phase 2 after glaciation.*

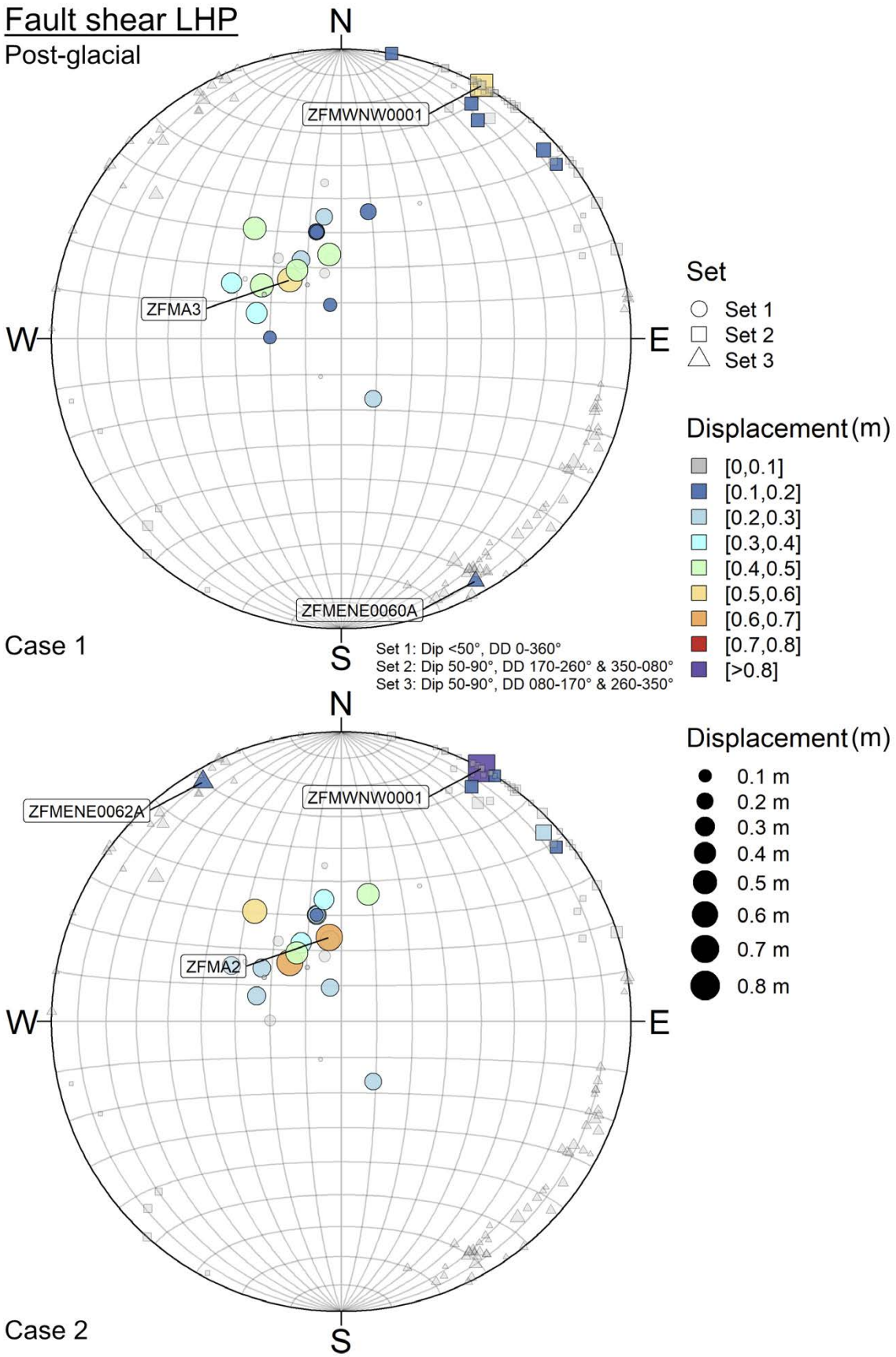

Figure 4-32. *Deformation zone shear after glaciation by set group on an equal area lower hemisphere projection (LHP) for Case 1 and 2. Both symbol size and colour indicate displacement magnitude in metres.*

Apart from the ±20° thrust rotation the depth distribution of the σ_1 magnitude and trend are very close to the Base case (Appendix 8, Appendix 11). The glacial cycle decreases the mean magnitude of σ_1 to a depth of 300 m and widens variation on both sides, being higher than in the Base case (Appendix 8). In the repository volume the σ_1, σ_2 and σ_1 trend median are practically equal to the Base case, but in Case 2 the variation of σ_1 is smaller than the Base case and the southernmost ends of the deposition tunnels may exhibit magnitudes 5 MPa to 10 MPa higher than the median (Appendix 13). In both cases σ_3 also has a higher variation resulting in magnitudes that are locally 2.5 MPa to 5 MPa higher or lower than the target.

Between a depth of 100 m and 300 m a high number of measured σ_1 values obtained from field stress measurements are below Case 1 95 % confidence limits while in Case 2 the amount is moderate. Below 300 m all measured σ_1 values are above Case 1 95 % confidence limits whereas in Case 2 the corresponding amount is moderate (Figure 4-33). In Case 1 a considerable number of σ_2 values obtained from field stress measurements up to a depth of 300 m are below the 95 % confidence limits and below 300 m almost all of them are above the 95 % confidence limits. In Case 2 a high number of measured σ_2 values are above the 95 % confidence limits (Figure 4-34). The σ_1 trend variation in Case 2 is closer to the measured variation above a depth of 100 m but even more narrow than in the Base case below this depth (Appendix 15, Appendix 17, Appendix 19, Appendix 21).

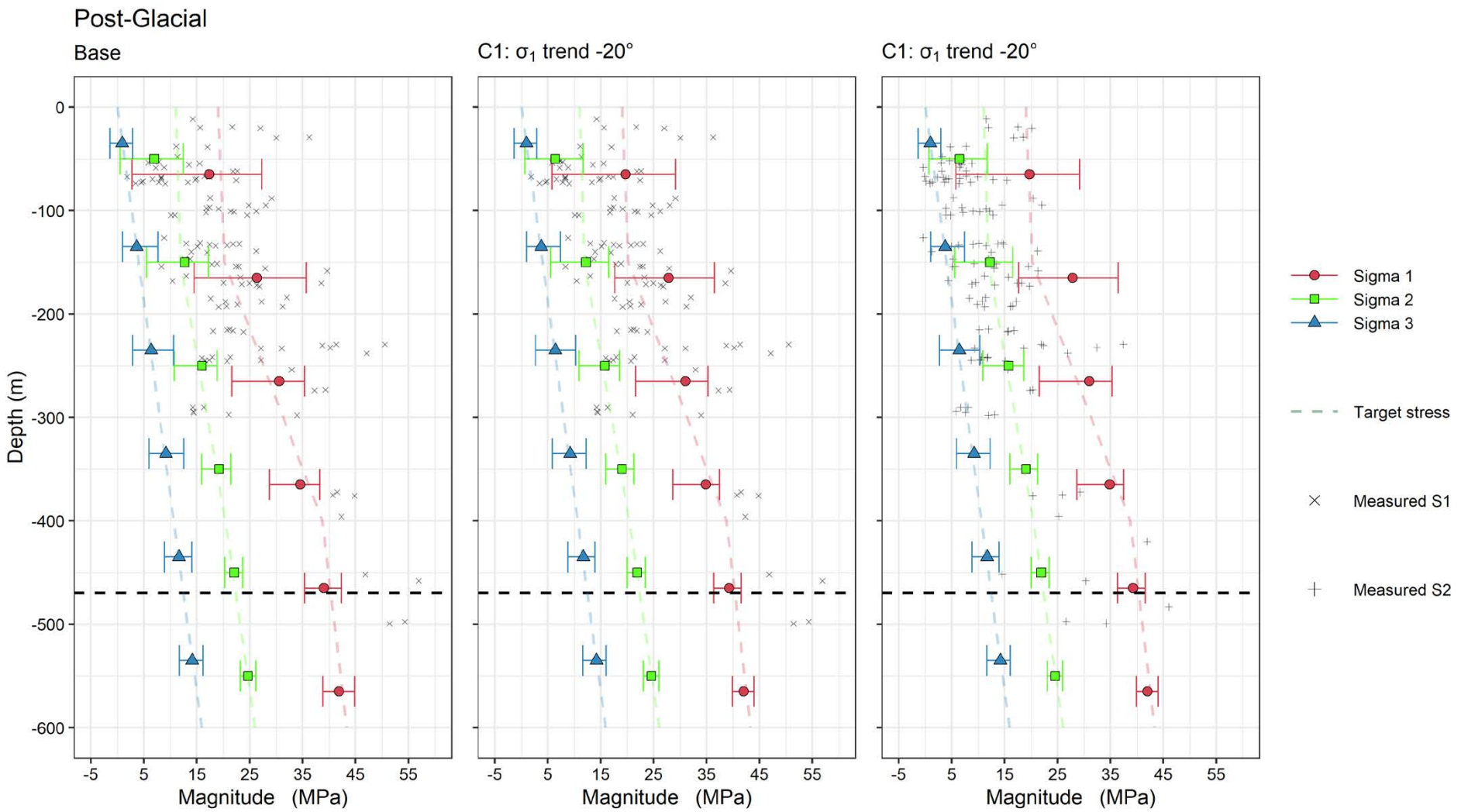

Figure 4-33. *Mean and 95 % variation interval of the principal stress magnitudes versus measured stresses at hundred meter intervals for the Base case and Case 1 (C1) of Phase 2 simulations after glaciation from a cylinder covering the repository. The Martin (2007) interpretation is indicated with a green dashed line and the repository depth with a horizontal dashed black line. Field stress measurements indicated with grey cross or plus symbols.*

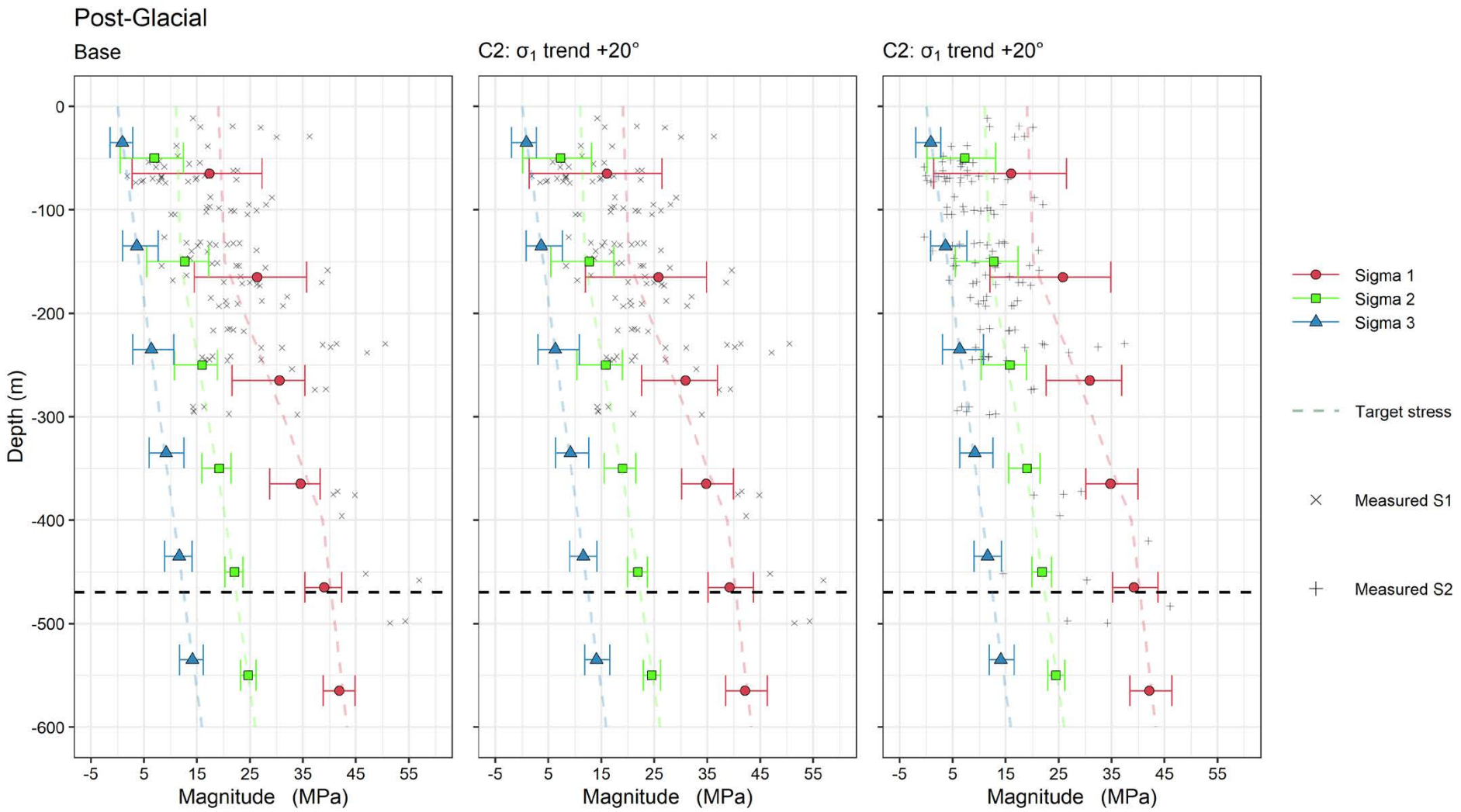

Figure 4-34. *Mean and 95 % variation interval of the principal stress magnitudes versus measured stresses at hundred meter intervals for the Base case and Case 2 (C2) of Phase 2 simulations after glaciation from a cylinder covering the repository. The Martin (2007) interpretation is indicated with a green dashed line and the repository depth with a horizontal dashed black line. Field stress measurements indicated with grey cross or plus symbols.*

Cases C3 and C6

In Cases 3 and 6, the minimum horizontal stress is decreased by 45 % compared to the Base case, being equal to the vertical stress component and in Case 6 the maximum horizontal stress is also increased by 15 %. Note that the increases or decreases are those applicable to a depth of 470 m, given the models are controlled according to the stresses monitored at this depth; e.g. a maximum horizontal stress that is increased by 15 % applies to all depth levels in Case 6. This reduces the deformation zone Set 2 normal stresses thereby inducing high plastic shear, one to three times the elastic shear observed in the Base case. The amount of elastic shear is still approximately the same. Due to its lower shear strength, the Singö deformation zone exhibits plastic shear extending to a depth over one kilometer. The other Set 2 deformation zones shear considerably less than Singö and shear does not extend as deep. Plastic shear of Set 1 is approximately the same as in the Base case. West and east dipping Set 3 deformation zones also exhibit minor plastic shear. A somewhat higher amount of plastic shear is evident in Case 6 because of increased shear stresses.

Glaciation increases plastic shear mainly of Set 2 but also of Set 1 and Set 3. The depth distribution of the σ_1 magnitude and trend is very close to the Base case, for both cases σ_1 is elevated only from a depth of 100 m to 200 m and below 300 m σ_1 is close to the target magnitude or even slightly below. The glacial cycle decreases the σ_1 mean magnitude to a greater depth than in the Base case: a major decrease is evident to a depth of 400 m but it extends to a depth of one kilometer. In the repository volume the median σ_1, σ_2 and trend of σ_1 practically match the target. The major differences are that glaciation decreases the σ_1 magnitude and increases magnitude variation more than in the Base case and rotates the trend a few degrees counterclockwise (Figure 4-35, Figure 4-36), resulting in a σ_1 and σ_3 magnitude that is locally 5 MPa lower in the northeastern part of the deposition tunnel volume (Figure 4-37, Figure 4-39). In Case 6, this is even 5 to 7.5 MPa lower than the target value (Figure 4-38, Figure 4-40).

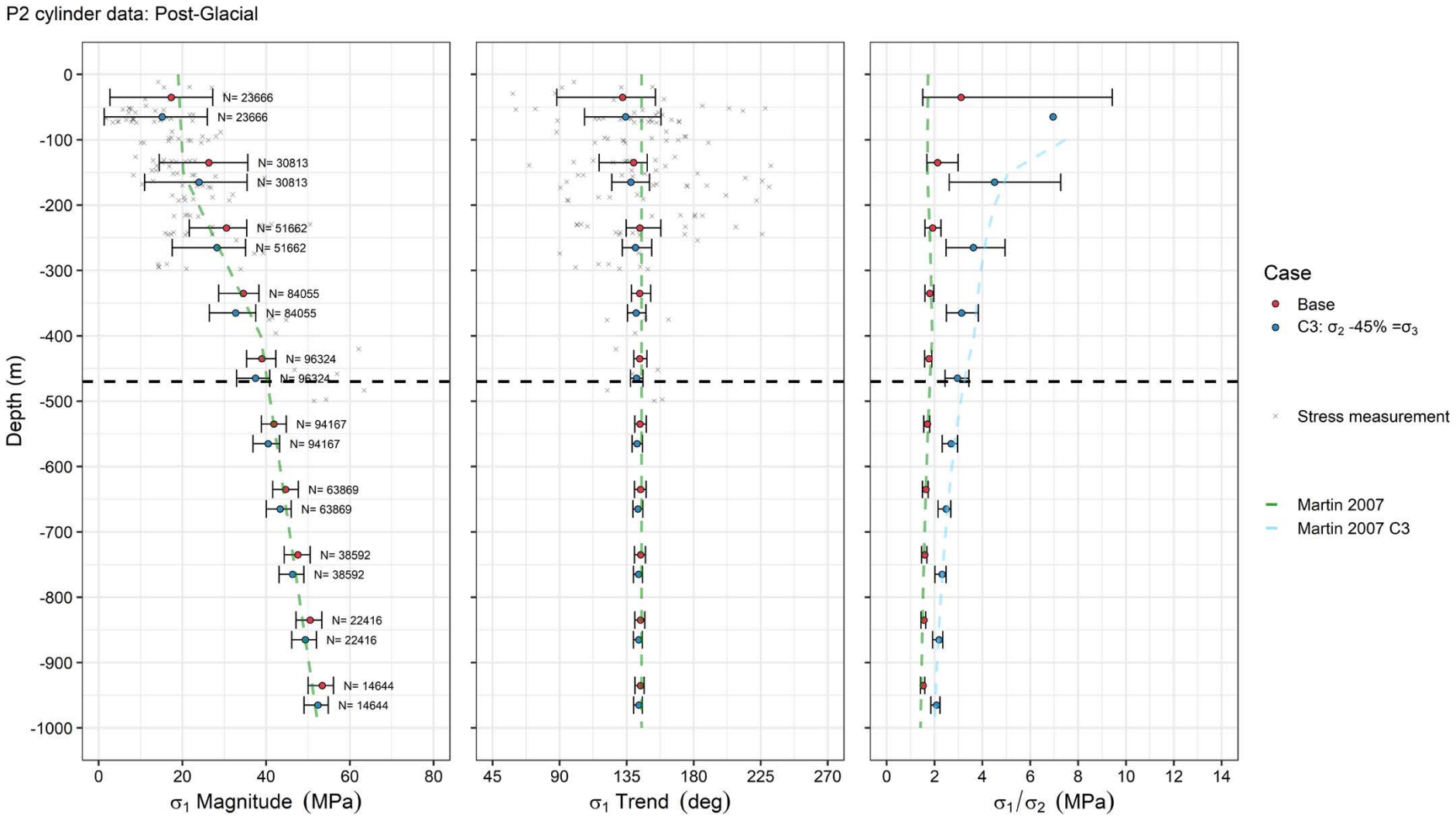

Figure 4-35. *Mean and 95 % variation interval of σ_1 magnitude,trend and the ratio of σ_1 and σ_2 at hundred meter intervals for the Base case and Case 3 (C3) of Phase 2 after glaciation for a cylinder covering the repository footprint (in blue in top right inset). The Martin (2007) interpretation is indicated with a green dashed line and the repository depth with a horizontal dashed black line. The blue dashed line indicates the target ratio of σ_1/σ_2 for Case 3. Field stress measurements indicated with grey markers.*

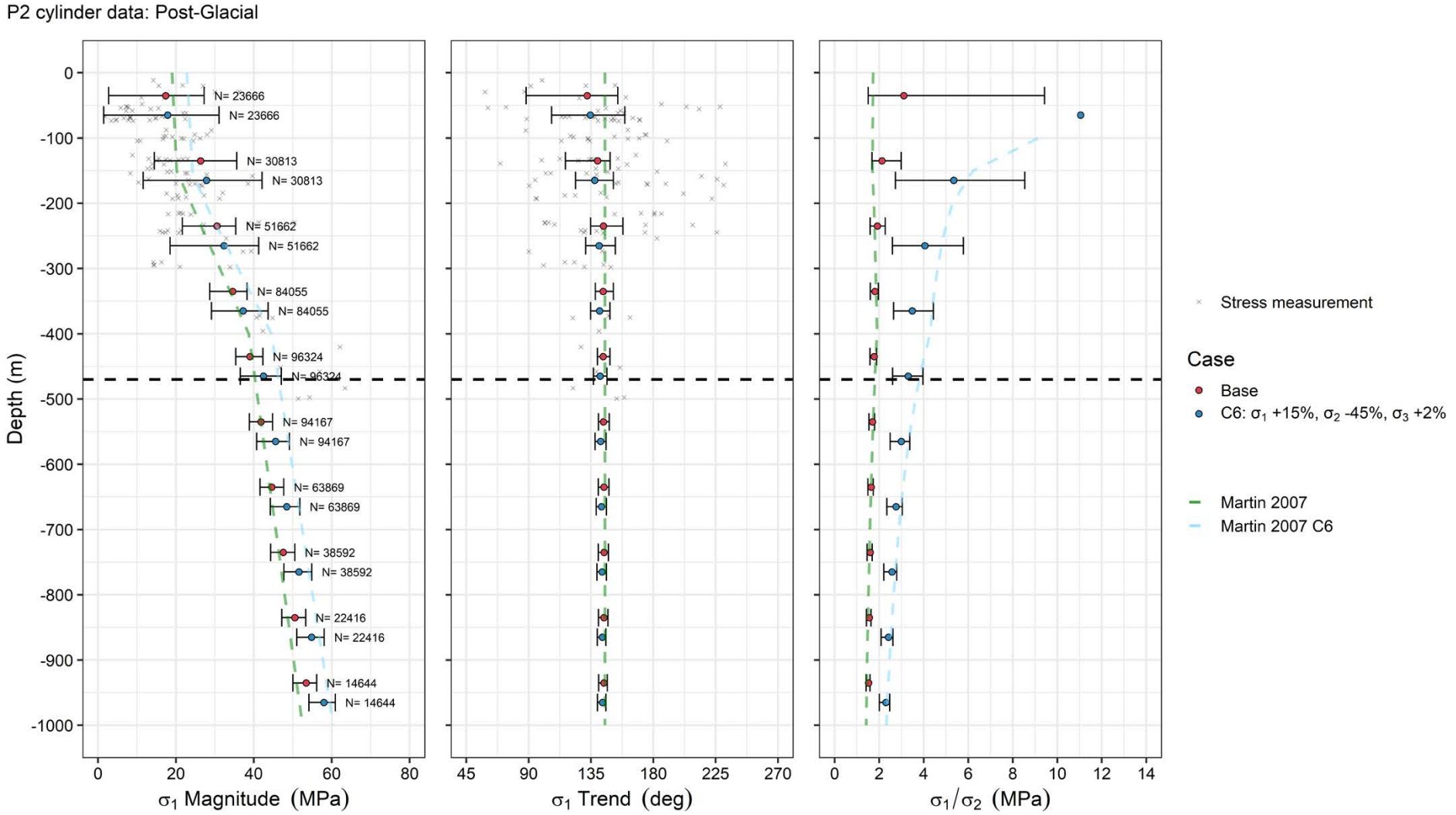

Figure 4-36. *Mean and 95 % variation interval of σ_1 magnitude,trend and the ratio of σ_1 and σ_2 at hundred meter intervals for the Base case and Case 6 (C6) of Phase 2 after glaciation for a cylinder covering the repository footprint (in blue in top right inset). The Martin (2007) interpretation is indicated with a green dashed line and the repository depth with a horizontal dashed black line. The blue dashed line indicates the target ratio of σ_1/σ_2 for Case 6. Field stress measurements indicated with grey markers.*

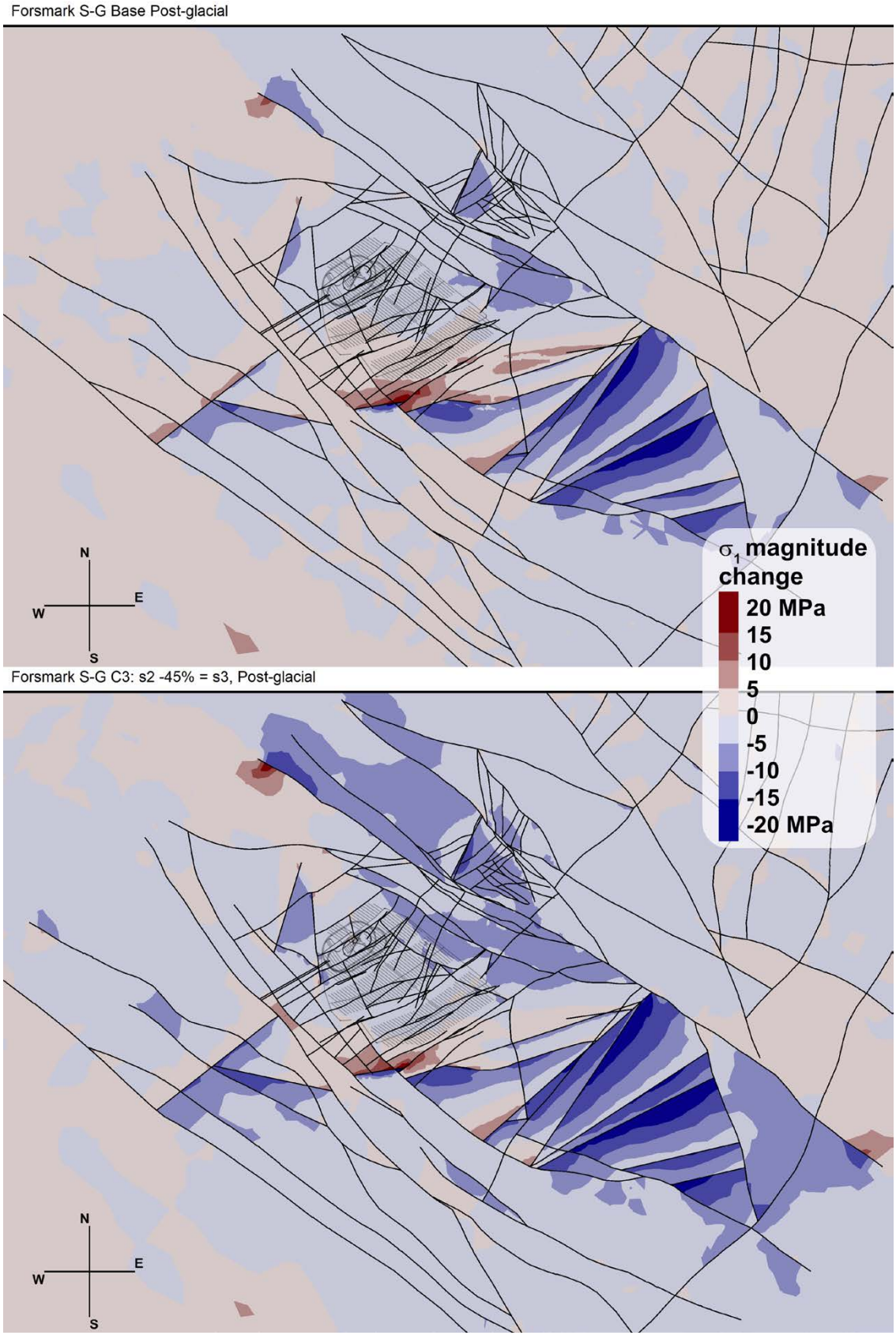

Figure 4-37. *The change in σ_1 magnitude after glaciation for the Base case and Case 3 (C3) of Phase 2 simulations in a horizontal cross-section at repository depth (470 m). The reference value is case-dependent.*

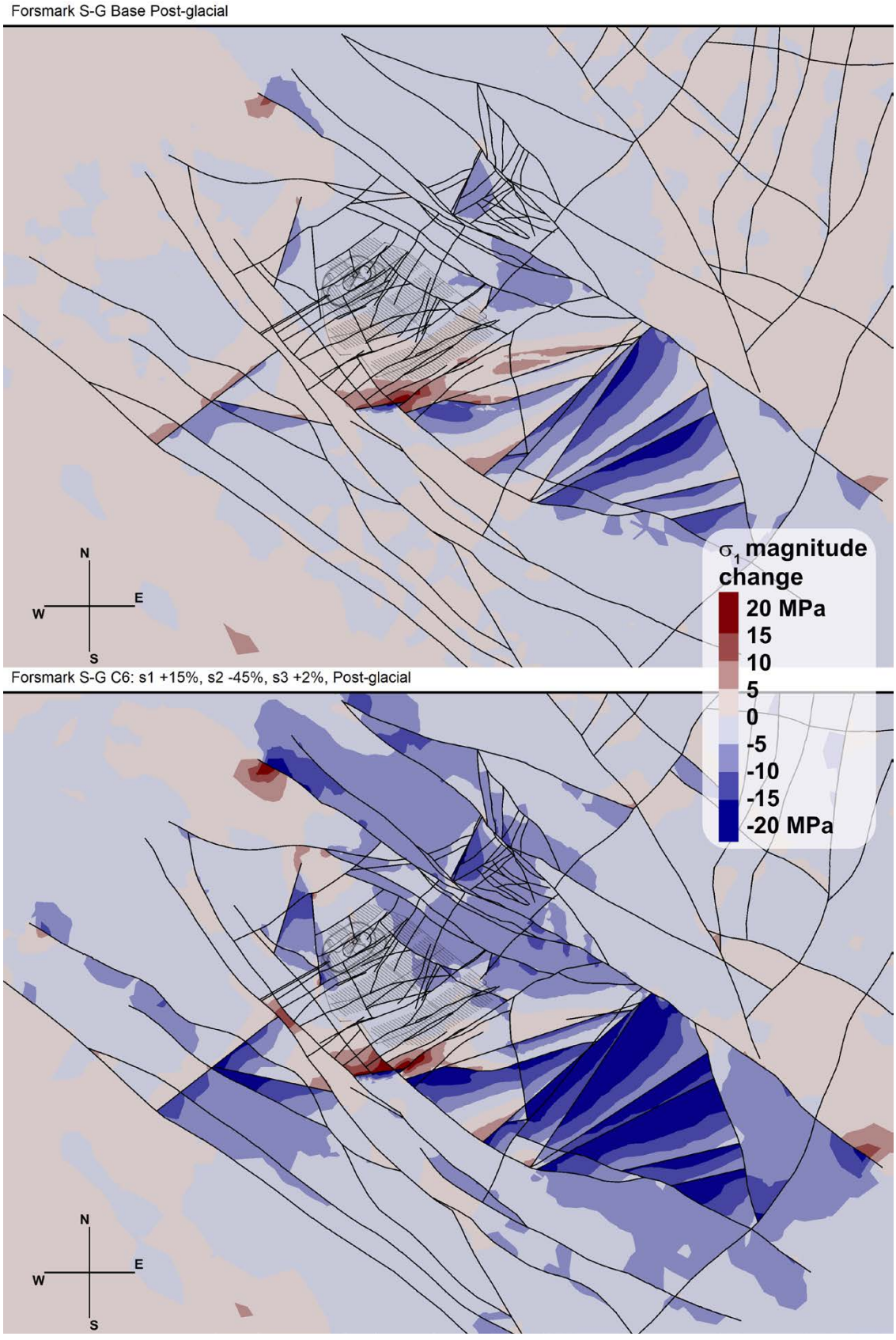

Figure 4-38. *The change in σ_1 magnitude after glaciation for the Base case and Case 6 (C6) of Phase 2 simulations in a horizontal cross-section at repository depth (470 m). The reference value is case-dependent.*

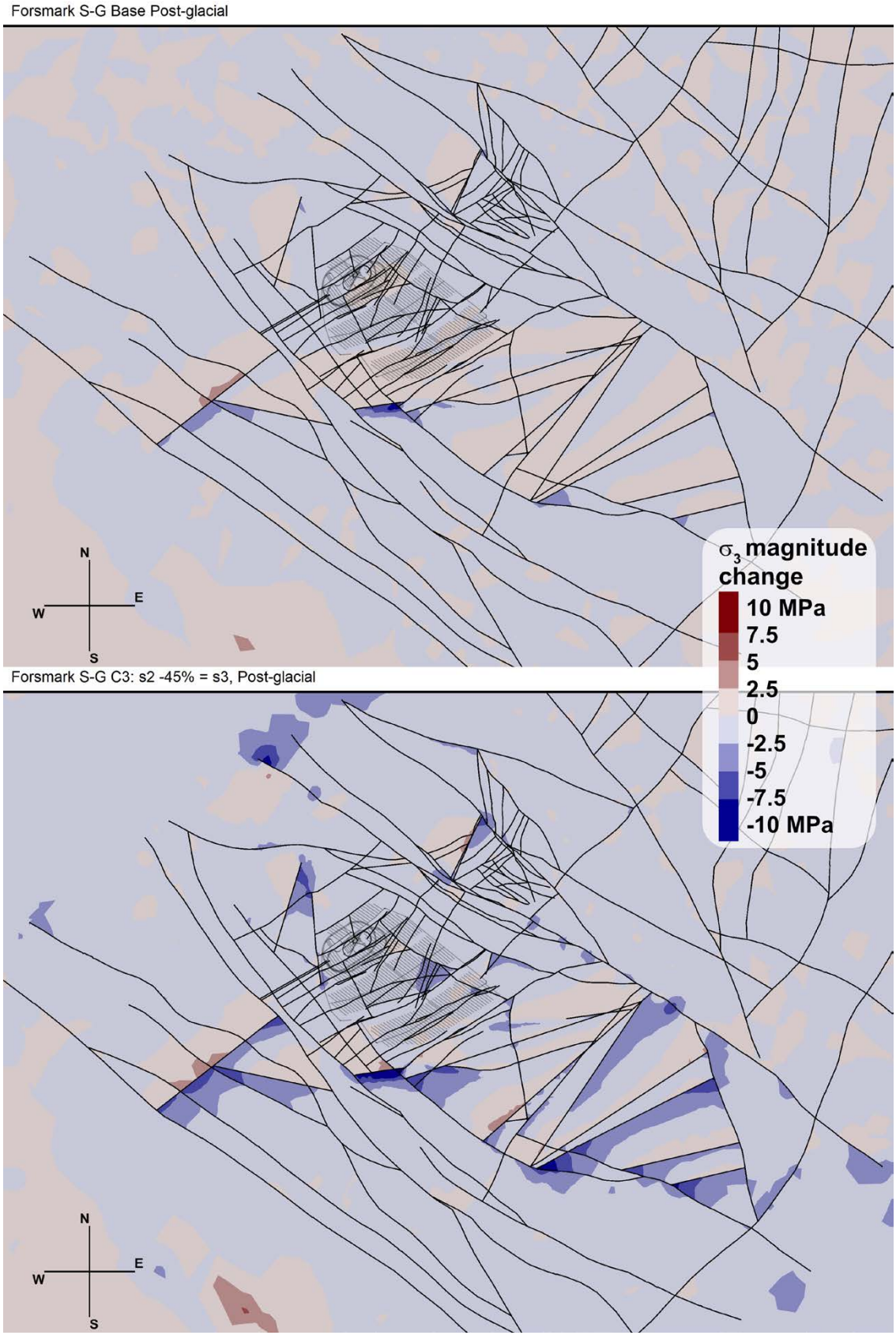

Figure 4-39. *The change in σ_3 magnitude after glaciation for the Base case and Case 3 (C3) of Phase 2 simulations in a horizontal cross-section at repository depth (470 m). The reference value is case-dependent.*

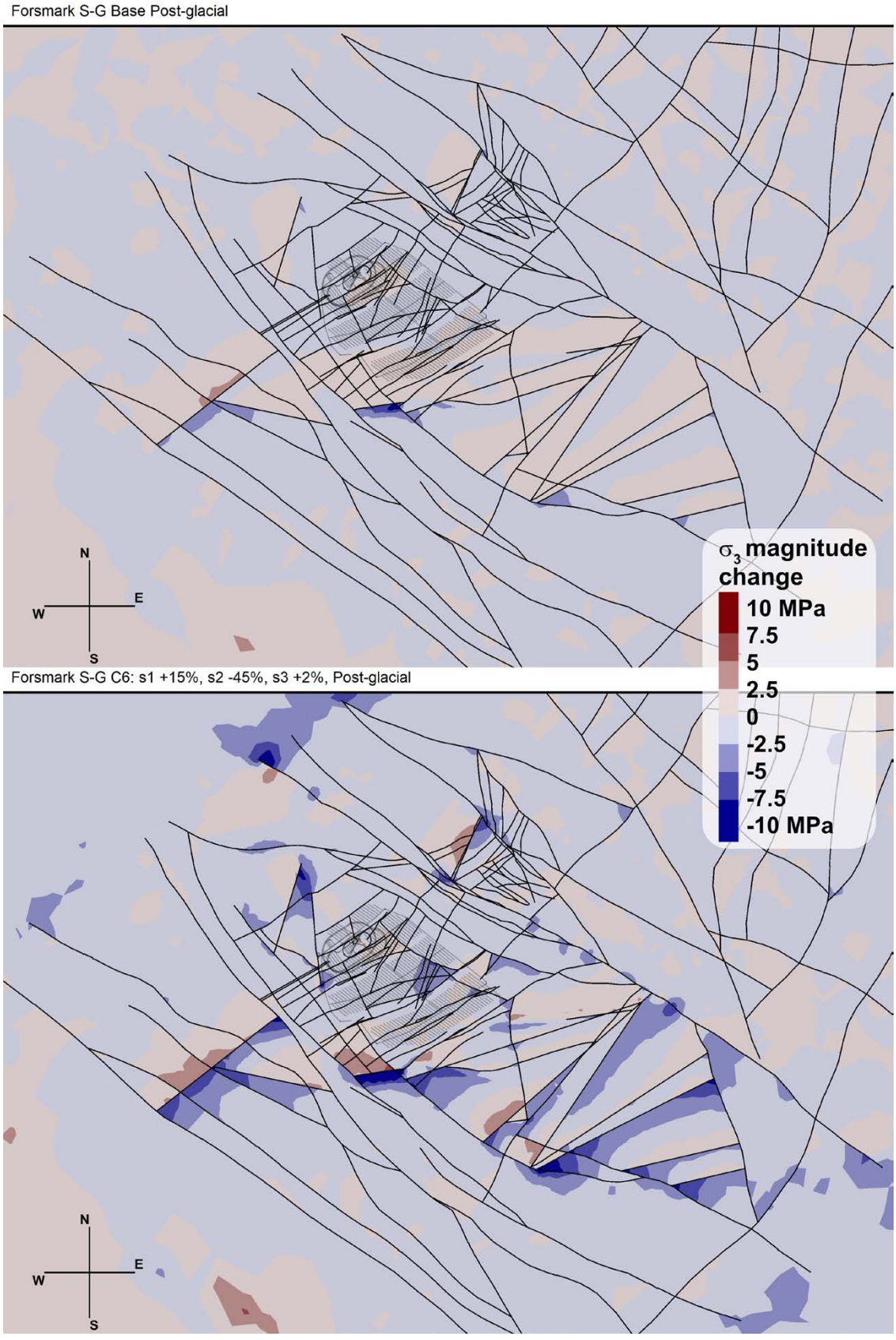

Figure 4-40. *The change in σ_3 magnitude after glaciation for the Base case and Case 6 (C6) of Phase 2 simulations in a horizontal cross-section at repository depth (470 m). The reference value is case-dependent.*

In Case 6, σ_2 is locally increased in several locations, at a maximum increase of 5 MPa. The maximum drop in the magnitude of σ_1 and σ_3 occurs in the same area but does not overlap with an increased σ_2 magnitude. The trend variation of σ_1 is in a range equal to that observed in the Base case. When comparing simulation results to stresses measured in the field, the major difference to the Base case is that almost all stresses measured in the field are above the upper 95 % confidence limit of σ_2 (Figure 4-41, Figure 4-42). After the glaciation cycle, the drop in the mean magnitude of σ_1 extends to a greater depth, in Case 3 to 600 m and in Case 6 to 800 m, with the variation of the simulated σ_1 increasing closer to the measured variation. In both cases the variation of the trend of σ_1 is narrower than in the Base case.

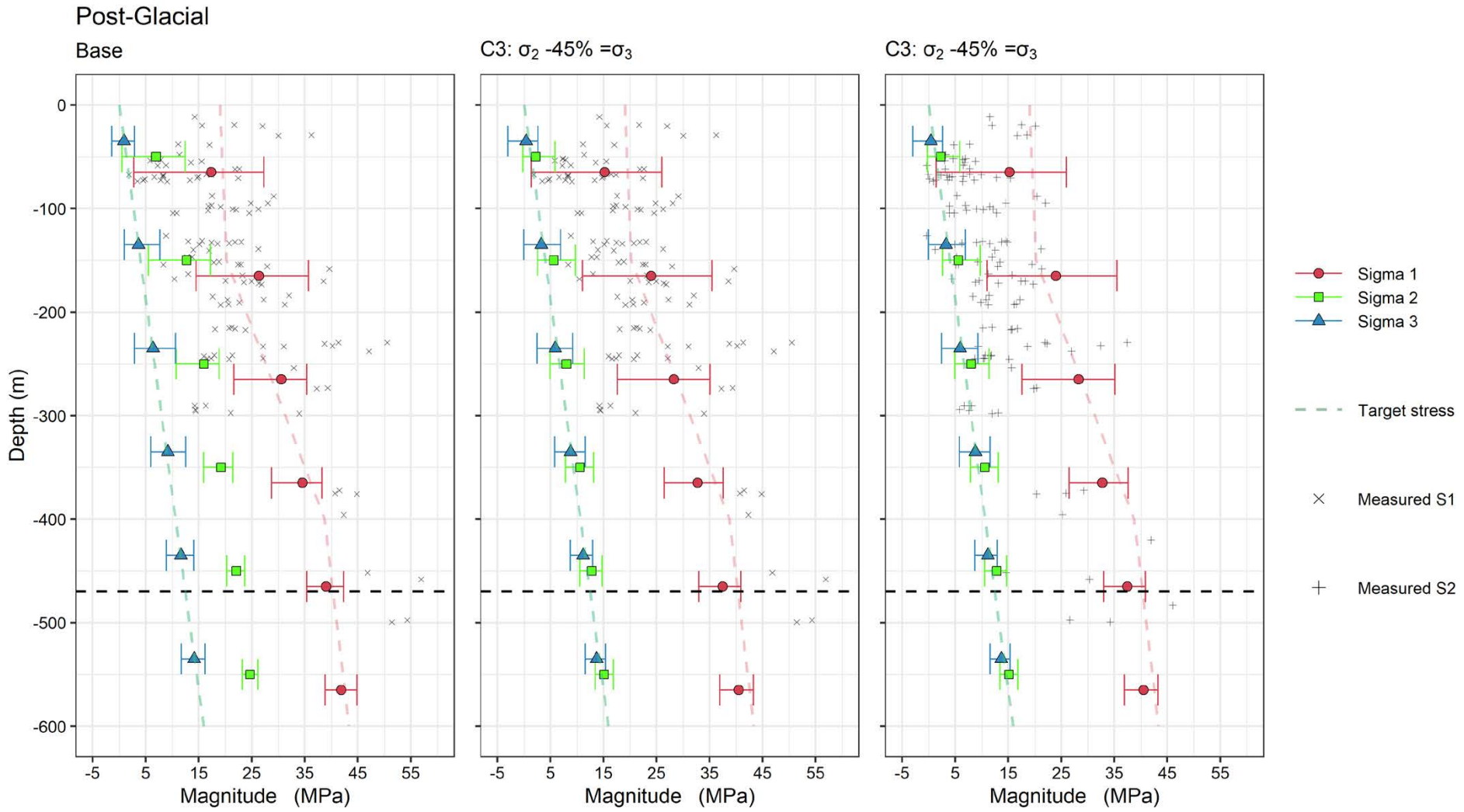

Figure 4-41. *Mean and 95 % variation interval of the principal stress magnitudes versus measured stresses at hundred-meter intervals for the Base case and Case 3 (C3) of Phase 2 simulations after glaciation from a cylinder covering the repository. The Martin (2007) interpretation is indicated with a green dashed line and the repository depth with a horizontal dashed black line. Field stress measurements indicated with grey cross or plus symbols.*

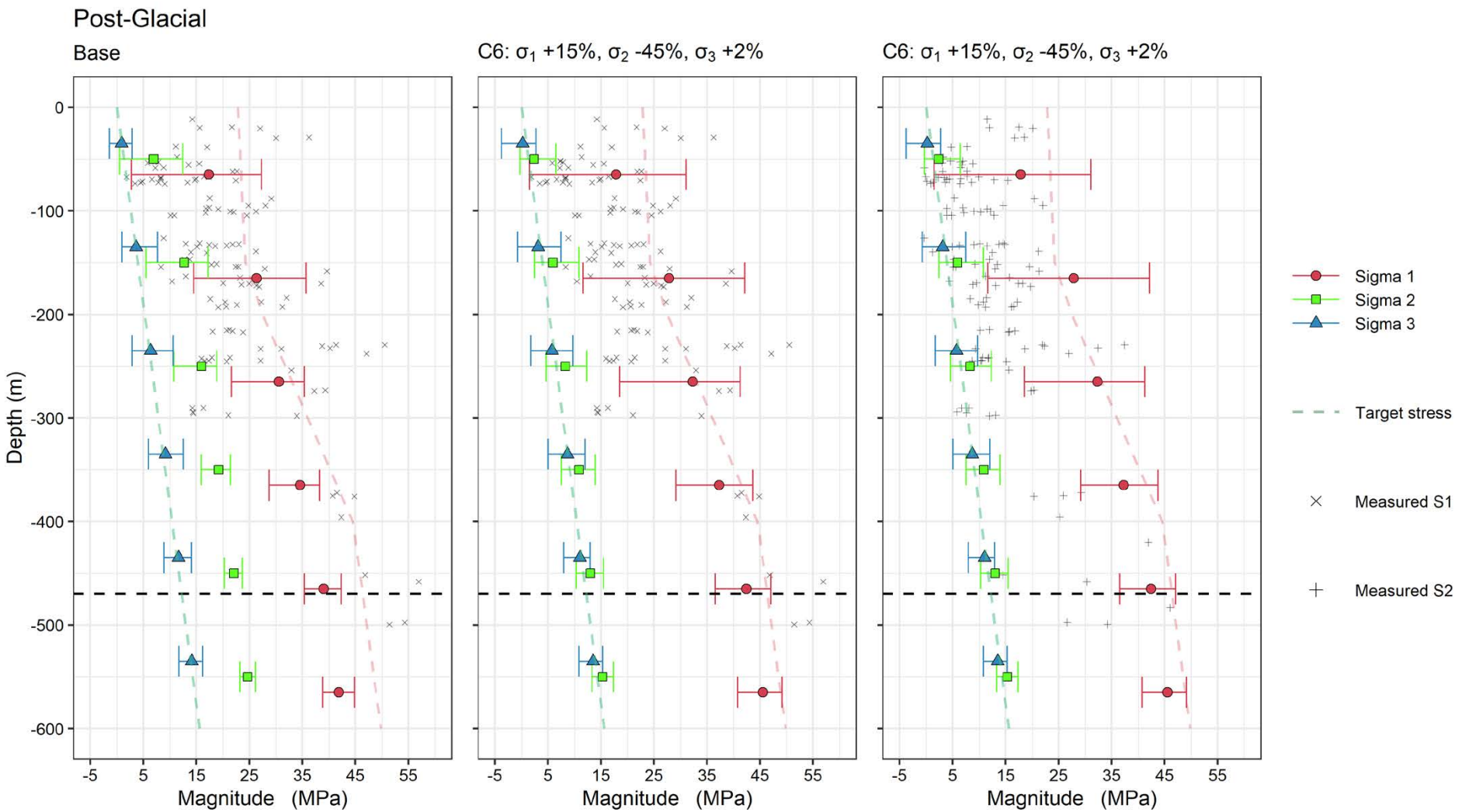

Figure 4-42. *Mean and 95 % variation interval of the principal stress magnitudes versus measured stresses at hundred meter intervals for the Base case and Case 6 (C6) of Phase 2 simulations after glaciation from a cylinder covering the repository. The Martin (2007) interpretation is indicated with a green dashed line and the repository depth with a horizontal dashed black line. Field stress measurements indicated with grey cross or plus symbols.*

Cases C4 and C5

In Cases 4 and 5, the maximum horizontal stress is elevated by 15 % and the minor horizontal stress either increased (Case 4) or decreased (Case 5) by 20 %. In both cases deformation zone Set 1 exhibits more plastic shear because of an increased σ_1 i.e., an increased shear stress. σ_2 is more or less oriented along the Set 1 deformation zones and does not affect deformation zone shear. The elastic shear of deformation zone Set 2 is increased only in Case 5 because of a decreased normal stress, with plastic shear also occurring. A few deformation zones of Set 3 that dip to the west also show minor plastic shear. The glaciation cycle increases deformation zone Set 1 and Set 2 shear and initiates Set 3 shear. For both cases the depth distribution of the σ_1 magnitude and trend is very close to the Base case. In Case 5 the σ_1 magnitude is below the target above a depth of 100 m and it is above the target only between a depth of 100 m to 200 m. At greater depths the σ_1 magnitude matches the target magnitude. The glaciation cycle increases the σ_1 magnitude and trend variation mainly down to a depth of 400 m, but it is apparent to a depth of 1 000 m. In the repository volume the median σ_1, σ_2 and trend of σ_1 are an almost exact match to the target values. Glaciation widens the variation of the magnitudes and orientation slightly more than in the Base case. The main difference to the Base case with regards to Case 4 is an increased variation in the σ_3 magnitude reaching up to ± 7.5 MPa, with the corresponding variation in Case 5 reaching ± 5 MPa. A comparison of the simulation results to the stresses measured in the field indicates that the main difference to the Base case is that a considerable number of measurements are below the lower 95 % confidence limits of σ_1, but at the 500 m level not all the measurements are above the upper 95 % confidence limits of σ_1. In Case 5 a high number of measurements are above upper 95 % confidence limits of σ_2. The effect of the glaciation cycle is similar to the effects apparent in the Base case but the variation of the magnitude of σ_1 and σ_2 is increased.

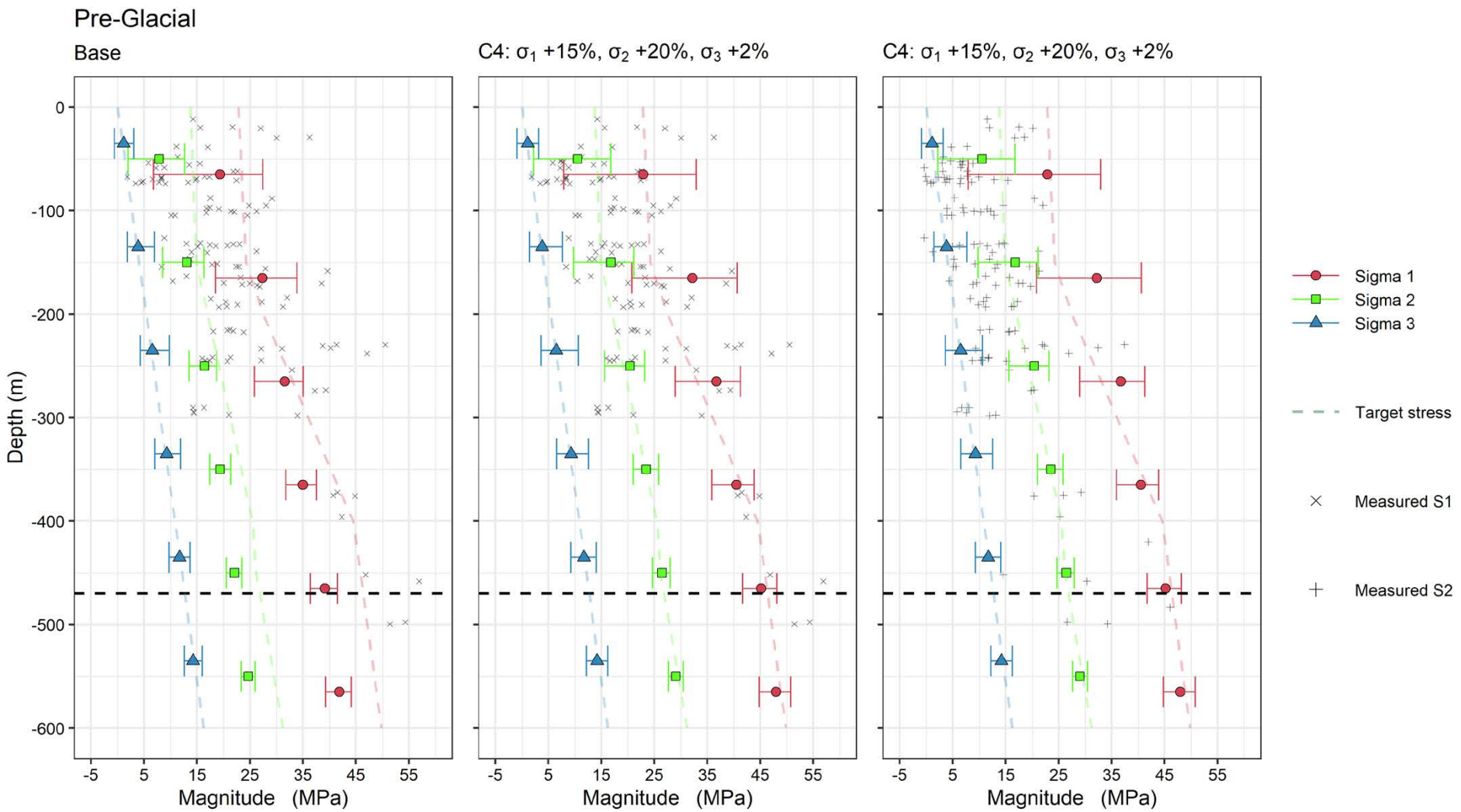

Figure 4-43. *Mean and 95 % variation interval of the principal stress magnitudes versus measured stresses at hundred meter intervals for the Base case and Case 4 (C4) of Phase 2 simulations before glaciation from a cylinder covering the repository. The Martin (2007) interpretation is indicated with a green dashed line and the repository depth with a horizontal dashed black line. Field stress measurements indicated with grey cross or plus symbols.*

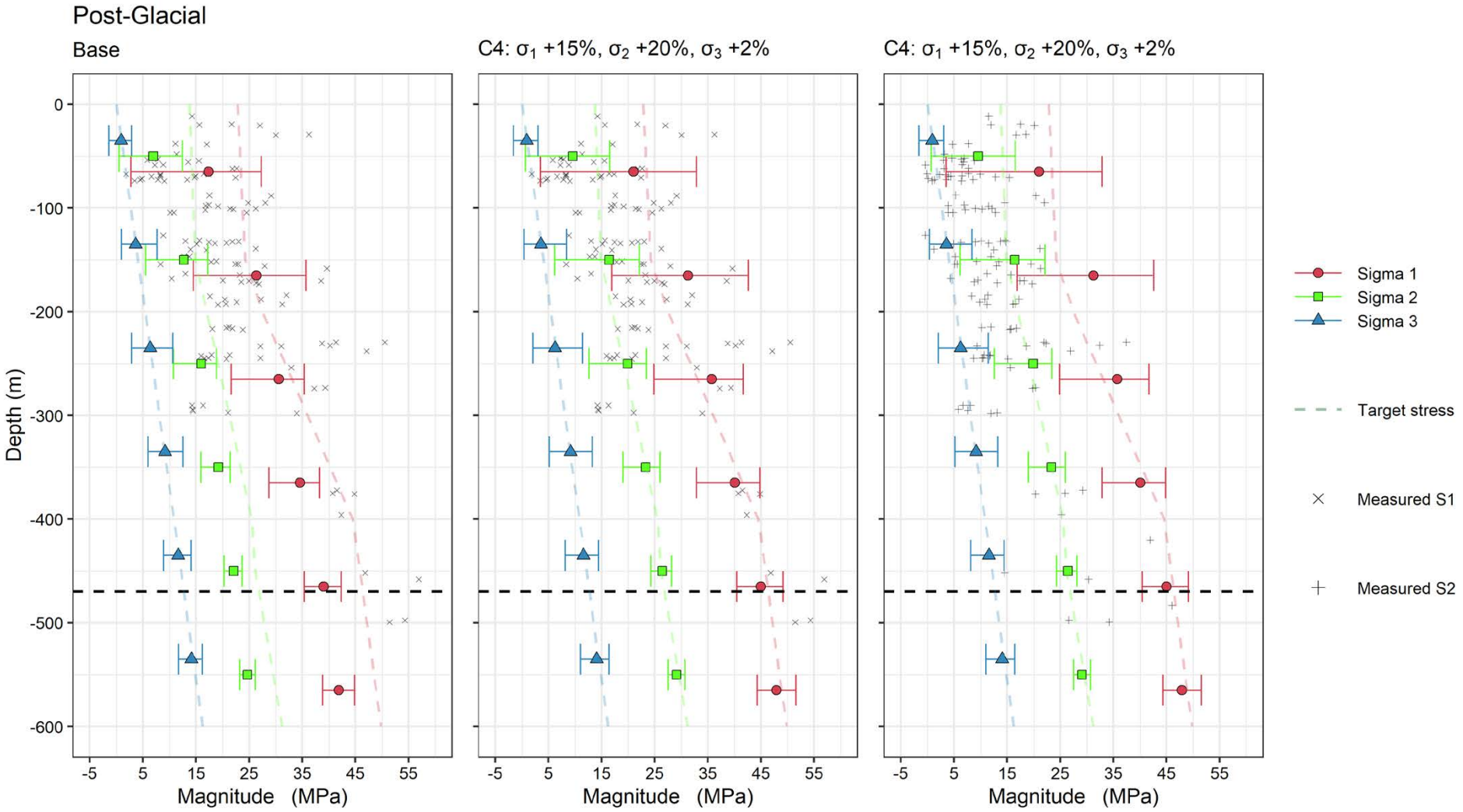

Figure 4-44. *Mean and 95 % variation interval of the principal stress magnitudes versus measured stresses at hundred meter intervals for the Base case and Case 4 (C4) of Phase 2 simulations after glaciation from a cylinder covering the repository. The Martin (2007) interpretation is indicated with a green dashed line and the repository depth with a horizontal dashed black line. Field stress measurements indicated with grey cross or plus symbols.*

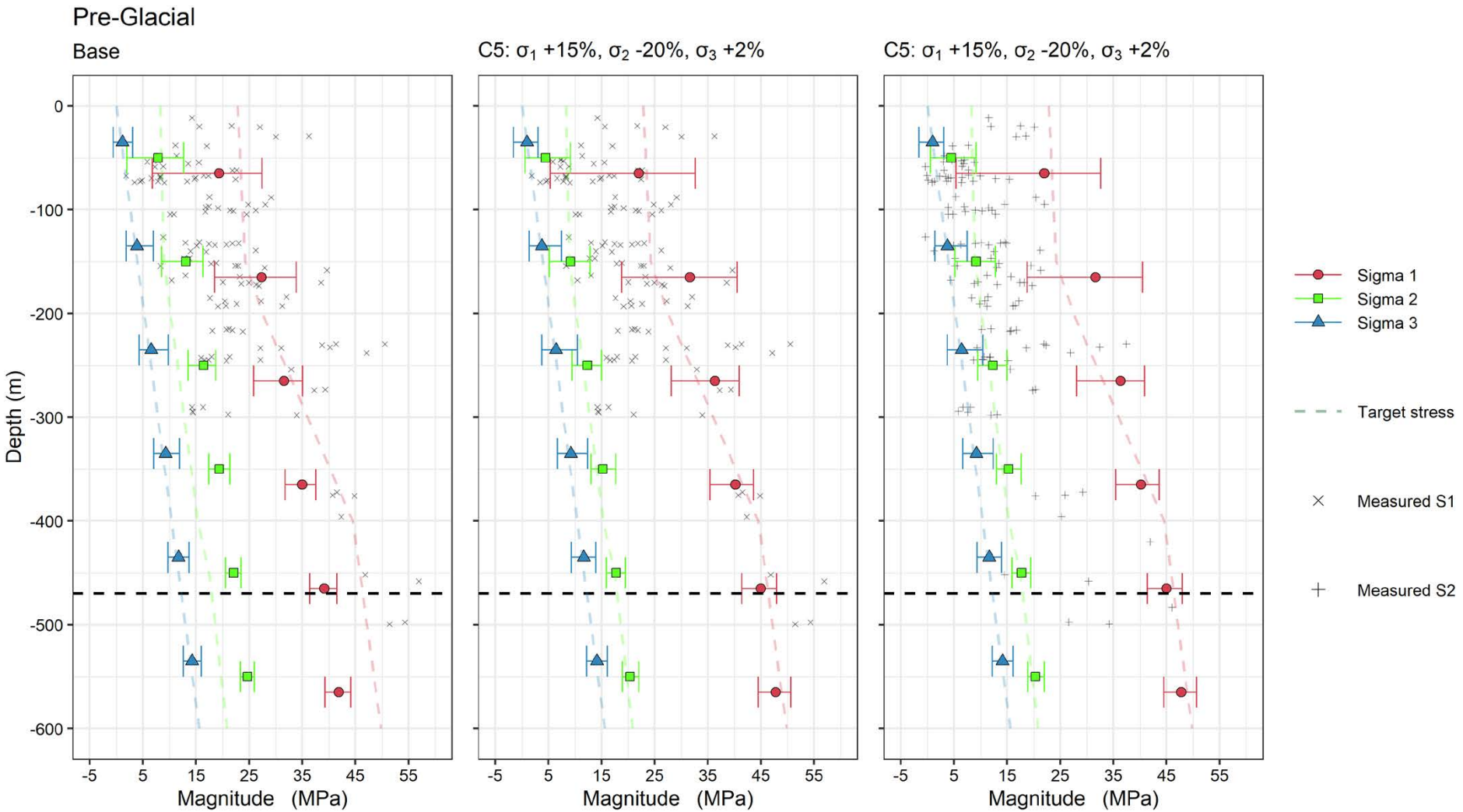

Figure 4-45. *Mean and 95 % variation interval of the principal stress magnitudes versus measured stresses at hundred meter intervals for the Base case and Case 5 (C5) of Phase 2 simulations before glaciation from a cylinder covering the repository. The Martin (2007) interpretation is indicated with a green dashed line and the repository depth with a horizontal dashed black line. Field stress measurements indicated with grey cross or plus symbols.*

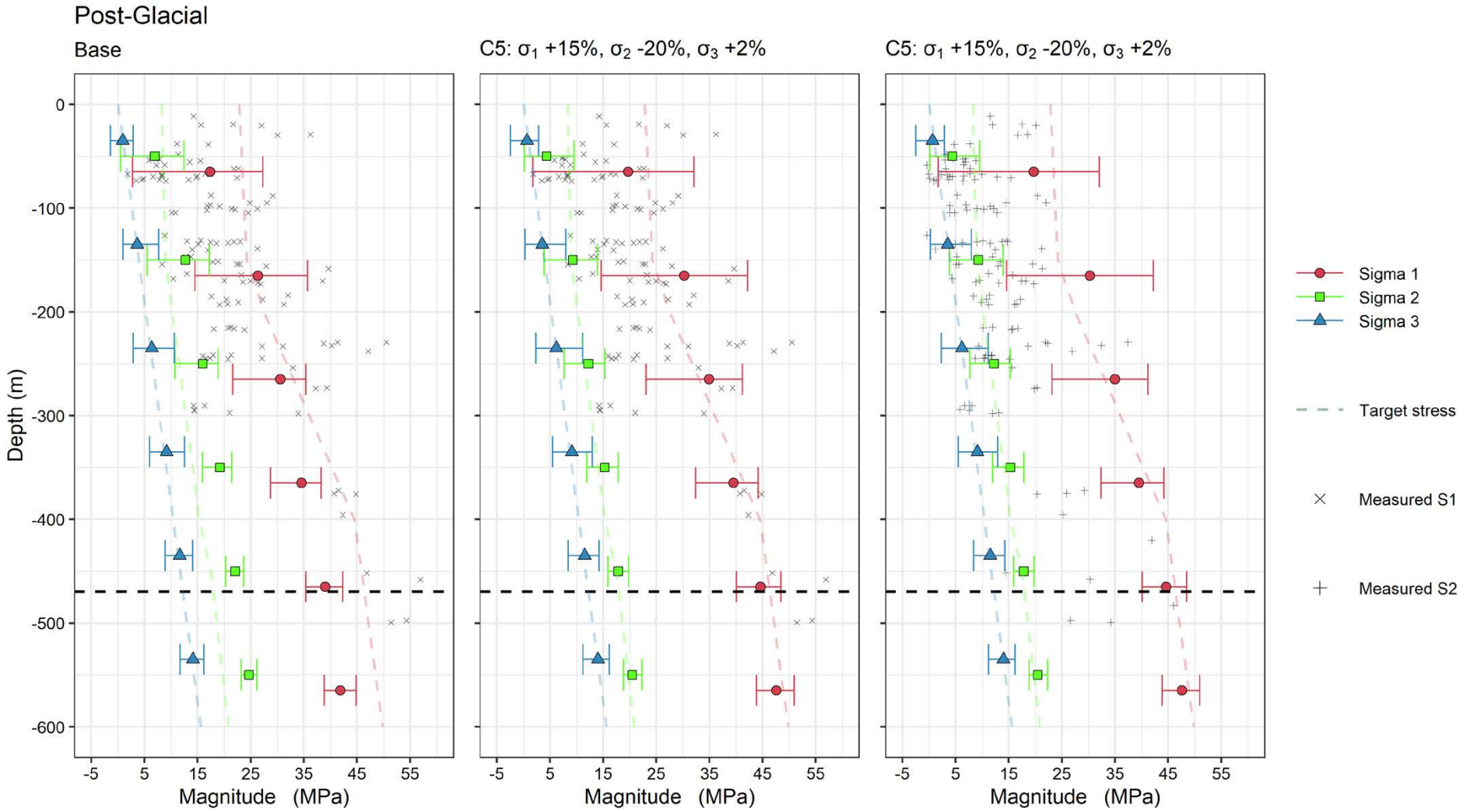

Figure 4-46. *Mean and 95 % variation interval of the principal stress magnitudes versus measured stresses at hundred meter intervals for the Base case and Case 5 (C5) of Phase 2 simulations after glaciation from a cylinder covering the repository. The Martin (2007) interpretation is indicated with a green dashed line and the repository depth with a horizontal dashed black line. Field stress measurements indicated with grey cross or plus symbols.*

5 Discussion, conclusions and recommendations

Phase 1 demonstrated a very similar stress state response between 3DEC and FLAC3D, although the deformation zone shear displacements differ when the glacial load is simulated. The difference can most likely be attributed to the difference in contact logic between the two codes but is acceptable considering the overall response of the models, particularly given deformation zone slip is not the focus in the current study. Given the significantly reduced computation time of FLAC3D, it was selected for use in Phase 2.

All the target stress states were achieved at the repository depth level (470 m) in Phase 2 using the applied boundary thrust approach together with the defined rock mass elastic parameters and deformation zone shear strength values. The depth-dependent principal stress magnitude gradients and orientations defined in the Martin (2007) stress model were also matched fairly well. Therefore, none of the studied cases can be deemed physically implausible.

Above a depth of 100 m all the simulation cases resulted in a mean σ_1 magnitude below the Martin (2007) stress model but above the mean of values obtained from field stress measurements. Furthermore, the simulated σ_1 mean magnitudes from a depth of 100 m to 200 m are above the Martin (2007) interpretation and values measured in the field. As a result, it can be concluded that if it is assumed that stresses measured in the field above the 300 m level are more or less reasonable then either *a)* shallow fractures have lower shear and normal stiffnesses and/or shear strength and/or *b)* deformation zones have a lower shear strength and normal stiffness than assumed. It is important to note that a constant normal stiffness has been assumed for the deformation zones and a constant modulus and Poisson's ratio for the rock mass, with the latter based on a constant fracture normal stiffness.

Alternatively, a rather high and almost constant σ_1 magnitude above a depth of 150 m according to Martin (2007) is unrealistic. The simulation results suggest that the σ_1 gradient would be more linear or lower near the surface with a gradual increase with depth up to 400 m. None of the simulation cases resulted in the highest measured σ_1 magnitudes, with the closest match obtained in Case 4 which exhibited reasonable σ_1 and σ_2 magnitudes and variation.

Deformation zone shear rotates the trend of σ_1 counterclockwise up to a depth of 200 m. The maximum rotation varies between 10° to 15° except in Case 2 where no rotation is evident. The measured rotation is over 50° from the surface to a depth of 75 m (Martin 2007, Figure 6-13). It is uncertain if increased rotation in the simulated trend of σ_1 could occur if a lower deformation zone shear strength was applied near the surface (the unpublished results from the latest Olkiluoto stress state simulations indicated that it could promote rotation). The trend of σ_1 matches the applied thrust orientation in all the simulation cases. The simulations of Cases 1 and 2 do not support a rotated thrust orientation as the mean trend of σ_1 as based on field measurements below a depth of 75 m is 145°.

Cases 3, 5 and 6 resulted in σ_2 mean magnitudes clearly below the field stress measurement results and can be considered less likely scenarios. Note that in Cases 3 and 6 the target value for the minimum horizontal stress was lower than the proposed variation limits in Martin (2007) and even below hydraulic fracturing results.

The minor stress component is vertical or subvertical in the simulations, deviating generally about ten degrees from vertical but in Case 5 the variation is up to twenty degrees. Cases 3 and 6 are exceptions as the vertical stress is equal to the minor horizontal stress and therefore σ_2 and σ_3 can easily rotate in a plane perpendicular to σ_1, but the variation in the orientation of σ_2 and σ_3 does not have any significant impact. Furthermore, Cases 3 and 6 were already considered less likely scenarios.

In the repository volume, a volume covering the excavation plan of the preliminary facilities, the variation in the magnitude of σ_1 and σ_2 was generally less than ± 10 %, but the relative variation of the minor component was higher, reaching at a maximum ± 20 %. In some cases the local variation can be even twice as much, but mainly this applies to the minor component. The trend of the major compression was always found to be within a range of ± 10°.

The Martin (2007) mean stress model always results in the highest shear stress occurring on the gently or moderately dipping Set 1 deformation zones (Base case and Cases 1 and 2). If the minor principal stress is reduced to the lower bound, as performed in Cases 3 and 6, the NW–SE trending Set 2 deformation zones, including the Singö deformation zone, shear most while Set 1 deformation zone shear is equivalent to Set 1 shear in the Base case. A reduction in the magnitude of σ_2 also activates most of the N–S trending Set 3 deformation zones. Although the slip/shear displacement of different deformation zone sets can be connected to the studied in situ stress magnitudes and ratios, it cannot be used to identify the most likely current in situ stress field. However, simulated deformation zone slip data could possibly be valuable with regards to the estimation of future slip during a glaciation period once the facilities are excavated and the in situ stress field has been confirmed.

A considerable number of field stress measurements have σ_1 magnitudes over the upper 95 % confidence limit of simulation results. Most of those are from boreholes KFK001, KFM001B and KFM07C (Appendix 22). When compared to the Base case simulation results, the magnitude correlation was poor with the measured results being on average 5–13 MPa higher. Overall, the amount of field stress measurements is low and additional data would be valuable for potential future studies.

To summarise the above, Base case and Case 4 yielded the best general match with the field stress measurement results. In Case 4 the σ_1 magnitude is elevated by 15 % and σ_2 by 20 % relative to the Base case (Table 3-7). It should, however, be noted that unfortunately the reliability of the field stress measurements is generally not very high. The simulated principal stresses of these two cases are in rather good agreement with the Martin (2007) stress model. The biggest difference is evident above a depth of 200 m where Martin (2007) proposes a rather constant σ_1 magnitude, whereas simulations indicate a steeper gradient. It should be noted that the major principal stress magnitude, according to measurements in Forsmark at repository depth, is high compared to the values generally measured in Sweden at this depth. For example, similarly high σ_1 magnitudes have been measured closer to a depth of one kilometer in the Garpenberg and Kiruna mine in Sweden and in the Pyhäsalmi, Kemi and Kittilä mine in Finland.

Before further simulations are performed it is recommended the elastic properties of the rock mass and the deformation zones are re-evaluated, especially at depths above 200 m. A stress dependent rock mass modulus or a normal stress dependent DZ normal stiffness would be more realistic. The shallow parts of the deformation zones have undergone more shear during past thrust phases and the glaciation period and could potentially have a lower shear strength. Moreover, there could be value in investigating if the seismic monitoring results could be linked with the current simulated mechanical state of the three major deformation zone sets.

References

SKB's (Svensk Kärnbränslehantering AB) publications can be found at www.skb.com/publications.

Glamheden R, Fredriksson A, Röshoff K, Karlsson J, Hakami H, Christansson R, 2007. Rock Mechanics Forsmark. Site descriptive modelling, Forsmark Stage 2.2. SKB R-07-31, Svensk Kärnbränslehantering AB.

Glamheden R, Lanaro F, Karlsson J, Lindberg U, Bygg B, Wrafter J, Hakami H, Johansson M, 2008. Rock Mechanics Forsmark. Modelling stage 2.3. Complementary analysis and verification of the rock mechanics model. SKB R-08-06, Svensk Kärnbränslehantering AB.

Hakala M, Ström J, Valli J, Juvani J, 2019. Structural control on stress variability at Forsmark. SKB R-19-23, Svensk Kärnbränslehantering AB.

Hakami H, 2006. Numerical studies on spatial variation of the in situ stress field at Forsmark – a further step. Site descriptive modelling Forsmark – stage 2.1. SKB R-06-124, Svensk Kärnbränslehantering AB.

Hakami H, Min K, 2009. Modelling of the state of stress. Preliminary site description Laxemar subarea – version 1.2. SKB R-06-17, Svensk Kärnbränslehantering AB.

Heidbach O, Rajabi M, Cui X, Fuchs K, Müller B, Reinecker J, Reiter K, Tingay M, Friedemann W, Xie F, Ziegler M O, Zoback M-L, Zoback M, 2018. The World Stress Map database release 2016: Crustal stress pattern across scales. Tectonophysics, 744, 484–498. https://doi.org/10.1016/j.tecto.2018.07.007

Hultgren P, Petersson J, 2022. DMS Baseline Forsmark v1 Surface.dgn, version 1.0. Model id:1968355. Forsmark: Svensk Kärnbränslehantering AB.

Hökmark H, Lönnqvist M, Fälth B, 2010. THM-issues in repository rock. Thermal, mechanical, thermo-mechanical and hydro-mechanical evolution of the rock at the Forsmark and Laxemar sites. SKB TR-10-23, Svensk Kärnbränslehantering AB.

Itasca, 2022a. FLAC3D Version 9.0: Continuum Modeling for Geomechanics. [Online] Available at: https://www.itascacg.com/software/flac3d [28 August 2023].

Itasca, 2022b. 3DEC Version 7.0: Distinct Element Modeling of Jointed and Blocky Material in 3D. Available at: https://www.itascacg.com/software/3dec [31 October 2022].

Itasca, 2022c. FLAC3D: Creation of Interface Geometry. Available at: http://docs.itascacg.com/flac3d700/flac3d/docproject/source/theory/interfaces/creationofgeometry.html?highlight=interface [31 October 2022].

Kaisko O, Mattila J, Valli J, Hakala M, 2023. Stress-geology interaction simulation of the Olkiluoto site. Working Report 2023-11, Posiva Oy, Finland.

Martin D, 2007. Quantifying in situ stress magnitudes and orientations for Forsmark. Forsmark stage 2.2. SKB R-07-26. Stockholm, Svensk Kärnbränslehantering AB.

SKB, 2008. Site description of Forsmark at completion of the site investigation phase. SDM-Site Forsmark. SKB TR-08-05, Svensk Kärnbränslehantering AB.

Stephansson O, Ljunggren C, Jing L, 1991. Stress measurements and tectonic implications for Fennoscandia. Tectonophysics, 189:1-4, 317–322.

Stephens M B, Simeonov A, 2015. Description of DZ model version 2.3, Forsmark. SKB R-14-28, Svensk Kärnbränslehantering AB.

Tonon F, Amadei B, Pan E, 2001. Bayesian estimation of rock mass boundary conditions with applications to the AECL underground research laboratory. International Journal of Rock Mechanics and Mining Sciences 38, 995–1027.

Tonon F, Amadei B, 2003. Stresses in anisotropic rock masses: an engineering perspective building on geological knowledge. International Journal of Rock Mechanics and Mining Sciences 40, 1099–1120.

Valli J, Hakala M, Kuula H, 2011. Modelling of the in situ stress state at the Olkiluoto site, western Finland. Working Report 2011-34, Posiva, Finland.

Valli J, Hakala M, Siren T, 2016. Stress-Geology Interaction Modelling at Olkiluoto. In Proceedings of the 7th International Symposium on In Situ Rock Stress International Society for Rock Mechanics, Tampere 10–12 May 2016. Tampere: ISRM, 352–361.

Appendix 1

Phase 1 deformation zone shear

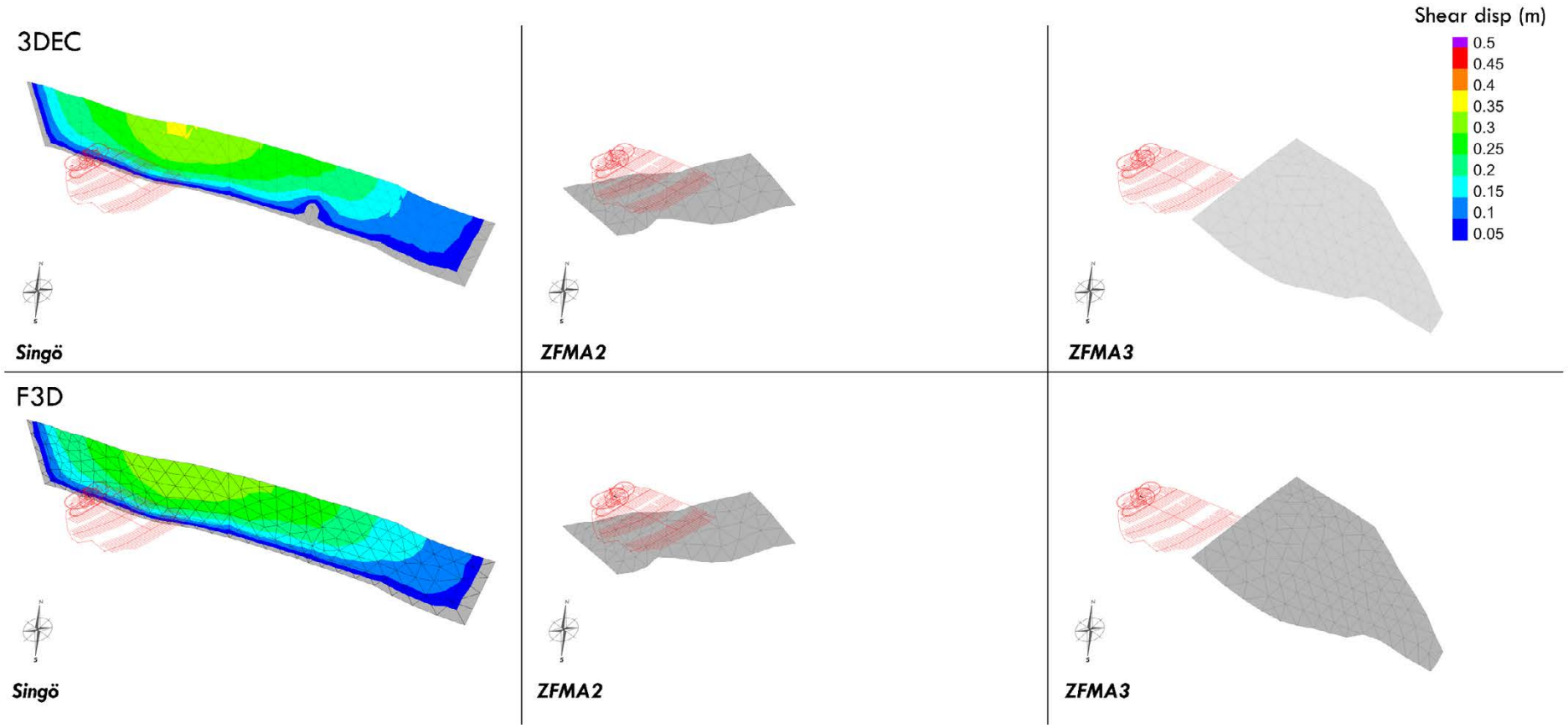

Figure A1-1. *Deformation zone shear contours for three selected deformation zones after the glacial maximum in fully elastic Phase 1 simulations.*

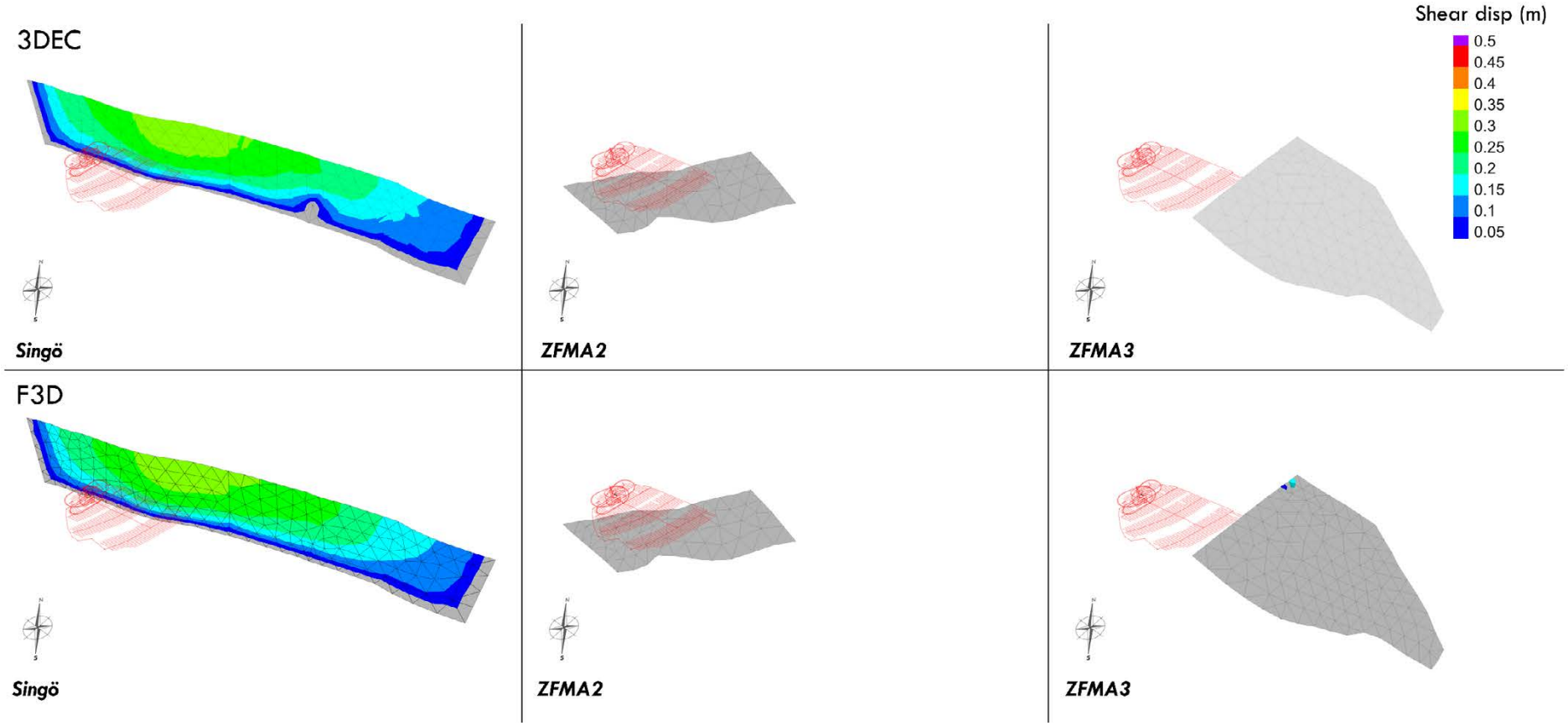

Figure A1-2. *Deformation zone shear contours for three selected deformation zones after the edge passing stage in fully elastic Phase 1 simulations.*

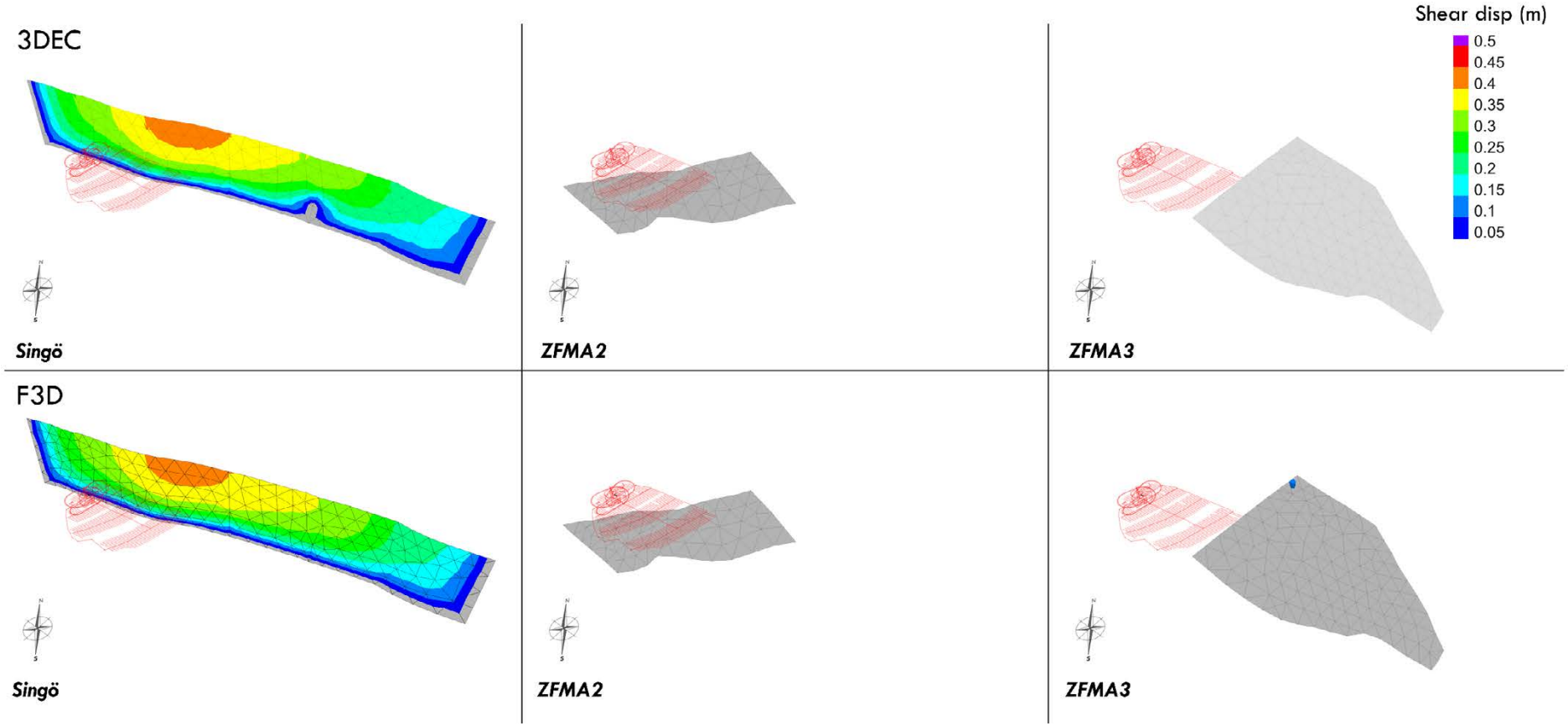

Figure A1-3. *Deformation zone shear contours for three selected deformation zones after glaciation in fully elastic Phase 1 simulations.*

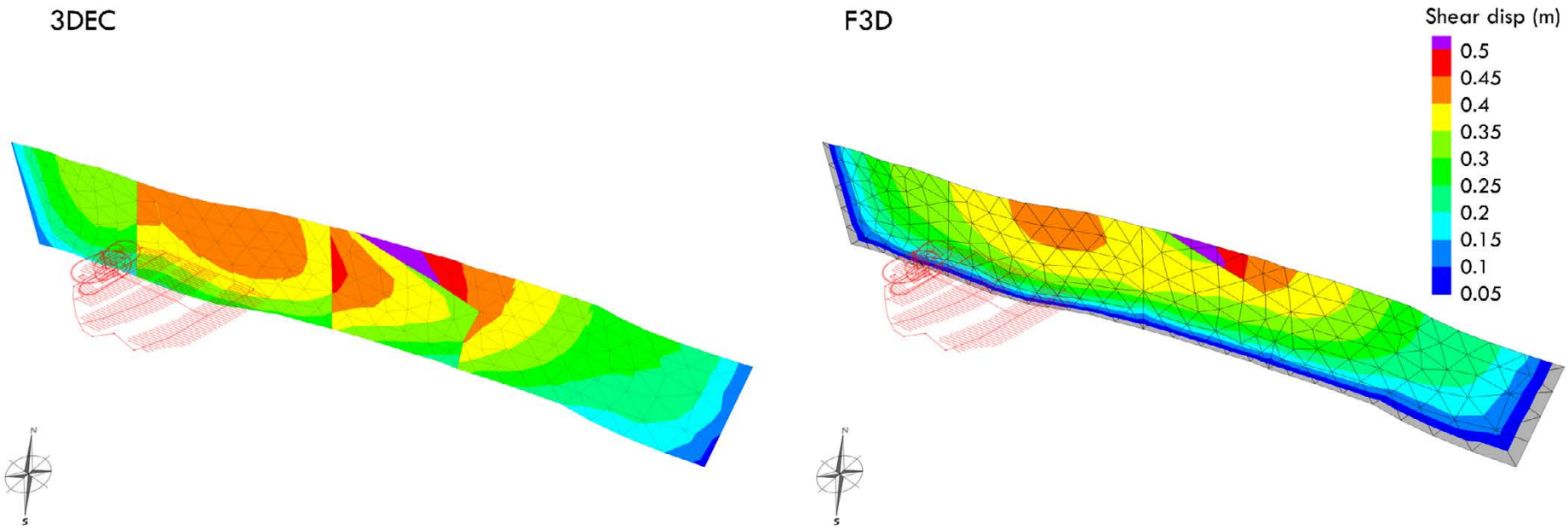

Figure A1-4. *Deformation zone shear contours for the Singö deformation zone before glaciation in elastoplastic simulation Phase 1 simulations.*

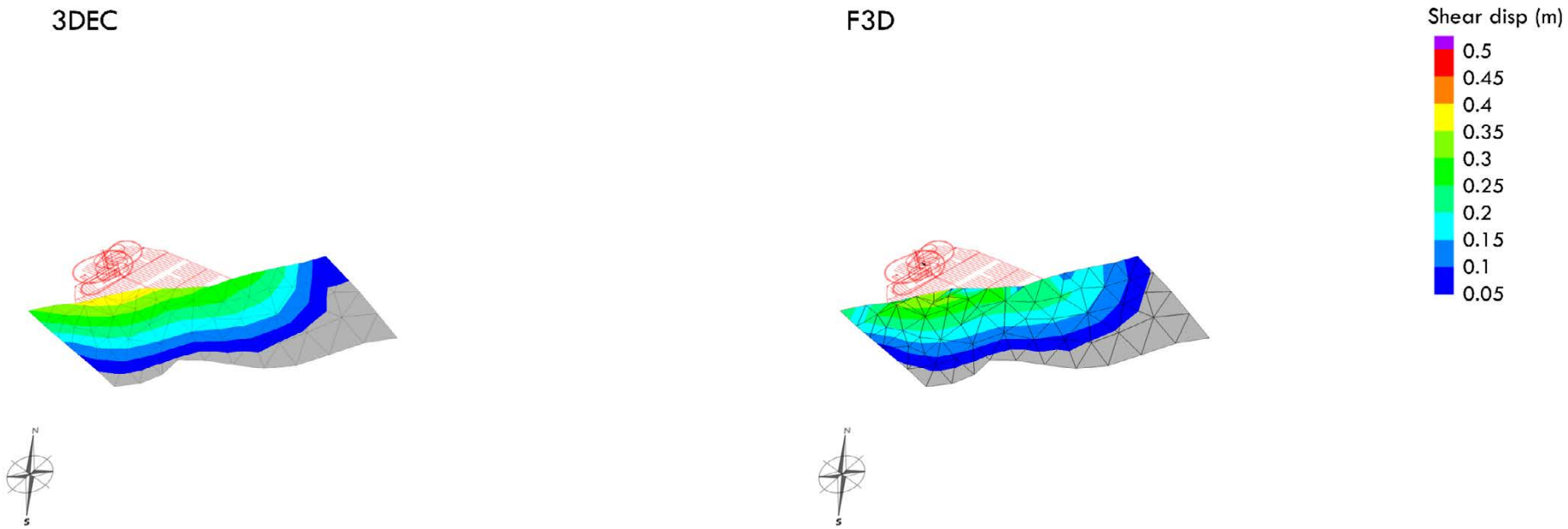

Figure A1-5. *Deformation zone shear contours for the ZFMA2 deformation zone before glaciation in elastoplastic simulation Phase 1 simulations.*

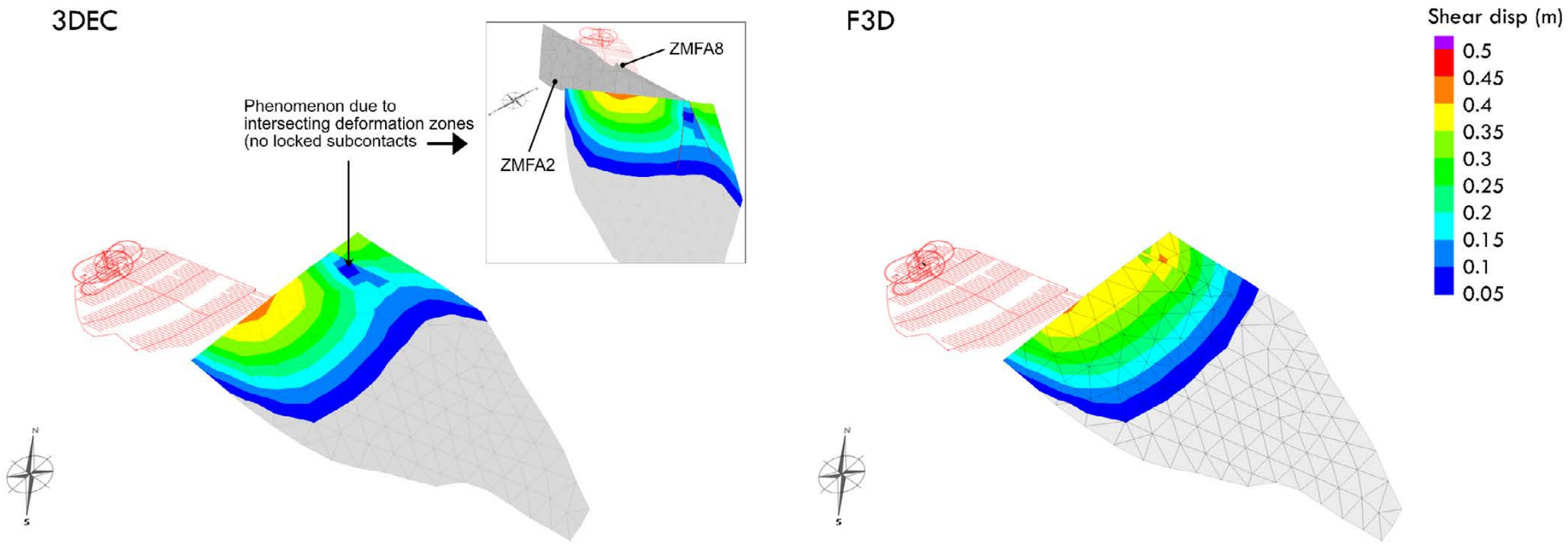

Figure A1-6. *Deformation zone shear contours for the ZFMA3 deformation zone before glaciation in elastoplastic simulation Phase 1 simulations.*

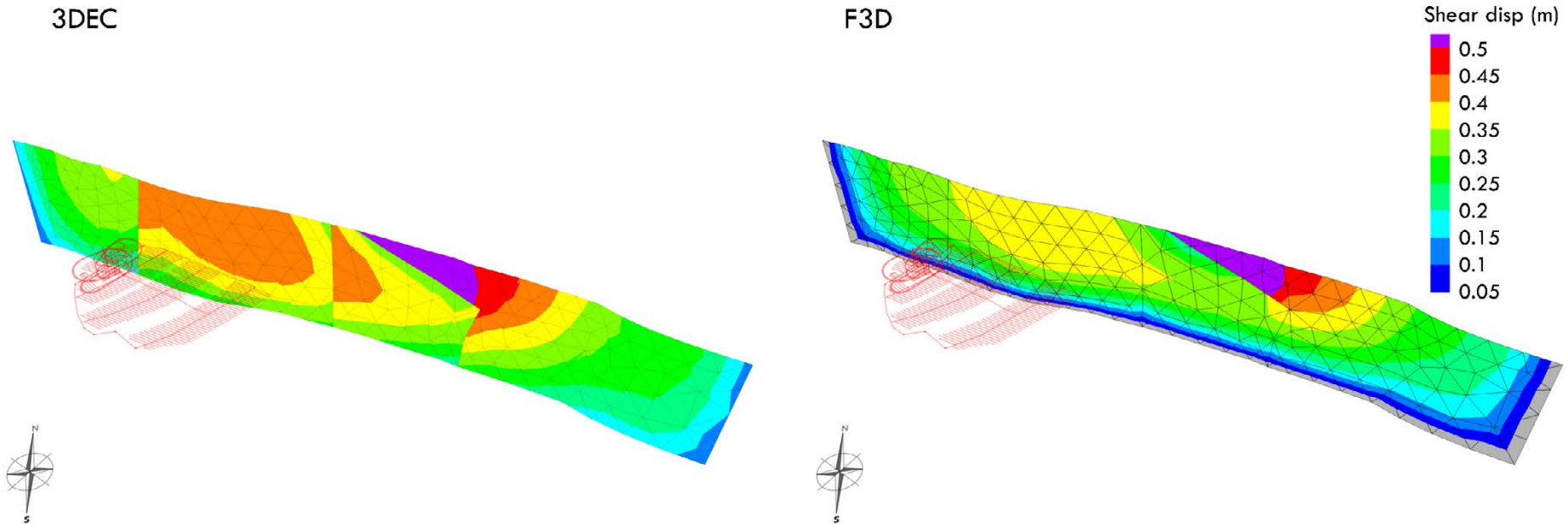

Figure A1-7. *Deformation zone shear contours for the Singö deformation zone after glaciation in elastoplastic simulation Phase 1 simulations.*

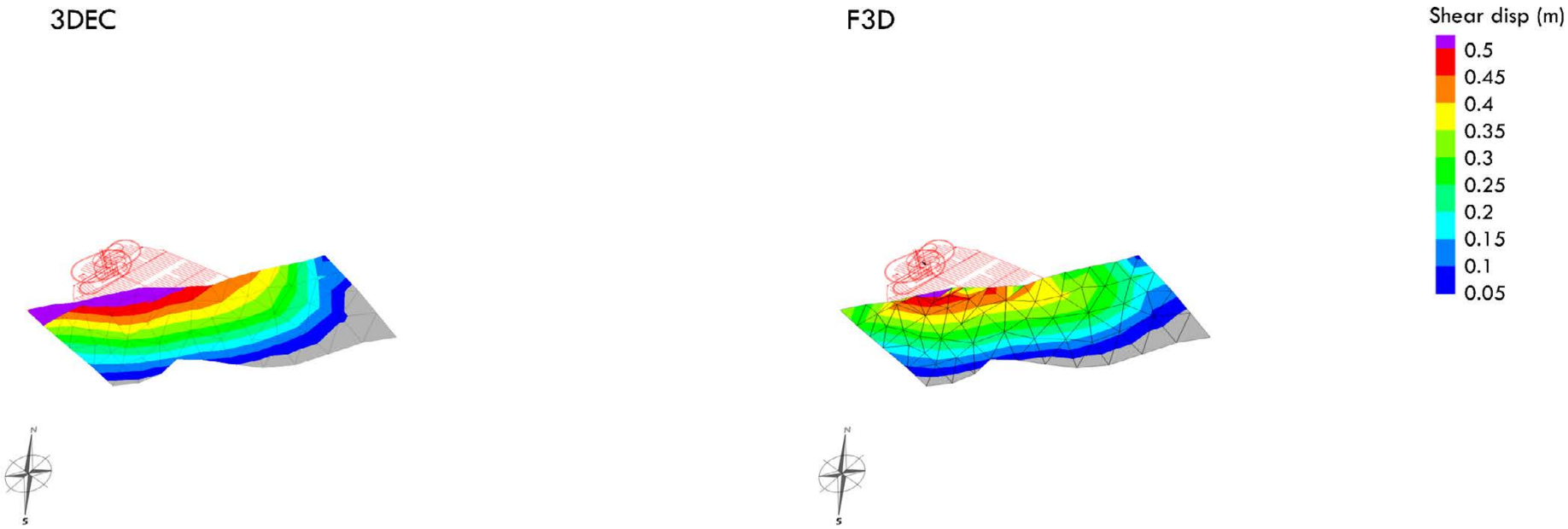

Figure A1-8. *Deformation zone shear contours for the ZFMA2 deformation zone after glaciation in elastoplastic simulation Phase 1 simulations.*

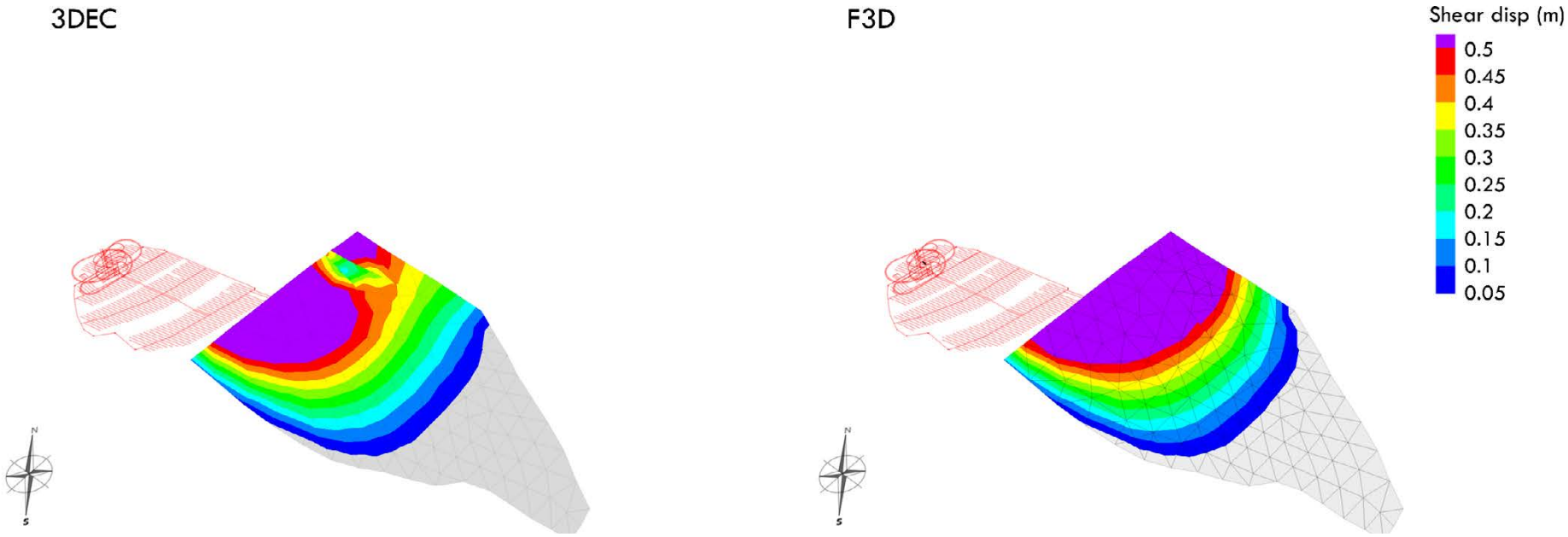

Figure A1-9. *Deformation zone shear contours for the ZFMA3 deformation zone after glaciation in elastoplastic simulation Phase 1 simulations.*

Appendix 2

Phase 2 deformation zone shear

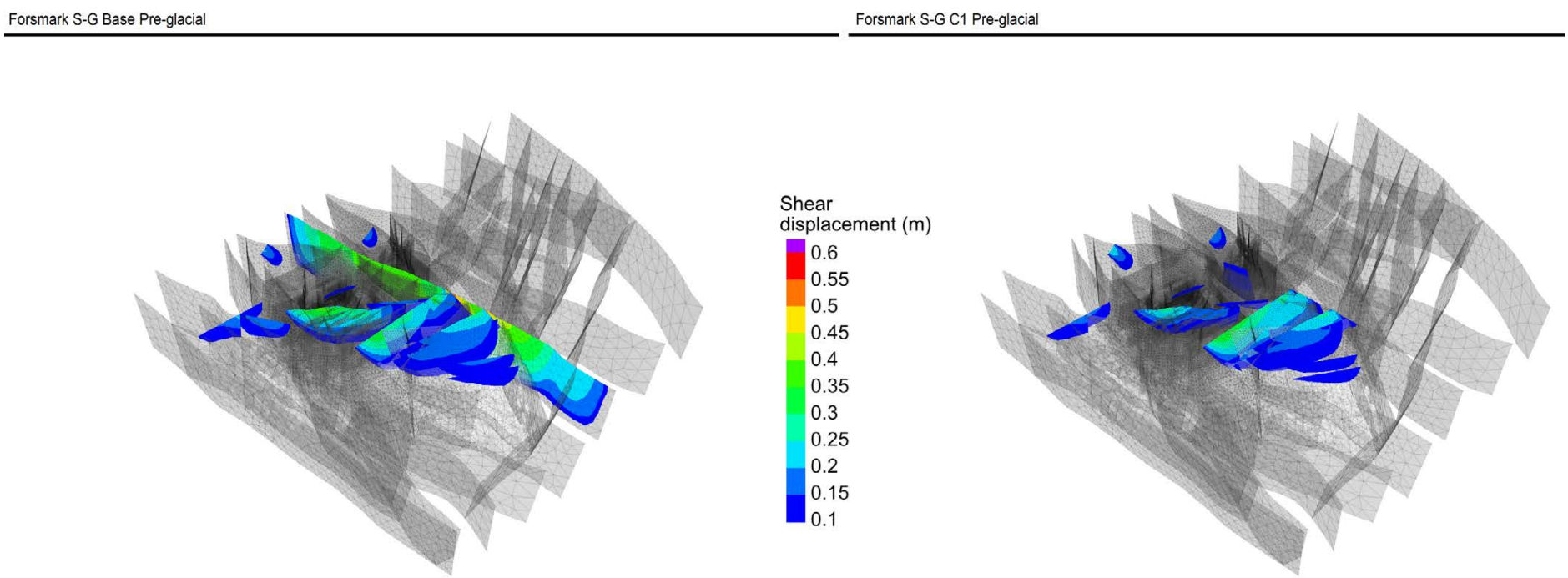

Figure A2-1. *Phase 2 deformation zone shear contours before glaciation for the Base case and Case 1.*

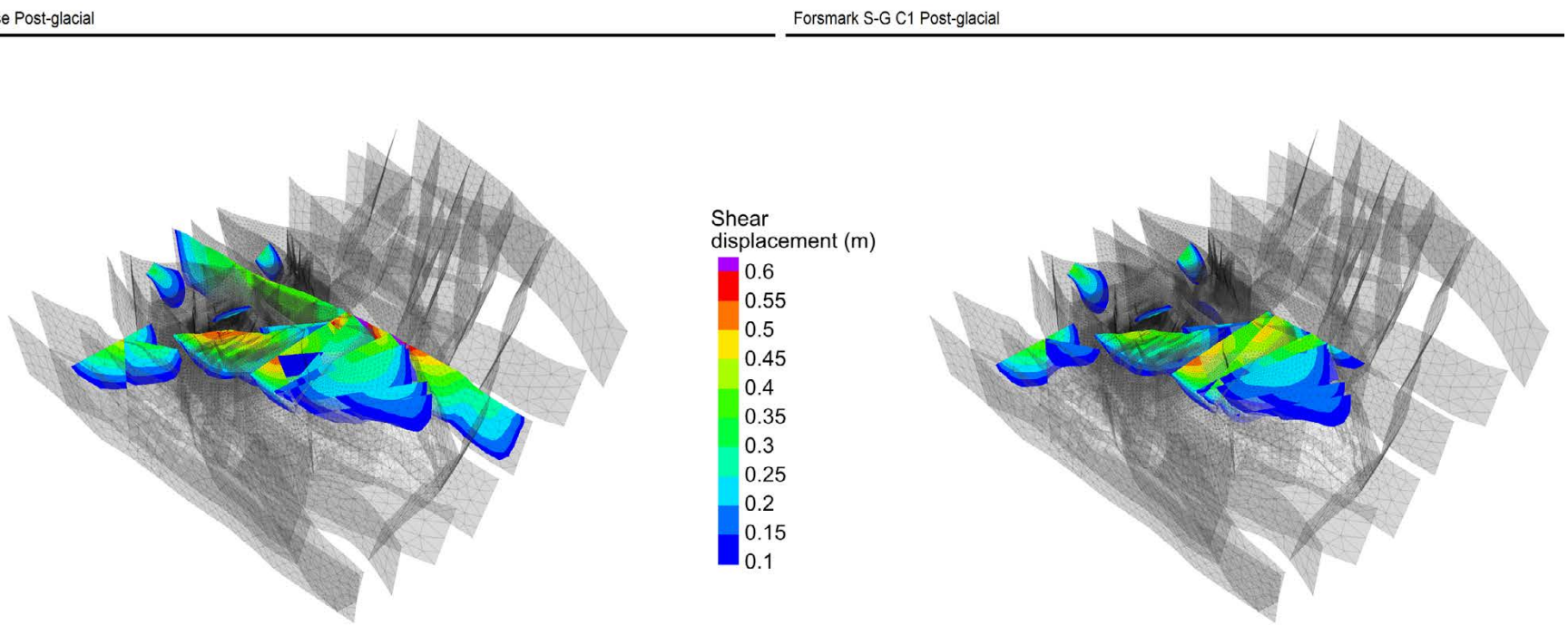

Figure A2-2. *Phase 2 deformation zone shear contours after glaciation for the Base case and Case 1.*

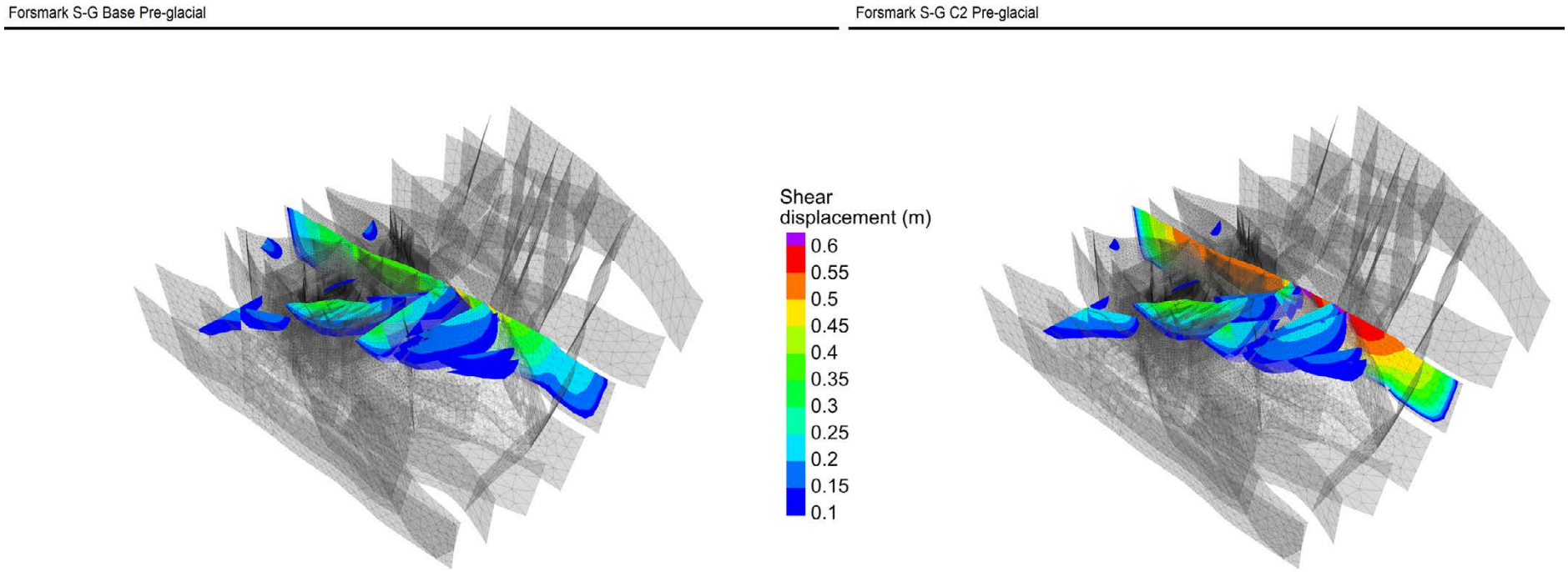

Figure A2-3. *Phase 2 deformation zone shear contours before glaciation for the Base case and Case 2.*

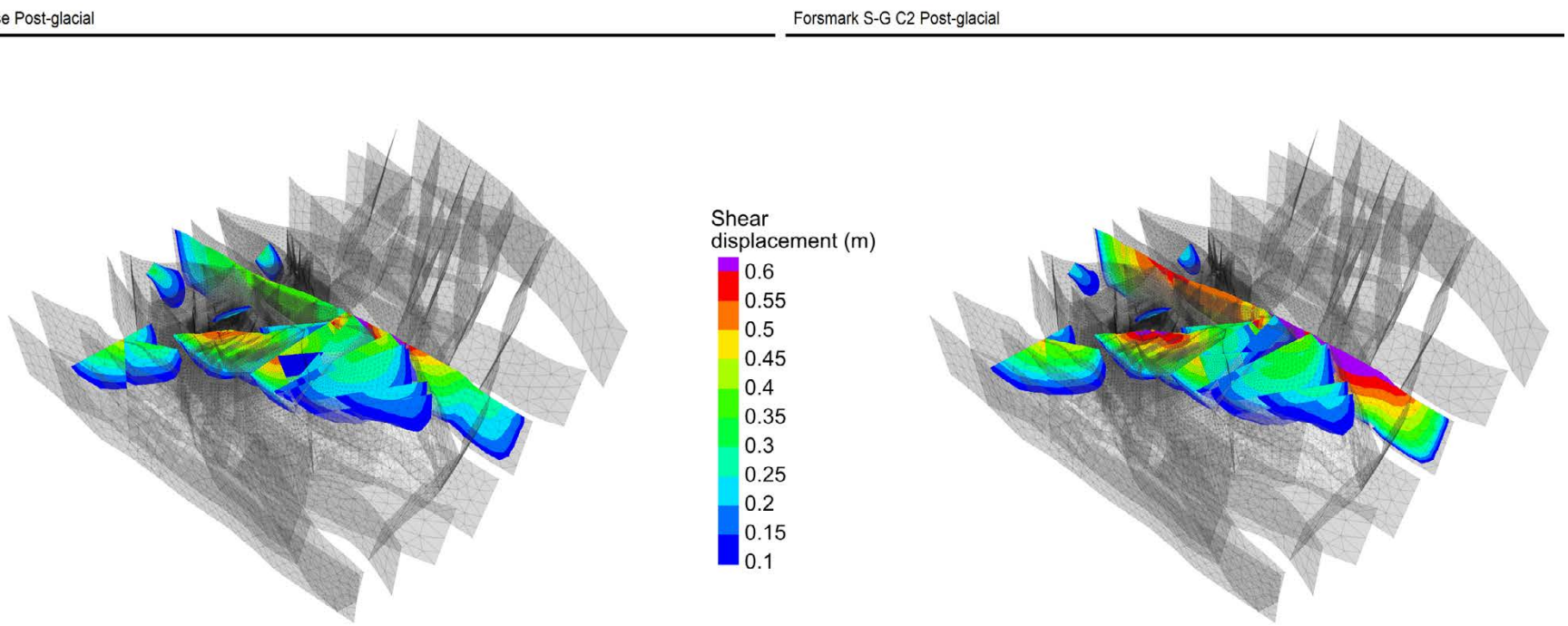

Figure A2-4. *Phase 2 deformation zone shear contours after glaciation for the Base case and Case 2.*

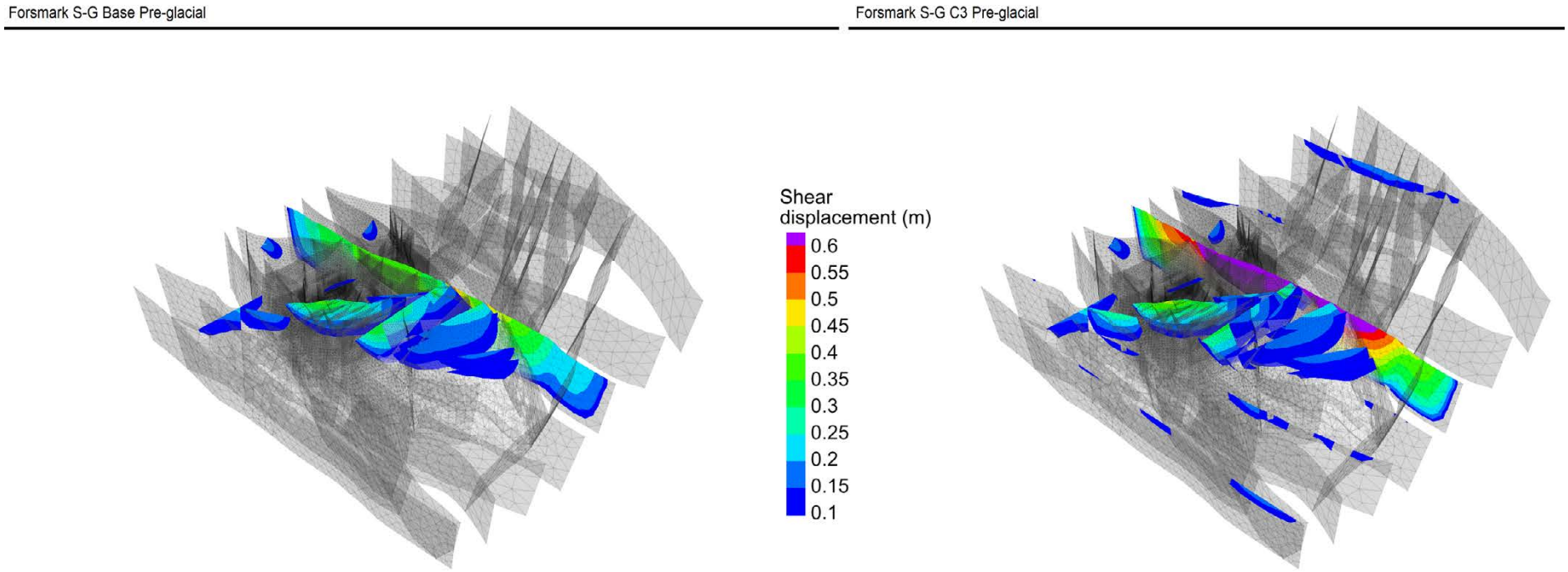

Figure A2-5. *Phase 2 deformation zone shear contours before glaciation for the Base case and Case 3.*

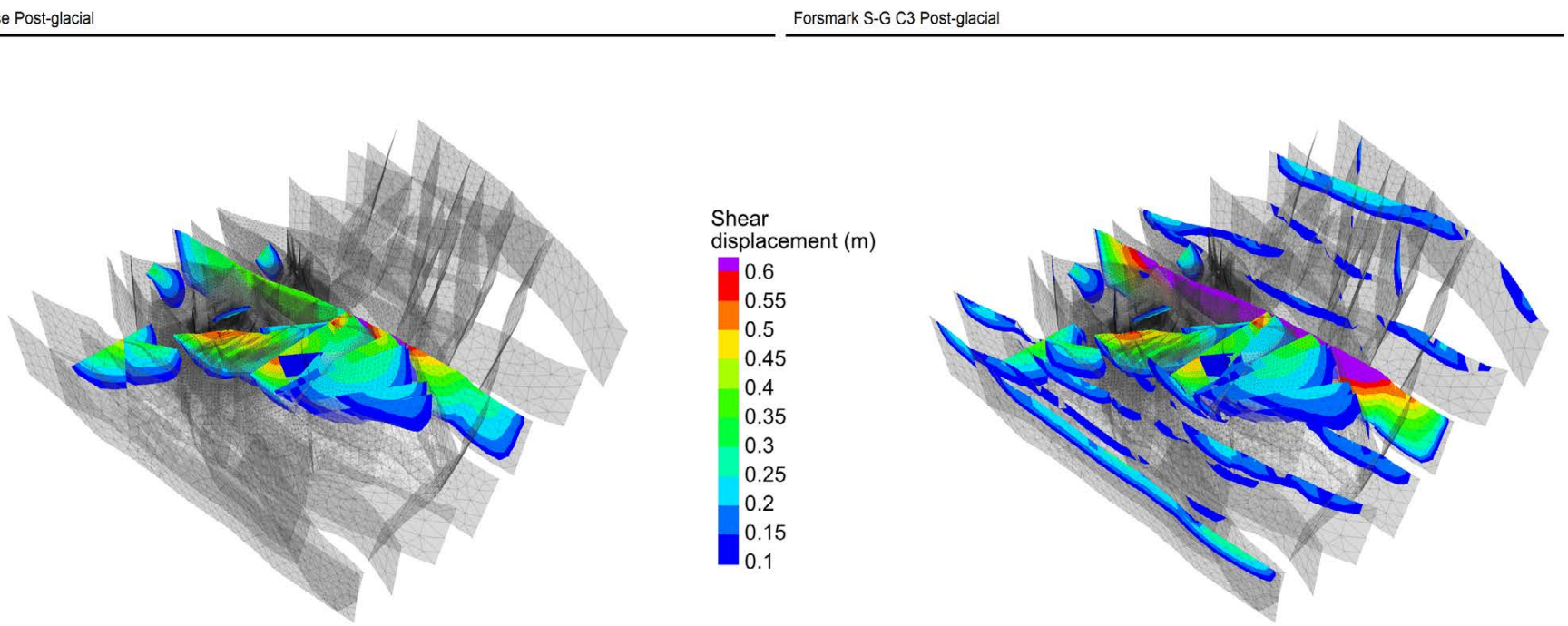

Figure A2-6. *Phase 2 deformation zone shear contours after glaciation for the Base case and Case 3.*

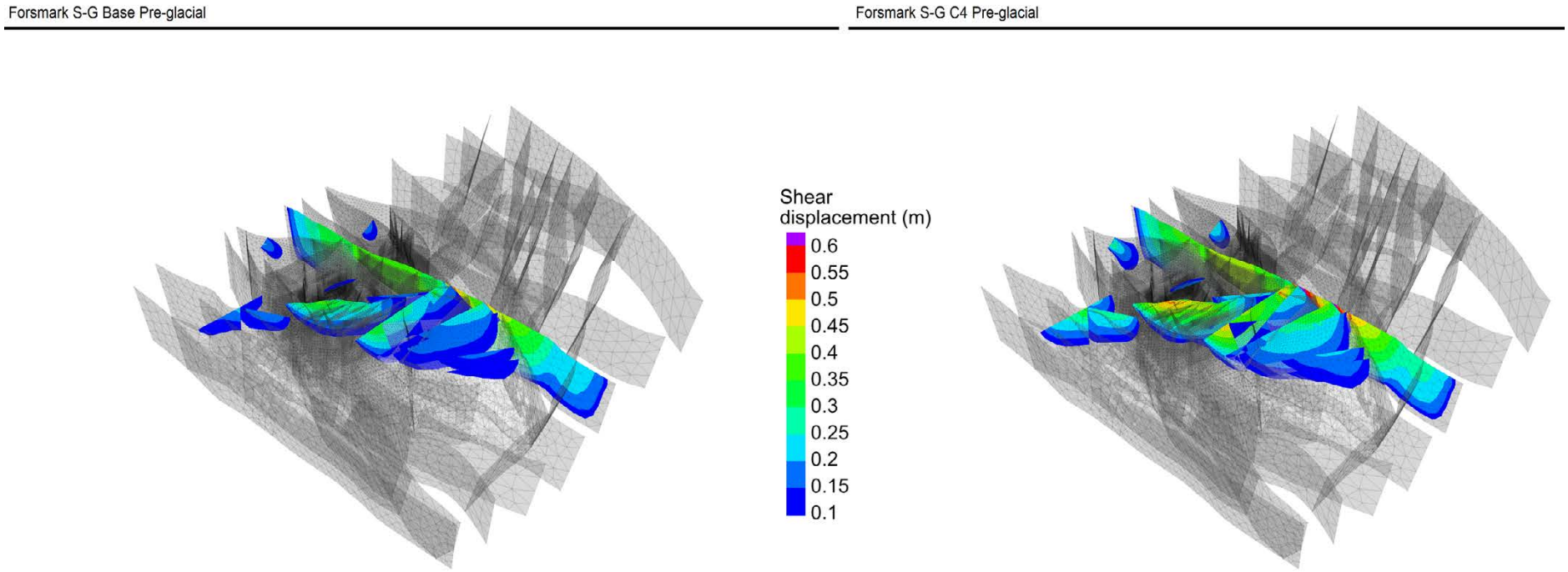

Figure A2-7. *Phase 2 deformation zone shear contours before glaciation for the Base case and Case 4.*

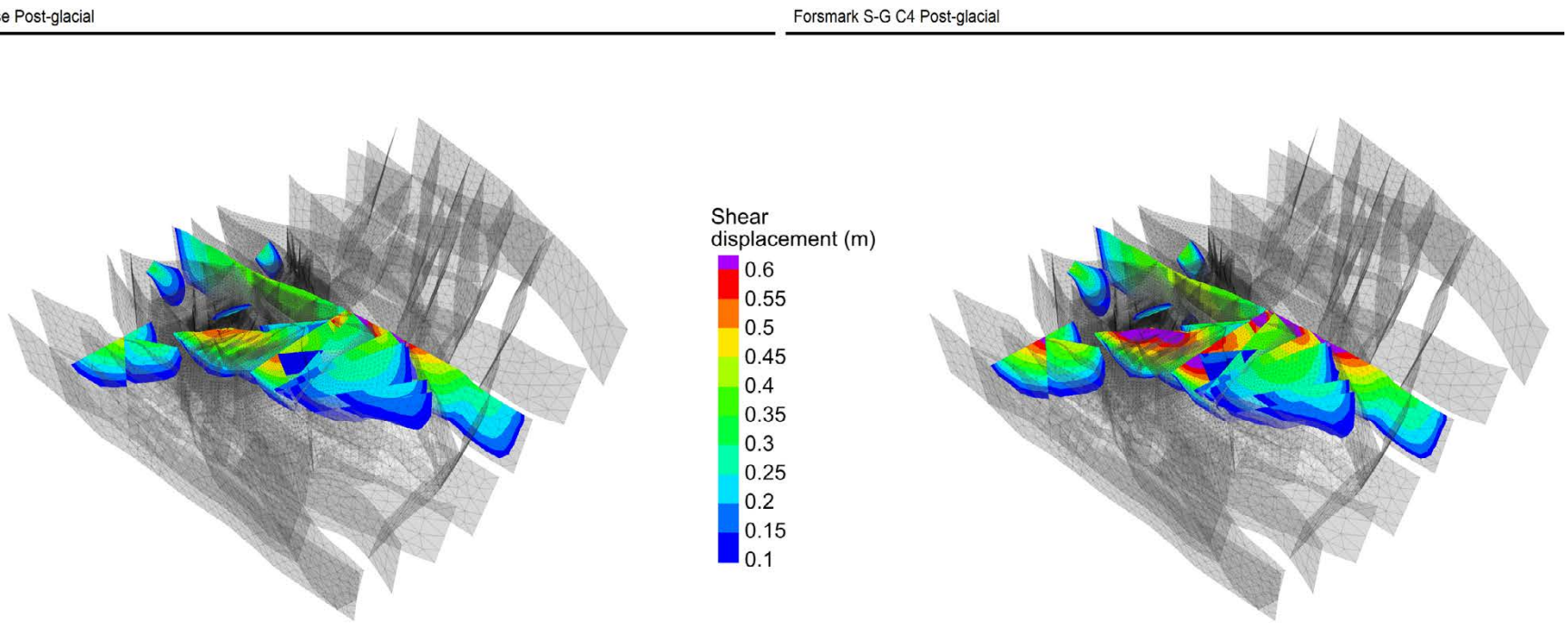

Figure A2-8. *Phase 2 deformation zone shear contours after glaciation for the Base case and Case 4.*

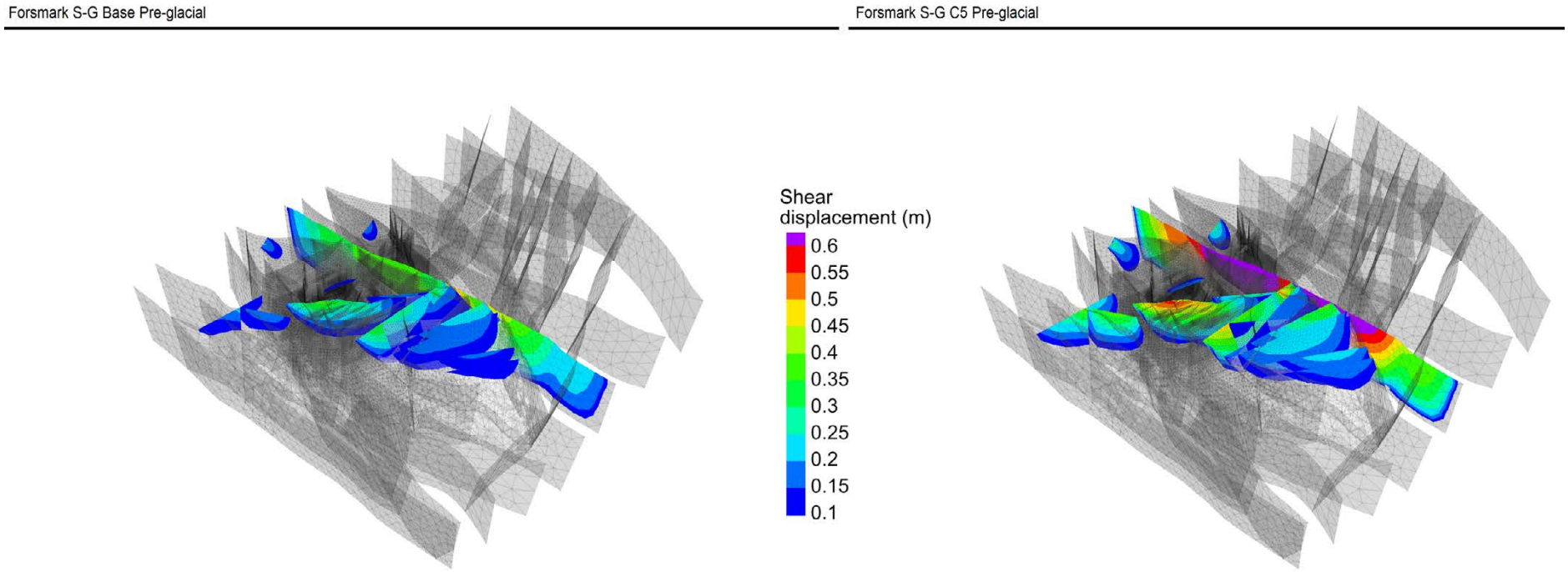

Figure A2-9. *Phase 2 deformation zone shear contours before glaciation for the Base case and Case 5.*

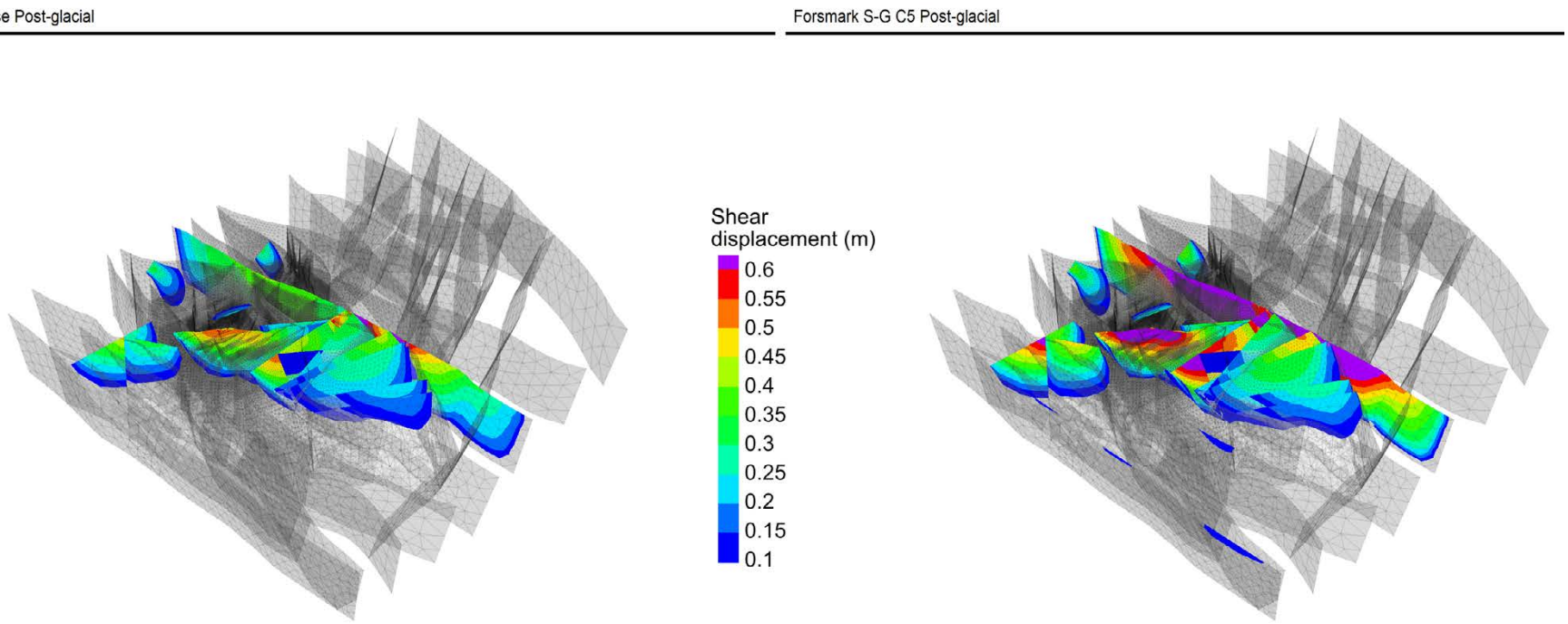

Figure A2-10. *Phase 2 deformation zone shear contours after glaciation for the Base case and Case 5.*

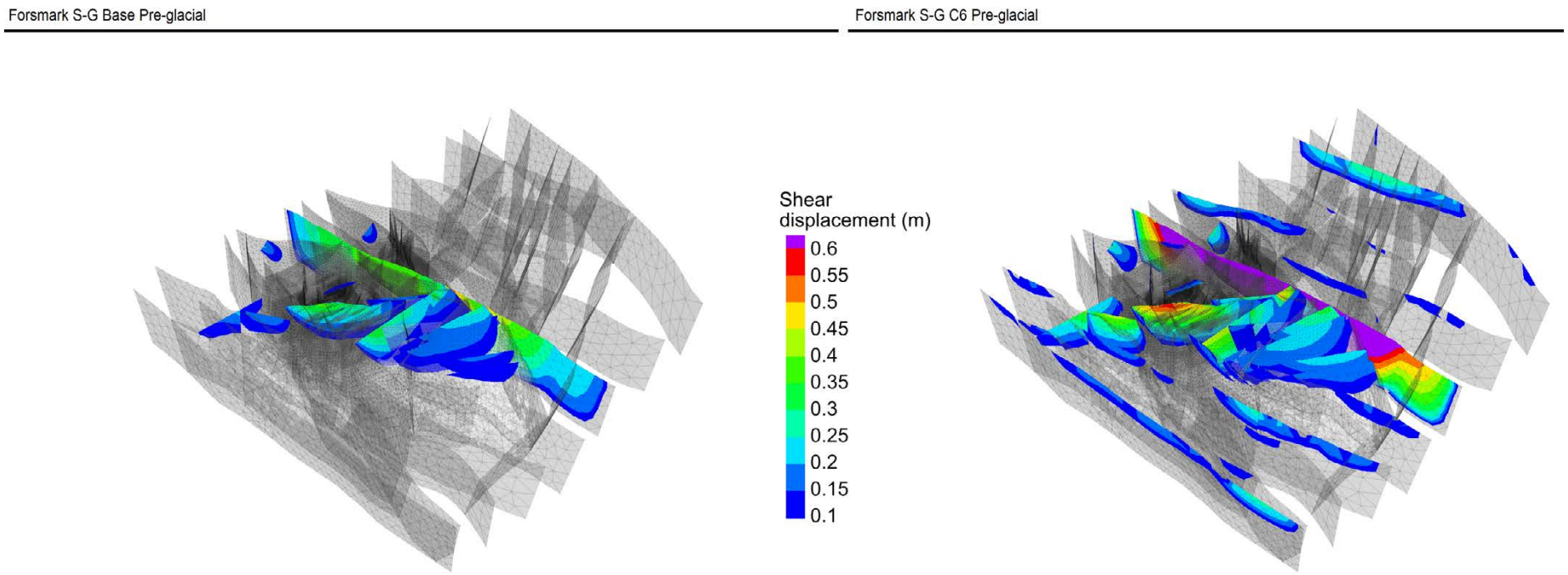

Figure A2-11. *Phase 2 deformation zone shear contours before glaciation for the Base case and Case 6.*

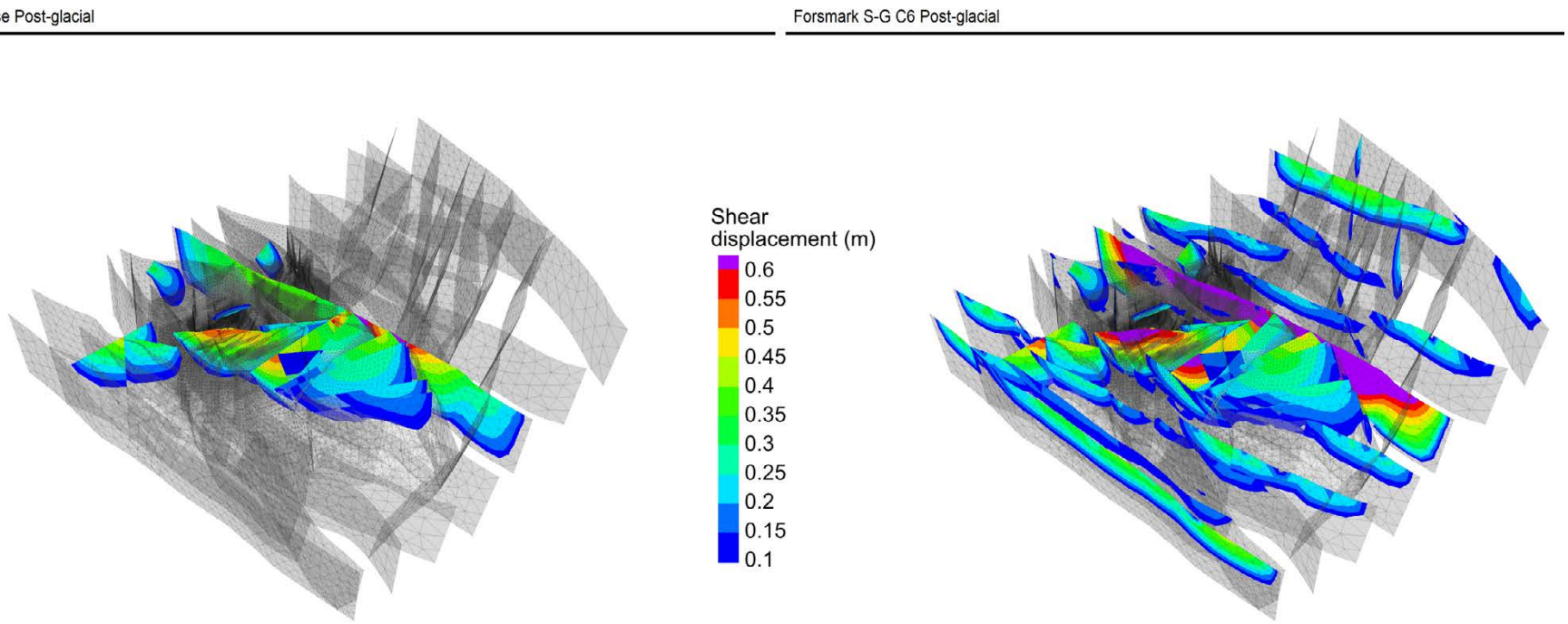

Figure A2-12. *Phase 2 deformation zone shear contours after glaciation for the Base case and Case 6.*

Appendix 3

Phase 1 deformation zone shear lower hemisphere projection

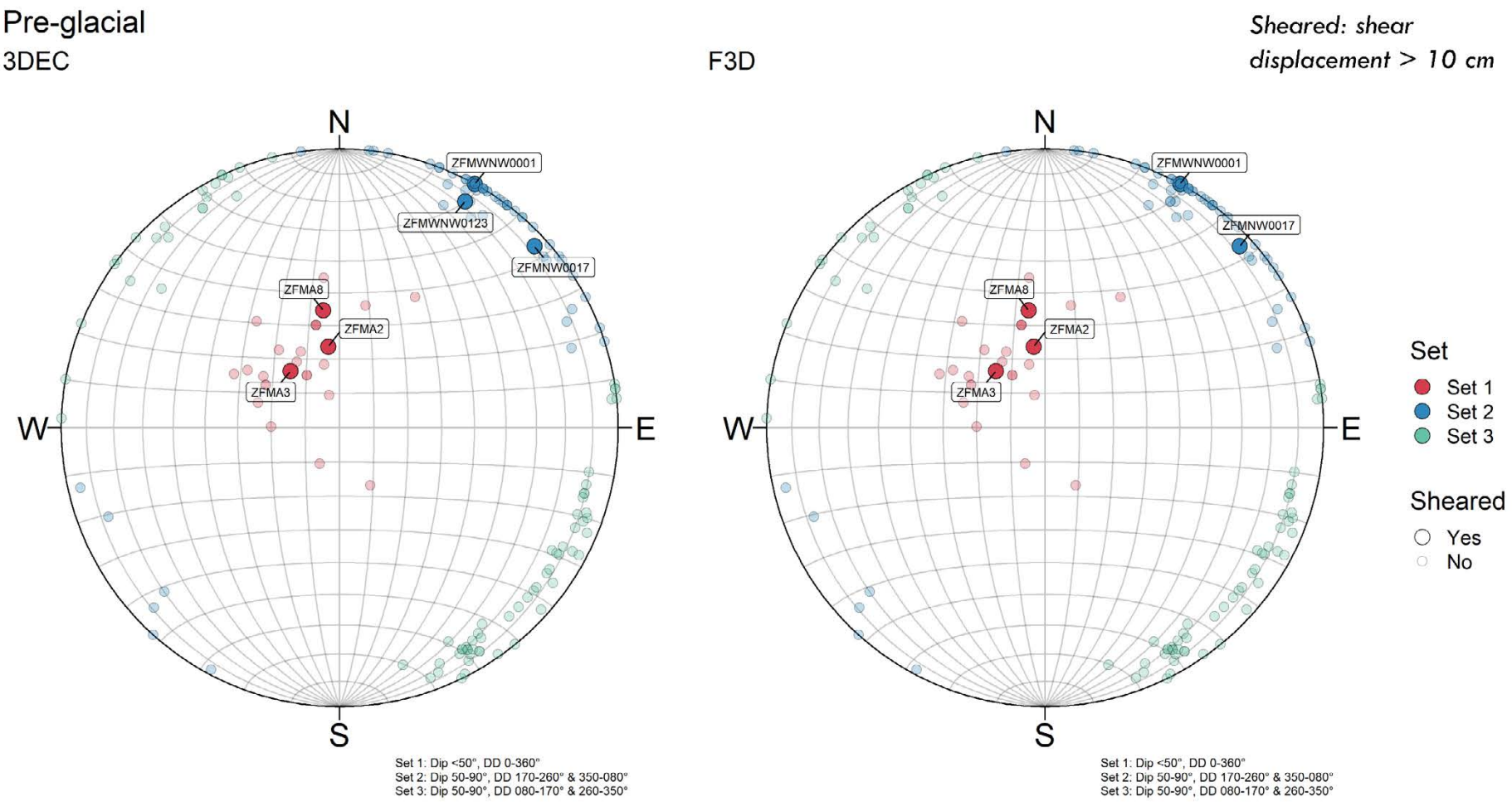

Figure A3-1. *Equal area lower hemisphere projection of sheared deformation zones according to set definitions before glaciation in an elastoplastic simulation for 3DEC and FLAC3D in Phase 1.*

Appendix 4

Phase 2 deformation zone shear lower hemisphere projections

Pre-glacial

Base

C1: σ_1 trend -20°

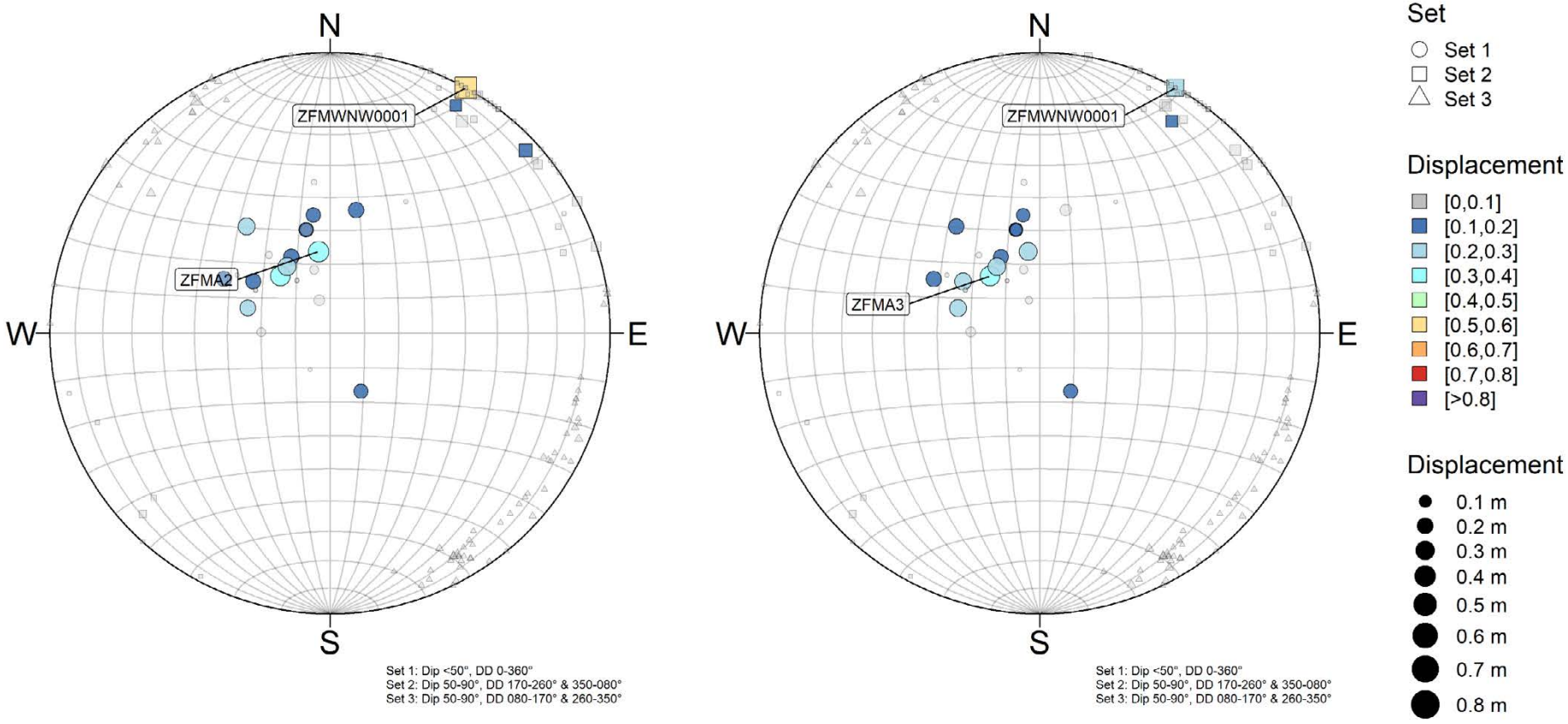

Figure A4-1. *Deformation zone shear before glaciation by set group on an equal area lower hemisphere projection (LHP) for the Base case and Case 1. Both symbol size and colour indicate displacement magnitude in metres.*

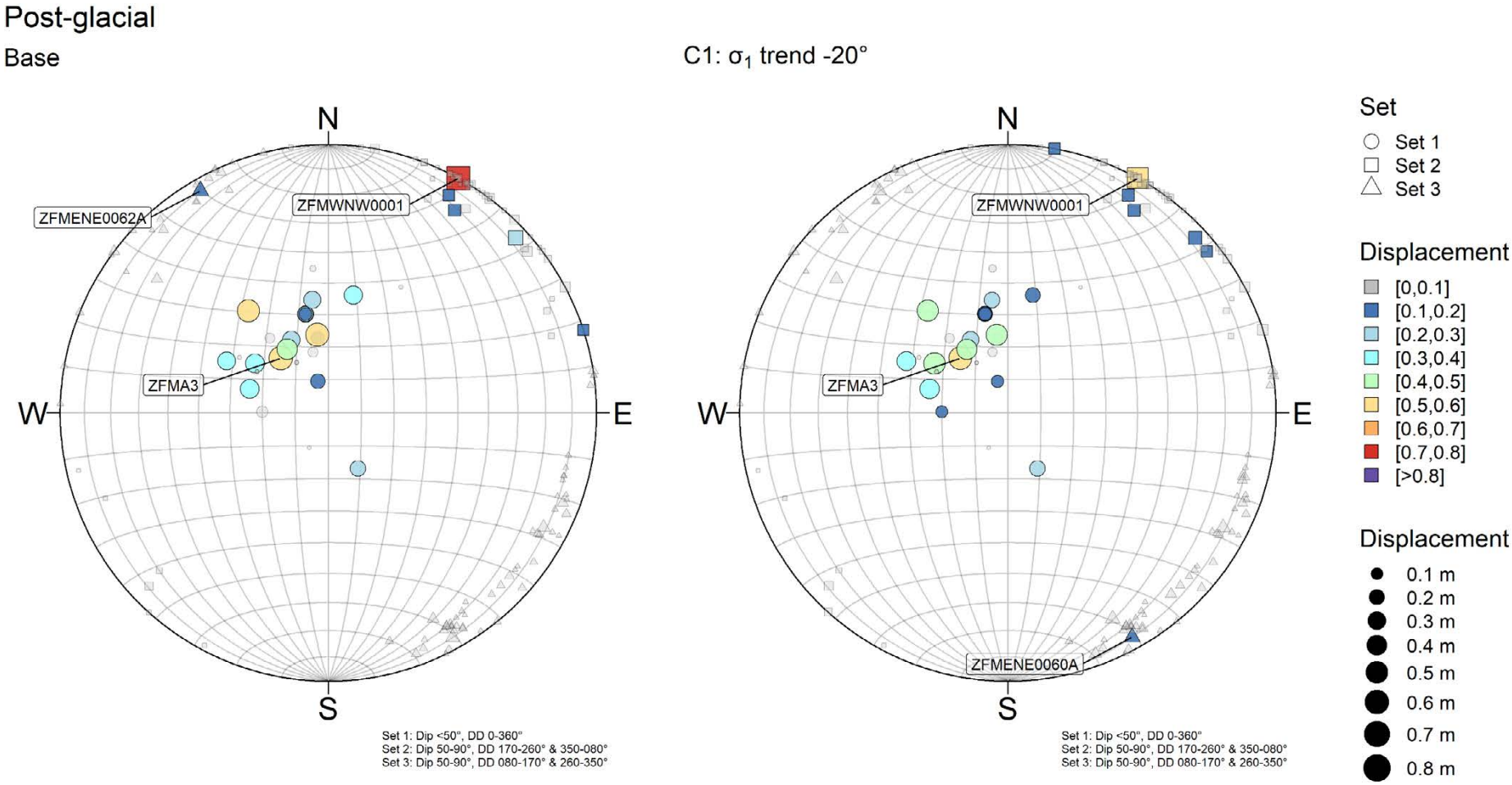

Figure A4-2. *Deformation zone shear after glaciation by set group on an equal area lower hemisphere projection (LHP) for the Base case and Case 1. Both symbol size and colour indicate displacement magnitude in metres.*

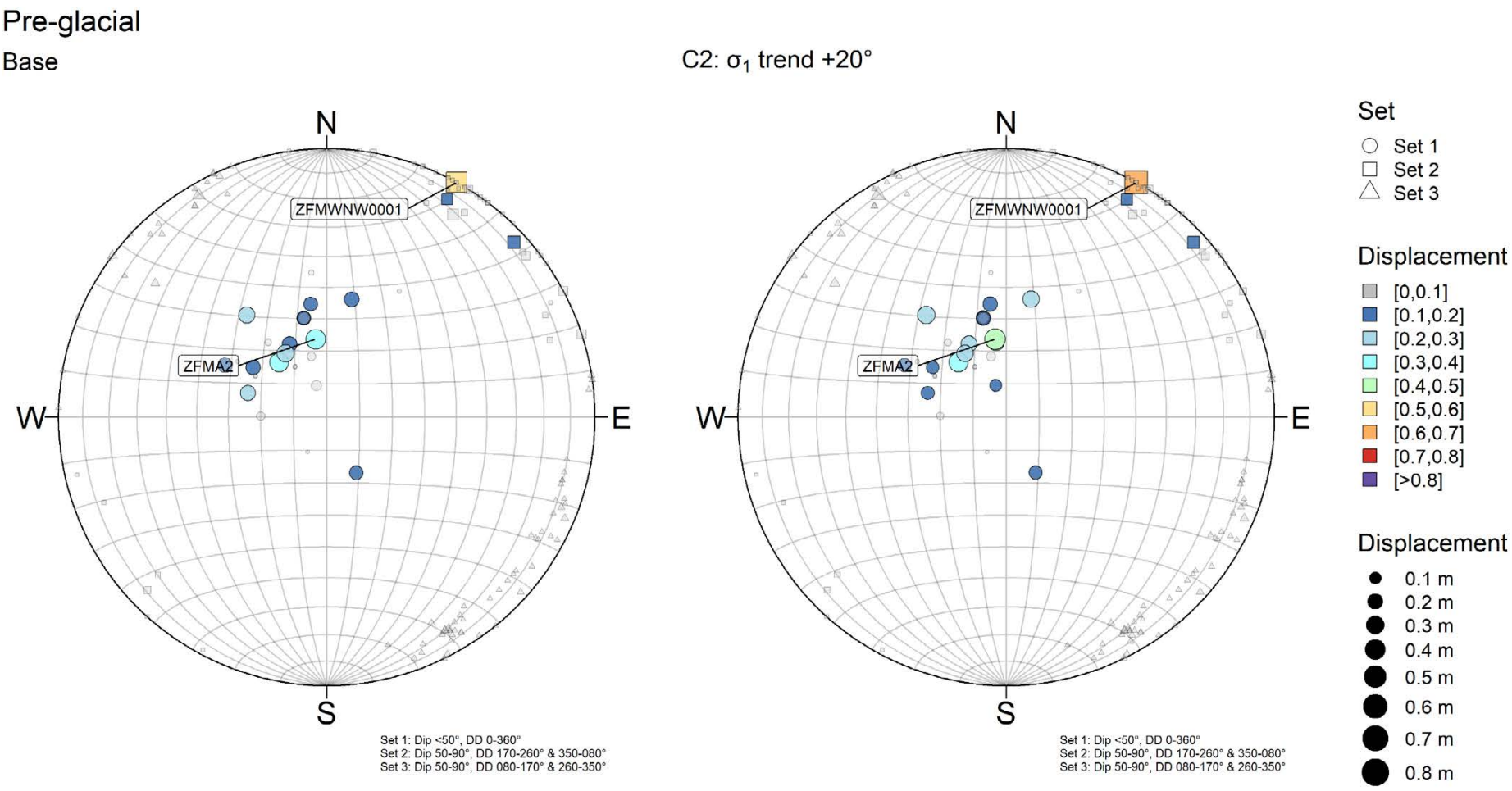

Figure A4-3. *Deformation zone shear before glaciation by set group on an equal area lower hemisphere projection (LHP) for the Base case and Case 2. Both symbol size and colour indicate displacement magnitude in metres.*

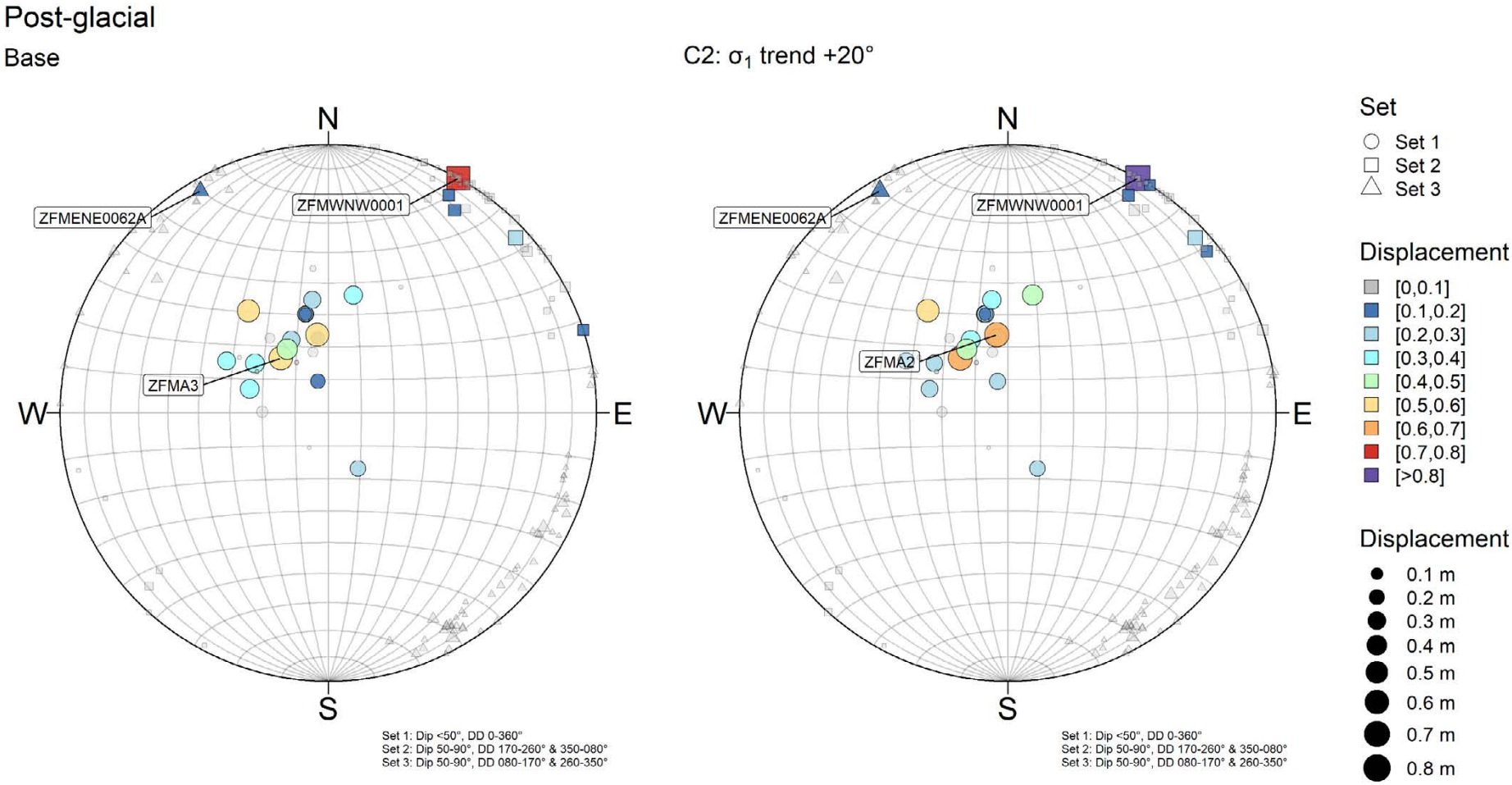

Figure A4-4. *Deformation zone shear after glaciation by set group on an equal area lower hemisphere projection (LHP) for the Base case and Case 2. Both symbol size and colour indicate displacement magnitude in metres.*

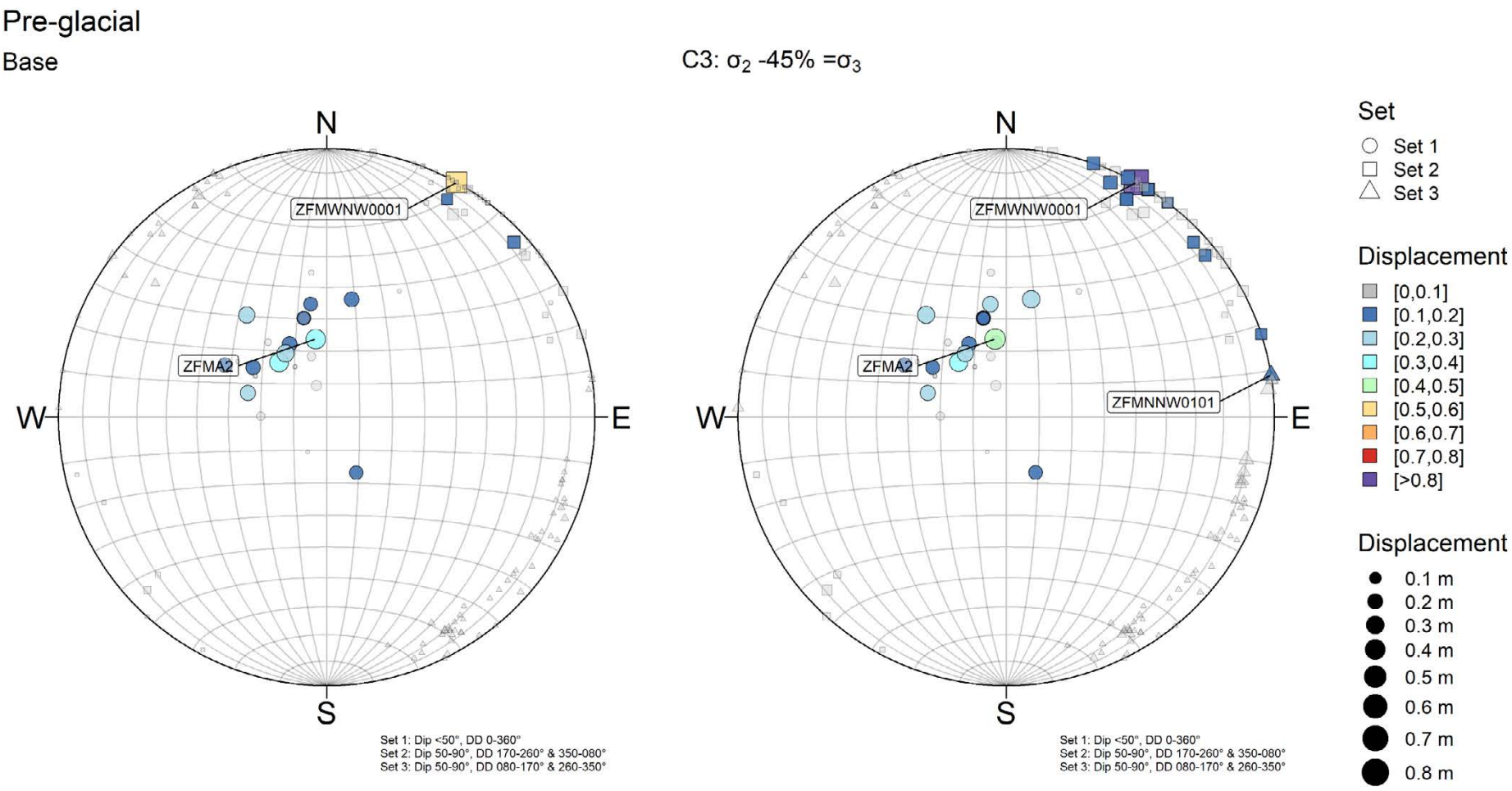

Figure A4-5. *Deformation zone shear before glaciation by set group on an equal area lower hemisphere projection (LHP) for the Base case and Case 3. Both symbol size and colour indicate displacement magnitude in metres.*

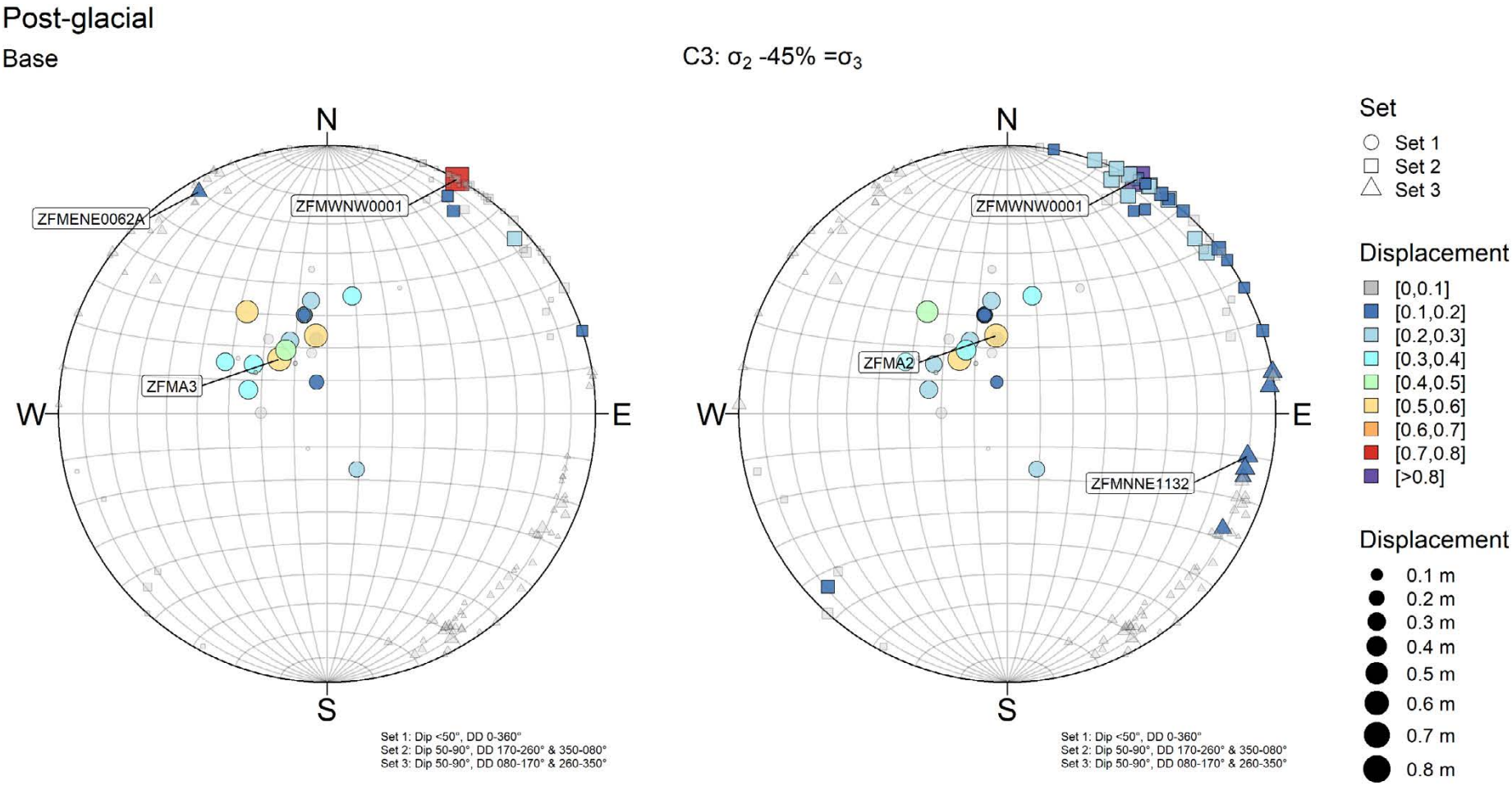

Figure A4-6. *Deformation zone shear after glaciation by set group on an equal area lower hemisphere projection (LHP) for the Base case and Case 3. Both symbol size and colour indicate displacement magnitude in metres.*

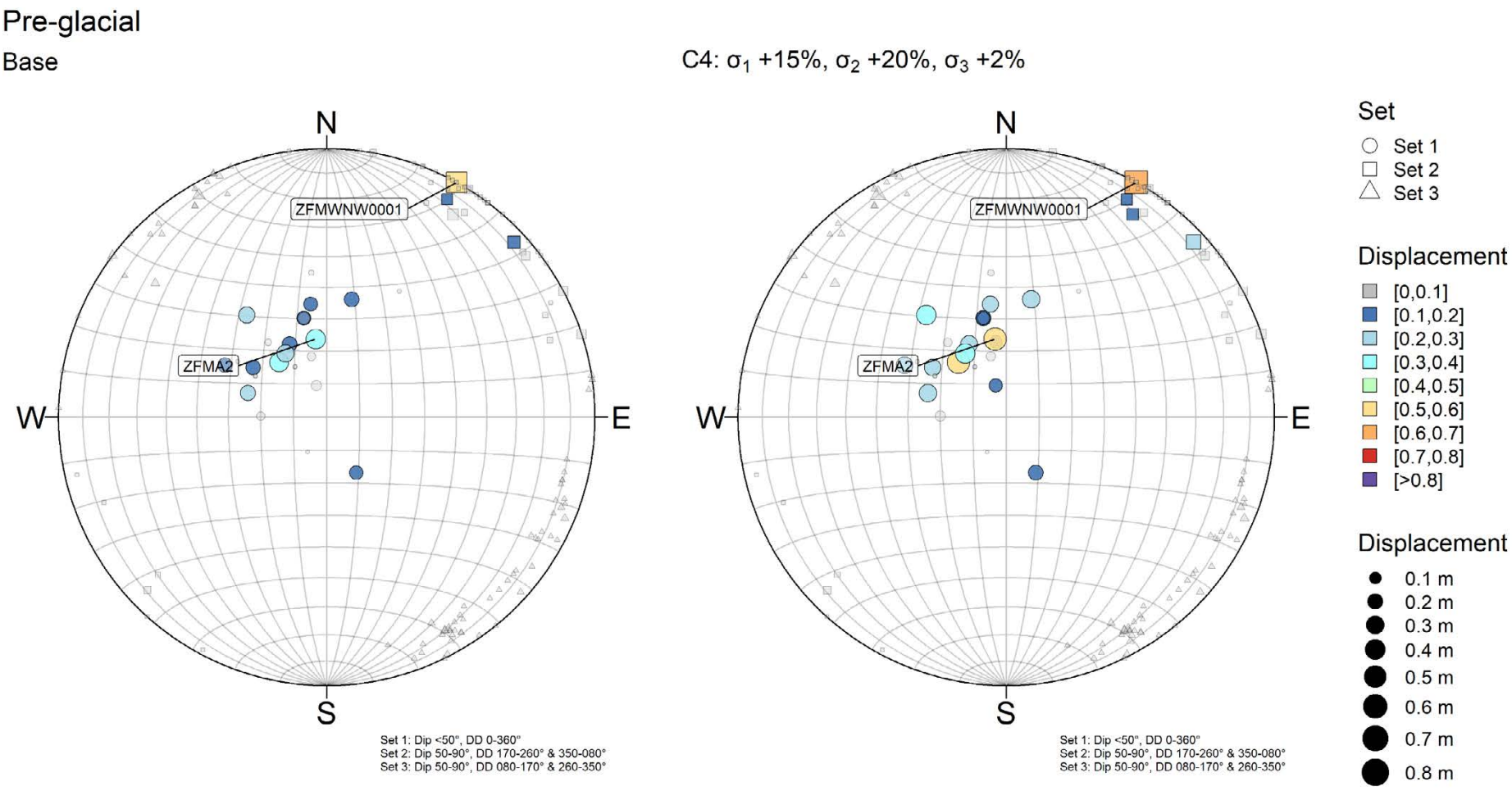

Figure A4-7. *Deformation zone shear before glaciation by set group on an equal area lower hemisphere projection (LHP) for the Base case and Case 4. Both symbol size and colour indicate displacement magnitude in metres.*

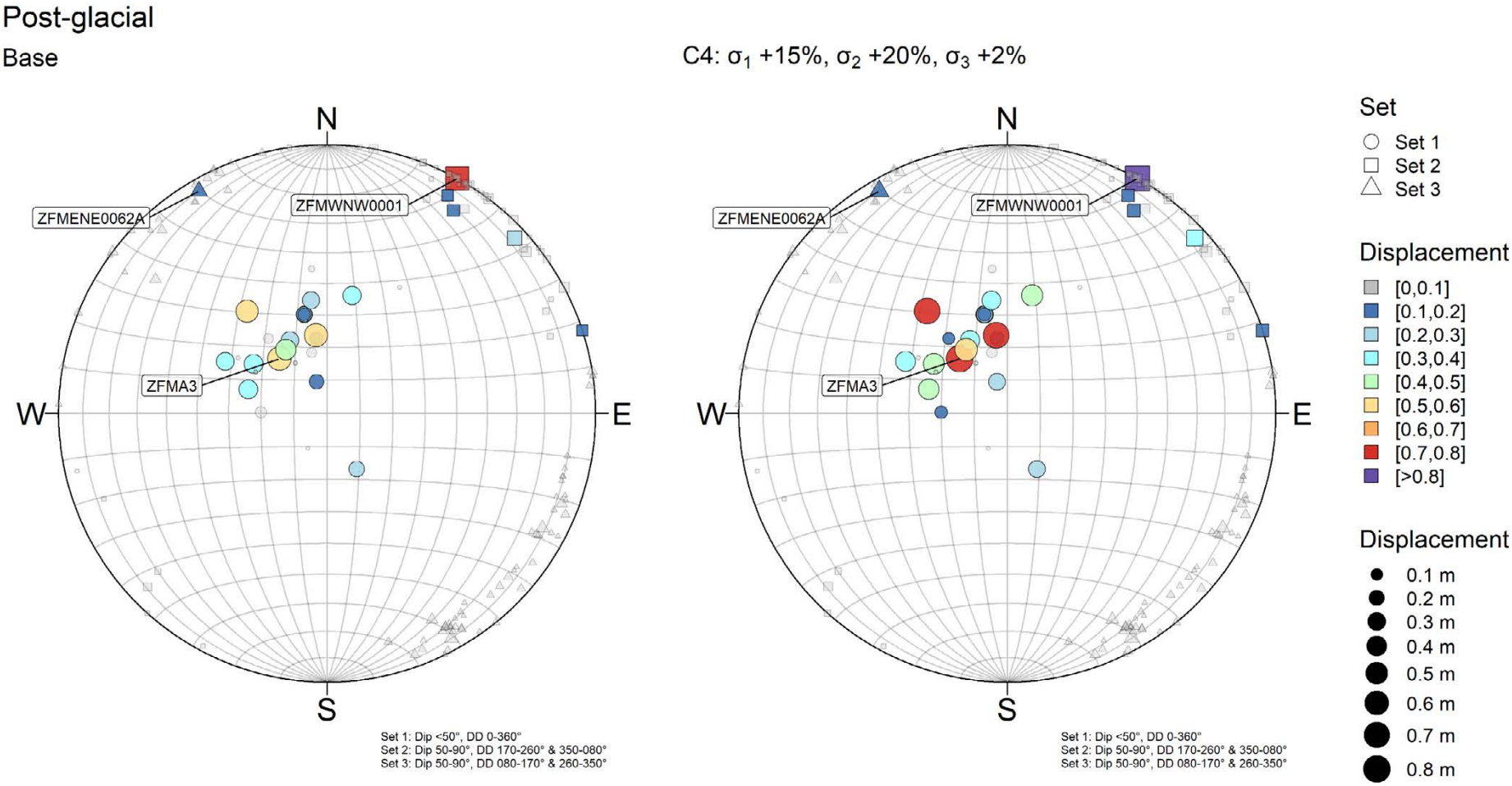

Figure A4-8. *Deformation zone shear after glaciation by set group on an equal area lower hemisphere projection (LHP) for the Base case and Case 4. Both symbol size and colour indicate displacement magnitude in metres.*

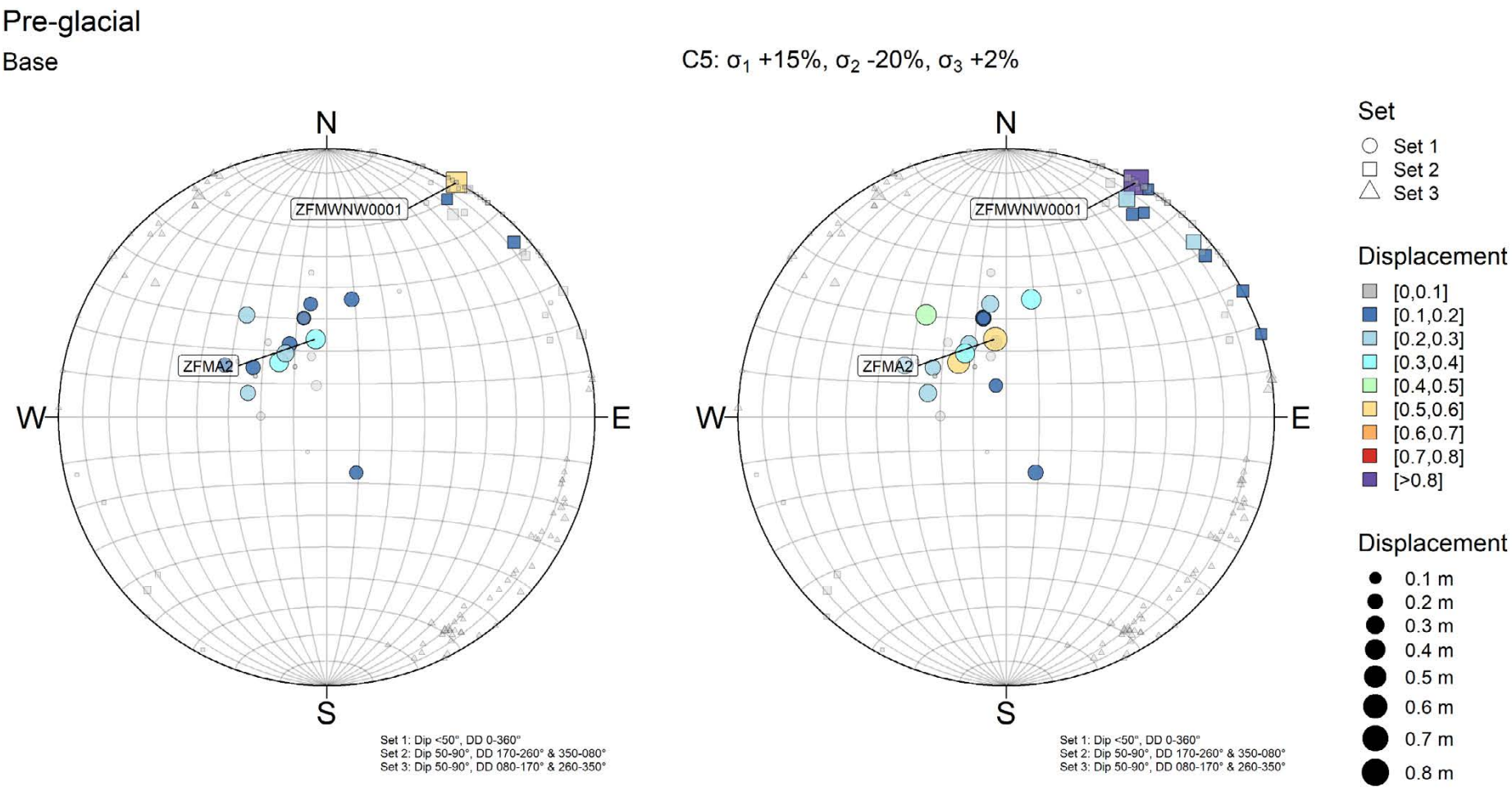

Figure A4-9. *Deformation zone shear before glaciation by set group on an equal area lower hemisphere projection (LHP) for the Base case and Case 5. Both symbol size and colour indicate displacement magnitude in metres.*

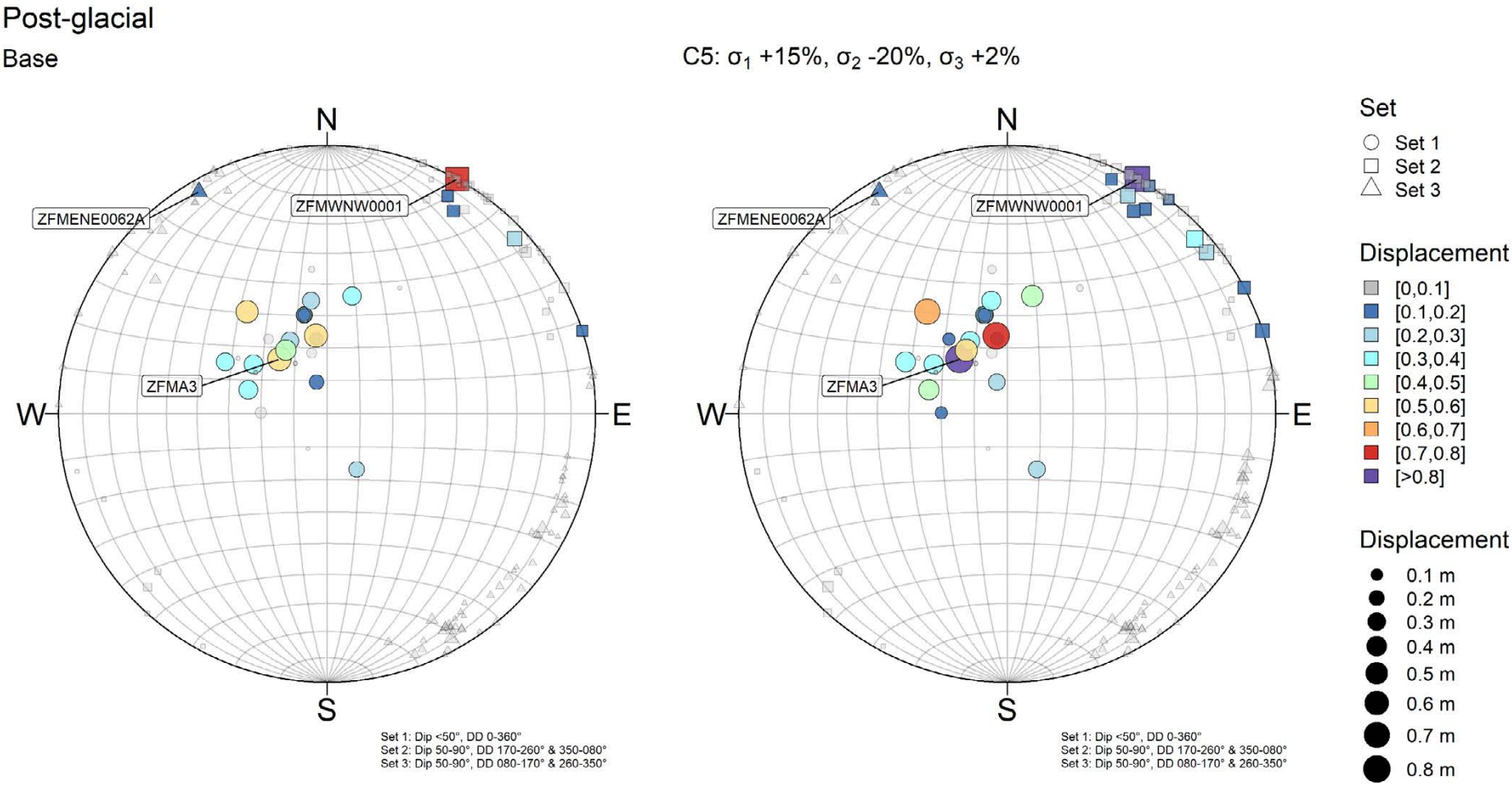

Figure A4-10. *Deformation zone shear after glaciation by set group on an equal area lower hemisphere projection (LHP) for the Base case and Case 5. Both symbol size and colour indicate displacement magnitude in metres.*

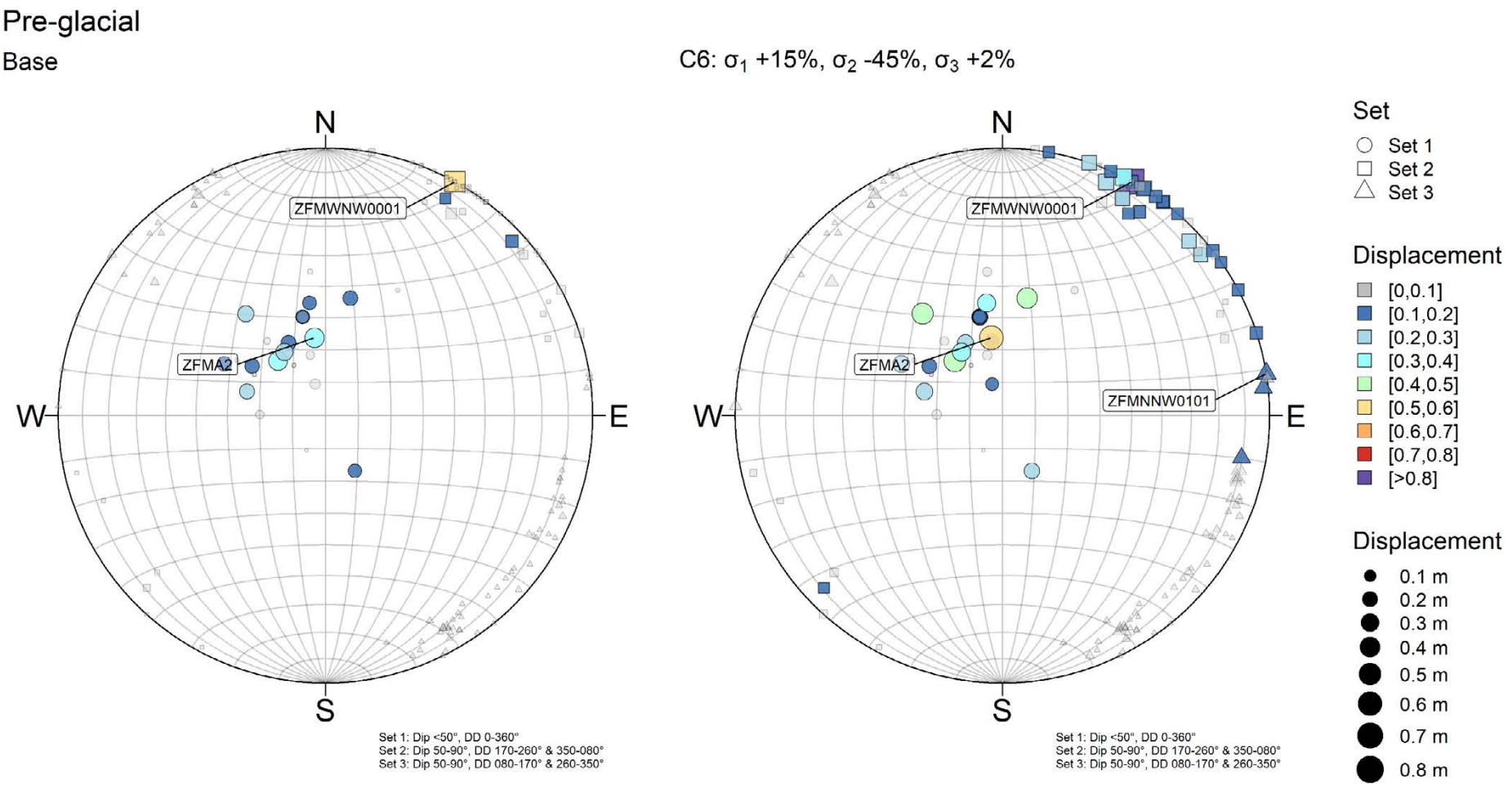

Figure A4-11. *Deformation zone shear before glaciation by set group on an equal area lower hemisphere projection (LHP) for the Base case and Case 6. Both symbol size and colour indicate displacement magnitude in metres.*

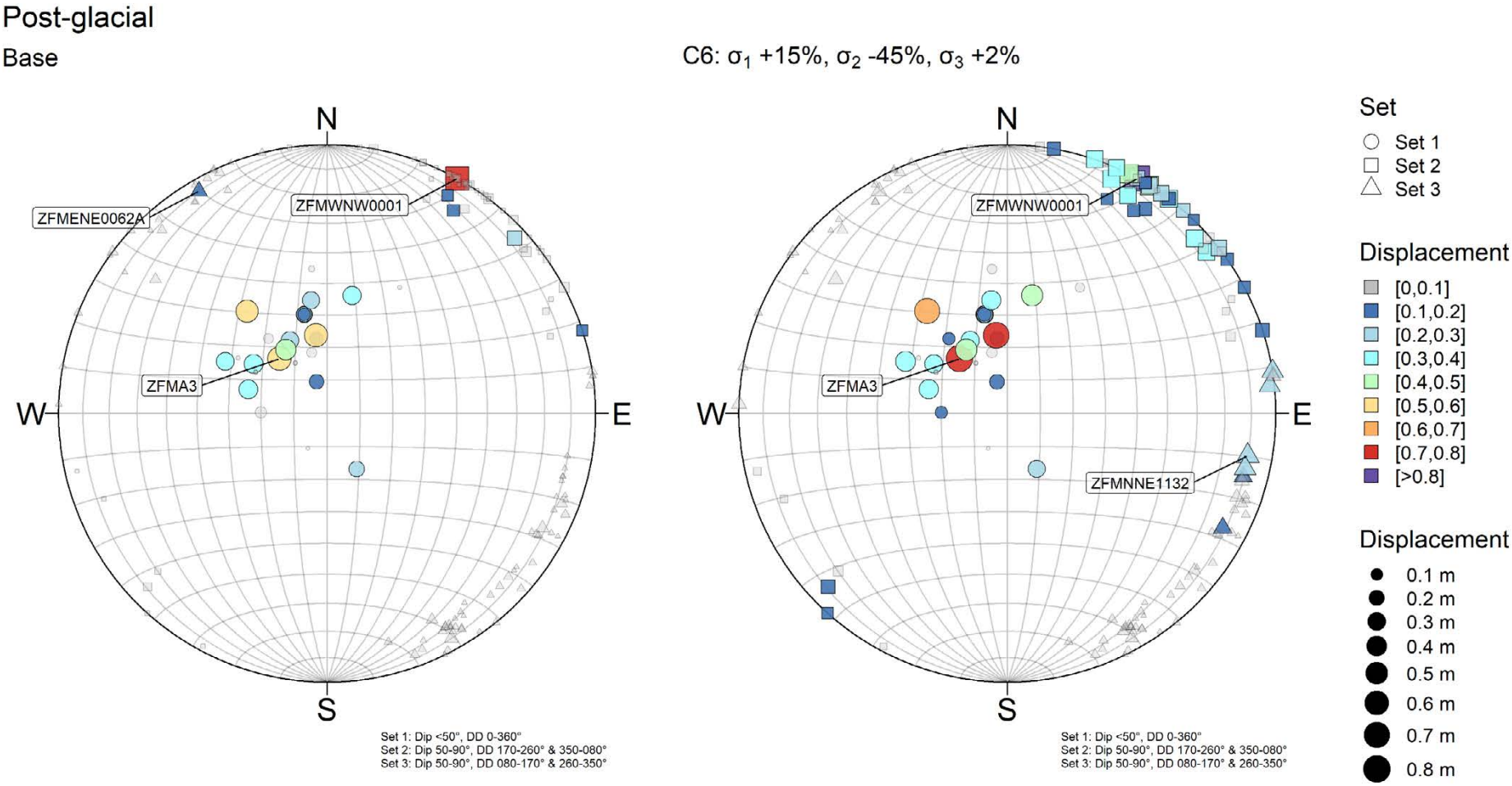

Figure A4-12. *Deformation zone shear after glaciation by set group on an equal area lower hemisphere projection (LHP) for the Base case and Case 6. Both symbol size and colour indicate displacement magnitude in metres.*

Appendix 5

Phase 1 deformation zone slip histograms

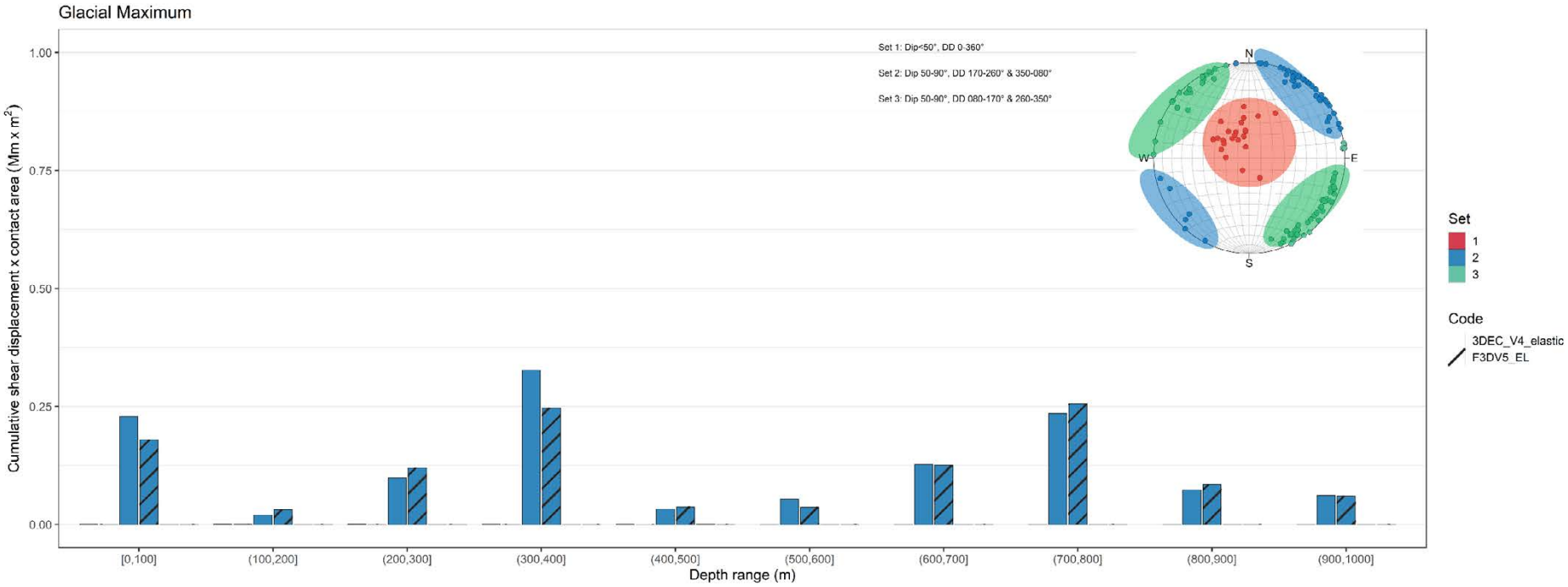

Figure A5-1. *Cumulative shear displacement multiplied by associated area versus depth for major orientations sets of DZ for 3DEC and FLAC3D after the glacial maximum in fully elastic Phase 1 simulations.*

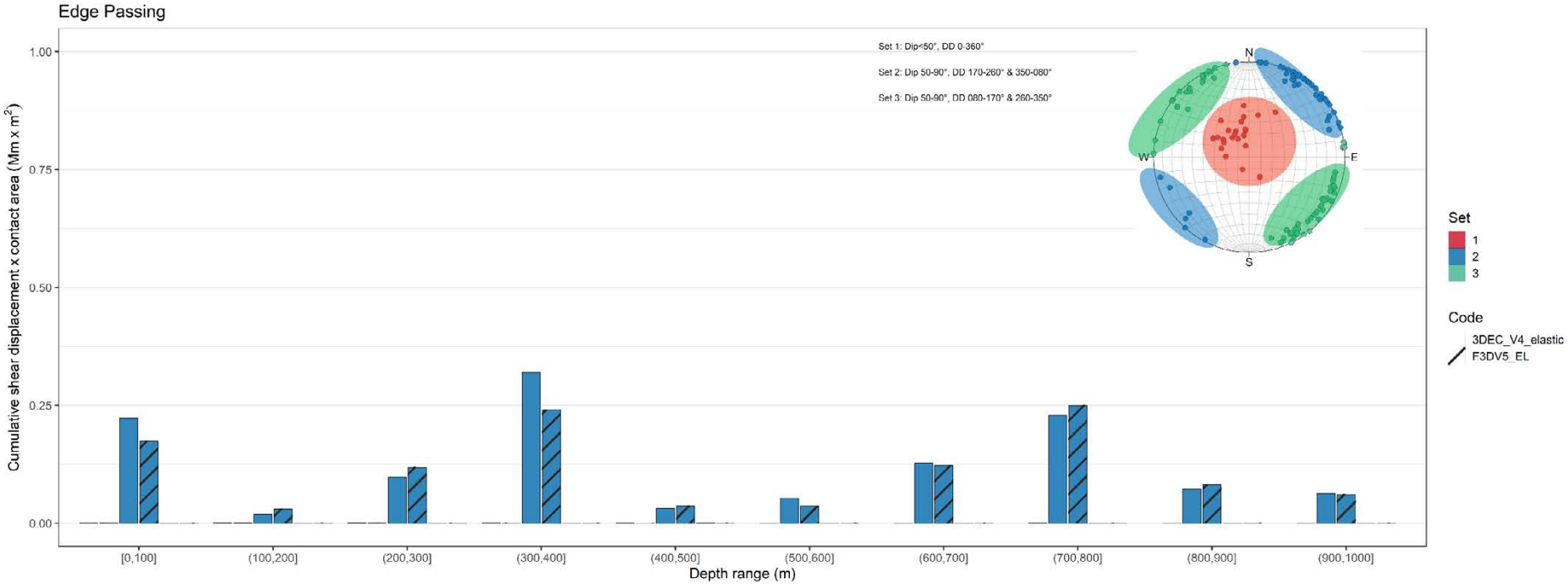

Figure A5-2. *Cumulative shear displacement multiplied by associated area versus depth for major orientation sets of DZ for 3DEC and FLAC3D after the edge passing stage in fully elastic Phase 1 simulations.*

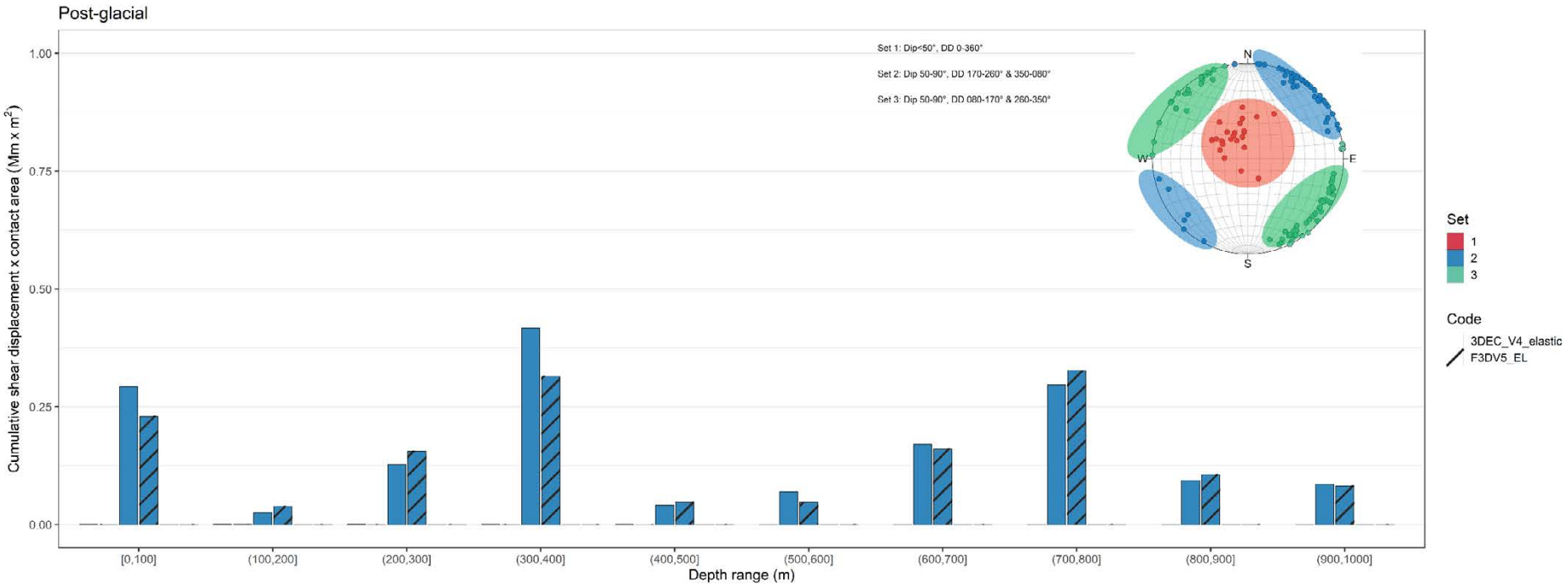

Figure A5-3. *Cumulative shear displacement multiplied by associated area versus depth for major orientation sets of DZ for 3DEC and FLAC3D after glaciation in fully elastic Phase 1 simulations.*

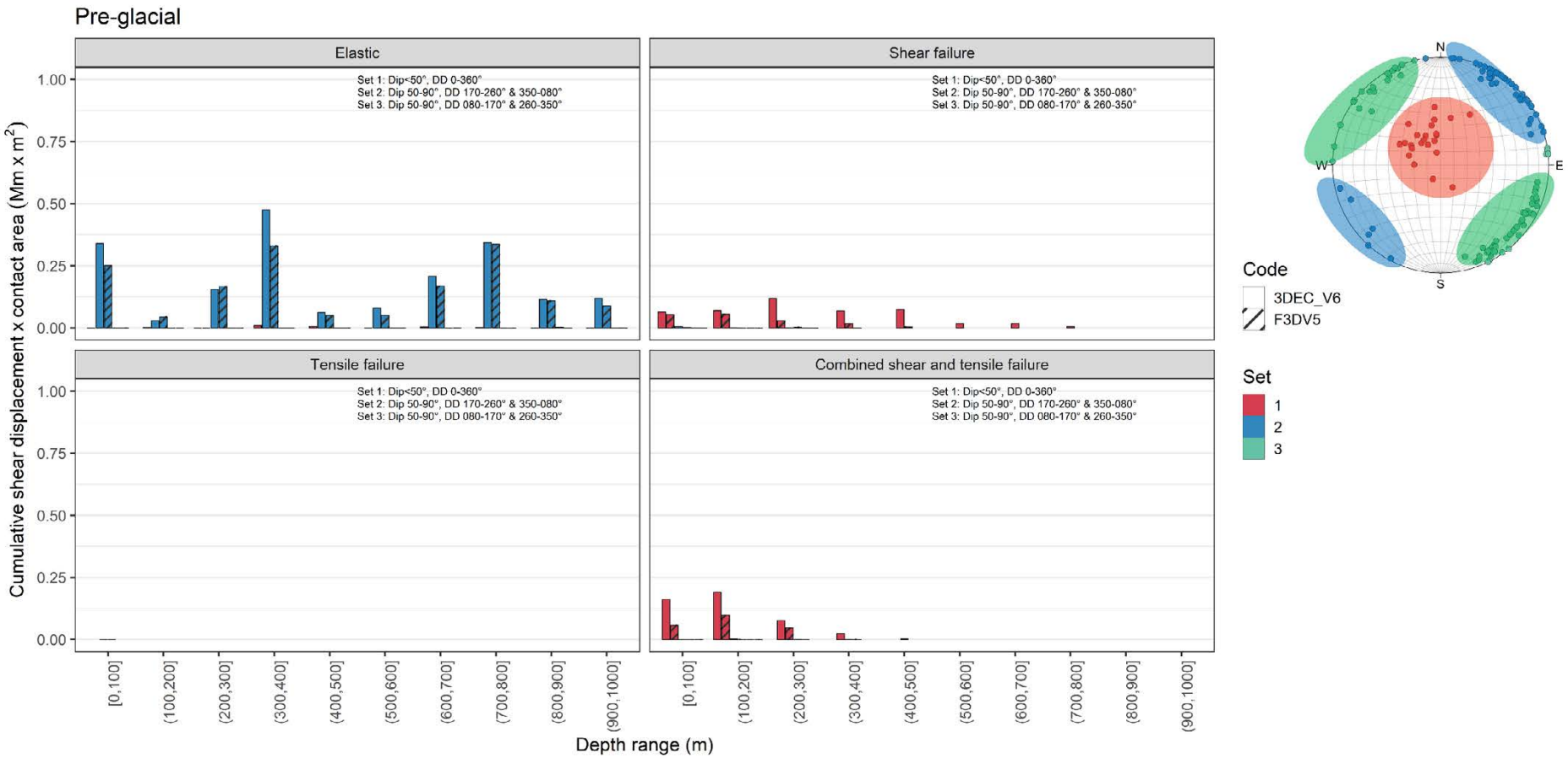

Figure A5-4. *Cumulative shear displacement multiplied by associated area versus depth for major orientation sets of DZ for 3DEC and FLAC3D before glaciation in elastoplastic Phase 1 simulations.*

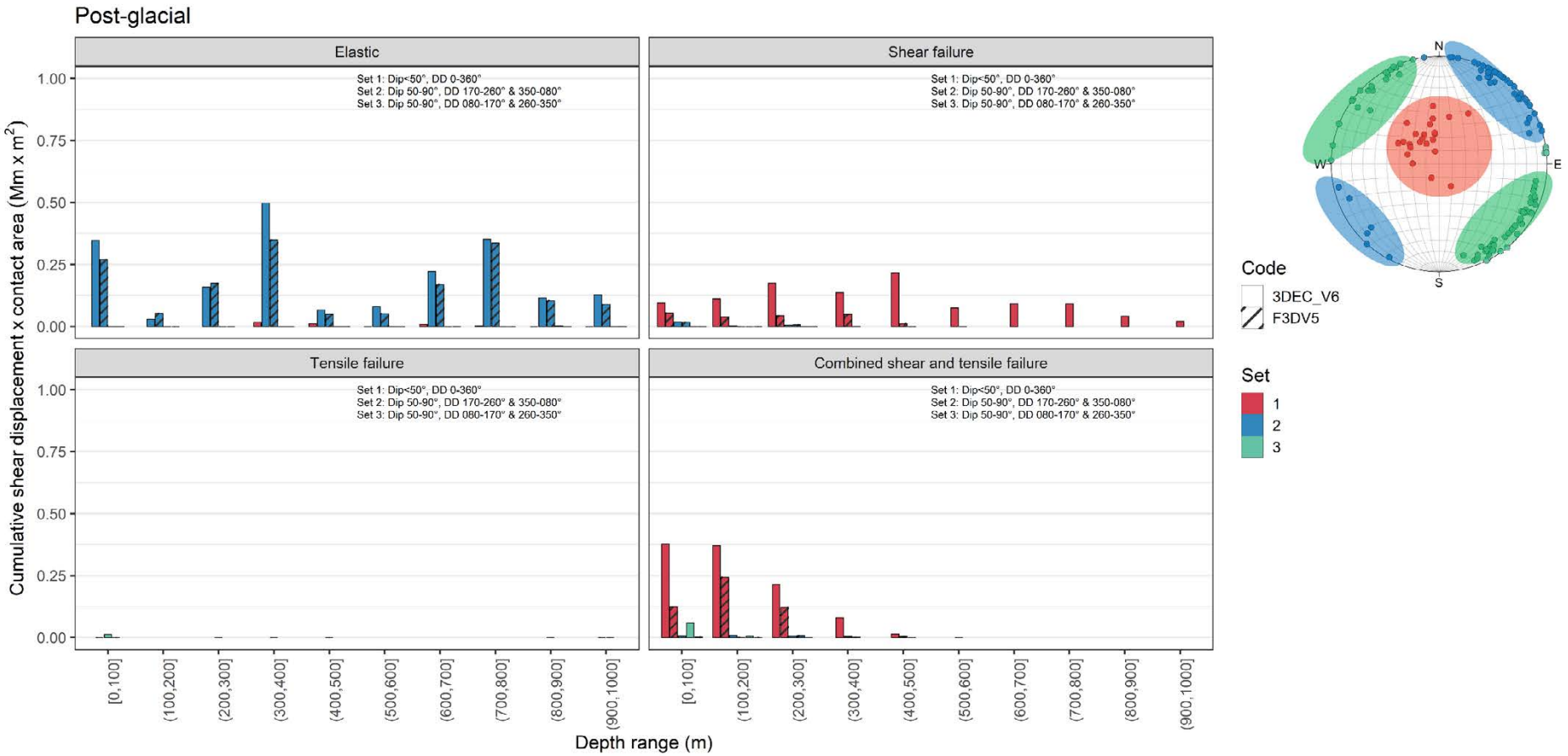

Figure A5-5. *Cumulative shear displacement multiplied by associated area versus depth for major orientation sets of DZ for 3DEC and FLAC3D after glaciation in elastoplastic Phase 1 simulations.*

Appendix 6

Phase 2 deformation zone slip histograms

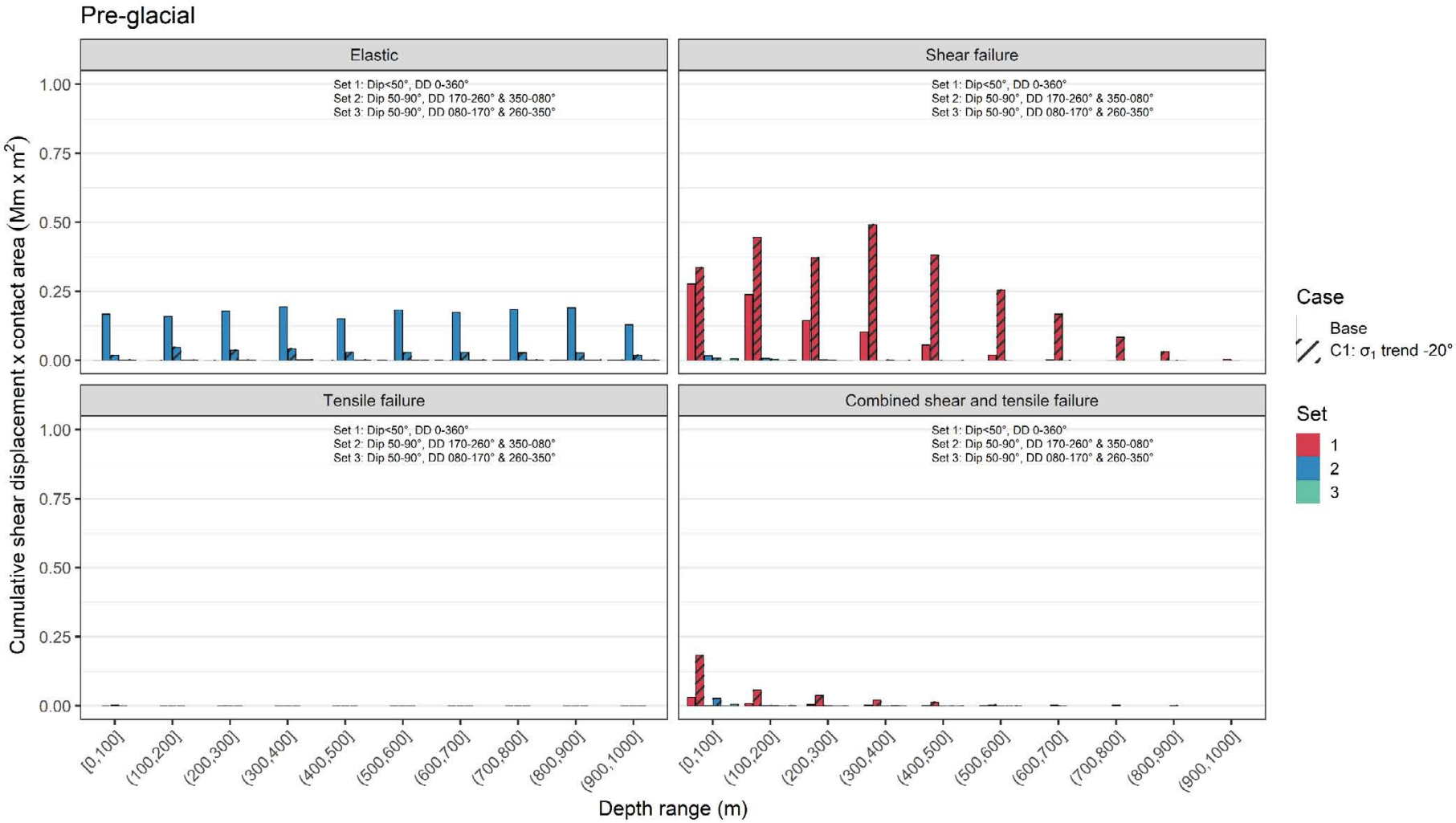

Figure A6-1. *Cumulative shear displacement multiplied by associated area versus depth for major orientation sets of DZ for the Base case and Case 1 of Phase 2 before glaciation.*

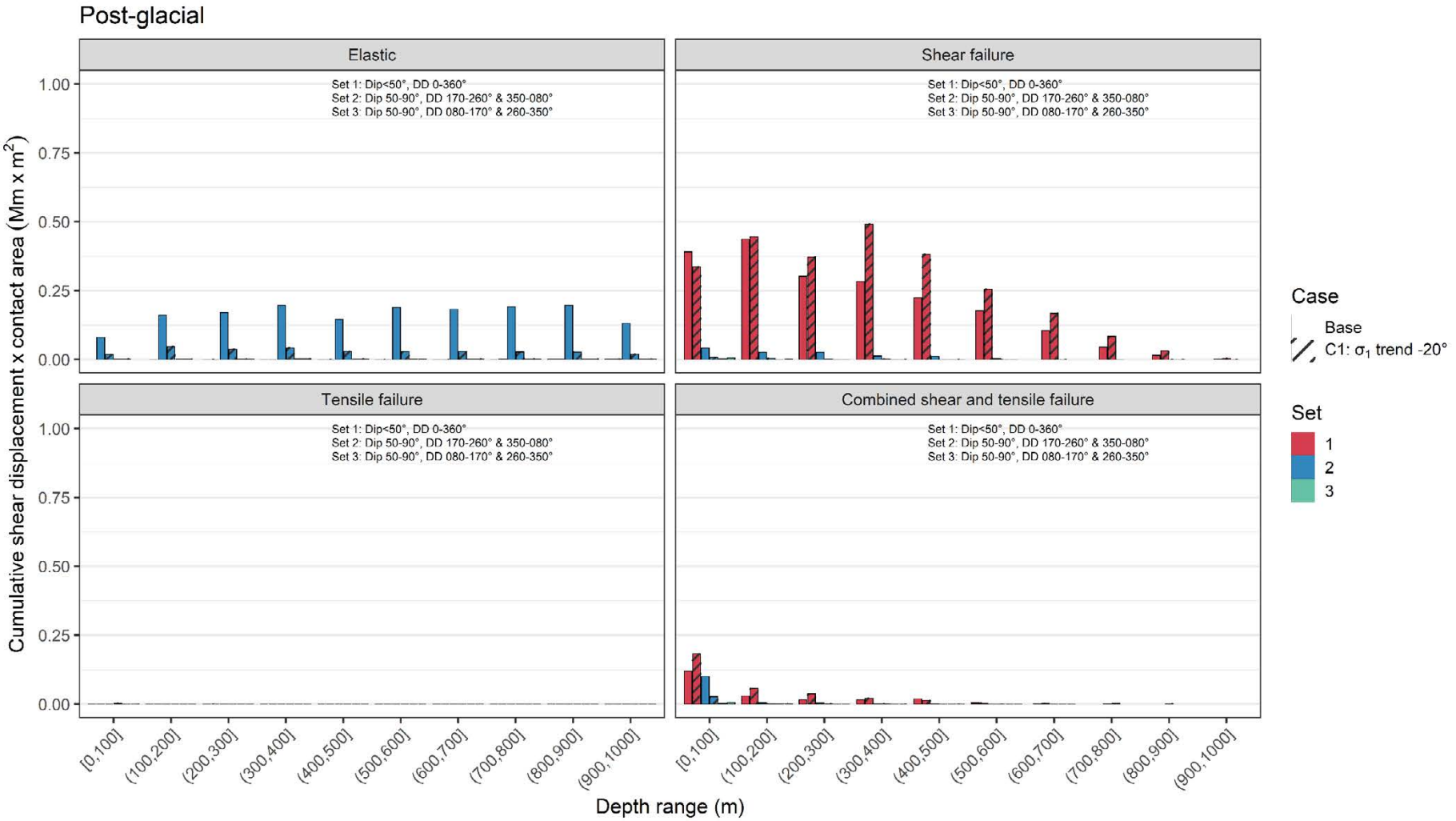

Figure A6-2. *Cumulative shear displacement multiplied by associated area versus depth for major orientation sets of DZ for the Base case and Case 1 of Phase 2 after glaciation.*

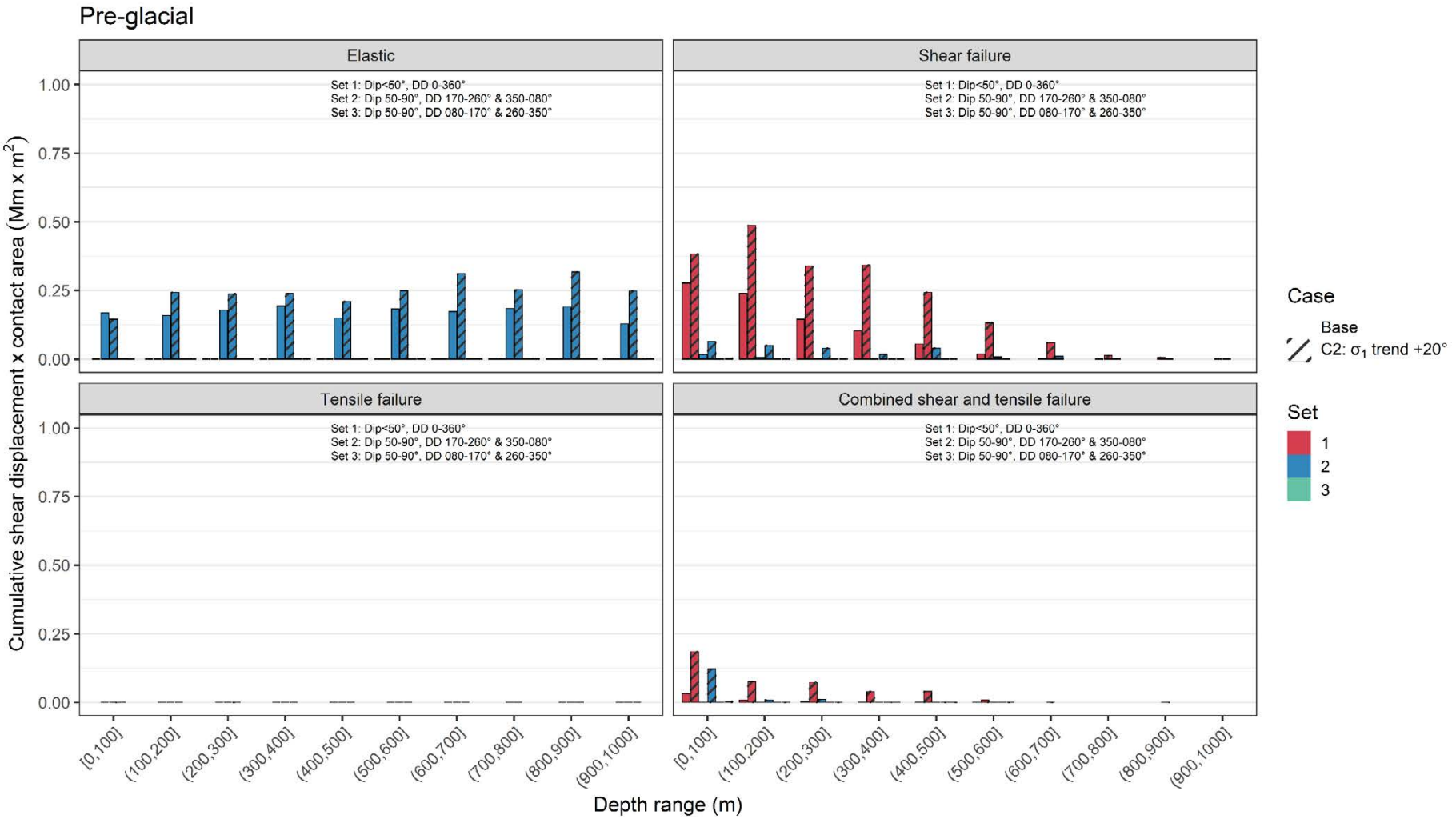

Figure A6-3. *Cumulative shear displacement multiplied by associated area versus depth for major orientation sets of DZ for the Base case and Case 2 of Phase 2 before glaciation.*

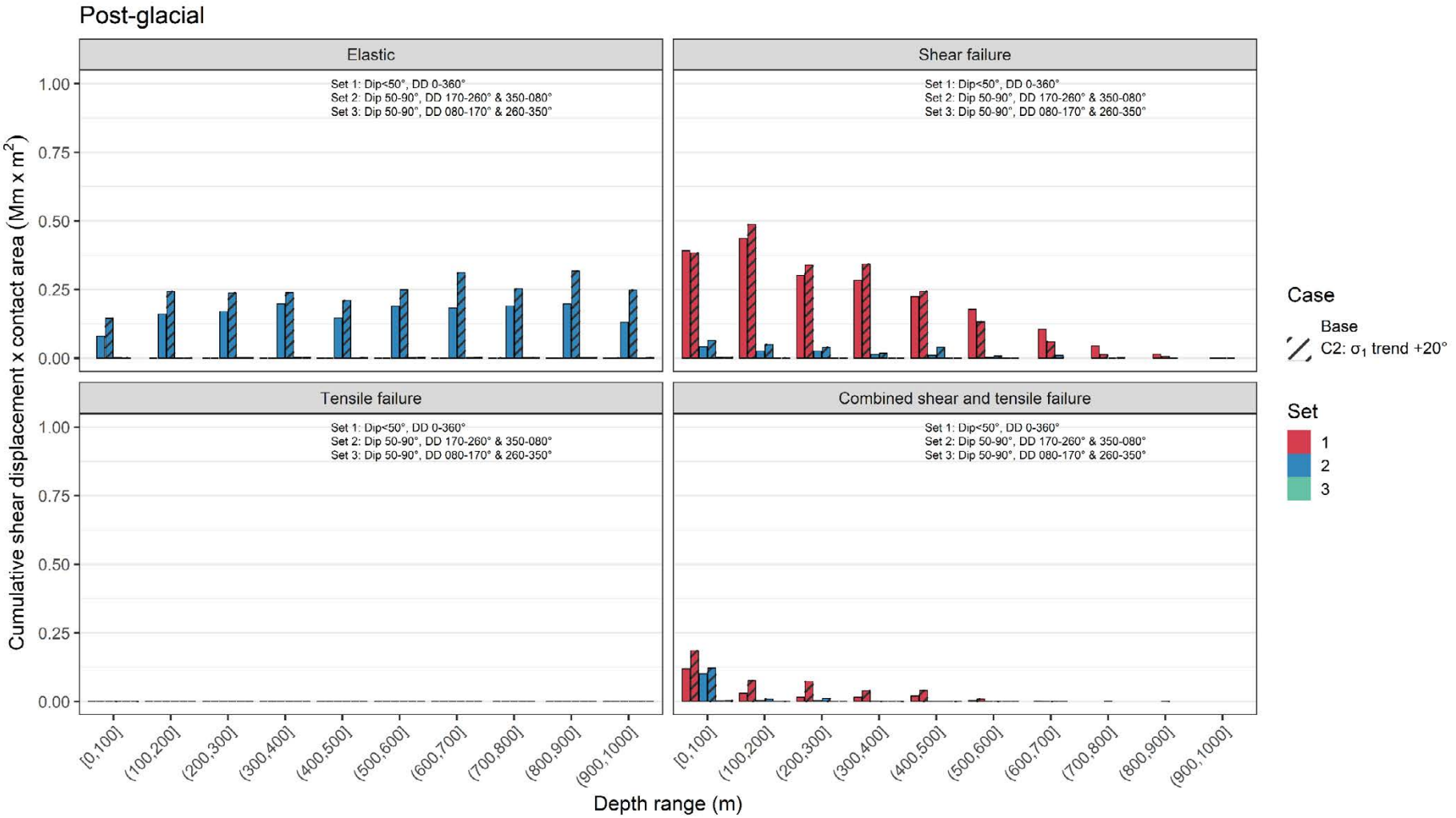

Figure A6-4. *Cumulative shear displacement multiplied by associated area versus depth for major orientation sets of DZ for the Base case and Case 2 of Phase 2 after glaciation.*

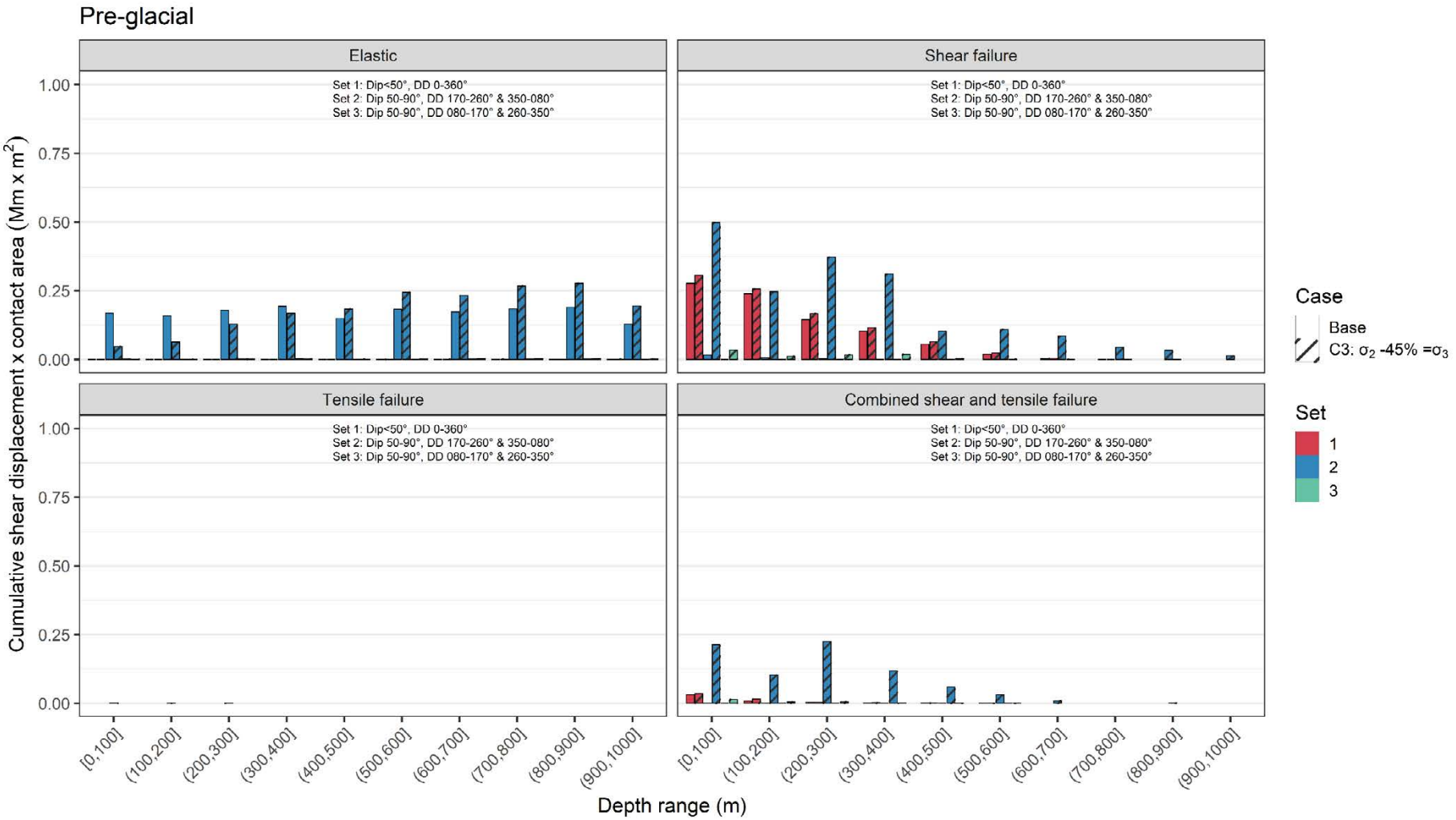

Figure A6-5. *Cumulative shear displacement multiplied by associated area versus depth for major orientation sets of DZ for the Base case and Case 3 of Phase 2 before glaciation.*

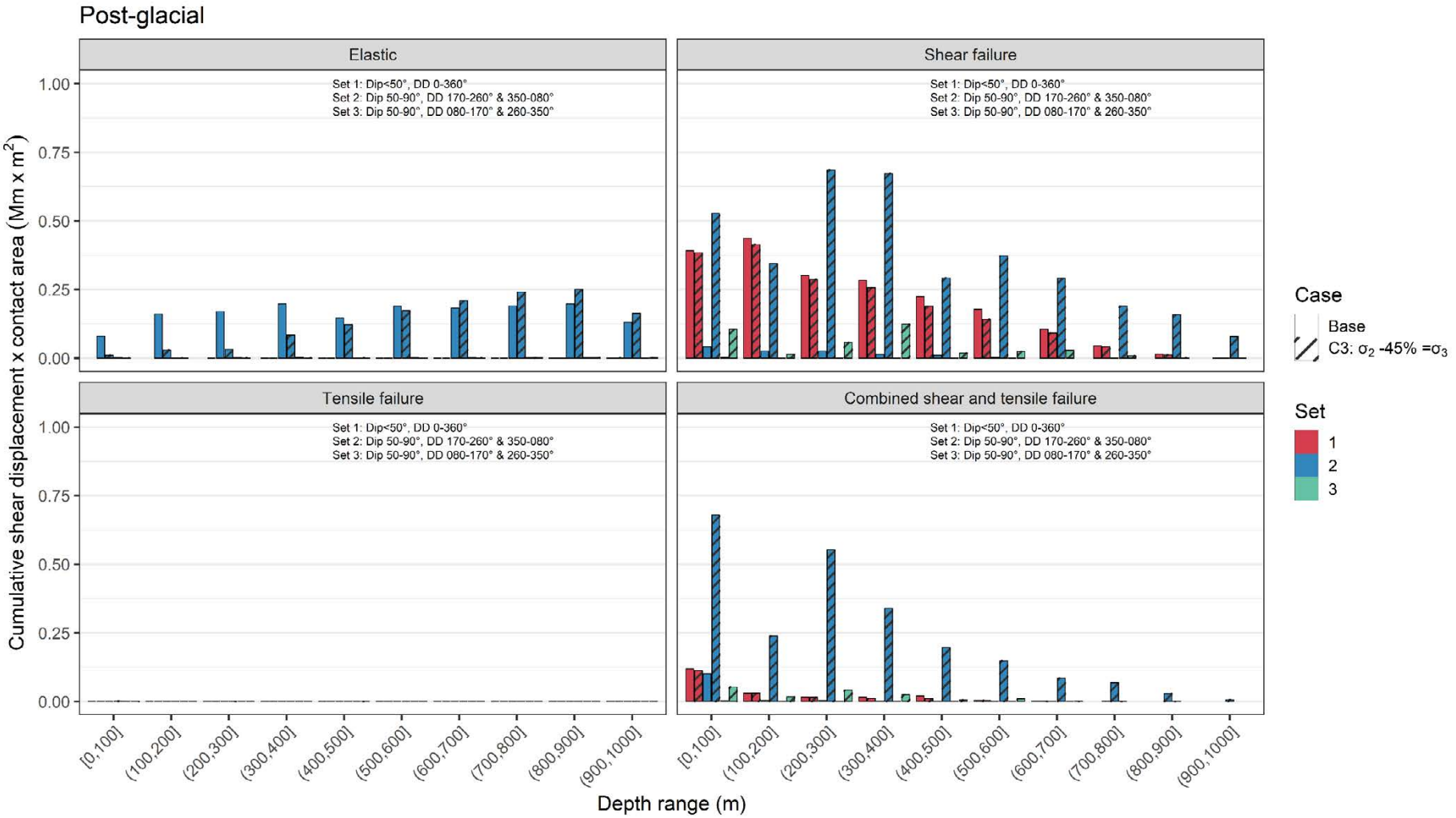

Figure A6-6. *Cumulative shear displacement multiplied by associated area versus depth for major orientation sets of DZ for the Base case and Case 3 of Phase 2 after glaciation.*

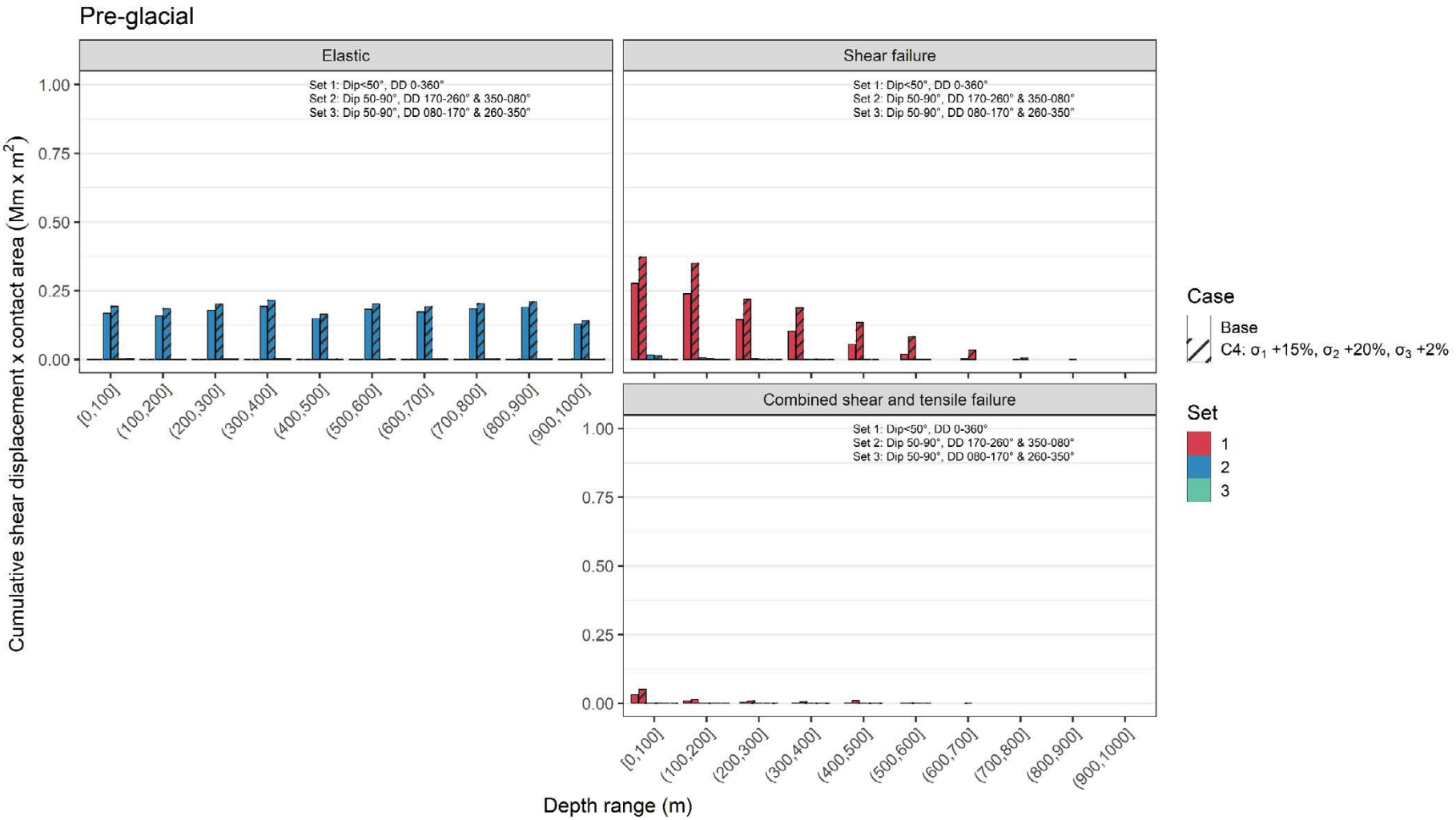

Figure A6-7. *Cumulative shear displacement multiplied by associated area versus depth for major orientation sets of DZ for the Base case and Case 4 of Phase 2 before glaciation.*

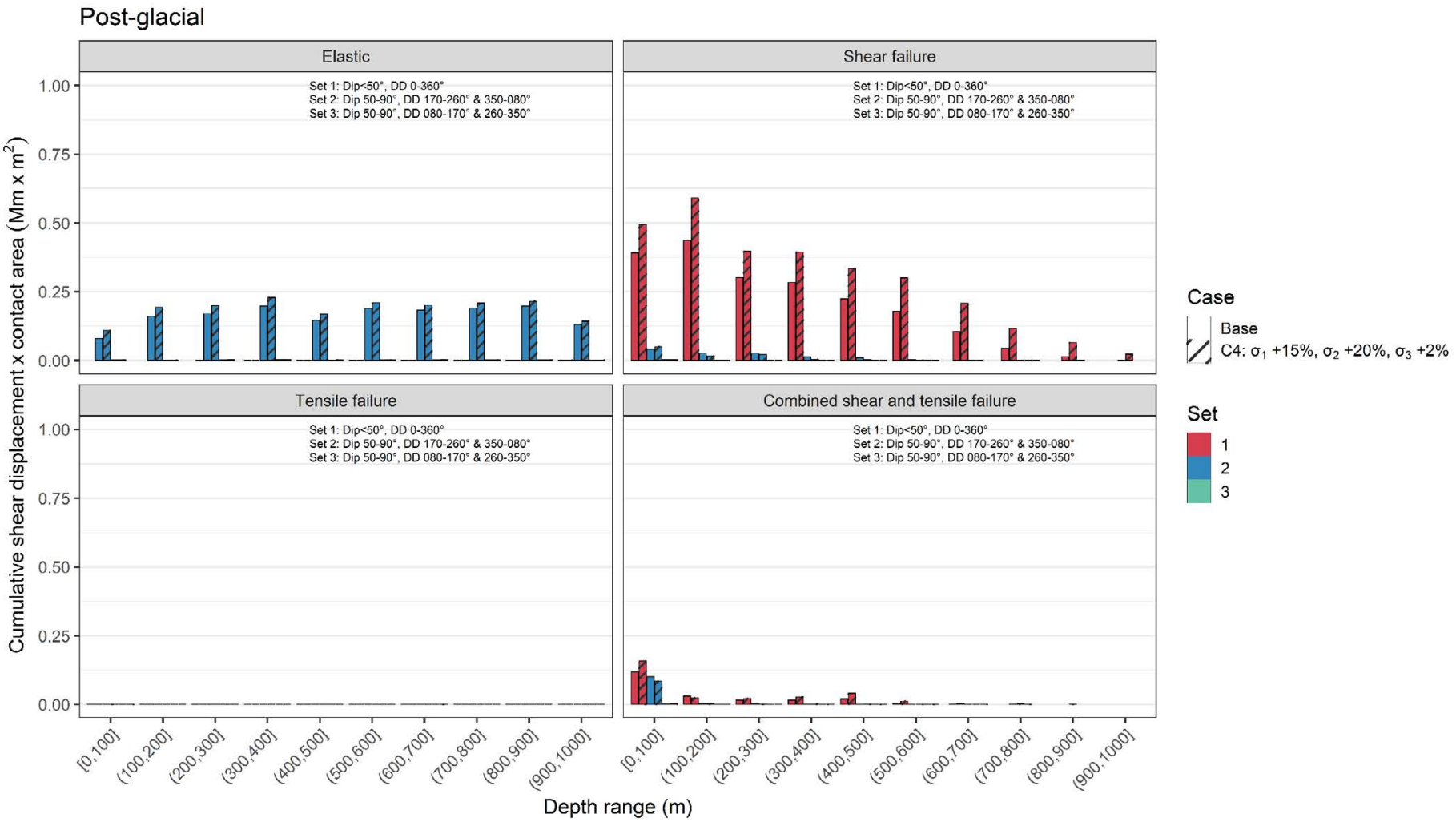

Figure A6-8. *Cumulative shear displacement multiplied by associated area versus depth for major orientation sets of DZ for the Base case and Case 4 of Phase 2 after glaciation.*

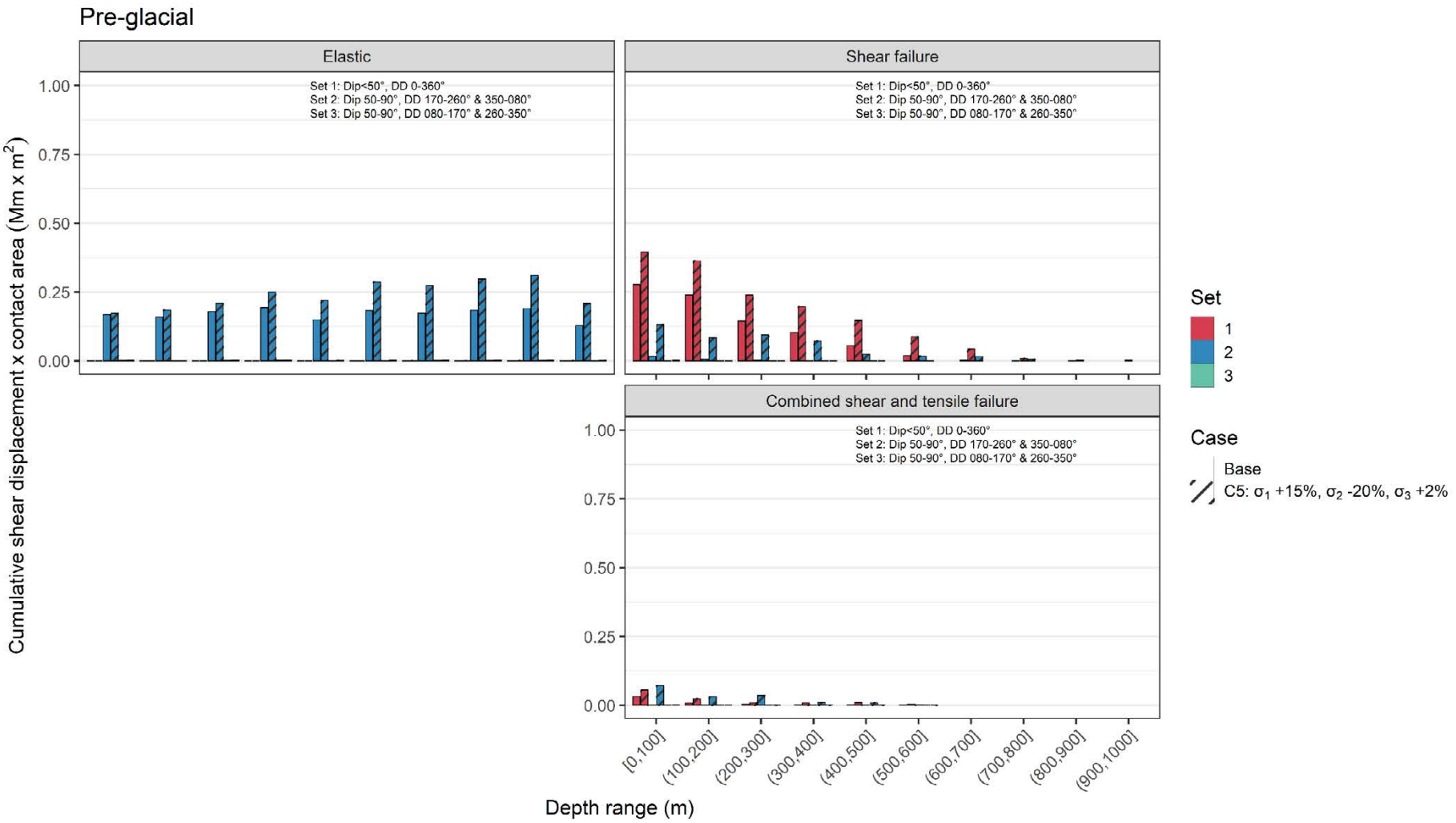

Figure A6-9. *Cumulative shear displacement multiplied by associated area versus depth for major orientation sets of DZ for the Base case and Case 5 of Phase 2 before glaciation.*

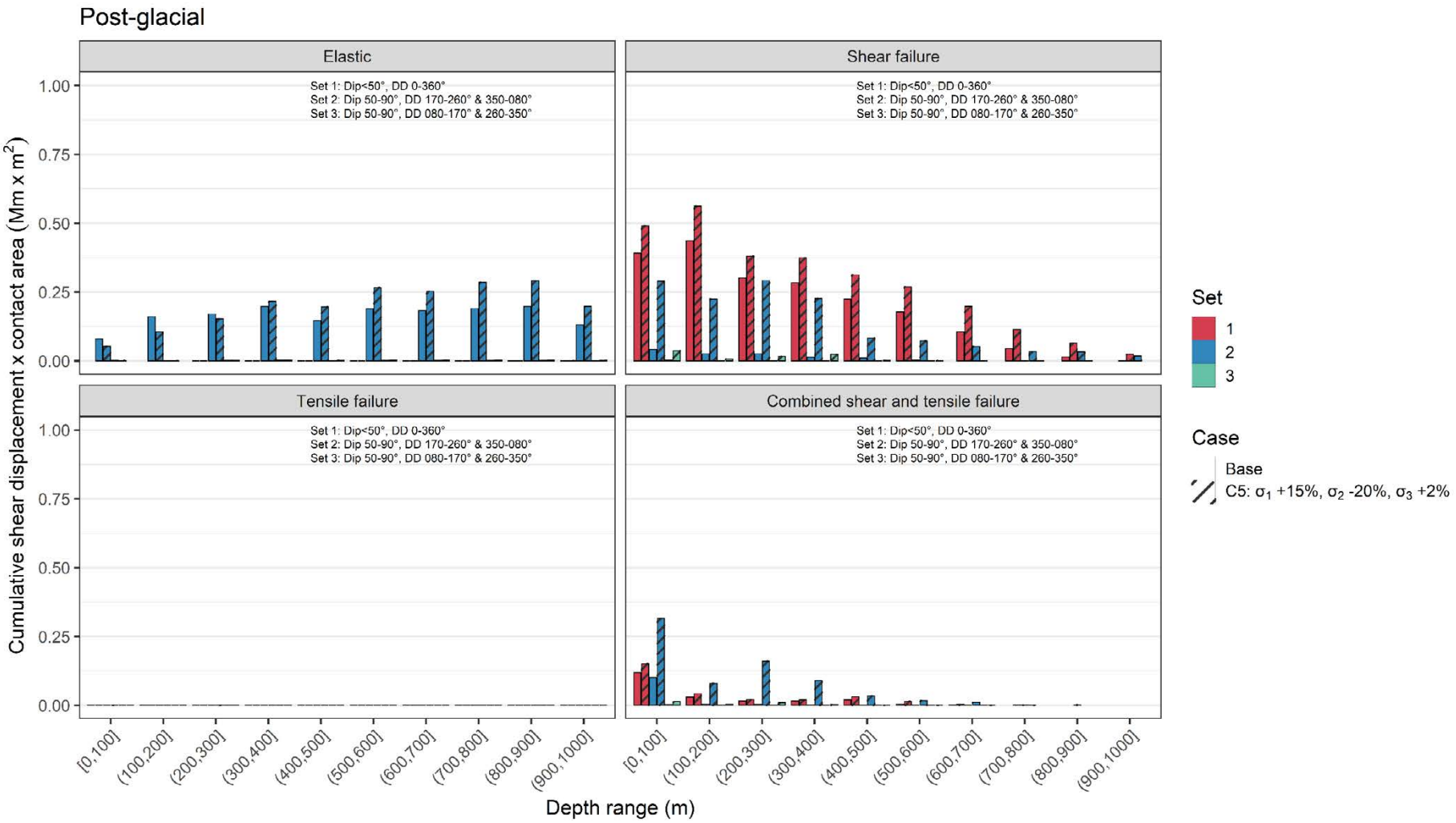

Figure A6-10. *Cumulative shear displacement multiplied by associated area versus depth for major orientation sets of DZ for the Base case and Case 5 of Phase 2 after glaciation.*

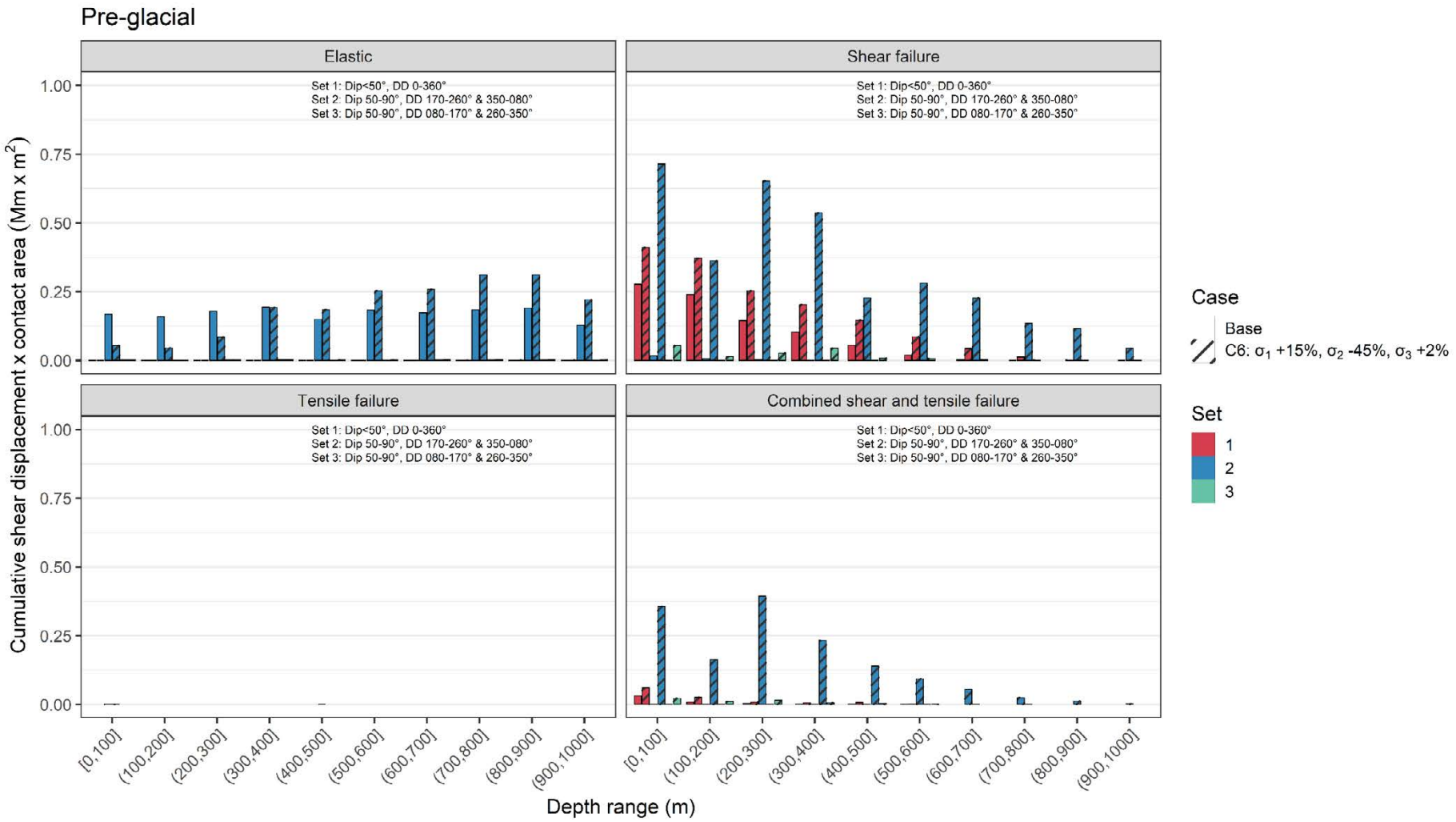

Figure A6-11. *Cumulative shear displacement multiplied by associated area versus depth for major orientation sets of DZ for the Base case and Case 6 of Phase 2 before glaciation.*

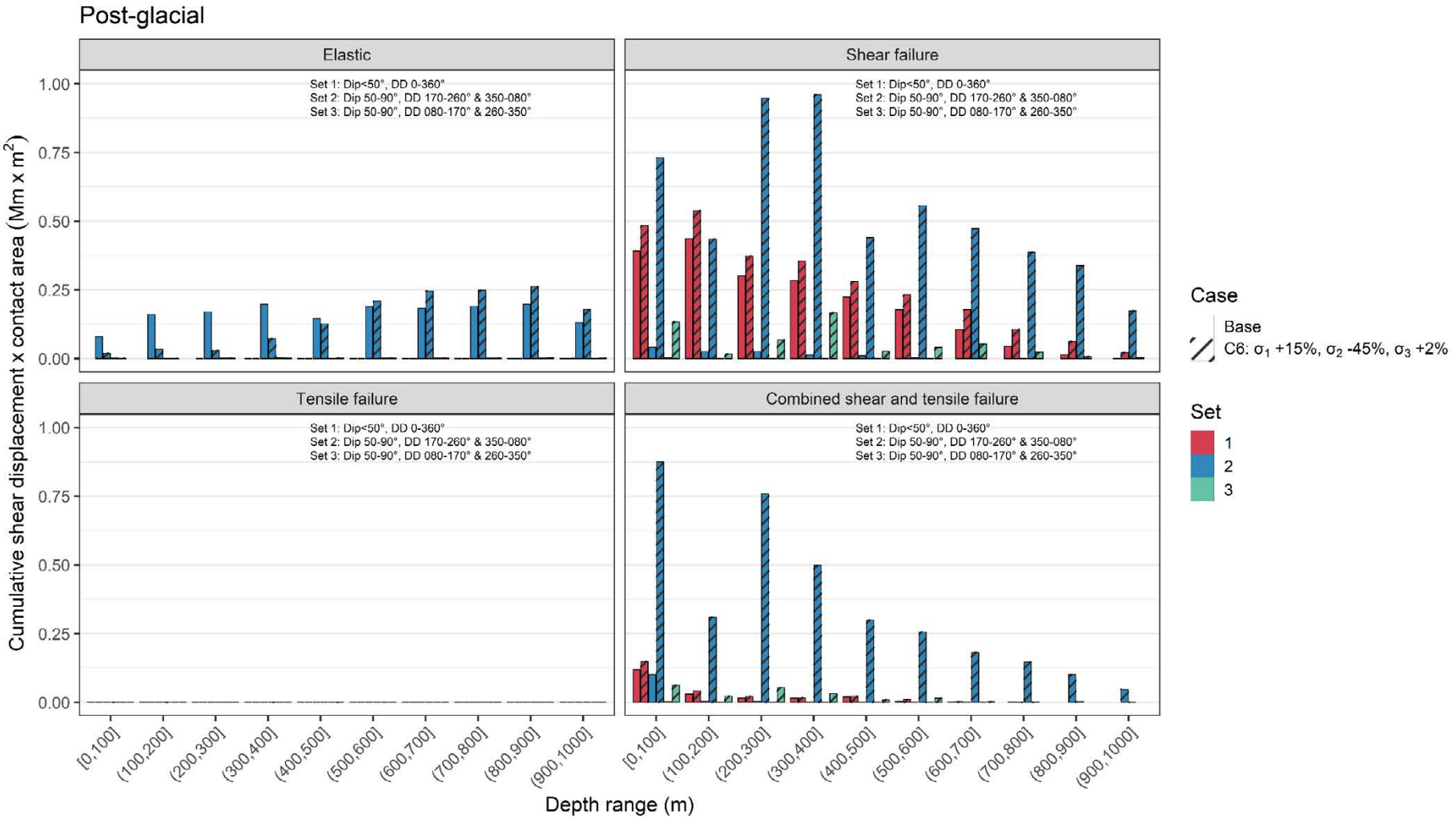

Figure A6-12. *Cumulative shear displacement multiplied by associated area versus depth for major orientation sets of DZ for the Base case and Case 6 of Phase 2 after glaciation.*

Appendix 7

Phase 1 mean and variation of σ_1 magnitude, trend and σ_1/σ_2 ratio for hundred meter intervals (95 % variation interval)

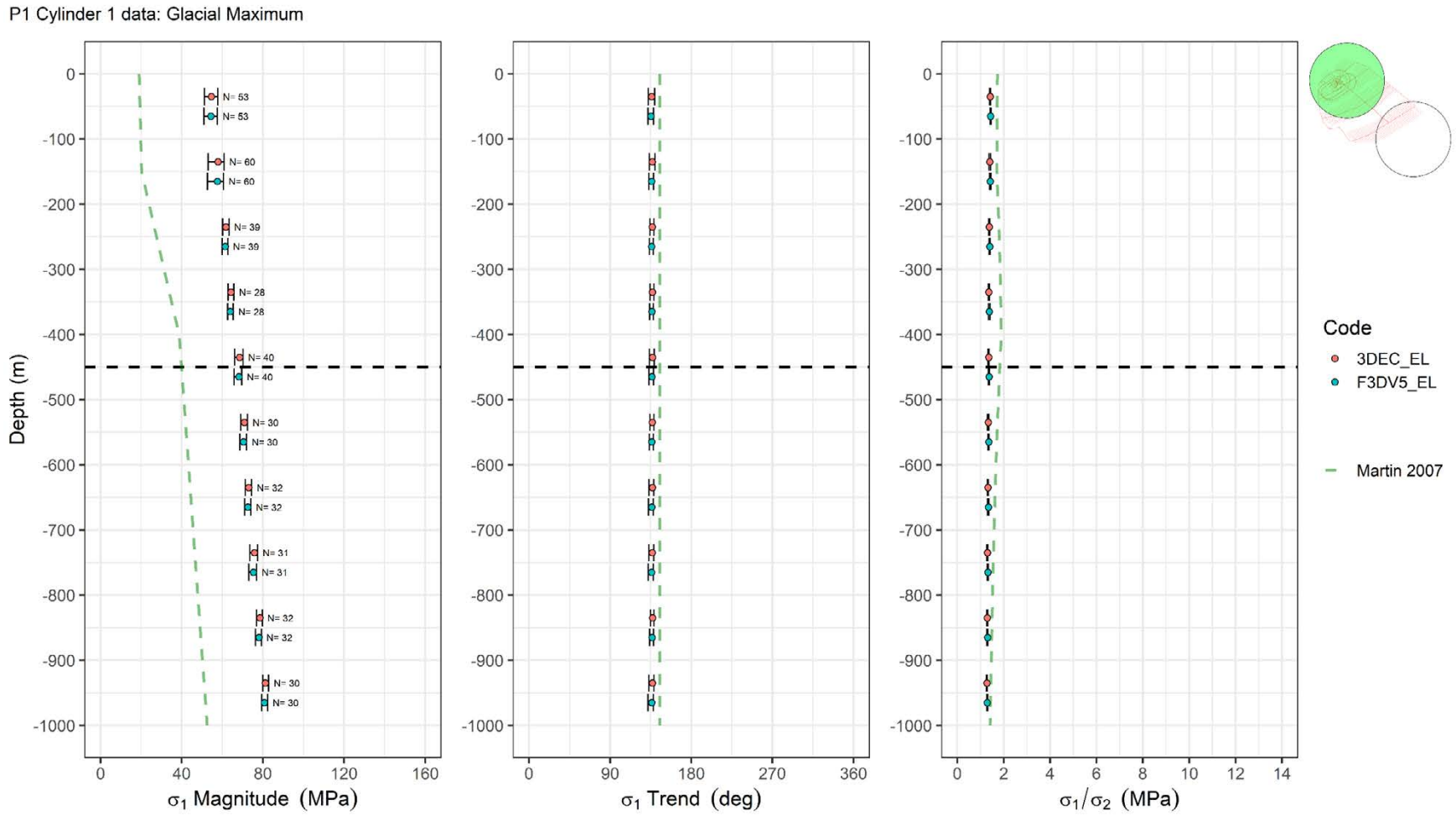

Figure A7-1. *Mean and 95 % variation interval of σ_1 magnitude and trend at hundred meter intervals for 3DEC and FLAC3D after the glacial maximum in Phase 1 elastic simulations for cylinder 1 (top right:green). The Martin (2007) interpretation is indicated with a green dashed line and the repository depth with a horizontal dashed black line.*

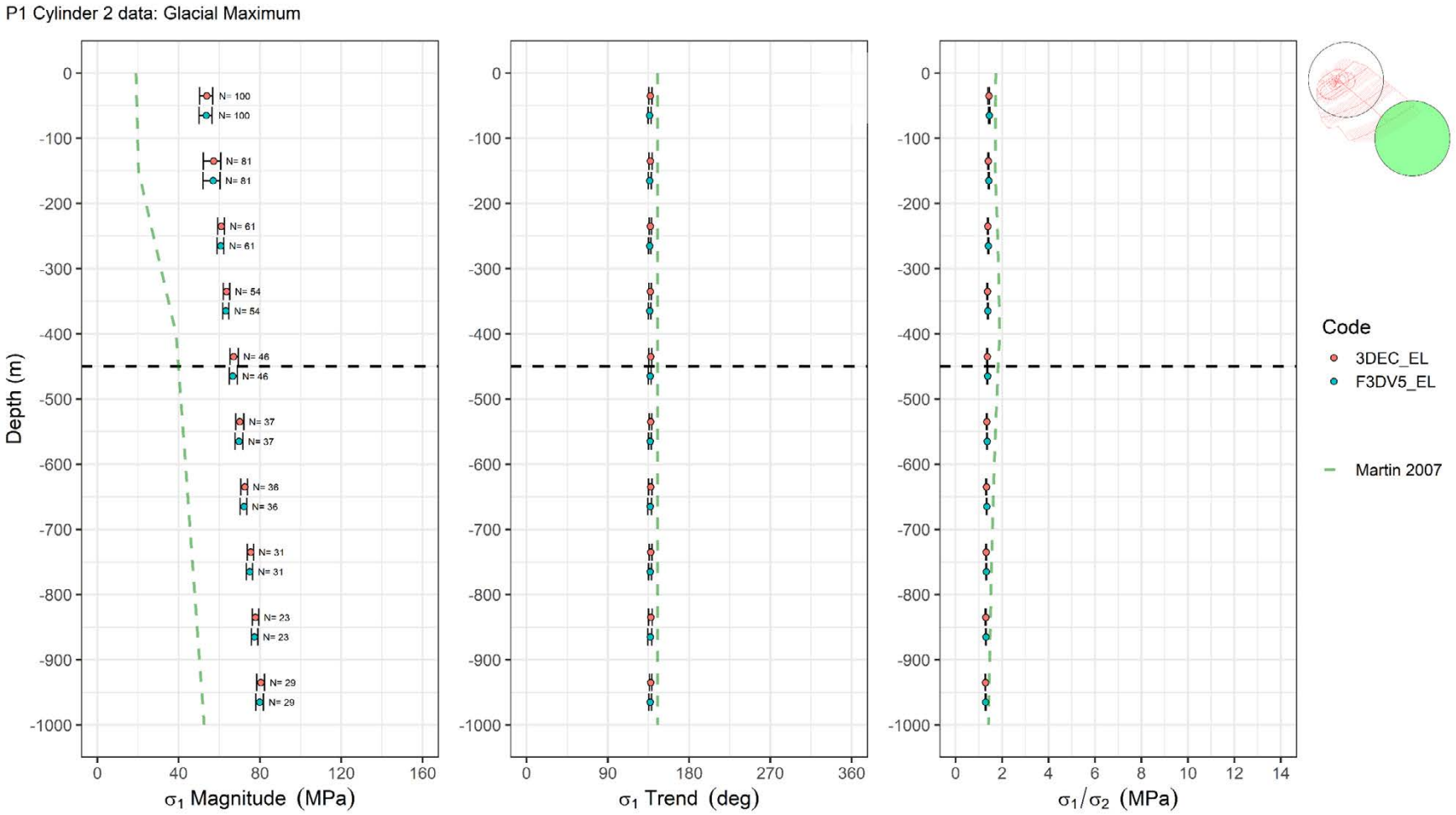

Figure A7-2. *Mean and 95 % variation interval of σ_1 magnitude and trend at hundred meter intervals for 3DEC and FLAC3D after the glacial maximum in Phase 1 elastic simulations for cylinder 2 (top right:green). The Martin (2007) interpretation is indicated with a green dashed line and the repository depth with a horizontal dashed black line.*

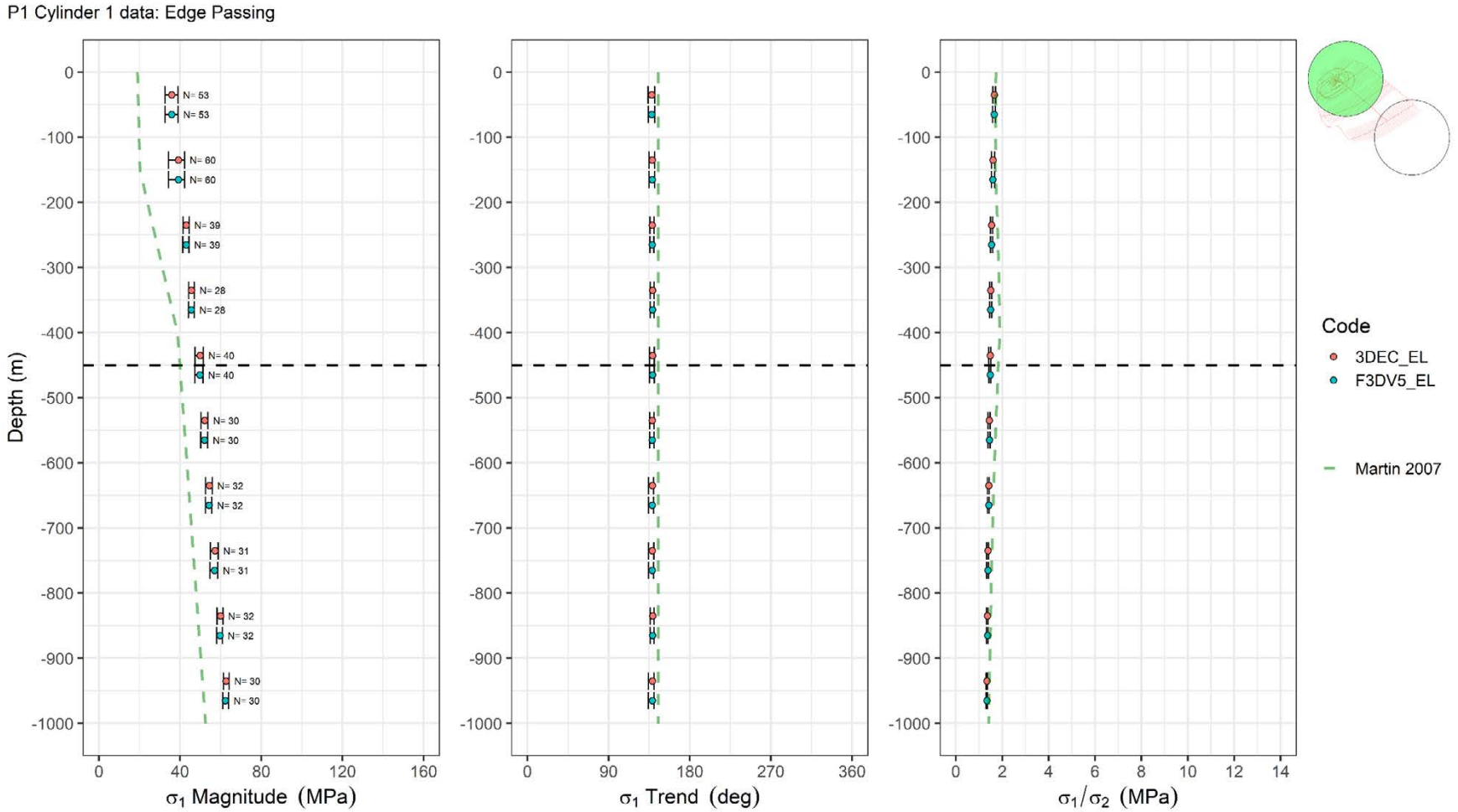

Figure A7-3. *Mean and 95 % variation interval of σ_1 magnitude and trend at hundred meter intervals for 3DEC and FLAC3D after the edge passing stage in Phase 1 elastic simulations for cylinder 1 (top right:green). The Martin (2007) interpretation is indicated with a green dashed line and the repository depth with a horizontal dashed black line.*

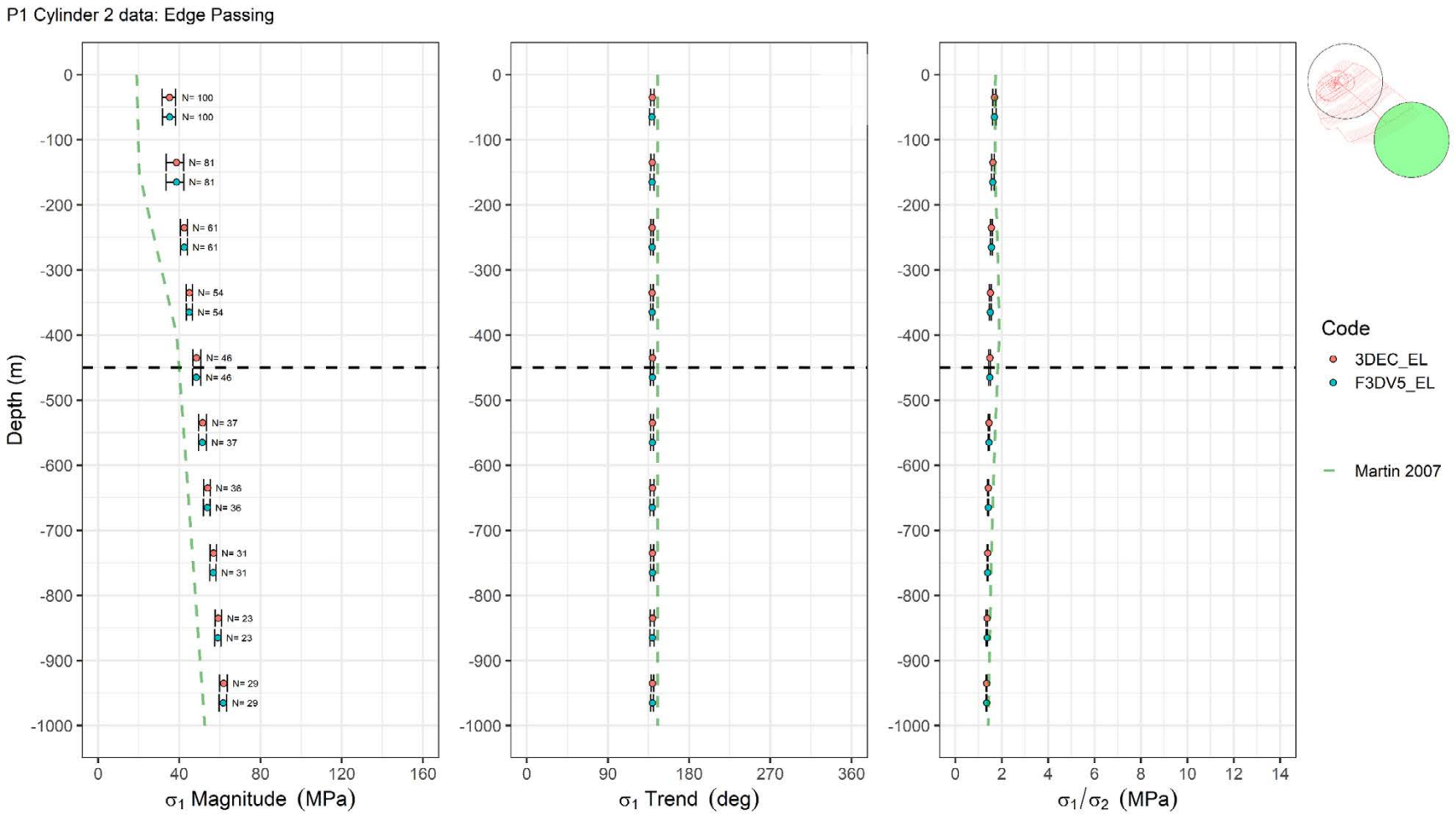

Figure A7-4. *Mean and 95 % variation interval of σ_1 magnitude and trend at hundred meter intervals for 3DEC and FLAC3D after the edge passing stage in Phase 1 elastic simulations for cylinder 2 (top right:green). The Martin (2007) interpretation is indicated with a green dashed line and the repository depth with a horizontal dashed black line.*

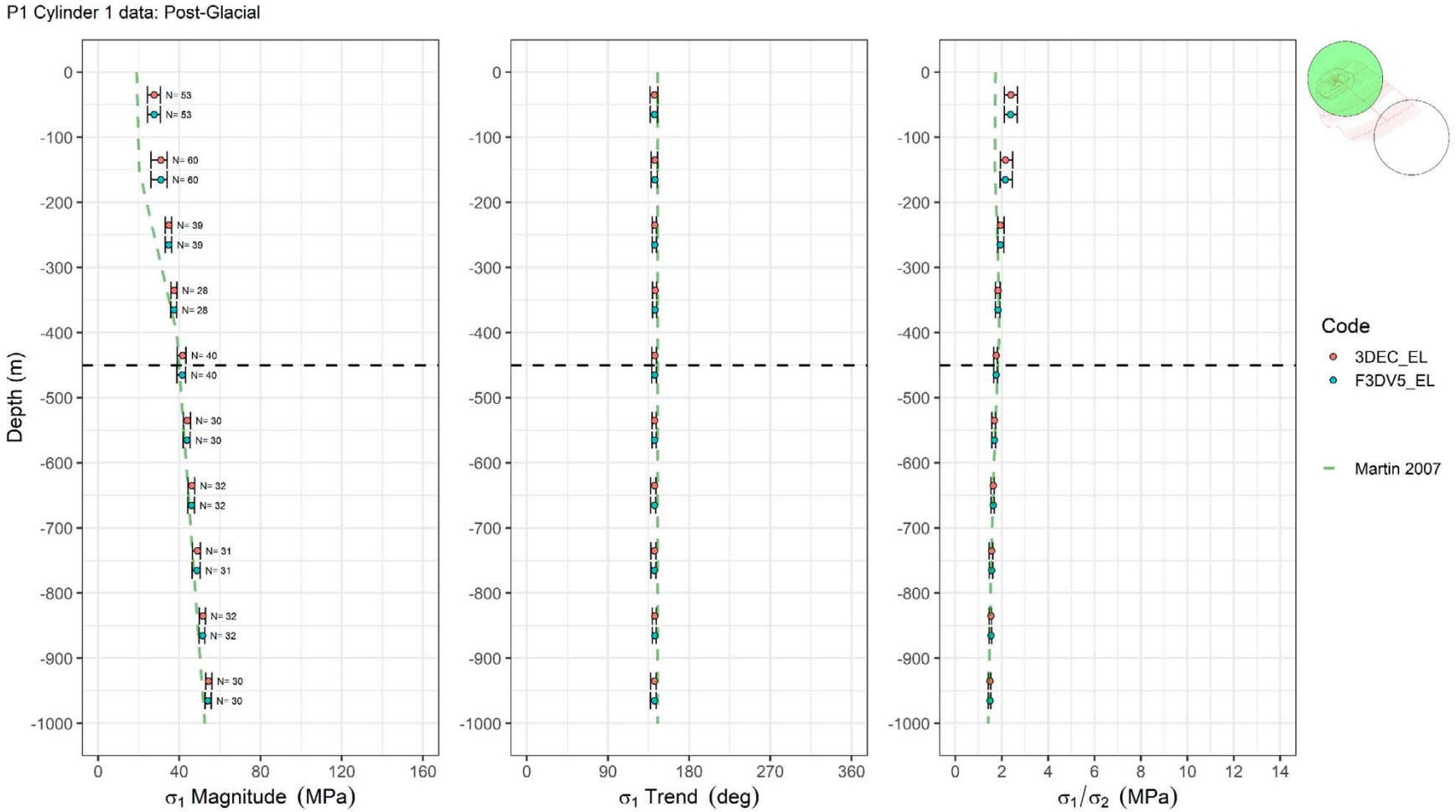

Figure A7-5. *Mean and 95 % variation interval of σ_1 magnitude and trend at hundred meter intervals for 3DEC and FLAC3D after glaciation in Phase 1 elastic simulations for cylinder 1 (top right:green). The Martin (2007) interpretation is indicated with a green dashed line and the repository depth with a horizontal dashed black line.*

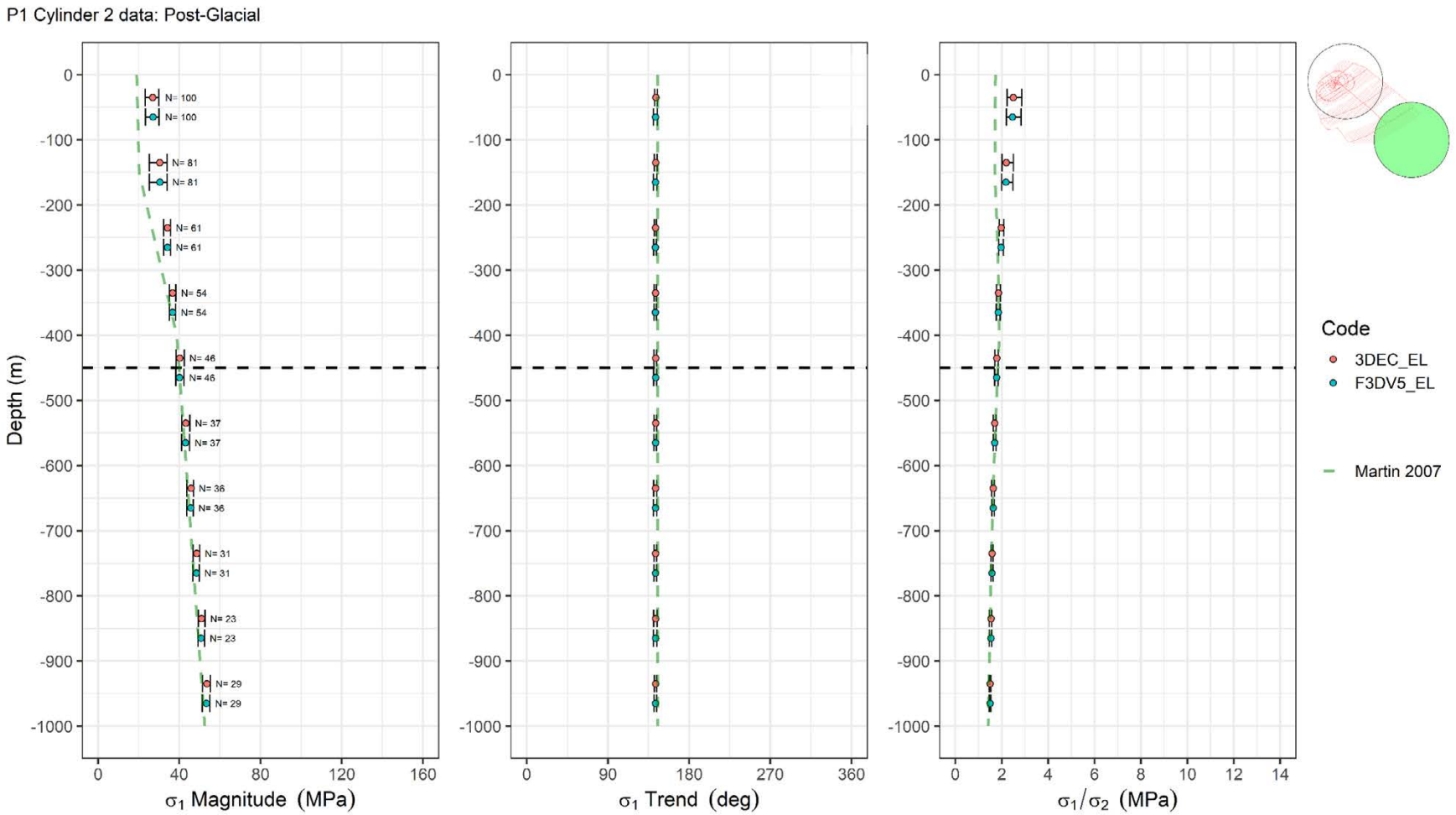

Figure A7-6. *Mean and 95 % variation interval of σ_1 magnitude and trend at hundred meter intervals for 3DEC and FLAC3D after glaciation in Phase 1 elastic simulations for cylinder 2 (top right:green). The Martin (2007) interpretation is indicated with a green dashed line and the repository depth with a horizontal dashed black line.*

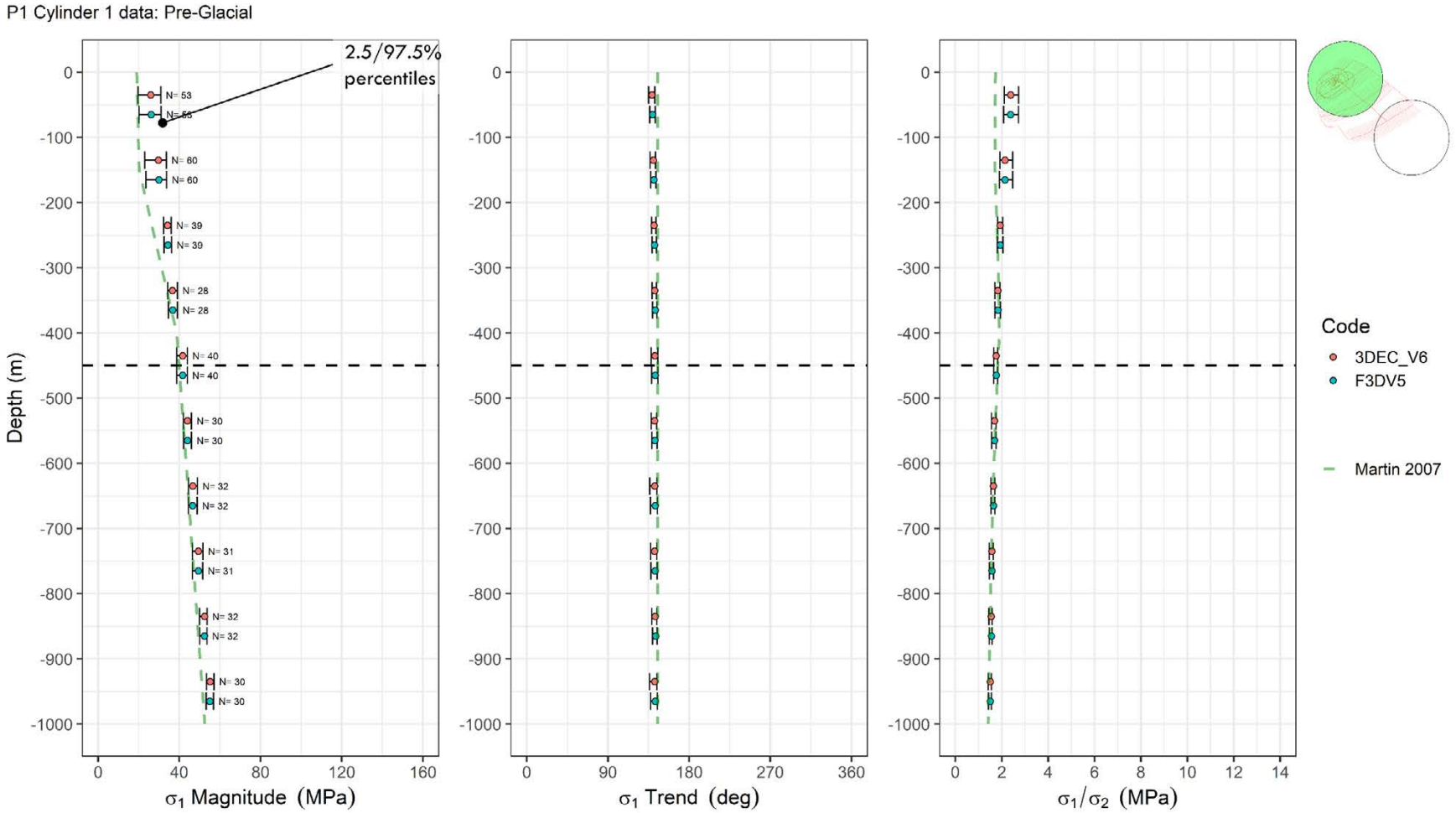

Figure A7-7. *Mean and 95 % variation interval of σ_1 magnitude and trend at hundred meter intervals for 3DEC and FLAC3D before glaciation in Phase 1 elastoplastic simulations for cylinder 1 (top right:green). The Martin (2007) interpretation is indicated with a green dashed line and the repository depth with a horizontal dashed black line.*

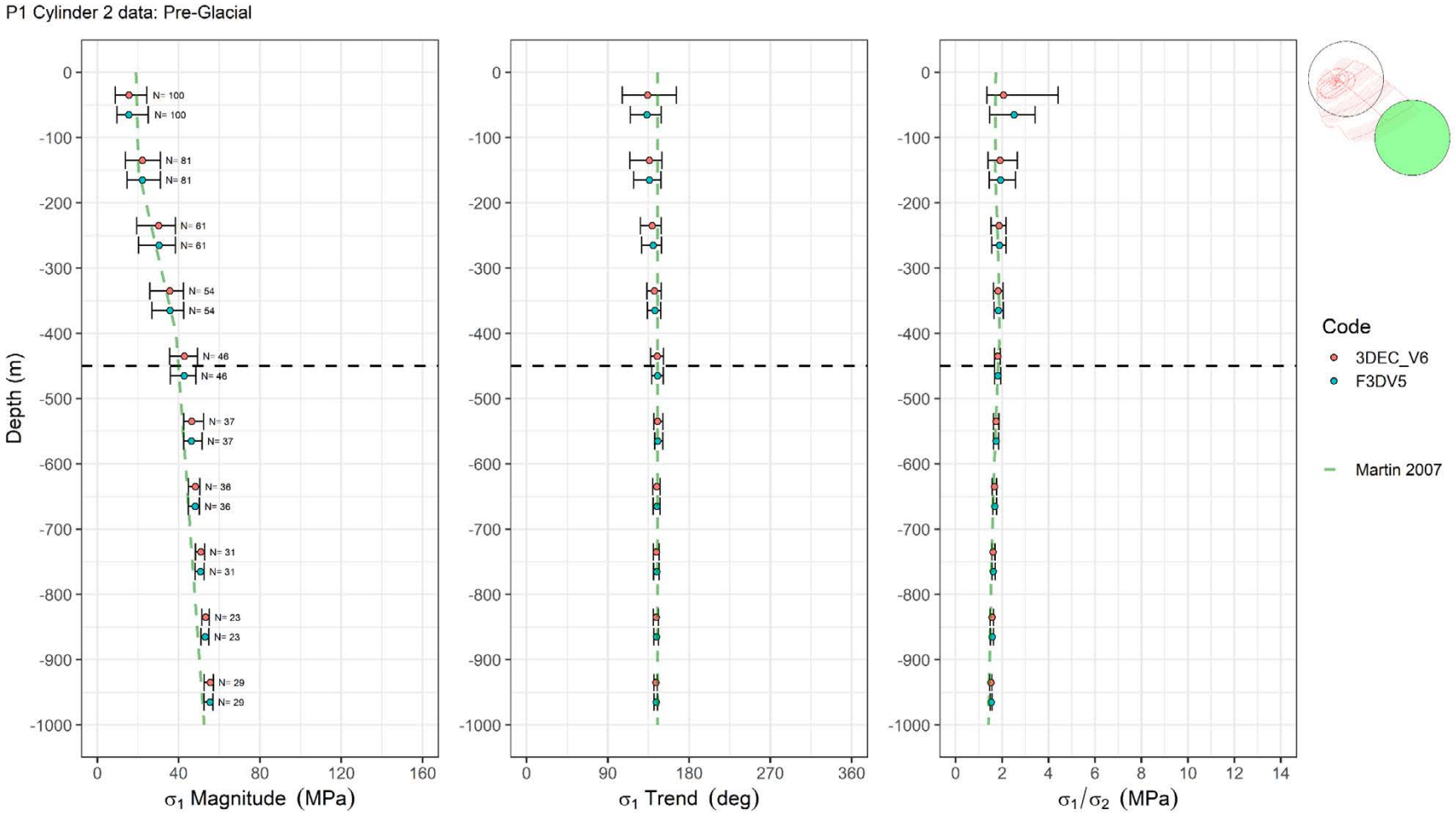

Figure A7-8. *Mean and 95 % variation interval of σ_1 magnitude and trend at hundred meter intervals for 3DEC and FLAC3D before glaciation in Phase 1 elastoplastic simulations for cylinder 2 (top right:green). The Martin (2007) interpretation is indicated with a green dashed line and the repository depth with a horizontal dashed black line.*

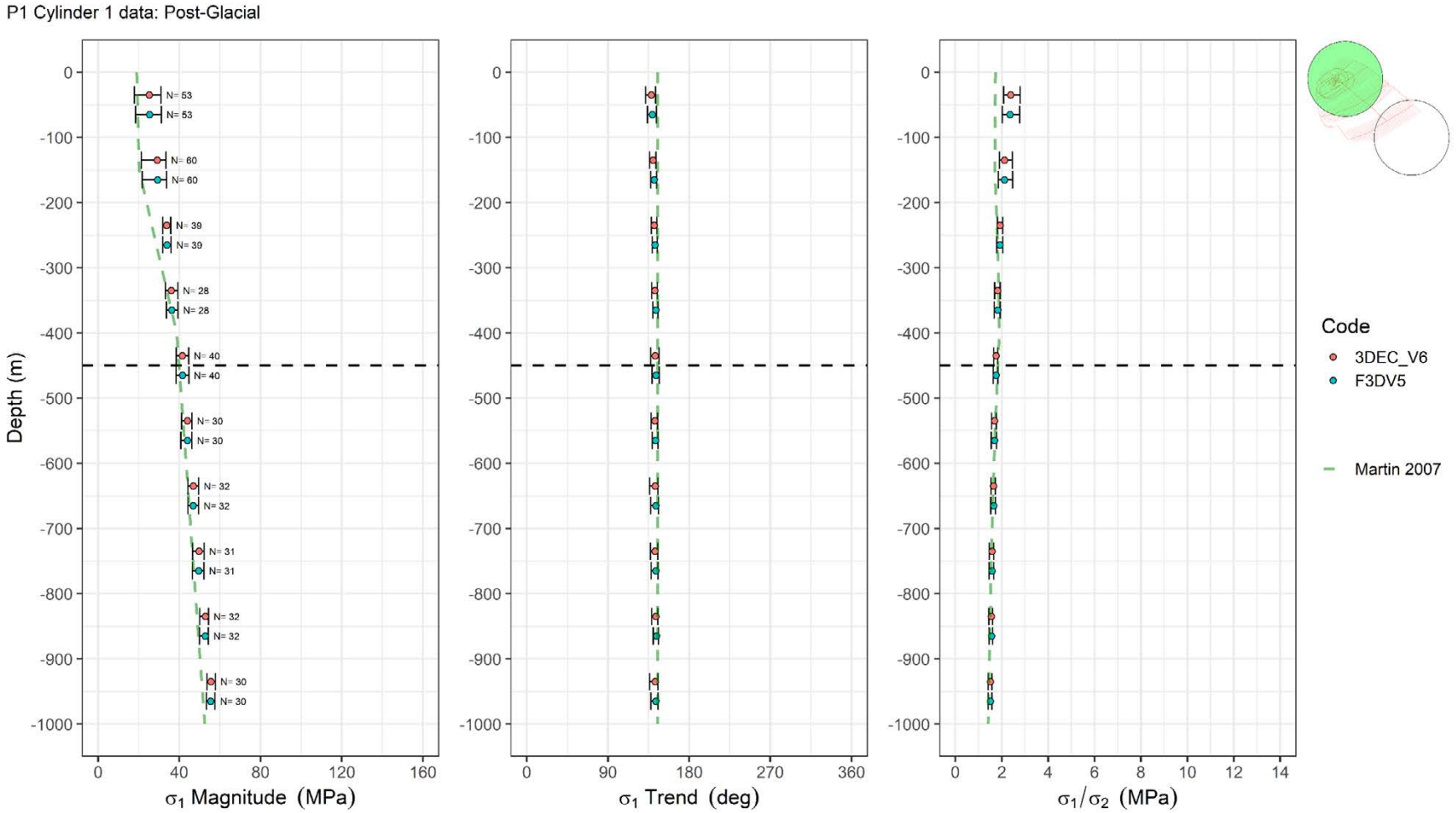

Figure A7-9. *Mean and 95 % variation interval of σ_1 magnitude and trend at hundred meter intervals for 3DEC and FLAC3D after glaciation in Phase 1 elastoplastic simulations for cylinder 1 (top right:green). The Martin (2007) interpretation is indicated with a green dashed line and the repository depth with a horizontal dashed black line.*

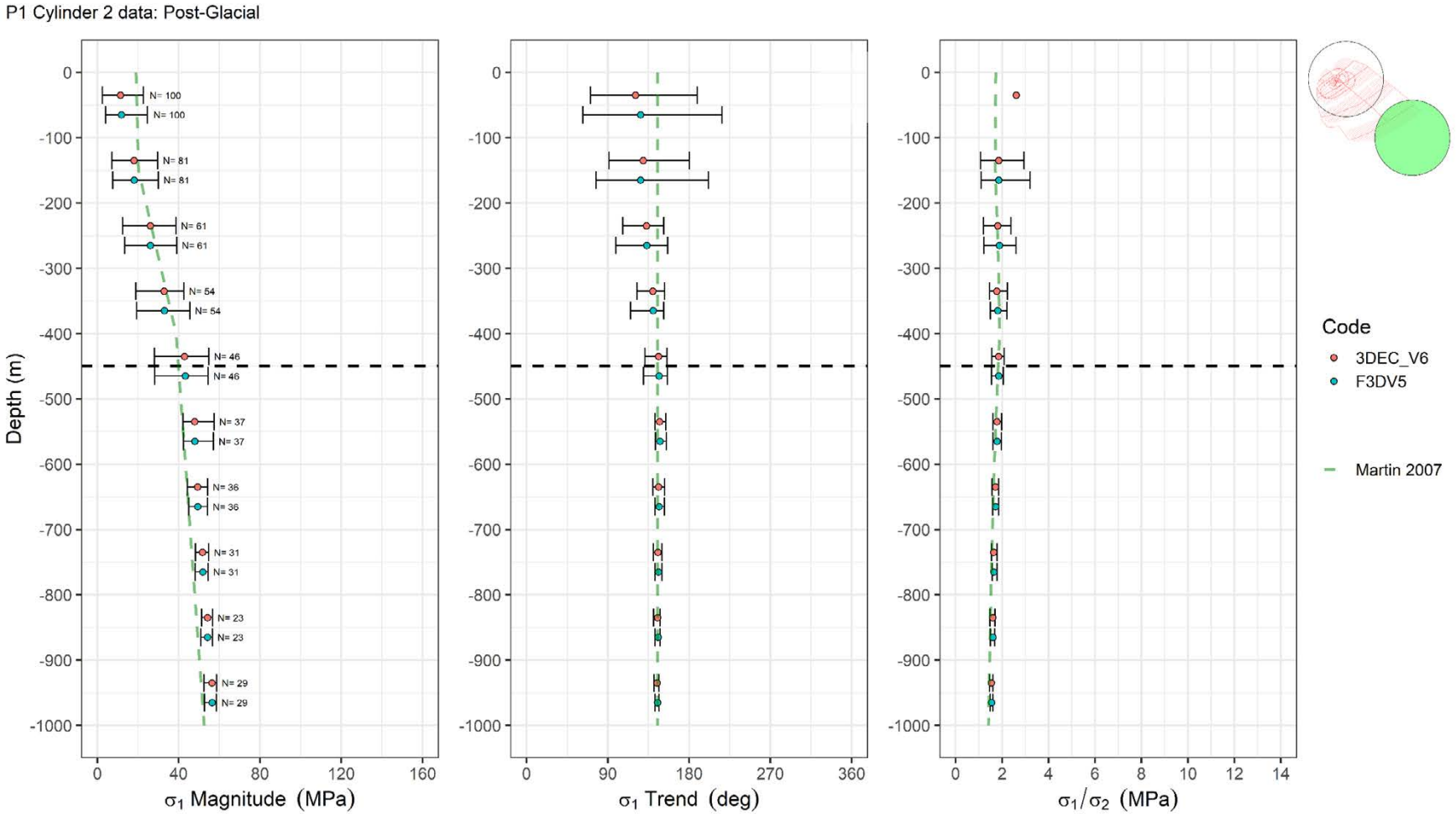

Figure A7-10. *Mean and 95 % variation interval of σ_1 magnitude and trend at hundred meter intervals for 3DEC and FLAC3D after glaciation in Phase 1 elastoplastic simulations for cylinder 2 (top right:green). The Martin (2007) interpretation is indicated with a green dashed line and the repository depth with a horizontal dashed black line.*

Phase 2 mean and variation of σ_1 magnitude, trend and σ_1/σ_2 ratio for hundred meter intervals (95 % variation interval)

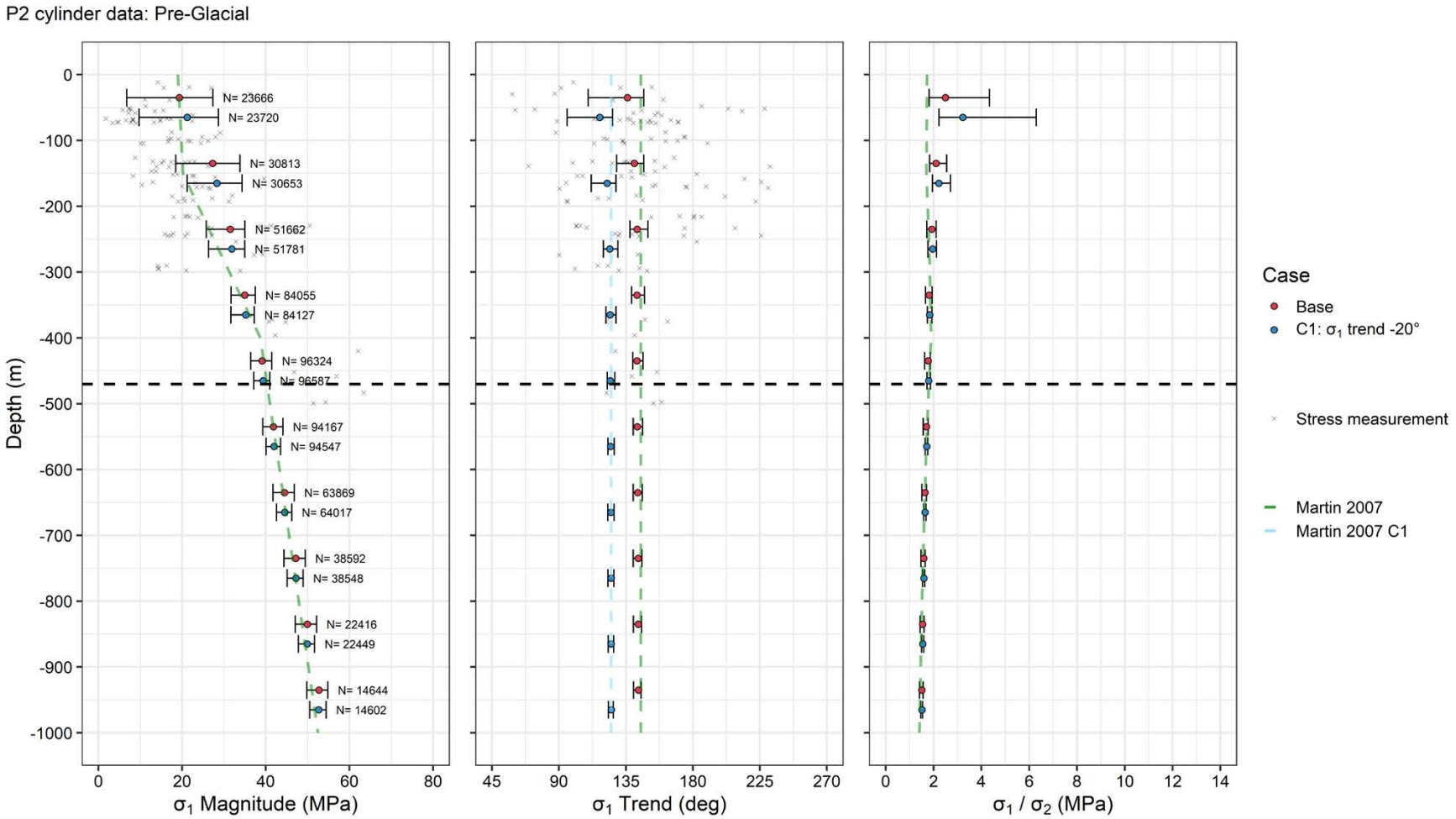

Figure A8-1. *Mean and 95 % variation interval of σ_1 magnitude,trend and the ratio of σ_1 and σ_2 at hundred meter intervals for the Base case and Case 1 of Phase 2 before glaciation for a cylinder covering the repository footprint. The Martin (2007) interpretation is indicated with a green dashed line and the repository depth with a horizontal dashed black line. The blue dashed line indicates the target trend of σ_1 for Case 1. Field stress measurements indicated with grey markers.*

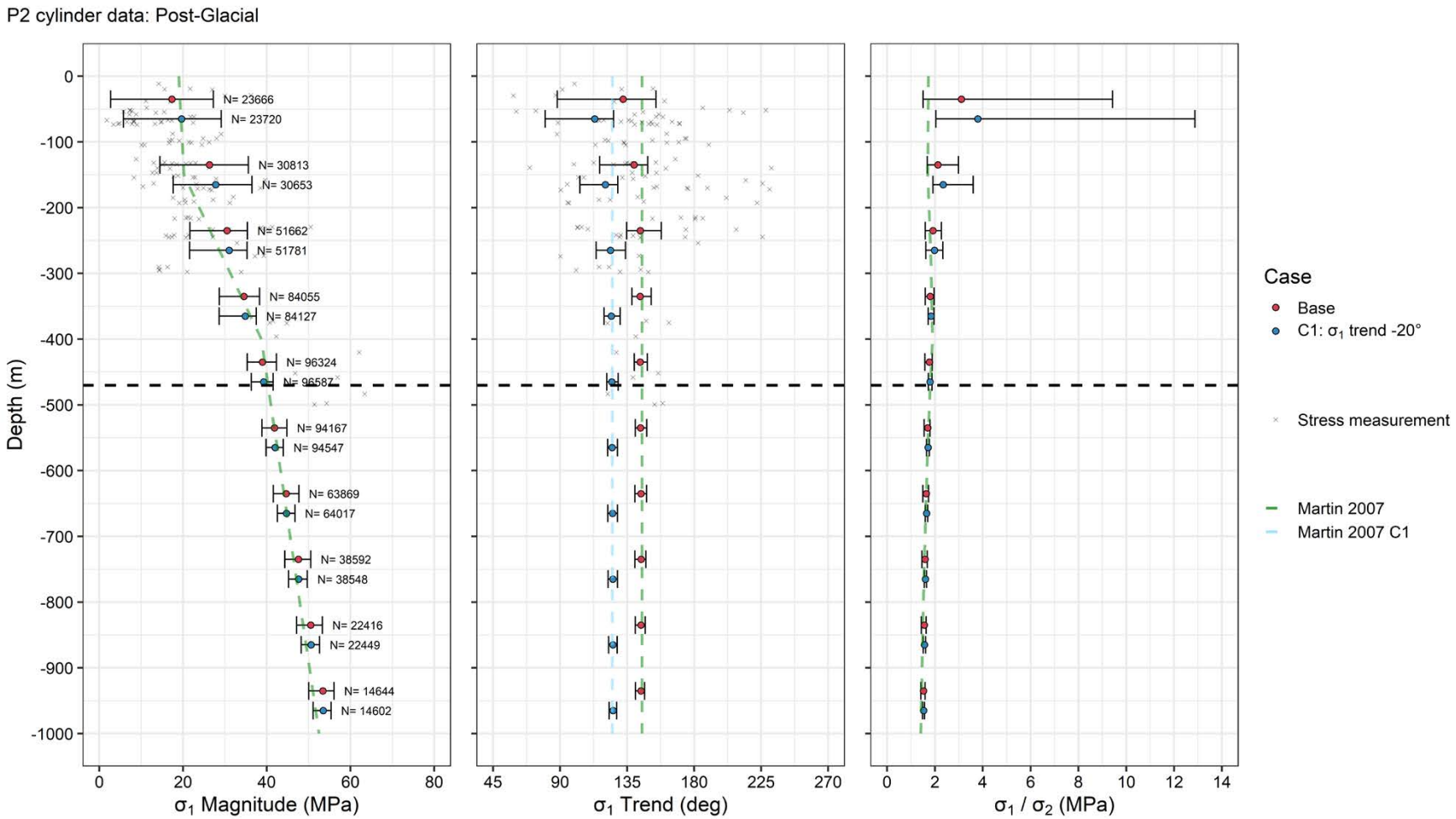

Figure A8-2. *Mean and 95 % variation interval of σ_1 magnitude,trend and the ratio of σ_1 and σ_2 at hundred meter intervals for the Base case and Case 1 of Phase 2 after glaciation for a cylinder covering the repository footprint. The Martin (2007) interpretation is indicated with a green dashed line and the repository depth with a horizontal dashed black line. The blue dashed line indicates the target trend of σ_1 for Case 1. Field stress measurements indicated with grey markers.*

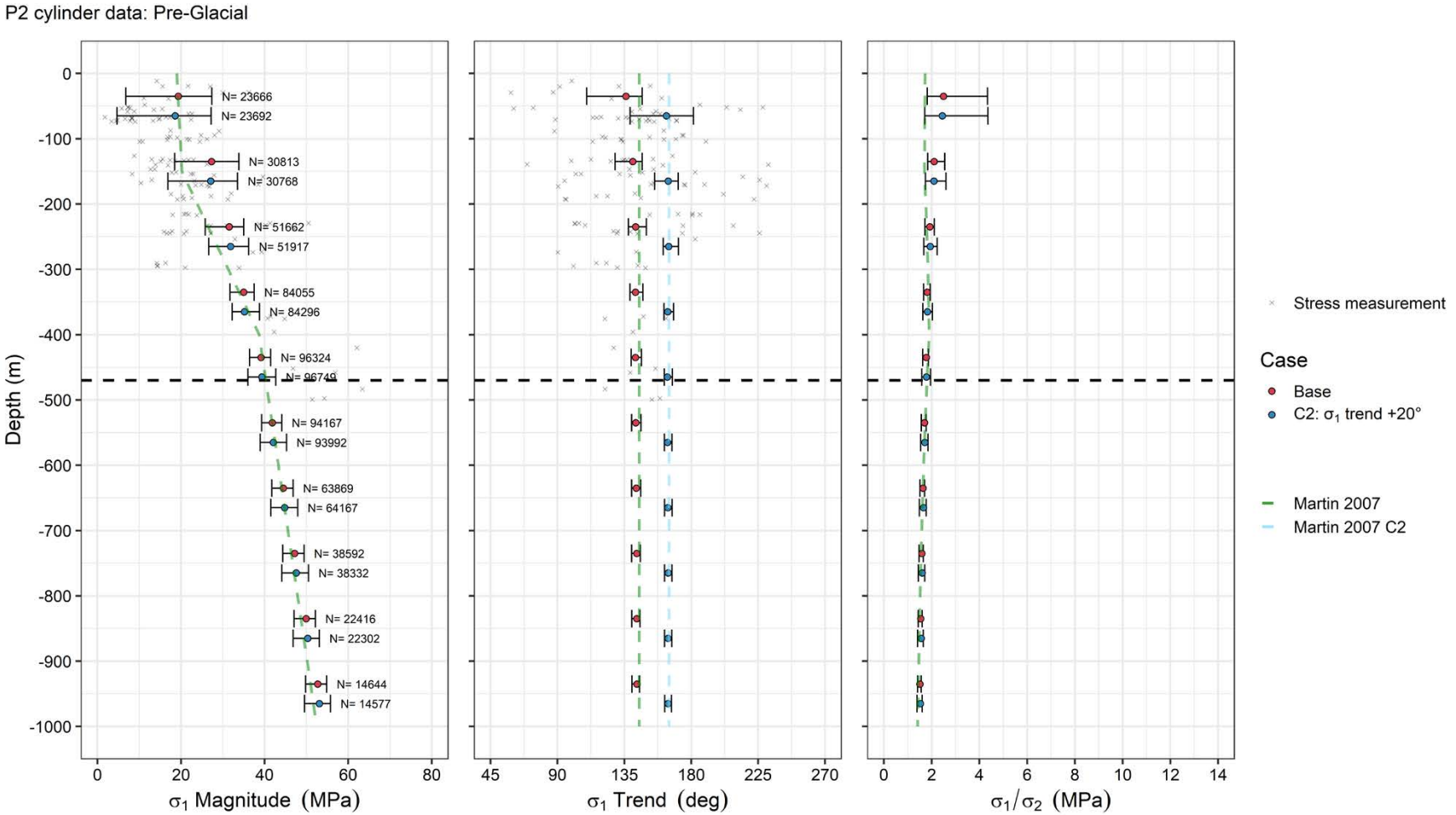

Figure A8-3. *Mean and 95 % variation interval of σ_1 magnitude,trend and the ratio of σ_1 and σ_2 at hundred meter intervals for the Base case and Case 2 of Phase 2 before glaciation for a cylinder covering the repository footprint. The Martin (2007) interpretation is indicated with a green dashed line and the repository depth with a horizontal dashed black line. The blue dashed line indicates the target trend of σ_1 for Case 2. Field stress measurements indicated with grey markers.*

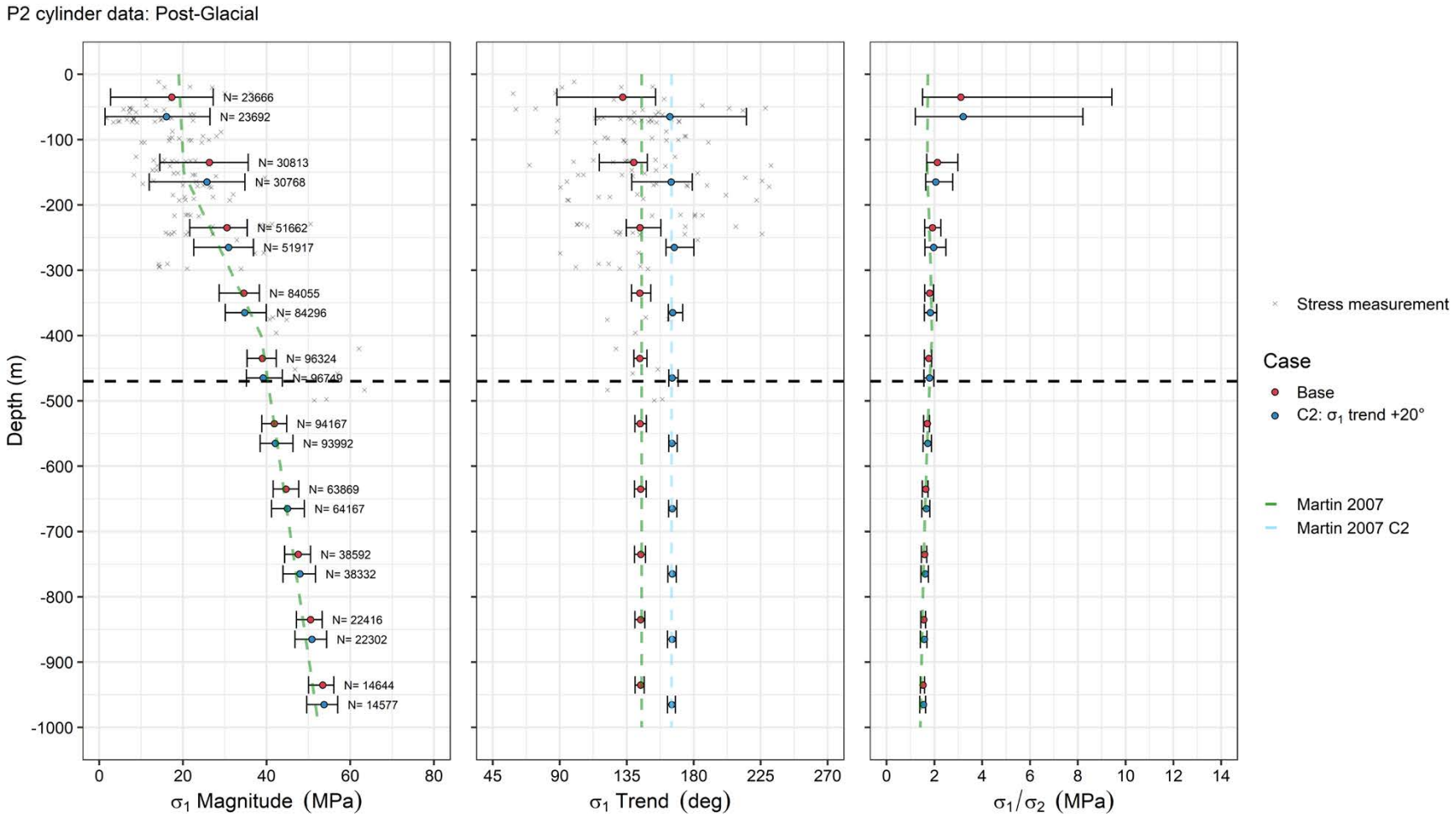

Figure A8-4. *Mean and 95 % variation interval of σ_1 magnitude,trend and the ratio of σ_1 and σ_2 at hundred meter intervals for the Base case and Case 2 of Phase 2 after glaciation for a cylinder covering the repository footprint. The Martin (2007) interpretation is indicated with a green dashed line and the repository depth with a horizontal dashed black line. The blue dashed line indicates the target trend of σ_1 for Case 2. Field stress measurements indicated with grey markers.*

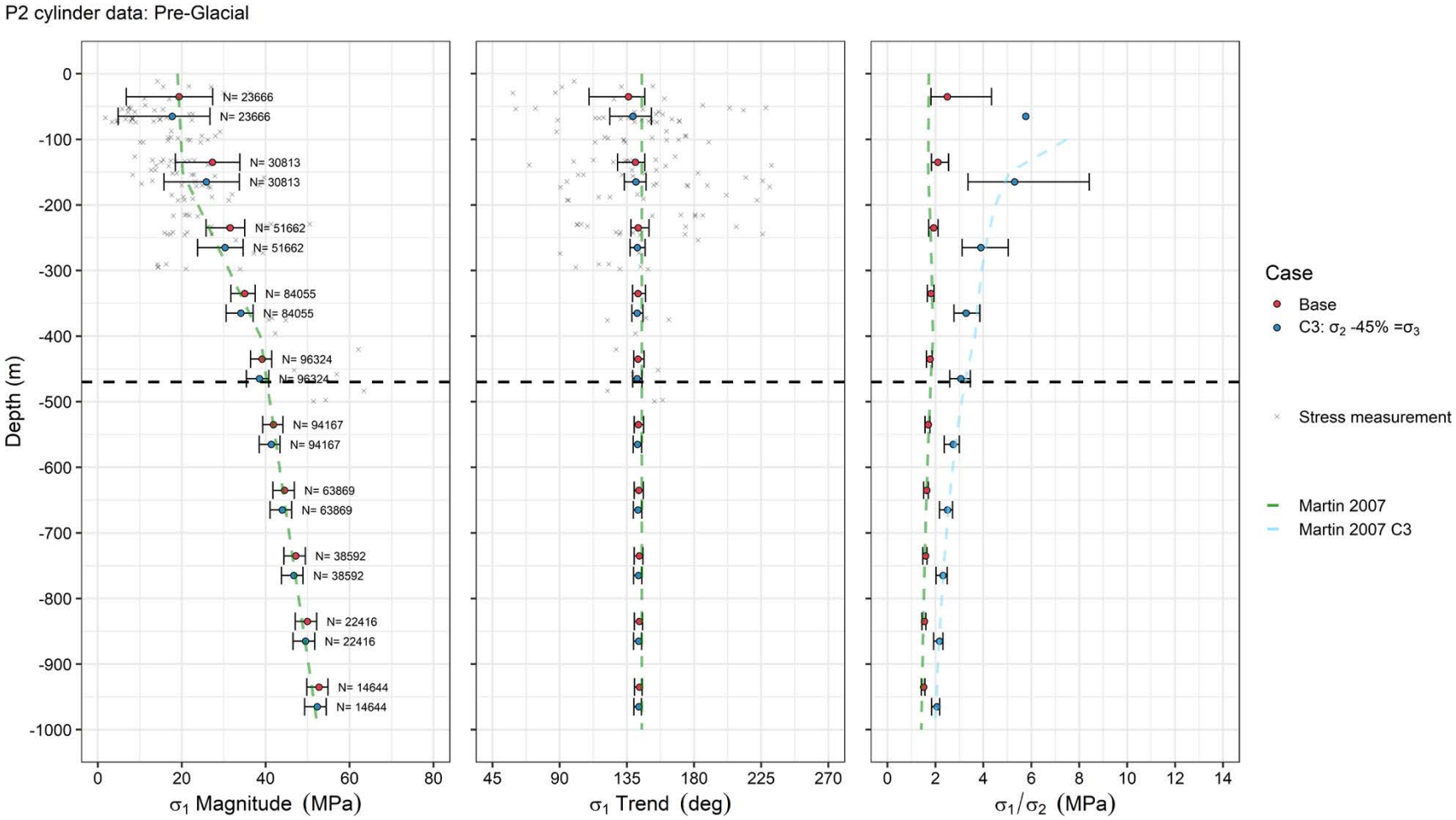

Figure A8-5. *Mean and 95 % variation interval of σ_1 magnitude,trend and the ratio of σ_1 and σ_2 at hundred meter intervals for the Base case and Case 3 of Phase 2 before glaciation for a cylinder covering the repository footprint. The Martin (2007) interpretation is indicated with a green dashed line and the repository depth with a horizontal dashed black line. The blue dashed line indicates the target ratio of σ_1/σ_2 for Case 3. Field stress measurements indicated with grey markers.*

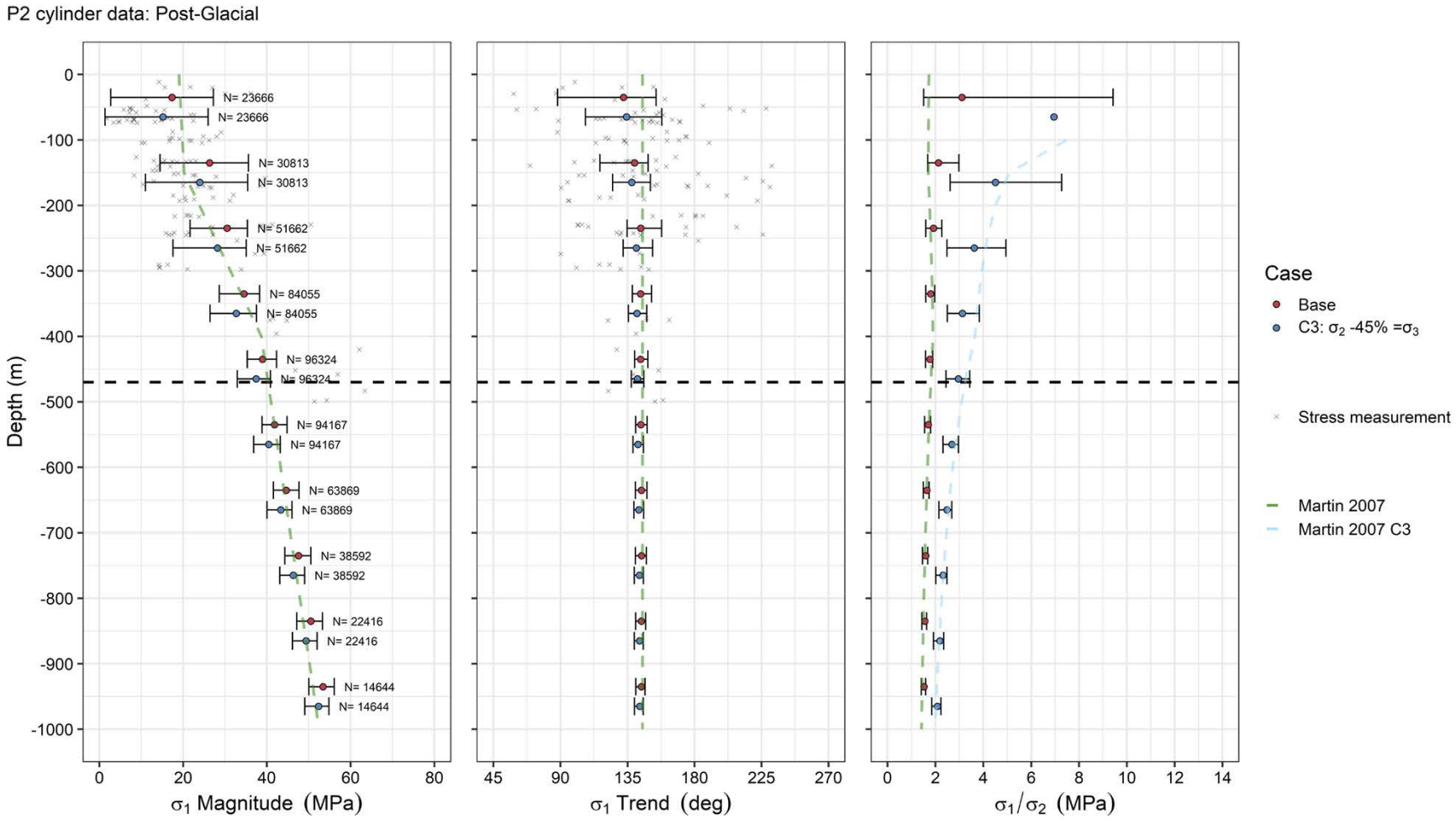

Figure A8-6. *Mean and 95 % variation interval of σ_1 magnitude,trend and the ratio of σ_1 and σ_2 at hundred meter intervals for the Base case and Case 3 of Phase 2 after glaciation for a cylinder covering the repository footprint. The Martin (2007) interpretation is indicated with a green dashed line and the repository depth with a horizontal dashed black line. The blue dashed line indicates the target ratio of σ_1/σ_2 for Case 3. Field stress measurements indicated with grey markers.*

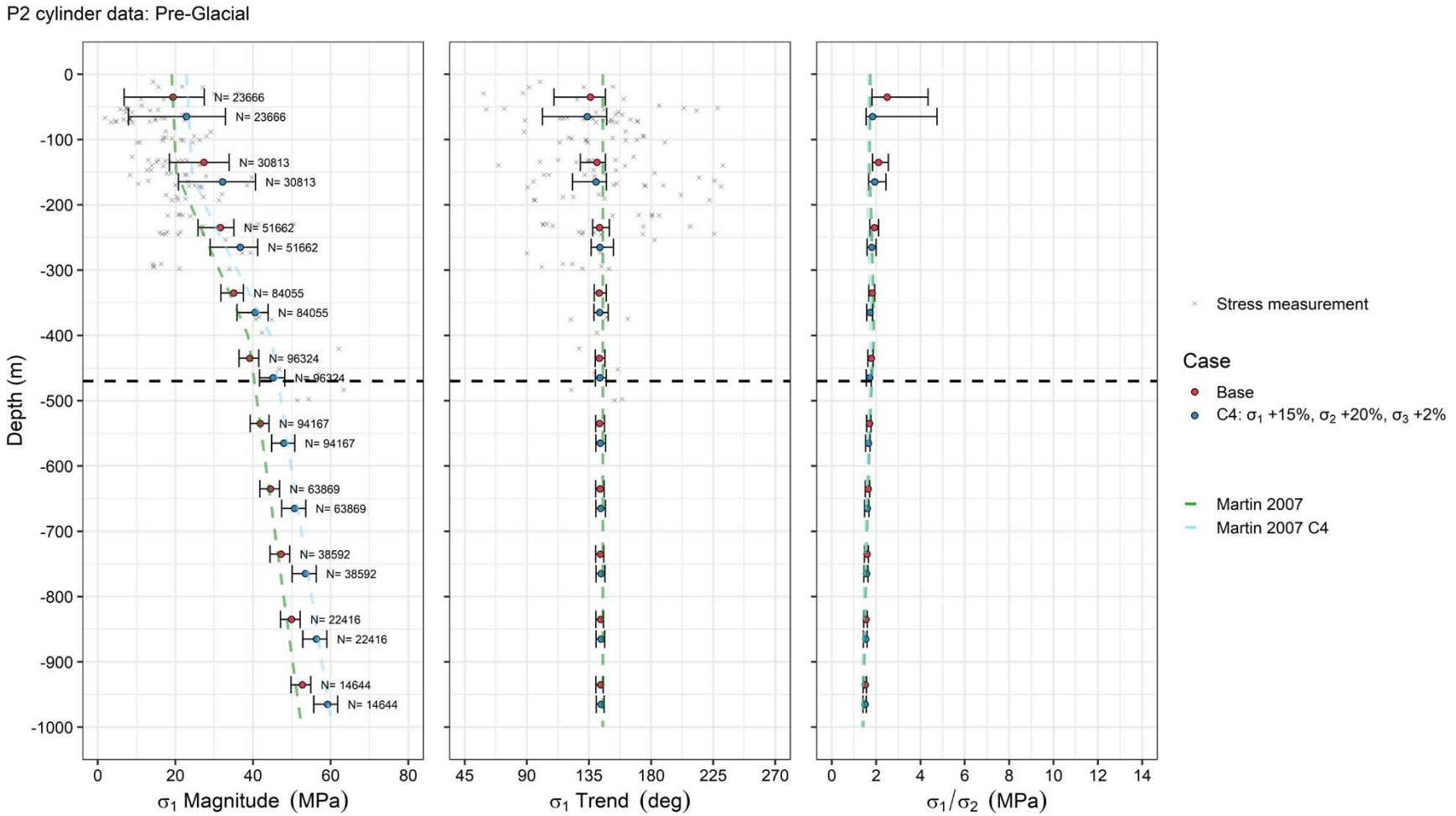

Figure A8-7. *Mean and 95 % variation interval of σ_1 magnitude,trend and the ratio of σ_1 and σ_2 at hundred meter intervals for the Base case and Case 4 of Phase 2 before glaciation for a cylinder covering the repository footprint. The Martin (2007) interpretation is indicated with a green dashed line and the repository depth with a horizontal dashed black line. The blue dashed line indicates the target ratio of σ_1/σ_2 for Case 4. Field stress measurements indicated with grey markers.*

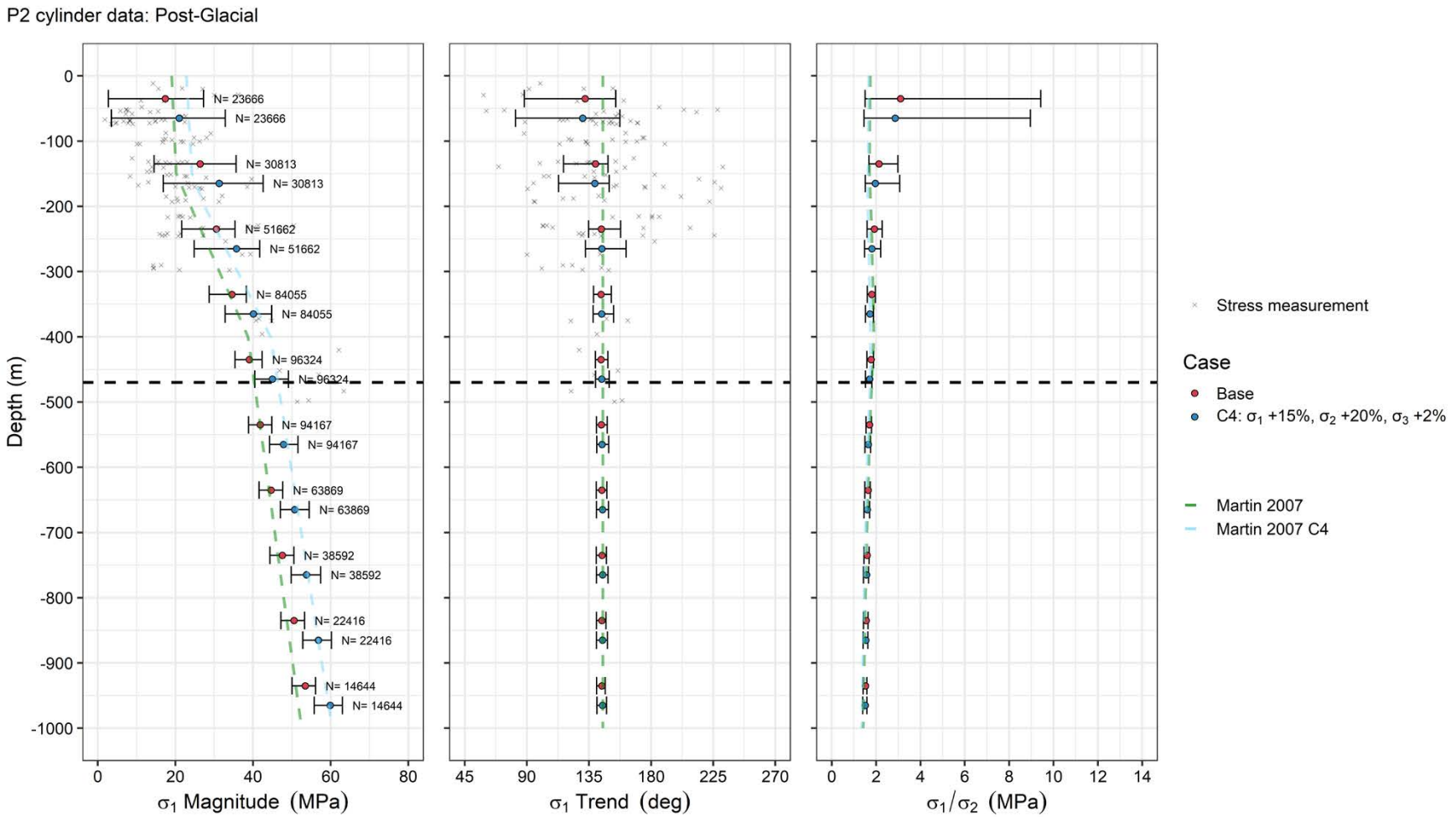

Figure A8-8. *Mean and 95 % variation interval of σ_1 magnitude,trend and the ratio of σ_1 and σ_2 at hundred meter intervals for the Base case and Case 4 of Phase 2 after glaciation for a cylinder covering the repository footprint. The Martin (2007) interpretation is indicated with a green dashed line and the repository depth with a horizontal dashed black line. The blue dashed line indicates the target ratio of σ_1/σ_2 for Case 4. Field stress measurements indicated with grey markers.*

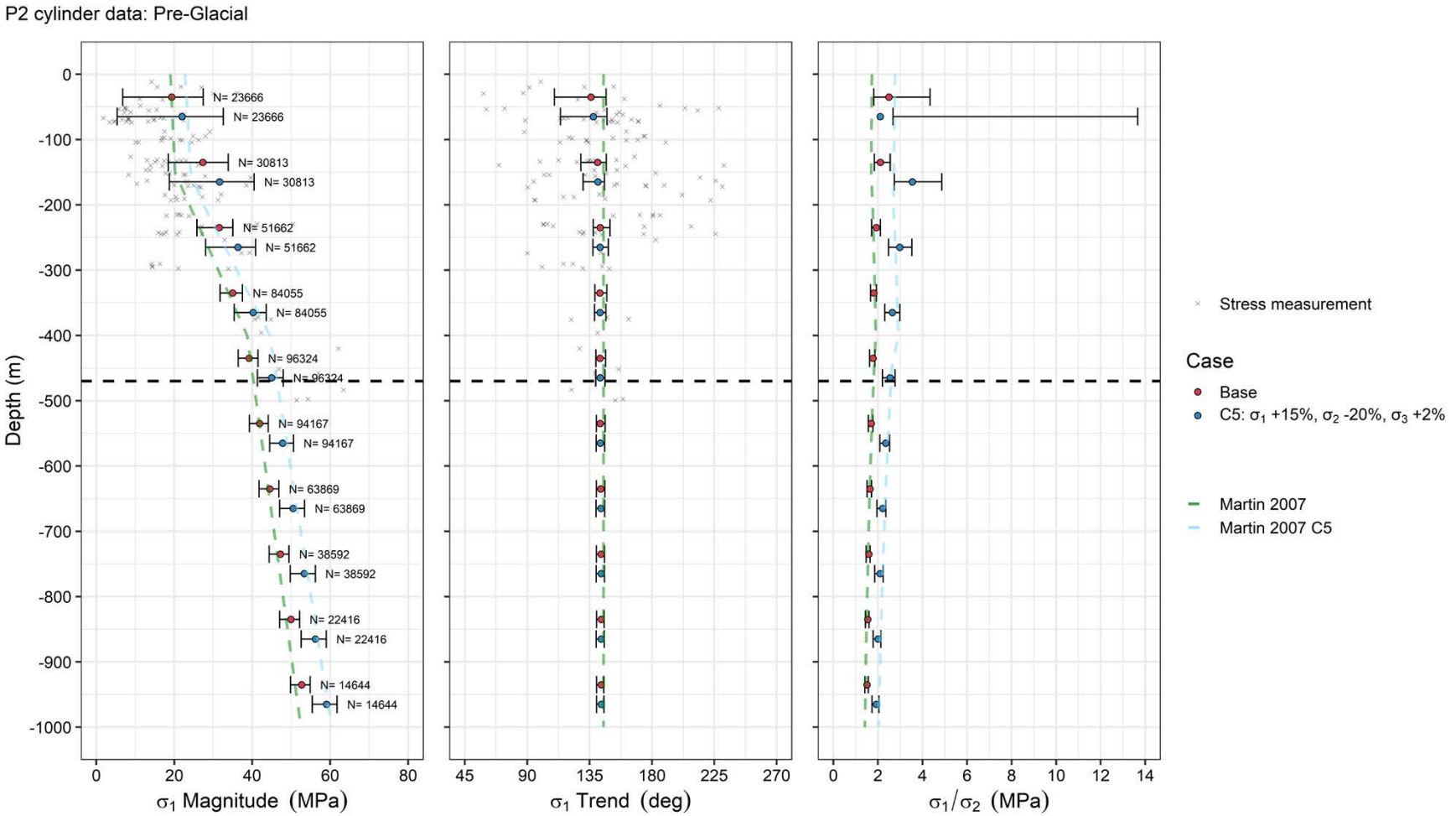

Figure A8-9. *Mean and 95 % variation interval of σ_1 magnitude,trend and the ratio of σ_1 and σ_2 at hundred meter intervals for the Base case and Case 5 of Phase 2 before glaciation for a cylinder covering the repository footprint. The Martin (2007) interpretation is indicated with a green dashed line and the repository depth with a horizontal dashed black line. The blue dashed line indicates the target ratio of σ_1/σ_2 for Case 5. Field stress measurements indicated with grey markers.*

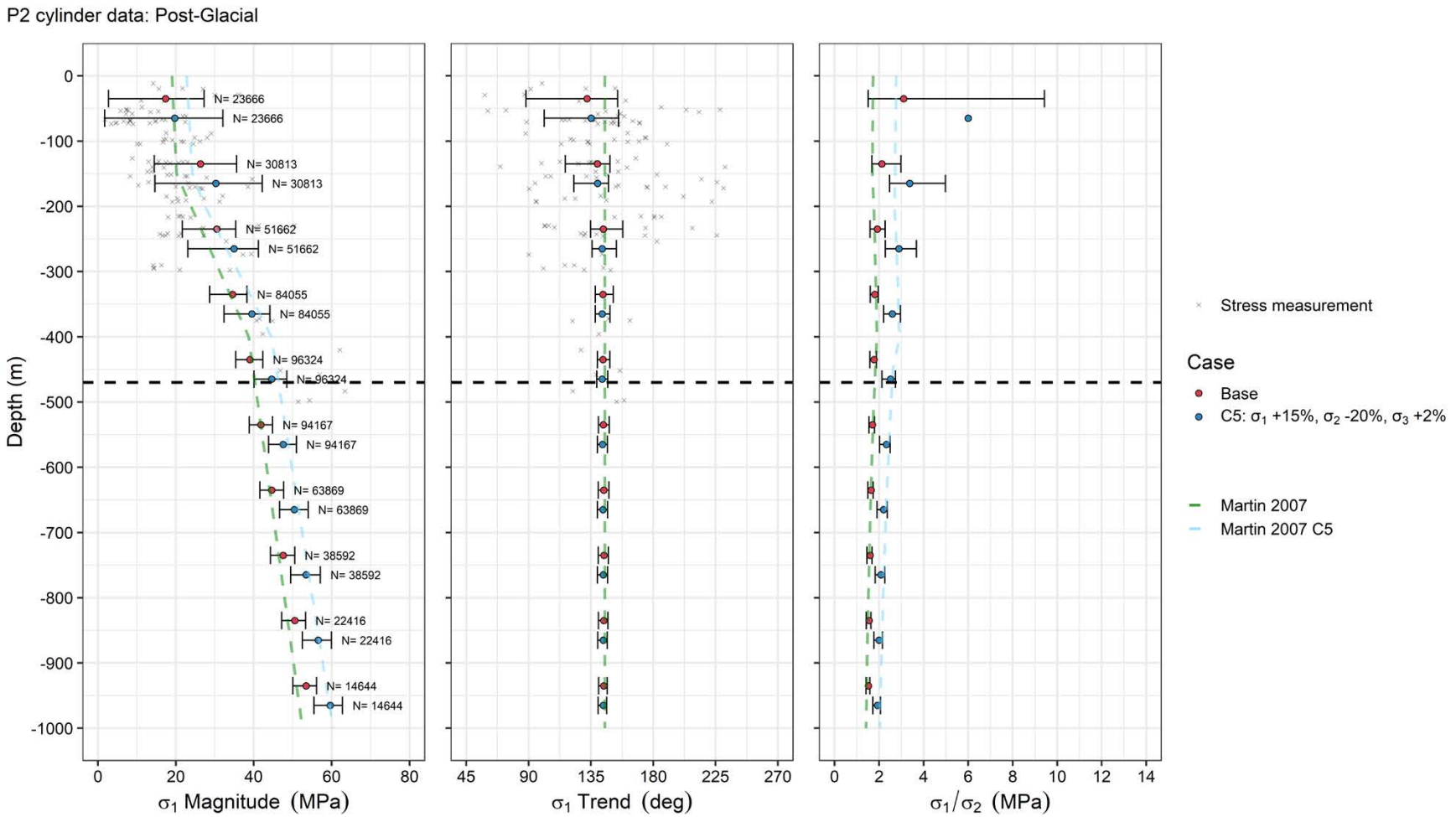

Figure A8-10. *Mean and 95 % variation interval of σ_1 magnitude,trend and the ratio of σ_1 and σ_2 at hundred meter intervals for the Base case and Case 5 of Phase 2 after glaciation for a cylinder covering the repository footprint. The Martin (2007) interpretation is indicated with a green dashed line and the repository depth with a horizontal dashed black line. The blue dashed line indicates the target ratio of σ_1/σ_2 for Case 5. Field stress measurements indicated with grey markers.*

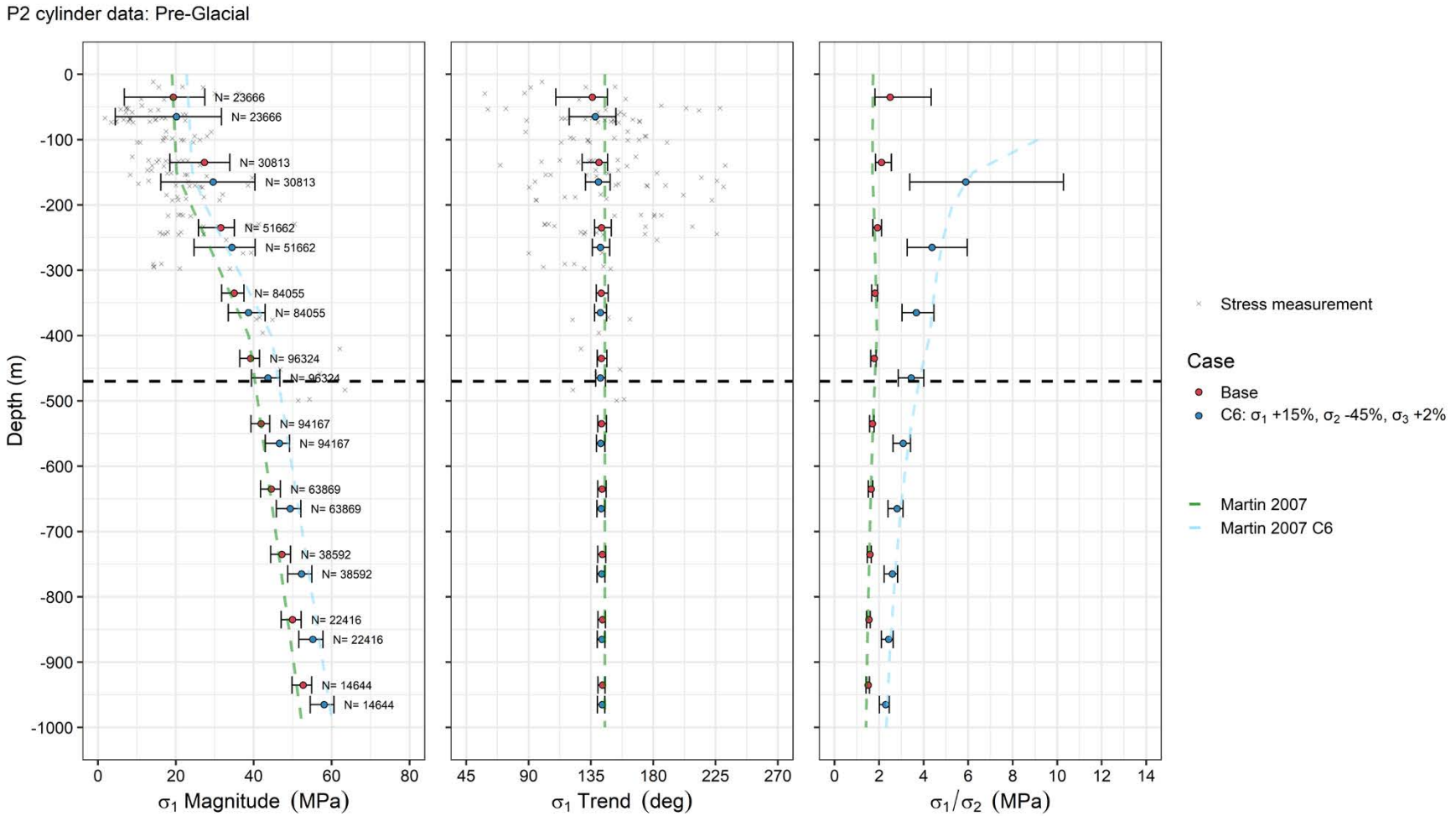

Figure A8-11. *Mean and 95 % variation interval of σ_1 magnitude,trend and the ratio of σ_1 and σ_2 at hundred meter intervals for the Base case and Case 6 of Phase 2 before glaciation for a cylinder covering the repository footprint. The Martin (2007) interpretation is indicated with a green dashed line and the repository depth with a horizontal dashed black line. The blue dashed line indicates the target ratio of σ_1/σ_2 for Case 6. Field stress measurements indicated with grey markers.*

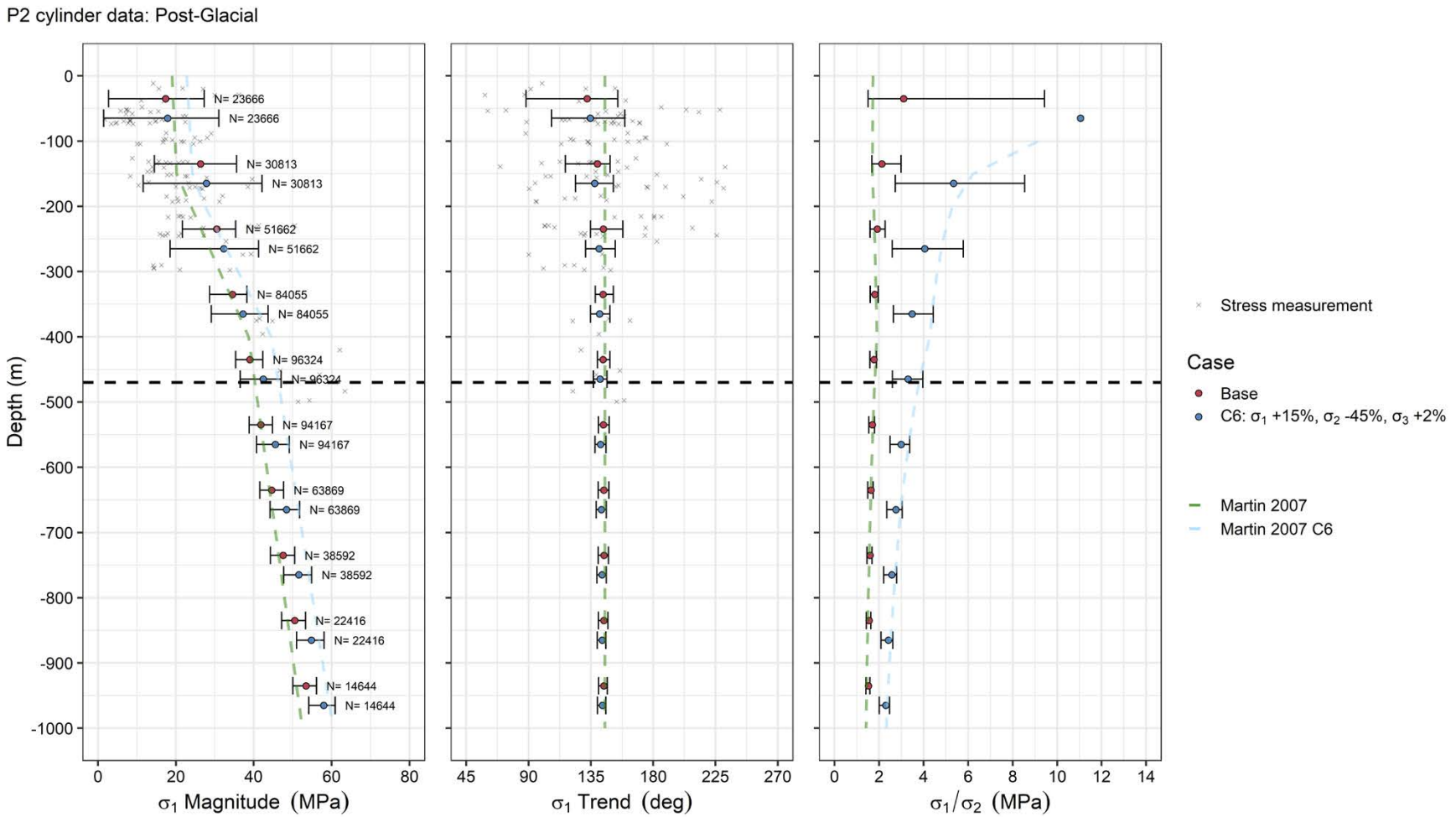

Figure A8-12. *Mean and 95 % variation interval of σ_1 magnitude,trend and the ratio of σ_1 and σ_2 at hundred meter intervals for the Base case and Case 6 of Phase 2 after glaciation for a cylinder covering the repository footprint. The Martin (2007) interpretation is indicated with a green dashed line and the repository depth with a horizontal dashed black line. The blue dashed line indicates the target ratio of σ_1/σ_2 for Case 6. Field stress measurements indicated with grey markers.*

Appendix 9

Phase 2 principal stress mean and variation for hundred meter intervals (95 % variation interval) versus stress measurements

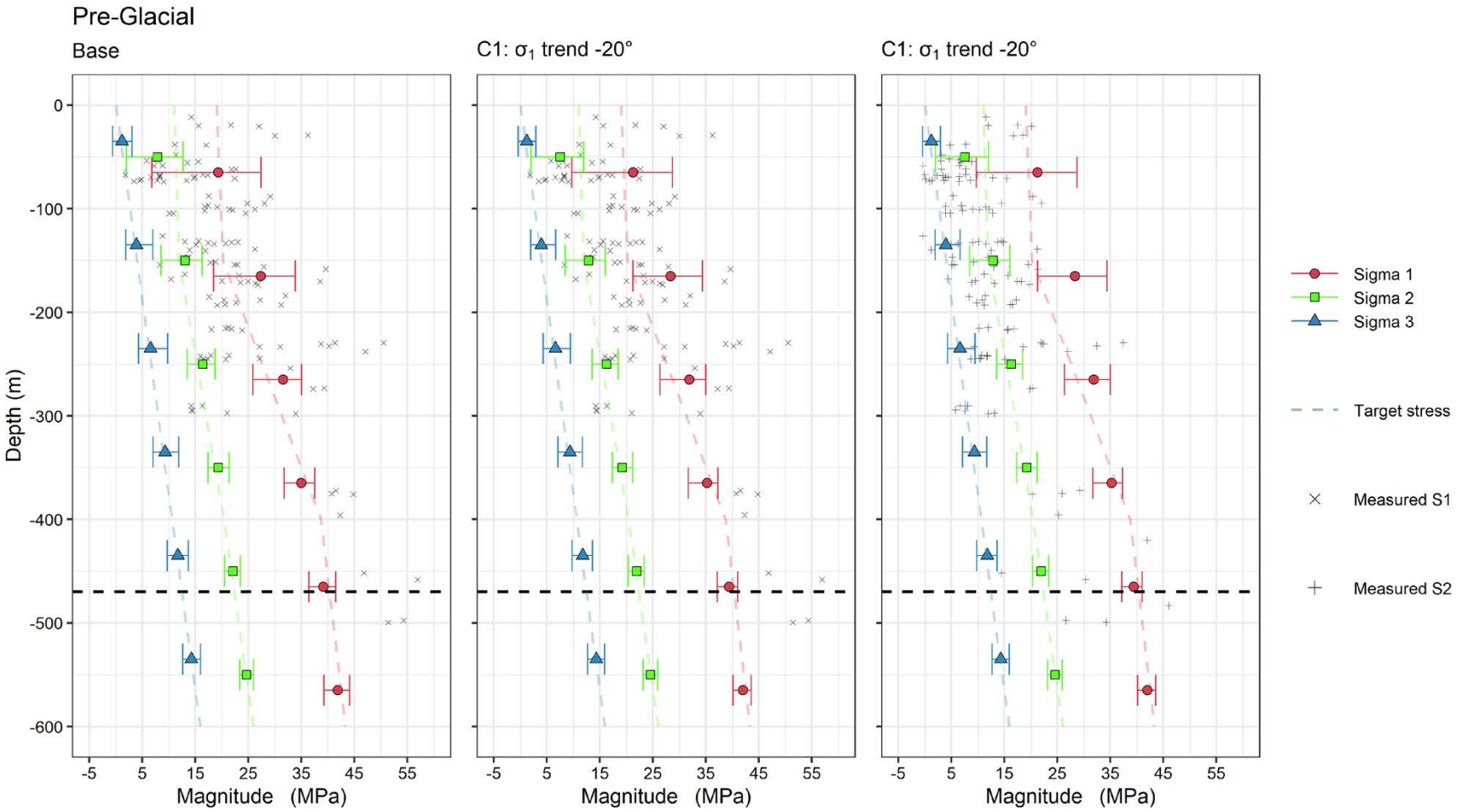

Figure A9-1. *Mean and 95 % variation interval of the principal stress magnitudes versus measured stresses at hundred meter intervals for the Base case and Case 1 of Phase 2 simulations before glaciation from a cylinder covering the repository. The Martin (2007) interpretation is indicated with coloured dashed lines and the repository depth with a horizontal dashed black line. Field stress measurements indicated with grey cross or plus symbols.*

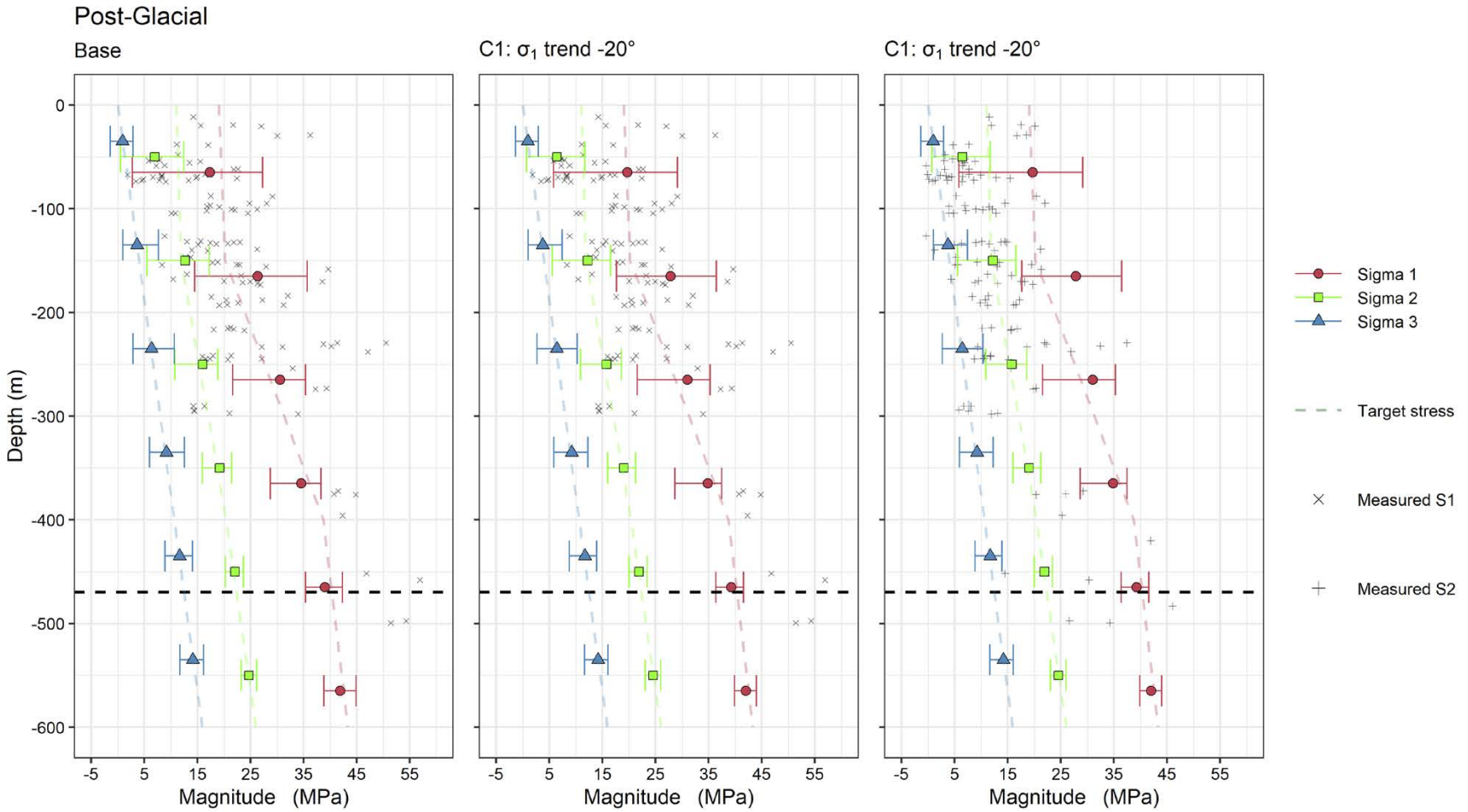

Figure A9-2. *Mean and 95 % variation interval of the principal stress magnitudes versus measured stresses at hundred meter intervals for the Base case and Case 1 of Phase 2 simulations after glaciation from a cylinder covering the repository. The Martin (2007) interpretation is indicated with coloured dashed lines and the repository depth with a horizontal dashed black line. Field stress measurements indicated with grey cross or plus symbols.*

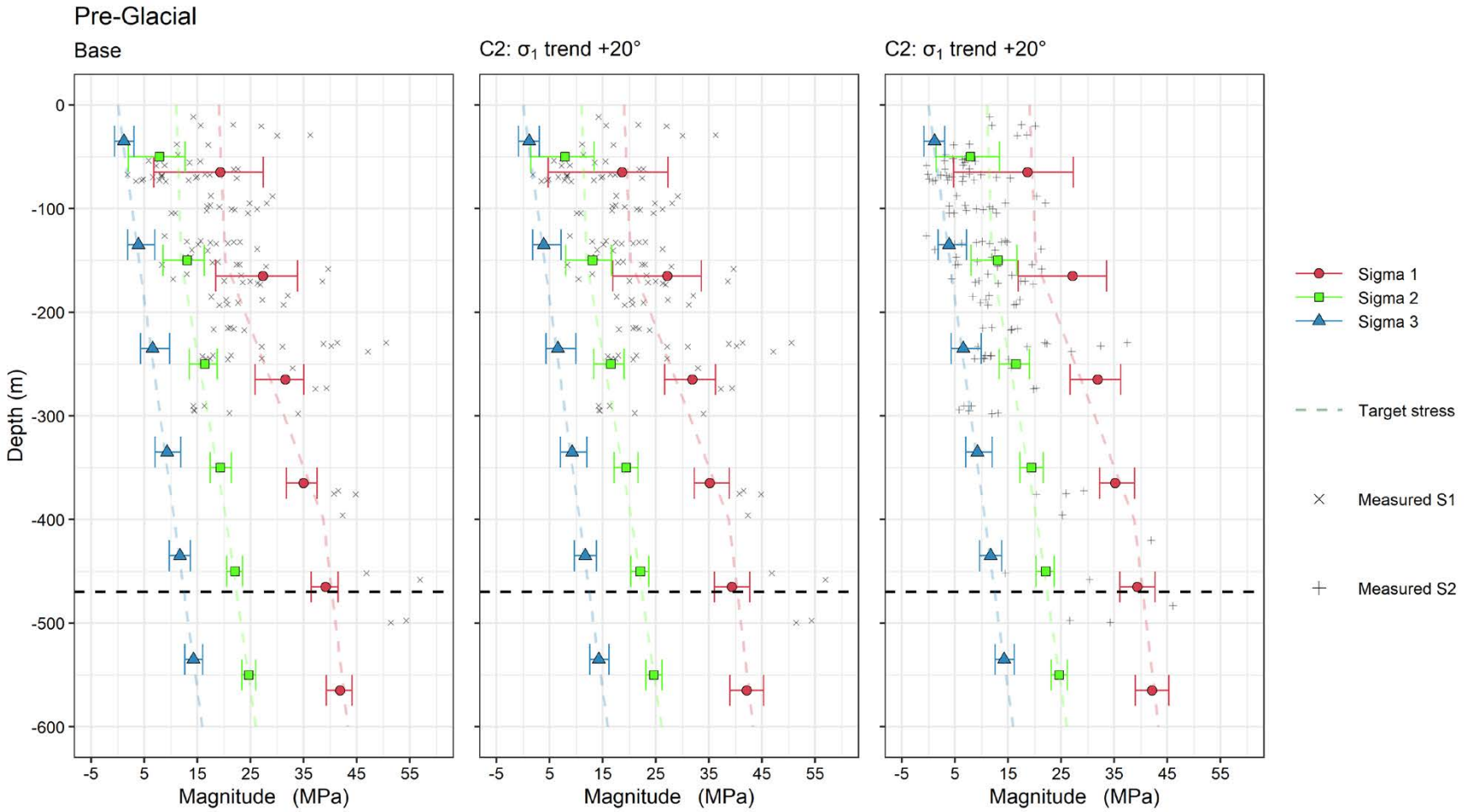

Figure A9-3. *Mean and 95 % variation interval of the principal stress magnitudes versus measured stresses at hundred meter intervals for the Base case and Case 2 of Phase 2 simulations before glaciation from a cylinder covering the repository. The Martin (2007) interpretation is indicated with coloured dashed lines and the repository depth with a horizontal dashed black line. Field stress measurements indicated with grey cross or plus symbols.*

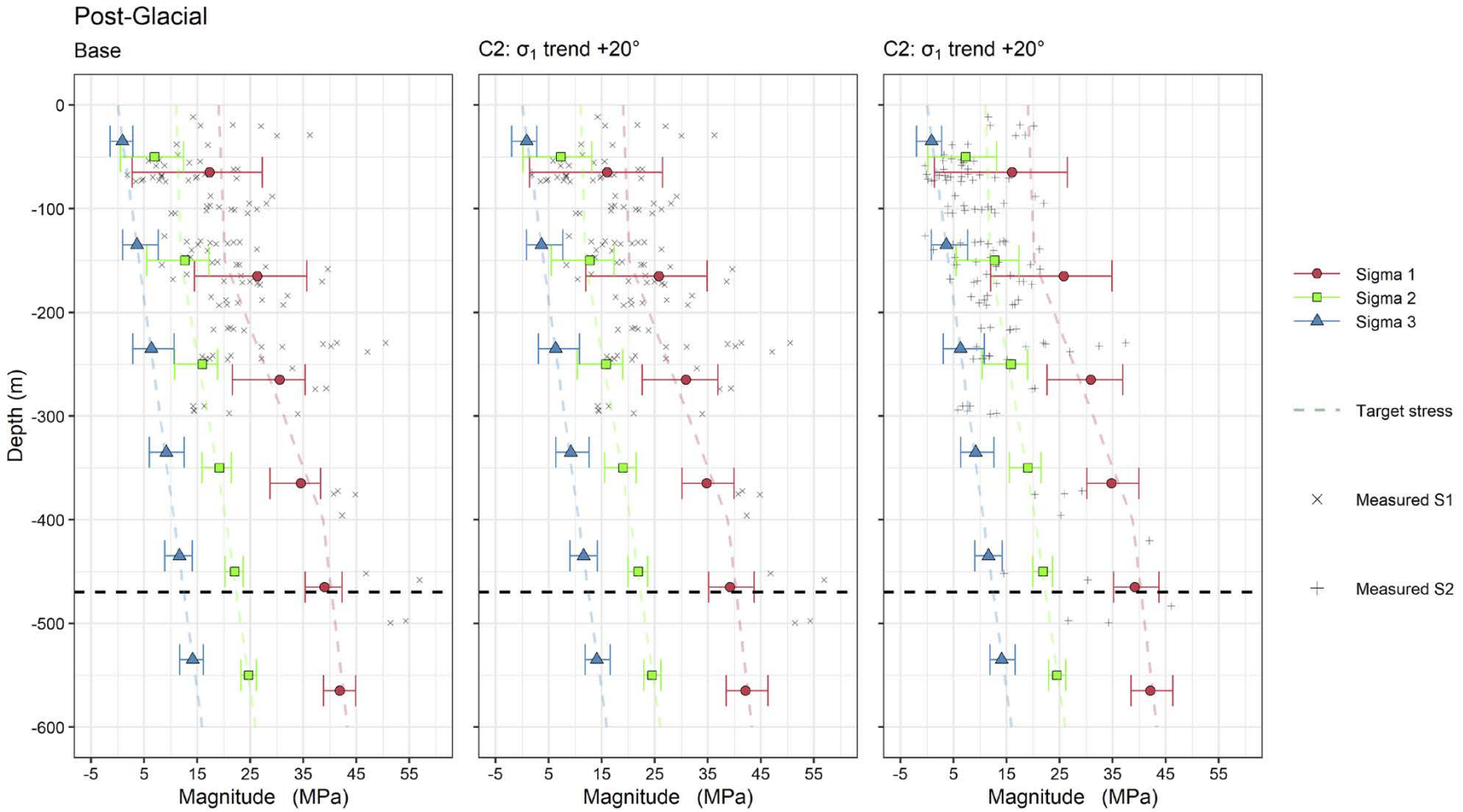

Figure A9-4. *Mean and 95 % variation interval of the principal stress magnitudes versus measured stresses at hundred meter intervals for the Base case and Case 2 of Phase 2 simulations after glaciation from a cylinder covering the repository. The Martin (2007) interpretation is indicated with coloured dashed lines and the repository depth with a horizontal dashed black line. Field stress measurements indicated with grey cross or plus symbols.*

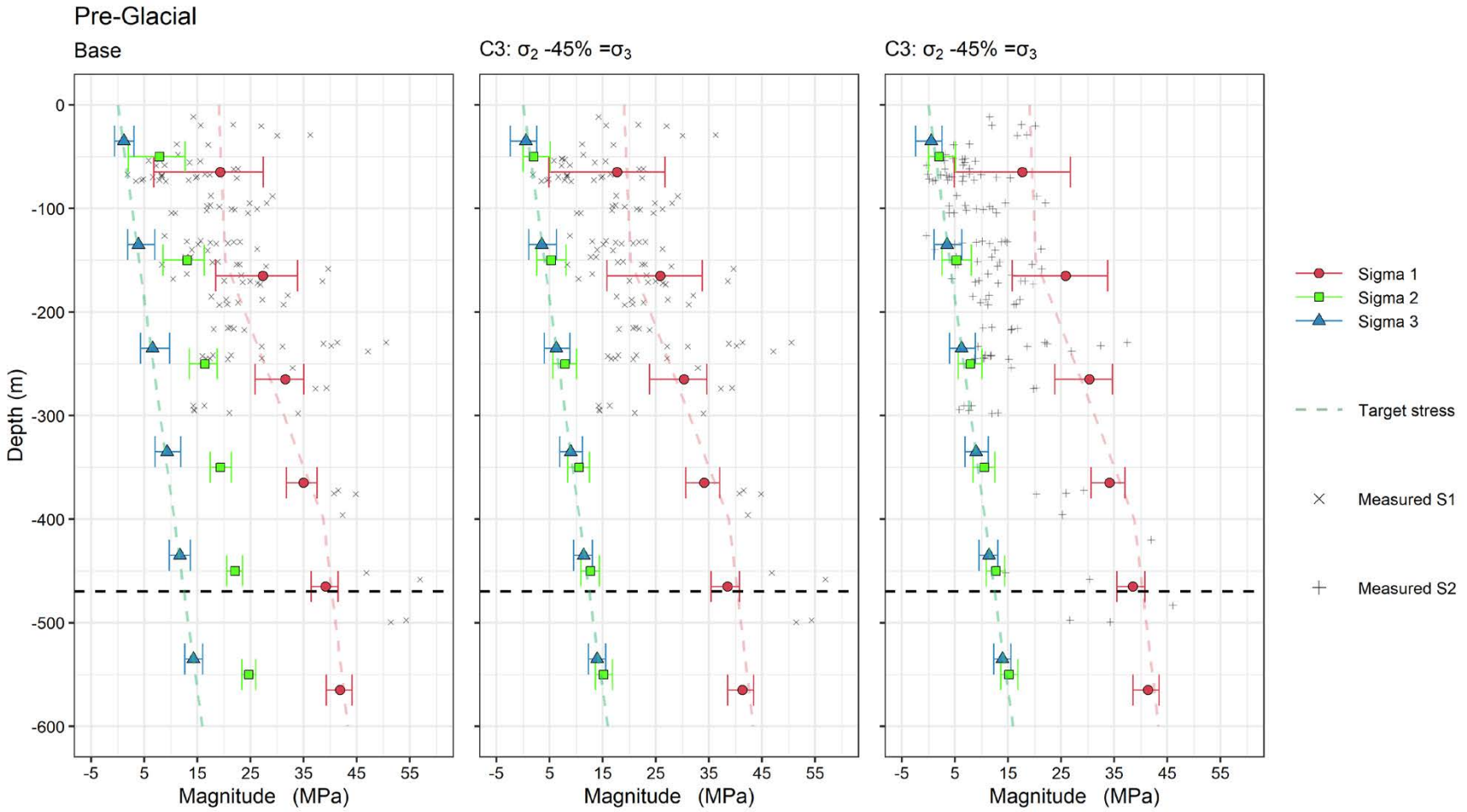

Figure A9-5. *Mean and 95 % variation interval of the principal stress magnitudes versus measured stresses at hundred meter intervals for the Base case and Case 3 of Phase 2 simulations before glaciation from a cylinder covering the repository. The Martin (2007) interpretation is indicated with coloured dashed lines and the repository depth with a horizontal dashed black line. Field stress measurements indicated with grey cross or plus symbols.*

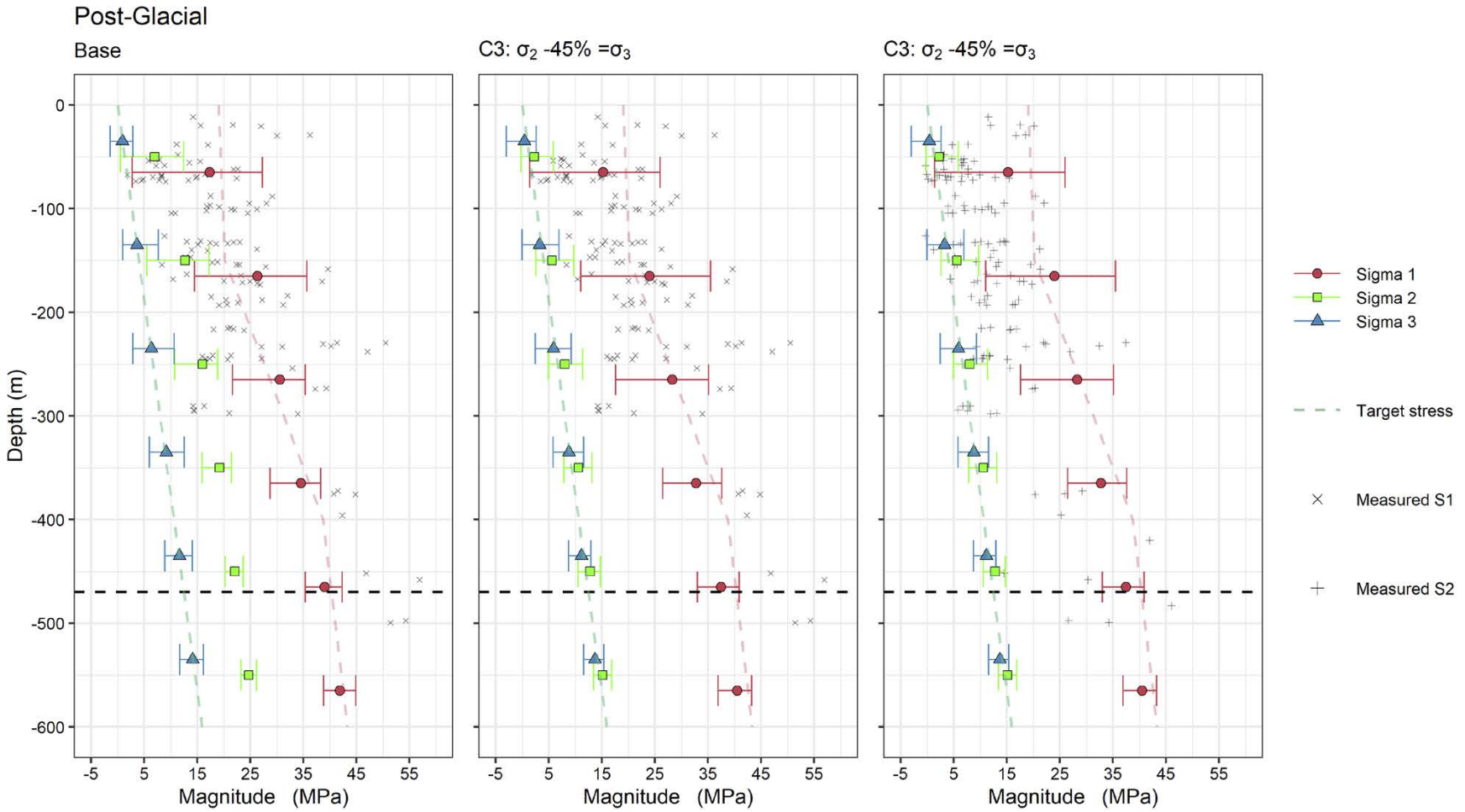

Figure A9-6. *Mean and 95 % variation interval of the principal stress magnitudes versus measured stresses at hundred meter intervals for the Base case and Case 3 of Phase 2 simulations after glaciation from a cylinder covering the repository. The Martin (2007) interpretation is indicated with coloured dashed lines and the repository depth with a horizontal dashed black line. Field stress measurements indicated with grey cross or plus symbols.*

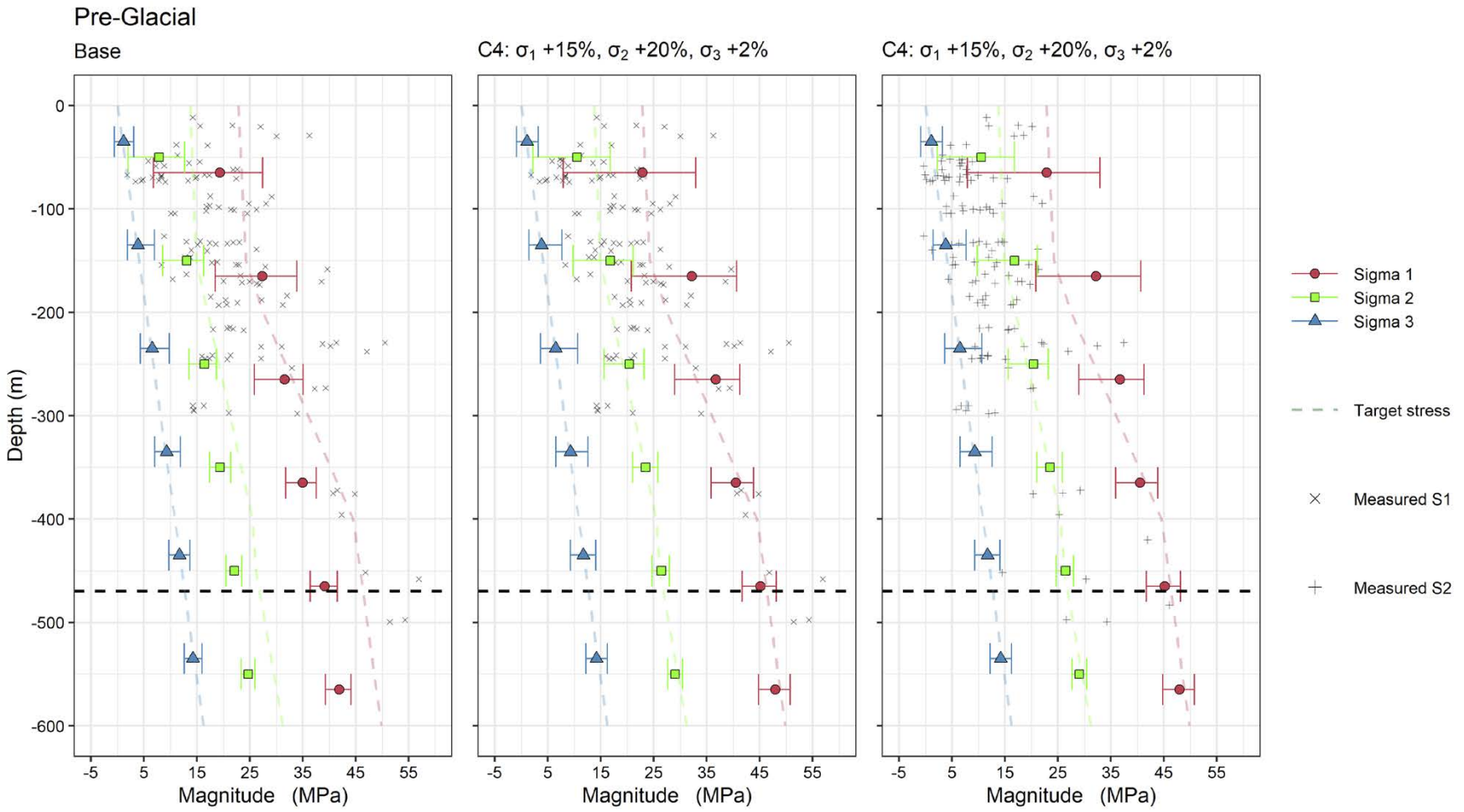

Figure A9-7. *Mean and 95 % variation interval of the principal stress magnitudes versus measured stresses at hundred meter intervals for the Base case and Case 4 of Phase 2 simulations before glaciation from a cylinder covering the repository. The Martin (2007) interpretation is indicated with coloured dashed lines and the repository depth with a horizontal dashed black line. Field stress measurements indicated with grey cross or plus symbols.*

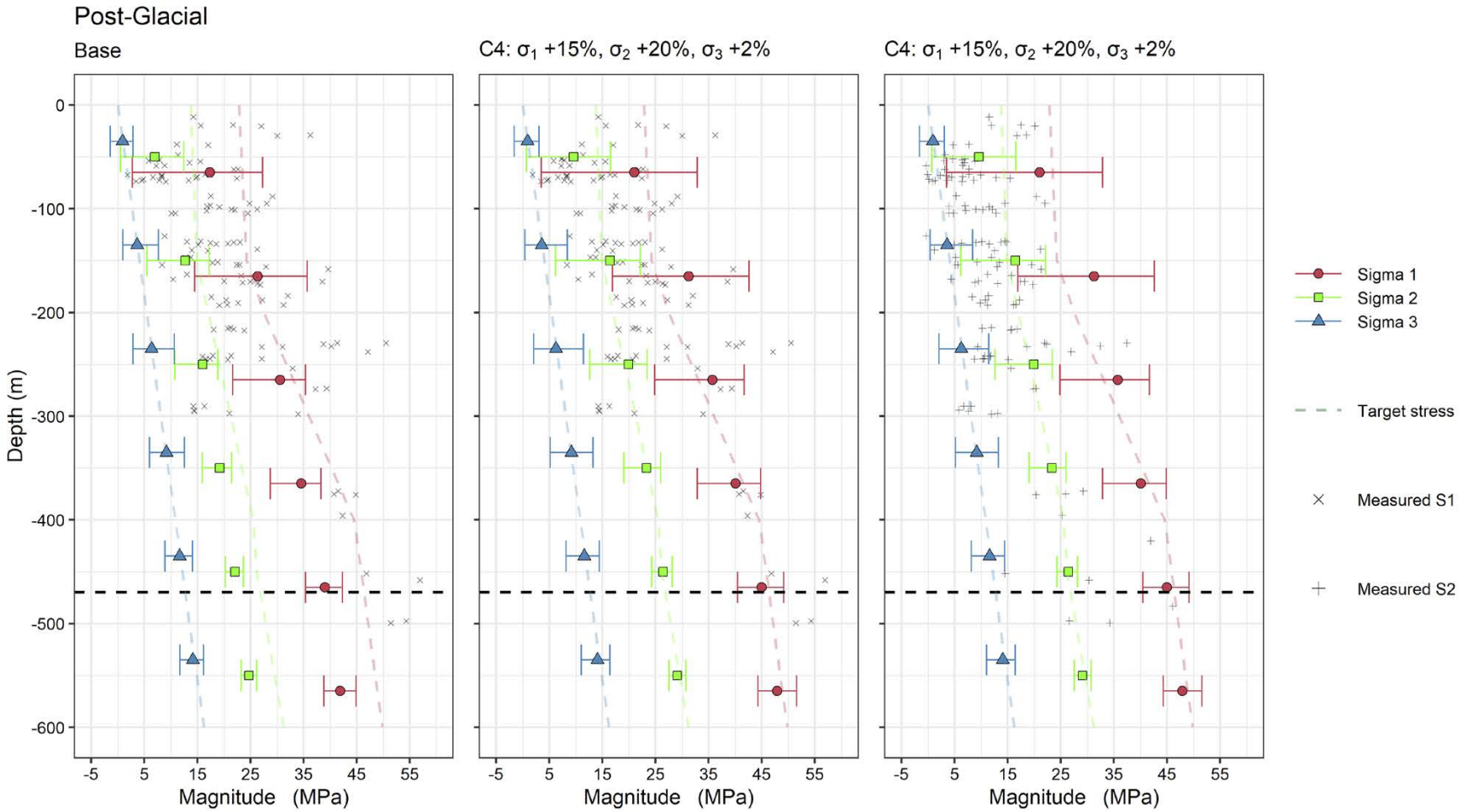

Figure A9-8. *Mean and 95 % variation interval of the principal stress magnitudes versus measured stresses at hundred meter intervals for the Base case and Case 4 of Phase 2 simulations after glaciation from a cylinder covering the repository. The Martin (2007) interpretation is indicated with coloured dashed lines and the repository depth with a horizontal dashed black line. Field stress measurements indicated with grey cross or plus symbols.*

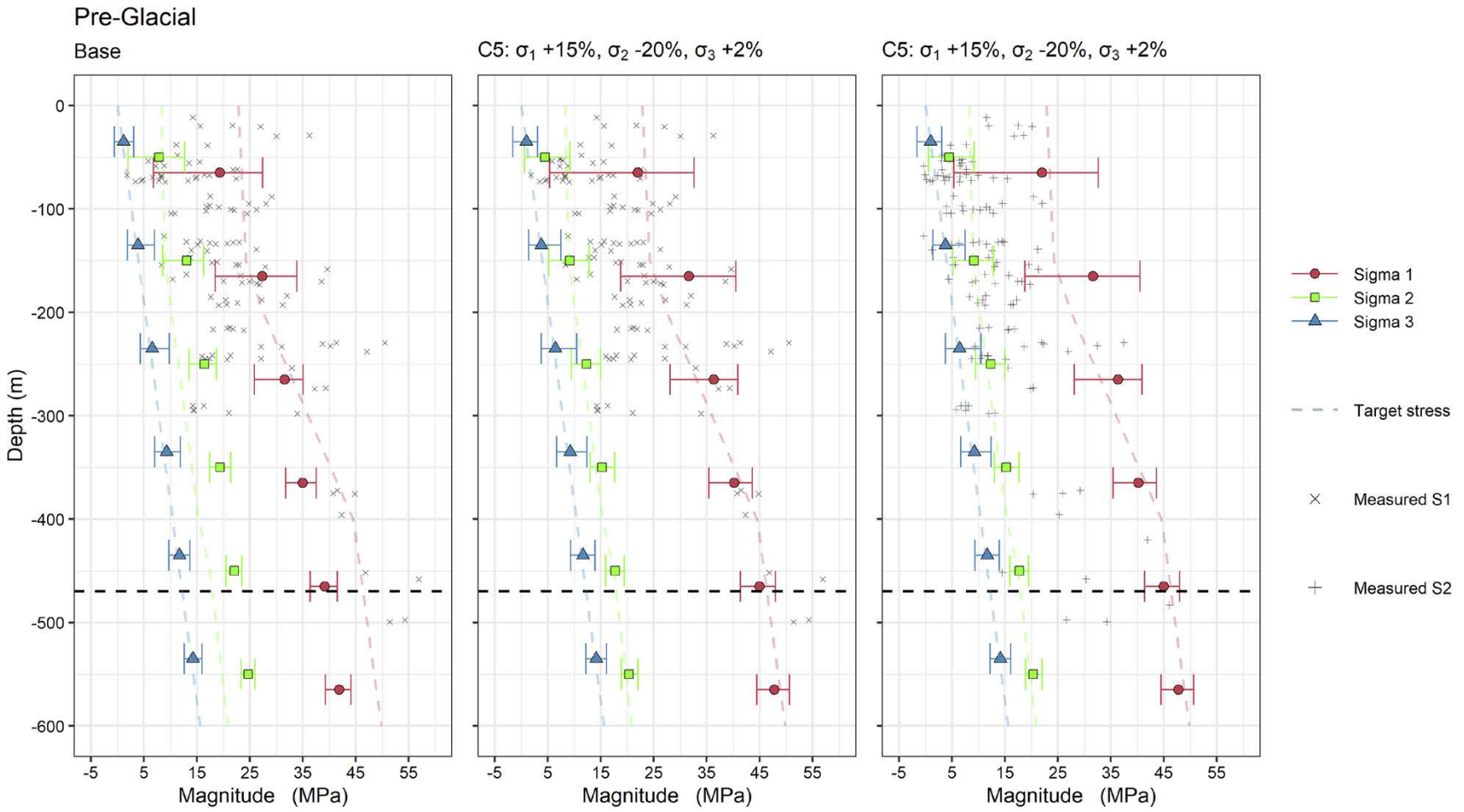

Figure A9-9. *Mean and 95 % variation interval of the principal stress magnitudes versus measured stresses at hundred meter intervals for the Base case and Case 5 of Phase 2 simulations before glaciation from a cylinder covering the repository. The Martin (2007) interpretation is indicated with coloured dashed lines and the repository depth with a horizontal dashed black line. Field stress measurements indicated with grey cross or plus symbols.*

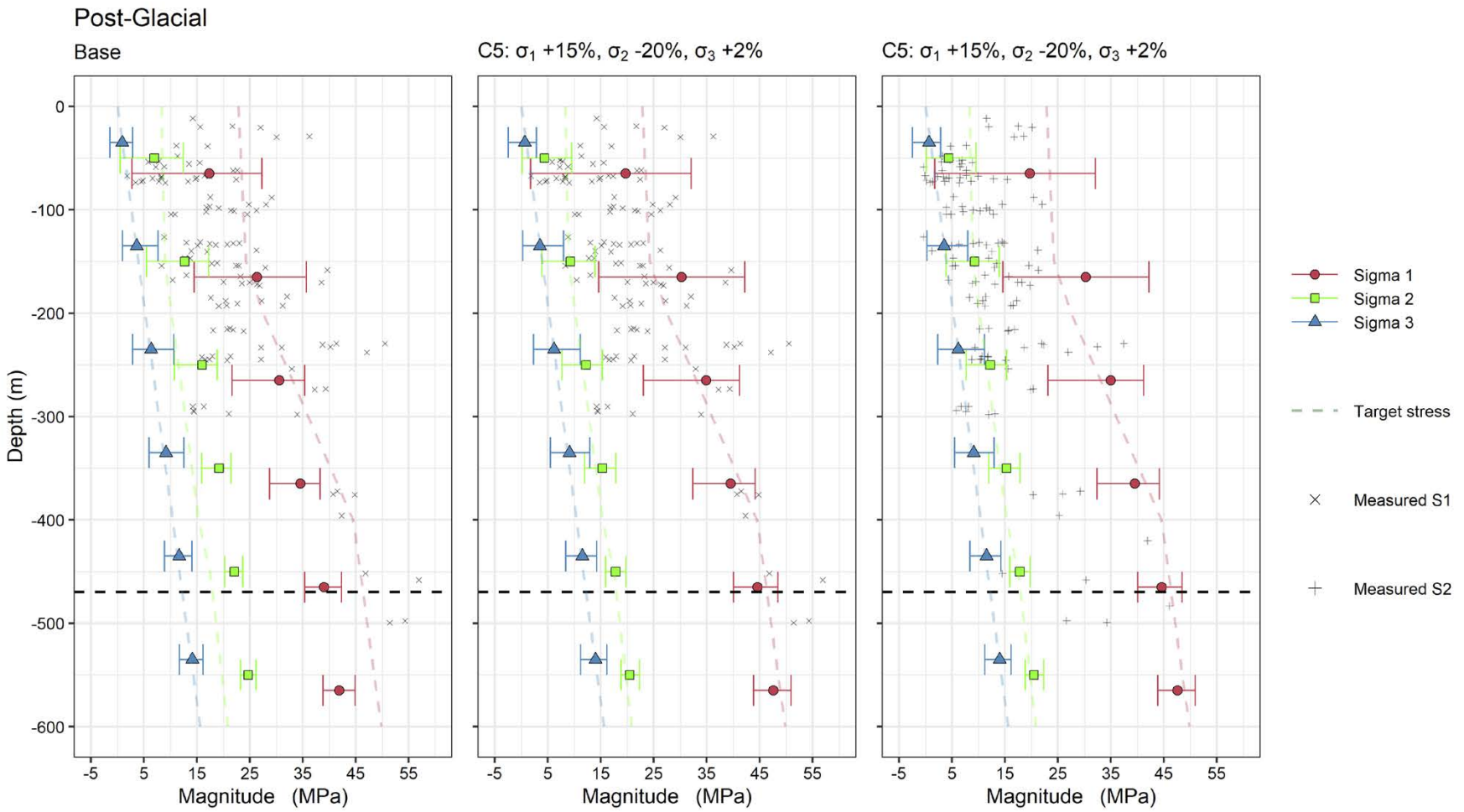

Figure A9-10. *Mean and 95 % variation interval of the principal stress magnitudes versus measured stresses at hundred meter intervals for the Base case and Case 5 of Phase 2 simulations after glaciation from a cylinder covering the repository. The Martin (2007) interpretation is indicated with coloured dashed lines and the repository depth with a horizontal dashed black line. Field stress measurements indicated with grey cross or plus symbols.*

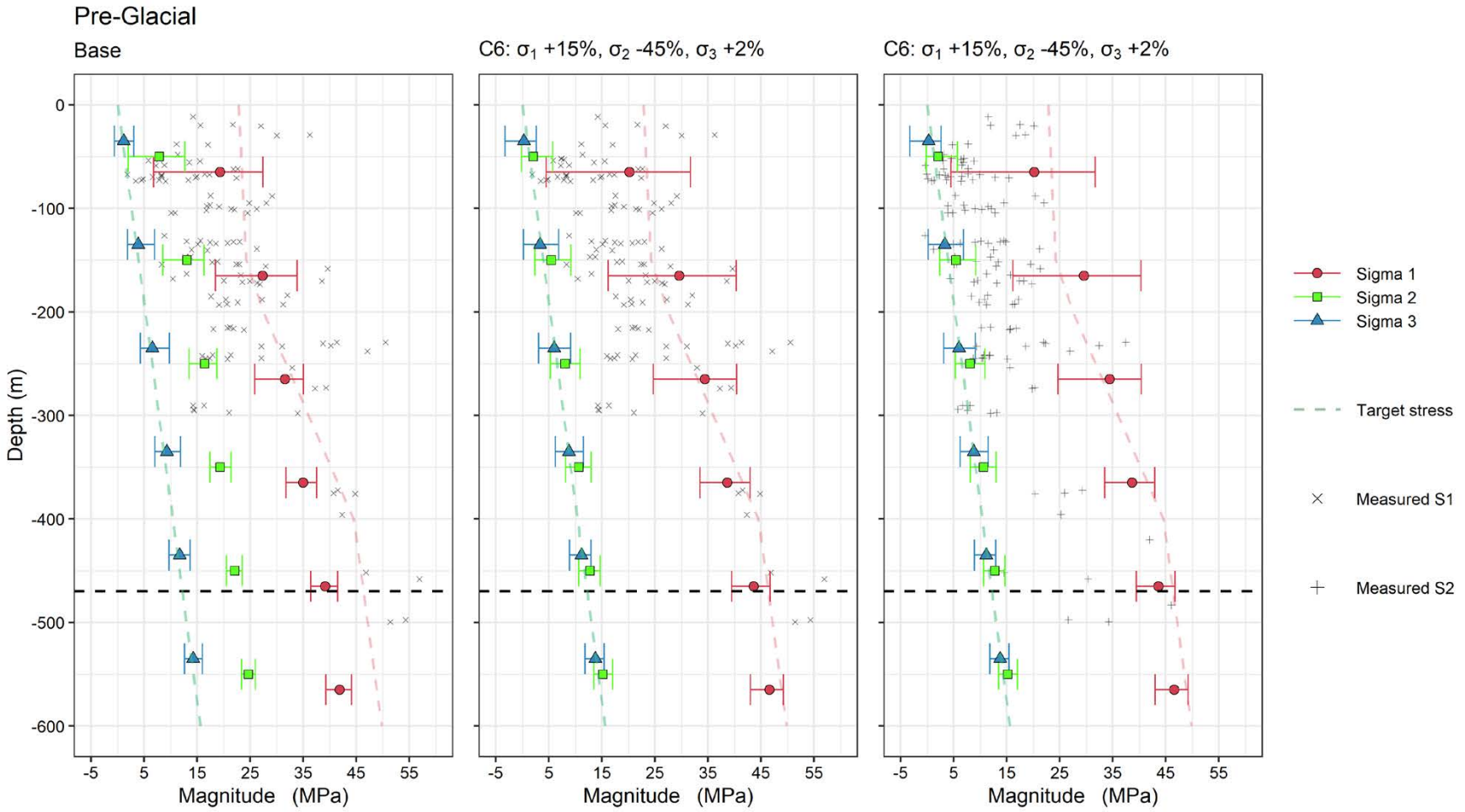

Figure A9-11. *Mean and 95 % variation interval of the principal stress magnitudes versus measured stresses at hundred meter intervals for the Base case and Case 6 of Phase 2 simulations before glaciation from a cylinder covering the repository. The Martin (2007) interpretation is indicated with coloured dashed lines and the repository depth with a horizontal dashed black line. Field stress measurements indicated with grey cross or plus symbols.*

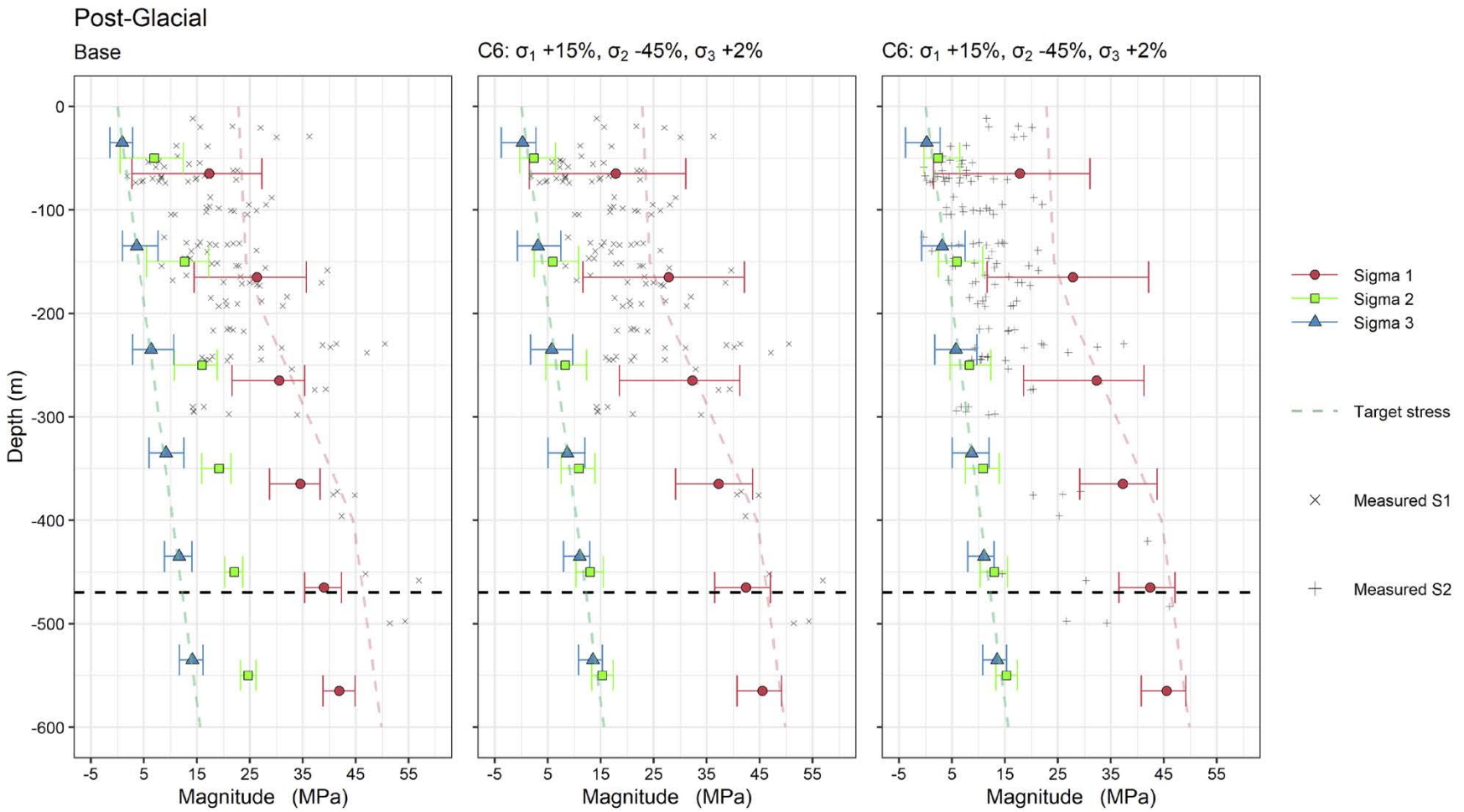

Figure A9-12. *Mean and 95 % variation interval of the principal stress magnitudes versus measured stresses at hundred meter intervals for the Base case and Case 6 of Phase 2 simulations after glaciation from a cylinder covering the repository. The Martin (2007) interpretation is indicated with coloured dashed lines and the repository depth with a horizontal dashed black line. Field stress measurements indicated with grey cross or plus symbols.*

Appendix 10

Phase 1 principal stress lower hemisphere projections

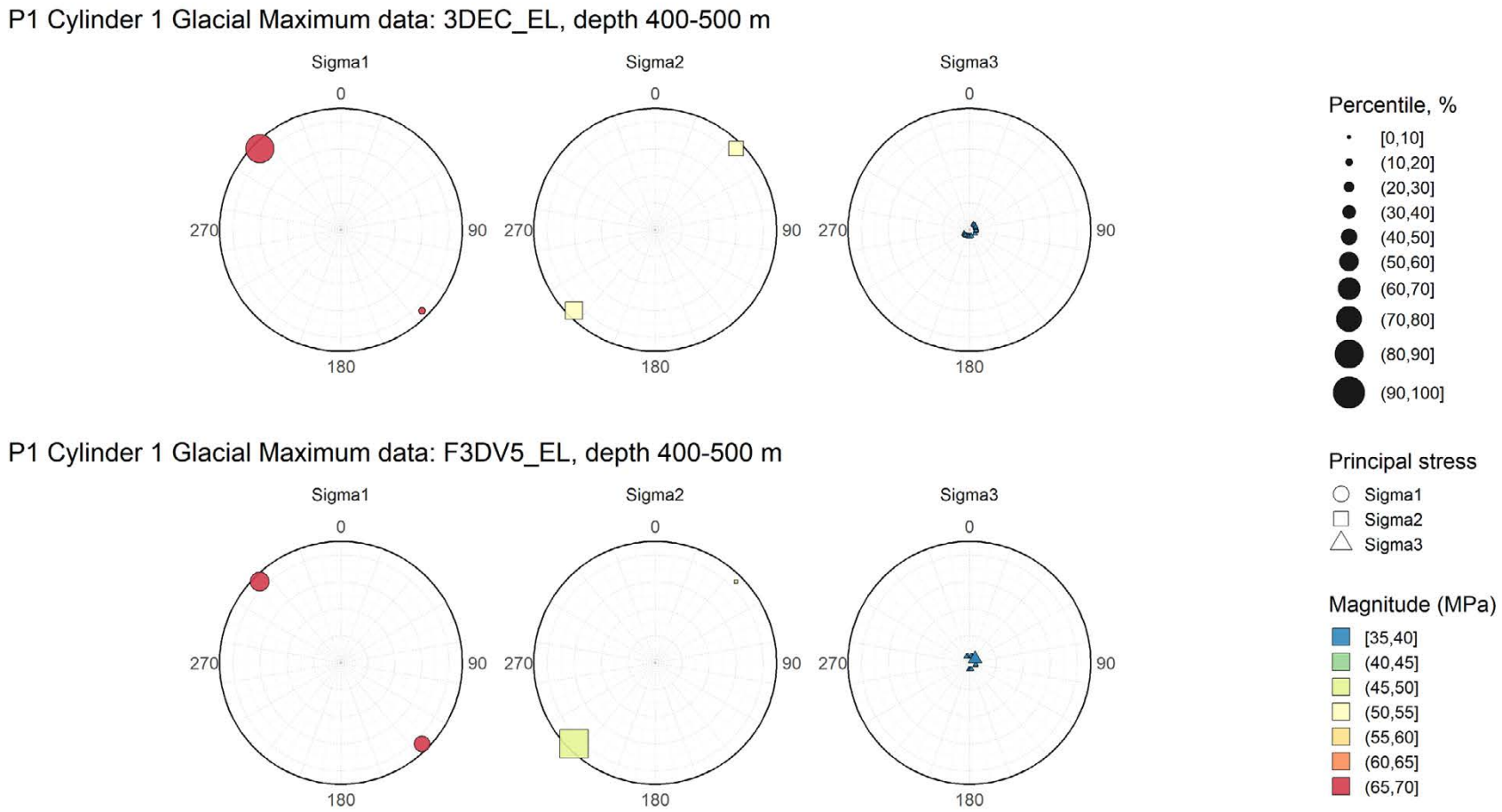

Figure A10-1. *Lower hemisphere projection polar plot of the principal stresses at 20° intervals obtained from cylinder 1 of fully elastic Phase 1 simulations after the glacial maximum, coloured according to magnitude and symbol sizes by percentile. z = 400–500 m.*

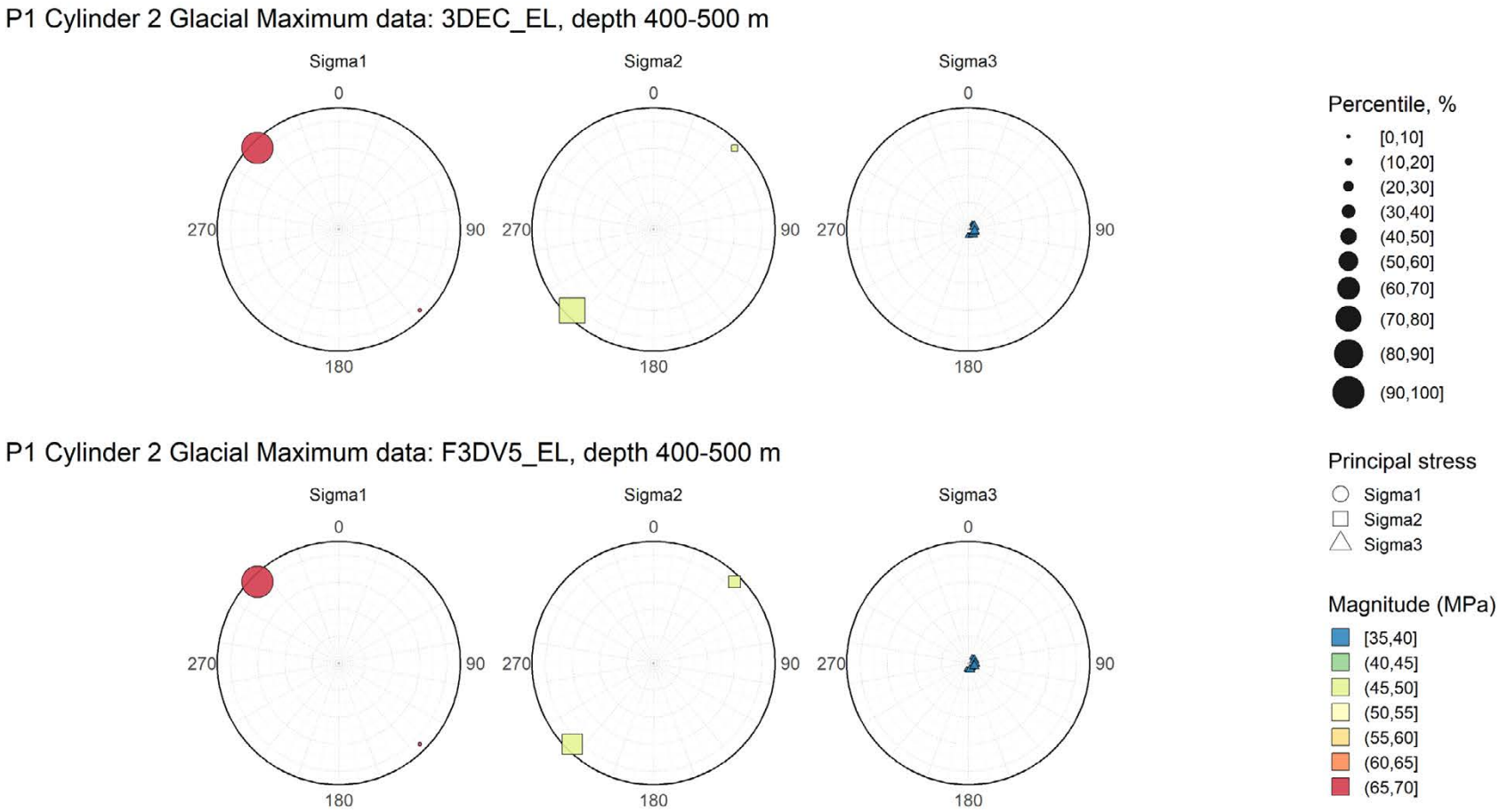

Figure A10-2. *Lower hemisphere projection polar plot of the principal stresses at 20° intervals obtained from cylinder 2 of fully elastic Phase 1 simulations after the glacial maximum, coloured according to magnitude and symbol sizes by percentile. z = 400−500 m.*

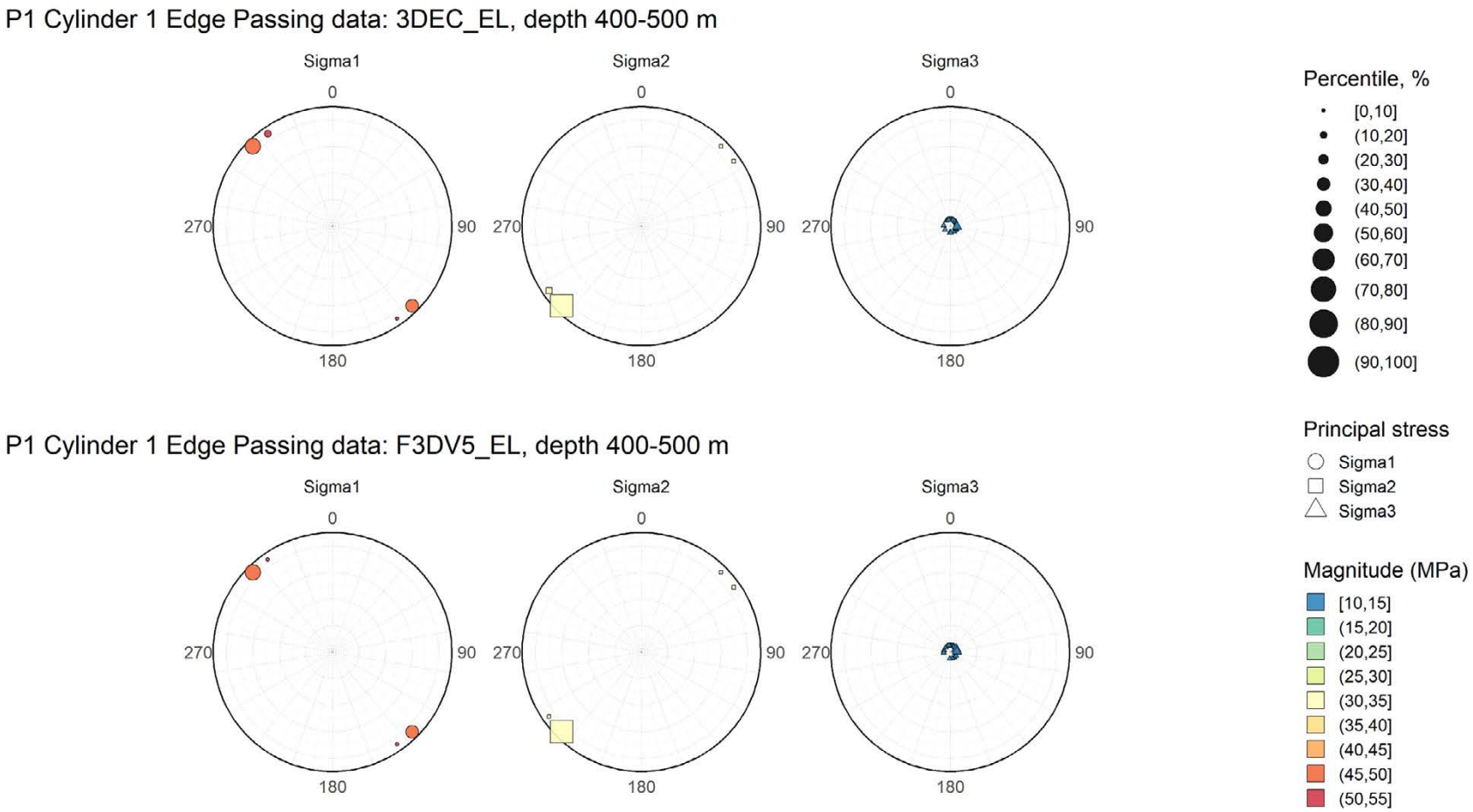

Figure A10-3. *Lower hemisphere projection polar plot of the principal stresses at 20° intervals obtained from cylinder 1 of fully elastic Phase 1 simulations after the edge passing stage, coloured according to magnitude and symbol sizes by percentile. z = 400–500 m.*

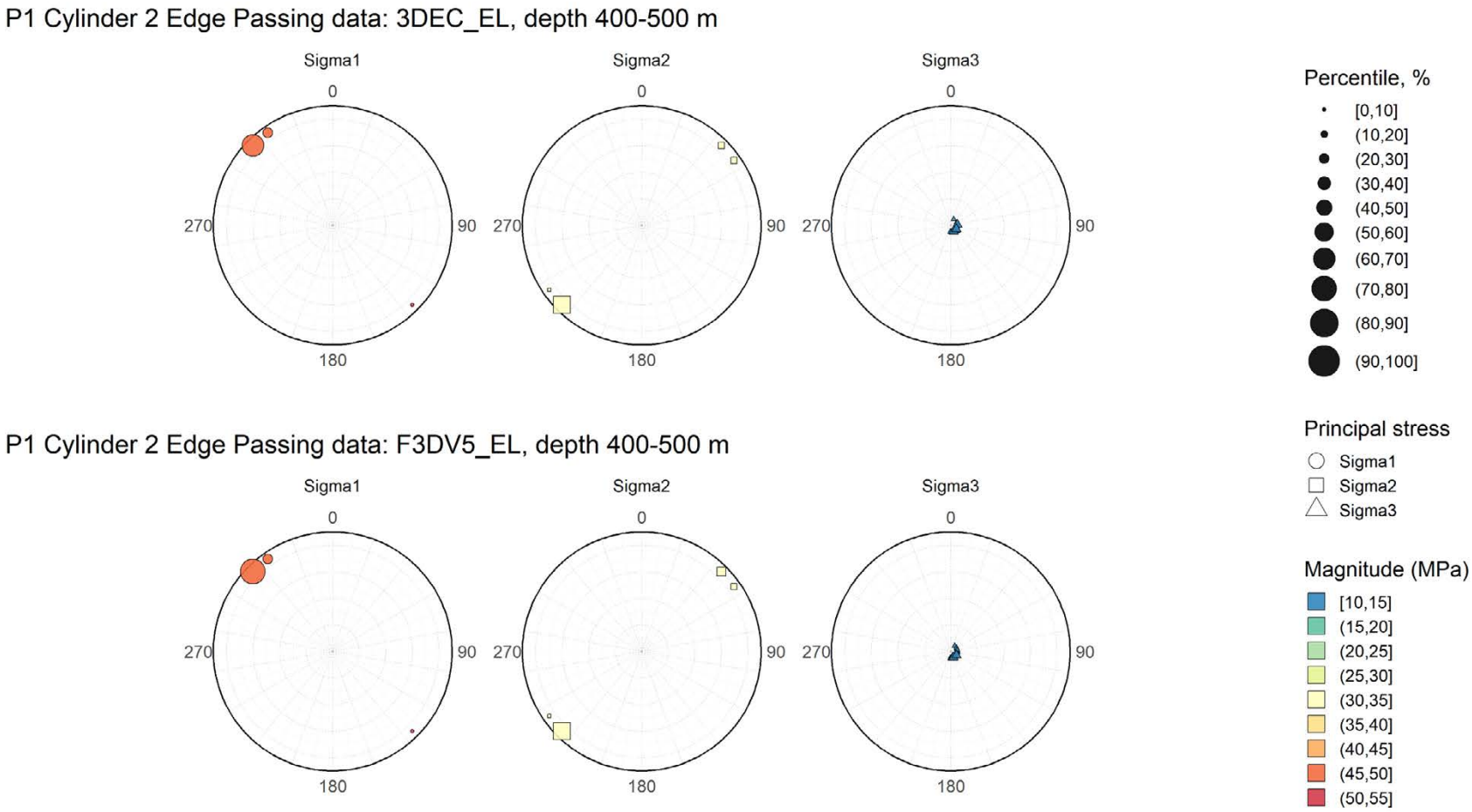

Figure A10-4. *Lower hemisphere projection polar plot of the principal stresses at 20° intervals obtained from cylinder 2 of fully elastic Phase 1 simulations after the edge passing stage, coloured according to magnitude and symbol sizes by percentile. z = 400−500 m.*

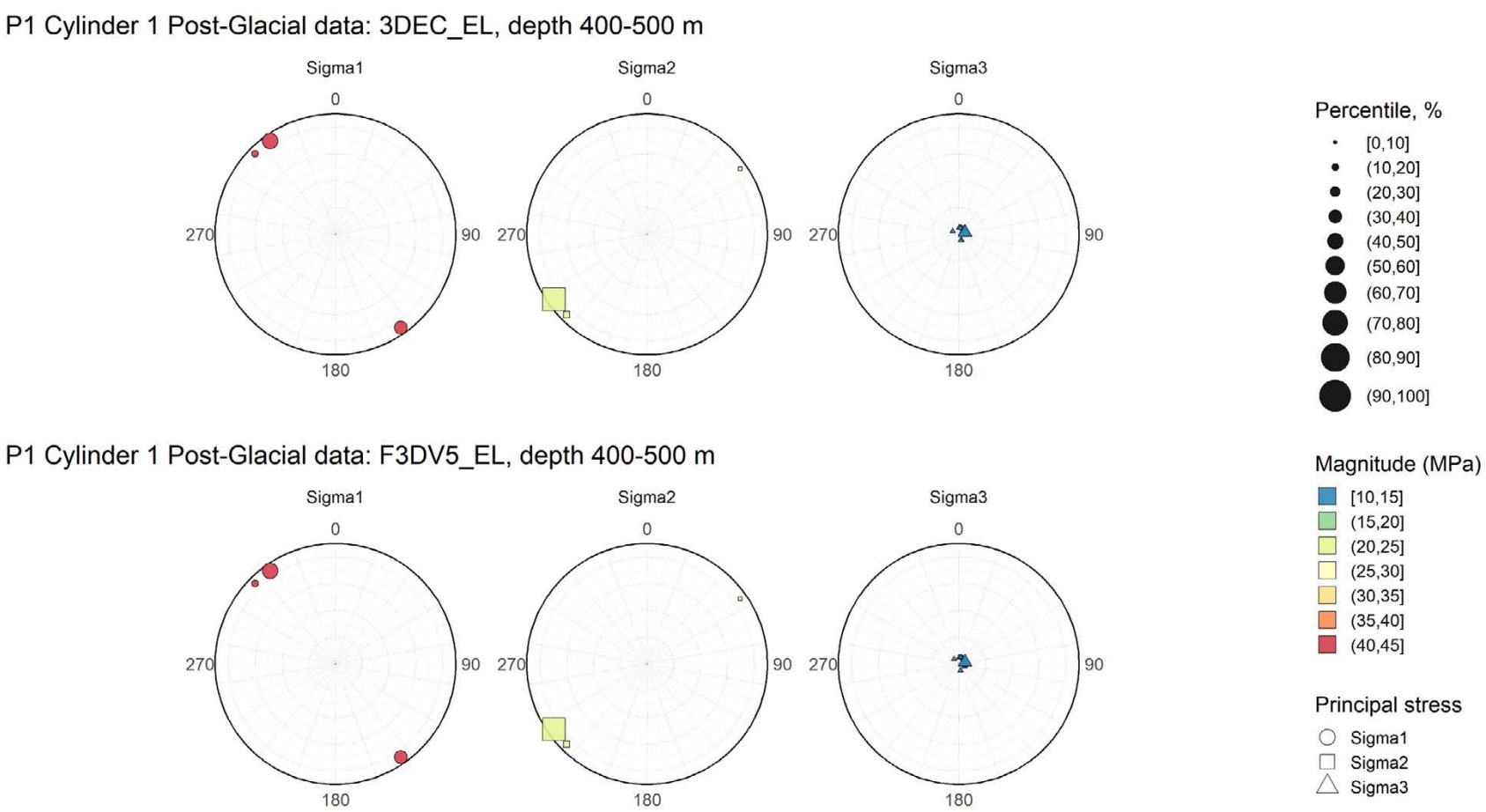

Figure A10-5. *Lower hemisphere projection polar plot of the principal stresses at 20° intervals obtained from cylinder 1 of fully elastic Phase 1 simulations after glaciation, coloured according to magnitude and symbol sizes by percentile. z = 400−500 m.*

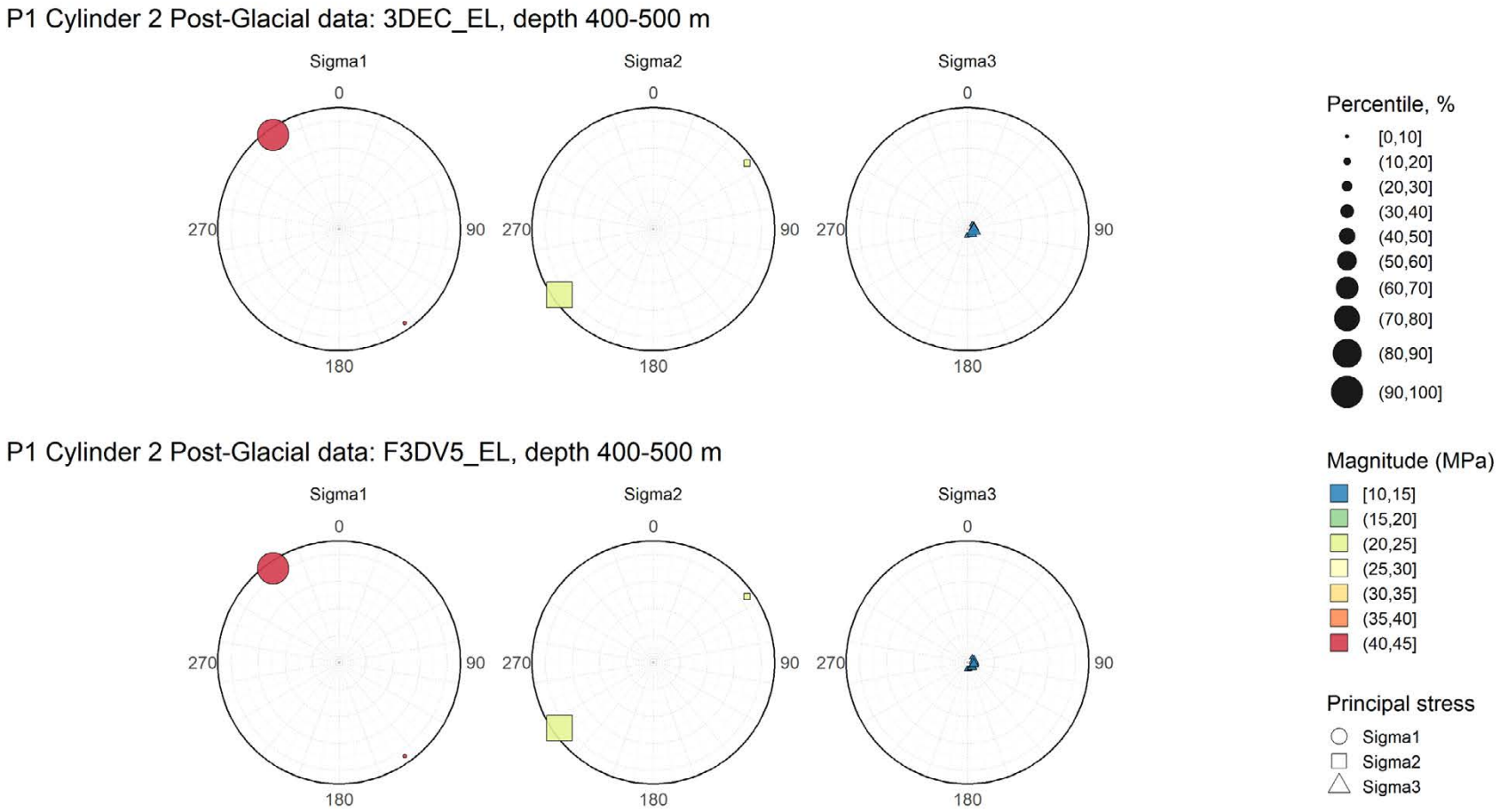

Figure A10-6. *Lower hemisphere projection polar plot of the principal stresses at 20° intervals obtained from cylinder 2 of fully elastic Phase 1 simulations after glaciation, coloured according to magnitude and symbol sizes by percentile. z = 400–500 m.*

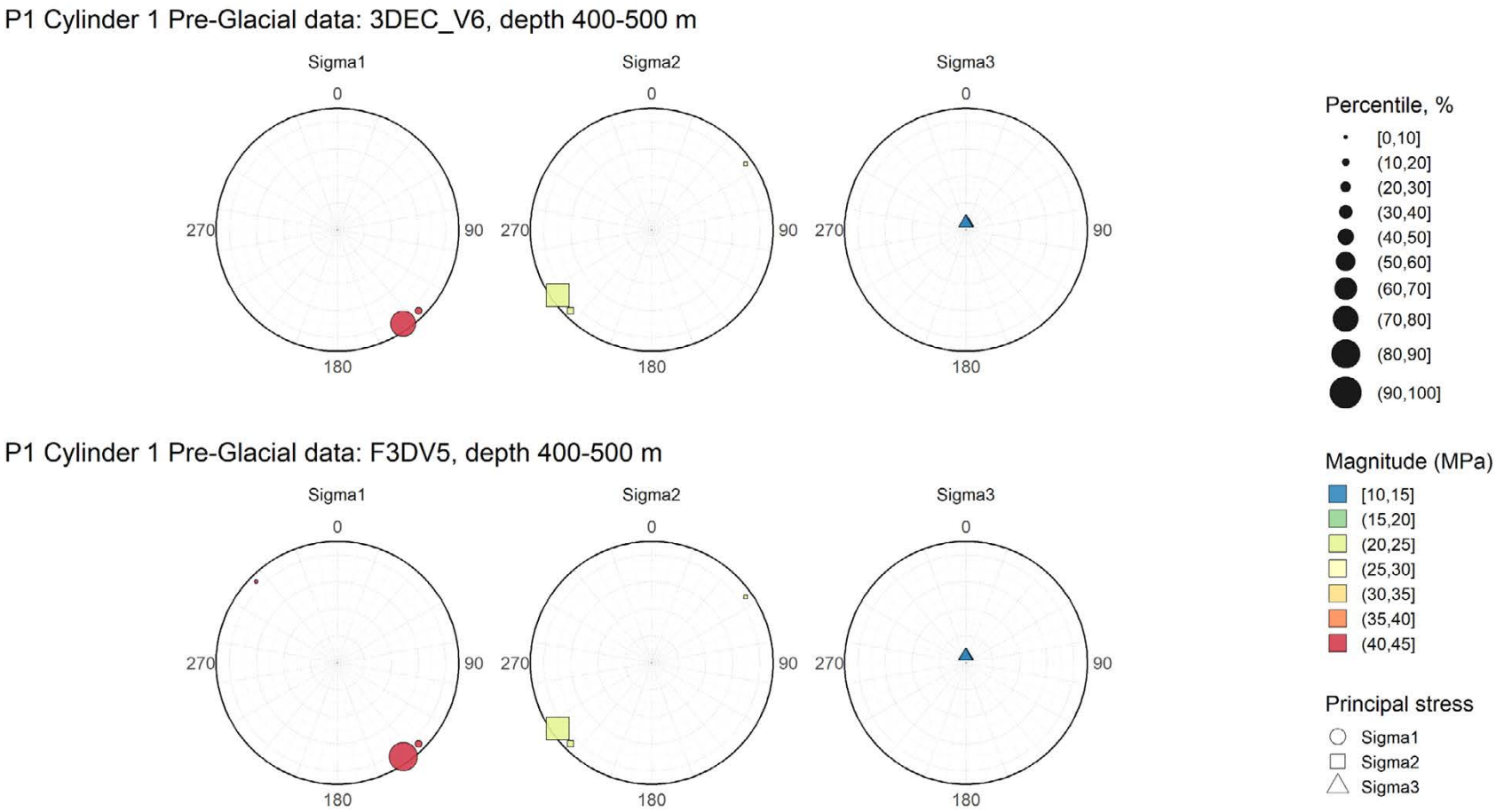

Figure A10-7. *Lower hemisphere projection polar plot of the principal stresses at 20° intervals obtained from cylinder 1 of elastoplastic Phase 1 simulations before glaciation, coloured according to magnitude and symbol sizes by percentile. z = 400–500 m.*

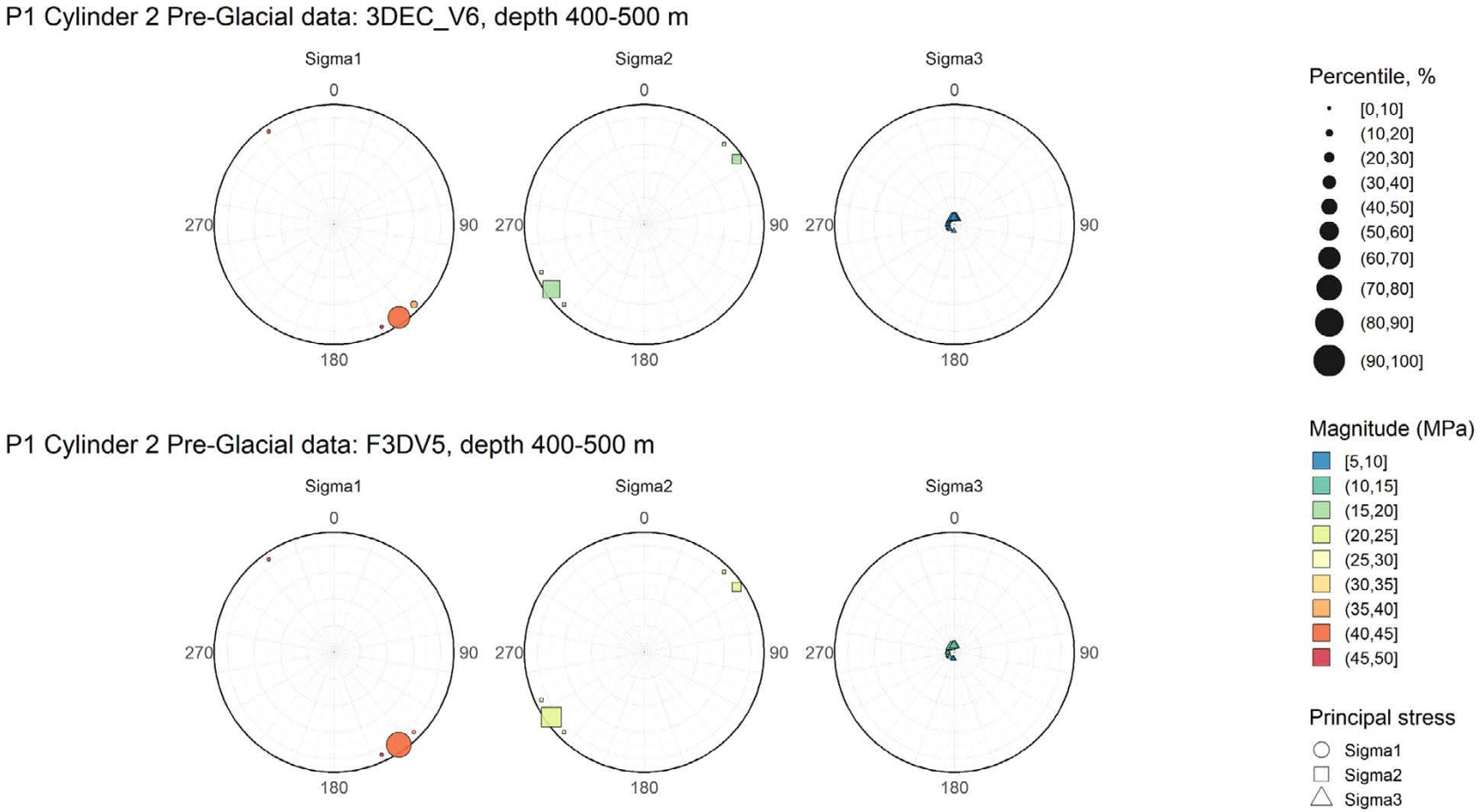

Figure A10-8. *Lower hemisphere projection polar plot of the principal stresses at 20° intervals obtained from cylinder 2 of elastoplastic Phase 1 simulations before glaciation, coloured according to magnitude and symbol sizes by percentile. z = 400–500 m.*

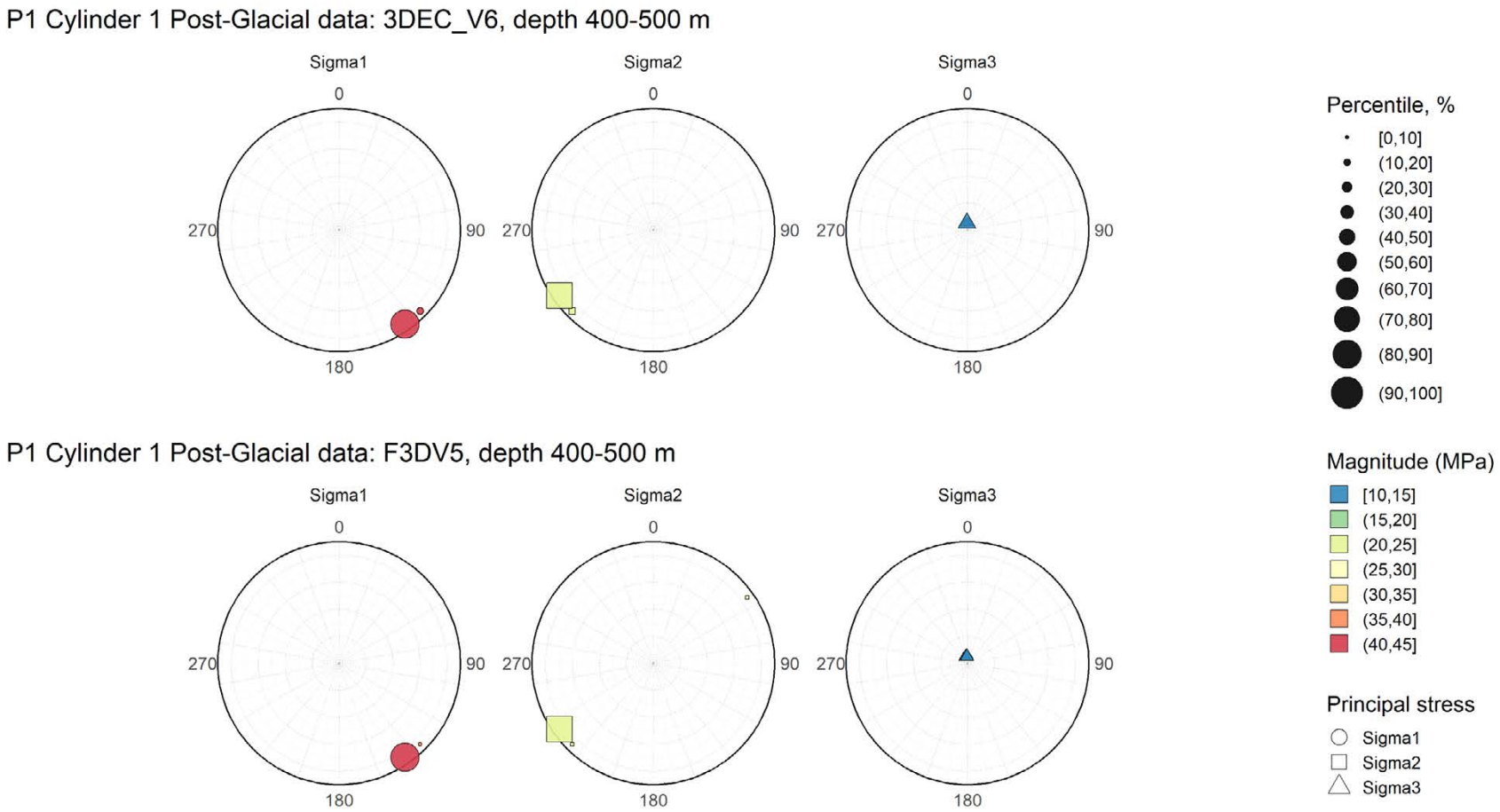

Figure A10-9. *Lower hemisphere projection polar plot of the principal stresses at 20° intervals obtained from cylinder 1 of elastoplastic Phase 1 simulations after glaciation, coloured according to magnitude and symbol sizes by percentile. z = 400–500 m.*

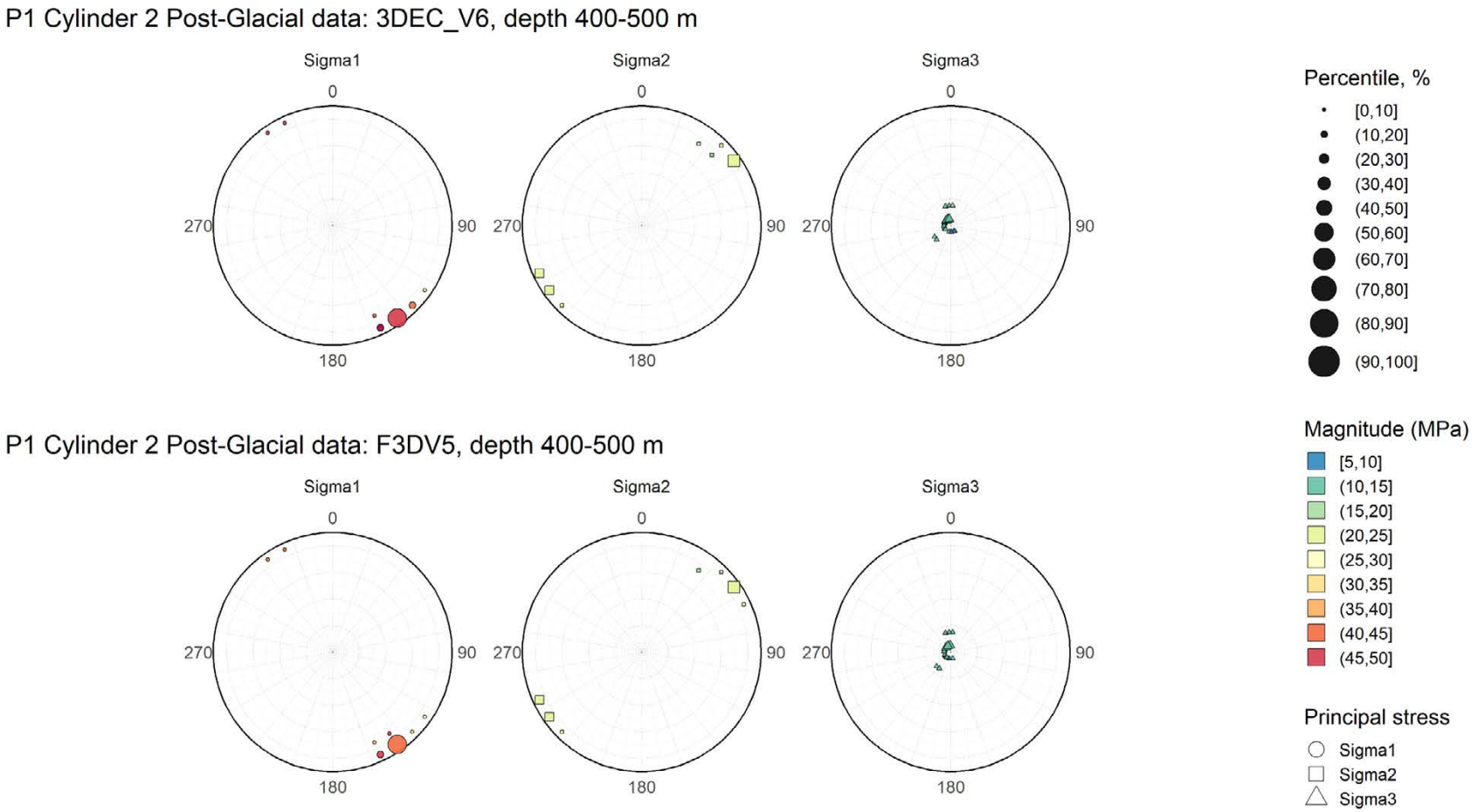

Figure A10-10. *Lower hemisphere projection polar plot of the principal stresses at 20° intervals obtained from cylinder 2 of elastoplastic Phase 1 simulations after glaciation, coloured according to magnitude and symbol sizes by percentile. z = 400–500 m.*

Appendix 11

Phase 2 principal stress lower hemisphere projections

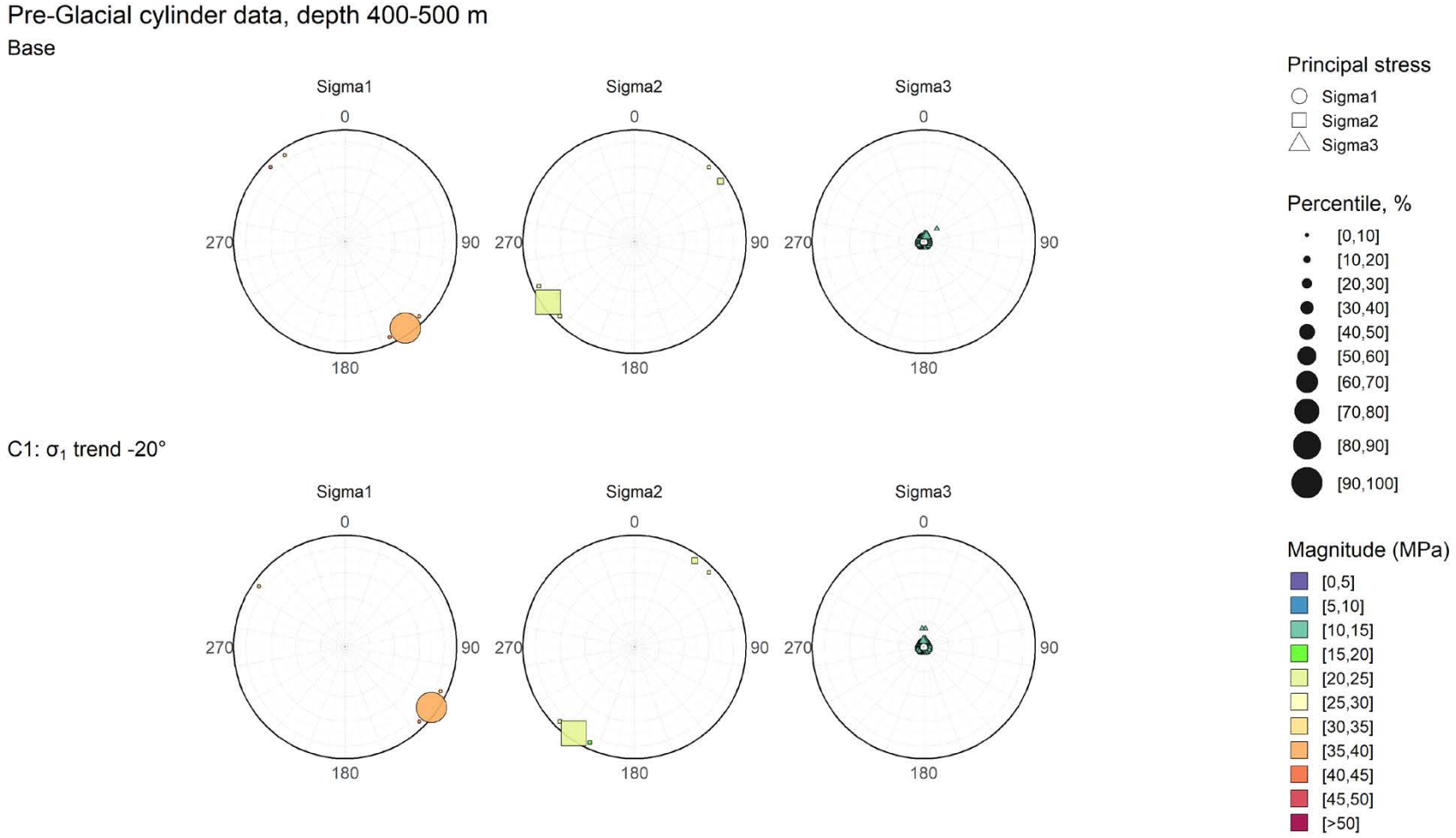

Figure A11-1. *Lower hemisphere projection polar plot of the principal stresses at 20° intervals obtained from a depth section of a cylinder covering the repository footprint (Figure 4-2) for the Base case and Case 1 of Phase 2 simulations before glaciation, coloured according to magnitude and symbol sizes by percentile. z = 400–500 m.*

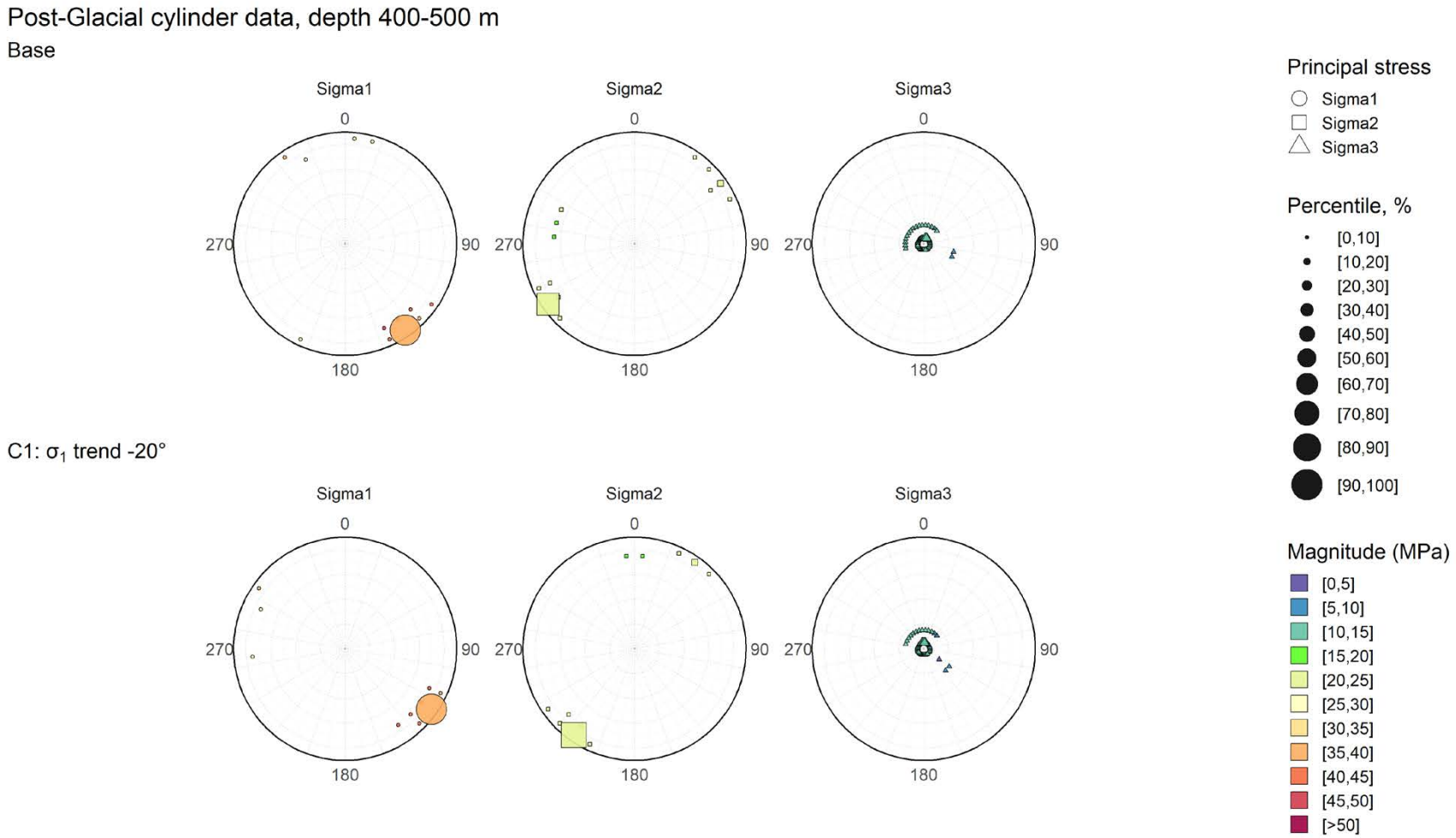

Figure A11-2. *Lower hemisphere projection polar plot of the principal stresses at 20° intervals obtained from a depth section of a cylinder covering the repository footprint (Figure 4-2) for the Base case and Case 1 of Phase 2 simulations after glaciation, coloured according to magnitude and symbol sizes by percentile. z = 400–500 m.*

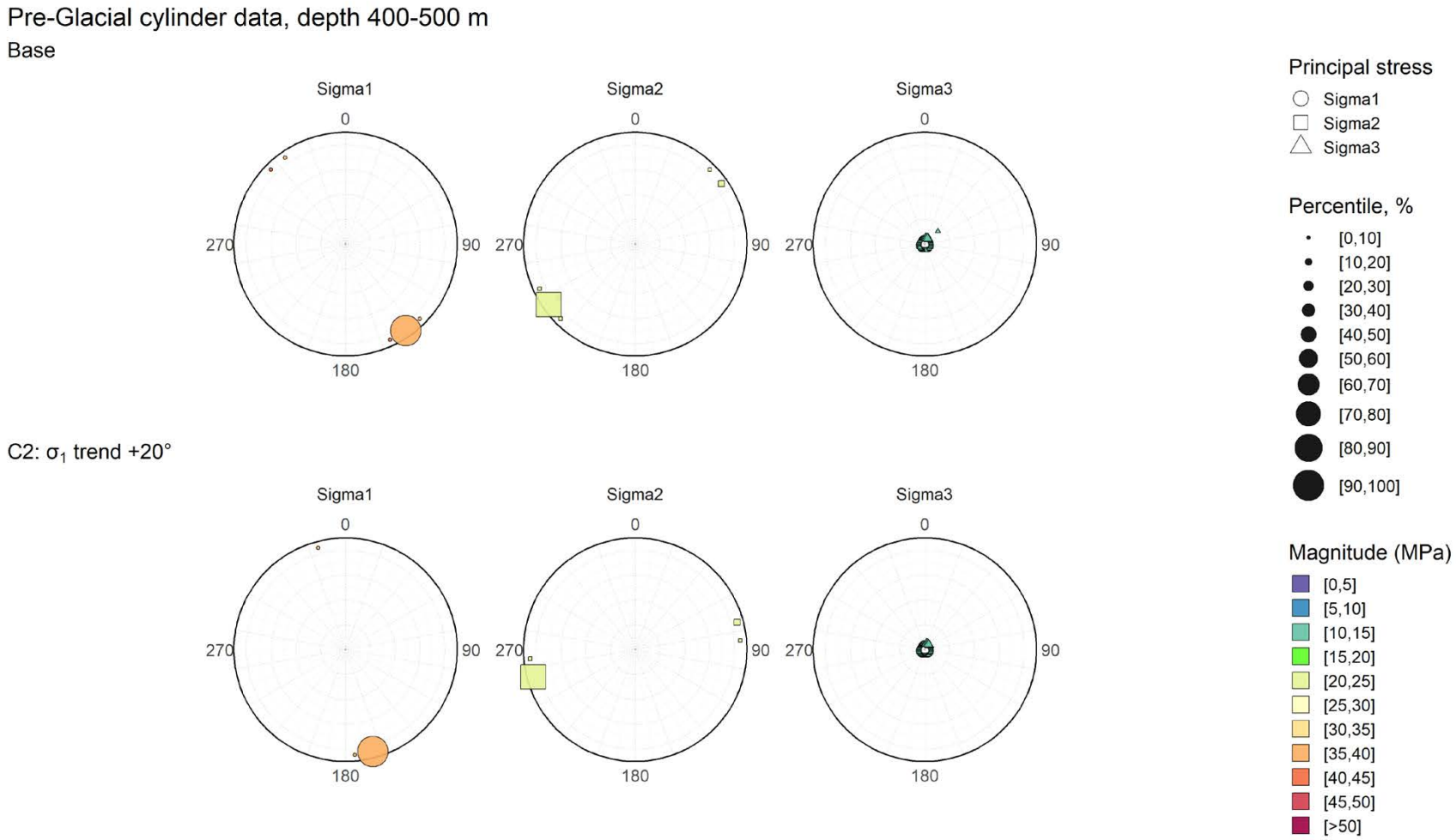

Figure A11-3. *Lower hemisphere projection polar plot of the principal stresses at 20° intervals obtained from a depth section of a cylinder covering the repository footprint (Figure 4-2) for the Base case and Case 2 of Phase 2 simulations before glaciation, coloured according to magnitude and symbol sizes by percentile. z = 400–500 m.*

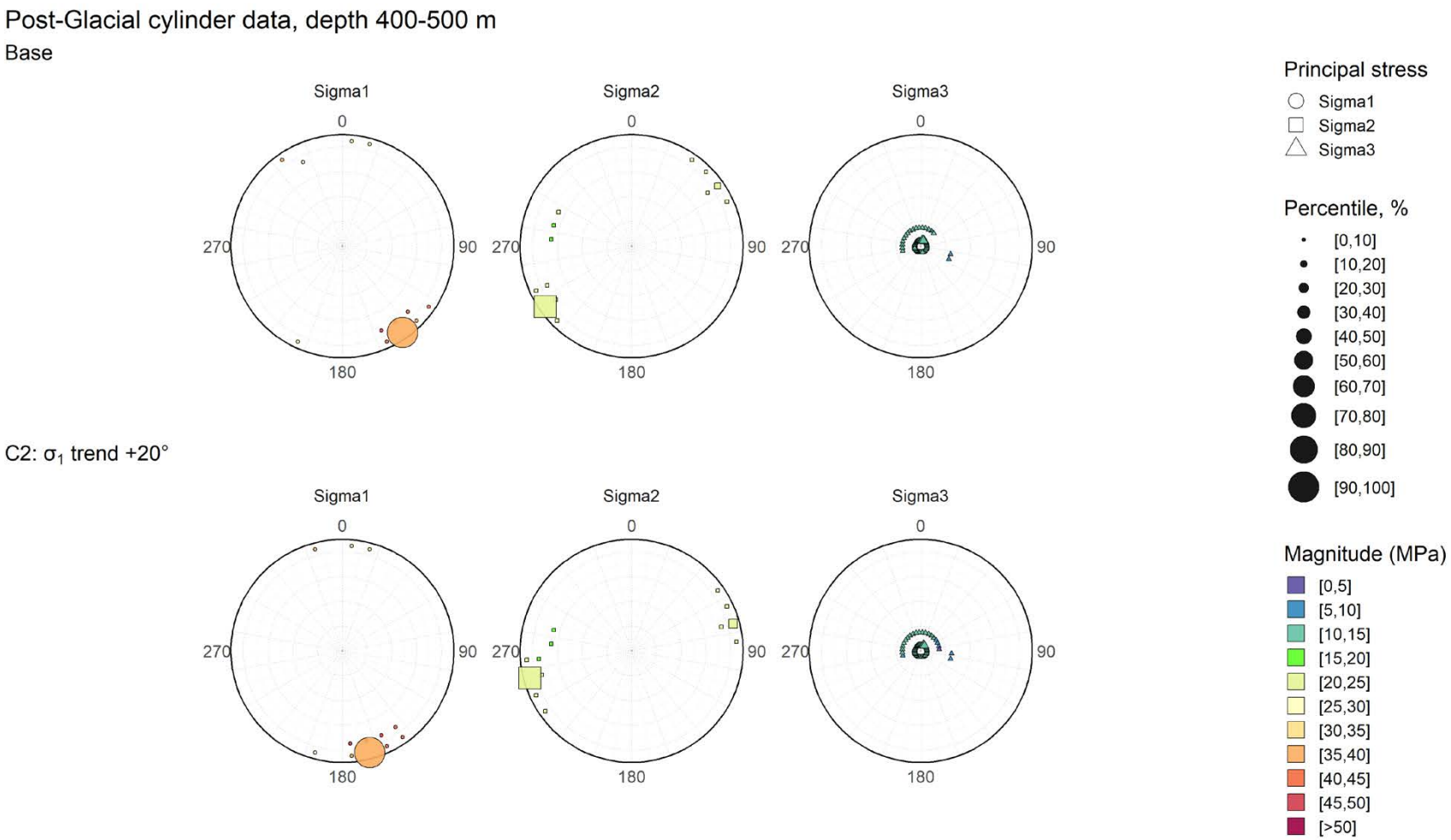

Figure A11-4. *Lower hemisphere projection polar plot of the principal stresses at 20° intervals obtained from a depth section of a cylinder covering the repository footprint (Figure 4-2) for the Base case and Case 2 of Phase 2 simulations after glaciation, coloured according to magnitude and symbol sizes by percentile. z = 400–500 m.*

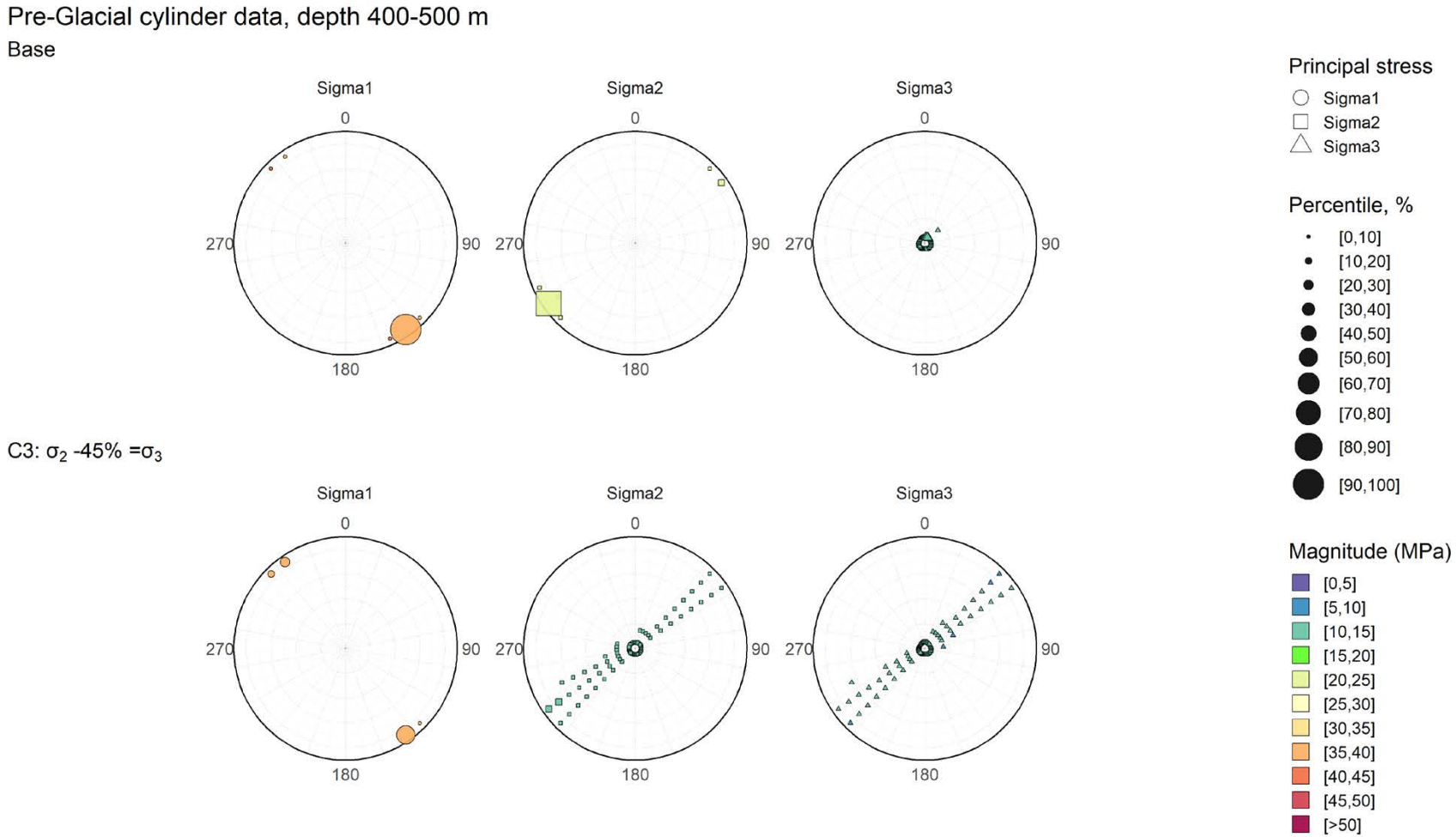

Figure A11-5. *Lower hemisphere projection polar plot of the principal stresses at 20° intervals obtained from a depth section of a cylinder covering the repository footprint (Figure 4-2) for the Base case and Case 3 of Phase 2 simulations before glaciation, coloured according to magnitude and symbol sizes by percentile. z = 400–500 m.*

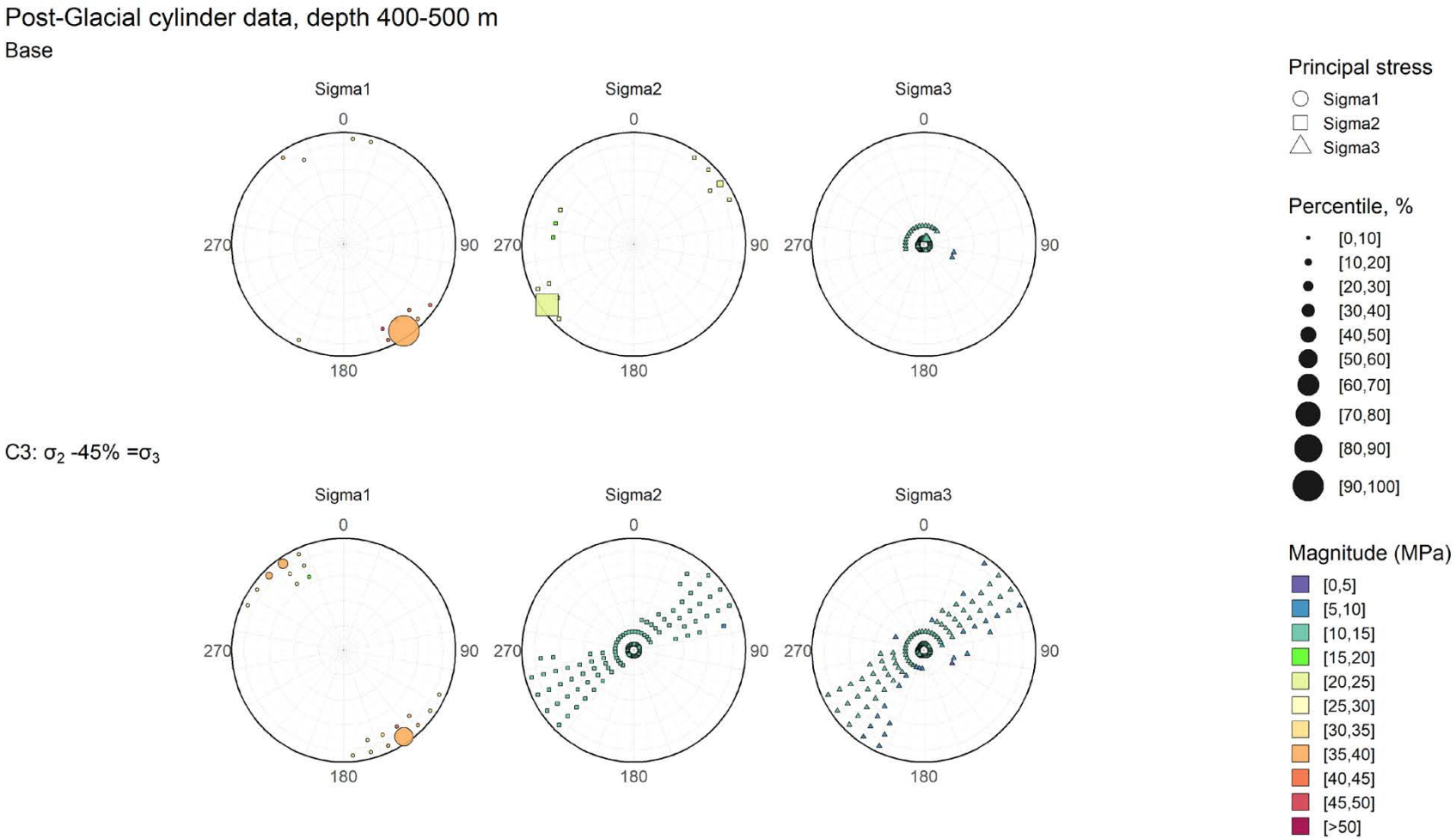

Figure A11-6. *Lower hemisphere projection polar plot of the principal stresses at 20° intervals obtained from a depth section of a cylinder covering the repository footprint (Figure 4-2) for the Base case and Case 3 of Phase 2 simulations after glaciation, coloured according to magnitude and symbol sizes by percentile. z = 400–500 m.*

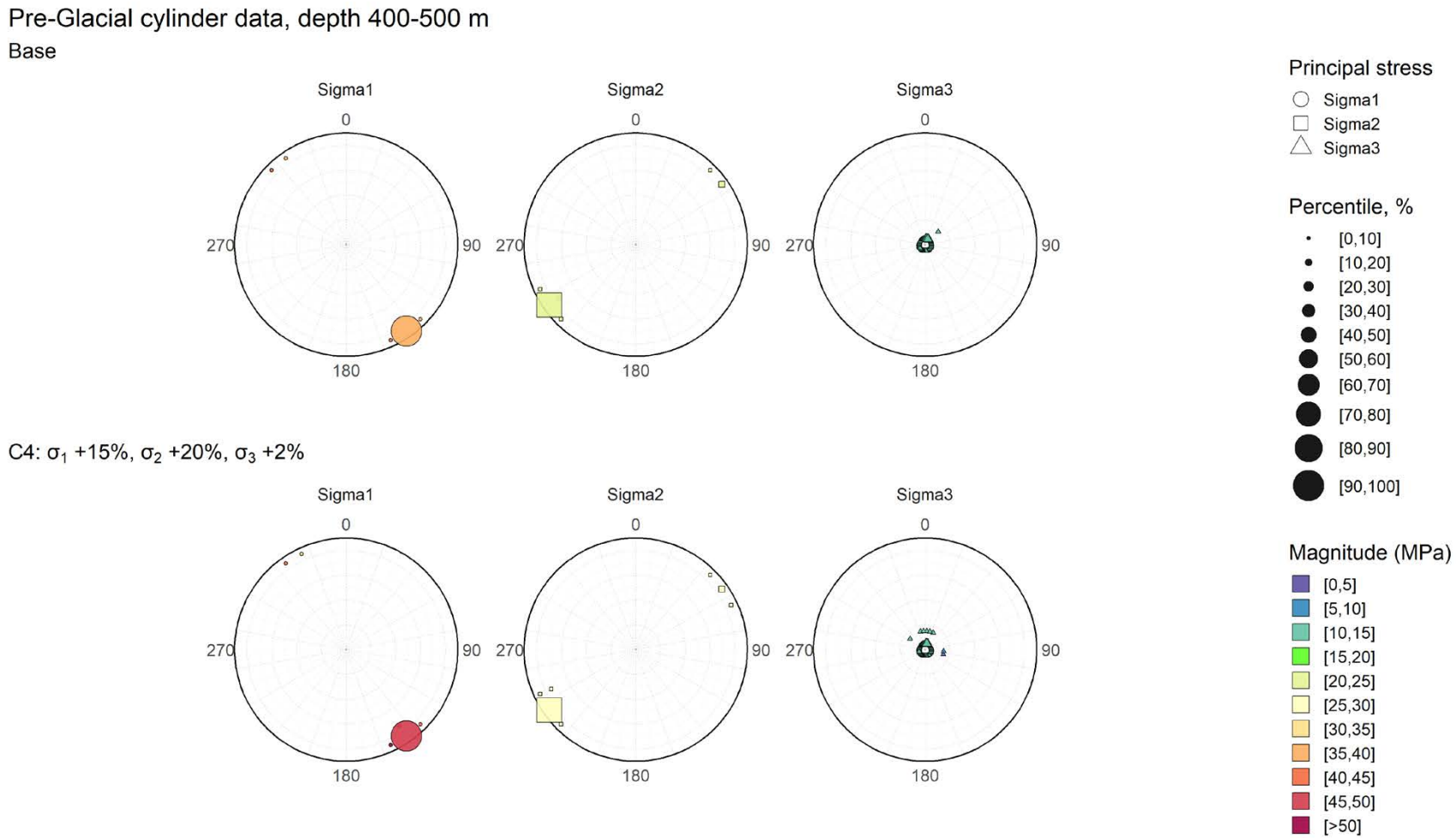

Figure A11-7. *Lower hemisphere projection polar plot of the principal stresses at 20° intervals obtained from a depth section of a cylinder covering the repository footprint (Figure 4-2) for the Base case and Case 4 of Phase 2 simulations before glaciation, coloured according to magnitude and symbol sizes by percentile. z = 400–500 m.*

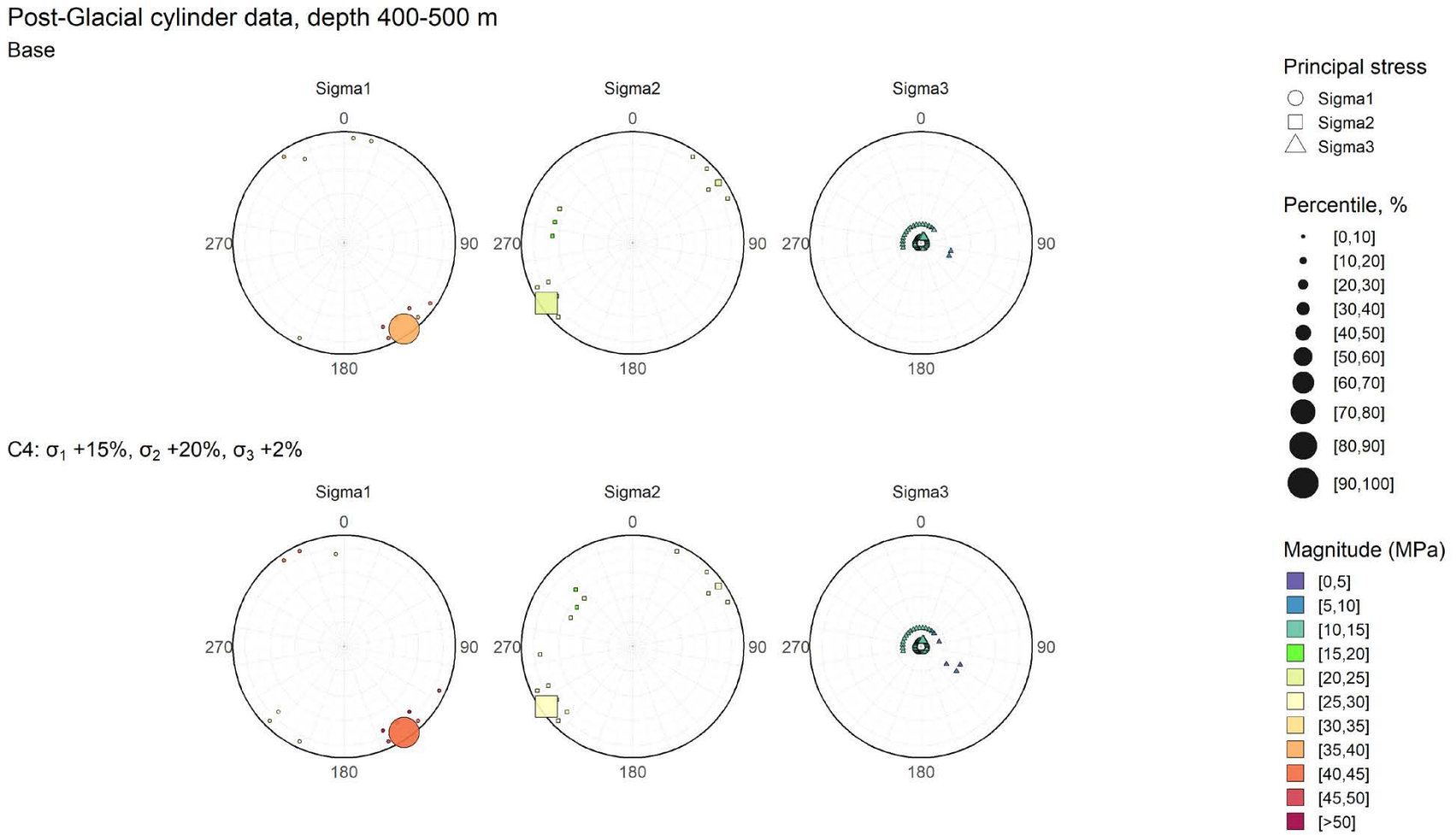

Figure A11-8. *Lower hemisphere projection polar plot of the principal stresses at 20° intervals obtained from a depth section of a cylinder covering the repository footprint (Figure 4-2) for the Base case and Case 4 of Phase 2 simulations after glaciation, coloured according to magnitude and symbol sizes by percentile. z = 400–500 m.*

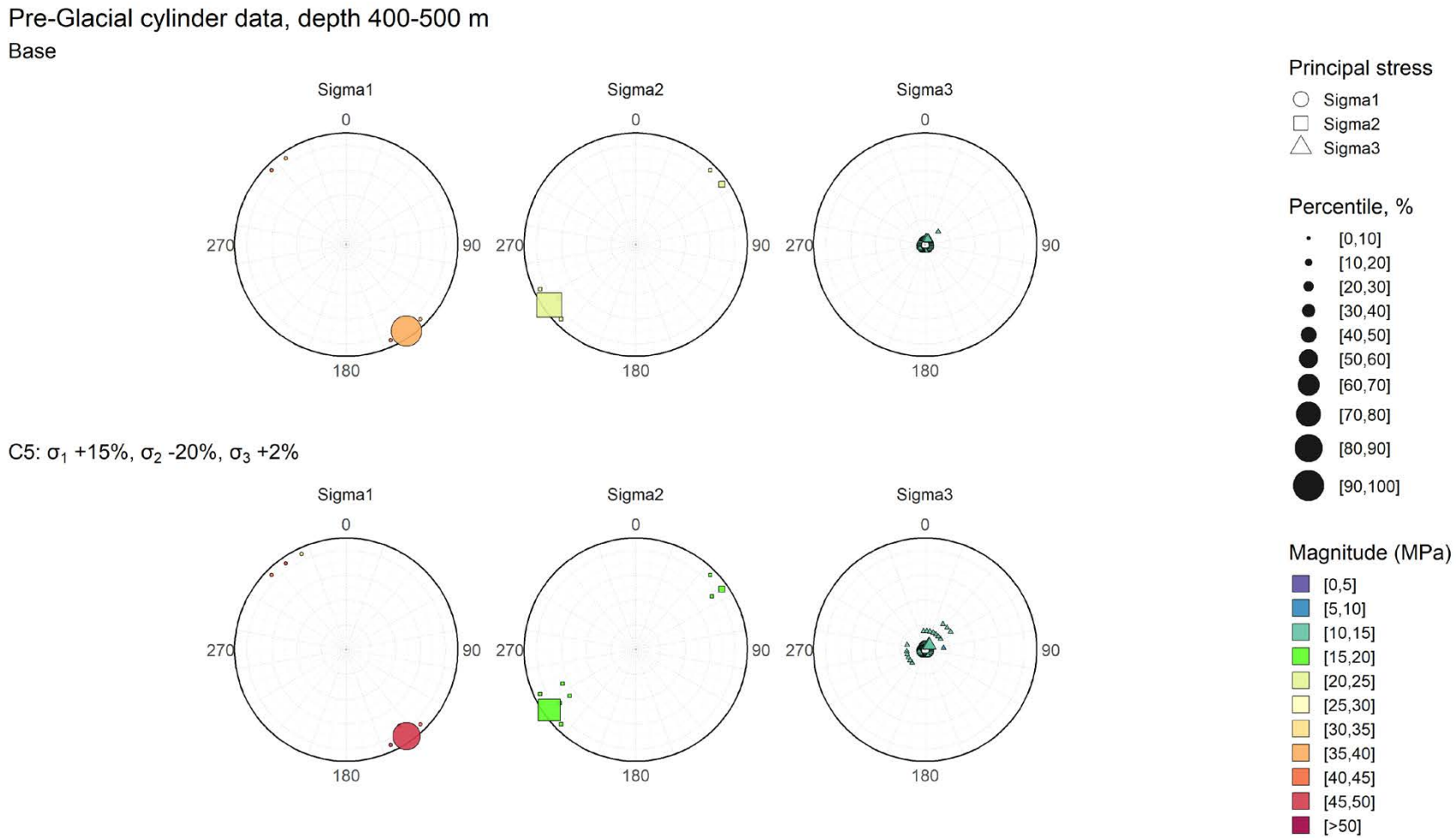

Figure A11-9. *Lower hemisphere projection polar plot of the principal stresses at 20° intervals obtained from a depth section of a cylinder covering the repository footprint (Figure 4-2) for the Base case and Case 5 of Phase 2 simulations before glaciation, coloured according to magnitude and symbol sizes by percentile. z = 400–500 m.*

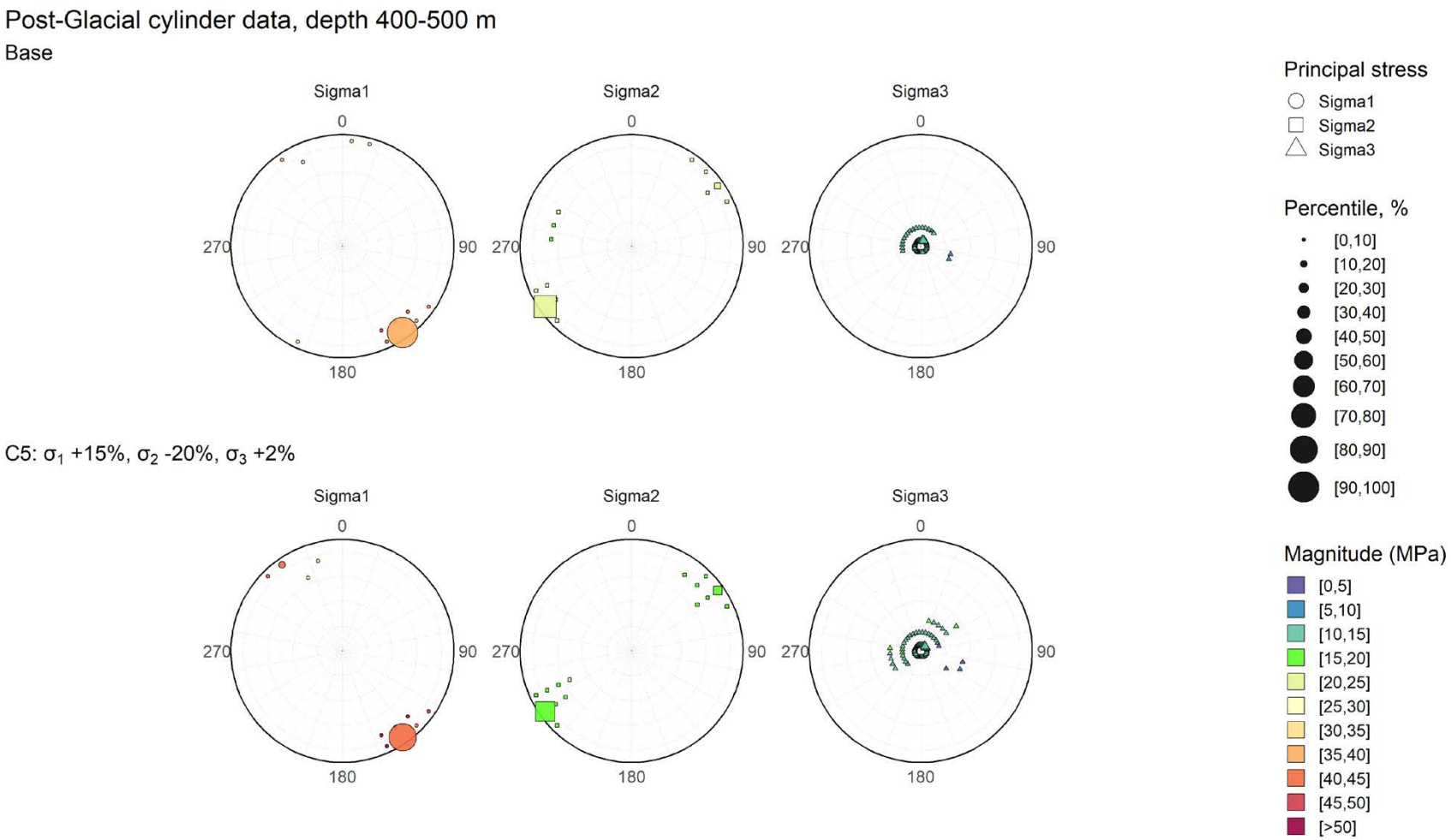

Figure A11-10. *Lower hemisphere projection polar plot of the principal stresses at 20° intervals obtained from a depth section of a cylinder covering the repository footprint (Figure 4-2) for the Base case and Case 5 of Phase 2 simulations after glaciation, coloured according to magnitude and symbol sizes by percentile. z = 400–500 m.*

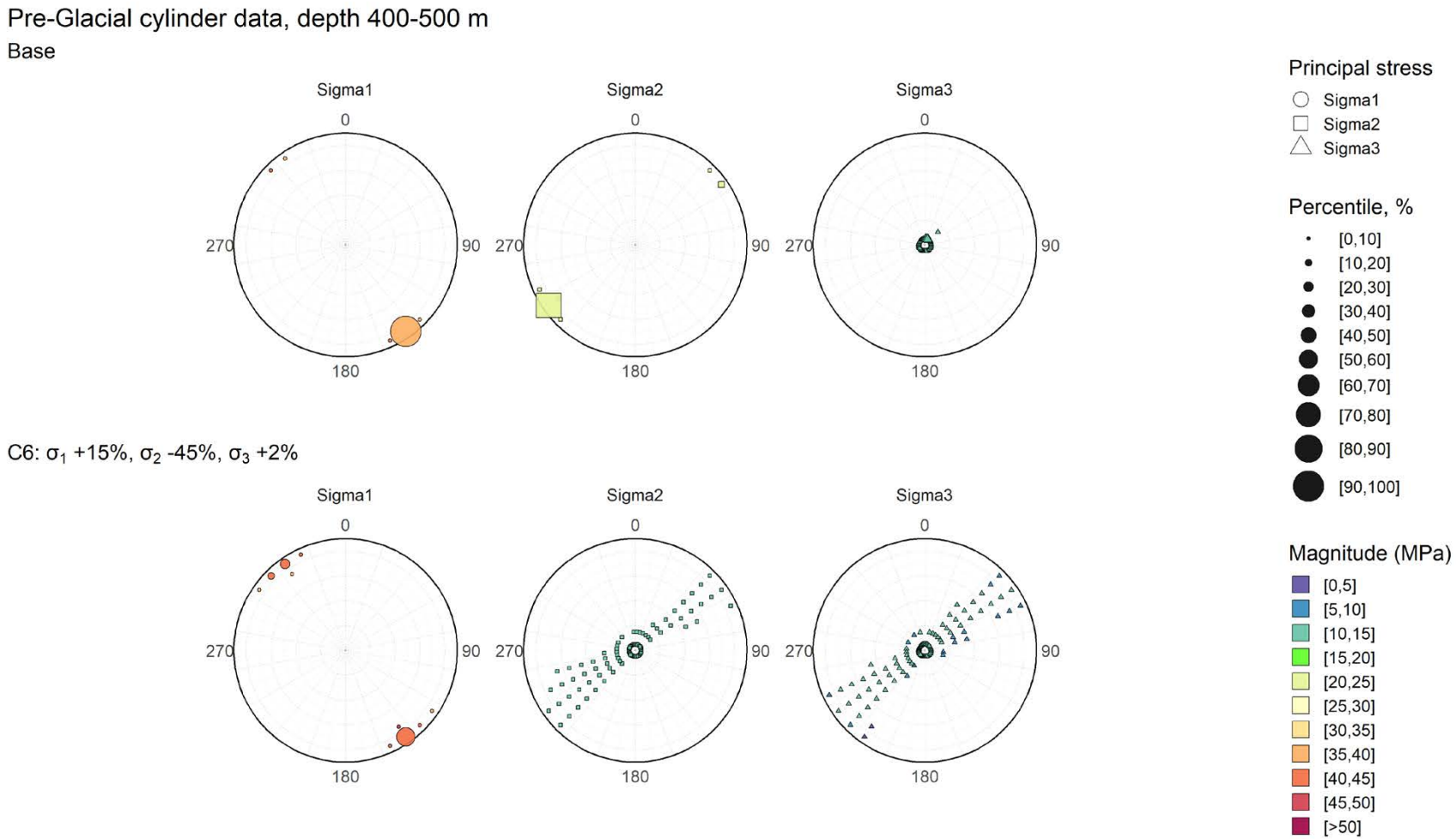

Figure A11-11. *Lower hemisphere projection polar plot of the principal stresses at 20° intervals obtained from a depth section of a cylinder covering the repository footprint (Figure 4-2) for the Base case and Case 6 of Phase 2 simulations before glaciation, coloured according to magnitude and symbol sizes by percentile. z = 400–500 m.*

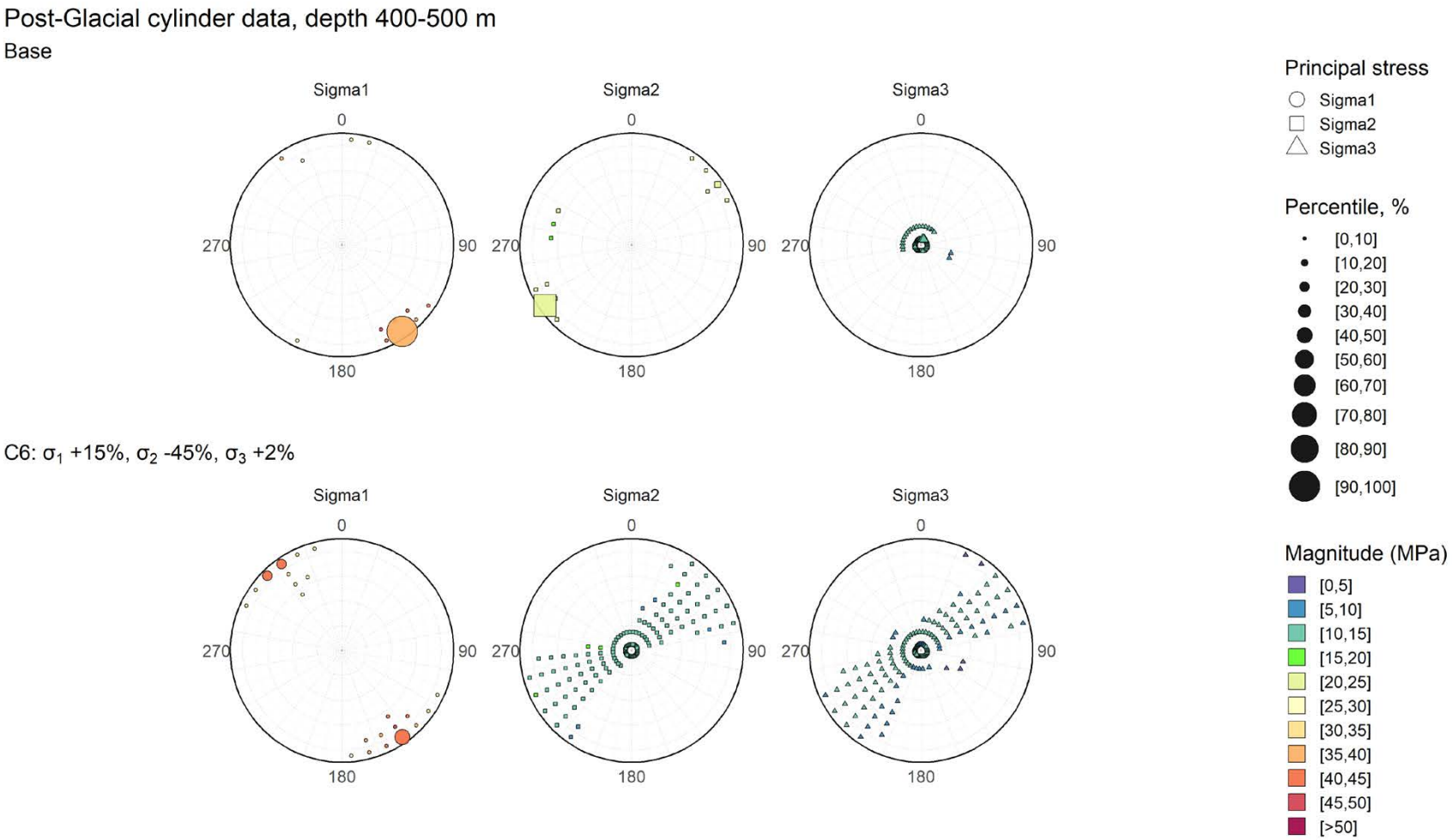

Figure A11-12. *Lower hemisphere projection polar plot of the principal stresses at 20° intervals obtained from a depth section of a cylinder covering the repository footprint (Figure 4-2) for the Base case and Case 6 of Phase 2 simulations after glaciation, coloured according to magnitude and symbol sizes by percentile. z = 400–500 m.*

Appendix 12

Phase 1 – frequency of σ_1 trend and magnitude variation at repository depth

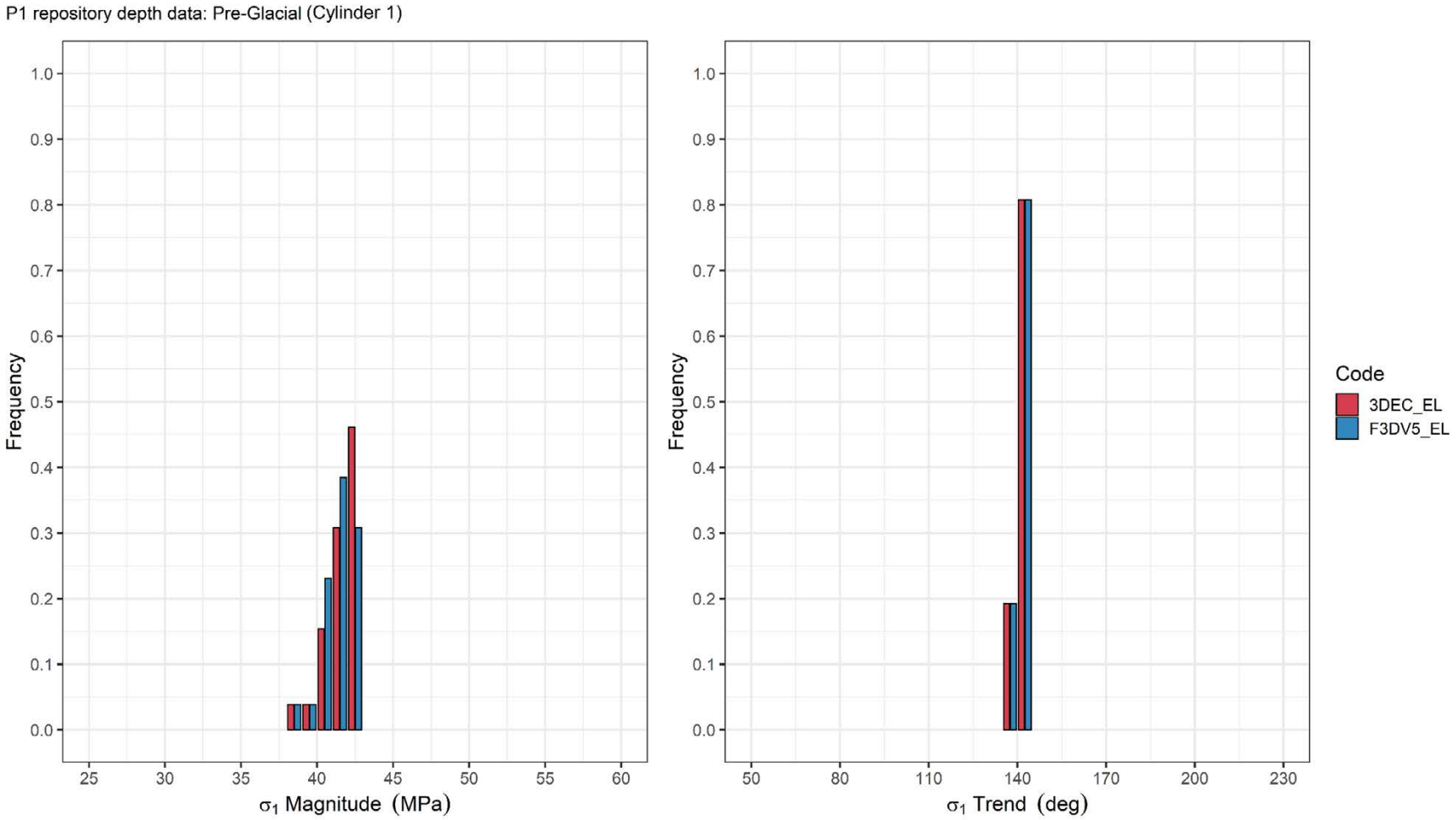

Figure A12-1. *Distribution of σ_1 trend and magnitude at repository depth from cylinder 1 before glaciation in a fully elastic simulation.*

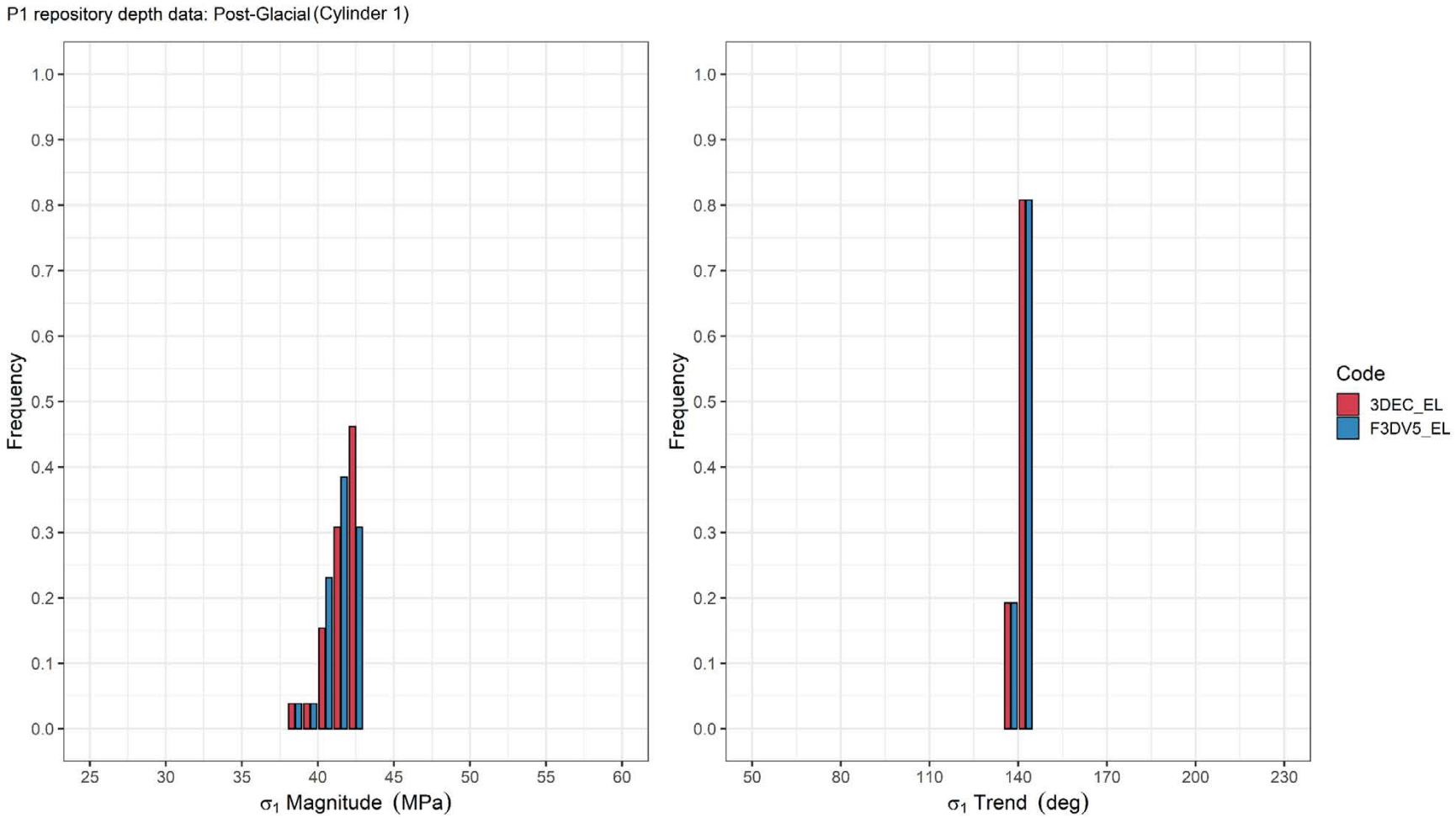

Figure A12-2. *Distribution of σ_1 trend and magnitude at repository depth from cylinder 1 after glaciation in a fully elastic simulation.*

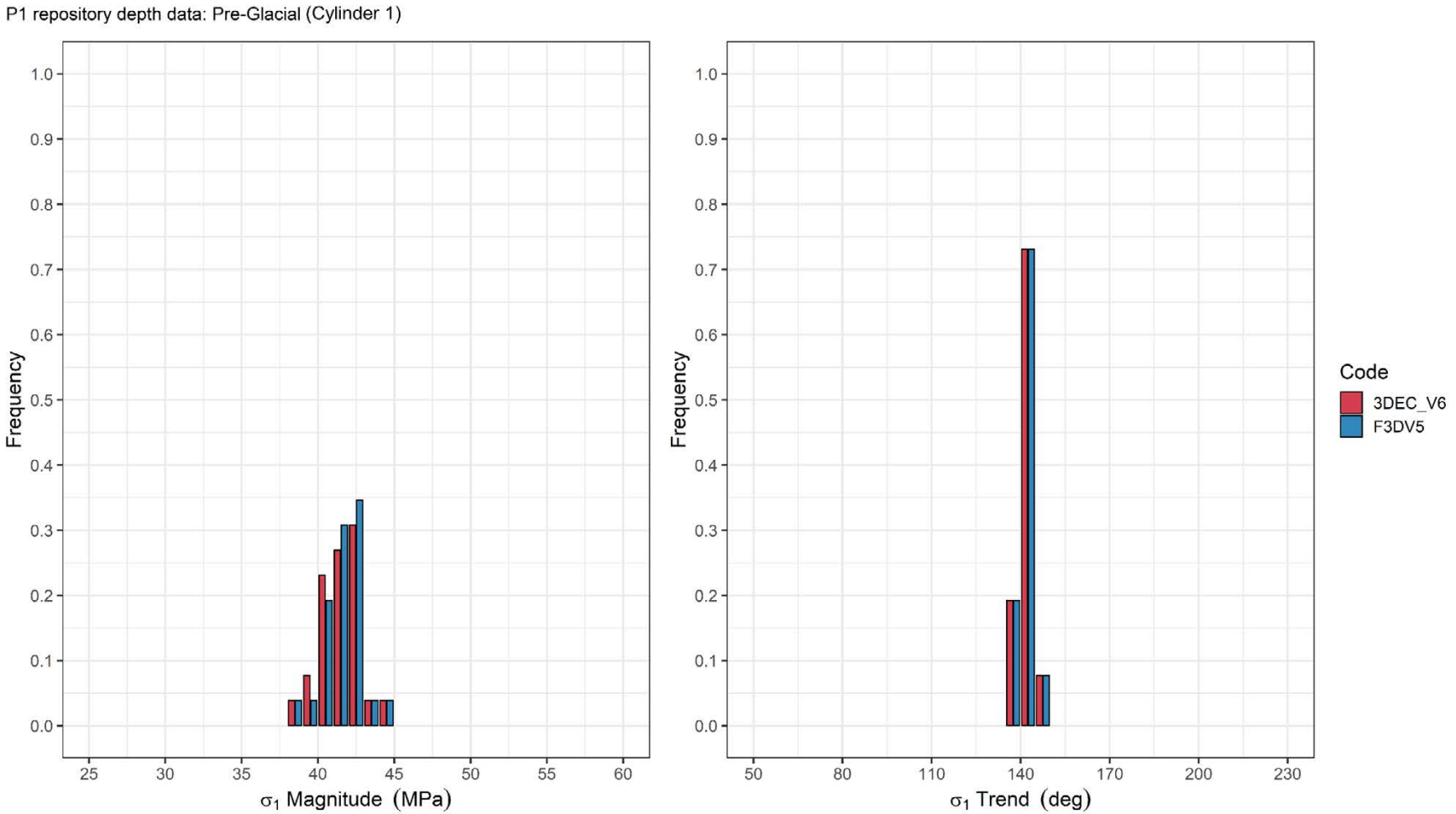

Figure A12-3. *Distribution of σ_1 trend and magnitude at repository depth from cylinder 1 after glaciation in an elastoplastic simulation.*

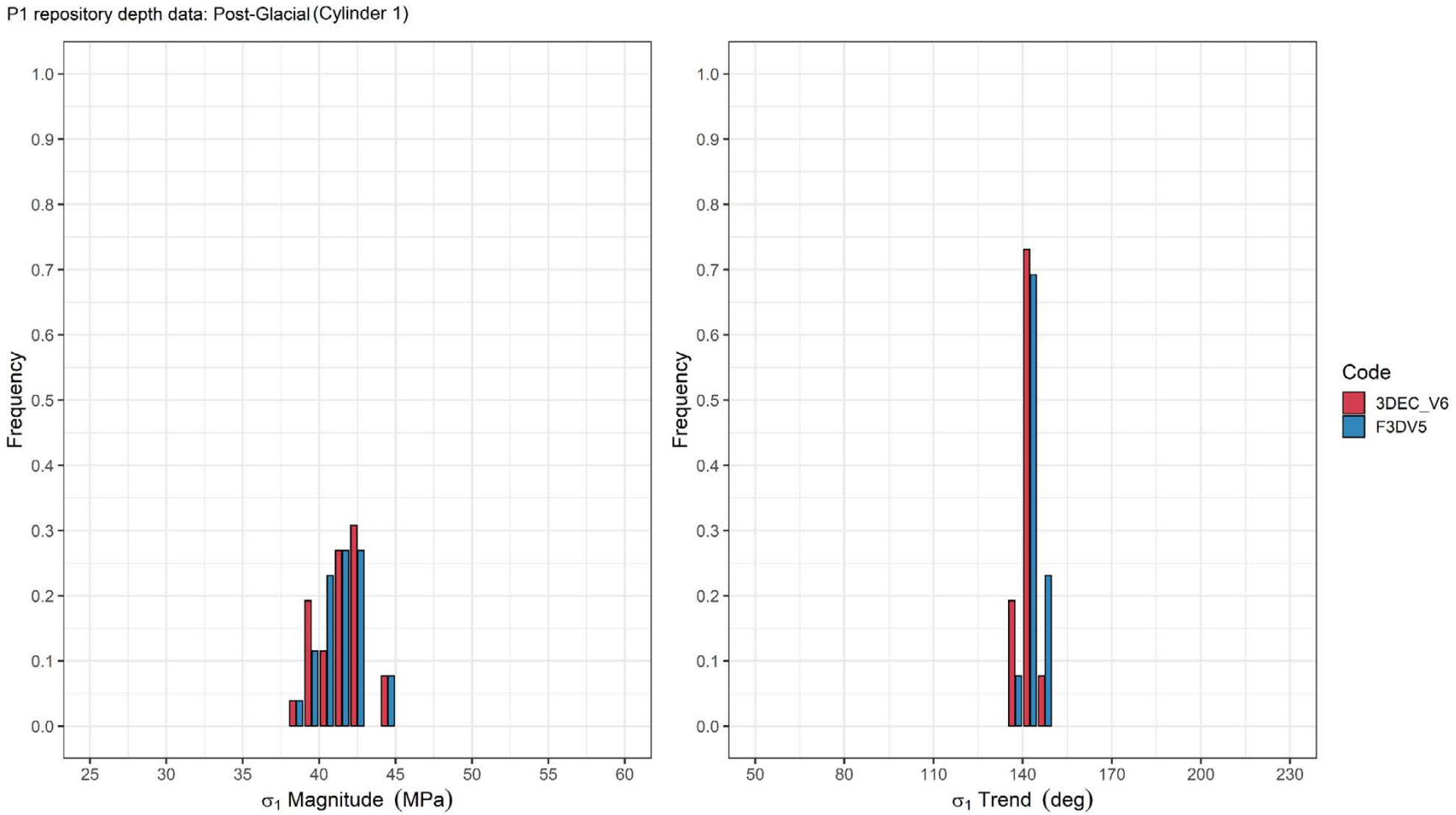

Figure A12-4. *Distribution of σ_1 trend and magnitude at repository depth from cylinder 1 after glaciation in an elastoplastic simulation.*

Phase 2 – frequency of σ_1 trend and magnitude variation at repository depth

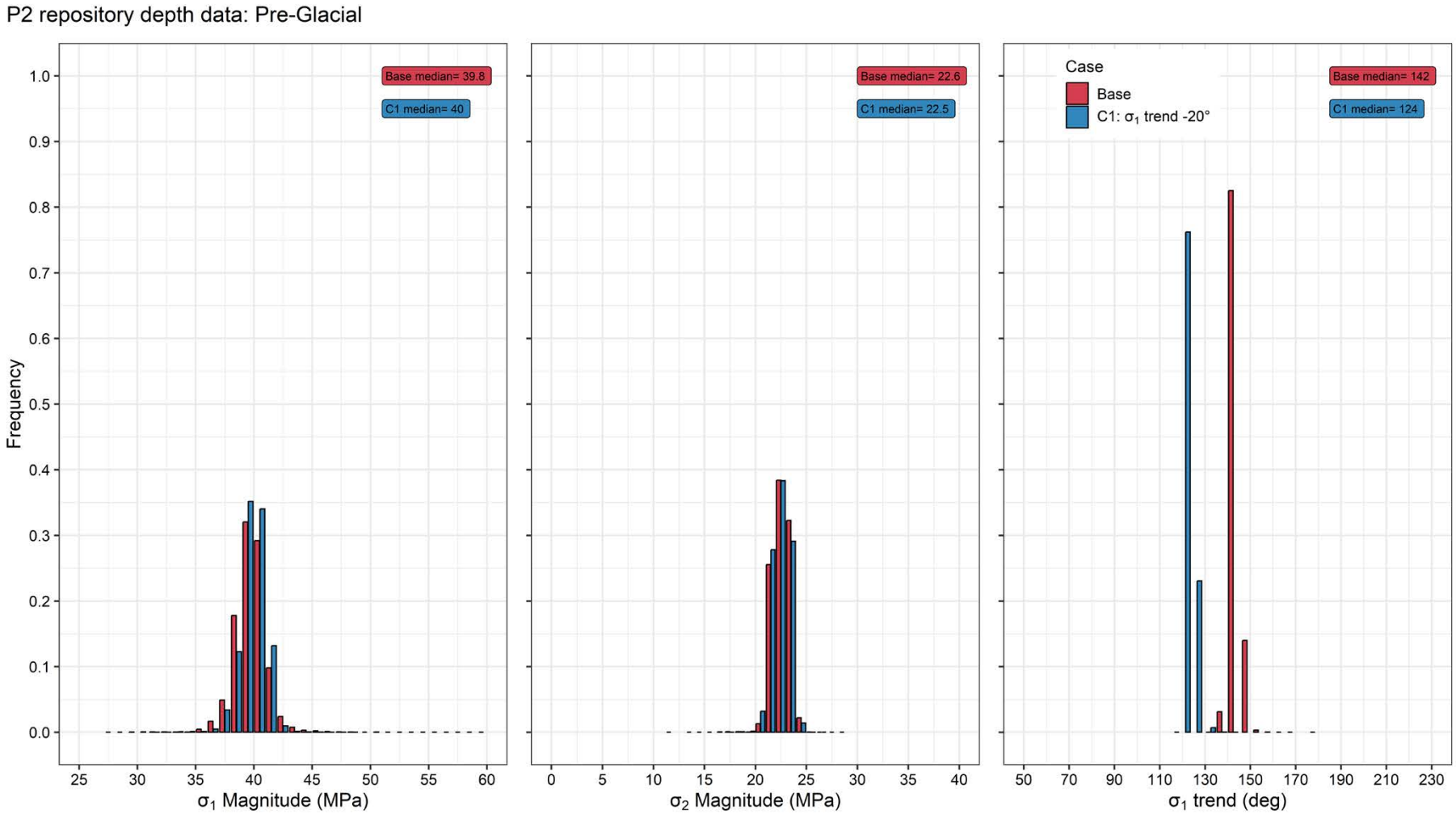

Figure A13-1. *Distribution of σ_1, σ_2 magnitude and σ_1 trend at repository depth from a cylinder covering the repository footprint (Figure 4-2) before glaciation for the Base case and Case 1 of Phase 2 simulations.*

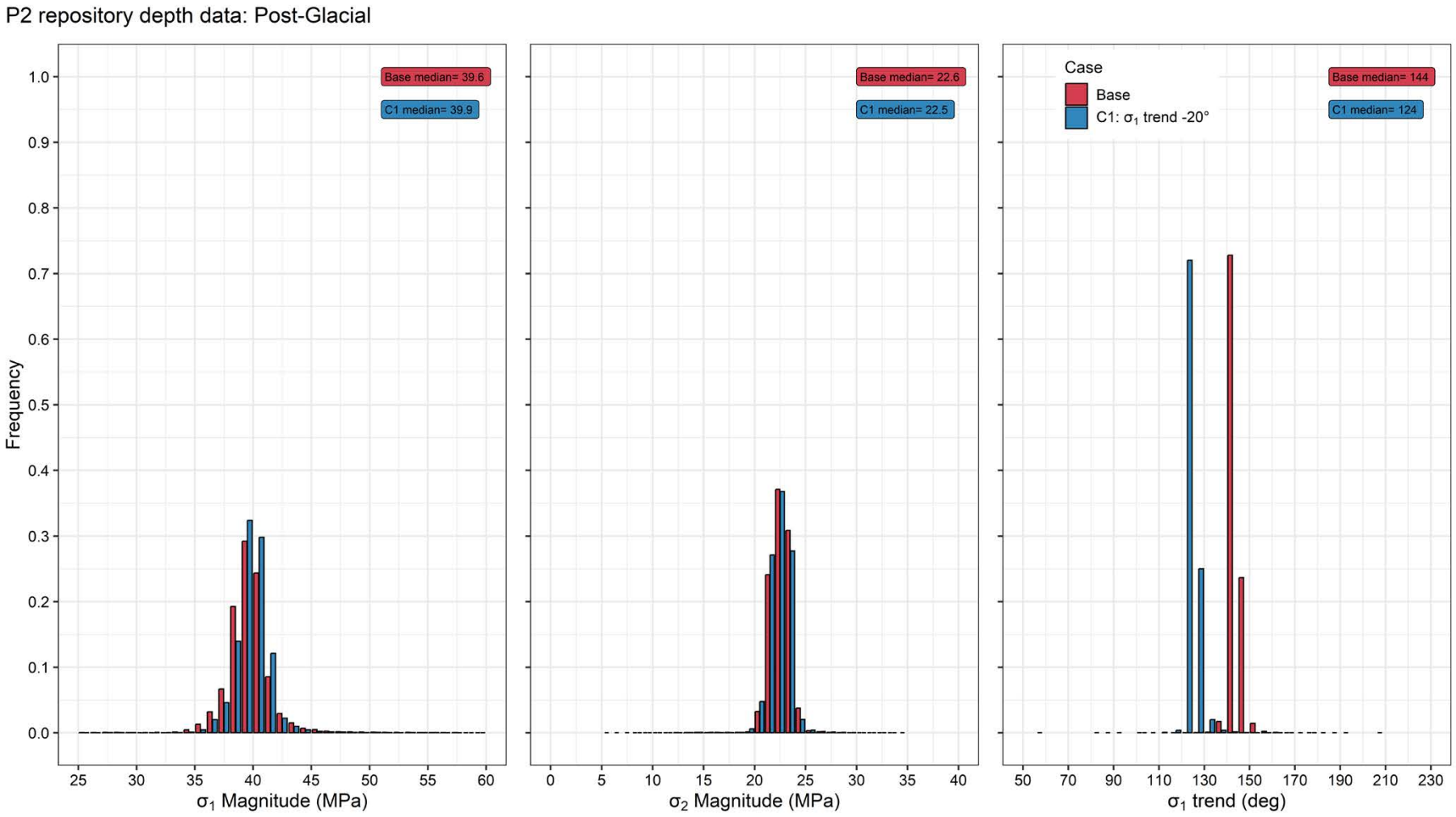

Figure A13-2. *Distribution of σ_1, σ_2 magnitude and σ_1 trend at repository depth from a cylinder covering the repository footprint (Figure 4-2) after glaciation for the Base case and Case 1 of Phase 2 simulations.*

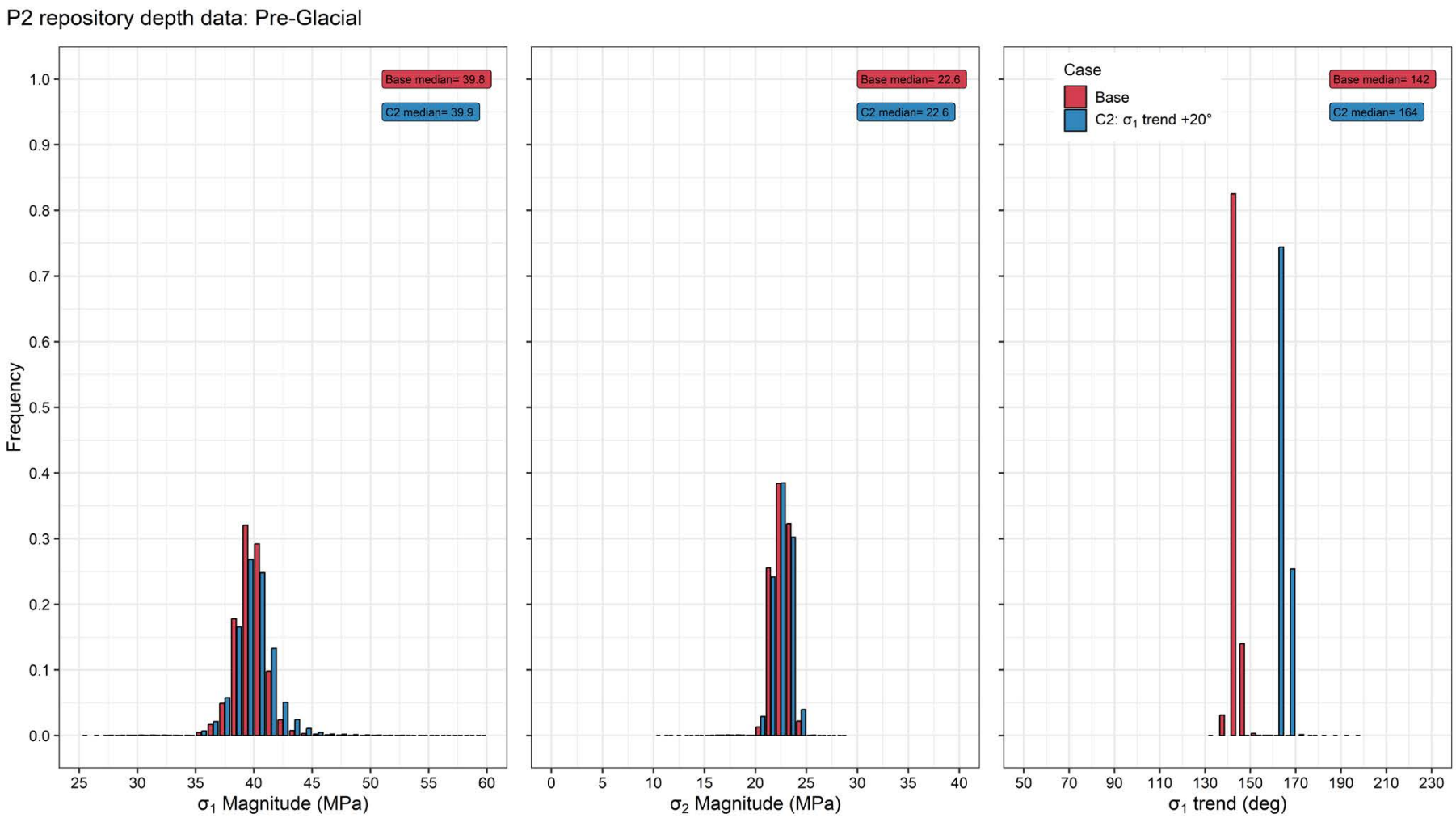

Figure A13-3. *Distribution of σ_1, σ_2 magnitude and σ_1 trend at repository depth from a cylinder covering the repository footprint (Figure 4-2) before glaciation for the Base case and Case 2 of Phase 2 simulations.*

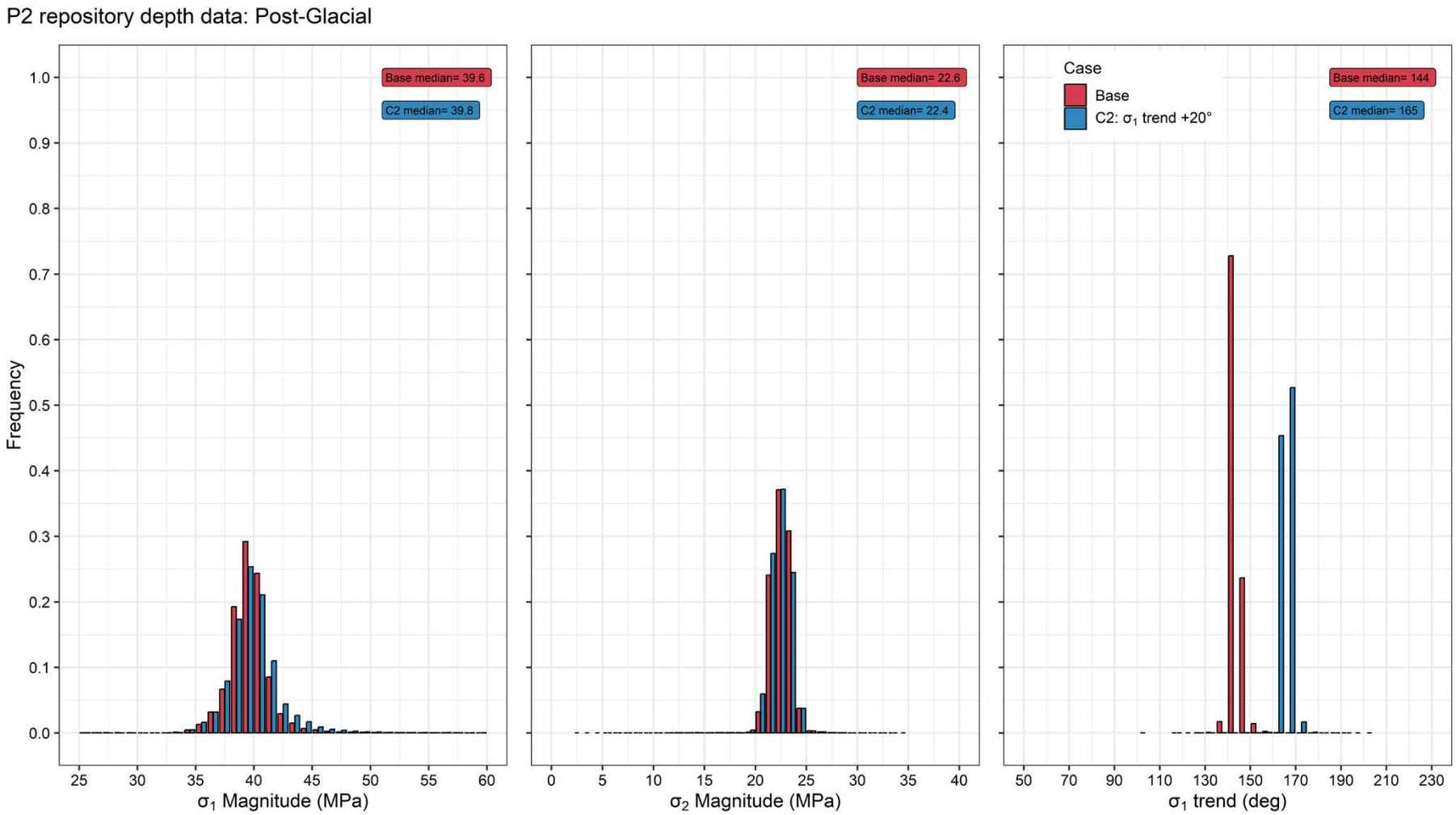

Figure A13-4. *Distribution of σ_1, σ_2 magnitude and σ_1 trend at repository depth from a cylinder covering the repository footprint (Figure 4-2) after glaciation for the Base case and Case 2 of Phase 2 simulations.*

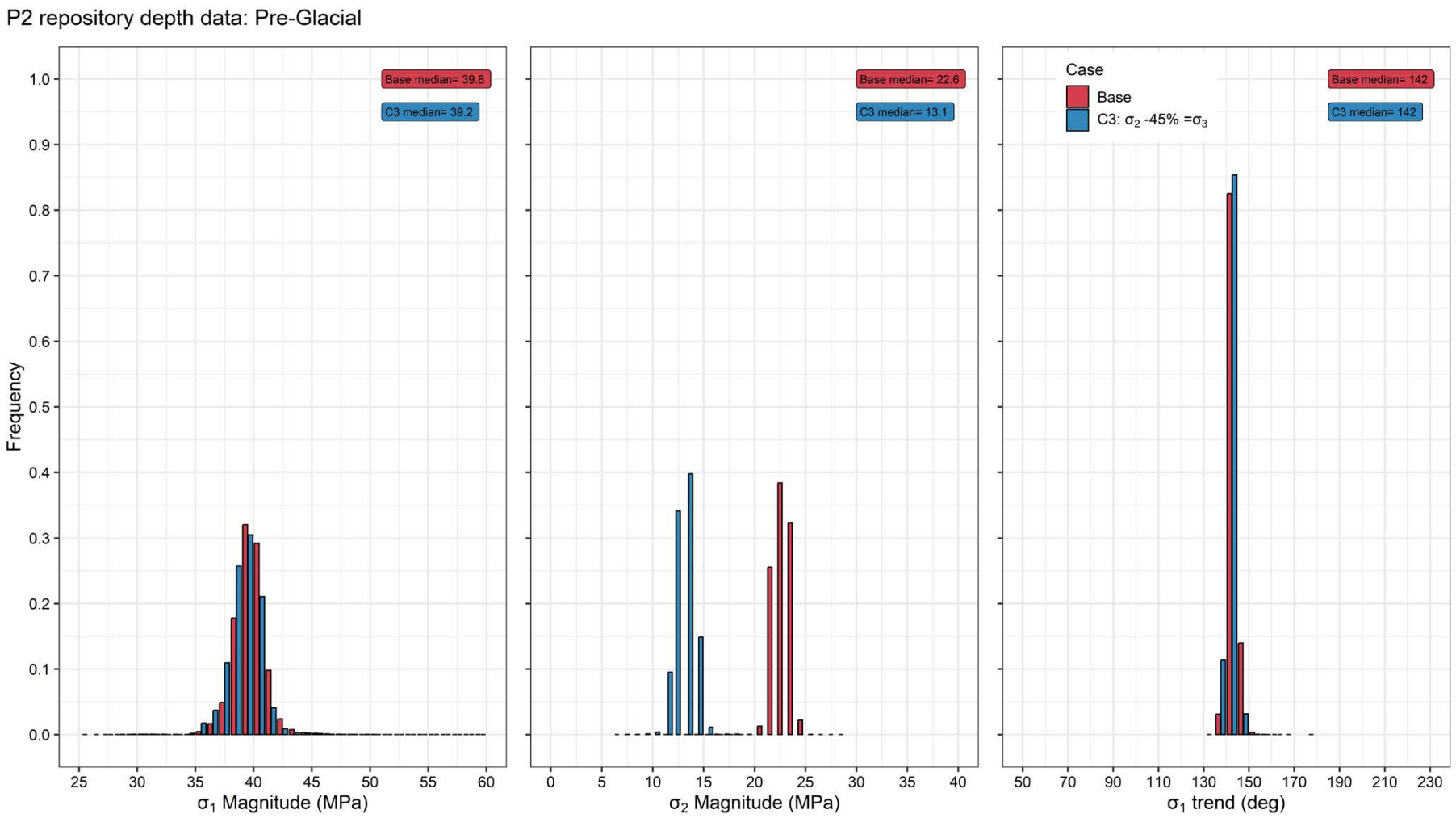

Figure A13-5. *Distribution of σ_1, σ_2 magnitude and σ_1 trend at repository depth from a cylinder covering the repository footprint (Figure 4-2) before glaciation for the Base case and Case 3 of Phase 2 simulations.*

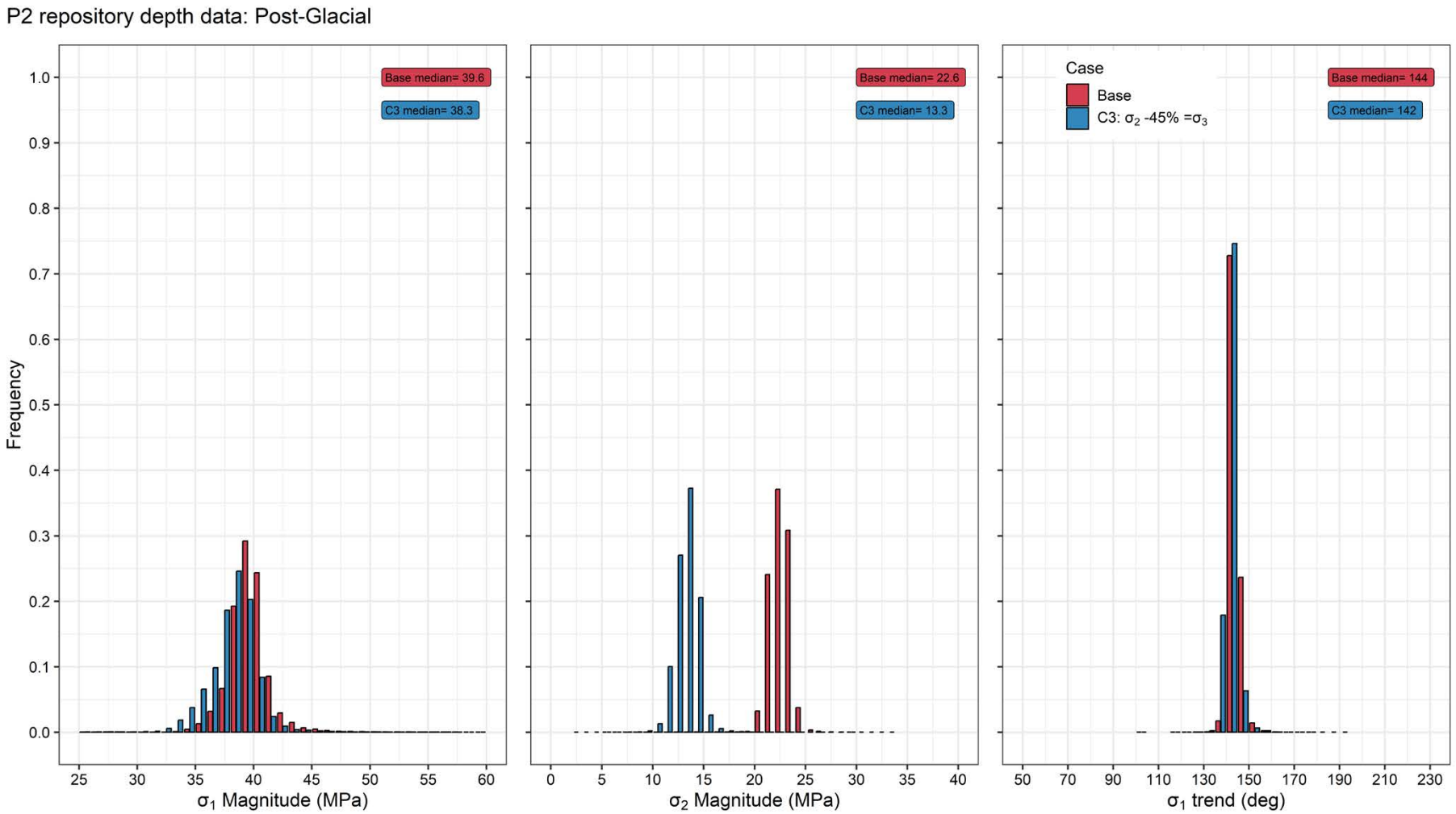

Figure A13-6. *Distribution of σ_1, σ_2 magnitude and σ_1 trend at repository depth from a cylinder covering the repository footprint (Figure 4-2) after glaciation for the Base case and Case 3 of Phase 2 simulations.*

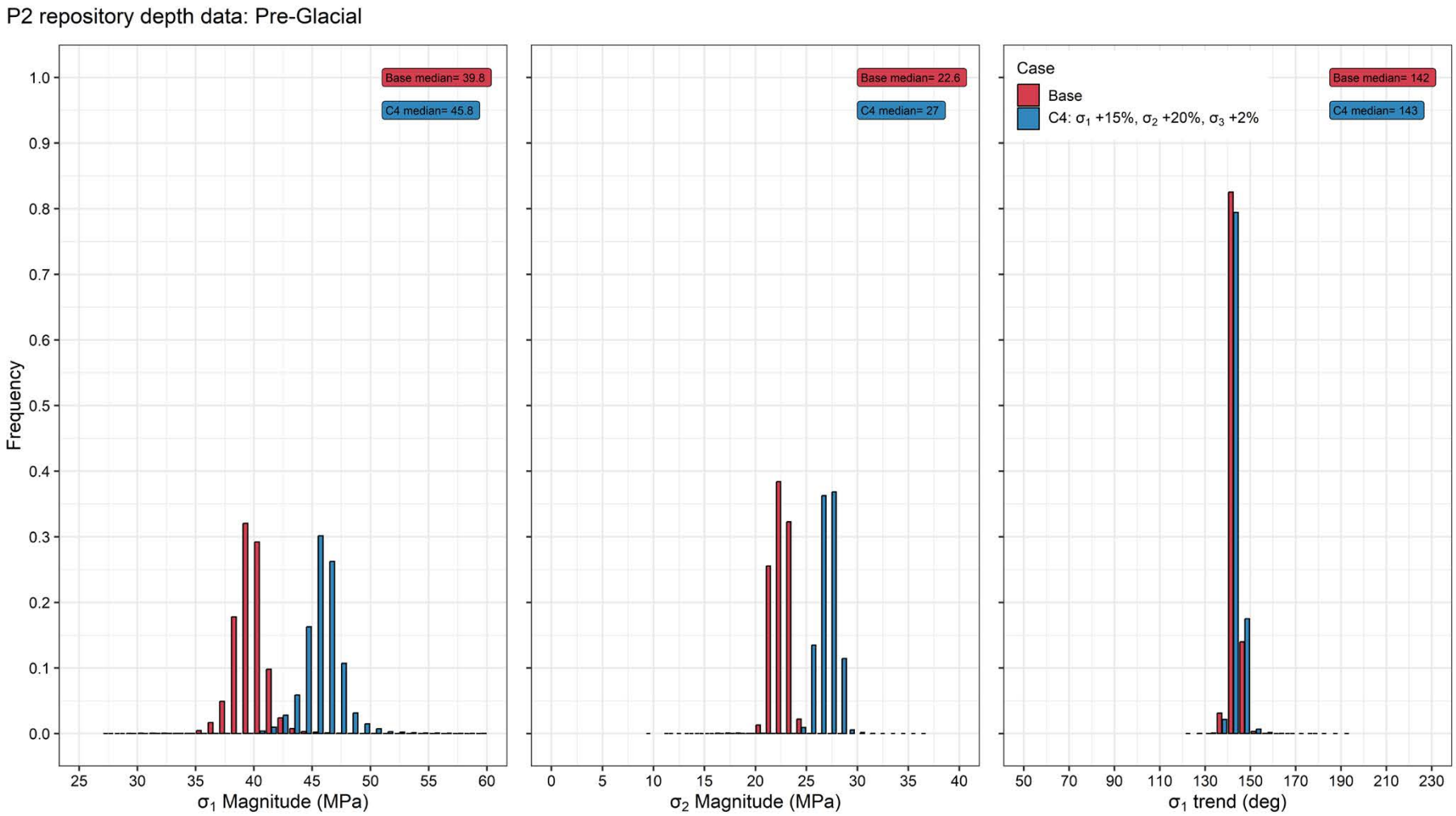

Figure A13-7. *Distribution of σ_1, σ_2 magnitude and σ_1 trend at repository depth from a cylinder covering the repository footprint (Figure 4-2) before glaciation for the Base case and Case 4 of Phase 2 simulations.*

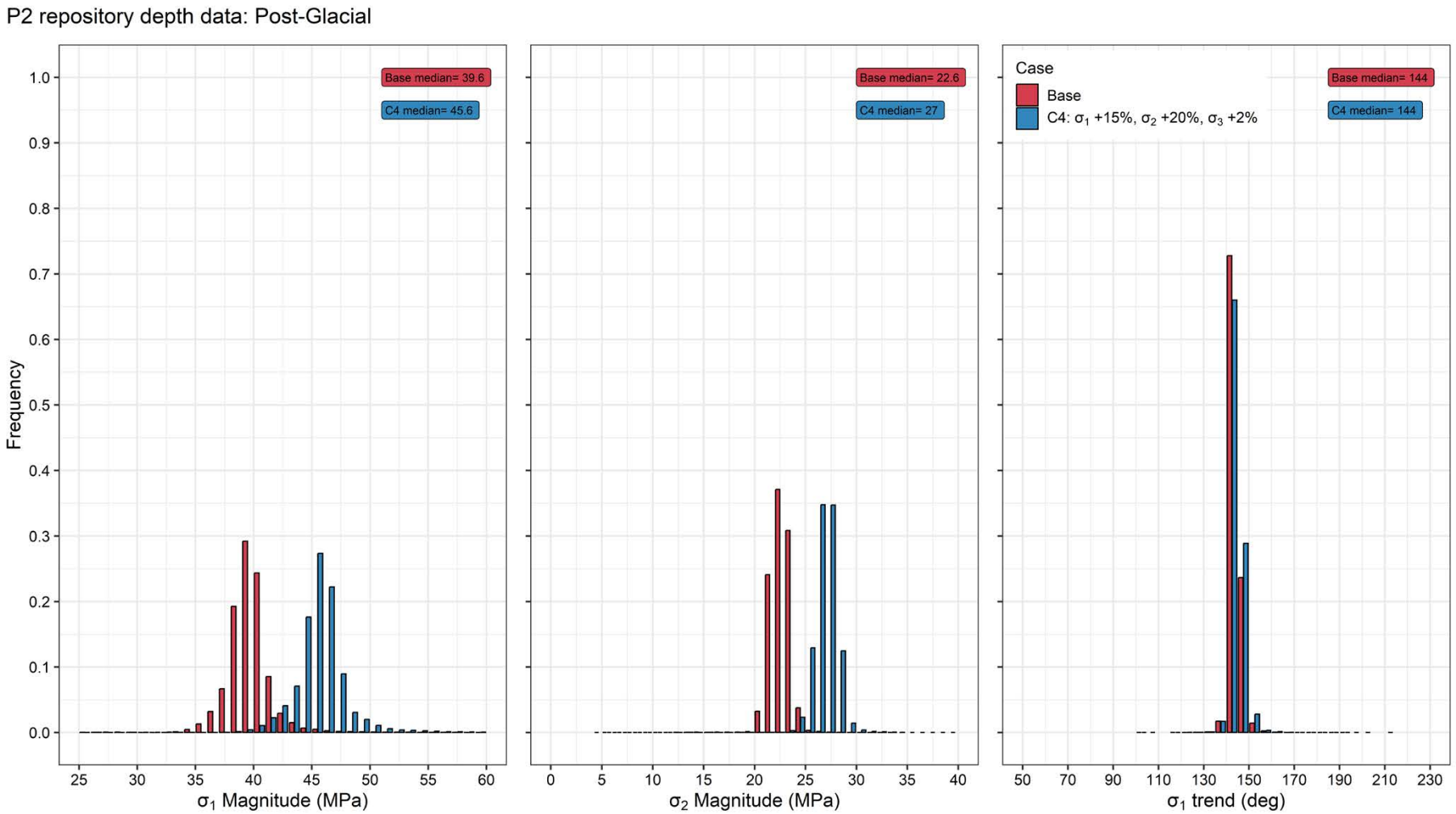

Figure A13-8. *Distribution of σ_1, σ_2 magnitude and σ_1 trend at repository depth from a cylinder covering the repository footprint (Figure 4-2) after glaciation for the Base case and Case 4 of Phase 2 simulations.*

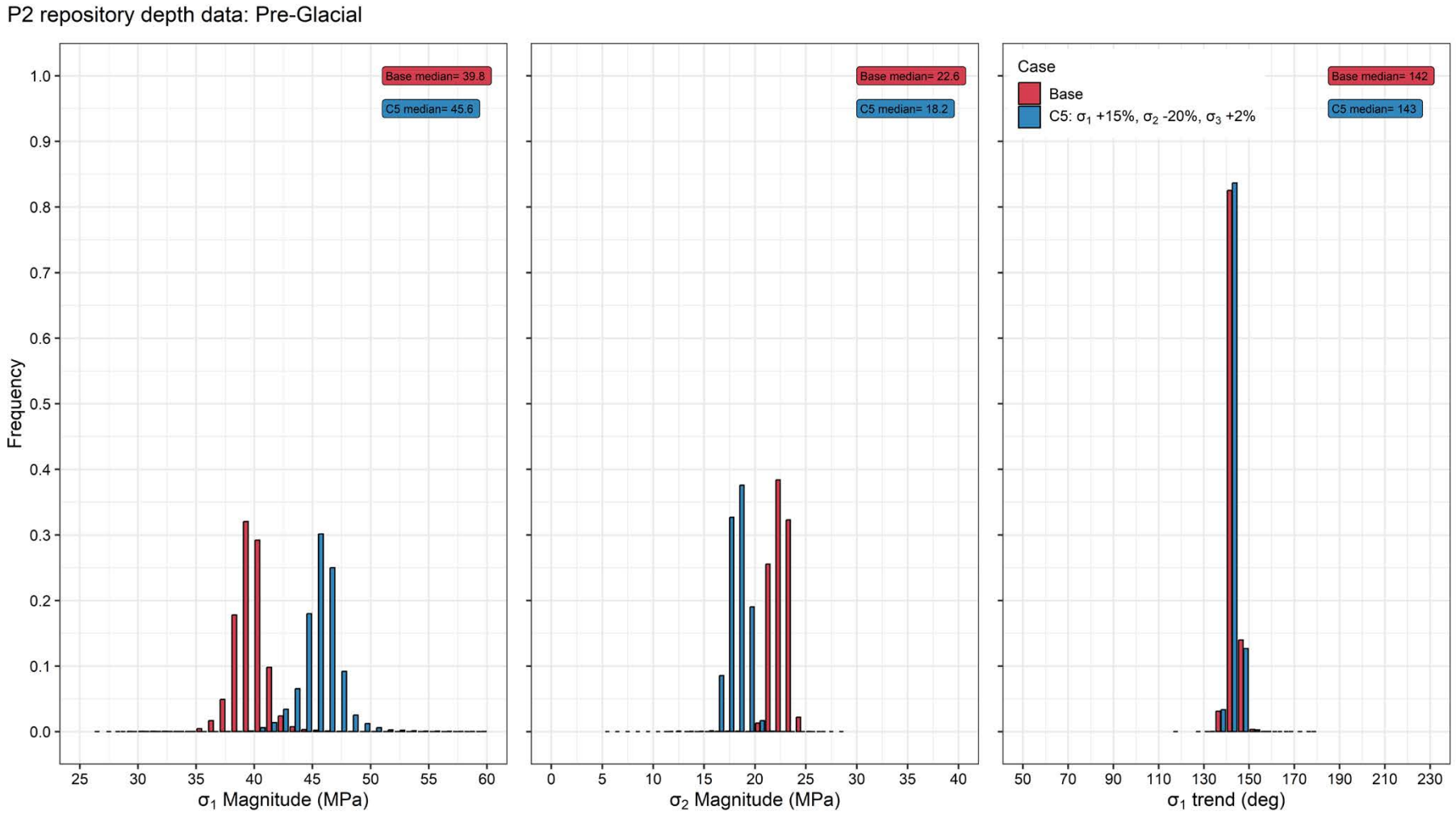

Figure A13-9. *Distribution of σ_1, σ_2 magnitude and σ_1 trend at repository depth from a cylinder covering the repository footprint (Figure 4-2) before glaciation for the Base case and Case 5 of Phase 2 simulations.*

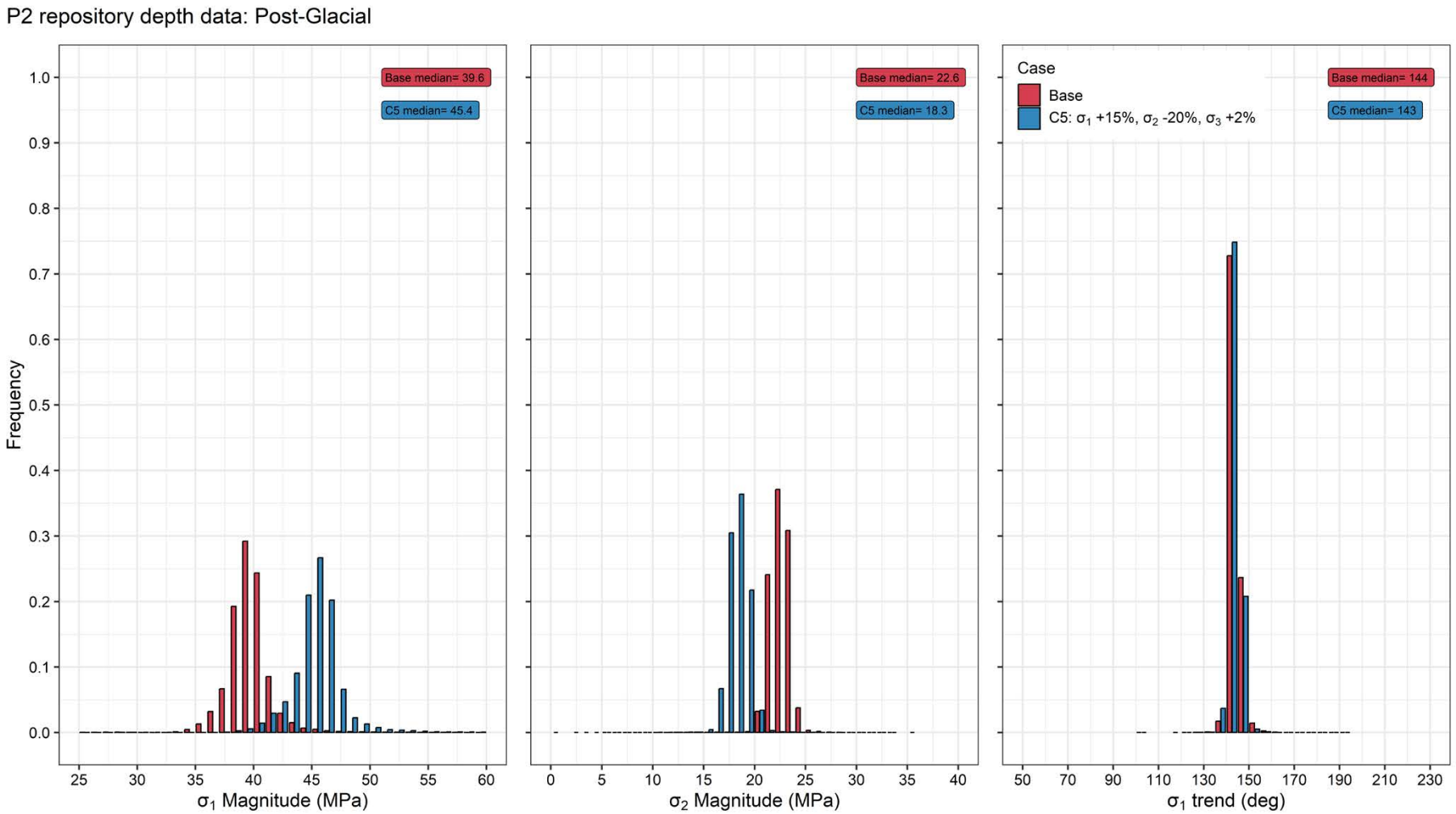

Figure A13-10. *Distribution of σ_1, σ_2 magnitude and σ_1 trend at repository depth from a cylinder covering the repository footprint (Figure 4-2) after glaciation for the Base case and Case 5 of Phase 2 simulations.*

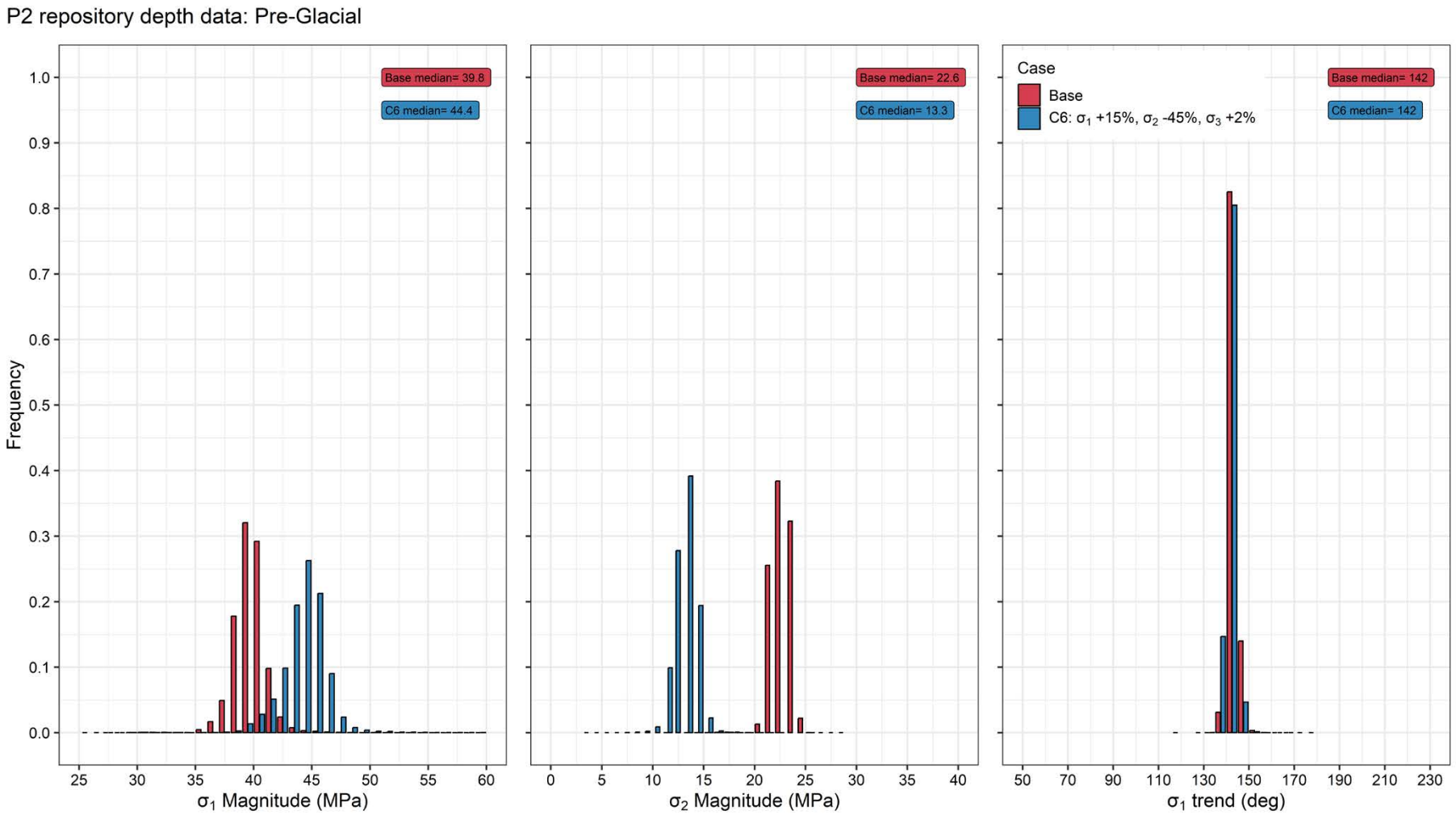

Figure A13-11. *Distribution of σ_1, σ_2 magnitude and σ_1 trend at repository depth from a cylinder covering the repository footprint (Figure 4-2) before glaciation for the Base case and Case 6 of Phase 2 simulations.*

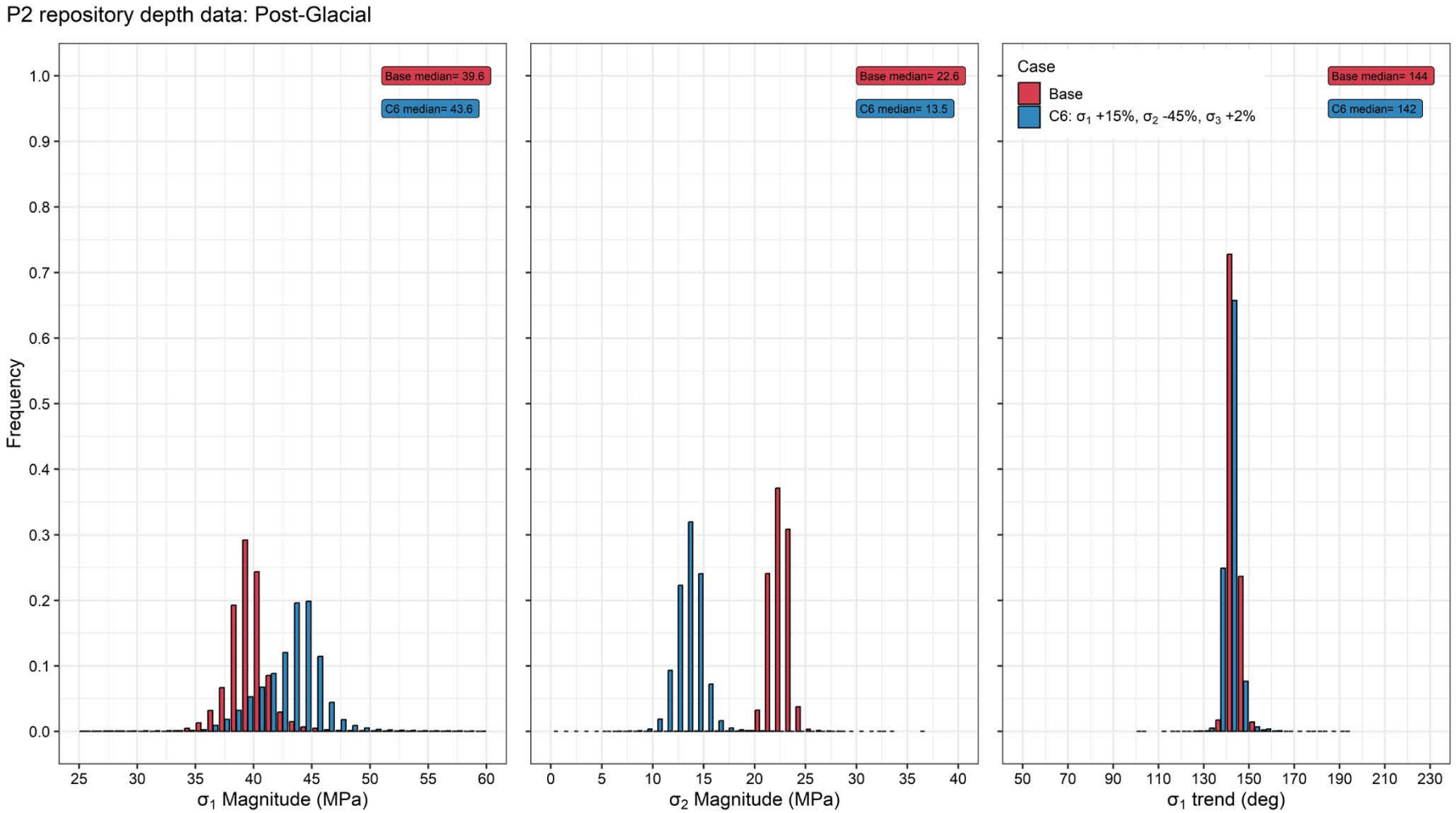

Figure A13-12. *Distribution of σ_1, σ_2 magnitude and σ_1 trend at repository depth from a cylinder covering the repository footprint (Figure 4-2) after glaciation for the Base case and Case 6 of Phase 2 simulations.*

Appendix 14

Phase 1 – Change in σ_1 magnitude at repository depth

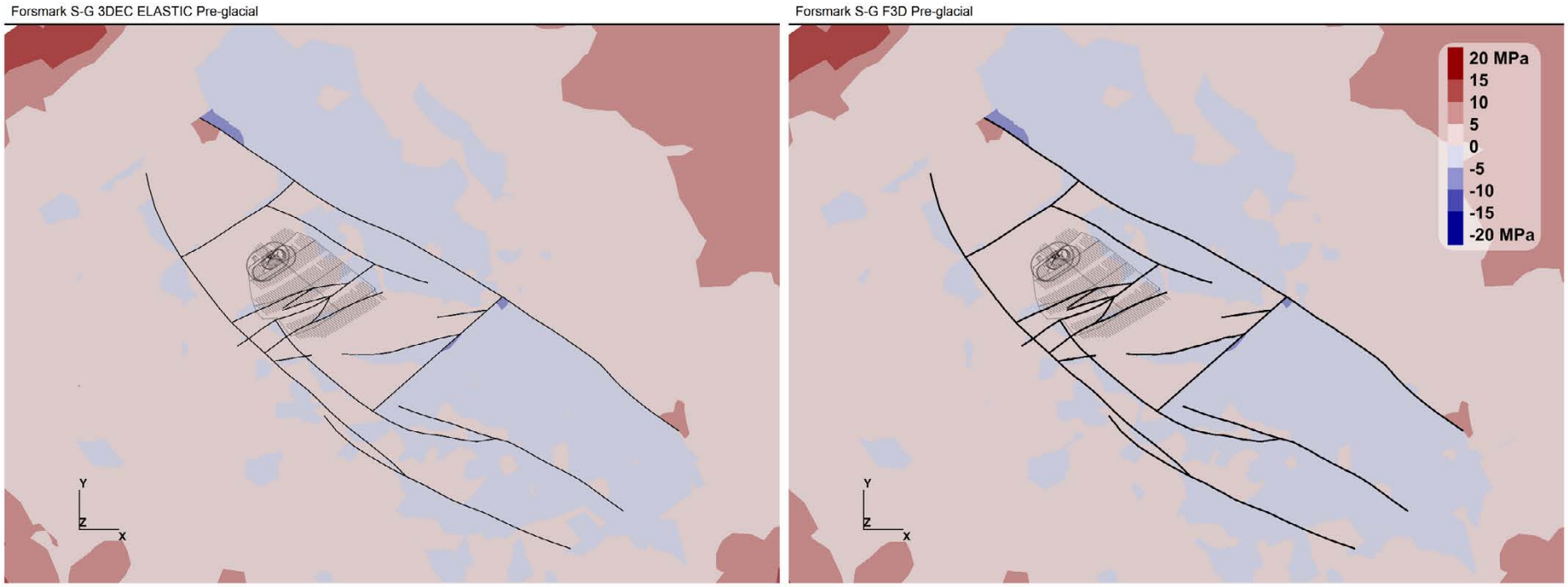

Figure A14-1. *Horizontal cross sections at repository depth −470 m of the maximum principal stress magnitude difference to the Martin (2007) interpretation before glaciation in a fully elastic simulation. The reference value is case-dependent.*

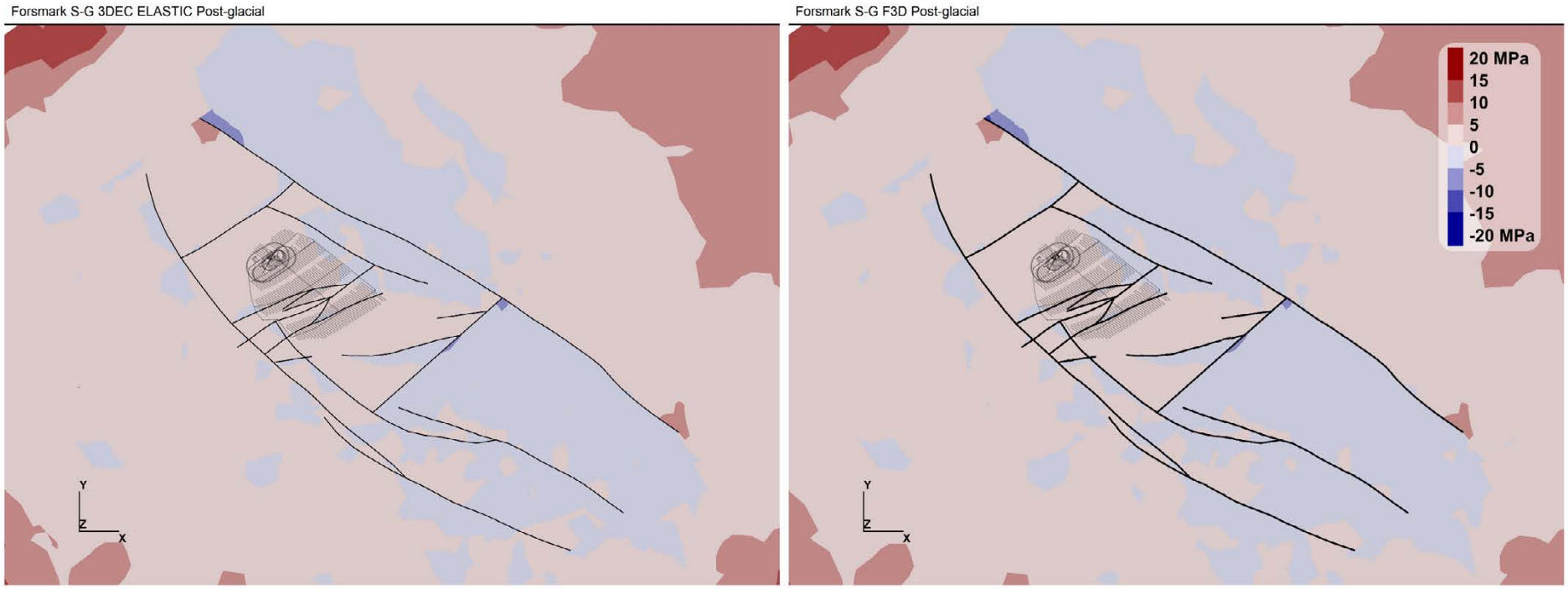

Figure A14-2. *Horizontal cross sections at repository depth −470 m of the maximum principal stress magnitude difference to the Martin (2007) interpretation after glaciation in a fully elastic simulation. The reference value is case-dependent.*

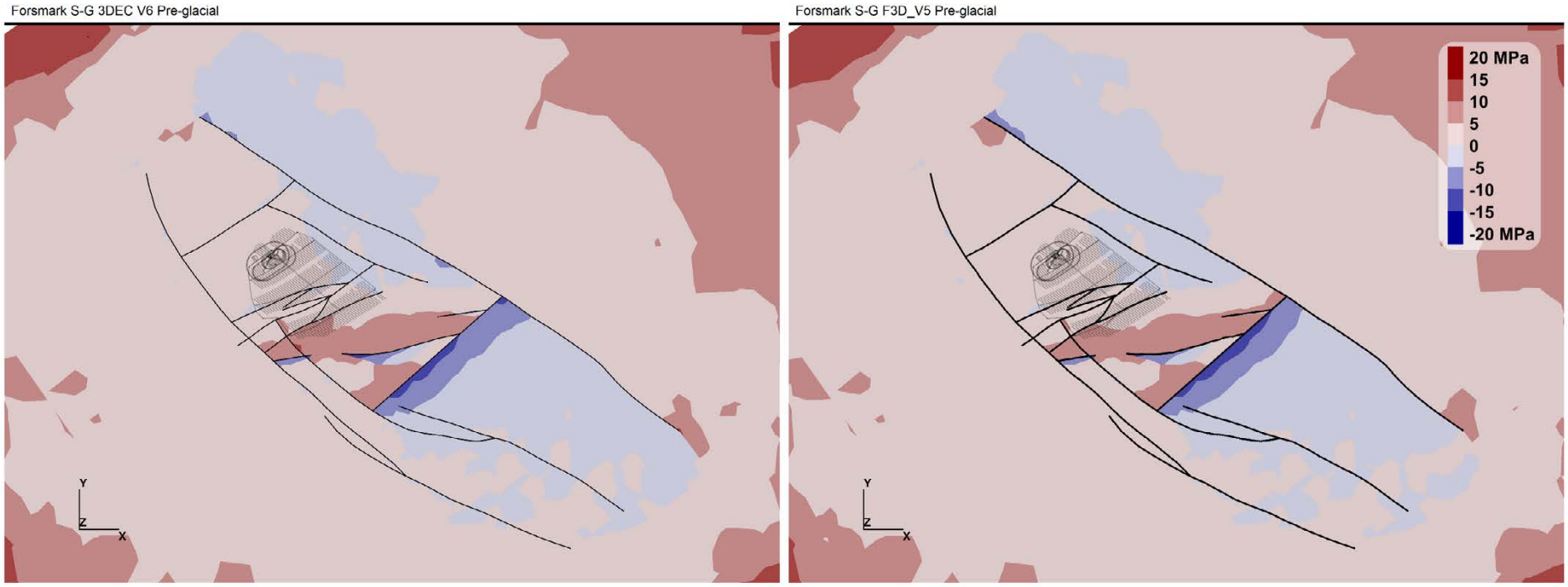

Figure A14-3. *Horizontal cross sections at repository depth −470 m of the maximum principal stress magnitude difference to the Martin (2007) interpretation before glaciation in an elastoplastic simulation. The reference value is case-dependent.*

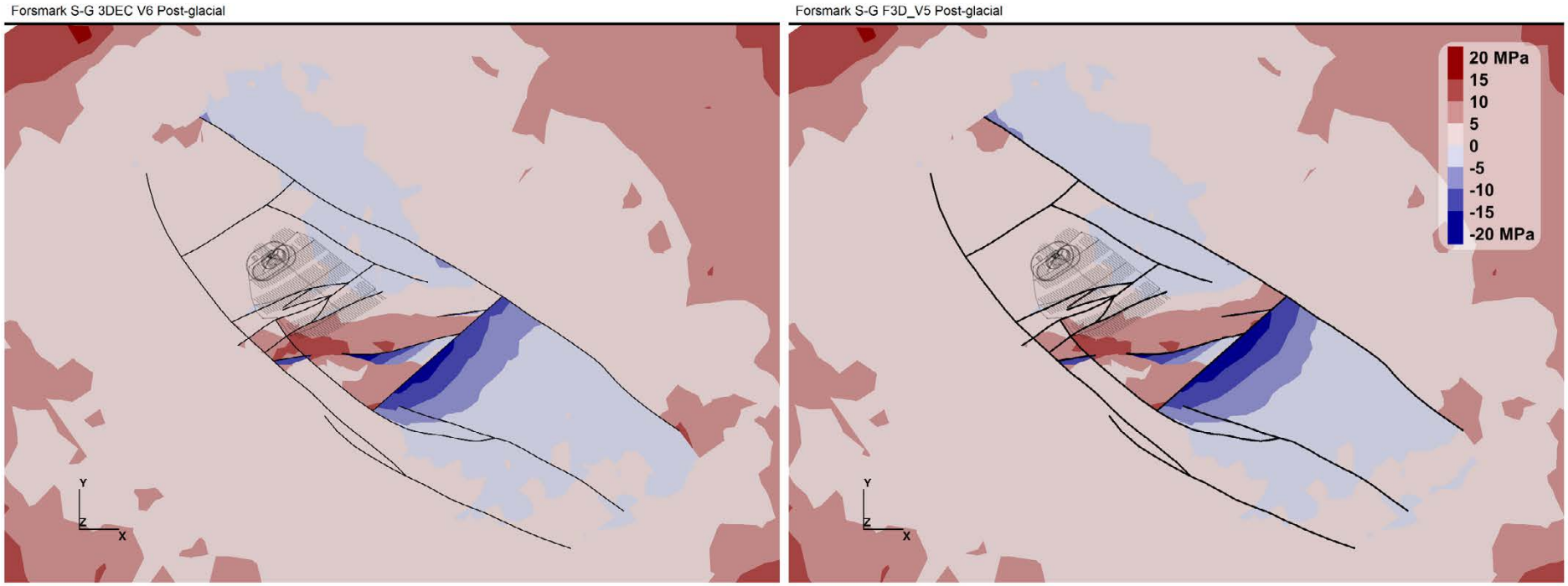

Figure A14-4. *Horizontal cross sections at repository depth −470 m of the maximum principal stress magnitude difference to the Martin (2007) interpretation after glaciation in an elastoplastic simulation. The reference value is case-dependent.*

Appendix 15

Phase 2 – Change in σ_1 magnitude at repository depth

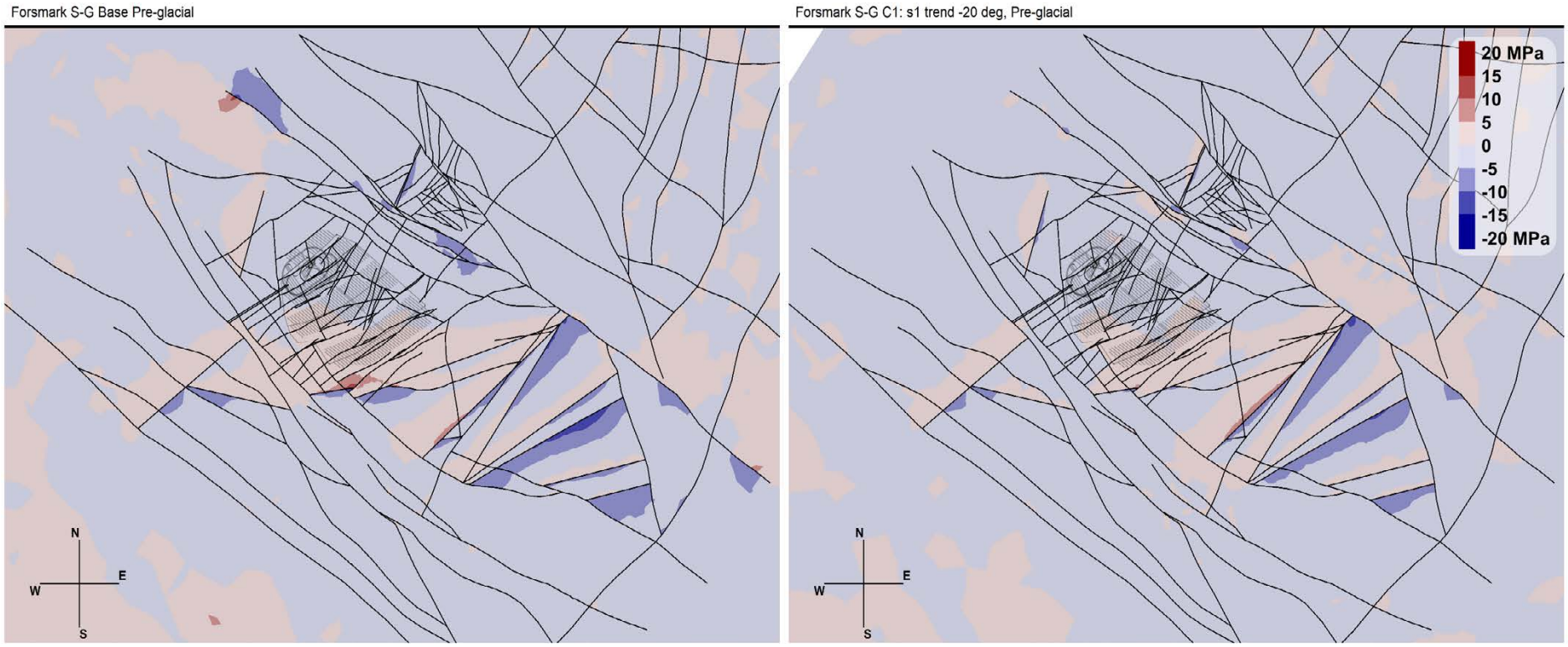

Figure A15-1. *The change in σ_1 magnitude before glaciation for the Base case and Case 1 of Phase 2 simulations in a horizontal cross-section at repository depth (470 m). The reference value is case-dependent.*

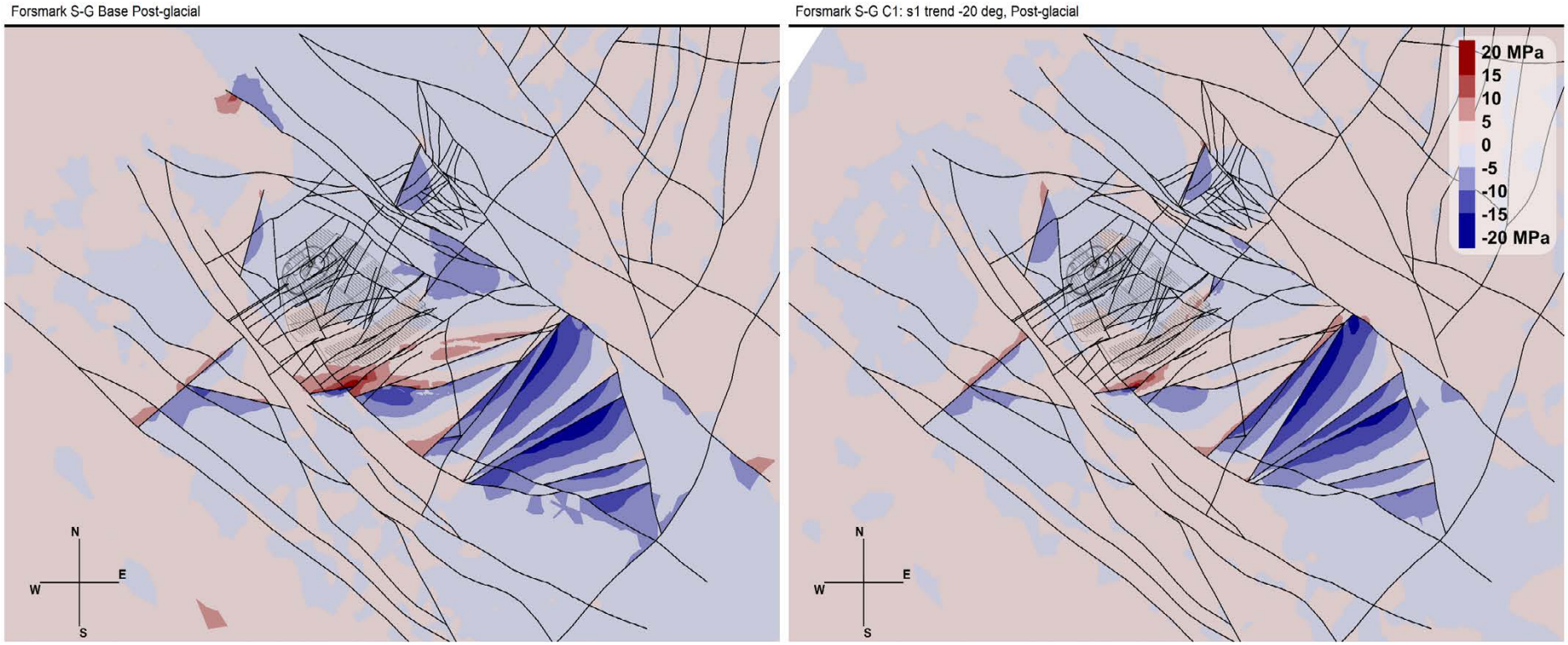

Figure A15-2. *The change in σ_1 magnitude after glaciation for the Base case and Case 1 of Phase 2 simulations in a horizontal cross-section at repository depth (470 m). The reference value is case-dependent.*

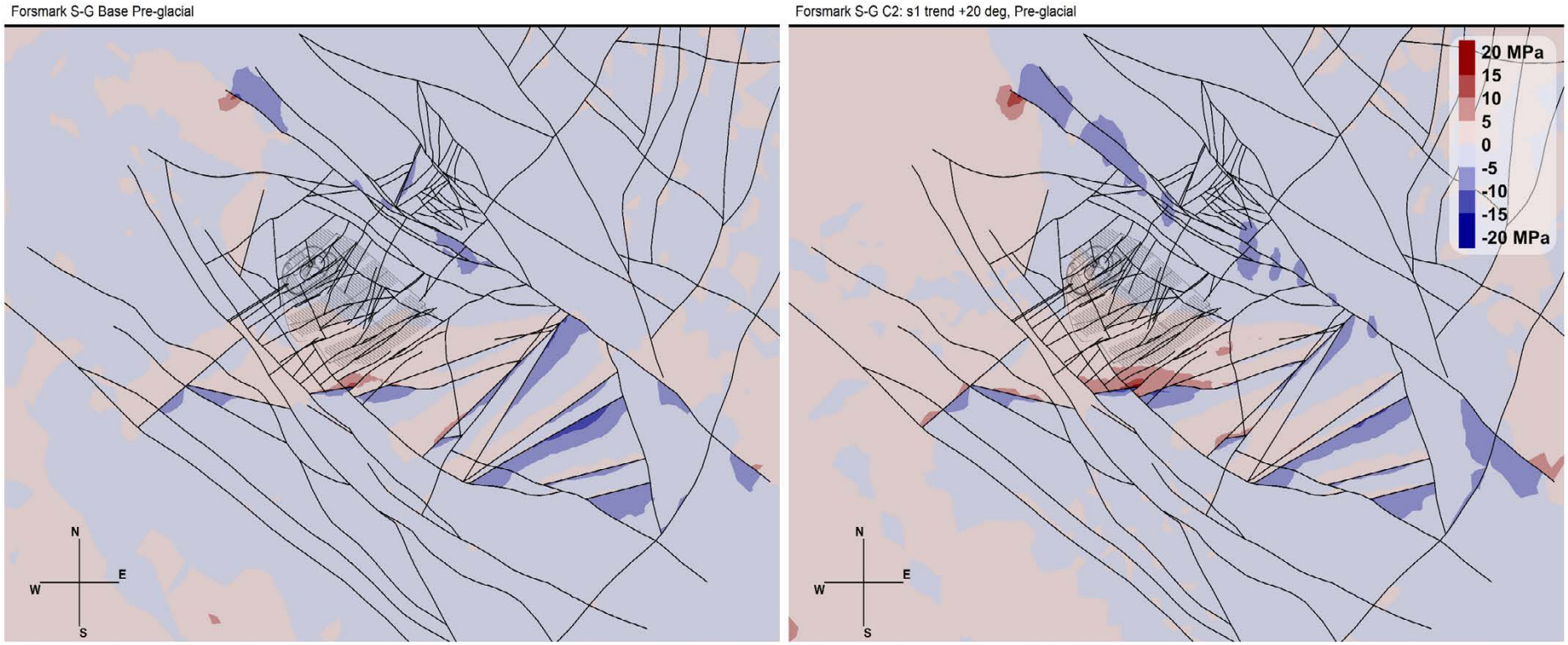

Figure A15-3. *The change in σ_1 magnitude before glaciation for the Base case and Case 2 of Phase 2 simulations in a horizontal cross-section at repository depth (470 m). The reference value is case-dependent.*

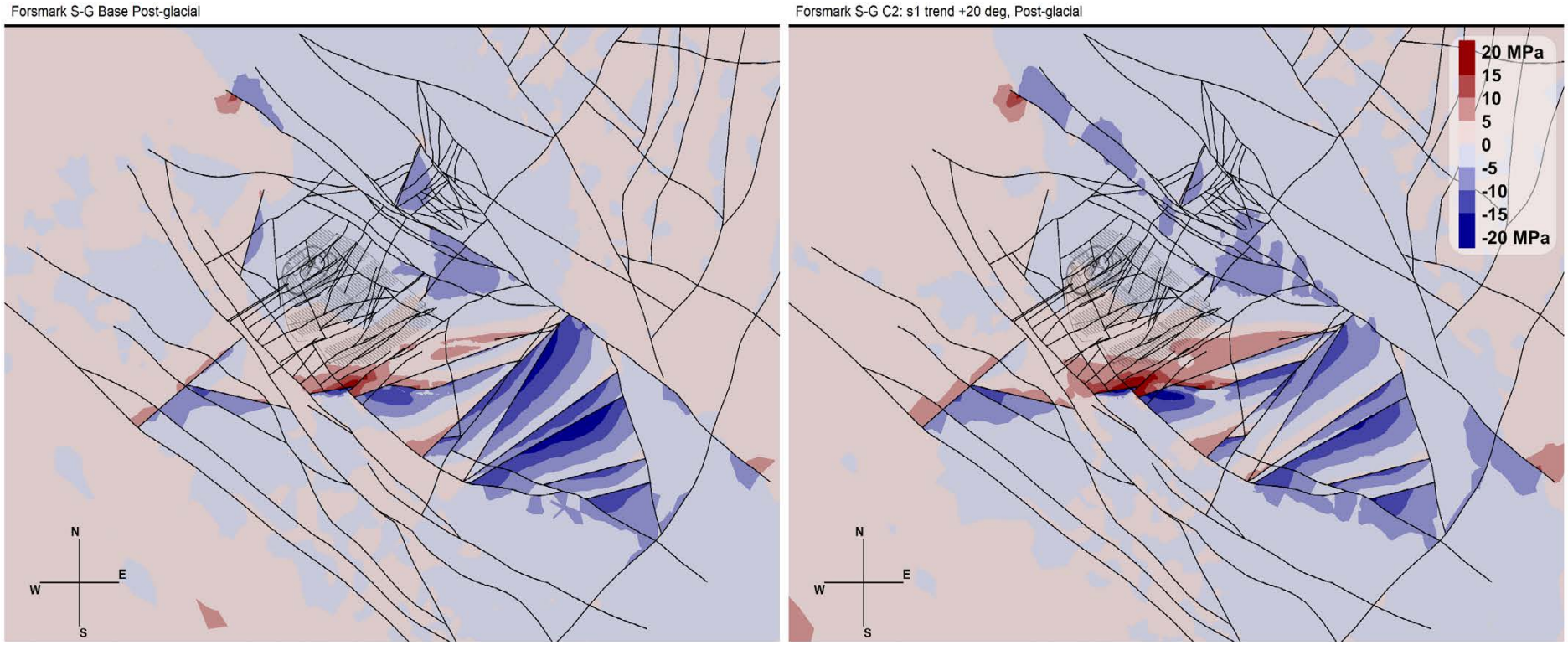

Figure A15-4. *The change in σ_1 magnitude after glaciation for the Base case and Case 2 of Phase 2 simulations in a horizontal cross-section at repository depth (470 m). The reference value is case-dependent.*

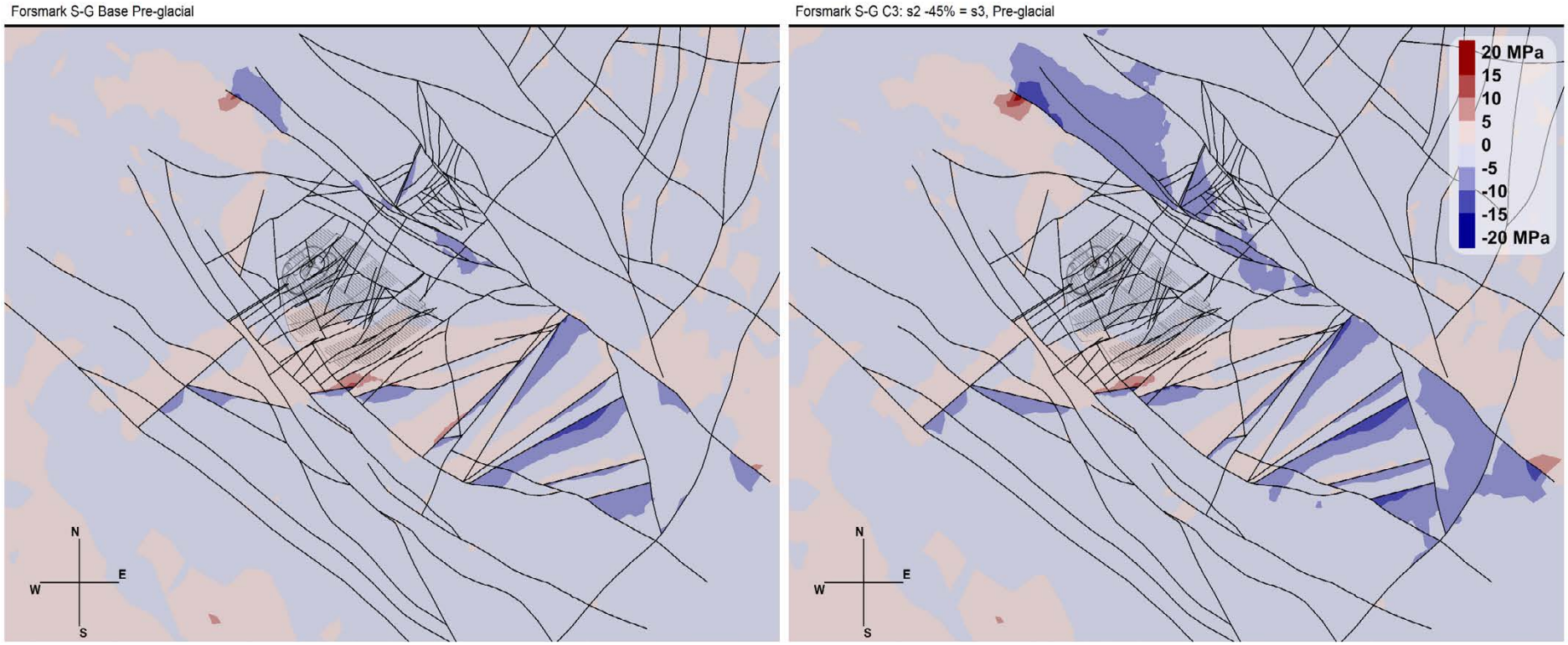

Figure A15-5. *The change in σ_1 magnitude before glaciation for the Base case and Case 3 of Phase 2 simulations in a horizontal cross-section at repository depth (470 m). The reference value is case-dependent.*

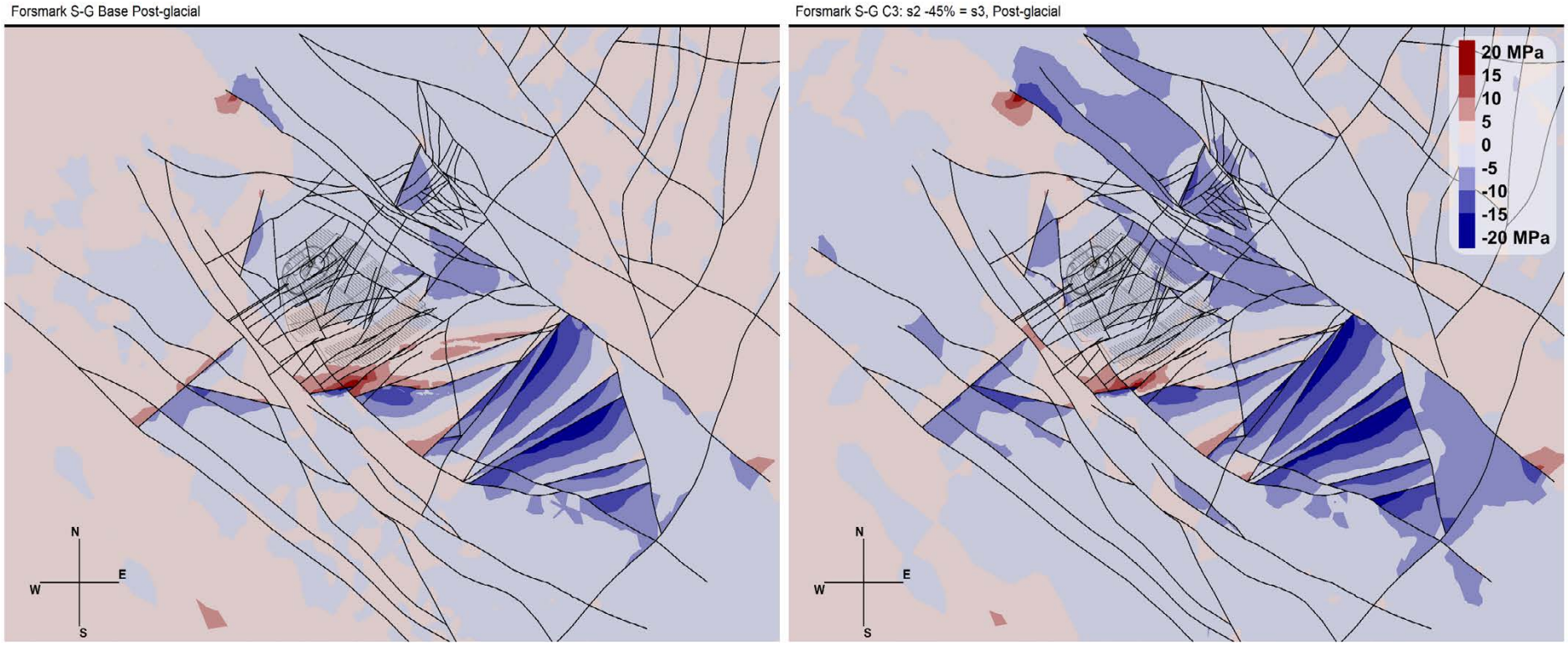

Figure A15-6. *The change in σ_1 magnitude after glaciation for the Base case and Case 3 of Phase 2 simulations in a horizontal cross-section at repository depth (470 m). The reference value is case-dependent.*

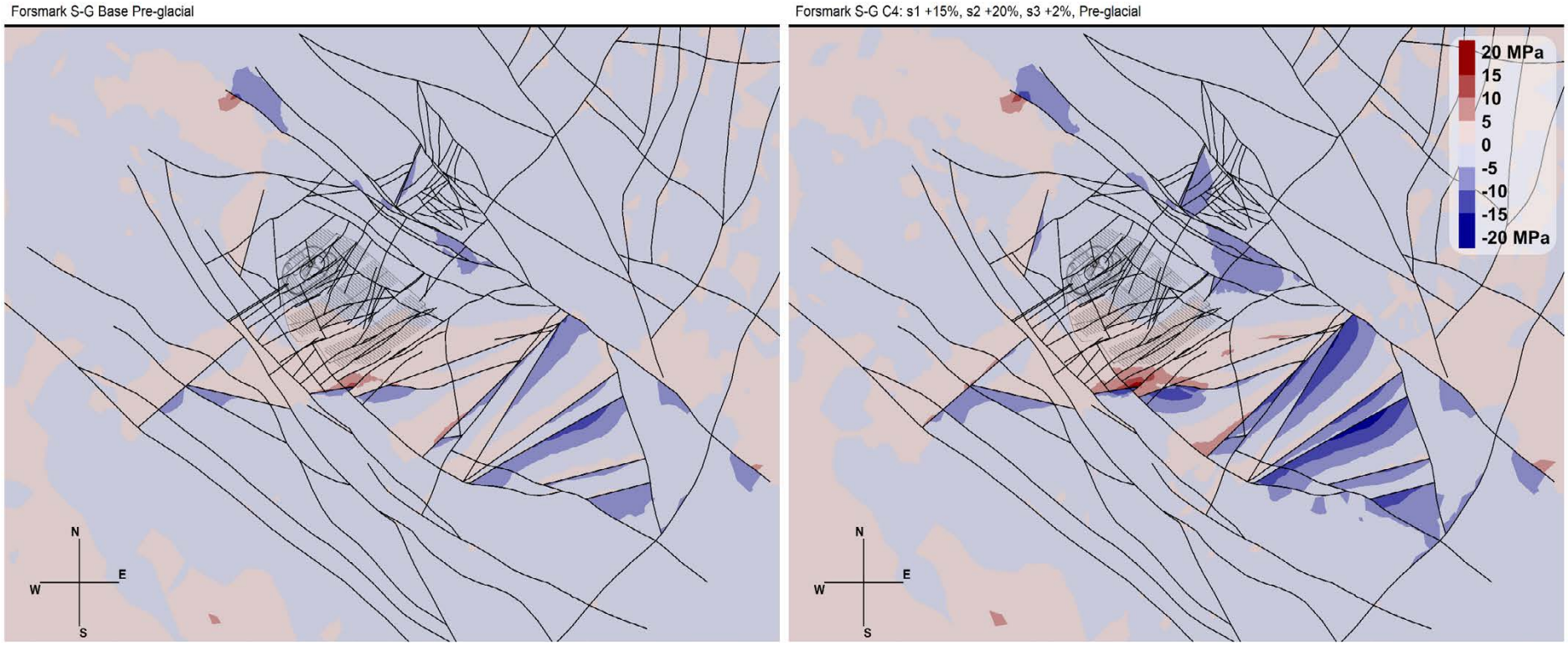

Figure A15-7. *The change in σ_1 magnitude before glaciation for the Base case and Case 4 of Phase 2 simulations in a horizontal cross-section at repository depth (470 m). The reference value is case-dependent.*

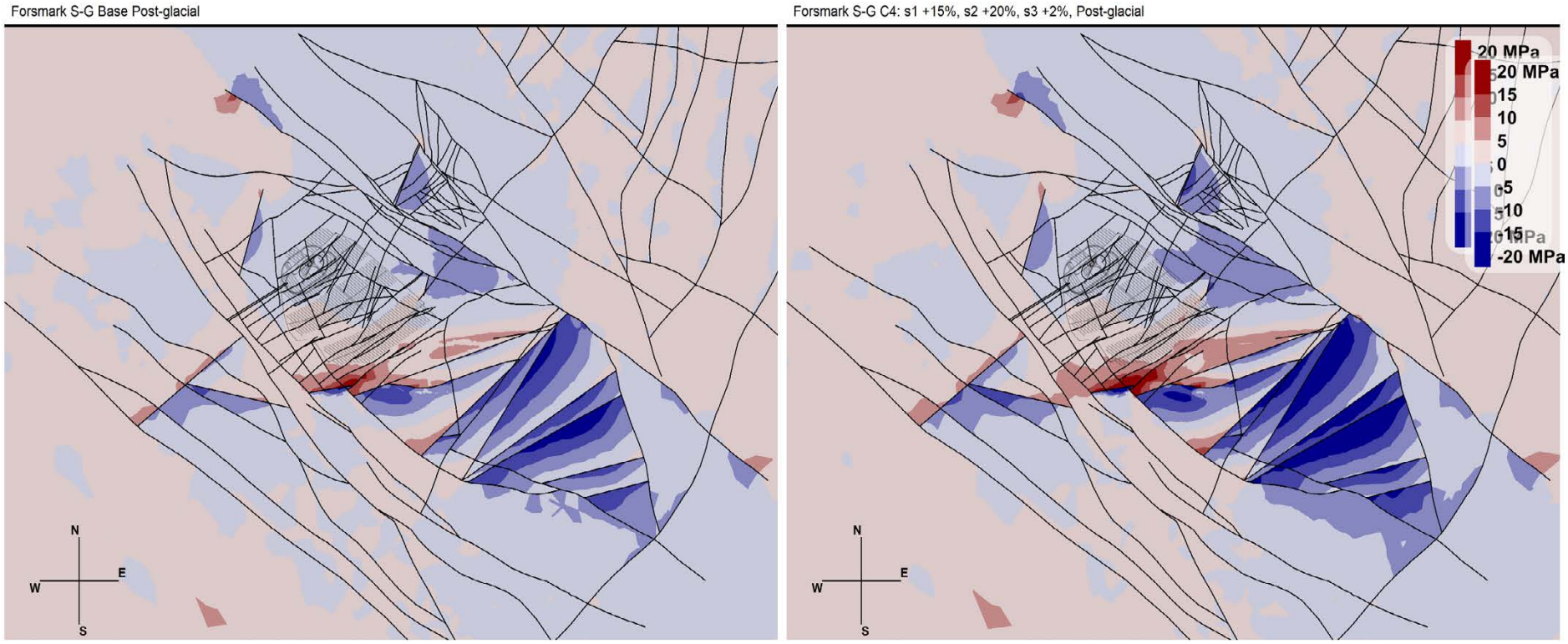

Figure A15-8. *The change in σ_1 magnitude after glaciation for the Base case and Case 4 of Phase 2 simulations in a horizontal cross-section at repository depth (470 m). The reference value is case-dependent.*

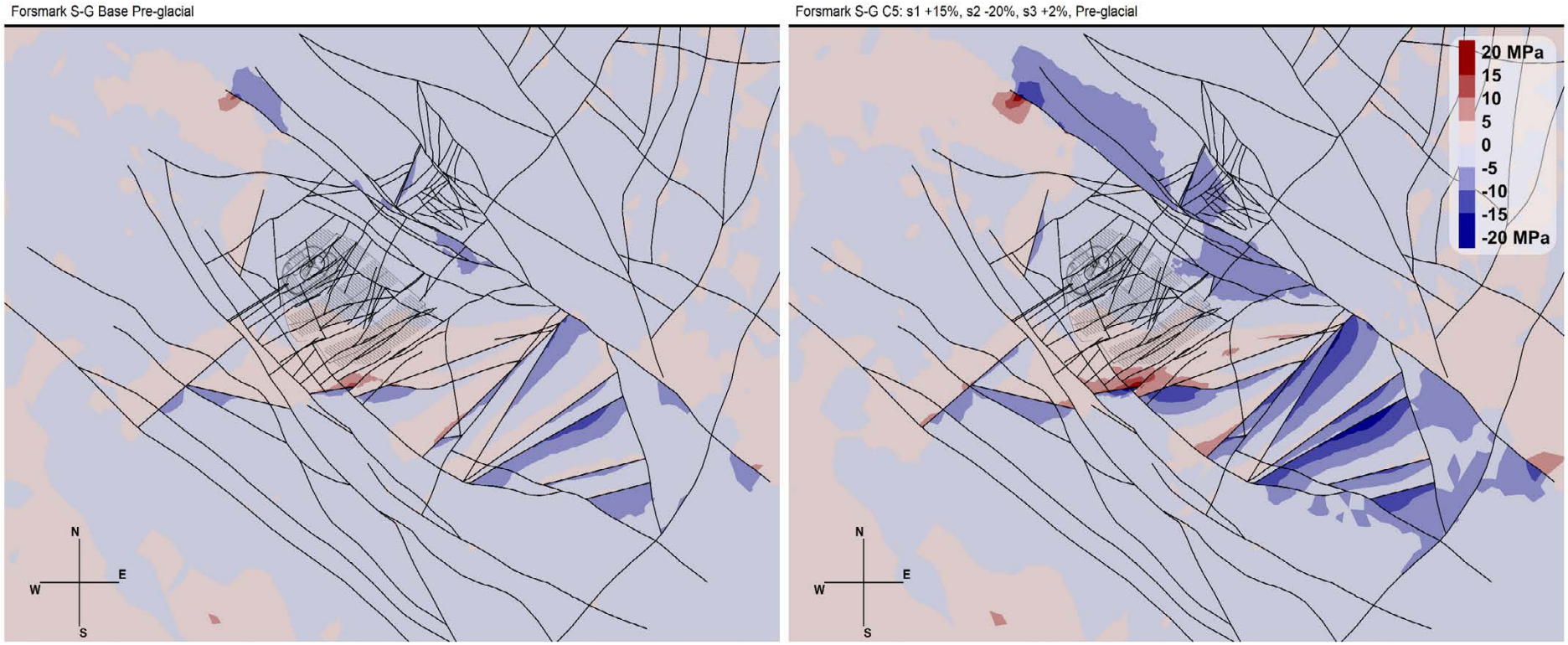

Figure A15-9. *The change in σ_1 magnitude before glaciation for the Base case and Case 5 of Phase 2 simulations in a horizontal cross-section at repository depth (470 m). The reference value is case-dependent.*

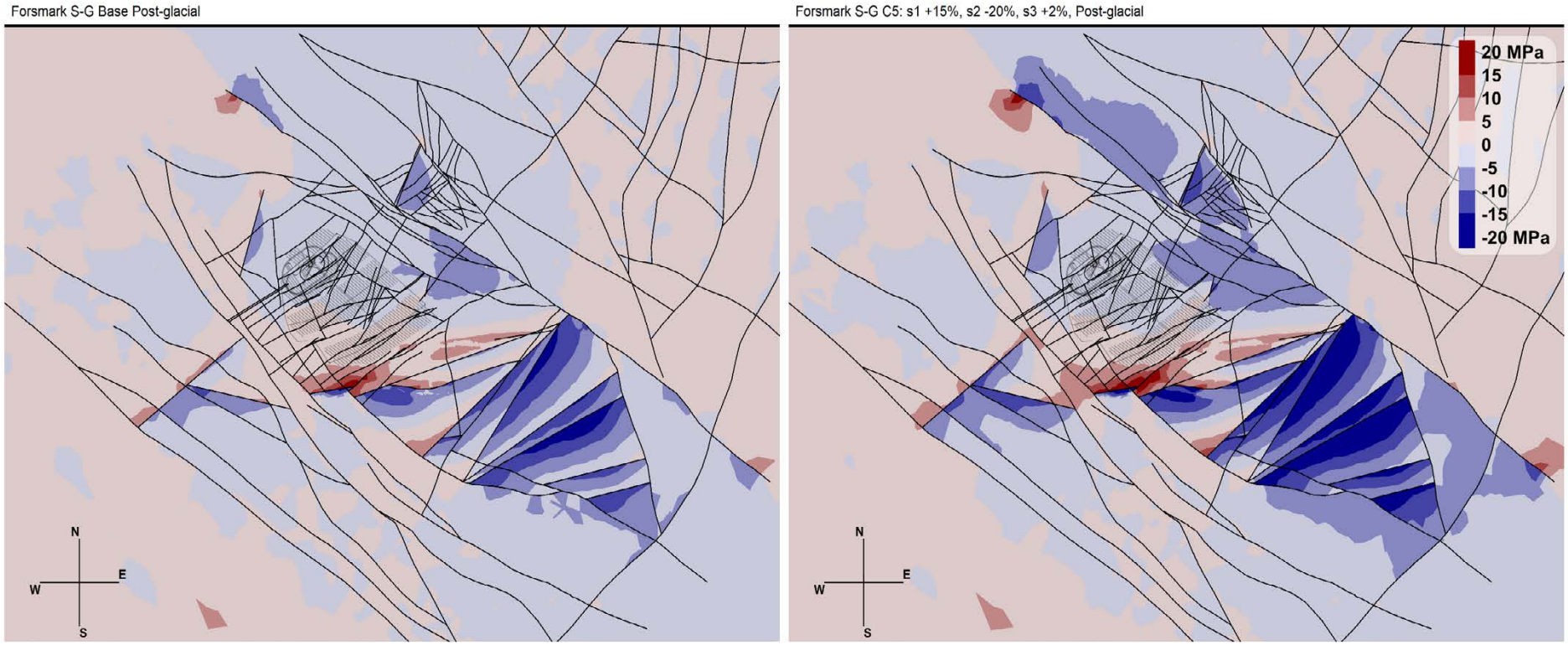

Figure A15-10. *The change in σ_1 magnitude after glaciation for the Base case and Case 5 of Phase 2 simulations in a horizontal cross-section at repository depth (470 m). The reference value is case-dependent.*

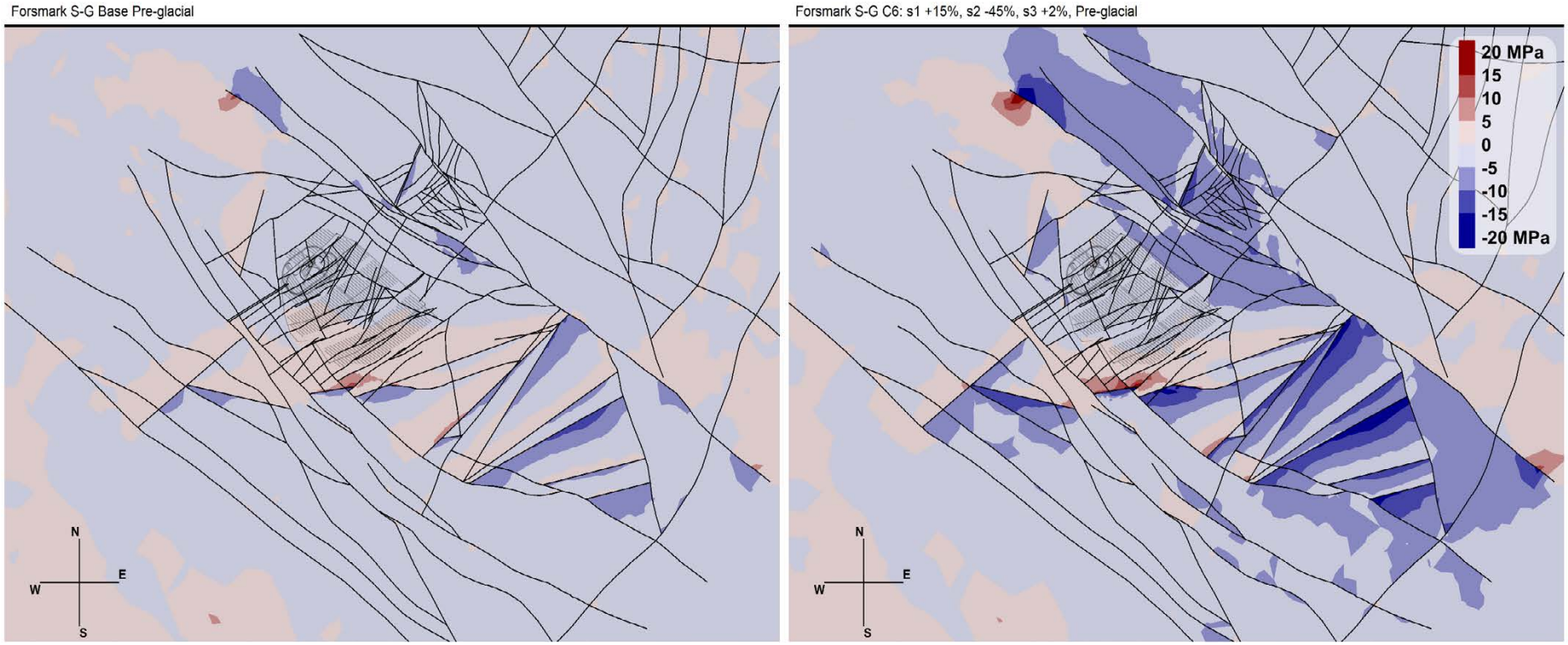

Figure A15-11. *The change in σ_1 magnitude before glaciation for the Base case and Case 6 of Phase 2 simulations in a horizontal cross-section at repository depth (470 m). The reference value is case-dependent.*

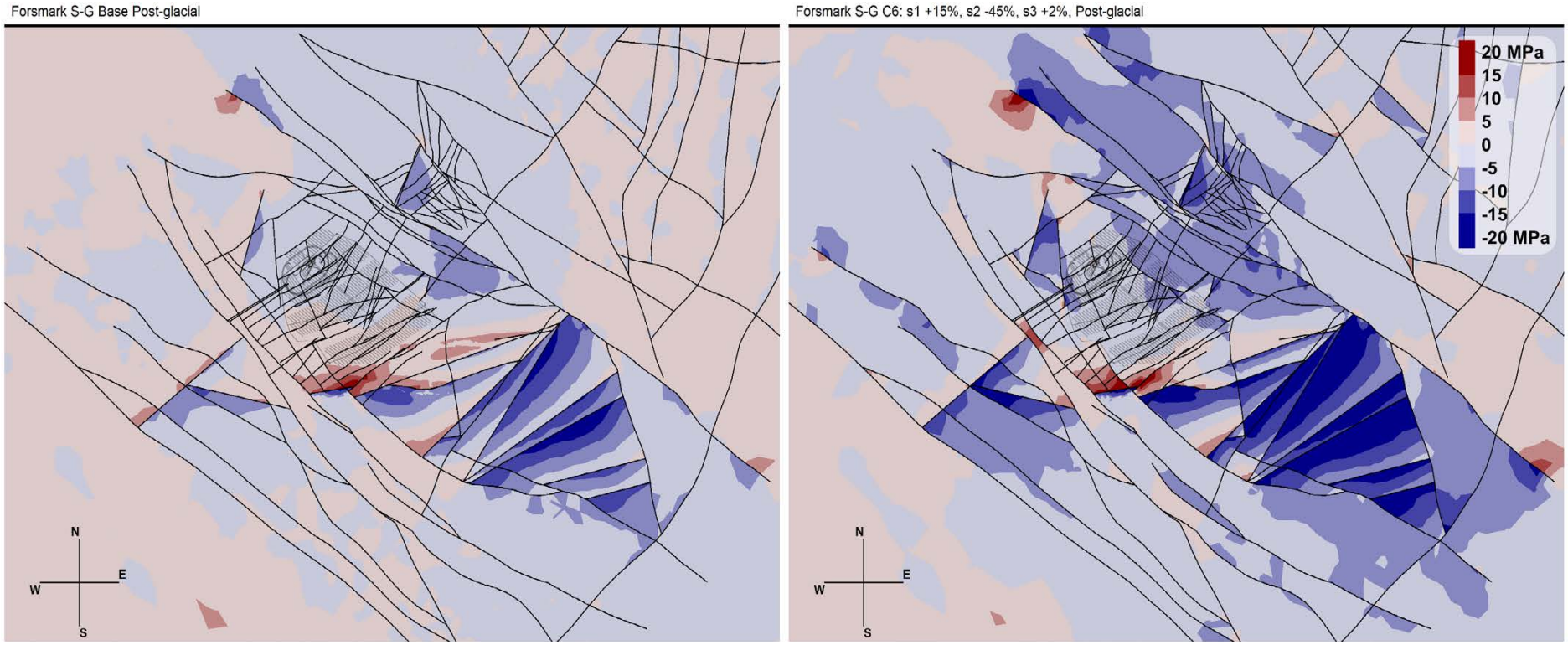

Figure A15-12. *The change in σ_1 magnitude after glaciation for the Base case and Case 6 of Phase 2 simulations in a horizontal cross-section at repository depth (470 m). The reference value is case-dependent.*

Appendix 16

Phase 1 – Change in σ_2 magnitude at repository depth

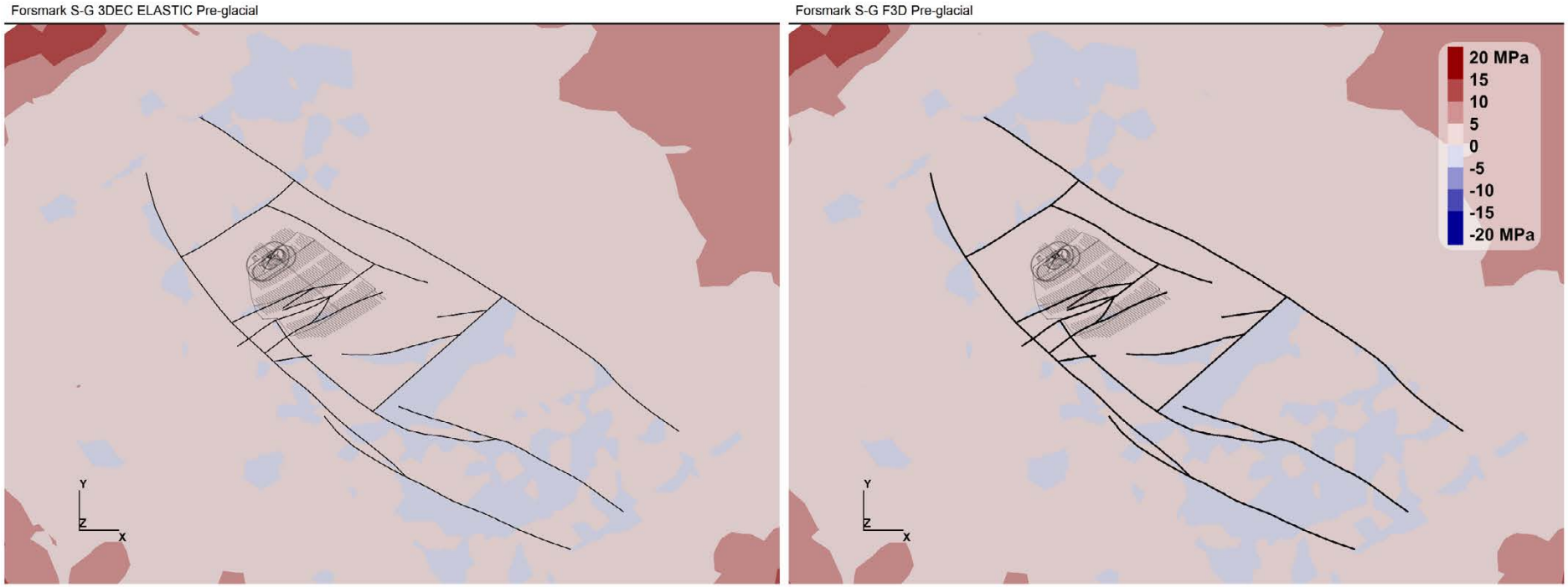

Figure A16-1. *Horizontal cross sections at repository depth −470 m of the intermediate principal stress magnitude difference to the Martin (2007) interpretation before glaciation in a fully elastic simulation. The reference value is case-dependent.*

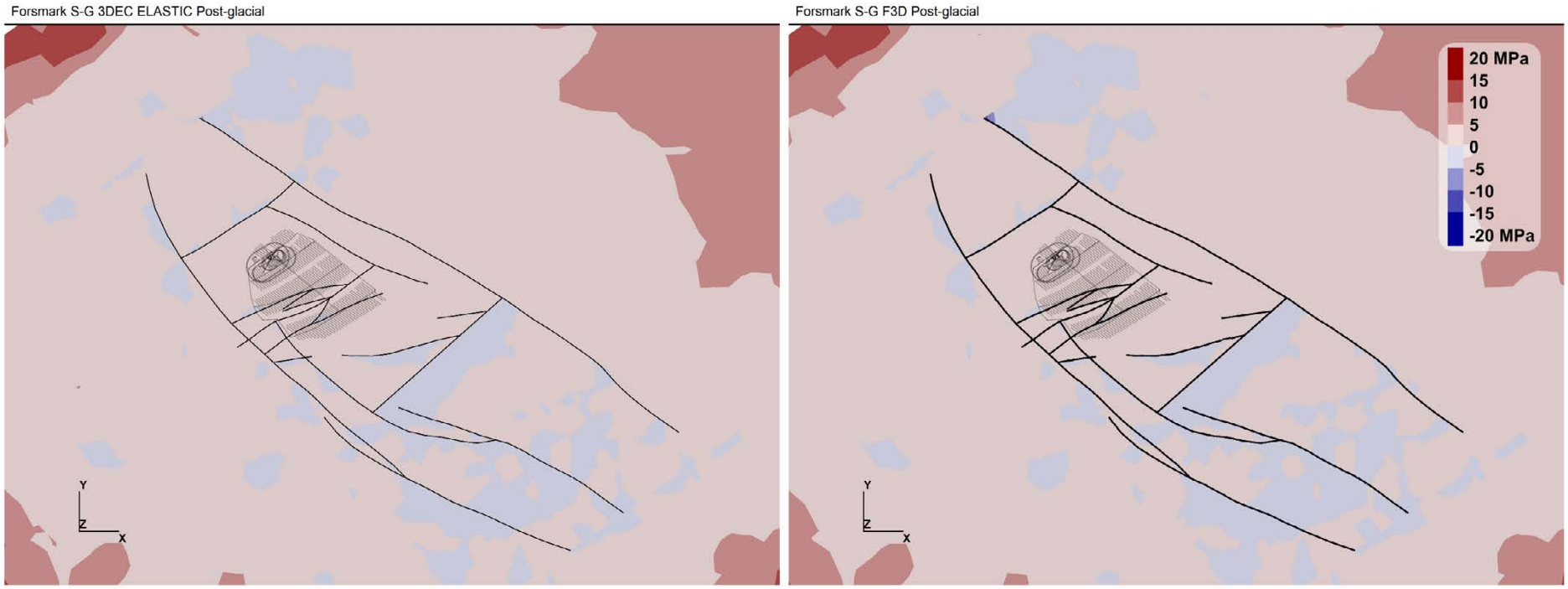

Figure A16-2. *Horizontal cross sections at repository depth −470 m of the intermediate principal stress magnitude difference to the Martin (2007) interpretation after glaciation in a fully elastic simulation. The reference value is case-dependent.*

Figure A16-3. *Horizontal cross sections at repository depth −470 m of the intermediate principal stress magnitude difference to the Martin (2007) interpretation before glaciation in an elastoplastic simulation. The reference value is case-dependent.*

Figure A16-4. *Horizontal cross sections at repository depth −470 m of the intermediate principal stress magnitude difference to the Martin (2007) interpretation after glaciation in an elastoplastic simulation. The reference value is case-dependent.*

Appendix 17

Phase 2 – Change in σ_2 magnitude at repository depth

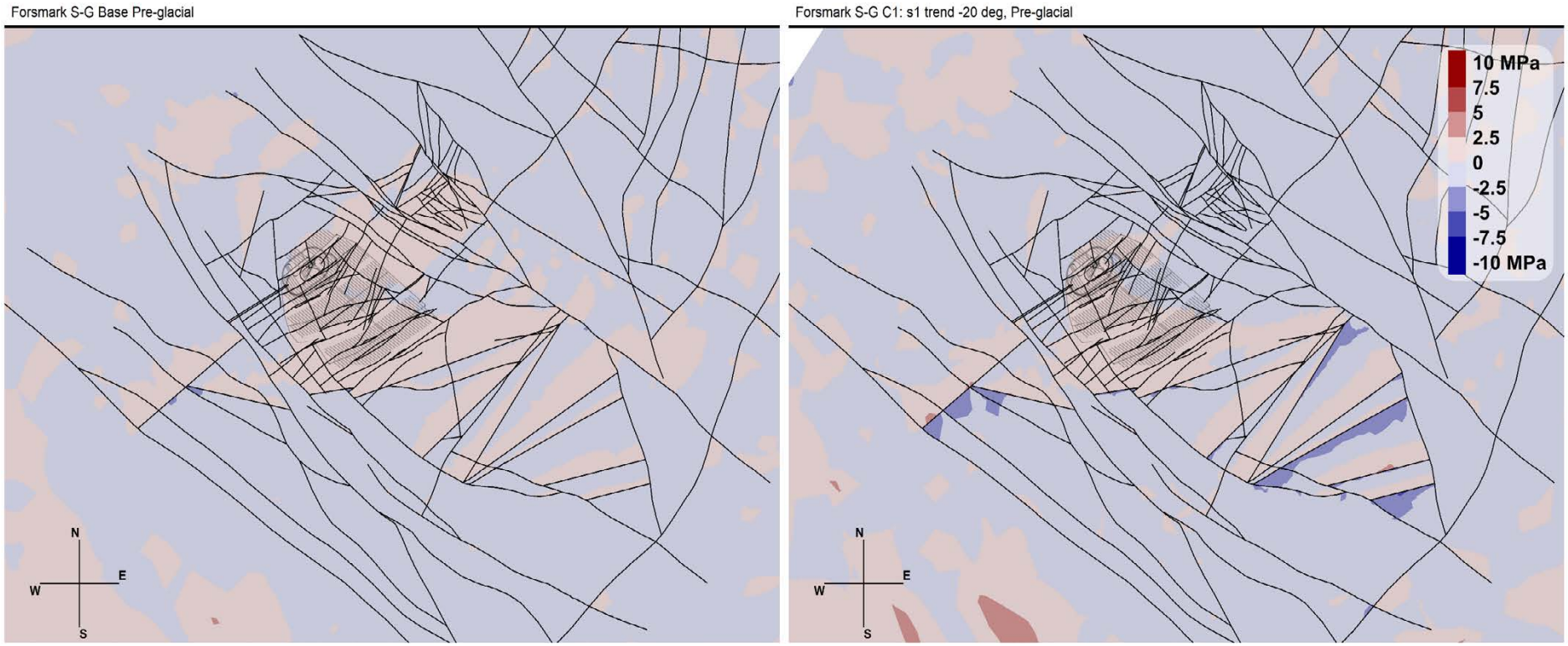

Figure A17-1. *The change in σ_2 magnitude before glaciation for the Base case and Case 1 of Phase 2 simulations in a horizontal cross-section at repository depth (470 m). The reference value is case-dependent.*

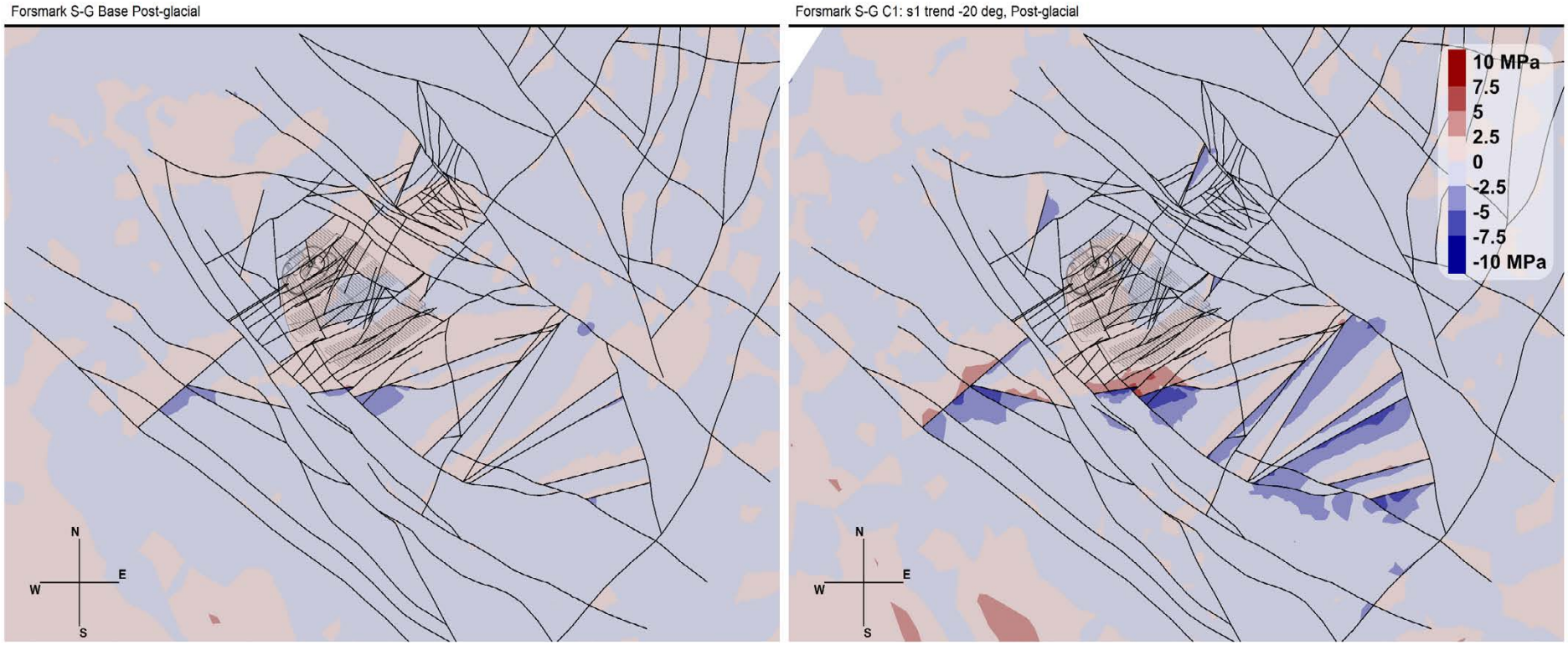

Figure A17-2. *The change in σ_2 magnitude after glaciation for the Base case and Case 1 of Phase 2 simulations in a horizontal cross-section at repository depth (470 m). The reference value is case-dependent.*

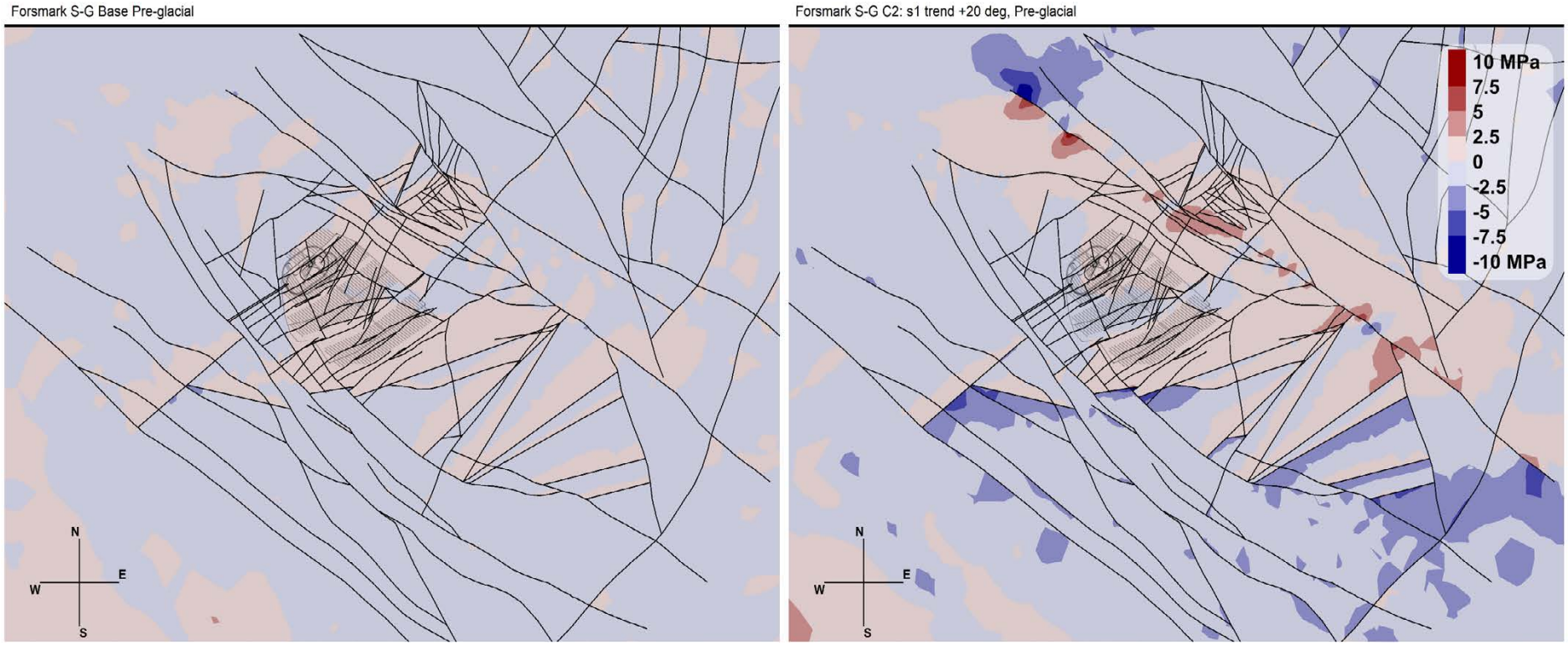

Figure A17-3. *The change in σ_2 magnitude before glaciation for the Base case and Case 2 of Phase 2 simulations in a horizontal cross-section at repository depth (470 m). The reference value is case-dependent.*

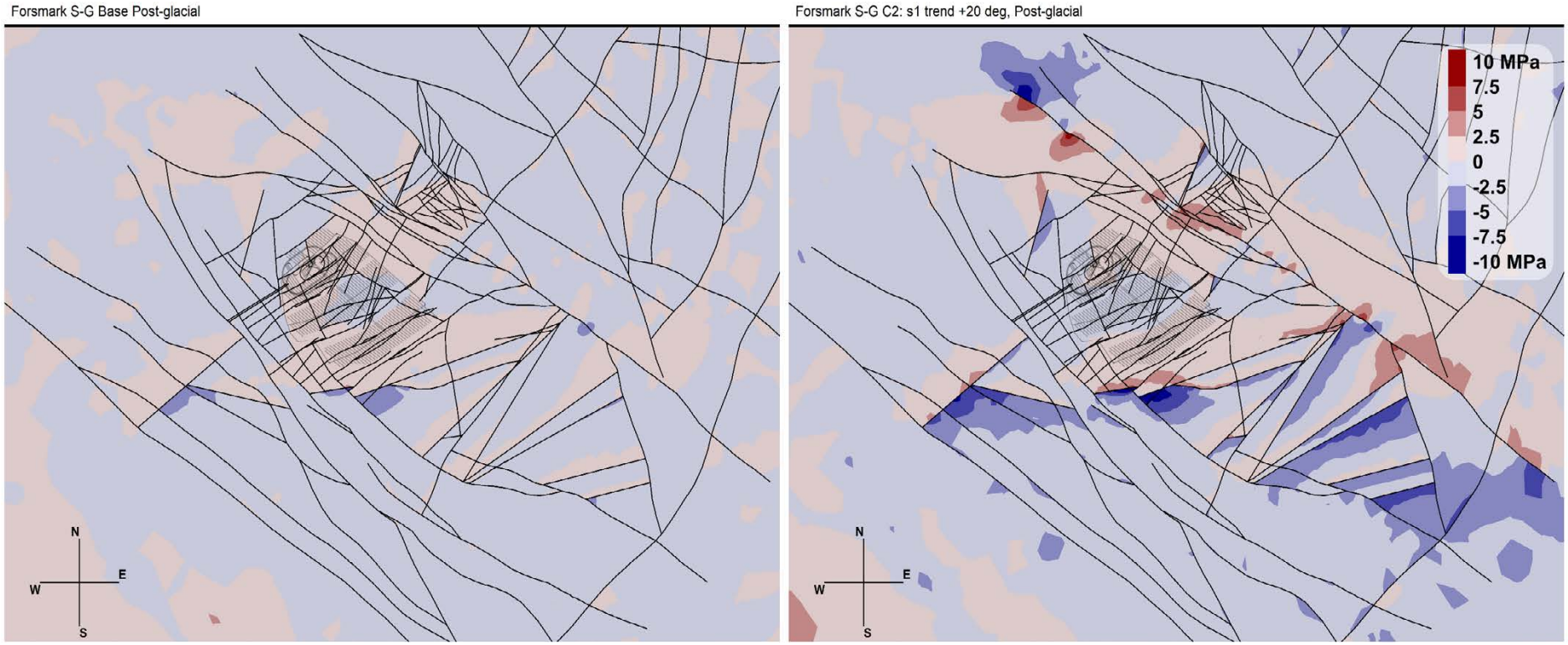

Figure A17-4. *The change in σ_2 magnitude after glaciation for the Base case and Case 2 of Phase 2 simulations in a horizontal cross-section at repository depth (470 m). The reference value is case-dependent.*

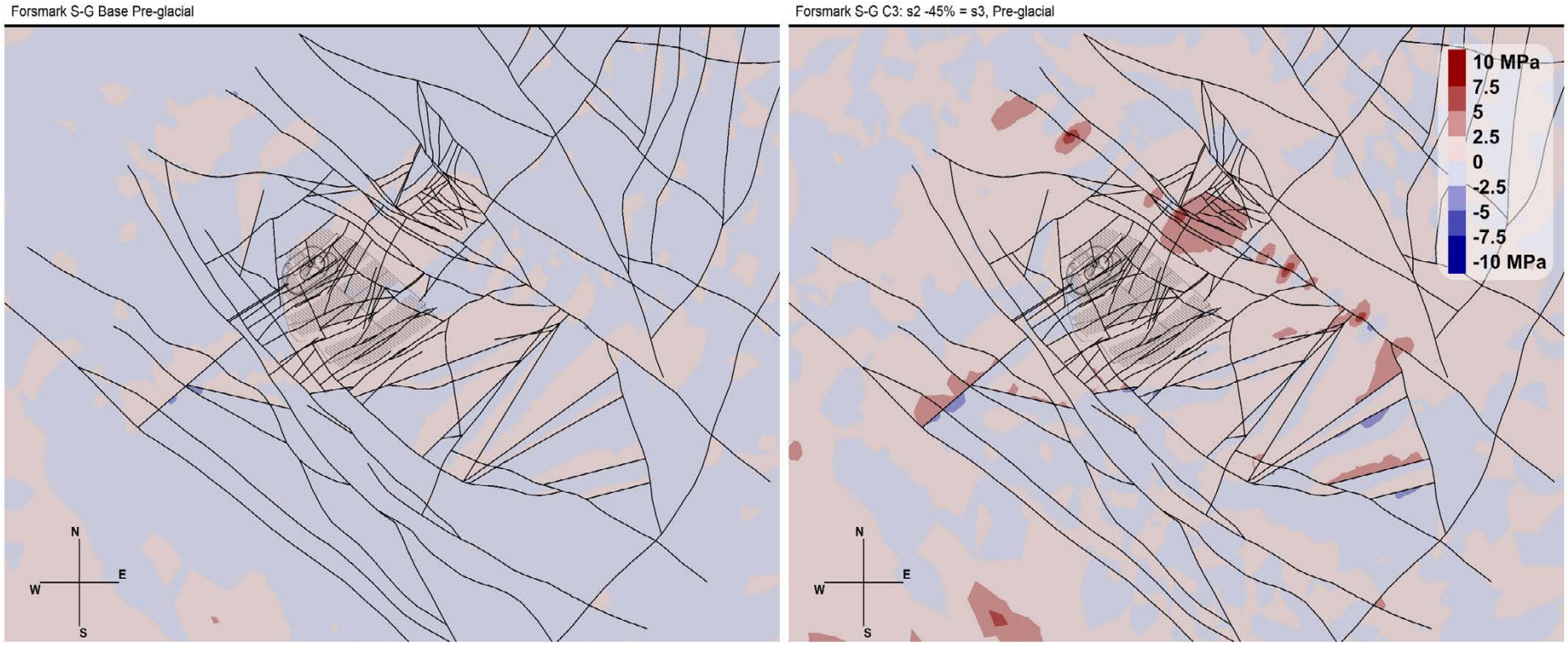

Figure A17-5. *The change in σ_2 magnitude before glaciation for the Base case and Case 3 of Phase 2 simulations in a horizontal cross-section at repository depth (470 m). The reference value is case-dependent.*

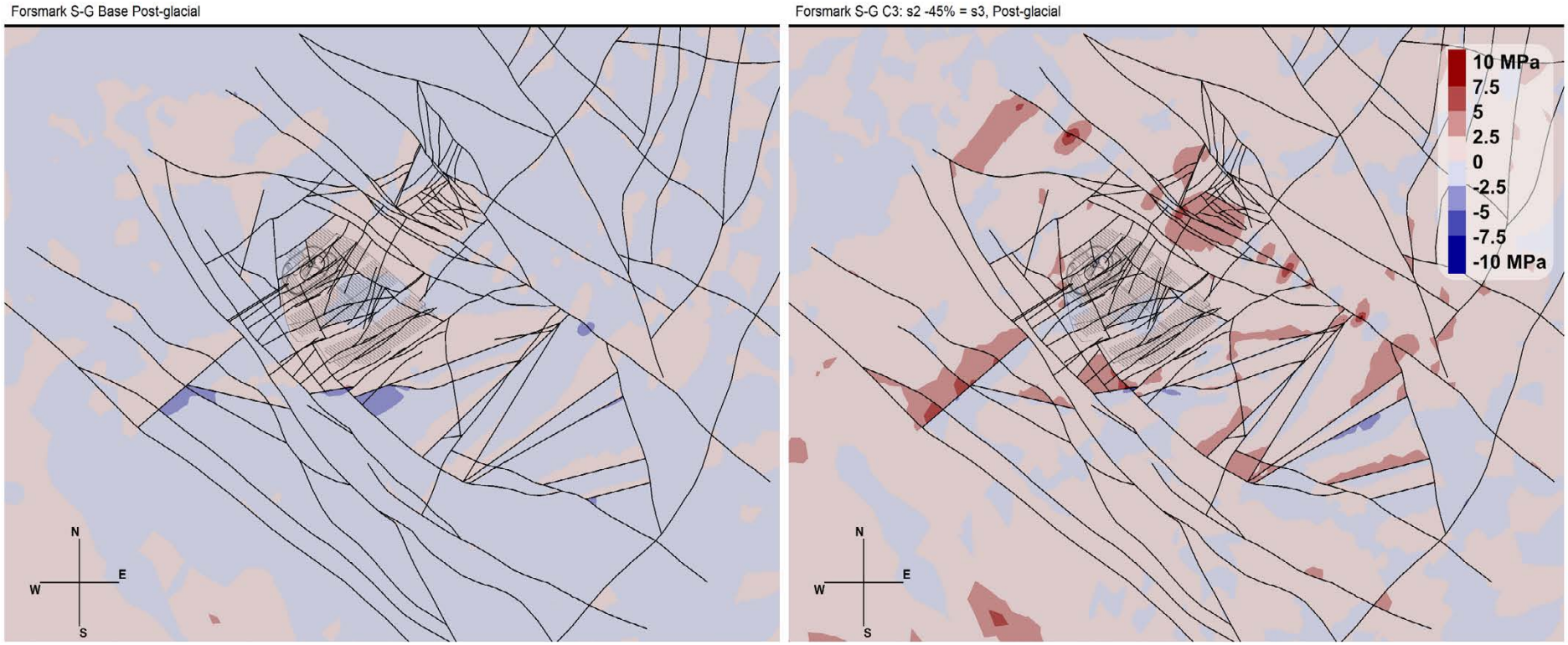

Figure A17-6. *The change in σ_2 magnitude after glaciation for the Base case and Case 3 of Phase 2 simulations in a horizontal cross-section at repository depth (470 m). The reference value is case-dependent.*

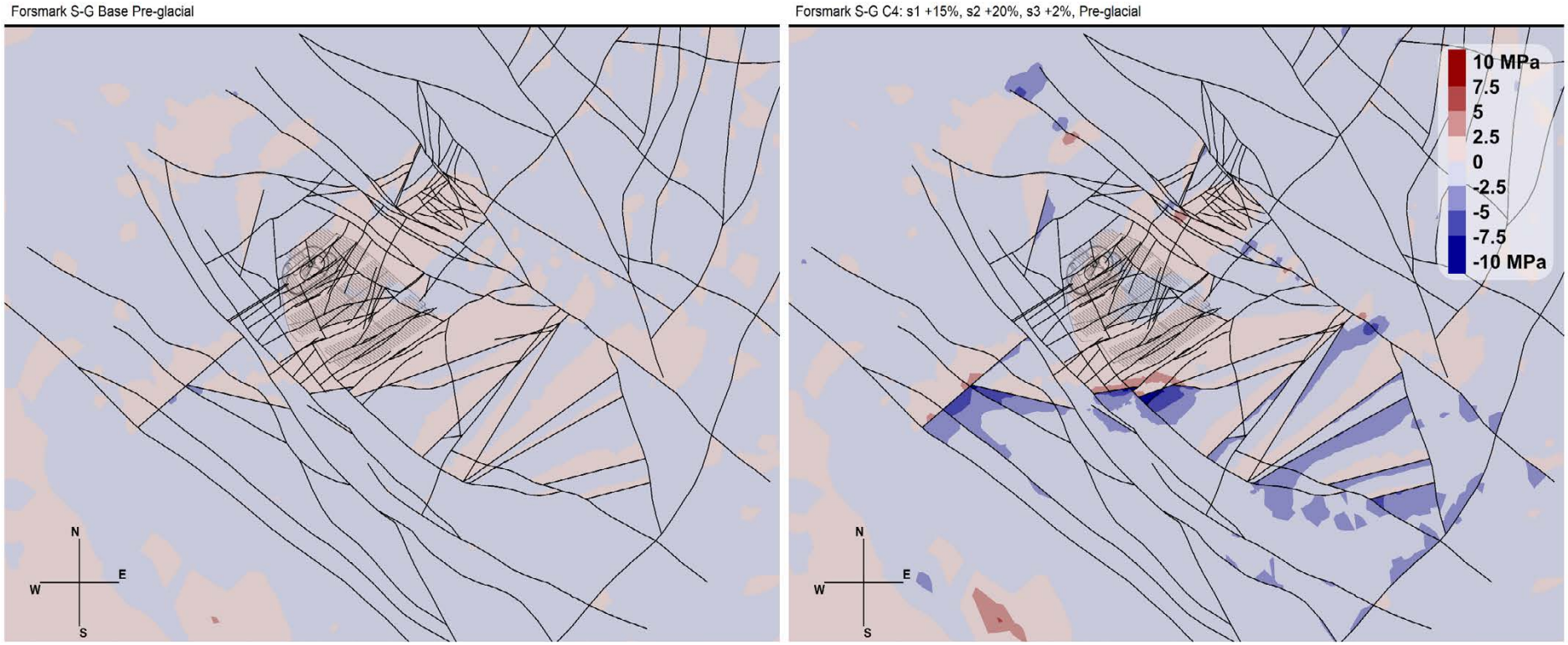

Figure A17-7. *The change in σ_2 magnitude before glaciation for the Base case and Case 4 of Phase 2 simulations in a horizontal cross-section at repository depth (470 m). The reference value is case-dependent.*

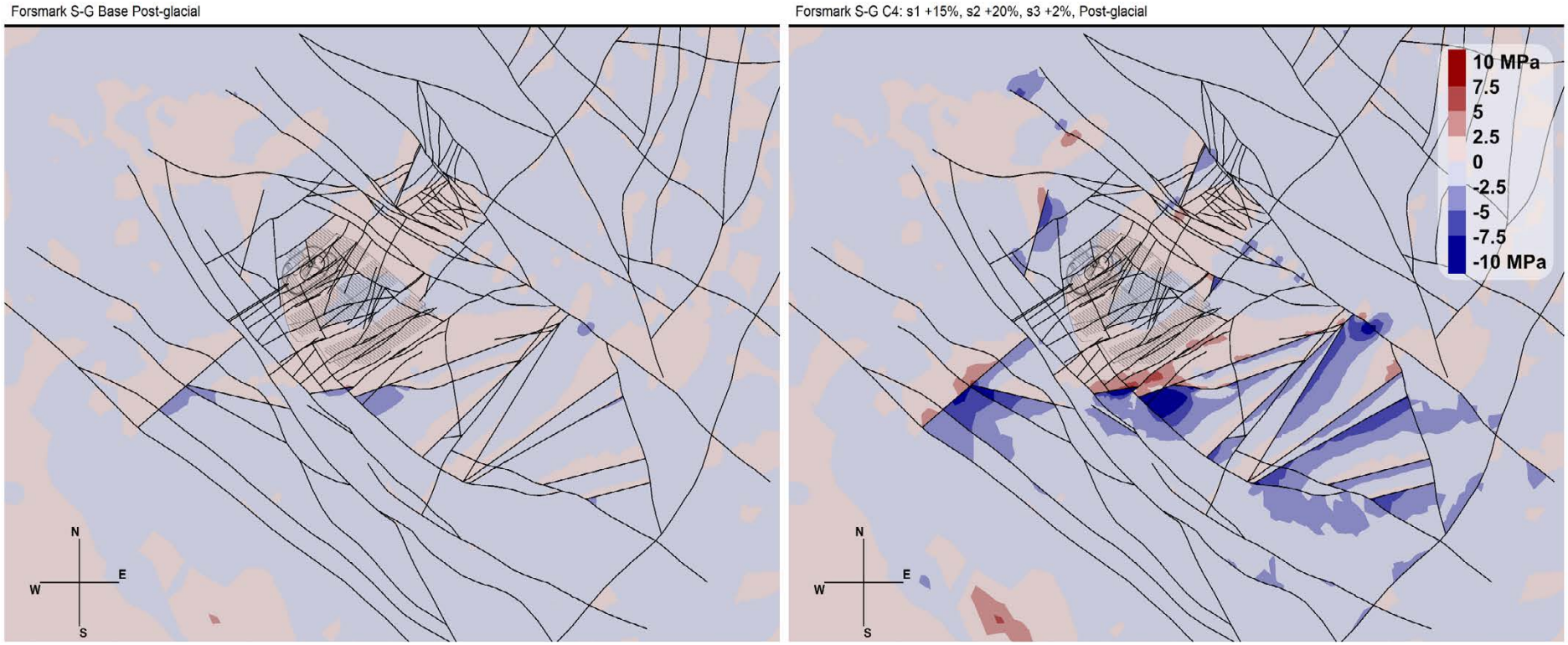

Figure A17-8. *The change in σ_2 magnitude after glaciation for the Base case and Case 4 of Phase 2 simulations in a horizontal cross-section at repository depth (470 m). The reference value is case-dependent.*

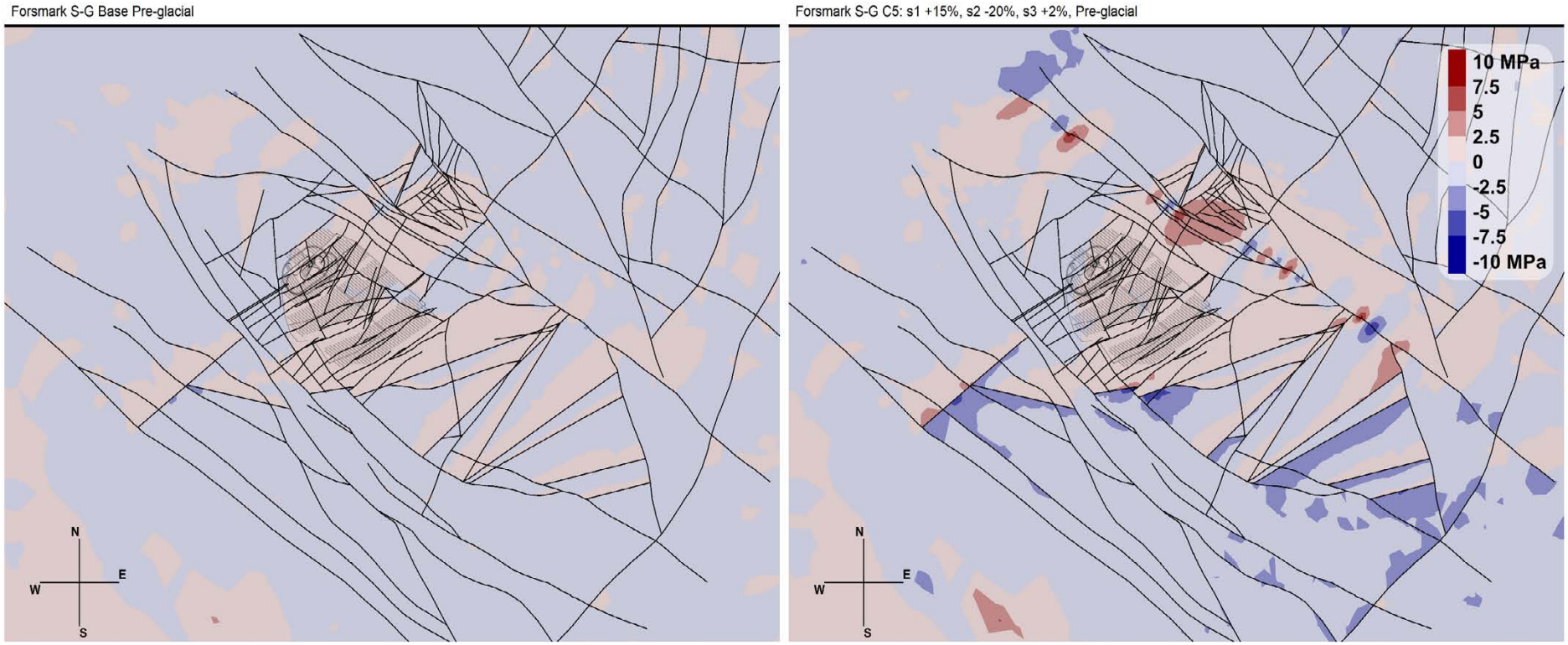

Figure A17-9. *The change in σ_2 magnitude before glaciation for the Base case and Case 5 of Phase 2 simulations in a horizontal cross-section at repository depth (470 m). The reference value is case-dependent.*

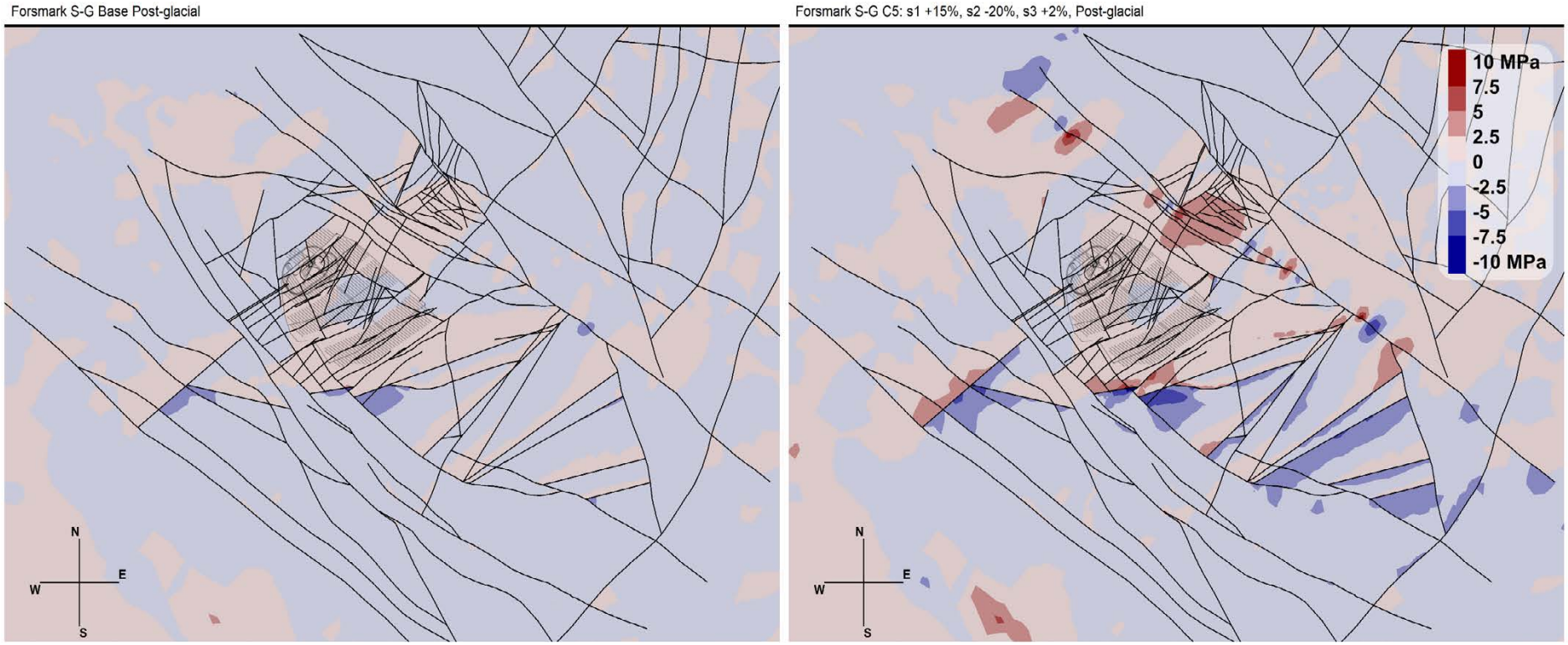

Figure A17-10. *The change in σ_2 magnitude after glaciation for the Base case and Case 5 of Phase 2 simulations in a horizontal cross-section at repository depth (470 m). The reference value is case-dependent.*

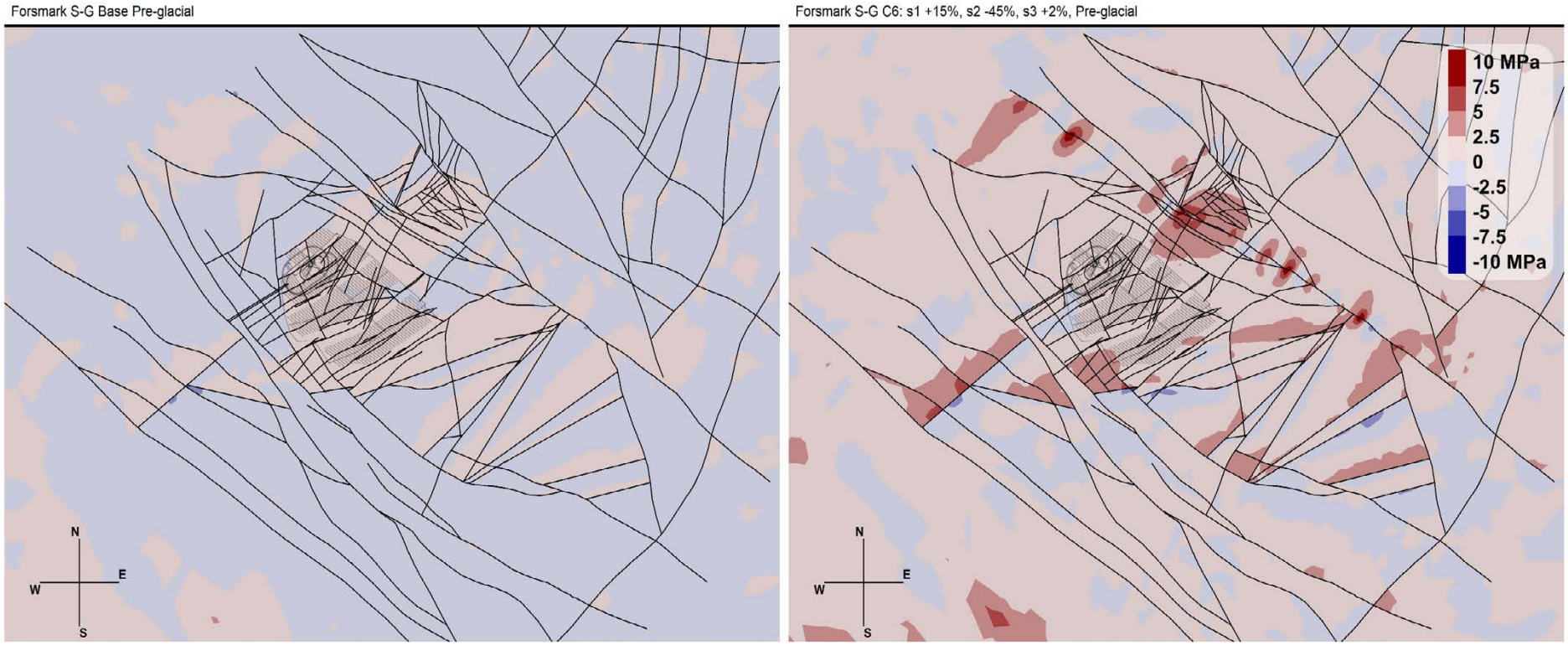

Figure A17-11. *The change in σ_2 magnitude before glaciation for the Base case and Case 6 of Phase 2 simulations in a horizontal cross-section at repository depth (470 m). The reference value is case-dependent.*

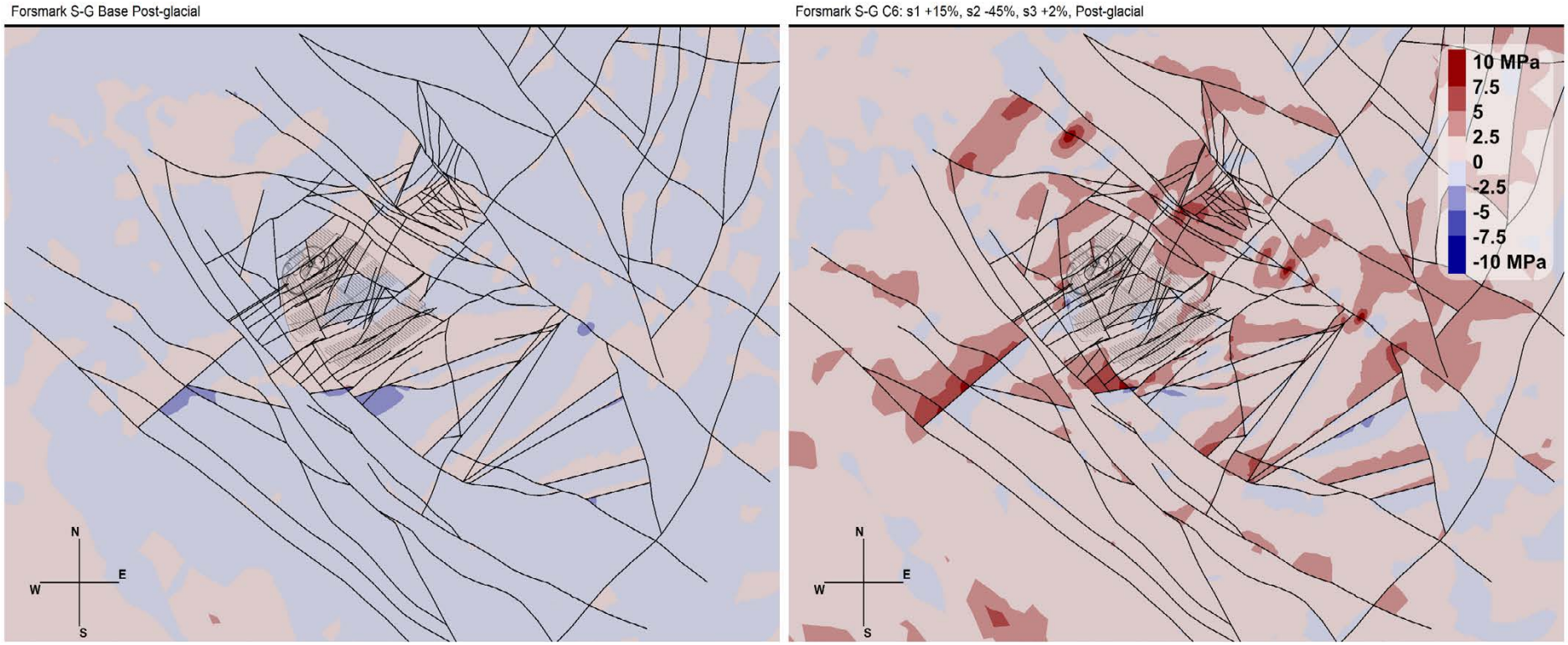

Figure A17-12. *The change in σ_2 magnitude after glaciation for the Base case and Case 6 of Phase 2 simulations in a horizontal cross-section at repository depth (470 m). The reference value is case-dependent.*

Appendix 18

Phase 1 – Change in σ_3 magnitude at repository depth

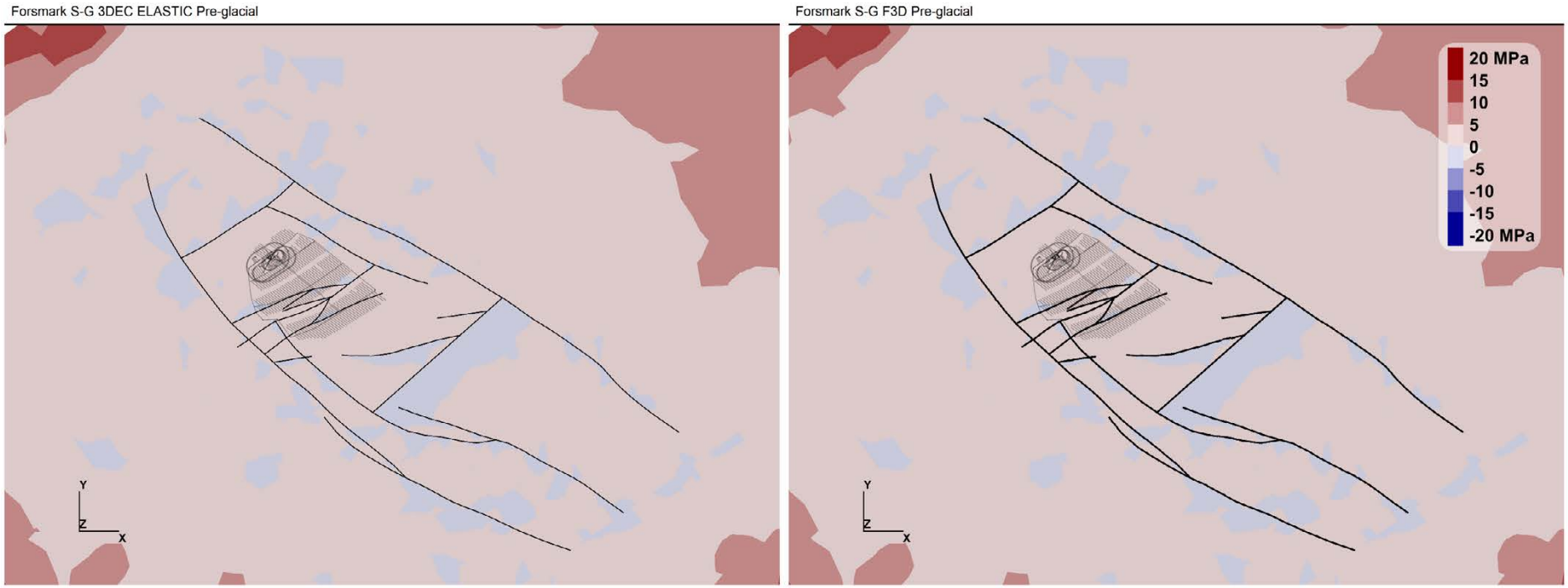

Figure A18-1. *Horizontal cross sections at repository depth −470 m of the minimum principal stress magnitude difference to the Martin (2007) interpretation before glaciation in a fully elastic simulation. The reference value is case-dependent.*

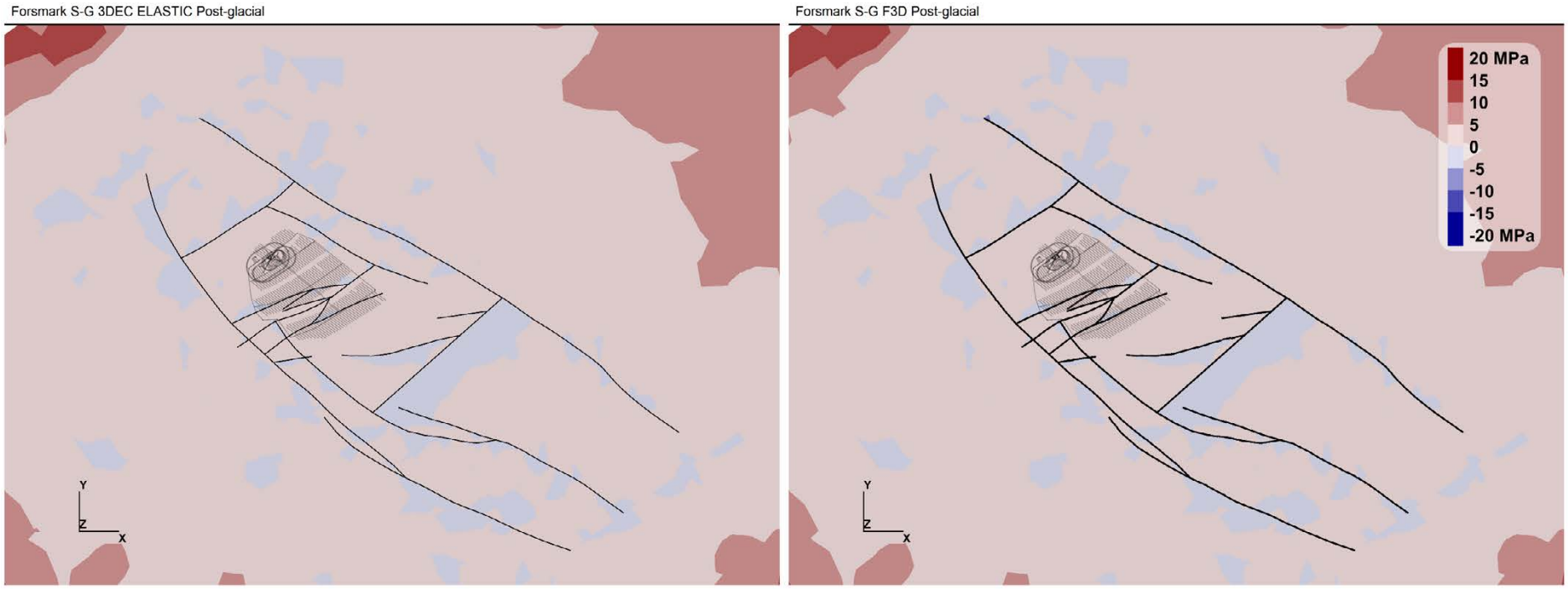

Figure A18-2. *Horizontal cross sections at repository depth −470 m of the minimum principal stress magnitude difference to the Martin (2007) interpretation after glaciation in a fully elastic simulation. The reference value is case-dependent.*

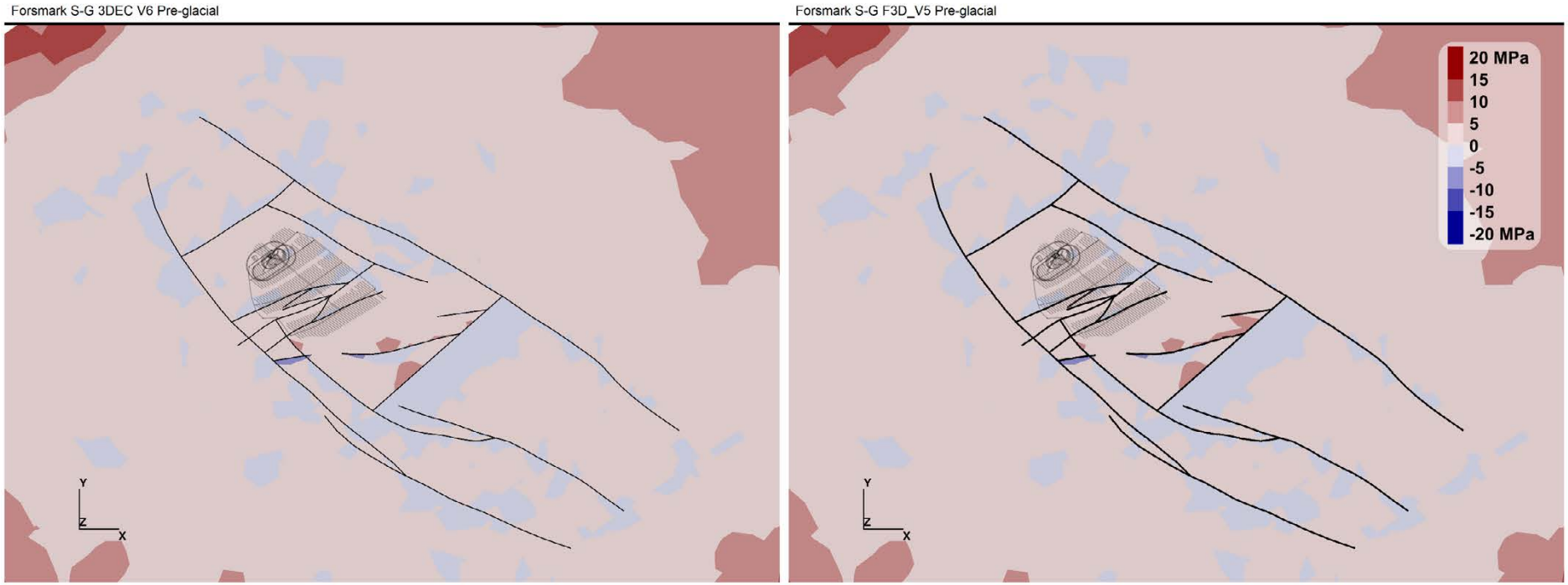

Figure A18-3. *Horizontal cross sections at repository depth −470 m of the minimum principal stress magnitude difference to the Martin (2007) interpretation before glaciation in an elastoplastic simulation. The reference value is case-dependent.*

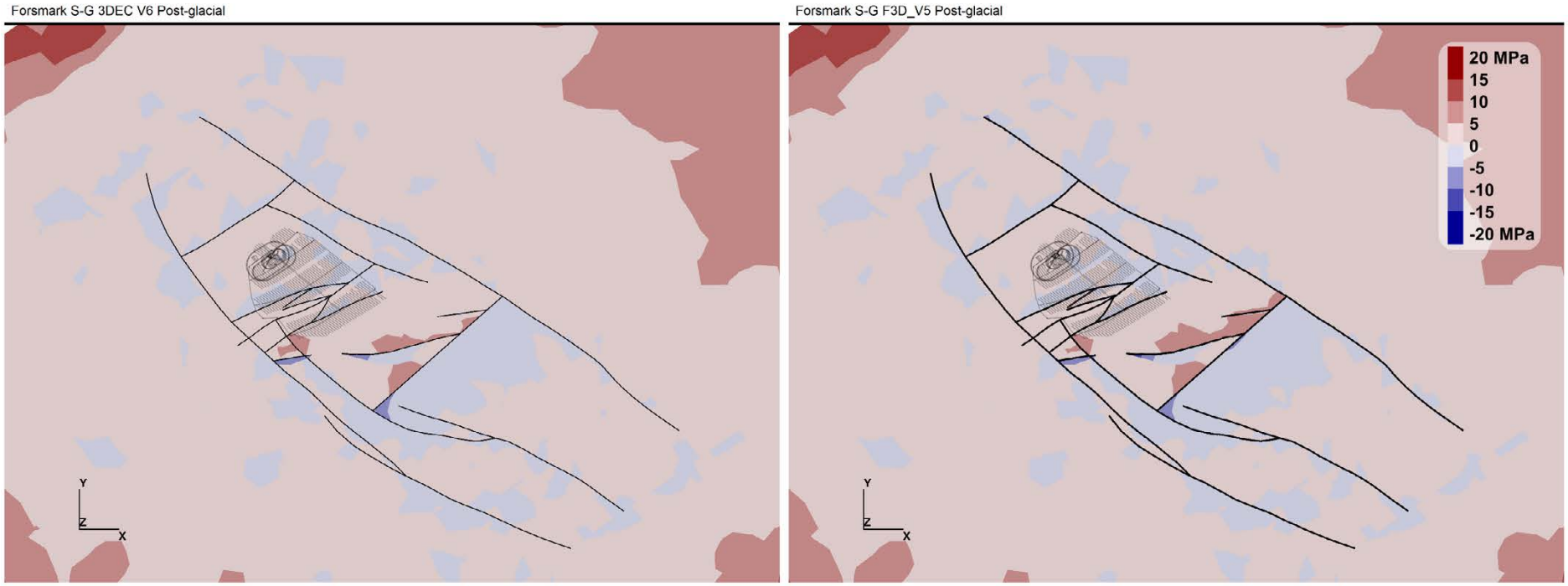

Figure A18-4. *Horizontal cross sections at repository depth −470 m of the minimum principal stress magnitude difference to the Martin (2007) interpretation after glaciation in an elastoplastic simulation. The reference value is case-dependent.*

Appendix 19

Phase 2 – Change in σ_3 magnitude at repository depth

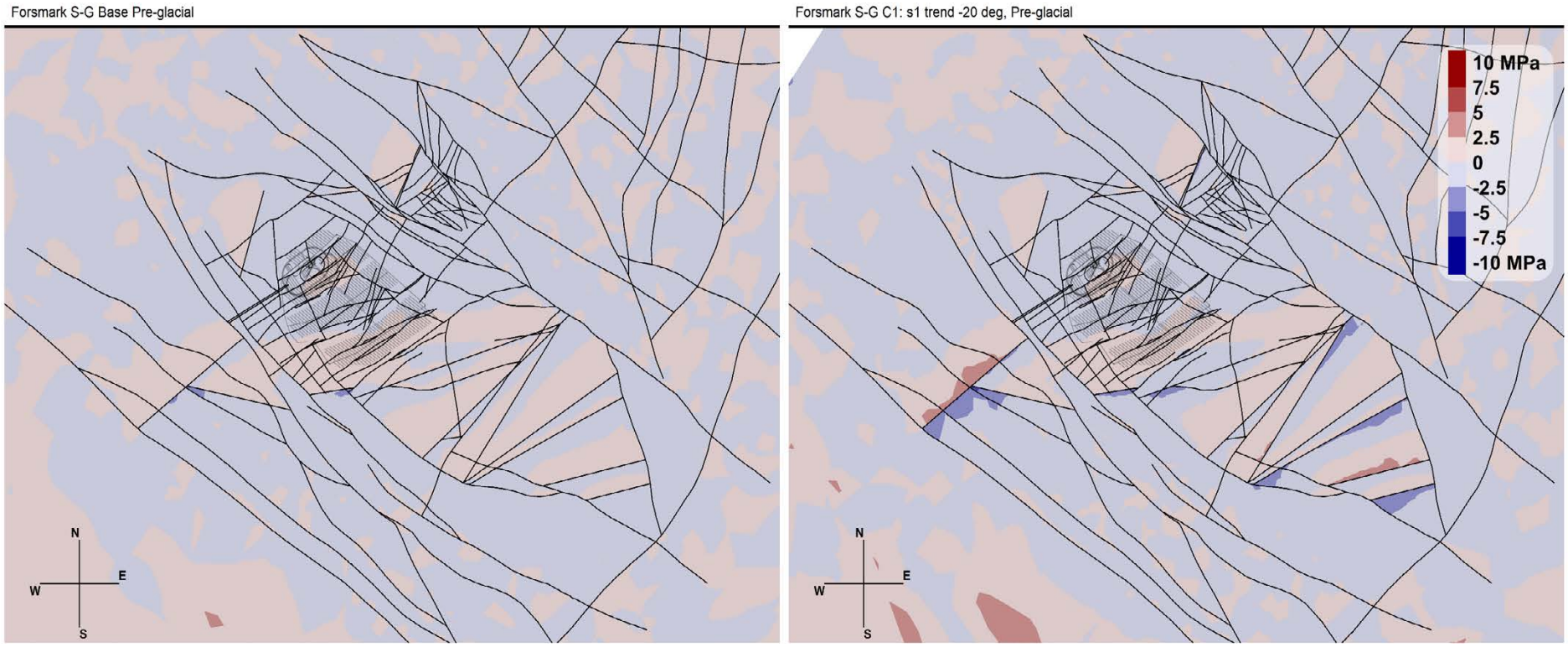

Figure A19-1. *The change in σ_3 magnitude before glaciation for the Base case and Case 1 of Phase 2 simulations in a horizontal cross-section at repository depth (470 m). The reference value is case-dependent.*

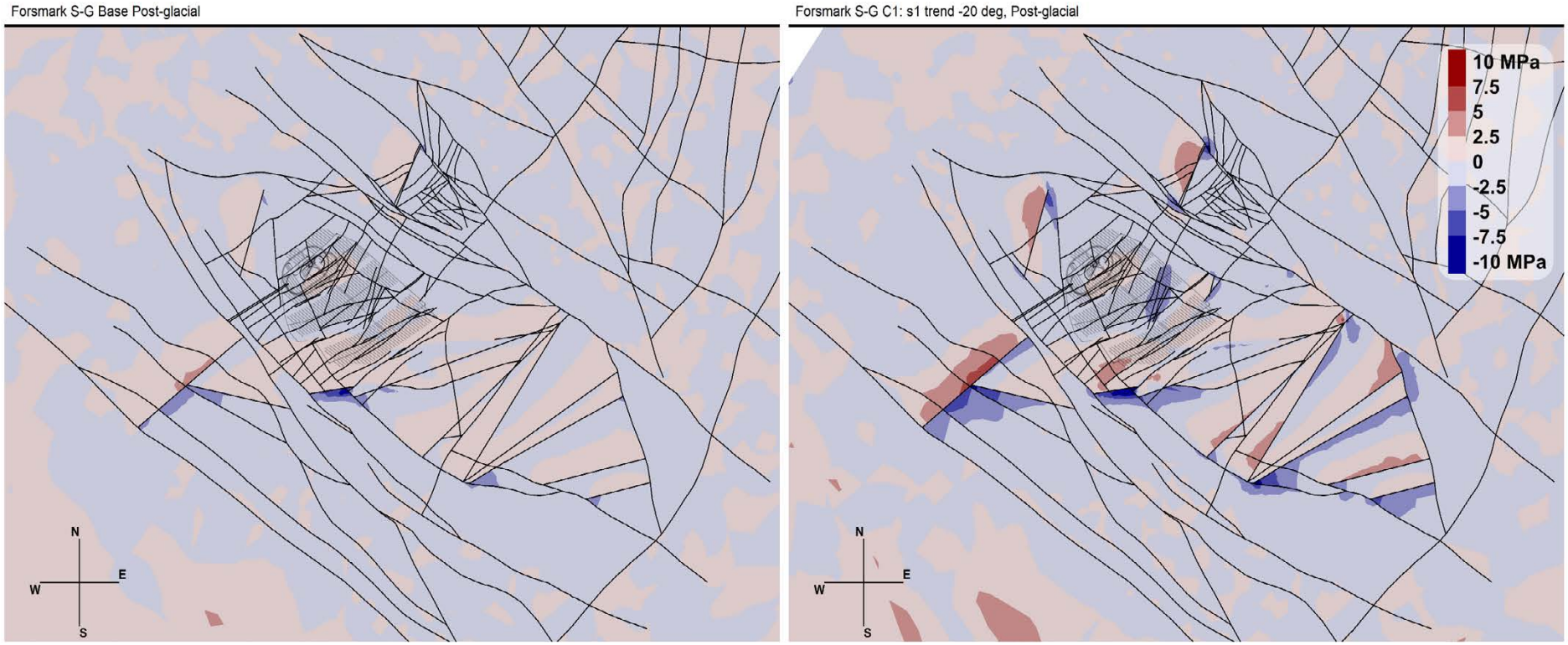

Figure A19-2. *The change in σ_3 magnitude after glaciation for the Base case and Case 1 of Phase 2 simulations in a horizontal cross-section at repository depth (470 m). The reference value is case-dependent.*

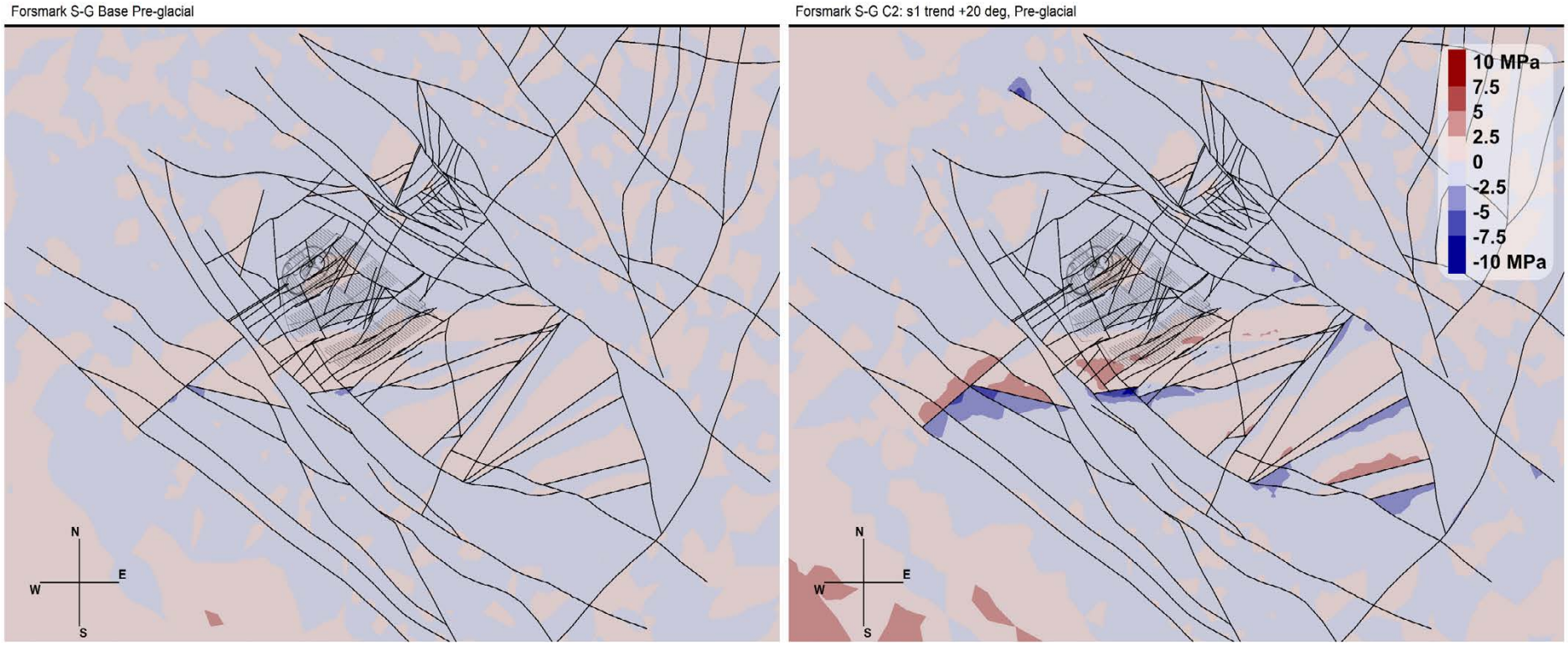

Figure A19-3. *The change in σ_3 magnitude before glaciation for the Base case and Case 2 of Phase 2 simulations in a horizontal cross-section at repository depth (470 m). The reference value is case-dependent.*

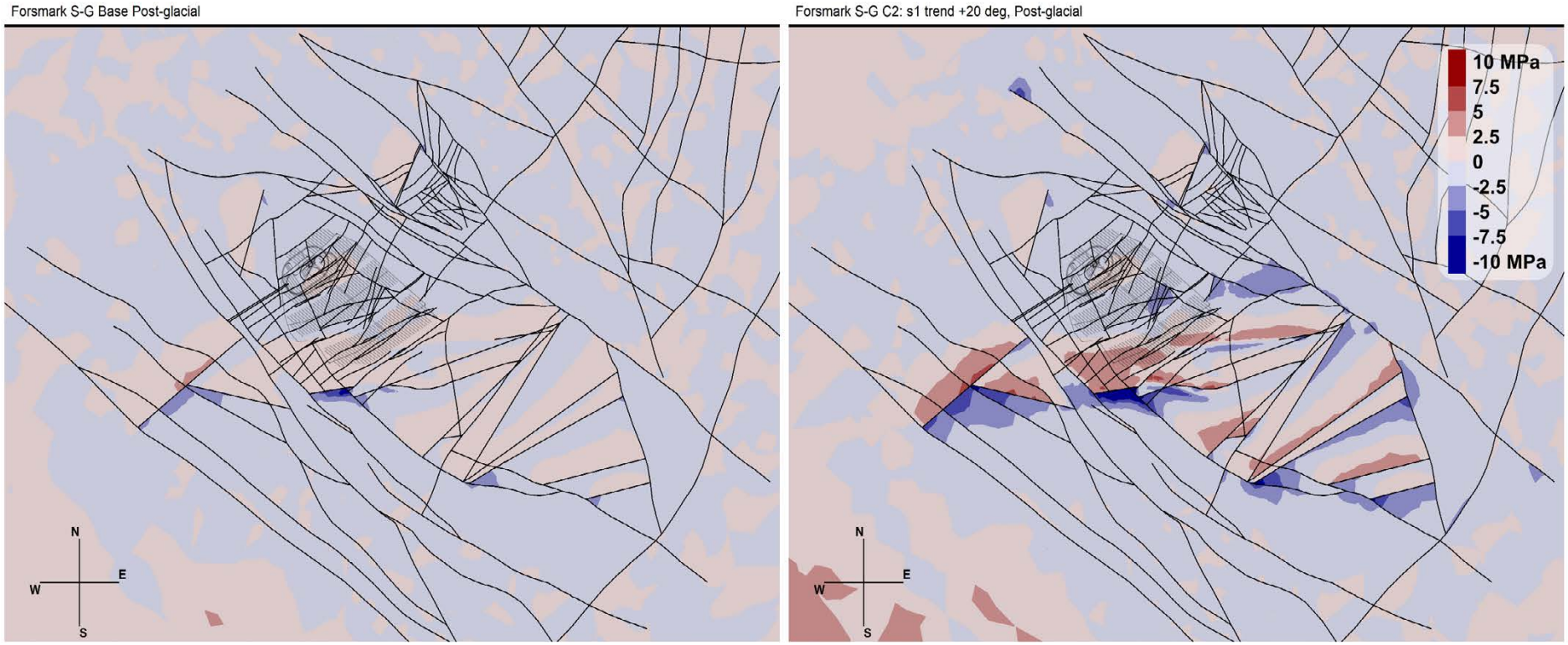

Figure A19-4. *The change in σ_3 magnitude after glaciation for the Base case and Case 2 of Phase 2 simulations in a horizontal cross-section at repository depth (470 m). The reference value is case-dependent.*

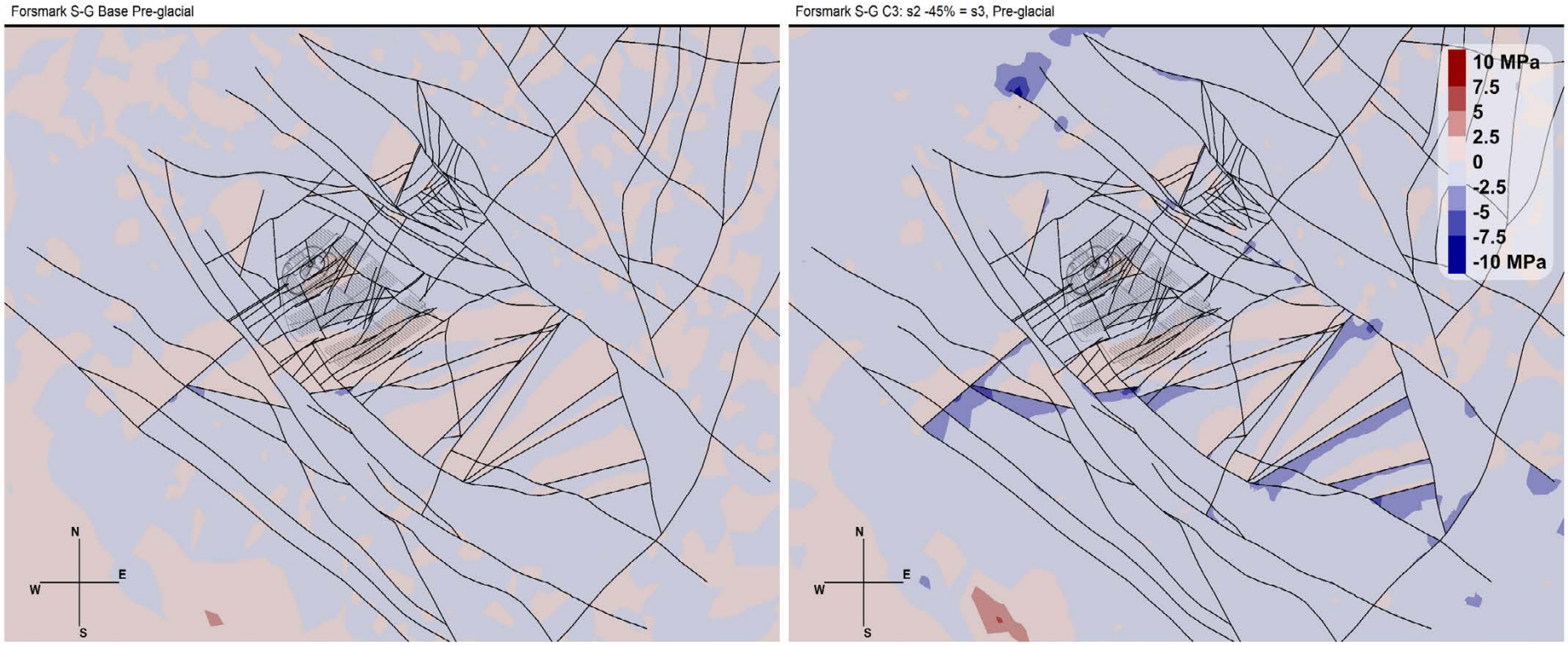

Figure A19-5. *The change in σ_3 magnitude before glaciation for the Base case and Case 3 of Phase 2 simulations in a horizontal cross-section at repository depth (470 m). The reference value is case-dependent.*

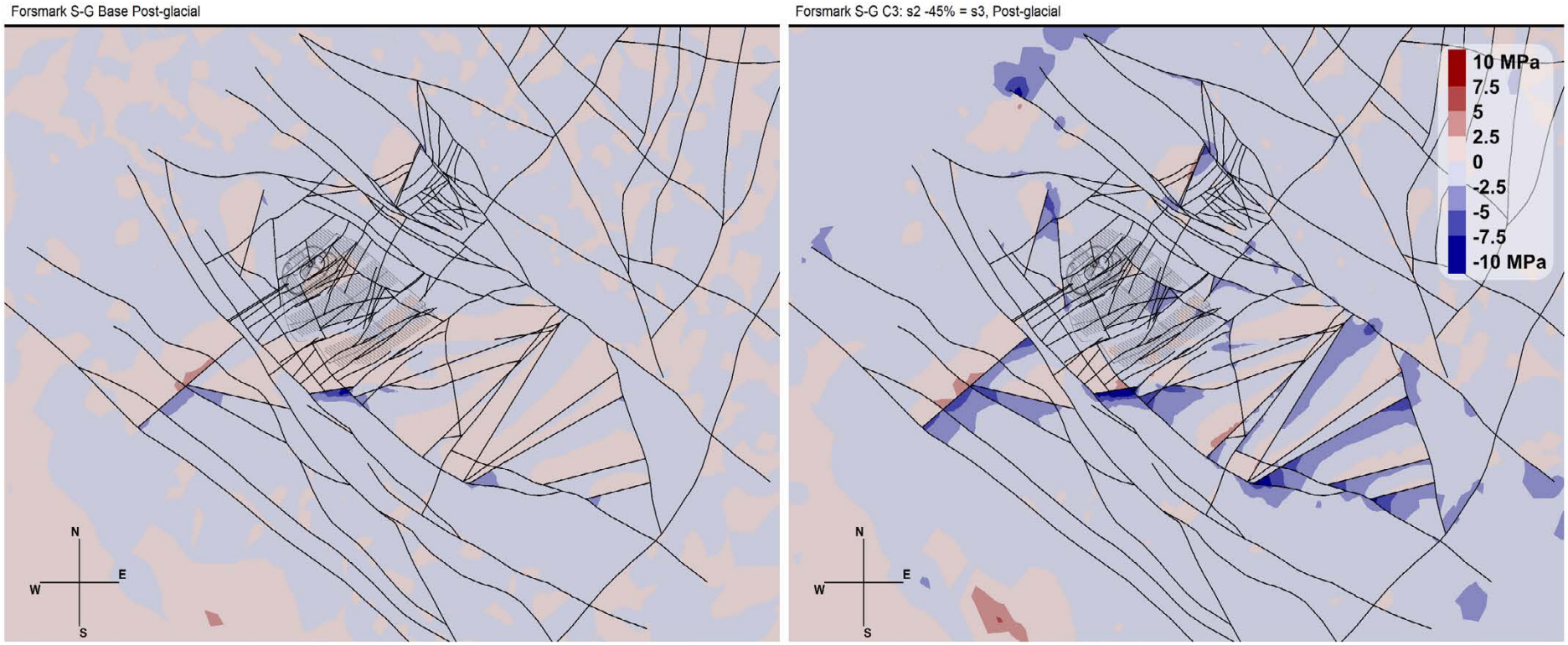

Figure A19-6. *The change in σ_3 magnitude after glaciation for the Base case and Case 3 of Phase 2 simulations in a horizontal cross-section at repository depth (470 m). The reference value is case-dependent.*

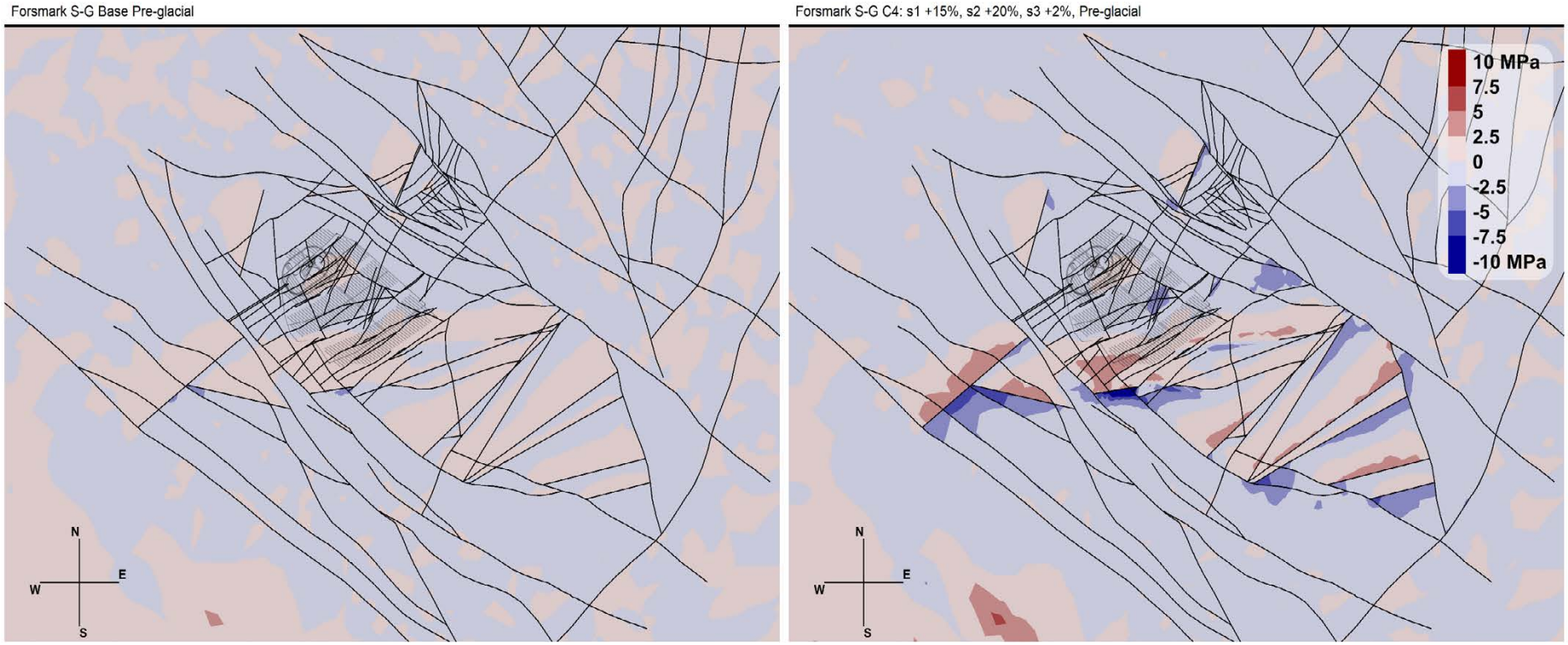

Figure A19-7. *The change in σ_3 magnitude before glaciation for the Base case and Case 4 of Phase 2 simulations in a horizontal cross-section at repository depth (470 m). The reference value is case-dependent.*

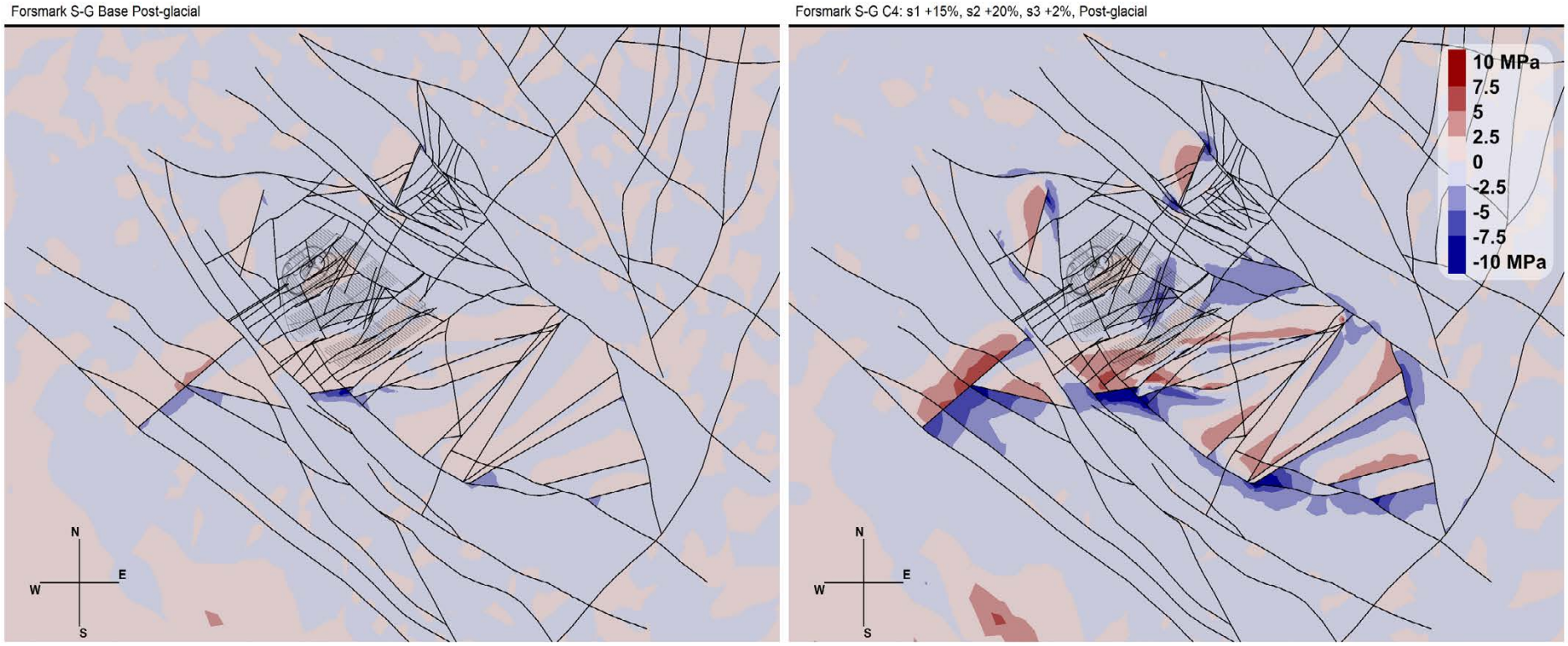

Figure A19-8. *The change in σ_3 magnitude after glaciation for the Base case and Case 4 of Phase 2 simulations in a horizontal cross-section at repository depth (470 m). The reference value is case-dependent.*

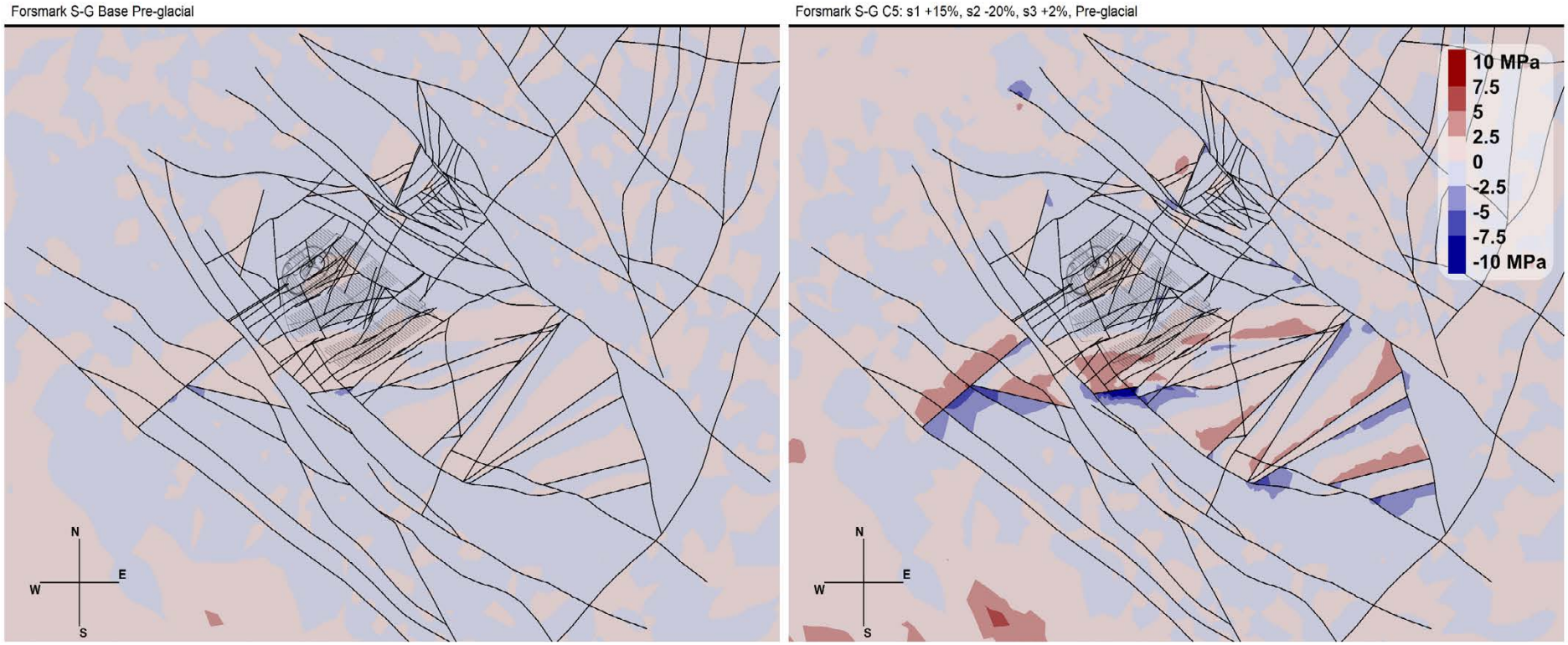

Figure A19-9. *The change in σ_3 magnitude before glaciation for the Base case and Case 5 of Phase 2 simulations in a horizontal cross-section at repository depth (470 m). The reference value is case-dependent.*

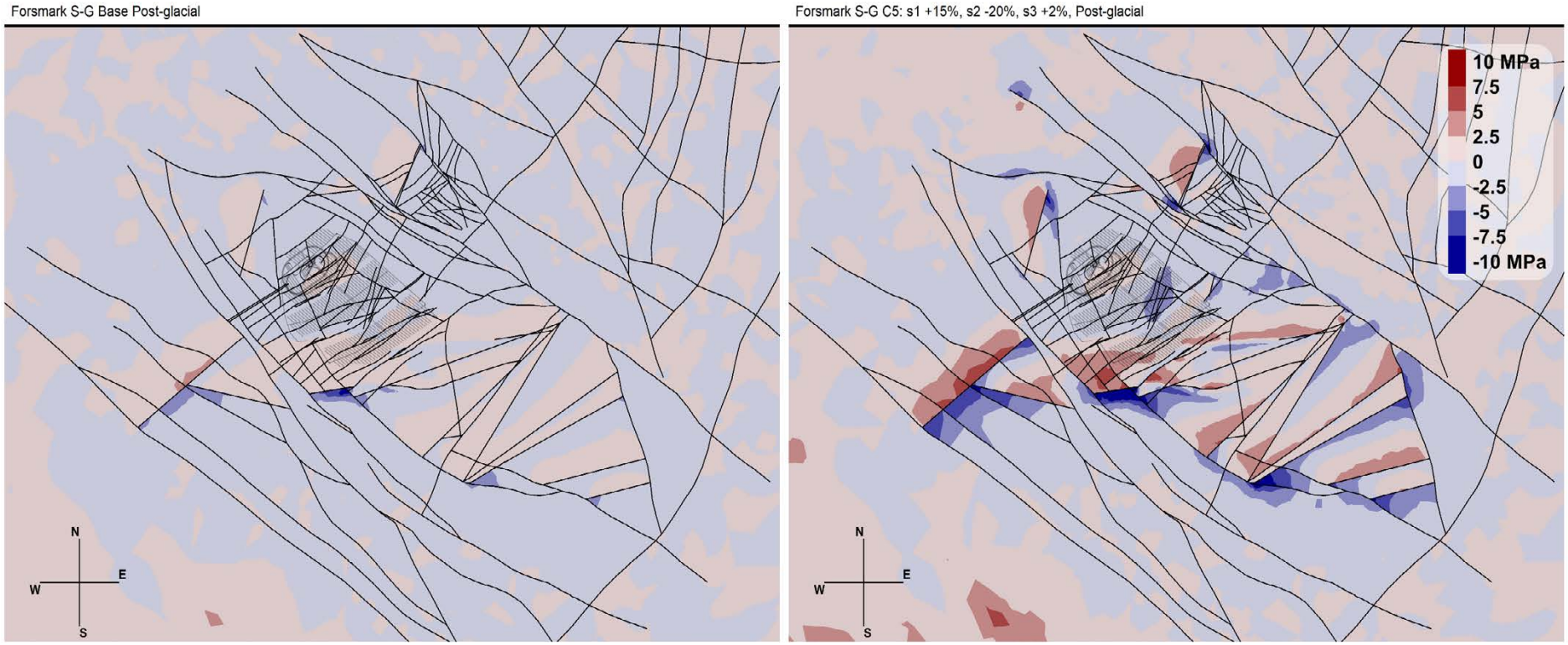

Figure A19-10. *The change in σ_3 magnitude after glaciation for the Base case and Case 5 of Phase 2 simulations in a horizontal cross-section at repository depth (470 m). The reference value is case-dependent.*

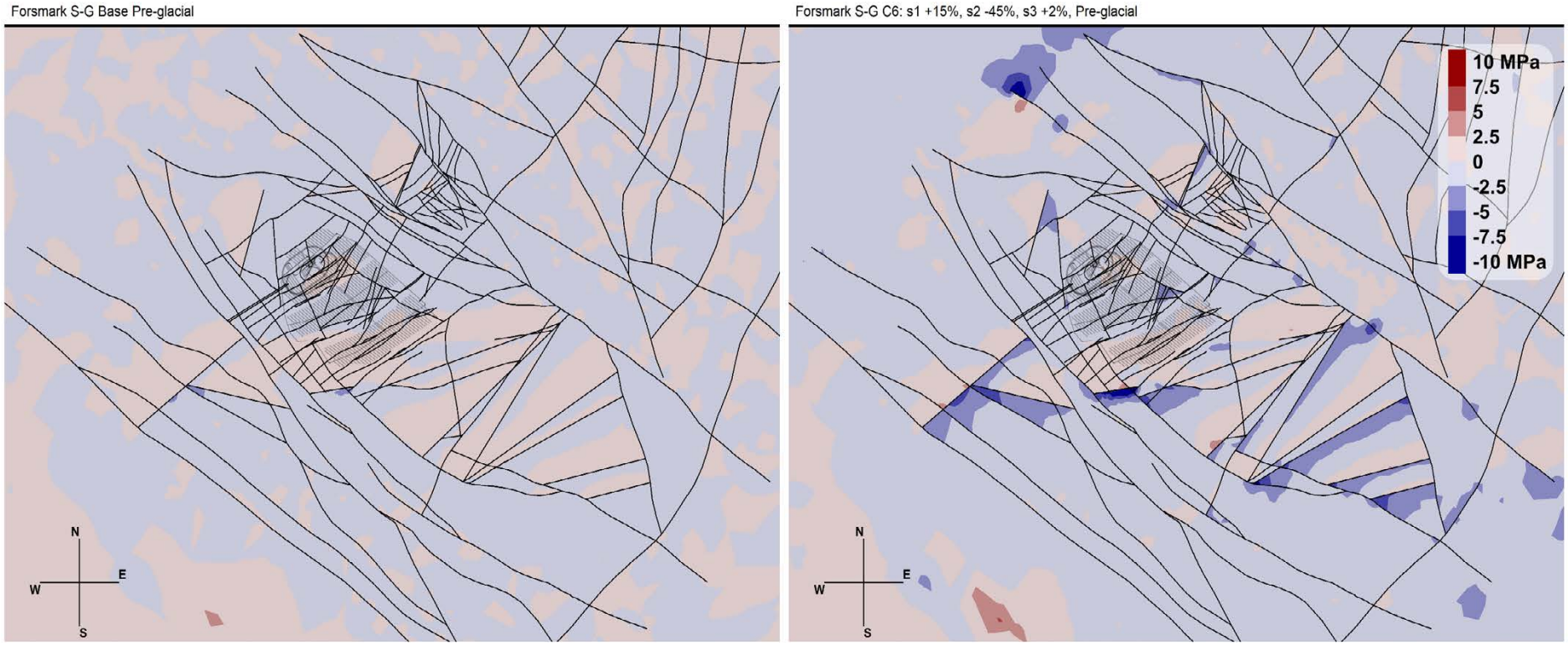

Figure A19-11. *The change in σ_3 magnitude before glaciation for the Base case and Case 6 of Phase 2 simulations in a horizontal cross-section at repository depth (470 m). The reference value is case-dependent.*

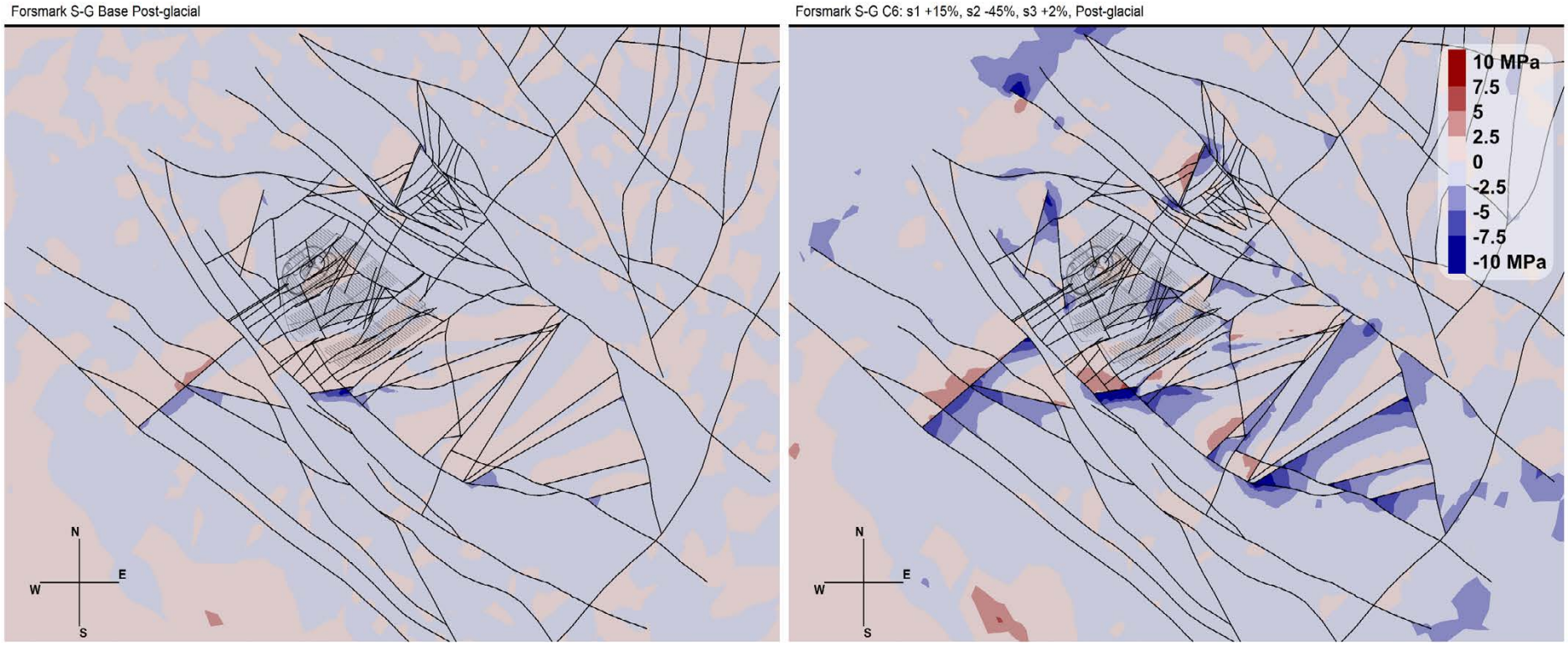

Figure A19-12. *The change in σ_3 magnitude after glaciation for the Base case and Case 6 of Phase 2 simulations in a horizontal cross-section at repository depth (470 m). The reference value is case-dependent.*

Appendix 20

Phase 1 – Change in σ_1 trend at repository depth

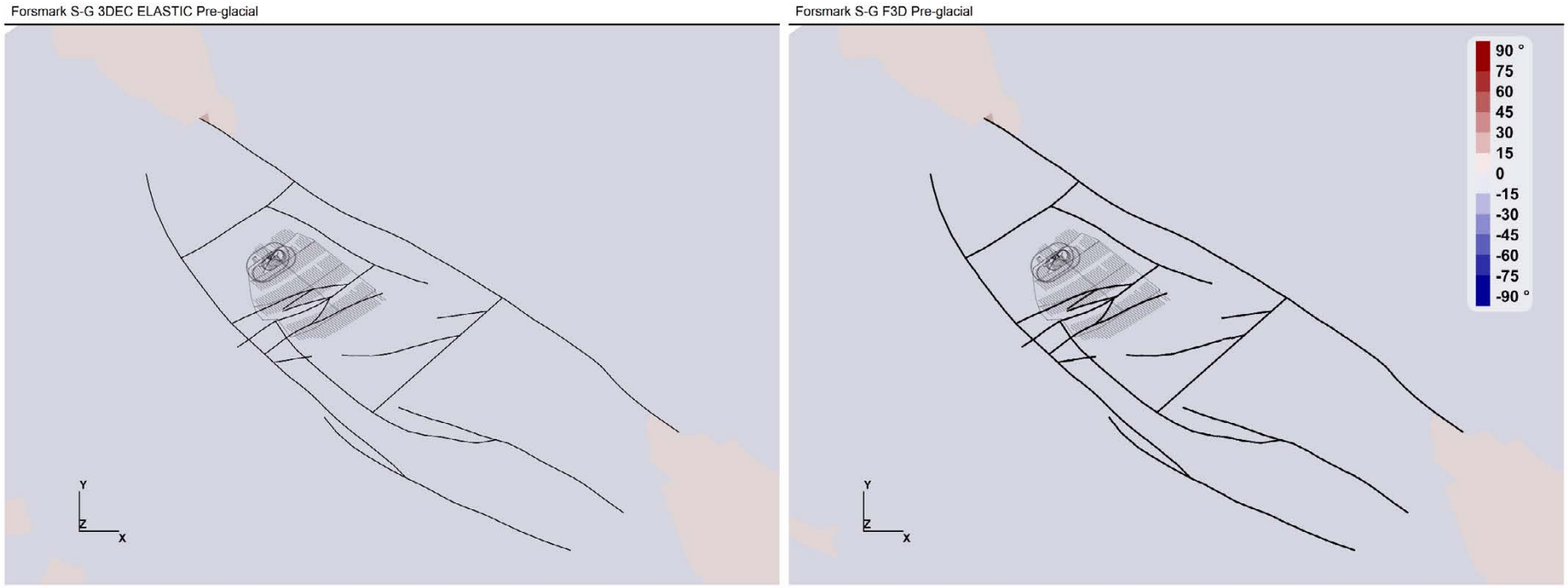

Figure A20-1. *Horizontal cross sections at repository depth −470 m of the maximum principal stress trend difference to the Martin (2007) interpretation before glaciation in a fully elastic simulation. The reference value is case-dependent.*

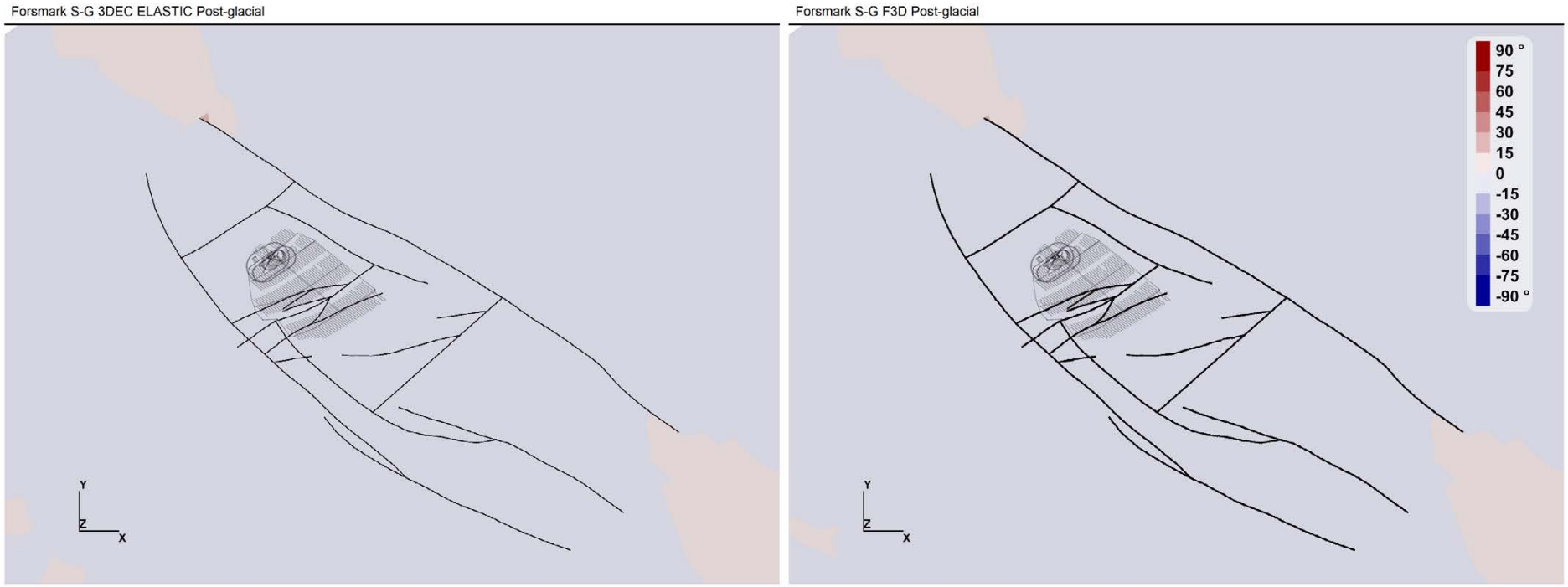

Figure A20-2. *Horizontal cross sections at repository depth −470 m of the maximum principal stress trend difference to the Martin (2007) interpretation after glaciation in a fully elastic simulation. The reference value is case-dependent.*

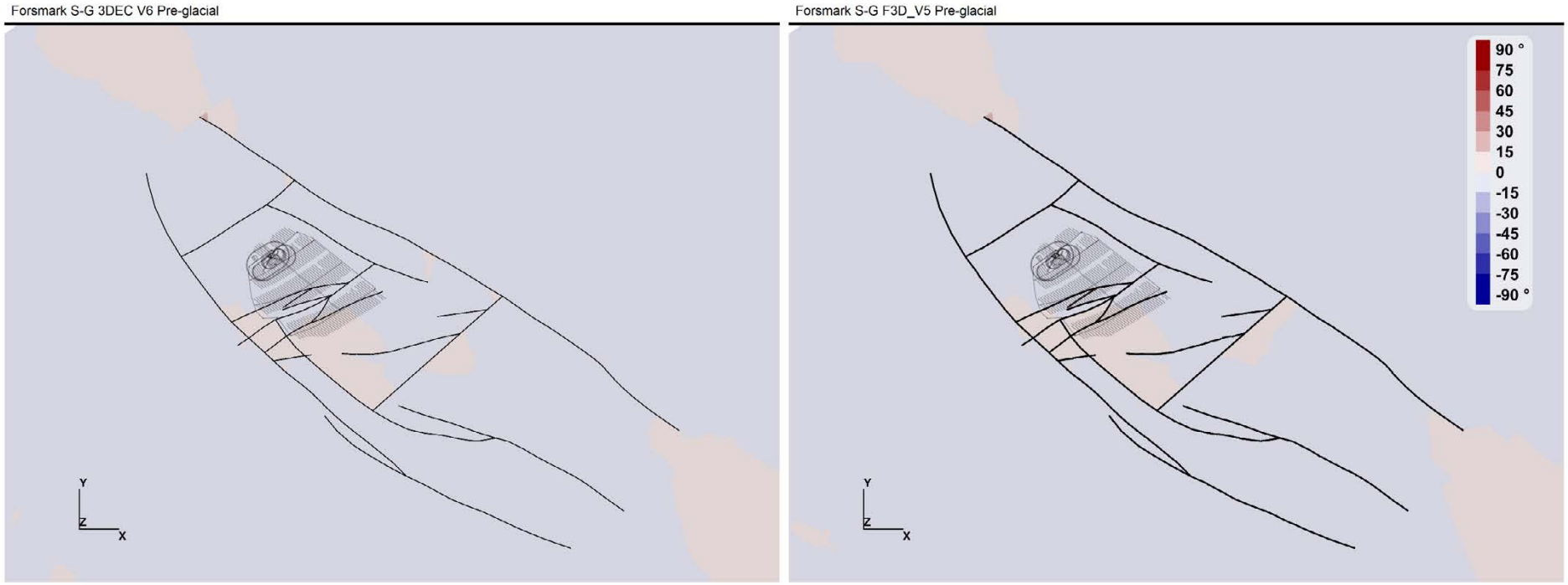

Figure A20-3. *Horizontal cross sections at repository depth −470 m of the maximum principal stress trend difference to the Martin (2007) interpretation before glaciation in an elastoplastic simulation. The reference value is case-dependent.*

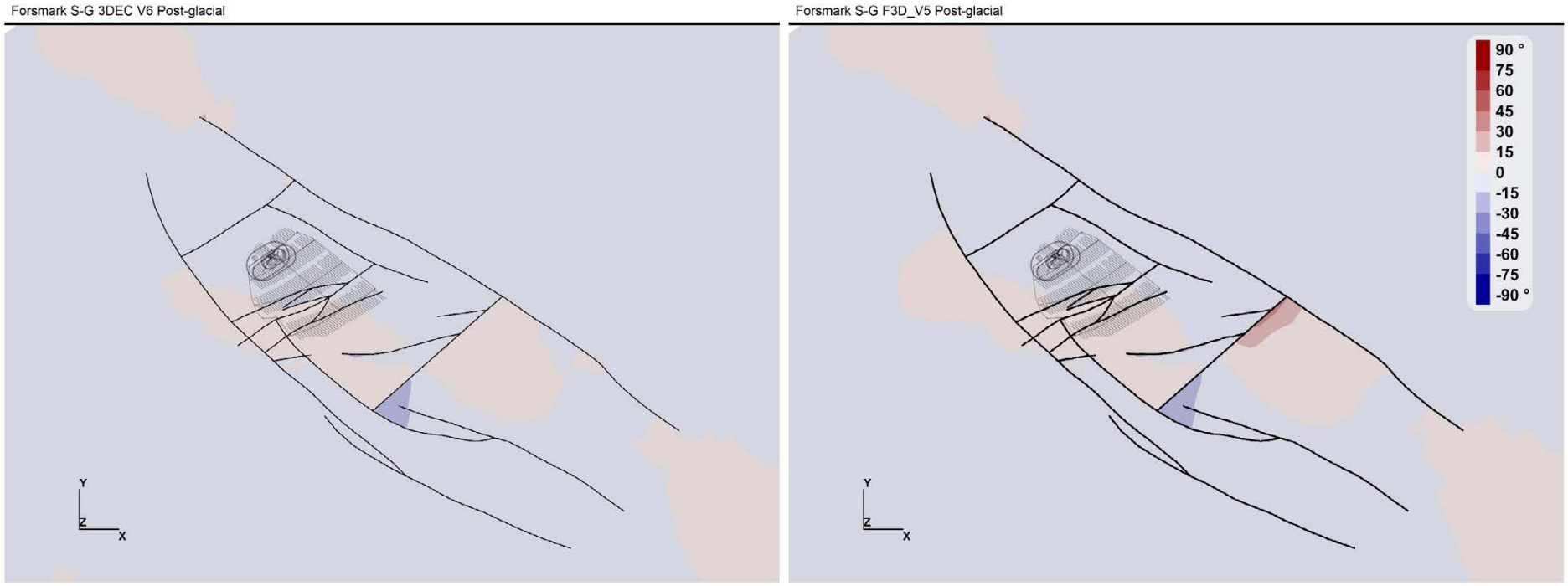

Figure A20-4. *Horizontal cross sections at repository depth −470 m of the maximum principal stress trend difference to the Martin (2007) interpretation after glaciation in an elastoplastic simulation. The reference value is case-dependent.*

Appendix 21

Phase 2 – Change in σ_1 trend at repository depth

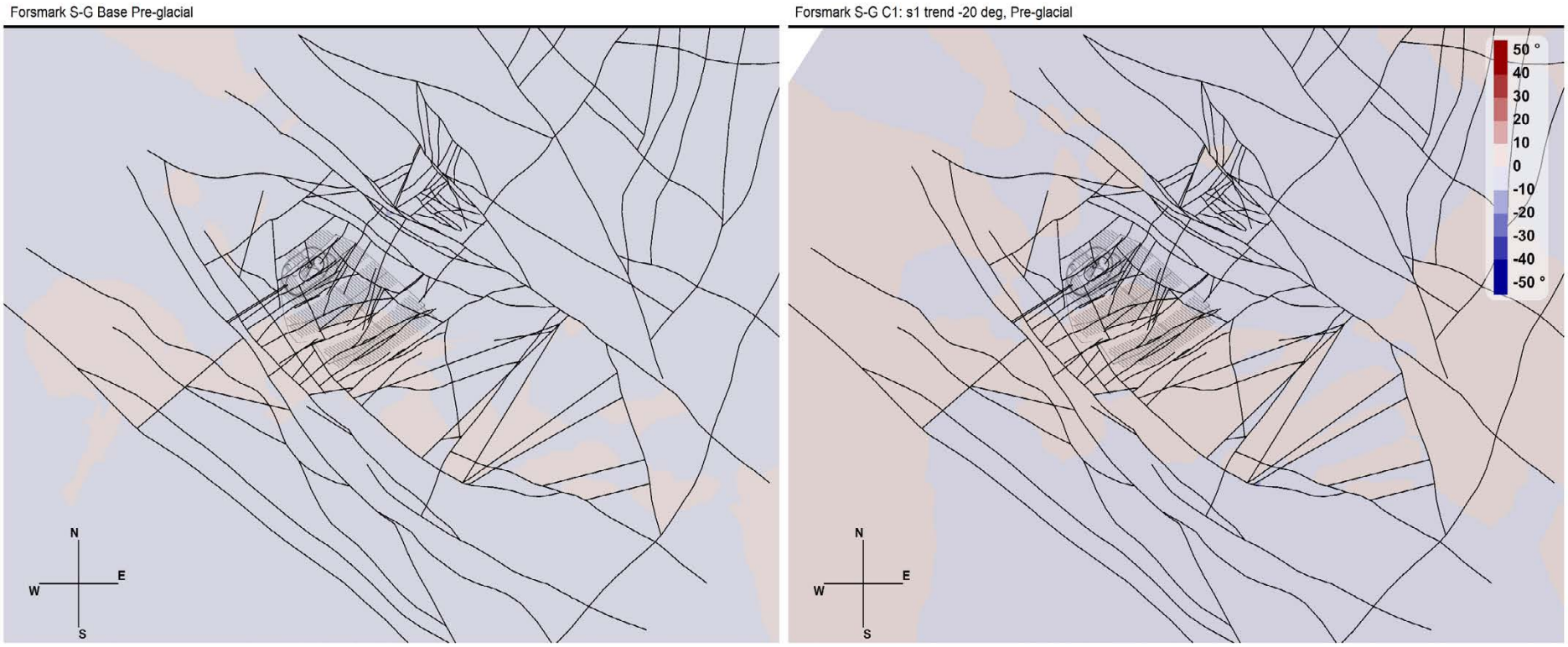

Figure A21-1. *The change in σ_1 trend before glaciation for the Base case and Case 1 of Phase 2 simulations in a horizontal cross-section at repository depth (470 m). The reference value is case-dependent.*

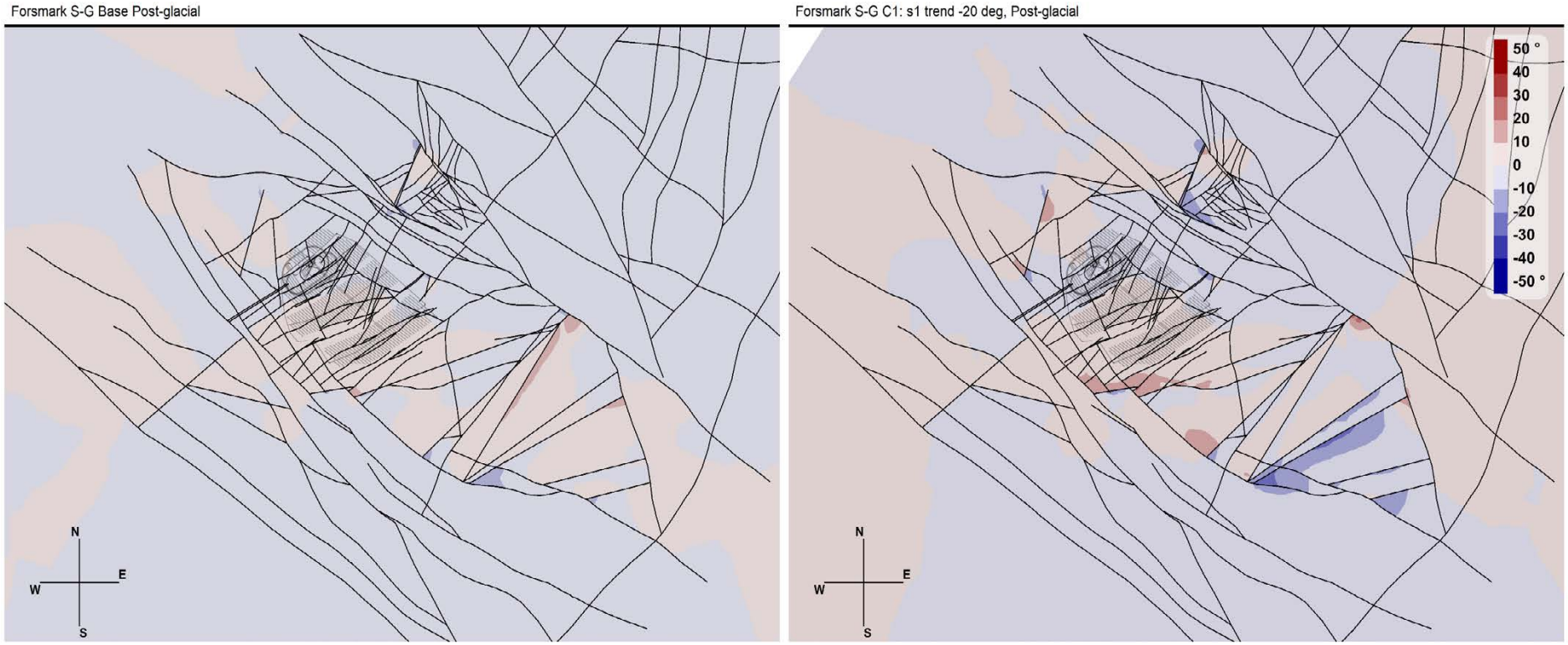

Figure A21-2. *The change in σ_1 trend after glaciation for the Base case and Case 1 of Phase 2 simulations in a horizontal cross-section at repository depth (470 m). The reference value is case-dependent.*

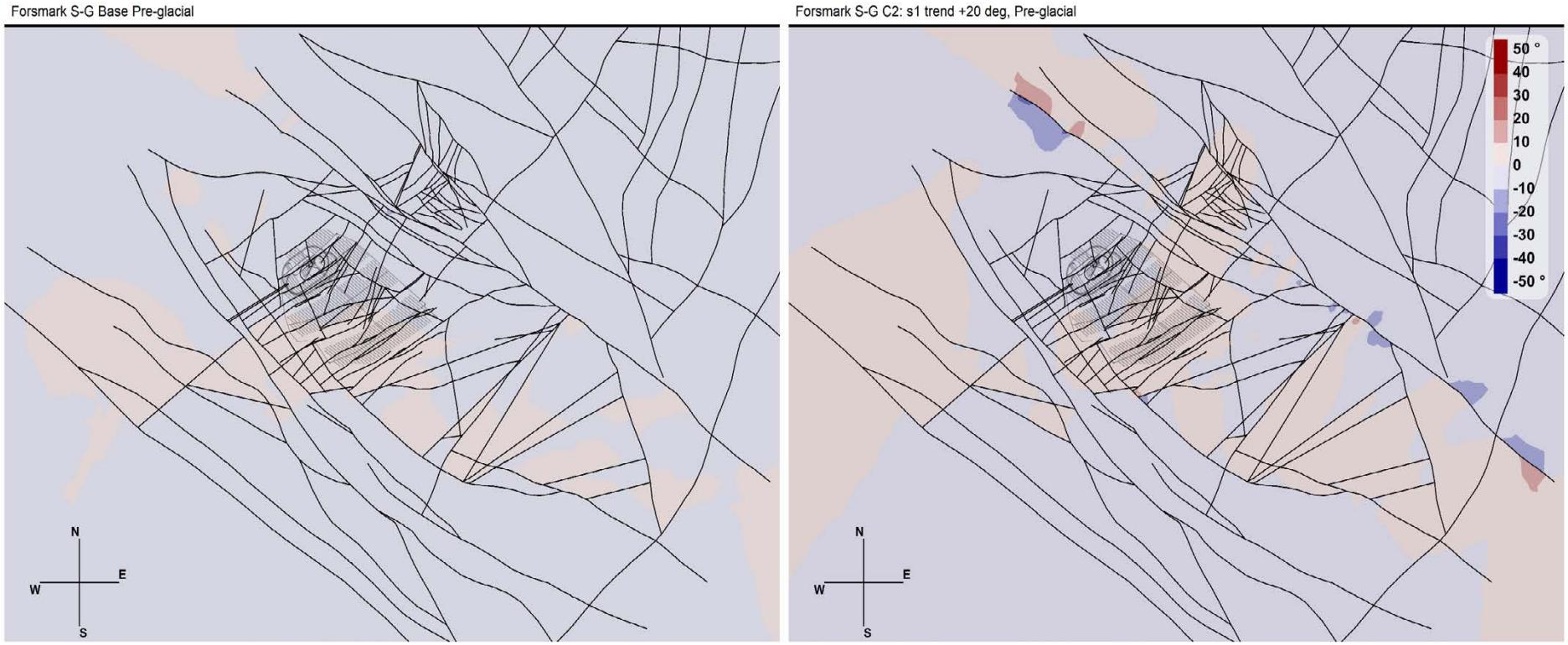

Figure A21-3. *The change in σ_1 trend before glaciation for the Base case and Case 2 of Phase 2 simulations in a horizontal cross-section at repository depth (470 m). The reference value is case-dependent.*

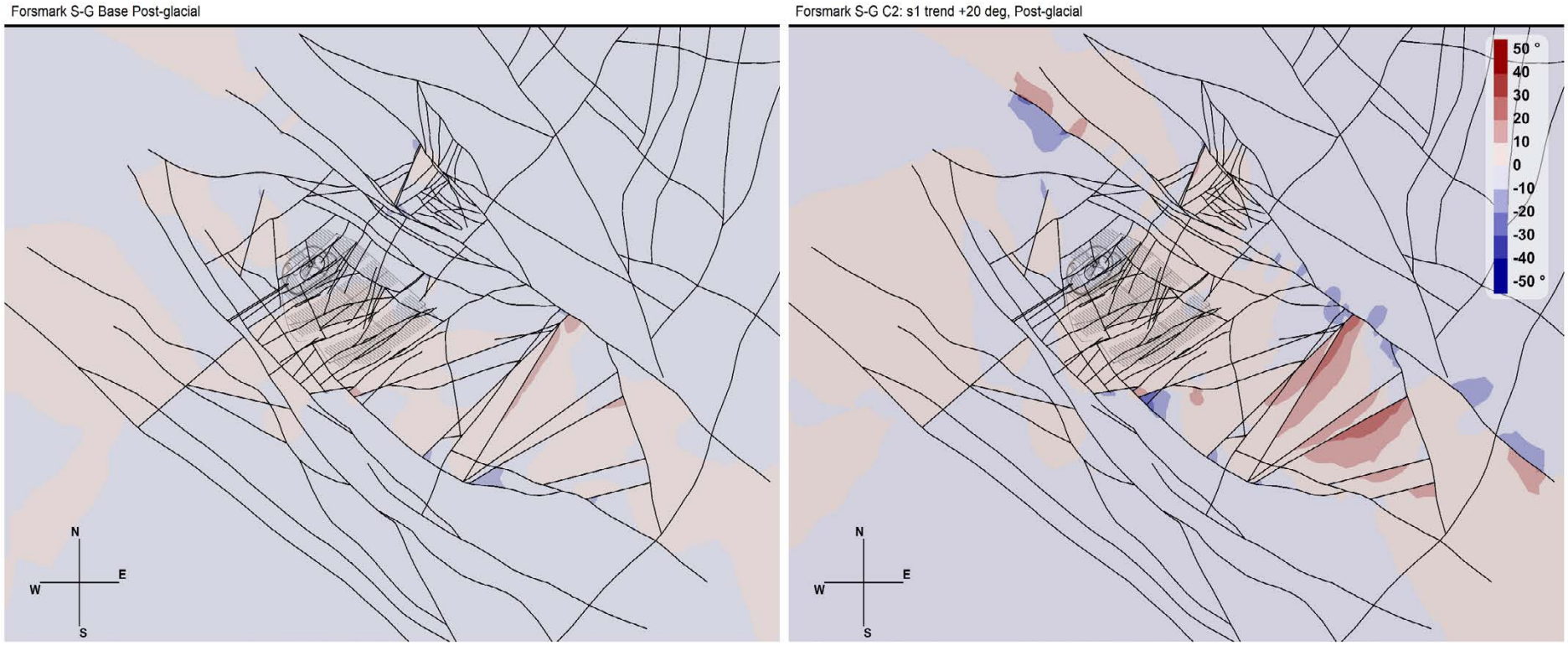

Figure A21-4. *The change in σ_1 trend after glaciation for the Base case and Case 2 of Phase 2 simulations in a horizontal cross-section at repository depth (470 m). The reference value is case-dependent.*

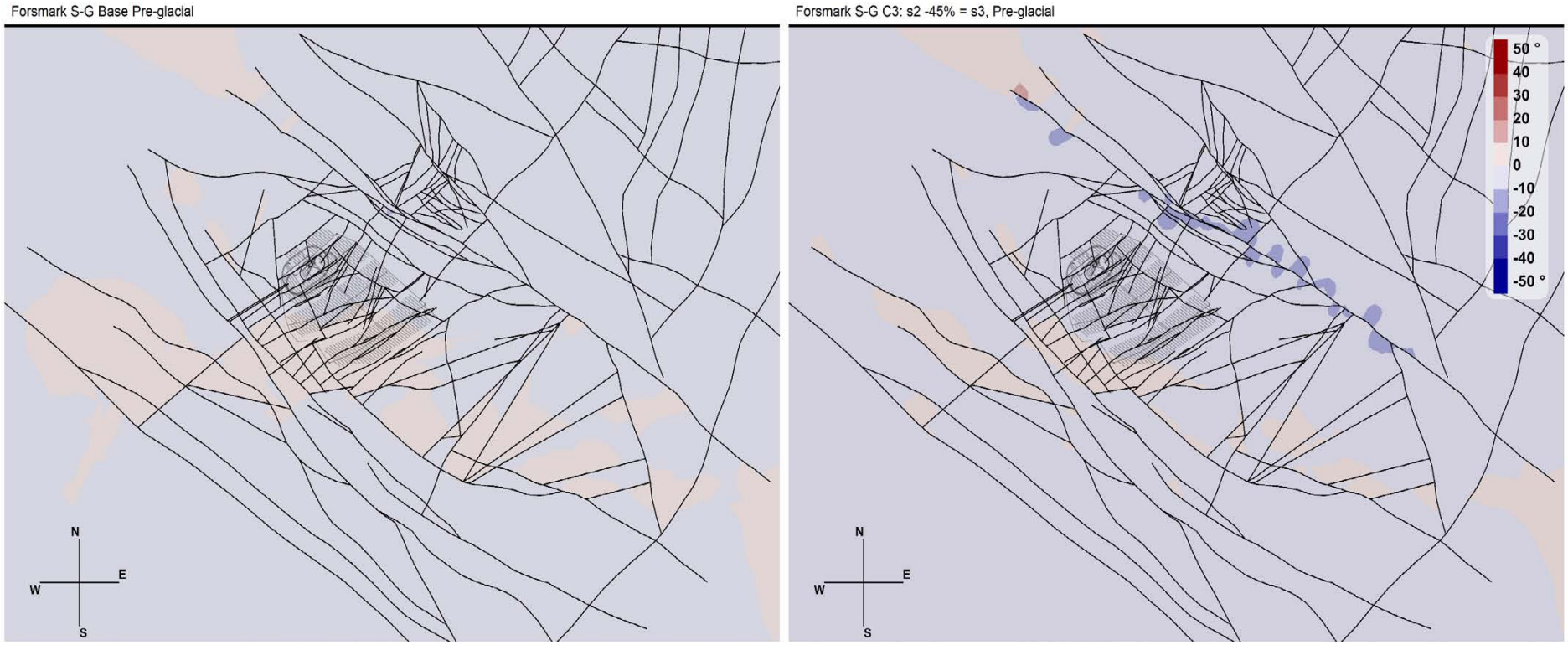

Figure A21-5. *The change in σ_1 trend before glaciation for the Base case and Case 3 of Phase 2 simulations in a horizontal cross-section at repository depth (470 m). The reference value is case-dependent.*

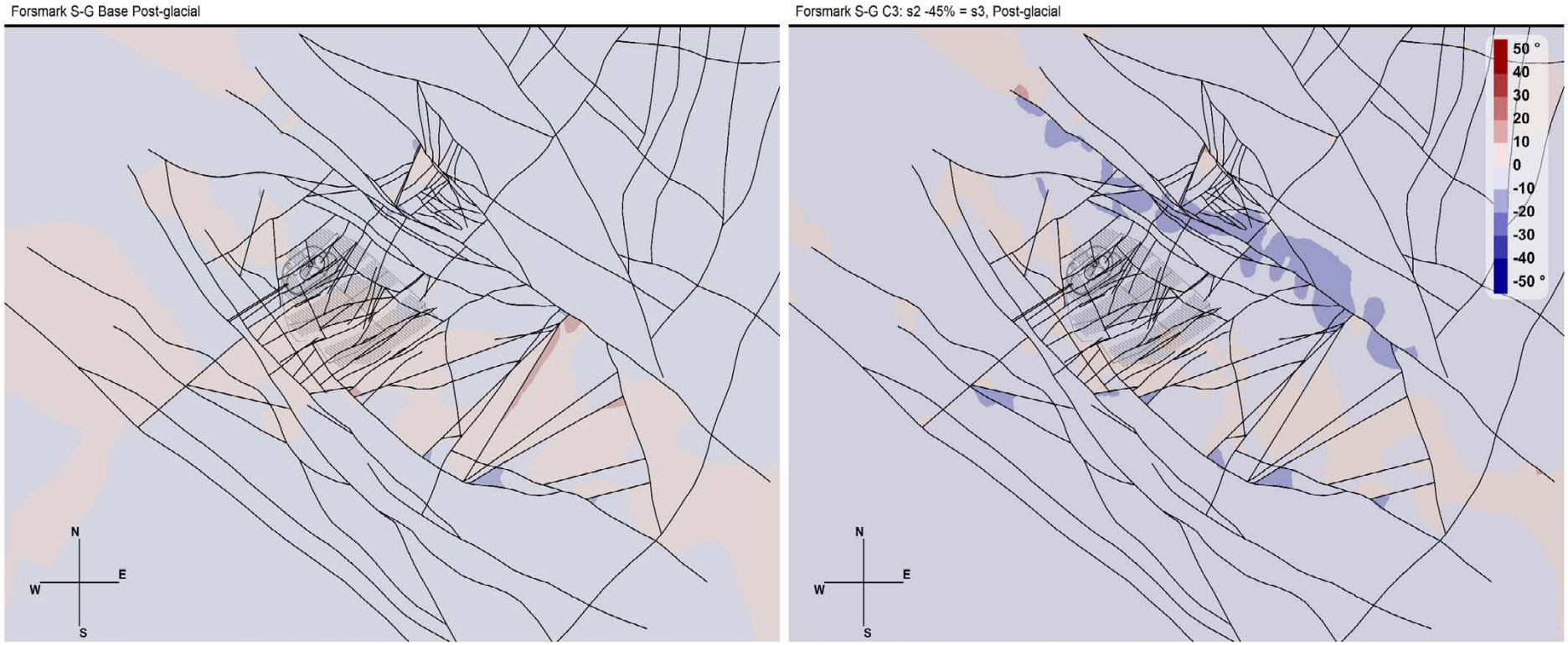

Figure A21-6. *The change in σ_1 trend after glaciation for the Base case and Case 3 of Phase 2 simulations in a horizontal cross-section at repository depth (470 m). The reference value is case-dependent.*

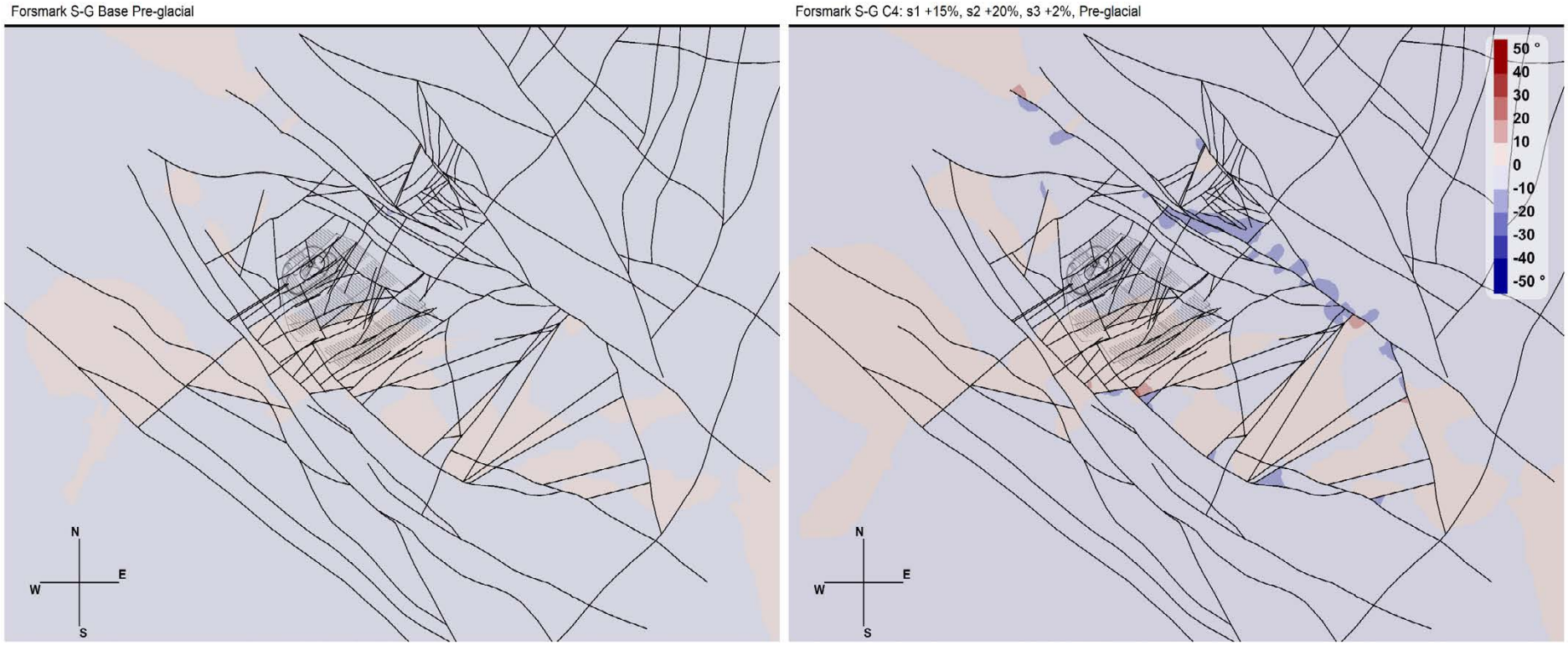

Figure A21-7. *The change in σ_1 trend before glaciation for the Base case and Case 4 of Phase 2 simulations in a horizontal cross-section at repository depth (470 m). The reference value is case-dependent.*

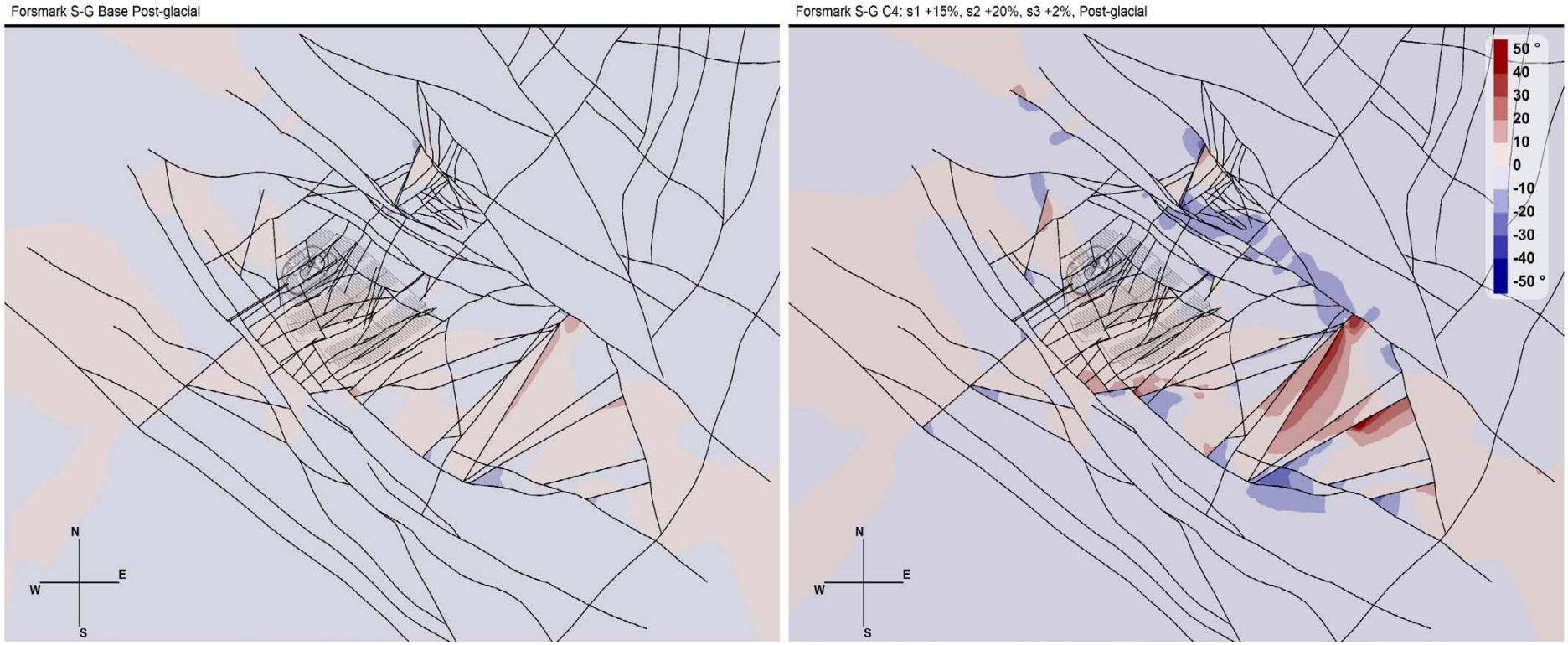

Figure A21-8. *The change in σ_1 trend after glaciation for the Base case and Case 4 of Phase 2 simulations in a horizontal cross-section at repository depth (470 m). The reference value is case-dependent.*

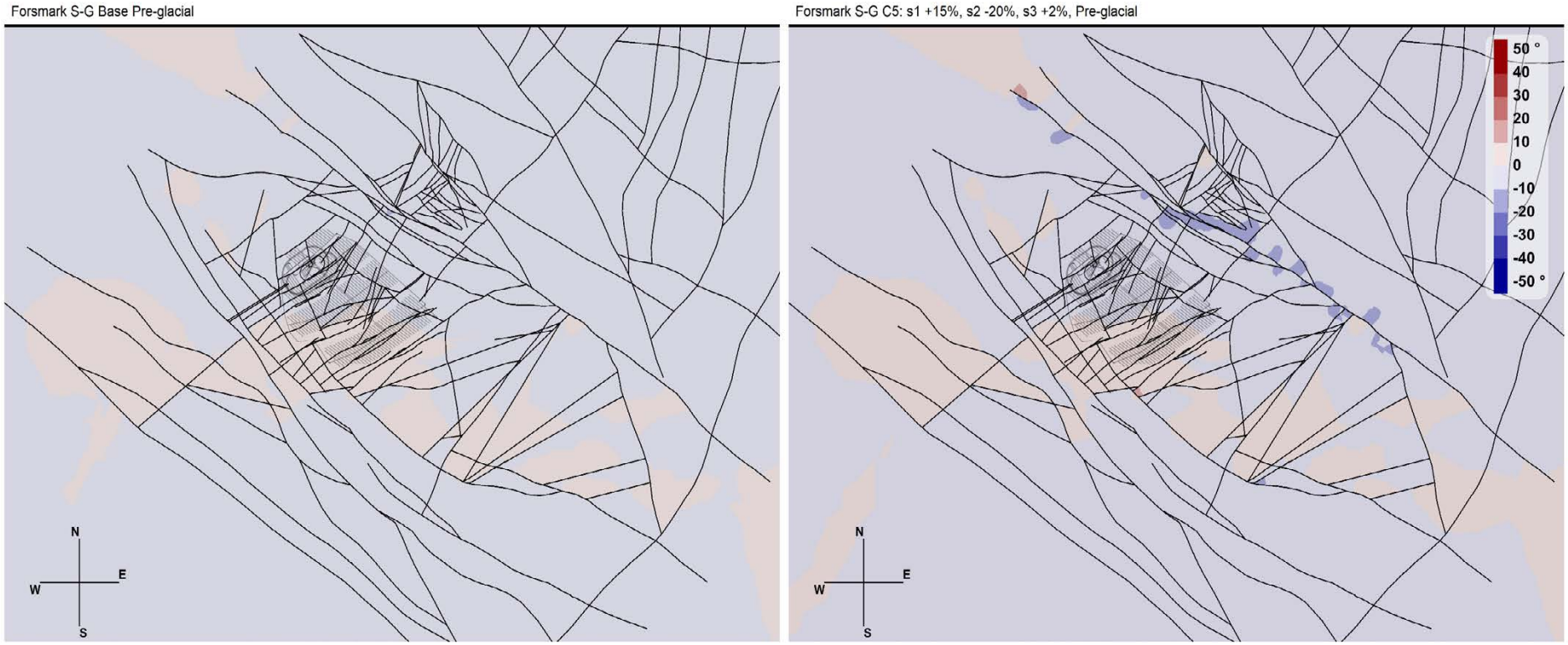

Figure A21-9. *The change in σ_1 trend before glaciation for the Base case and Case 5 of Phase 2 simulations in a horizontal cross-section at repository depth (470 m). The reference value is case-dependent.*

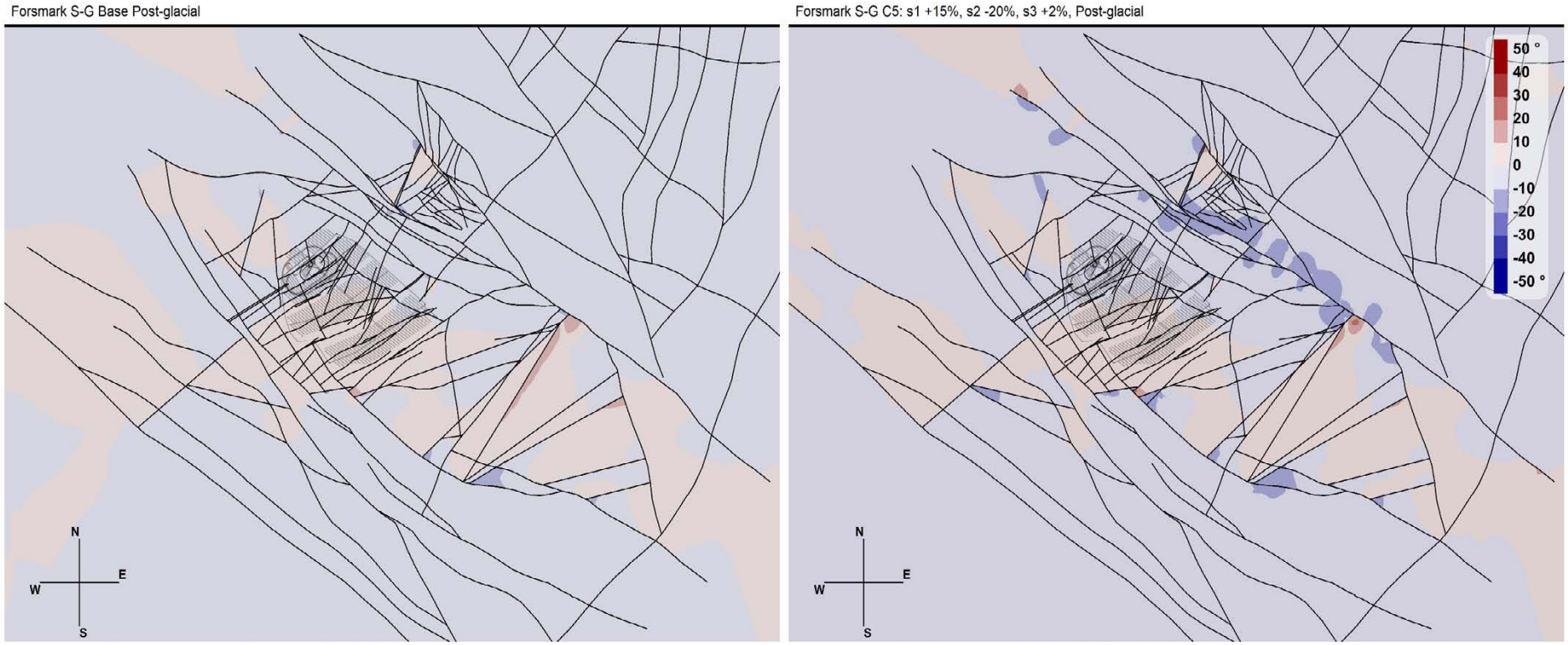

Figure A21-10. *The change in σ_1 trend after glaciation for the Base case and Case 5 of Phase 2 simulations in a horizontal cross-section at repository depth (470 m). The reference value is case-dependent.*

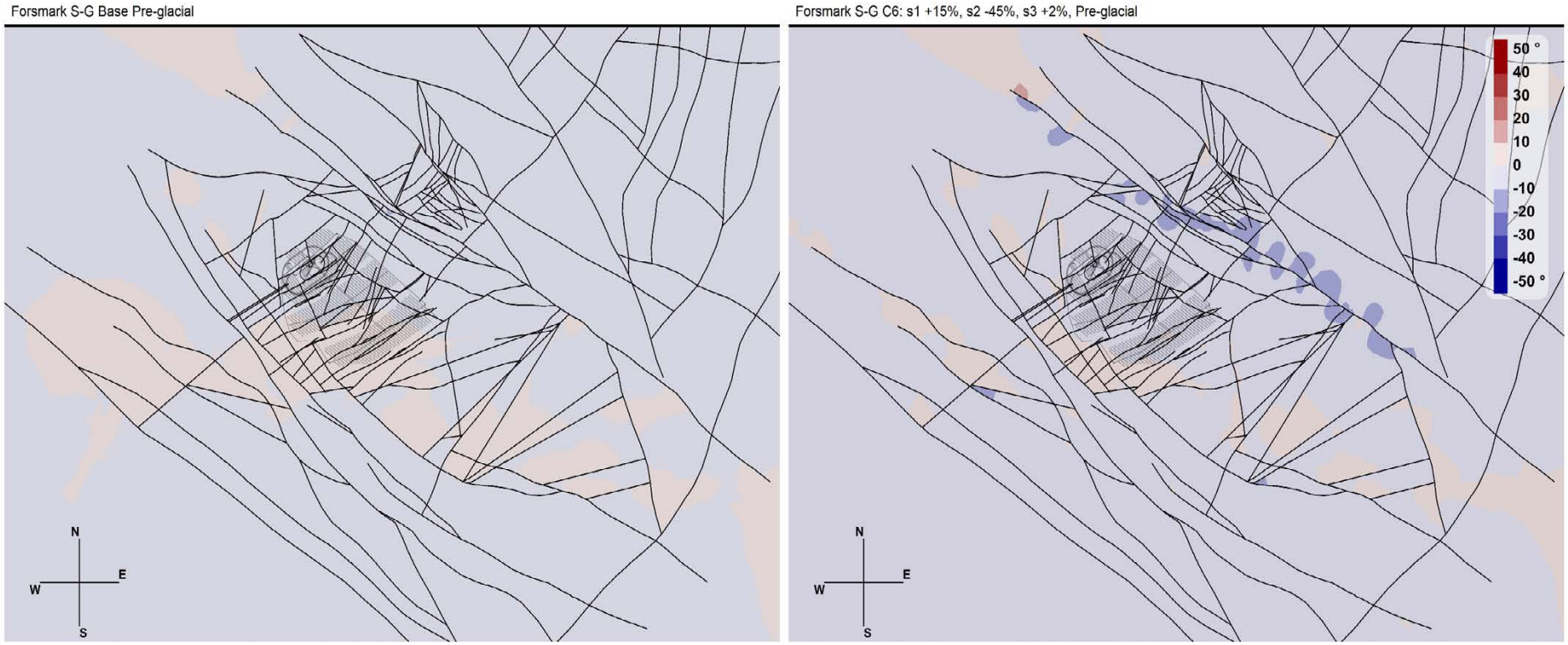

Figure A21-11. *The change in σ_1 trend before glaciation for the Base case and Case 6 of Phase 2 simulations in a horizontal cross-section at repository depth (470 m). The reference value is case-dependent.*

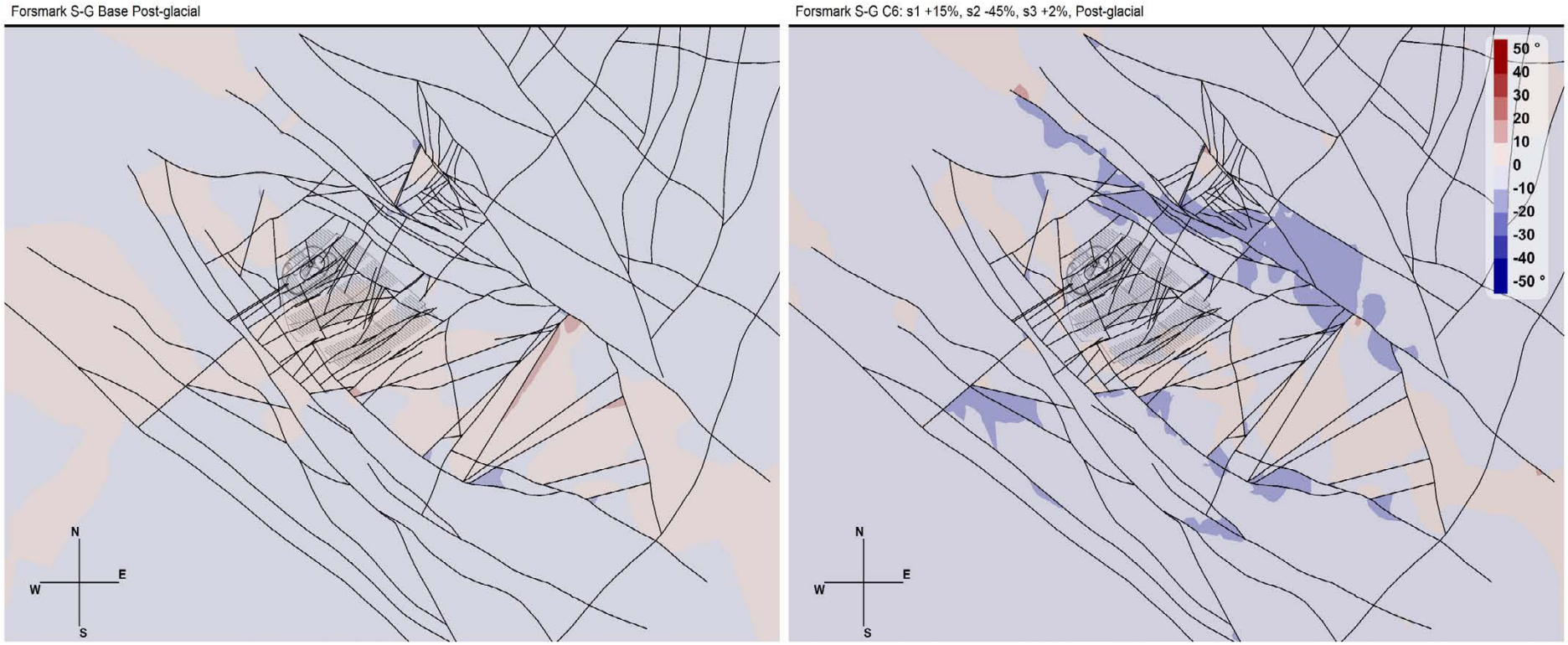

Figure A21-12. *The change in σ_1 trend after glaciation for the Base case and Case 6 of Phase 2 simulations in a horizontal cross-section at repository depth (470 m). The reference value is case-dependent.*

Selected stress measurements in vertical cross sections of the maximum principal stress at selected borehole locations

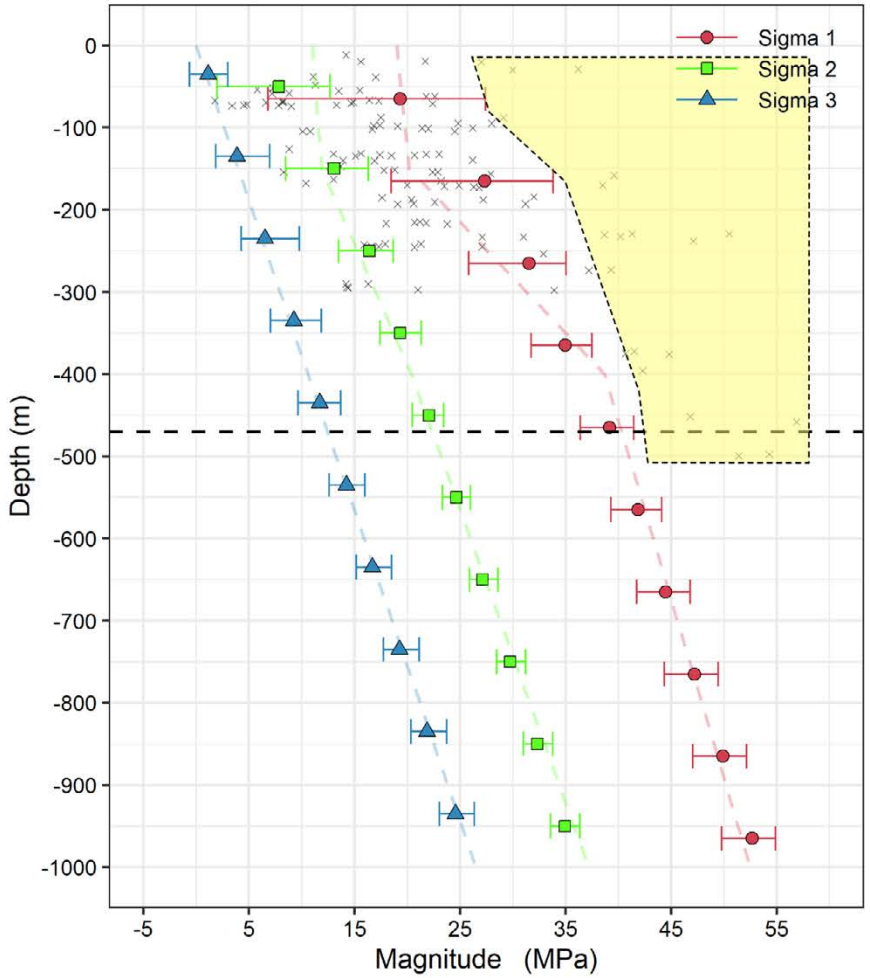

Selected stress measurements inside highlighted area

IDCODE	SIGMA_1 (MPa)	NORTHING_SECUP	EASTING_SECUP	ELEVATION_SECUP
KFK001	30	6699413.43	158810.29	-29.57
KFK001	36.2	6699413.43	158810.29	-28.97
KFK001	39.3	6699413.43	158810.29	-273.26
KFK001	40.7	6699413.43	158810.29	-374.99
KFK001	41.5	6699413.43	158810.29	-372.25
KFK001	44.8	6699413.43	158810.29	-375.78
KFK001	51.4	6699413.43	158810.29	-499.38
KFK001	54.3	6699413.43	158810.29	-497.49
KFK001	56.9	6699413.43	158810.29	-458.1
KFK003	27	6699501.93	158894.11	-20.32
KFM01B	38.7	6697810.79	160331.24	-230.49
KFM01B	40.2	6697810.79	160330.69	-232.46
KFM01B	41.301	6697810.79	160331.53	-229.46
KFM01B	42.3	6697811.54	160281.23	-395.86
KFM01B	46.8	6697812.26	160262.87	-451.82
KFM07C	24.9	6698392.17	160059.95	-170.15
KFM07C	39.6	6698393.33	160059.42	-158.31

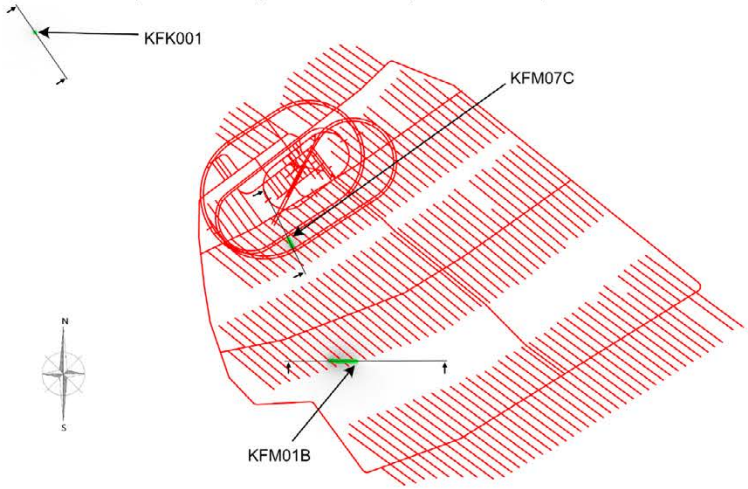

Figure A22-1. *Selected stress measurements that fall into the area highlighted in yellow. The bottom left illustrates the locations of the vertical cross-sections and their orientations for boreholes KFK001, KFM01B, KFM07C. Field stress measurements indicated with grey markers.*

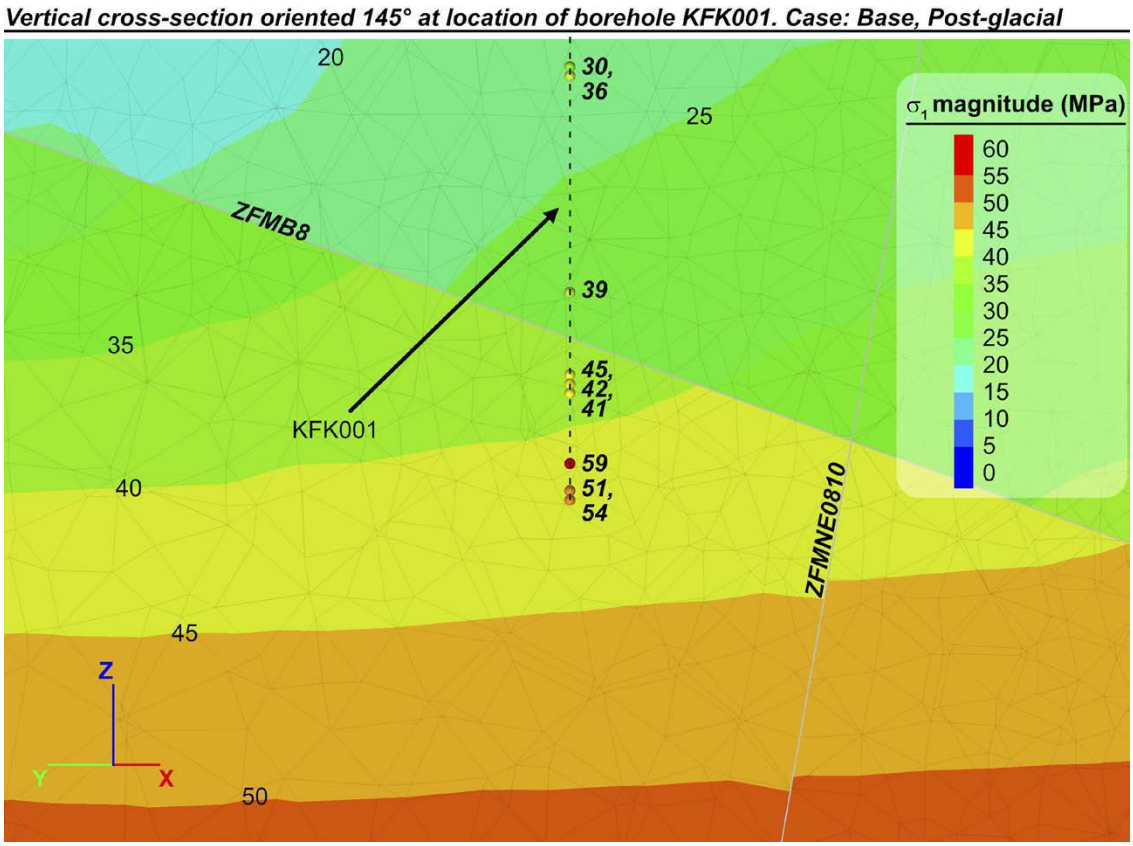

Figure A22-2. *Vertical cross section of σ_1 magnitude at location of KFK001 for the Base case after glaciation. Stress measurements are illustrated as spheres coloured and labelled by the measured σ_1 magnitude. KFK001 is illustrated with a black dashed line.*

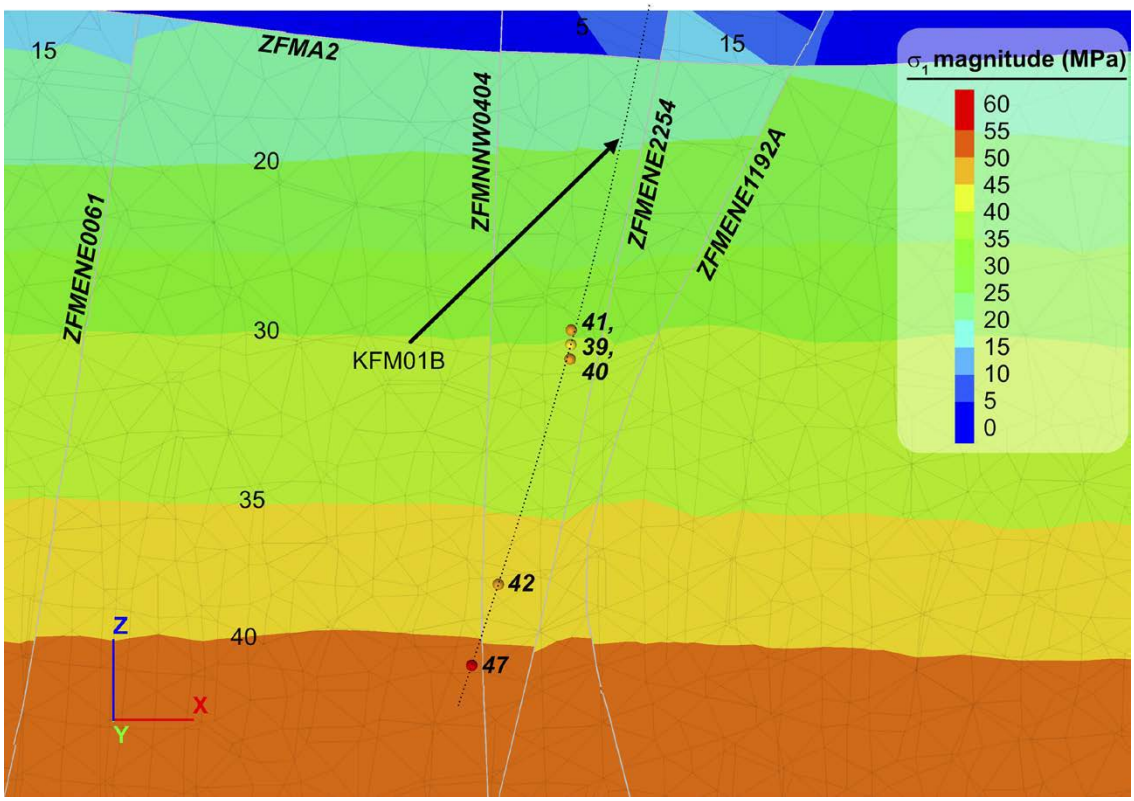

Figure A22-3. *Vertical cross section of σ_1 magnitude at location of KFM01B for the Base case after glaciation. Stress measurements are illustrated as spheres coloured and labelled by the measured σ_1 magnitude. KFM01B is illustrated with a black dotted line.*

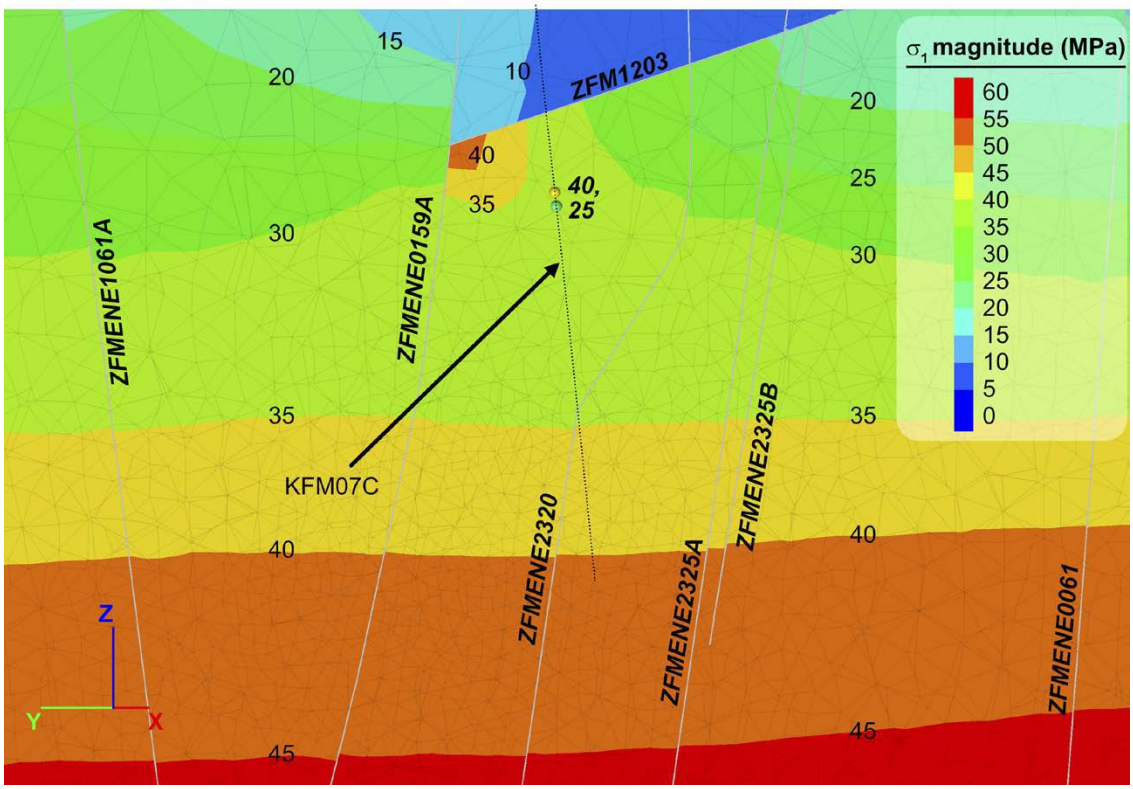

Figure A22-4. *Vertical cross section of σ_1 magnitude at location of KFM07C for the Base case after glaciation. Stress measurements are illustrated as spheres coloured and labelled by the measured σ_1 magnitude. KFM07C is illustrated with a black dotted line.*

Arkitektkopia AB, Bromma, 2023

SKB is responsible for managing spent nuclear fuel and radioactive waste produced by the Swedish nuclear power plants such that man and the environment are protected in the near and distant future.

skb.se